中国科学院上海应用物理研究所

年　报

2013-2014

(第 26 卷)

《中国科学院上海应用物理研究所年报》

编辑委员会

前　言

2013-2014 年，我所扎实推进“一三五”规划，迎来建所 55 周年并顺利完成了领导班子换届。中国科学院启动和推进“率先行动”计划，实施“四类机构”改革方案试点，全院首批共设 12 个试点机构，依托我所成立了中科院上海大科学中心和中科院先进核能创新研究院。我所成为全院唯一同时承担两个试点的单位，迎来了新的发展机遇。

一、扎实推进“一三五”规划，着力践行“四个率先”

以党的十八大精神为指导，深入实施院“创新 2020”和研究所“一三五”规划，进一步凝练战略目标，加大力度推进钍基熔盐堆核能系统战略性先导专项的实施，力争尽快掌握钍基熔盐堆核能系统的核心技术；积极开展上海光源大科学装置集群建设，促进国际一流水平的光子科学研究基地的形成，助力重大科研成果的产出；冲击核科学和基础交叉创新研究的世界前沿，解决基础和应用研究中的重大和关键科学问题。我所不断提升综合实力和竞争力，科技创新成效明显，在院发展规划局组织的研究所“一三五”国际专家诊断评估中取得高度评价。

二、科研工作取得重要突破，科研项目和经费稳步增长

钍基熔盐堆核能（TMSR）先导专项工作扎实推进，在人才队伍建设、嘉定园区（冷）实验基地建设、实验堆设计与关键技术研究及关键设备样机研制、国际合作等方面取得重要进展，顺利通过中科院组织的先导专项中期进展评估，获得继续支持；国际国内合作取得重大突破，与美国橡树岭国家实验室正式签订熔盐堆技术合作研究与开发协议（CRADA），与麻省理工大学签订科技合作意向书。完成 10MW 固态燃料钍基熔盐实验堆（TMSR-SF1）、仿真实验堆（TMSR-SF0）、2MW 液态燃料钍基熔盐实验堆（TMSR-LF1）三种钍基熔盐实验堆（均为世界首堆）概念设计，启动 TMSR-SF1 工程设计，完成了 TMSR-SF0 首轮工程设计。

上海光源大科学装置持续高效、稳定运行，用户数量和成果产出都超过了国际同类装置建成同期的水平。上海光源二期、蛋白质设施 5 线 6 站、“梦之线”、基于上海同步辐射光源的能源环境新材料原位电子结构综合研究平台、巴西直线

加速器等上海光源后续建设项目正在按照计划实施、推进，其中 X 射线自由电子激光试验装置和首台国产质子治疗示范装置研制项目已经正式开工建设。

核科学技术与前沿交叉学科领域开展广泛研究，在高能核物理、同步辐射细胞成像、DNA 纳米结构相关研究等方面做出了特色工作，获得了丰硕成果。核物理团队在相对论重离子对撞机 STAR 国际合作中，首次测量获得了 200GeV/c 金-金对撞中的双电子的产额，解决了长期困扰 RHIC 能区低质量区间双轻子产额增强的机制问题；物理生物学研究室与上海光源生物成像中心合作，清晰展示了一类自组装 DNA 四面体结构在活细胞中的摄取与转运过程，为其在药物载运和治疗方面的应用奠定了良好的基础；水科学研究室采用量子计算、同步辐射能谱实验等方法，研究了铝对蛋白结构的影响，提出了一种铝对人体生物毒性的新分子机制。

2013-2014 年，全所新争取各类科研项目 199 项、科研经费总额 7.55 亿元（上海光源运行费 2 亿元和核能专项经费 6.96 亿元除外）。获批国家基金委项目 97 项，其中重点项目 1 项、国际科技合作专项 2 项，新增 973 项目（课题）2 项。在重要项目争取上有较大突破，首次获得国家自然科学基金委创新研究群体项目。院重点实验室“微观界面物理与探测重点实验室”获得批准。发表论文 490 余篇，其中 SCI 论文 351 篇，以第一作者单位发表影响因子大于 5 的高水平论文 65 篇。申请专利 96 件，专利授权 68 件。

2013-2014 年，我所获得主要奖项如下：2013 年，上海光源国家重大科学工程获国家科技进步一等奖；2014 年，“相对论重离子碰撞中的反物质探测与夸克物质的强子谱学与集体性质研究”（马余刚、陈金辉）、“多元、协同生物传感界面的设计、组装及生物分析应用研究”（樊春海、王丽华、李迪）分别获上海市自然科学奖一等奖；樊春海获得 2014 年度上海市自然科学牡丹奖。

三、实施人才强所战略，凝聚和打造精锐科技团队

围绕研究所“一三五”规划的战略目标，持续推进人才强所战略，以凝聚和造就创新人才队伍为重点，采取多种措施建设满足本所跨越发展需求的人才队伍。

2013-2014 年，引进与招收各类工作人员 213 名，其中具有博士学位人员 105 名，受聘正高级岗位 8 名。骨干队伍中中科院“百人计划”23 名、国家级“百千万

人才”5 名、中科院“青年科学家奖”2 名。引进本所首位“青年千人计划”入选者，1 人入选“百千万人才”国家级人选并荣获国家“有突出贡献的中青年专家”称号、1 人入选国家“万人计划”之“青年拔尖人才”、2 人获得中科院“百人计划”择优支持、1 人获得中科院“现有关键技术人才”称号、1 人获得中科院“青年科学家奖”、1 人入选中科院“引进杰出技术人才”、2 人获得中科院“王宽诚教育基金会卢嘉锡青年人才奖”、8 人获得“中国博士后科研基金”和“上海市博士后科研资助”（其中 1 人获得中国博士后科研基金一等资助）、8 人获得人社部和教育部“留学回国人员科技项目资助”、1 人荣获上海市“青年科技英才”称号。

研究生教育和管理工作不断取得新进展，2014 年我所被评为国科大招生工作先进单位。拓展研究生培养新模式，获得直博生培养资格；打开专业硕士考博新途径，获得专硕考博英语自命题许可；实施“联合培养研究生计划”；与中国科学技术大学联合创办“赵忠尧应用物理科技英才班”，形成一套所系联合办学新模式；渗透本科教育，在复旦大学核科学与技术系设立“应用物理奖学金”，促使更多的优秀学生投身核科学与技术领域高水平科学研究和创新研究。教学管理方面，建立在读博士生退出机制；设立“梦想奖学金”和“学业奖学金”。2013-2014 年共计招收硕士生 208 名、博士生 120 名，毕业硕士 58 名、博士 85 名。

四、纵深拓展国际合作，提升国际影响力和竞争力

围绕研究所“一三五”规划和院“率先行动”计划，积极拓展和深化国际合作与交流，系统谋划我所国际化推进战略。两年共计派出 700 余人次执行因公出访任务；外宾来访 1000 余人次，创历史新高；新签署国际合作协议 13 项，成功举办“第四届国际粒子加速器大会”、“第五届原子力显微镜生物医学国际会议”、“第十五届全国核物理大会暨第十一届会员代表大会”、“高温高密核物质形态研究和奇特粒子寻找”研讨会、第三届两岸同步辐射研讨会等一系列高水平学术会议。其中“第四届国际粒子加速器大会”（简称 IPAC13）由我所出任大会主席，是国际加速器领域规模最大的学术会议，共有 33 个国家的 1300 余位代表参会，境外代表约 900 人，是我所主办的规模最大的一次国际会议。

我所目前正处于历史上发展最快的时期和“一三五”实施攻坚的关键阶段，也面临着严峻的挑战，使命光荣、目标远大，任务艰巨。我们要在认真组织和实

施“率先行动”计划的过程中，发奋图强、扎实工作、凝心聚力、开拓进取，建设好中科院上海大科学中心和中科院先进核能创新研究院，提高我所核心竞争力，打造核科技强所，使我所成为我国独具特色、不可替代和具有国际竞争力的研究机构，为中国科技的创新发展做出新的贡献。

目 录

大科学装置

钍基熔盐堆核能系统

基础与交叉

附录

大科学
装置

上海光源高频低电平的升级改造

高频组

高频低电平控制器采用反馈算法来控制加速结构的幅度和相位，工作频率等稳定运行，以及实现加速器需要的加速腔压和加速频率等的要求。最初采用的技术基于基带控制，采用模拟的反馈放大器来实现，在本世纪初，由于大规模集成电路的发展，以及现场可编程门阵列的成熟应用，采用数字技术来实现反馈控制，可以得到更高的控制精度和结构更紧凑的硬件框架。

上海光源从 2005 年开始数字化低电平的研制工作，硬件上采用商业化的数字信号处理开发板，加上时钟分布板卡构成了数字信号处理的核心硬件，由同轴混频器，放大器，功分器等器件构成了上下变频部分，开发了幅度，相位和频率控制环路，在 2007 年成功应用于储存环的调束中。

经过近几年的运行，深切的感受到采用商业化的硬件带来了接线较多，结构还不够紧凑的缺点，故障偶有发生。因此，开发了我们自己的硬件，最终的硬件结构由两个板卡组成：数字信号处理板和射频处理前端板卡。在数字信号处理板中，集成了 4 路高速的模数转换器通道，和 2 路高速数模转换器通道以及现场可编程门阵列。在接口方面，设计了控制马达运行的数字 I/O 通道，用于数据传输的网络通讯口等。射频前端包括 6 路变频通道，根据需要，都可以用来做上变频通道，也可以全部用于下变频通道，通过更改不同的外围器件来实现。整个控制器的精度有了很大的提高，幅度和相位稳定度(RMS)分别是：0.015%，0.014 度，(P-P) 0.1%和 0.1 度。在人机交互界面也从以前的 Labview+share_memory 的方式改成了加速器通常使用的 EPCIS 界面，运行平台从 windows 改成了 linux，这些改变提高了运行的可靠性。

图 1 所示为升级换代后的低电平实物，控制精度和 EPICS 界面。

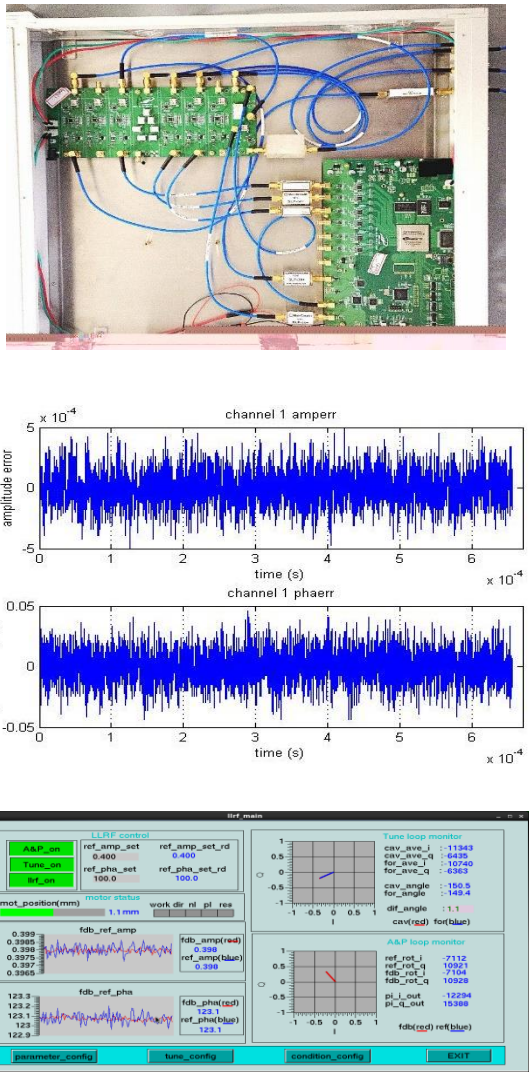

图 1 低电平实物，控制精度和 EPICS 界面

Update of digital LLRF in SSRF

LLRF (Low level radio frequency) is used to control the amplitude, phase and operation frequency of accelerator architecture. In additional, it need to realize the ramp of amplitude and frequency in some special accelerator. Before the beginning of this century, the analog and baseband technique are used in the LLRF, but with development of large scale IC, such as Field program gate array (FPGA) especially. The algorithm of feedback can be programmed in the FPGA, so the digital and immediate frequency technique are used in the LLRF. The virtue of digital technique make it better precision.

From 2005, the LLRF had been developed based on digital technique at SSRF. The commercial digital signal process board which include FPGA, ADCs and DAC was adopted to build the hardware architecture. The coaxial RF elements such as mixer, amplifier and splitter were used to build the RF front-end. The algorithm of field feedback loop, tuning loop was developed in this stage. In the end of 2007, this digital LLRF controller was operated successfully in the SSRF storage.

It was operated after six years. The shortcoming of commercial board is showed up Because the board and independent RF element are connected by several cables, the release of some connection result the trip of LLRF so that we develop the compact hardware board which only include RF front-end board and DSP board. In the DSP board, it is consisted of four ADC channels, two DAC channels, FPGA, digital I/O and ethernet port. The RF front-end have six channels of up- converter or down-converter which can be changed according to your requirement. The coaxial RF element were replaced by surface chips. The precision of LLRF controller was improved. The stability of amplitude and phase respectively are (RMS) 0.015%, 0.014 degree. The peak to peak is 0.1% and 0.1 degree. The data transfer and GUI are changed from LabView+ Share_memory on windows platform to EPCIS on Linux platform. Those updates improve the robustness and stability of LLRF.

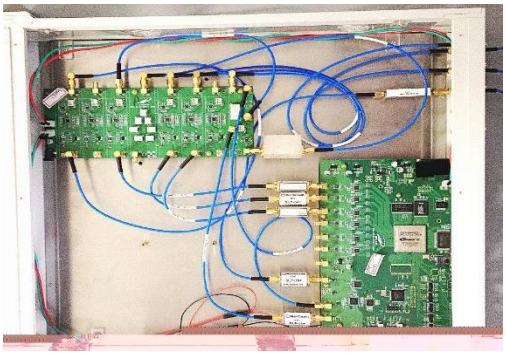

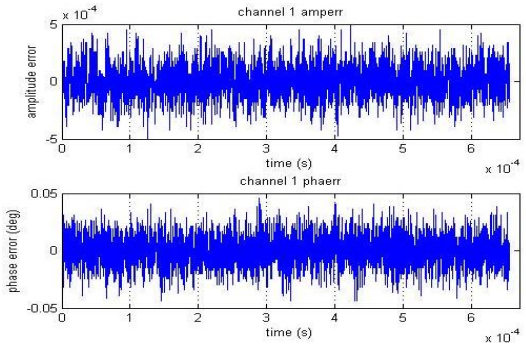

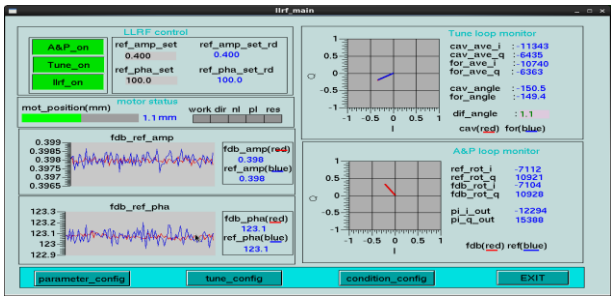

Fig.1 Shows the updated LLRF controller, stability and GUI

2013–2014 年度电源部脉冲组工程技术研究研制情况

电源部 脉冲组

2013–2014 年度，脉冲组所承担工程研制任务较为繁重，这些工程研制任务主要包括：1) SXFEL、DCLS 以及巴西 SIRIUS 直线加速器调制器系统研制任务工程设计，核能加速器调制器系统设计及安装调试；2) 上海先进质子治疗装置注入引出系统以及 RFKO 系统研制的工程设计；3) SSRF 插入件控制及前馈，SXFEL 以及 DCLS 插入件及段间设备（BBA，移相器）以及 Chicane 的控制；4) 调制器相关技术研究。下面就部分内容展开介绍。

1 高功率脉冲调制器研制

各个项目工程中高功能脉冲调制器的功率参数以及研制阶段如下表：

表 1 各项目调制器类型

参数 / 项目	类型	数量	功率	进展情况
核能加速器	S-Band	1	25 MW	调试验收
SXFEL	S-Band	4	50 MW	工程设计
	C-Band	7	50 MW	工程设计
	X-Band	1	6 MW	工程设计
DCLS	S-Band	2	50 MW	工程设计
	S-Band	2	80 MW	工程设计
巴西 SIRIS	S-Band	2	50 MW	工程设计
C 波段样机	C-Band	1	50 MW	调试验收

核能加速器调制器的关键技术技术指标如重复频率、平均功率、峰值功率分别为 266 Hz、120 kW、75 MW。设计中采用多个充电电源并联技术，硬件控制电路设计着重考虑了充电电源在大充电电流和高重复频率条件下工作的情况，同时完成 PFN 等功率元件的参数选择和散热设计[1]。本地控制采用触摸屏等。这些工作可应于以后的调制器系统设计中，特别是为 SXFEL 项目高功率调制器性能提升做了一定技术积累。

图 1 核能调制器布局及脉冲变压器油缸组件

初步技术指标的测试如表 2。

表 2 调制测试参数

	峰值功率	重复频率	底部平坦度	幅度稳定度
设计指标	70 MW	266 Hz	1%	0.2%
测试指标	71 MW	133 Hz	0.5%	0.1%

2 SAPT 注入引出

注入引出系统由两台静电切割板、两台凸轨磁铁（图 2）、三台静磁切割磁铁以及它们的激励电源和控制组成。由于低能下空间电荷效应很严重，且单圈注入的流强达不到环的流强要求，因此采用多圈涂抹注入，即每圈注入到相空间的不同位置，从而达到整个相空间近似均匀的填充方式。多圈注入由静磁切割磁铁、静电切割板和形成储存束流凸轨的 bump 磁铁组成，凸轨控制采用两块 bump，可以减少元件数目。为了使低能输运线的注入管道躲开束流前进方向上端的二极铁，并适当降低静电切割板的高压强度，采用了静磁切割铁和静电切割板相结合的方式[2]。慢引出利用水平方向接近于三阶共振的自由震荡频率，通过环中的共振六极铁提供的三阶共振驱动项使得水平方向稳定区域逐渐减小，首先超出接受度的那些粒子会沿着稳定区分界线运动，逐渐远离正常束流轨道[3]，在合适的位置放置静电切割板就会将束流偏离循环轨道而到达引出轨道。切割磁铁磁场仿真见图 3。

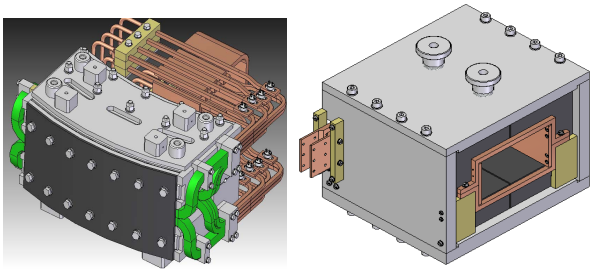

图 2 切割磁铁及凸轨磁铁

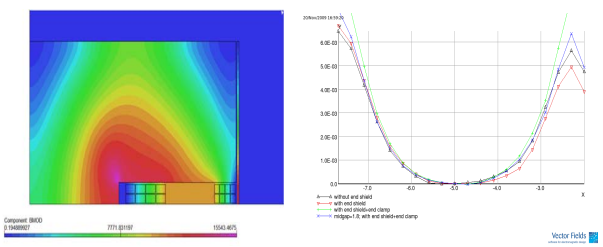

图 3 切割磁铁磁场仿真

3 SAPT RFKO

慢引出 RFKO 控制总体框图如图 4 所示，其按照功能划分，主要包括 RFKO 控制器、FM 发生器、电压控制放大器(VCA)、RF 开关、RF 放大器(RFA)、信号调理及 RFKO 电极。RFKO 控制器根据治疗控制系统的流强设置及能量设置计算激励信号的中心频率和带宽，并控制 FM 发生器产生相应的信号[6]。在获取流强反馈信号后，进行前馈、反馈控制激励信号的幅度[4]。在 RFKO 控制器发送 Beam on/off 信号的作用下，可以启动或停止束流引出，同时将相应的状态发送治疗控制系统。RFKO 控制器通过 RF on/off 信号控制 RF 开关，使得治疗流强可以快速切断（在无束要求期间不引出粒子）。RF-Kicker 3D 静态电场仿真如下图：

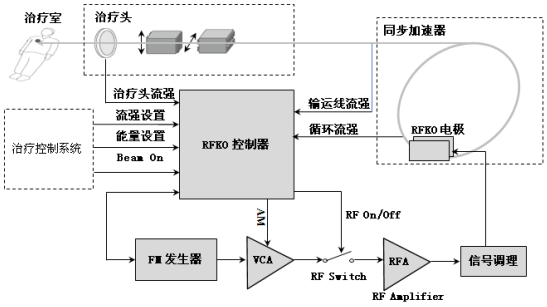

图 4 SAPT RFKO 控制总体框图

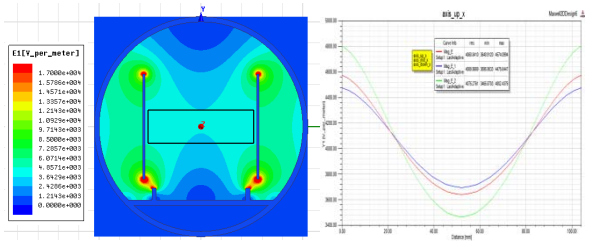

图 5 RF-Kicker 3D 静电场仿真

4 插入件控制及前馈

插入件的控制工作主要包括 SXFEL、DCLS 插入件及其段间设备运动控制系统的工程设计，国内首台低温波荡器温度监测及控制，微系统所 EPU200 运动控制，以及 DEPU 的前馈。EPU200 的运动控制采用六台步进电机驱动波荡器上、下大梁运动，用四个光栅尺检测大梁出、入口的上、下间隙，用两个光栅尺检测大梁的左右间隙。采用 PLC 实现运动控制和极限位置保护。系统设计了三重限位保护，另外还有机械挡块保护。图 6 是 EPU200 的控制框图。

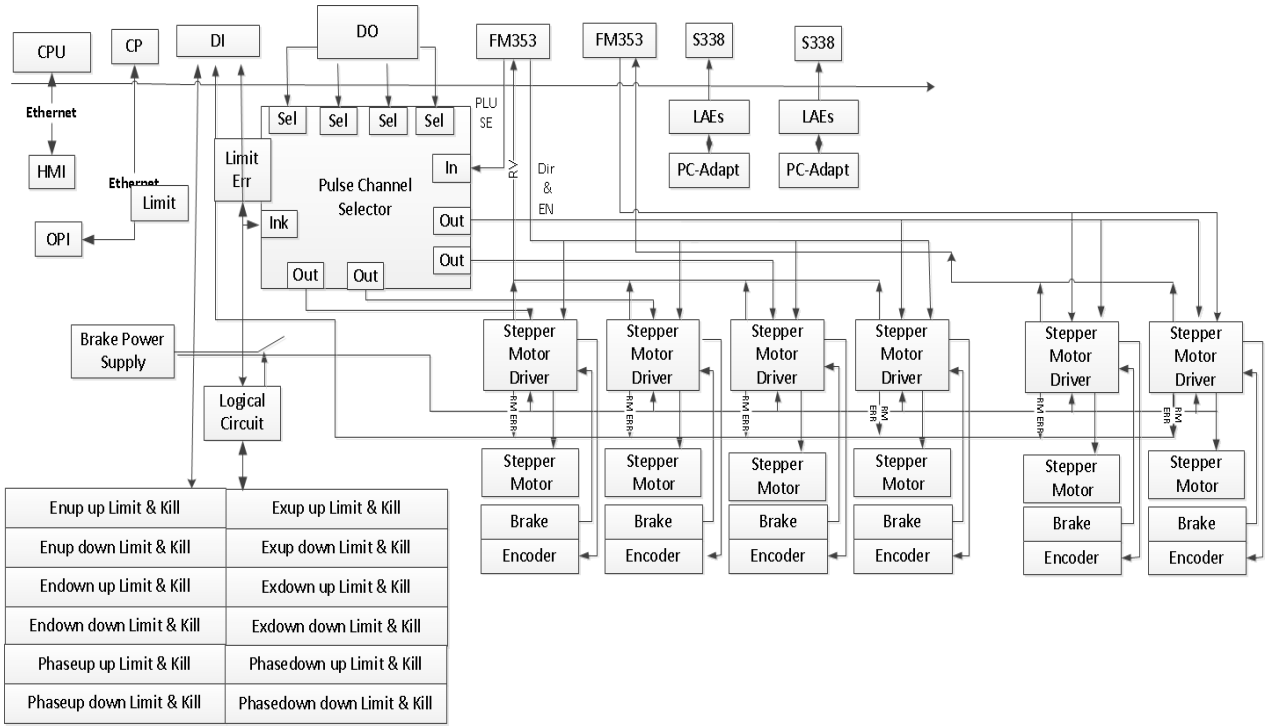

图 6 EPU200 运动控制框图

由于光源中太多的插入件 Gap 或 Shift 的运动，导致闭轨畸变，必须通过插入件入口及出口校正线

圈前馈控制抑制插入件磁极运动对束流轨道带来的影响。DEPU 的前馈包括两套二维数据表(Gap, Shift)，一套一维数据表(Frame)[5]。图 7 是 DEPU 示意及前馈算法示意。

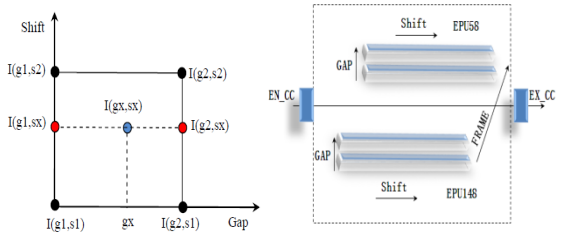

图 7 DEPU 及前馈示意图

5 调制器相关技术研究

XFEL 装置对电子束品质有很高的要求。高稳定性脉冲调制器的设计，是保证微波功率源 RF 性能（稳定的幅度及相位）、保证束流高品质的关键。提高调制器稳定性的措施包括高精度 PFN 采样、脉冲电源电压幅度高精度高速采样及反馈控制前级恒流充电电源。目前首要解决的问题是高精度 PFN 采样及脉冲电源电压的高精度采样，相关软硬件正在研制之中[7]。同时展开了高功率固态调制器相关技术研究，包括电路仿真以及 IGBT 驱动电路的设计等等[8]。

参考文献

1. 吴勇华. 中子核反应数据测量系统研制之加速器系统调制器系统研制, 内部报告, 2014.
2. 欧阳联华, 上海先进质子治疗装置注入引出系统设计, 内部报告, 2014.
3. Ouyang L, *et al*. Transverse RF Kicker Excitation and Longitudinal RF Noise Diffusion For Slow Extraction From SAPT. Proceedings of IPAC 2013, Shanghai, China.
4. 袁启兵. 上海先进质子治疗装置慢引出 RFKO 系统设计, 内部报告, 2014.
5. Yuan Q B, *et al*. The Feed-Forward Control Design for Correction Coil Power Supply For SSRF DEPU, Proceedings of IPAC2013, Shanghai, China.
6. 童金, 等. 基于 FPGA 和 DDS 的质子同步加速器共振慢引出信号源设计, 核技术, 2014.
7. 刘永芳, 等. 脉冲调制器稳定性监控中的信号调理电路研制, 核技术, 2013.
8. 李锋, 等. 高功率固态脉冲调制器关键技术研究, 核技术, 2013.

2013−2014 annual report of pulse group on engineer technical development

Power Division, Pulse Group

During 2013 and 2014, Pulse Group undertakes more tedious engineer development tasks. These tasks mainly include:

1) Engineer design report on high-power pulse modulator systems (HPMS) in LINAC of SXFEL, DCLS and Brazil SIRIUS. Installation, verification test and commissioning of modulation system in nuclear datum analysis accelerator (NDAA).

2) Engineer design report on injection& extraction system and slow extraction RFKO(RF-Knock out) system of Shanghai Advacned Proton Therapy Facility (SAPT);

3) Motion control of insertion devices (IDs) and feed-forward control (FFC) of correction coil power supplies (CCPS) in SSRF. Motion control of IDs, intersection devices (BBA, phase shifter) and chicane in SXFEL and DCLS

4) Modulator-related technologies research on high pulse-to-pulse amplitude stabilities and solid modulator.

Partly development contents are presented in the following texts.

1 High-power pulse modulator systems

Power parameters and development phase of HPMS in different projects are as follows:

Para. / Project	Type	Quan.	Power	Prog.Phase
NDAA	S-Band	1	25 MW	Veri.Test
SXFEL	S-Band	4	50 MW	Eng.Design
	C-Band	7	50 MW	Eng.Design
	X-Band	1	6 MW	Eng.Design
DCLS	S-Band	2	50 MW	Eng.Design
	S-Band	2	80 MW	Eng.Design
SIRIS	S-Band	2	50 MW	Eng.Design
Prot.Mod.	C-Band	1	50 MW	Veri.Test

Several key technical parameters of modulator in NDAA such as repetition frequency, average power and peak power are respectively 266 Hz, 120 kW and 75 MW. Because of large average power, parallel connection method is applied in integrating capacitor charging power supply. Large charging current and high repetition frequency are taken in to elaborate consideration in hardware control circuit. In addition, parameters confirmation of power components in PFN and heat dissipation design are accomplished[1]. Local operator is based on touch screen. All these modulator design would be applied in the later modulator system, especially offer some technical accumulations for modulator system design in SXFEL. Some pictures about NDAA modulator are seen in Fig.1. Preliminary technical parameters test results are listed in Table 2.

Fig.1 Layouts of modulator and assembly parts of oil-tank

Table 2 Test parameters of modulator

	Peak Power	Repetition Frequency	Flat-top Flatness	Amplitude stability
Design	70 MW	266 Hz	1%	0.2%
Test	71 MW	133 Hz	0.5%	0.1%

2 Injection and Extraction Systems of SAPT

Injection and extraction system is composed of two electric septums(ES), two bumps, three magnetic septums (MS) and their exciting power supplies and control (Fig.2). Because of severe space charge influence of particle under low energy condition, single turn injection cannot meet higher ring current requirement, multi-turn injection technology is adopted. That is to say, each turn is injected into the different position in the same phase space, thus uniform particle distribution in phase space is acquired. Multi-turn injection components are consisted of one ES, one MS and two bumps[2]. Application of combination ES with MS are adopted in the design, in order to make injection orbit (from low energy transfer line to storage ring) keep way from dipole magnet located in beam transferring direction, and reduce amplitude of ES exciting power supply. Under the excitation of resonant sextupole magnet, a triangular phase space is formed. As the increment of the horizontal emittance of particles, particles which become unstable would move towards triangular separatrix of phase space[3]. MS (Magnetic field simulation result is illustrated in Fig.3) placed at the appropriate position would deflect particles into extraction orbit.

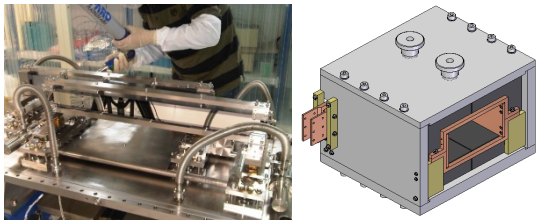

Fig.2 Septum and Bump

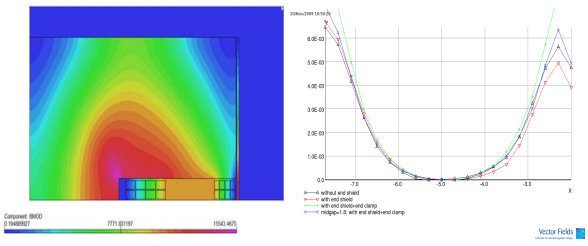

Fig.3 Magnetic field simulation of septum

3 RFKO system of SAPT

The overall diagram of slow extraction RFKO system is illustrated in Fig.4. The RFKO system is mainly composed of RFKO controller based on PXI with Labview RT system, FM generator, voltage control amplifier (used for AM), RF switch, RF power amplifier, signal conditioning and RF-Kicker. RFKO controller calculates the center frequency and band-

width of exciting signal according to the setting energy and beam current from treatment control system, and generates relating signal through FM generator[6]. After getting the feedback beam current, the RFKO controller would take feedback and feedforward control to alter exciting amplitude[4]. The beam on/off command is used to stop or start beam transferring, meanwhile, the stop function is required to get a 10 μs response time. The RF-Kicker electric simulation is as follows:

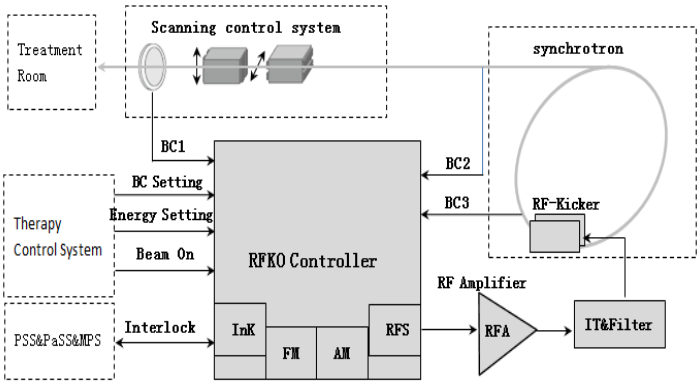

Fig.4 The overall control diagram of RFKO

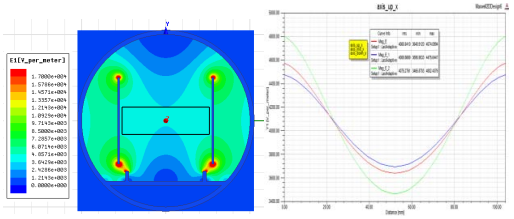

Fig.5 Static electric field simulation of RF-Kicker

4 Control of IDs and FFC of CCPS

Control tasks of IDs and intersection devices are mainly consisted of engineer design on project of SXFEL and DCLS, temperature monitoring and control of the first cryogenic permanent magnet undulator (CPMU) in China, motion control of EPU200 for Shanghai Institute of Microsystem and Information Technology, and feedforward control of DEPU. Six stepper motors are adopted to drive the movement of upper girder and down girder of EPU200. Every axis is equipped with one linear absolute encoder with 0.1 μm resolution to measure its displacement. The core controller is based on S7-300 PLC. In addition, apart from mechanic stop, three layers of limit protection are offered to fully guarantee safety motion. The overall control diagram is illustrated in Fig.6.

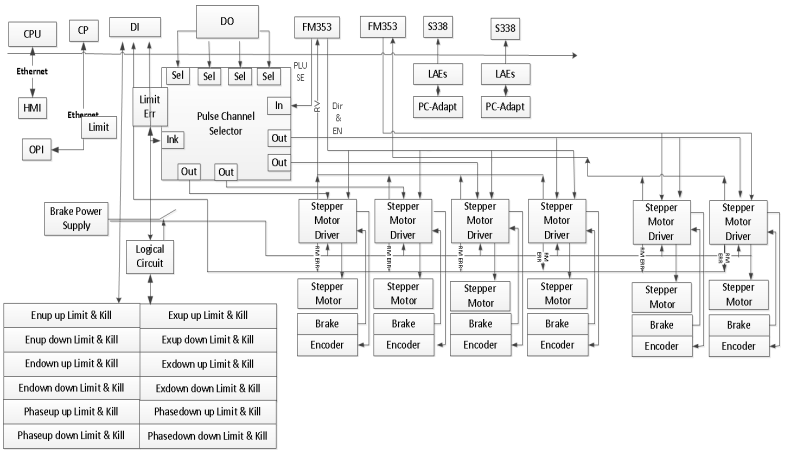

Fig.6 Control diagram of EPU200

In order to reduce the orbit distortion during movement of the DEPU gap and shift, the feed-forward correcting magnetic field must be put at the entrance and exit of the DEPU must be taken[5]. According to one 2D look-up table (LUT) CCPS controller calculates the excitation currents for entrance and exit coils of the DEPU(Fig.7).

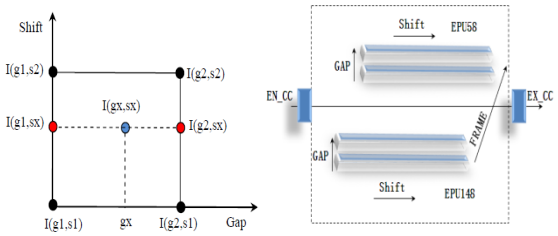

Fig.7 Schematics of DEPU and FFC

5 Research on modulator-related tehcnologis

XFEL facility has strong requirements about high-quality beam. High stability modulator design poses a crucial role for guaranteeing high stable amplitude, phase and high-quality beam. The measures taken to enhance modulator's stability are consisted of high precision data acquisition of PFN, high speed and precision data acquisition of pulse voltage and feedback control of charging supply. Presently, design of hardware and software on high precision data acquisition system is in progress[7]. In addition, circuit simulation and IGBT drive circuit design with relation to solid modulator are also being carried out[8].

Reference

1. Wu Yonghua, *et al*. The Research for LINAC Modulator, TMSR, Internal Report, 2014.
2. Ouyang L, Injection and Extraction System Design for SAPT, Internal Report, 2014
3. Ouyang L, *et al*. Transverse RF Kicker Excitation and Longitudinal RF Noise Diffusion For Slow Extraction From SAPT. Proceedings of IPAC 2013, Shanghai, China.
4. Yuan Q B, *et al*. Slow Extraction RFKO System Design for SAPT, Internal Report, 2014
5. Yuan Q B, *et al*. The Feed-Forward Control Design for Correction Coil Power Supply For SSRF DEPU, Proceedings of IPAC2013, Shanghai, China.
6. Tong Jin, *et al*. Design of slow-extraction signal source within proton-synchrotron based on FPGA&DDS, Nuclear Techniques, 2014.
7. Liu Yongfang, *et al*. Designing signal conditioning circuit for stability control system of LINAC modulator, Nuclear Techniques, 2013.
8. Li Feng, *et al*. Research on the key technology of high-power solid-state pulse modulator, Nuclear Techniques, 2013.

电子学组

2013 年 12 月份，电子学组访问 LNLS。介绍了 SSRF 定时系统的设计和运行情况；介绍了 SINAP 定时硬件的结构、功能和性能指标；调研了 SIRIUS 定时系统需求；讨论了 SIRIUS 定时系统的设计框架。在此基础上，在访问期间完成了 SIRIUS 定时系统的初步设计报告，最终 LNLS 决定采用 SINAP 定时硬件。双方讨论后，在 SIRIUS 定时系统合作中，我所将承担 SIRIUS 定时系统的初步设计报告和设计报告；提供 SINAP 定时硬件作为 SIRIUS 定时系统的主要硬件；设计 SIRIUS 定时系统软件；协助 LNLS 设计 SIRIUS 定时系统部分硬件；为 SIRIUS 定时系统的测试、安装、调试和运行提供技术支持。2014 年初，双方签署了 SIRIUS 定时系统合作的谅解备忘录。

Sirius 定时系统的硬件由 STD-EVO、STD-EVE、STD-MOE、STD-SOE 和 SOE 组成，储存环 BPM 电子学的定时模块由 LNLS 自行研发。STD-EVO、STD-EVE、STD-MOE 和 STD-SOE 为 1U 19 英寸标准独立模块，SOE 为 3U 独立模块。STD-EVO 可以通过软件配置成 EVG（事件发生器）、EVR（事件接收器）和 FOUT（扇出模块）；STD-EVE 功能为 EVR（事件接收器）；STD-MOE 是多模光纤定时信号解调器，与 STD-EVO（配置为 EVR）配合使用；STD-SOE 和 SOE 是塑料光纤定时信号解调器。各个硬件设备如下图所示：

STD-EVO

STD-EVE

STD-MOE

STD-SOE

SOE

在 Sirius 定时系统中采用独立模块，每个独立模块具备网络接口；定时系统软件运行在服务器中，采用 softIOC 模式。根据这种运行模式，我们重新设计了软件和 FPGA firmware，用于满足在网络数据传输的环境中。我们于 2015 年 1 月向 LNLS 交付整个定时系统软硬件。

2013 年 11 月 21 日，上海光源组织加速器和光束线的相关运行负责人和专业组负责人召开了快轨道反馈系统验收评审会。光束线和加速器相关人员共十人组成专家组对快轨道反馈系统设计方案、现场测试情况等进行了验收评审。该系统已经投入上海光源日常运行，目前运行稳定，使上海光源的轨道稳定性到达了一个新的水平，在 100 Hz 以内的束流轨道可以稳定在亚微米量级，使上海光源的性能得到进一步提升。

同时轨道反馈系统采用慢速轨道反馈+快速轨道反馈混合运行模式。混合轨道反馈系统采用数据交互的方法消除两套轨道反馈系统独立运行引入的 cross-talk，数据交互算法在慢速轨道反馈系统的上层软件中。

混合轨道反馈系统对束流轨道噪音的抑制能力如下图所示：

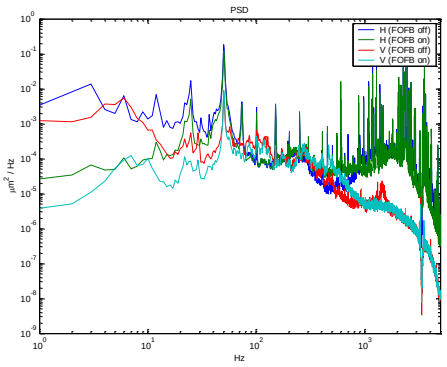

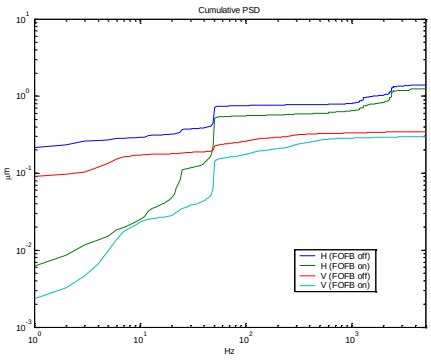

轨道快、慢反馈系统同时运行，通过慢反馈对快反馈实时设置参考轨道，以实现长时间稳定运行。其参考轨道为慢反馈系统的计算值，在试验中比较了实测值和计算值的运行效果，实践证明通过慢反馈校正铁的改变量计算出的轨道要比实测的轨道更稳定。混合轨道反馈系统运行 1 h 的轨道变化如下图所示：（左图为垂直方向；右图为水平方向）

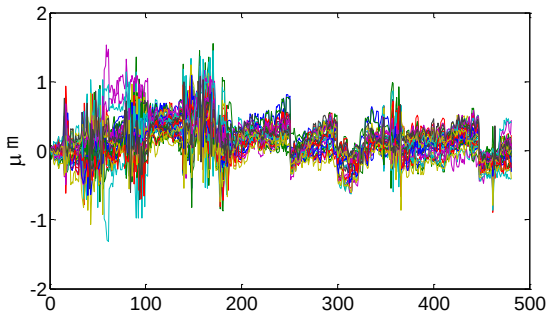

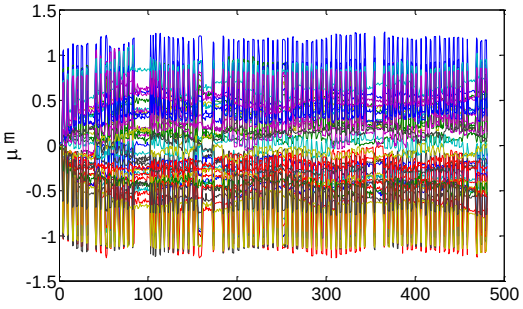

运行 1 h 的快校正子强度如下图所示：

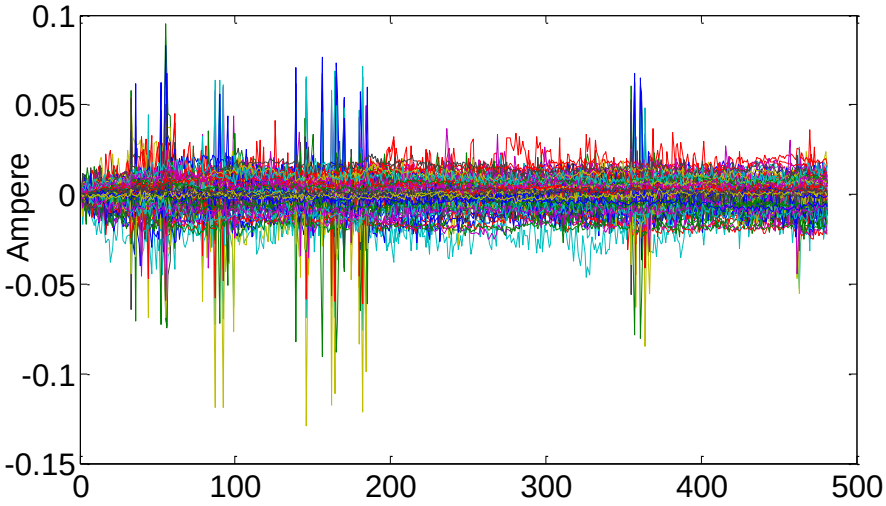

title

Electronics group

In December 2013, the electronics group visited LNLS. We introduced the development and operation situation of SSRF timing system. We introduced the hardware structure, function and specification of SINAP timing system. We investigated the requirement of SIRIUS timing system and discussed the framework of SIRIUS timing system. On the basis above, we completed the preliminary design report of SIRIUS timing system. LNLS decided to use hardware of SINAP timing system. After the discussion, our institute would undertake the responsibility of preliminary design report and design report of SIRIUS timing system, providing SINAP timing modules as hardware of SIRIUS timing system, software development of SIRIUS timing system, giving assistance to LNLS in part of hardware development of SIRIUS timing system, providing technical support for test, installation, commissioning and operation of SIRIUS timing system. At the beginning of 2014, we signed the MOU for collaboration of SIRIUS timing system.

We provided main hardware of SIRIUS timing system, including STD-EVO, STD-EVE, STD-MOE, STD-SOE and SOE. LNLS would design the timing modules for BPM electronics in storage ring by themselves. STD-EVO, STD-EVE, STD-MOE and STD-SOE are standalone modules with 1U height and 19U width. STD-EVO can be configured as EVG, EVR and FOUT by software. STD-EVE is used as EVR. STD-MOE is multimode fiber O/E demodulator, which is used with STD-EVO in pairs. STD-SOE and SOE are plastic fiber O/E mo demodulator. All of the hardware modules are illustrated in Fig.?.

STD-EVO

STD-EVE

STD-MOE

STD-SOE

SOE

We used the independent modules in Sirius timing system, and every independent module has the network interfaces; the software of the timing system was running in the server, using the model of soft IOC. According to this running model, we redesigned the software and the FPGA firmware, to meet the requirement of the network data transmission. We had delivered the whole timing system including the software and the hardware to LNLS in January of 2015.

On 21 November of 2013, SSRF organized the relevant operation leaders of the accelerator and the beam line and the leaders of the professional team to hold a review meeting for the acceptance inspection of the fast orbit feedback system. The 10 people from the beam line and the accelerator formed an expert group to inspect and review the design scheme and the field test situation of the fast orbit feedback system. The system had already been put into operation in SSRF, and it is running stably now. It made the orbit stability of SSRF reach a new level, for example, the beam orbit can be stable in sub-micron scale within 100 Hz, and improved the performance of SSRF.

At the same time, the orbit feedback system operated in the model of mixing slow orbit feedback and fast orbit feedback. The mixed orbit feedback system adopted the methods of data interaction to eliminate the cross-talk when these two orbit feedback system was running independently and the algorithm of the data interaction was in the upper software of the slow orbit feedback system.

We can see the inhibiting ability of the mixed orbit feedback system over the noise of the beam orbit as below:

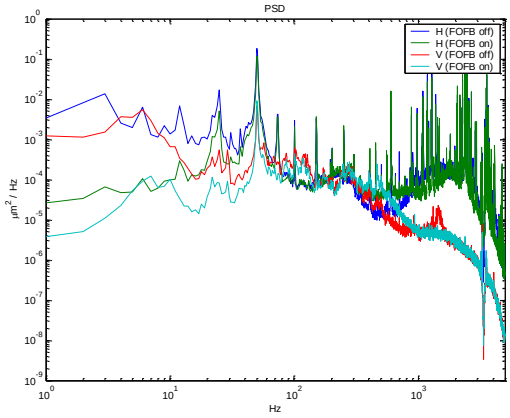

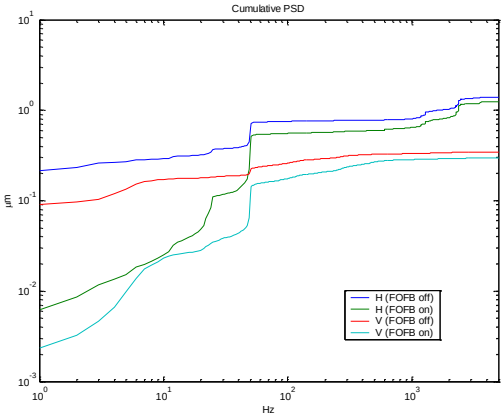

The fast orbit feedback system was running with the slow orbit feedback system, and we can set the reference orbit of the fast feedback in real time through the slow feedback, so that we can realize the steady running in a long term. The reference orbit was the calculated value of the slow feedback system, and we compared the running effect of the measured value with the one of the calculated value. Then we found that the calculated orbit according to the variation of the slow feedback corrector was more stable than the measured orbit through the practice. We can see the orbit changes as below when the mixed orbit feedback system had run for an hour: (the figure on the left is the vertical direction; while the figure on the right is the horizontal direction).

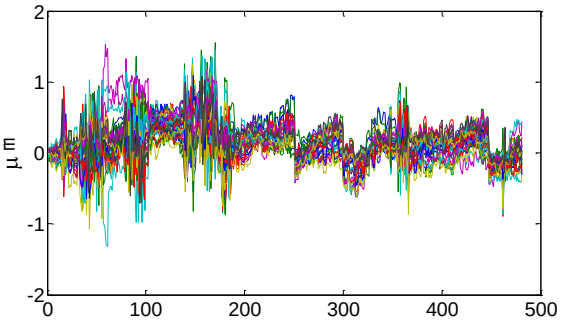

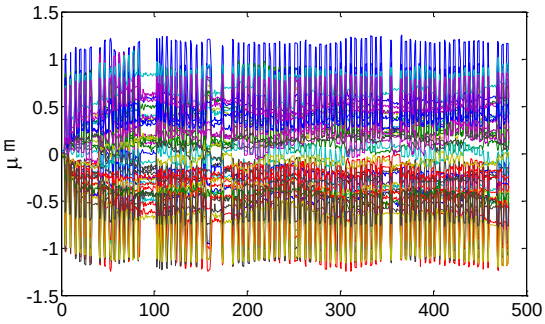

The intensity of the fast corrector running for an hour is shown below:

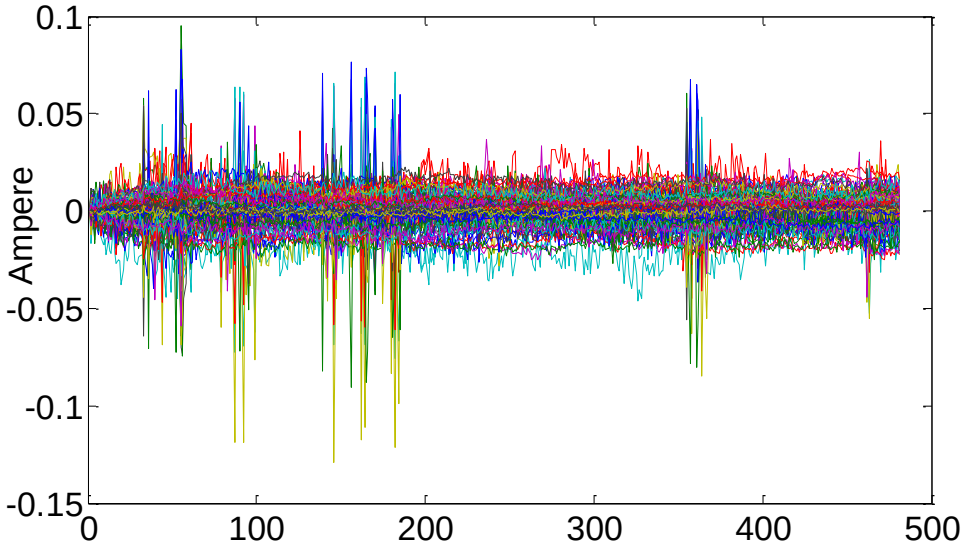

束流诊断技术

束流测量及控制技术部　束测组

本年度束测组的核心工作是上海光源束测系统的高效运行维护，以及配合升流强所做的系统升级改造。此外，结合加速器性能提升以及机器研究的需求，对全局数据关联分析、Online MIA 分析、数字化 BPM 信号处理、逐束团诊断等若干关键技术展开了研究。开展了 CBPM、质子 BPM 等关键样机的研制。

上海光源束测系统运行维护

上海光源束测系统2013年度设备故障共计8次（含不影响供束故障），年度 MTBF 约 303×24/8=909 h，优于 2012 年度；2014 年度设备故障共计 10 次（含不影响供束故障），年度 MTBF 约 306×24/8=734 h，与 2013 年度相比略有降低。主要为硬件故障，更换备件解决[1]。

上海光源束测系统升级改造

针对流强提高做了相关的束测系统升级改造，Libera Brilliance 电子学输入端加装 6 dB 衰减器，BPM 电子学硬件、软件升级，针对强流时噪声问题，增加 BPM 和信号测流强的冗余数据通道。

其他装置束测系统建设

- 核数据平台束测系统研制：
- 更新工程设计报告（机械 & 电气设计）
- 完成探头到货验收、真空检漏、现场安装
- 完成电子学到货验收与测试，现场安装
- 完成电缆铺设、接头制作、设备接线
- 完成 EPICS 软件开发与调试
- 质子治疗装置束测系统
- 初步设计定稿，工程设计第一版
- 关键样机测试分析，BPM 0.1 mm 分辨率，符合设计预期
- Faraday Cup 初步设计
- 完成 BPM，profile 样机研制。
- FEL 项目束测系统
- 完成关键技术研究，包括 CBPM 探头样机加工与实验室测试，profile 系统设计等。
- 4 MeV 加速器控制系统改造：
- 完成设备采购
- 完成工艺设计
- 完成软件开发及设备实验室联调

束流诊断关键技术研究

利用搭建的束测数据仓库进行了加速器运行性能评估[2]，研究了光源长期工作点稳定性，观察到不同运行周期内阻尼时间不同；研究注入后的残余振荡及其可能原因；分析 240 mA 丢束问题；测量流强累积过程中束流频谱变化。图 1 是工作点稳定性测试。

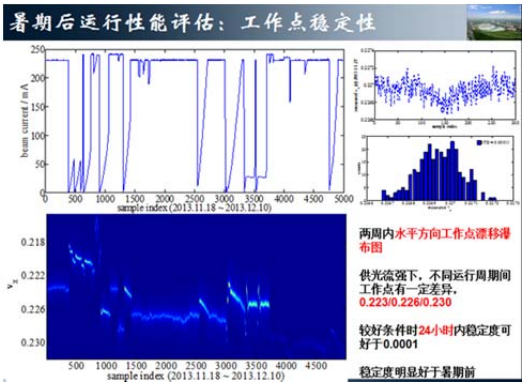

图 1　束测仓库工作点稳定性测试

基于 MIA 算法，开发了 Online MIA 系统，可用于机器参数监测，观察到 8、9 单元（新装 DEPU 后工作点补偿）β 函数随流强的变化，如图 2 所示。该系统可用于 BPM 故障定位[3]。

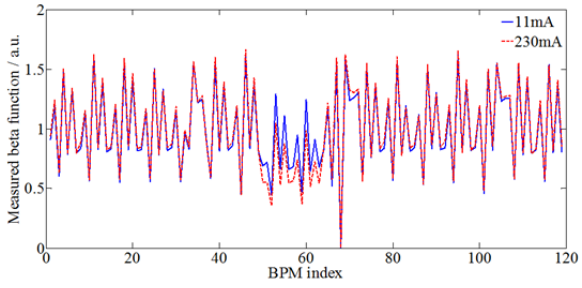

图 2　Online MIA 测试 8, 9 单元 β 函数

开展逐束团位置诊断技术实验研究[4–5]，基于该技术评估注入性能，分析注入瞬态过程不同模式，并重建了注入漏场分布，如图 3 所示。与物理组合作进行强流不稳定性丢束问题的实验研究。同时，开展了逐束团专用处理器研制工作，进行了 RF 前

端的束流仿真和带束测试，成功实现束流展宽。

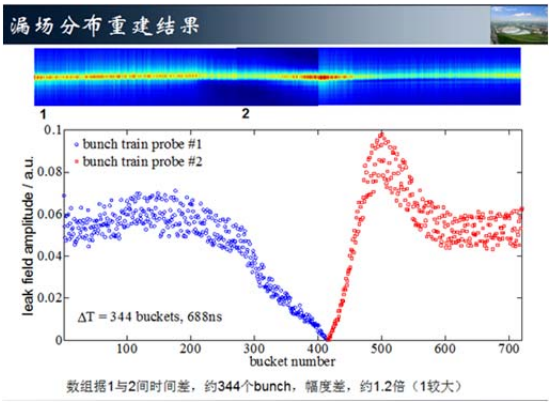

图 3　逐束团诊断技术用于漏场分布重建

研制的数字化 BPM 处理器完成小批量（5 台）工程样机完成测试，投入应用研究，各项技术指标满足同步辐射光源/FEL 装置需求，逐圈位置分辨率好于 2 μm，其他各项功能齐备，可确认用于上海光源/其他 FEL 装置后续应用搭建，图 4 为处理器束流测试结果[6]。

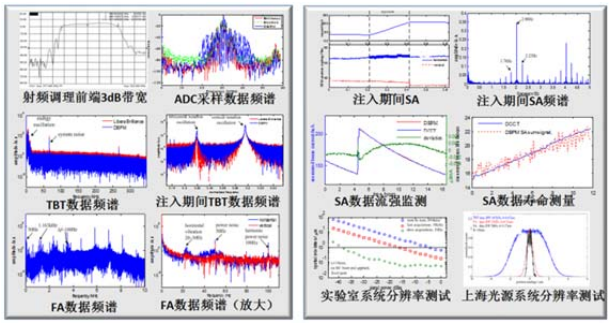

图 4　数字化 BPM 处理器束流测试

以 DBPM 处理器为平台，开发了基于 FPGA 开发智能触发模式，可捕捉随机事件，用于异常事件的锁存及后分析，如图 5 所示。

完成 FEL 项目关键设备 CBPM 探头样机加工与实验室测试，如图 6 所示，完成质子治疗装置 BPM，Profile 样机研制[7]。

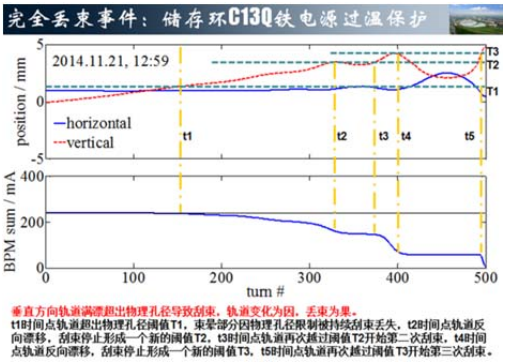

图 5　智能触发平台进行束流测试

图 6　CBPM 探头加工

参考文献

1. 上海光源束测系统运行年会报告，上海应用物理研究所, 2014.
2. Chen Z C, Leng Y B, Yuan R X, Study of algorithms of phase advance measurement between BPMs and its application in SSRF[J], NST, 2013, **24**(1): 7-11.
3. Chen Z C, Leng Y B, Yan Y B. Performance evaluation of BPM system in SSRF using PCA method[J], CPC, **38**(7): 112-116.
4. Chen Z C, Yang Y, Leng Y B. Wakefield measurement using principal component analysis on bunch-by-bunch information during transient state of injection in a storage ring[J], PRST, 2014, **17**(11): 112803.
5. Leng Y B. Bunch by bunch transverse beam position observation and analyze during injection at SSRF[C], UK: IBIC2013: 746-758.
6. 赖龙伟, 冷用斌, 易星, 等. 数字束流位置信号处理算法优化[J], 2013, **1**(25): 109-113.
7. Wang B P, Leng Y B, Yuan R X, *et al*. Development of cavity beam position monitor system IPAC2013[C], Shanghai, China, IPAC2013. 2013: 51.

Beam instrumentaion techenologies

Department of Beam Instrumentation and Control BI Group

The major missions of the beam diagnostics team this year were to maintain the effective operation of the beam diagnostics system and to upgrade the system for the higher beam current in SSRF. Meanwhile, key techniques such as global data analysis, Online MIA analyzing system, digital BPM signal processing, bunch by bunch diagnostics were studied with the performance improvement of the accelerator and the growing requirements of the machine studies. Meanwhile, the prototypes of Cavity BPM for FEL and BPM for proton accelerator were designed successfully at this year.

Operation of the beam diagnostics system of SSRF

There were 8 equipment failures at 2013, including those that did not affect the operation of the accelerator. The MTBF is 909 hours, which is a bit better than 2012. There were 10 failures at 2014, including those that did not affect the operation of the accelerator. The MTBF is 734 h. Most failures are caused by hardware, and solved by replaced with spare part[1].

Upgrade of the beam diagnostics system of SSRF

In order to meet the requirements of the higher beam current, a 6 dB attenuators were added on each channel of Libera Brilliance, and BPM hardware and software were upgraded. Additional noise appeared on the DCCT signal when the storage ring run at high beam current. To avoid the affection introduced by the noise, an extra data channel of BPM sum signal is added to measure beam current.

- Beam diagnostics system of other accelerators
- Nuclear data platform
- Updated engineering design report.
- Detectors arrived, examined and installed.
- Electronics arrived, and examined and installed.
- Cable laying and connection.
- EPICS development and commissioning.
- Proton accelerator
- Preliminary design, version I engineering design report.
- Key instruments prototype tested, BPM reached 0.1 mm resolution.
- Preliminary design of Farady Cup.
- FEL accelerator
- Key instruments prototypes design, including CBPM and profile.
- 4 MeV accelerator
- Equipment procurement
- System design, software development and lab tests.

Key techniques research of the beam diagnostics

Based on the beam diagnostic data warehouse, SSRF operation performance was evaluated[2], the long term stability of the tune value was studied (Fig.1). Damping time difference was observed during different operation cycle. At the same time, the warehouse was applied on the study of the injection residual oscillation, analysing beam lost reasons at 240 mA, and measuring the spectrum changing during current increasing.

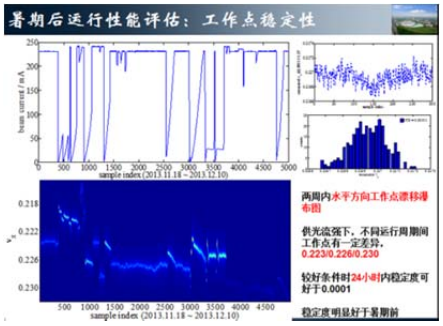

Fig.1 The long term stability of the tune value tests with diagnostic data warehouse.

An online MIA system has been designed based on MIA algorithm, which was applied on monitoring machine parameters. The beta function of 8,9 unit changing with current was observed(Fig.2). The system can also be used on fault BPM location[3].

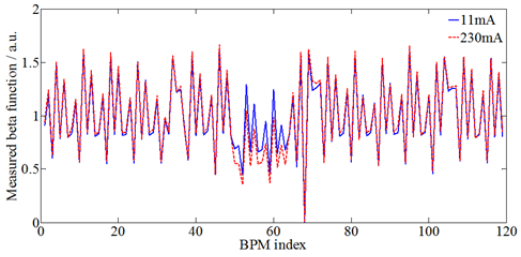

Fig.2 The measurement of beta function of 8,9 unit with Online MIA.

The application of bunch by bunch diagnostic method was studied[4,5]. The injection performance and modes on injection transit process were studied. And rebuilt the injection leak field(Fig.3). Made cooperative study with physics group on beam lost that introduced by strong current instability. The RF front-end of the dedicated BPM processor was studied, simulation and beam tests were carried on. The bunch signal was broadened successfully.

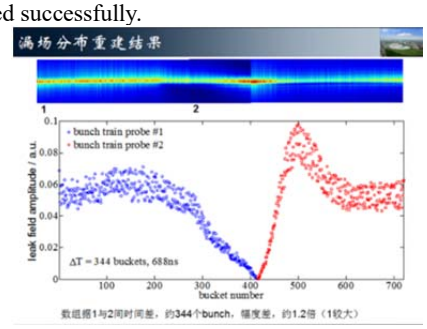

Fig.3 Injection leak field rebuilt with bunch by bunch diagnostic method.

A small batch (5) self-designed digital BPM processors were completed and tested. Performance evaluation showed that they meet the requirements of SSRF and FEL, turn-by-turn resolution is better than 2 μm. Fig.4 shows the beam test results[6].

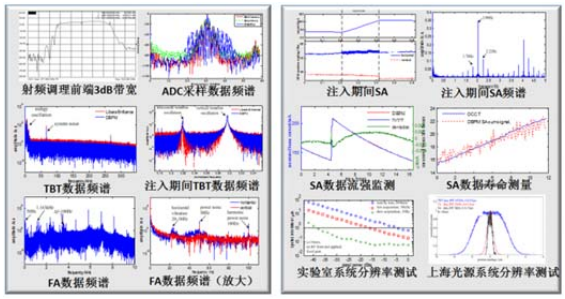

Fig.4 The beam tests of digital BPM processor.

A self-triggered module has been developed on the DBPM hardware platform, it could be used to capture the data when abnormal events appeared for analyzing(Fig.5).

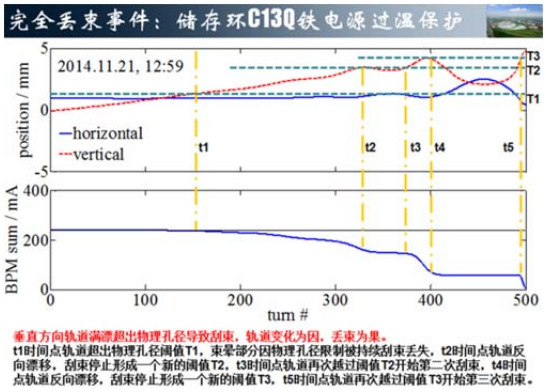

Fig.5 The beam tests of the self-trigger module.

Cavity BPM(Fig.6) and shoebox BPM are the key detectors on FEL and proton accelerator respectively. Their prototypes have been completed and made lab tests[7].

Fig.6 The CBPM processing

Reference

1. 上海光源束测系统运行年会报告，上海应用物理研究所，2014.
2. Chen Z C, Leng Y B, Yuan R X, Study of algorithms of phase advance measurement between BPMs and its application in SSRF[J], NST, 2013, **24**(1): 7-11.
3. Chen Z C, Leng Y B, Yan Y B. Performance evaluation of BPM system in SSRF using PCA method[J], CPC, **38**(7): 112-116.
4. Chen Z C, Yang Y, Leng Y B. Wakefield measurement using principal component analysis on bunch-by-bunch information during transient state of injection in a storage ring[J], PRST, 2014, **17**(11): 112803.
5. Leng Y B. Bunch by bunch transverse beam position observation and analyze during injection at SSRF[C], UK: IBIC2013: 746-758.
6. 赖龙伟，冷用斌，易星，等. 数字束流位置信号处理算法优化[J], 2013, **1**(25): 109-113.
7. Wang B P, Leng Y B, Yuan R X, *et al*. Development of cavity beam position monitor system IPAC2013[C], Shanghai, China, IPAC2013. 2013: 51.

束流测量与控制技术控制系统

控制组

2013−2014 年度，上海光源控制系统在保持稳定可靠运行的同时，专注于系统的维护与优化，并根据新的要求及新技术的发展，开展控制系统升级改造工作，主要包括虚拟服务器系统升级测试、存储系统升级改造、容错 IOC 测试、MPS 系统优化升级、新插入件控制等方面工作，同时，在 SXFEL 实验装置、大连相干光源 DCLS、巴西 SIRIUS 光源直线加速器等项目控制系统取得了一定的进展。

1　虚拟服务器系统升级测试

上海光源虚拟化服务器系统已经运行三年，其中虚拟机系统使用的 Dell 服务器已经运行 6 年，存在设备老化，虚拟化软件版本陈旧等问题，为确保光源控制系统环境的正常运行，计划将此系统更新到新的软硬件平台上。在 2014 年度 7 月底高温假期间对现有虚拟化系统及设备进行升级，虚机迁移等测试事项。

通过本次虚拟化系统升级、设备更新，新的主机服务器、存储均正常工作，虚拟服务器均可来回迁移，且工作正常，稳定性、性能大大增加。系统升级成 VMware ESXi 5.5 后，对于单个磁盘可分配的空间限制从原来的 2 T 增加至 16 T。整个存储空间足够满足当前数据存储。对于 CPU 要求不高的应用，虚拟机可以启用 FT 容错功能，可以保证应用不会应该硬件故障而中断服务。通过测试证明升级方案可行，具有较好的性能改进，计划 2015 年暑期将原有虚拟化系统升级至新版虚拟化系统。

2　数据存储系统改造工作

目前光源数据存储采用 Channel Archiver 系统。Channel Archiver 系统为文件存储类型，其驱动 2009 年后停止维护更新。RDB Archiver 是 CSS (Control system studio)的数据存储部分，其数据存储为关系型数据库。CSS 为一个工具集，它将数据存储，数据浏览，控制系统诊断工具及操作界面整合为一个整体，使 OPI 端的操作变得简洁高效。考虑到今后驱动的维护更新，数据存储系统需要从 Channel Archiver 系统升级为 RDB Archiver 系统。

2013 年对基于云存储的(Cloud storage system)分布式数据库系统进行了历史数据库的测试。本次 CSS 基础测试配置由一个 ISM Server、两个 MDS 与 OSN 的混合节点、4 个 OSN 节点、一个交换机和客户端组成。配置使用 ArchiveConfigTool 将 xml 配置文件中的通道配置导入 CSS-D 数据库中，使用 RDB ArchiveEngine 采集多通道数据或由现场编写程序生成多通道数据，然后通过 CSS Data-Browser 读取和展示通道数据。从现场网关获取通道数据，同时模拟现场生产环境，生成部分实验数据。总共包含 10 071 个 Channel。模拟数据采用四种不同频率的数据生成速度，生成一年的数据，数据总量约 1.85 T Bytes。

2014 年我们对 RDB Archiver 系统的硬件软件进行了升级。硬件方面采用两台华为 Tecal RH2288H V2 机架服务器，512 GB 内存，18 TB 裸盘。软件方面采用 Oracle Timesten 内存数据库存储数据和 Oracle 数据库检索数据。数据存储过程为 RDB Archiver 驱动采集的数据写入 Timesten，Timesten 再写入 Oracle 数据库；数据检索过程通过并行处理机制从 Oracle 数据库读取数据。存储操作通过 Timesten，检索操作通过并行处理机制使数据存储和检索速度大大提高。经测试数据写入速度可达到 10 万行每秒，可满足我们的性能要求。目前已完成硬件系统搭建；Oracle 服务器安装；Timesten 数据库安装；Oracle 数据库安装；RDB Archiver 驱动修改，增加 timesten 通讯接口和并行检索功能。通过调试目前已实现 Timesten 数据存储和数据并行检索（图 1）。

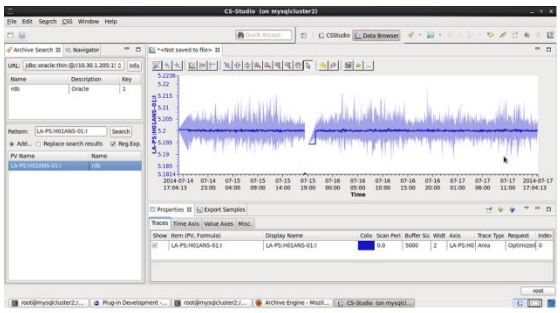

图 1　新存储系统数据检索

3　IOC 池化系统测试

EPICS IOC 容错系统是目前 EPICS 系统应用

于高可用性控制系统中的研发热点，提供冗余的 IOC 可大幅度提高系统的可用性，确保关键系统的长期稳定性，提高整个控制系统 MTBF，特别是类似目前光源 TOP-UP 联锁系统中存在的部分软件联锁，实施容错 IOC 系统具有很大的实际意义。

当前已经在进行过多轮测试，并联合池化系统开发厂家进行了多次改进，在 2014 年光源暑期维护期间又进行了一次测试，主要目的是问了改进相关 CA 在冗余 IOC 系统中的数据同步问题。

IOC 池化系统包含两台 IOC 服务器，同时运行着 IOC Server 程序；其中一台 IOC 服务器为主，另一台为辅。池化器将 IOC Client 的请求转发给主 IOC Server 的同时，也发送给辅 IOC Server，但池化器仅将主 IOC Server 的返回结果转发给 IOC Client，辅 IOC Server 的返回结果将被池化器丢弃。前端两台池化器#1 和#2，共用一个虚拟 IP 地址(VIP)，IOC 用户直接以 VIP 作为目标地址，通过池化器进行负载均衡及同步将用户请求同时发送至后端的两台 IOC Server 上。

测试结果如下：

故障迁移：完成主辅 IOC 互相切换测试，在单个 IOC 发生故障时，客户端能成功切换到另一个 IOC，系统可正常服务。

IOC 之间的数据同步：客户端向 IOC 发起一个 CA Put 写操作时，能将写入数据同步到辅 IOC 上。

后续还需解决在一个 IOC 发生故障后，重启此 IOC 的数据同步问题，修改处理主辅 IOC 之间的 SID 问题。

4 MPS 系统优化升级

4.1 储存环真空联锁修改

为了延长一个单元真空规灯丝的更换周期，同时避免因真空计故障造成相邻两个真空点同时误报警而导致踢束的问题，真空组提出了对单元真空联锁，以原设计所有真空点都参与联锁的方案，调整为任意取两个真空点参与联锁的方案。针对该需求，暑期维护期间我们对储存环所有单元的真空联锁逻辑进行了修改。修改后，真空组可直接在各单元联锁界面的真空联锁区域（图 2）进行设置每个真空点是否参与联锁 (Enable/Disable)。

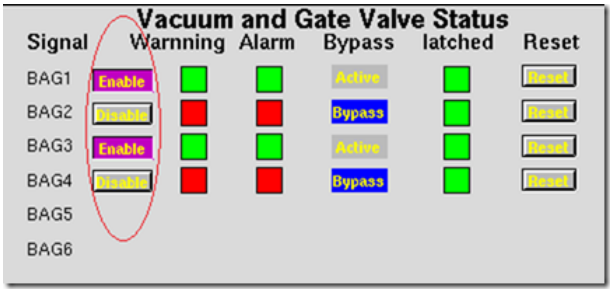

图 2 单元联锁界面设置

4.2 canted 联锁工作

C19 单元双插入件架构中的 canted 联锁实施，经过方案调整，又回归纳入 MPS 系统。同时，为了避免第一次实施所采用的软件联锁的不可靠性，本次实施采用了完全的硬件联锁方案。为了不影响标准单元联锁系统结构，MPS 在 C19 单元增加了一套补充联锁 PLC，将 canted 联锁内容在单独的 PLC 软硬件系统中实现。这种解决方案可推广到其他单元解决标准单元 MPS 架构中不能实现的增补联锁需求问题上，图 3 为实施系统的架构示意图。

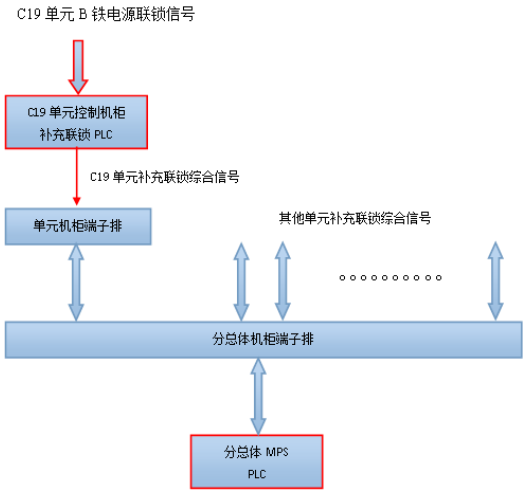

图 3 Canted 硬联锁实施方案架构

5 新插入件控制

5.1 DEPU

对于矫正线圈电源的前馈处理由 PLC 模拟模块实现，难点在于前馈表在上层控制系统和下层 PLC 之间的传输和更新。为此必须修改驱动程序，使 EPICS 驱动支持大数组方式的传送，同时根据物理组的要求前馈表进行了的多次更新。

实现 DEPU 工作点补偿功能，并根据物理组的要求随时更新数据表。

DEPU 长线圈控制功能基本实现，并完成测试。

5.2 IVU25

IVU25 的运动控制主要由上层 EPICS 对底层西门子 PLC 进行监控实现。利用主控界面结合 AUTOSAVE 函数，操作员在界面上的电源表中输入/修改 GAP 对应的 4 个校正线圈电流，将设置后的电流值下载到 PLC 中，完成前馈功能的实现。该实现方法具有数据保存，操作简单等特点。

5.3 IVU20

IVU20 的运动控制主要由上层 EPICS 对底层西门子 PLC 进行监控实现，主控界面包含多个子功能界面。

由于 IVU20 采用 PLC 控制模拟电源实现前馈的方式，因此如何将前馈数据表按照 EPICS 驱动方式传输给 PLC 成为主要问题。重新修改了 PSI 实验室开发的 EPICS 驱动程序，针对 RECORD DRIVER 和 DEVICE DRIVER，新增了 WAVEFORM 数据的支持，目前已经实现了对大数据数组的传输。

原电源无 CYCLE 功能，目前光源其他电源采用的 CYCLE 功能通过繁琐的 DB 实现，因此重新利用经典的 SNL 语言，实现并测试了针对 19 单元弯铁电源的 CYCLE 功能。经测试实现了物理组的要求。

6 SXFEL 实验装置及 DCLS 控制系统

SXFEL 控制系统完成了可研报告和初步设计报告，确定了总体设计方案：1) 基于 EPICS 分布式架构的系统设计；2) 基于全开源软件的控制系统工程目标。

根据初步设计报告，完善了 SXFEL 控制系统预算；确定了磁铁电源、真空、各种运动控制等的设备控制方案、安全联锁系统方案、加速器主定时系统设计方案；编制了 SXFEL 控制系统电气结构图，组织对电源、真空监控、调制器、波荡器、BBA、定时系统进行了控制信号的统计。

对控制系统关键设备进行了设备选型：基于 OMRON PLC 的安全联锁系统；基于 BNC 高精度数字延时器的加速器主定时系统；基于嵌入式控制器的 IOC 控制器； 基于 NIS 和 NFS 的控制系统运行环境；基于 Python 的物理计算平台。对关键设备 IOC 进行了软件集成开发与测试，达到了使用一种 IOC 控制器满足所有设备控制需求的目标。

DCLS 控制系统采用与 SXFEL 控制系统的相同方案，包括技术方案、设备选型及其控制软件。

完成了 DCLS 技术设计报告中英文版的控制系统部分编写；在与同步、束测、微波、功率源讨论后，形成了 DCLS 时序需求联系单；对 DCLS 安全联锁系统进行了需求分析，形成了 MPS 联锁逻辑表和真空保护逻辑表；使用服务器，工作站和 DA662 IOC 建立了物理开发应用平台，通过建立 DCLS 主加速器的虚拟 PV 通道，包括电源，调制器高压及相位，供 Linac 调束软件开发。确定了 DCLS 控制网络，设备底层通讯的网络地址分配。

根据关键首件任务书要求，完成了 DCLS 控制系统工程样机研制，涵盖了物理调束软件、控制系统运行环境、上层 OPI 操作界面，设备控制 IOC 控制软件等的完整工程样机研制。按照工程设计方案进行了 Timing、调制器、真空、电源、波荡器及 BBA Mover 等设备控制工程样机的开发。

对 FEL 操作界面进行了总体设计：edm 界面+WebOPI 两种方案。edm 采用横向 Global+物理分段、纵向设备控制子菜单选项的图形化集成界面方案（图 4）。WebOPI 用于基于 Internet Browser 的访问。样机研制中，WebOPI 界面实现了以波荡器和 BBA 电移平台为例的技术开发，并用 PC、IPAD 平板与手机都进行了访问测试。

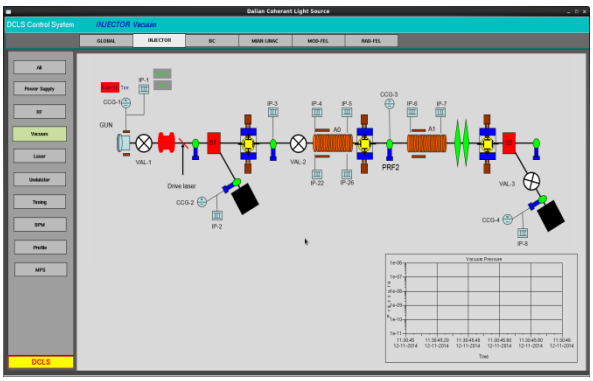

图 4 FEL 界面设计

7 巴西 SIRIUS 光源直线加速器控制系统

巴西 SIRIUS 光源直线加速器项目的控制系统于 2013 年中旬开始系统设计并于 2013 年底完成。该控制系统全部基于网络设备构成（图 5），符合 EPICS 规范。

样机研制从 2014 年初开始，在光源控制系统基础上，大量升级修改了设备驱动程序，新增系统管理软件等控制技术。2014 年底基本完成样机的研制和测试，同时，主要设备也采购到位并部分开

始安装调试。

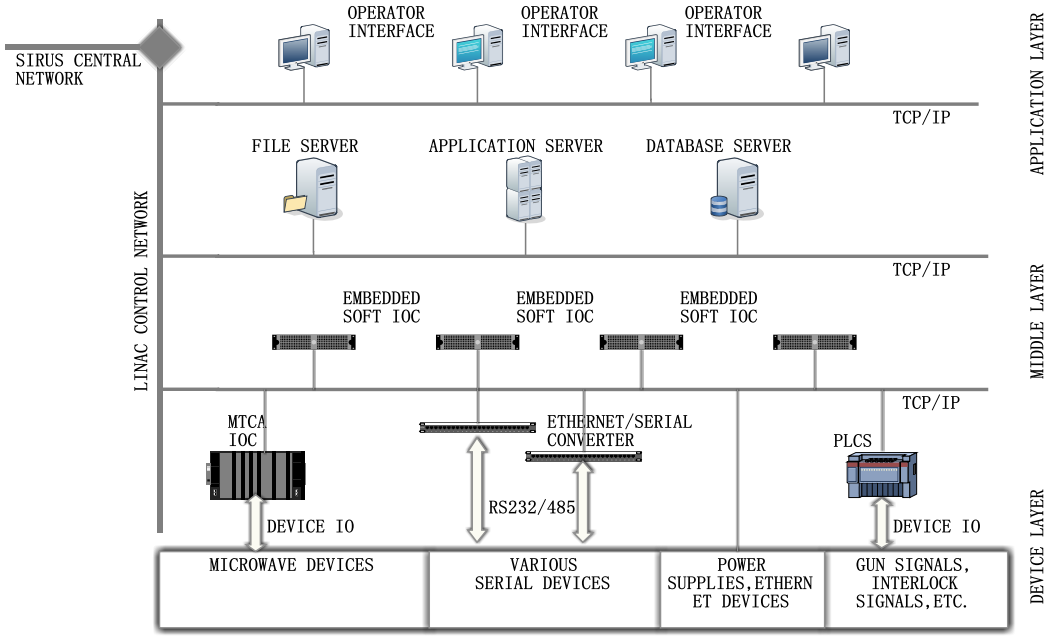

图 5　SIRIUS 光源直线加速器控制系统设计

8　质子治疗装置控制系统

质子治疗装置控制系统 2013−2014 年在开展了大量的调研工作的基础上进一步细化了设计方案和接口文件。技术路线和方案最终确定，完成系统设计报告简本，完成网络工程报告、服务器系统工程设计报告。并且和部分系统如真空、电源等，初步开展了部分样机的研制等工作；对各种质子治疗所需控制系统软件如驱动、服务器管理、GUI 等组织技术力量开始进行编写和调试。

9　医用电子直线加速器控制系统研发项目

完成首台 CMAX 机器的控制系统研发并通过药监局第三方检测，目前已进入医院临床阶段。完成 IGRT（图像引导治疗系统）机型的控制系统研发及调试，包括国内首台基于 FPGA 的多叶光栅 MLC 研制及 IGRT 接口，标准访问程序库供 IGRT 程序调用以及设备控制仲裁管理，共享数据库接口完成与 TPS（治疗计划系统）的对接。

Control group of beam instrument and control department

Control Group

From the year 2013 to 2014, the control group of Shanghai Light Source keeps the stable and reliable running. Meanwhile, they focus on the system maintenance and optimization and according to the new requirements and the development of new technology, we start the control system upgrade work. The development of the control system mainly including the upgrade testing of virtual server system, upgrade transformation of storage system, fault-tolerance IOC testing, upgrade optimization of MPS system, control of the new insertion device, and so forth. In the meantime, the control group makes progress in SXFEL experimental apparatus, relevant light source DCLS at Dalian, Brazil SIRIUS light source linear accelerator, etc.

1 Upgrade testing of virtual server system

Shanghai light source virtualized server system has run for 3 years. Dell server, used in virtual machine system, has run for 6 years, existing the defect of aging equipment, obsolete virtualization software version, and so on. In order to ensure the normal operation of light source control system, we are intended to transfer and update this system to a new software and hardware platform. During high-temperature vacation in July, 2014, we upgrade owned virtualized system and equipment and upgrade the testing events of virtual machine migration.

Owing to the upgrade of virtualized system and updating of devices, the new host server functions well and the virtual server can migrate back and forth, and also, it works well, together with an increment of stability and performance. The allocated space restriction of single disk increases from 2 T to 16T after upgrading to VMware ESXi 5.5. The whole storage space satisfies the current data storage. As to the application with a low CPU requirement, virtual machine can use FT fault-tolerance function to ensure that the application won't interrupt service when the hardware breakdown occurs. According to the testing, it proves to be a feasible scheme, along with good property improvement, planning to upgrade the old virtualized system to a new one in summer vacation, 2015.

2 Transformation project of data storage system

Recently, light source data takes advantage of Channel Archiver system. It is a file-storage category, its Driver cease maintenance and updating after 2009. RDB Archiver is the data storage part of CSS, its data storage is relational database. CSS, as a toolset, integrates the data storage, data browsing, control system diagnosis tools and operation interface, generating a concise and efficient OPI port operation. Considering the maintenance and updating of Driver in the future, the data storage system requires to upgrade from Channel Archiver system to RDB Archiver system.

In 2013, we conduct the historical-database testing based on the distributed database system of Cloud Storage System. This CSS primary testing configuration is consist of one ISM Server, two mixed nodes of MDS and OSN, four OSN nodes, one interchanger and one client. ArchiverConfigTool imports channel configuration of xml configuration file into CSS-D database, utilizing RDB ArchiverEngine to collect multi-channel data or write programs to create multi-channel data, and then, read and display channel data by CSS DataBrowser. Obtaining channel data from field gateway, simultaneously simulate on-site production environment, and generate a portion of experimental data. Totally it contains 10 071 channels. Analog data use four types of velocity in different frequencies to create one-year data, the entire data is around 1.85 T Bytes.

In 2014, we upgrade the hardware and software of RDB Archiver system. In the respect of hardware, we use two Huawei Tecal RH2288H V2 rack server with 512 GB memory. In the respect of software, we use Oracle Iimesten memory database to store data, use Oracle database to search data. Data storage process is RDB Archiver, the collected data from Driver write into Timesten, and then, Timesten writes it into Oracle database. The process of data searching read data from Oracle database by parallel processing mechanism. Storage operation by Timesten. Searching operation of parallel processing mechanism makes a great growth of data storage and searching speed. It can definitely meet our requirements ascribed to the writing speed reaching 100,000 lines per seconds. In current, hardware system building, Oracle server installation, Timesten database installation, Oracle database installation, RDB Archiver driver revision, coupled with the added Timesten communication interface and parallel searching function are accomplished. Nowadays, we achieve data storage as well as data parallel searching of Timesten via debugging (Fig.1).

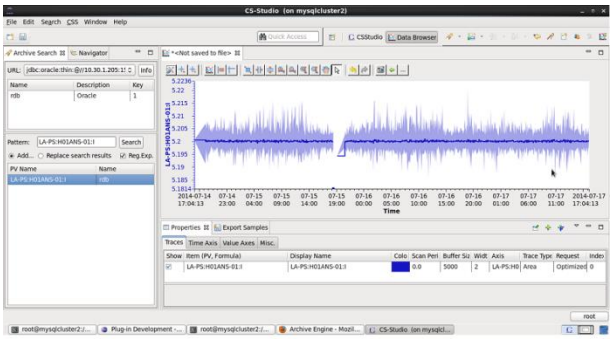

Fig.1 New data searching of storage system

3 IOC polling system testing

EPICS IOC fault-tolerance system is now a study hotspot of effectively available control system applied by EPICS system, which offers redundant IOC that promotes availability of system dramatically, ensures the long-term stability of key system, boosts the whole control system MTBF particularly for the part of software interlock existing in the current light source TOP-UP interlock system. Implementing fault-tolerance IOC system has huge and realistic significance.

In present, we have done several rounds of testing, uniting polling-system developing manufacturer to improve and conducting the testing again during summer vacation, 2014 for the purpose of improving data synchronization of relevant CA in redundant IOC system.

IOC polling system includes two IOC server, running IOC server program at the same time. One of the server is primary, the other one is auxiliary. The pooling instrument relays the request of IOC Client to the primary IOC Server, meanwhile, transmits to auxiliary one. However, the pooling instrument only relays returning results of primary IOC Server to IOC Client. The returning results of auxiliary one will be discarded by pooling instrument. The two front-end pooling instrument #1 and #2, both use the same virtual IP address (VIP). IOC users use VIP as destination address, operates load balancing and simultaneously transmits users' requests to the two rear-end IOC Servers by pooling instrument.

3.1 The testing results shows below:

Breakdown migration: complete the mutual switch of primary and auxiliary IOC. Client can shift to another IOC successfully including a system of normal service when the single IOC break down.

Data synchronization among data: Client can synchronize the writing data to the auxiliary IOC when trigger an AC Put writing operation to IOC.

Later, we need to figure out the rebooting of IOC data synchronization and the revision of SID between primary and auxiliary IOC after an IOC breaks down.

4 Optimization and upgrade of MPS system

4.1 Revision of storage ring vacuum interlock

In order to prolong the replacement period of a unit vacuum filament, avoid to cause play beam problem resulted from false alarm at the same time of two adjacent vacuum points ascribed to the breakdown of vacuum gauge, the vacuum group put forward vacuum interlock to the unit, the scheme of all vacuum points joining interlock via previous design, and adjust to the plan that randomly get two vacuum points joining interlock. Aiming to this request, we rectify all the units of vacuum interlock logic belonging to storage ring in the maintenance period of summer vacation. After rectification, vacuum group is able to set whether each vacuum point joins the interlock (Enable/Disable) directly in the vacuum interlock region (Fig.2) of each unit interlock interface.

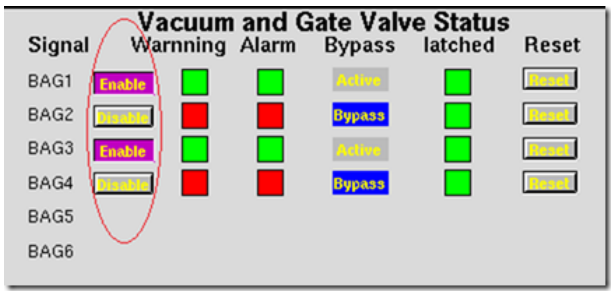

Fig.2 Unit interlock interface settings

4.2 Canted interlock work

Canted interlock implementation of C19 unit double insertion architecture is merged into MPS system after adjustment of the scheme. Meanwhile, in order to avoid unreliability of software interlock used in the first implementation, we completely use hardware interlock plan. In order to not impact the standard unit interlock system structure, MPS adds a set of complementary interlock PLC in C19 unit, and makes the canted interlock content achieved in single PLC software and hardware system. This solution can be popularized to other unit solving complementary interlock requests that standard unit MPS can't achieve. Fig.3 is the architecture schematic diagram of implementation system.

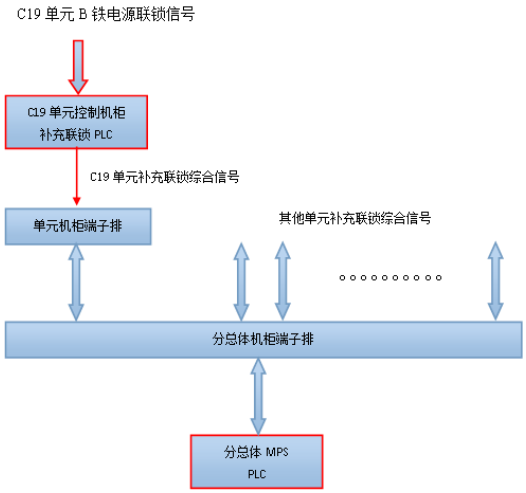

Fig.3 Canted hard interlock implementation scheme architecture

5 New insertion device control

5.1 DEPU

The feedforward disposal of corrective coil power source is achieved by PLC analog module. The difficulty lies in the transportation and updating of feedforward list between PLC on the upper and lower layer control system. Based on this, we must modify driver program, which drives the EPICS driver supporting transmission of big array. According to the requirement of physics group, we update feedforward lists several times.

Achieving compensation function of DEPU working spot, control function of DEPU long coil. Completing testing.

5.2 IVU25

The movement control of IVU25 mainly achieved via the supervision of upper layer EPICS to bottom layer Siemens PLC. Taking advantage of the master-control interface combination AUTOSAVE function, the operators import or correct four corrective coils corresponding to GAP in the power source list of interface, download the set current value to PLC, finish feedforward function. This method has some merits such as data storage, simple operation, etc.

5.3 IVU20

The movement control of IVU20 mainly achieved via the supervision of upper layer EPICS to bottom layer Siemens PLC. The master-control interface contains several subfunction interface.

Because IVU20 uses PLC control analog power source to achieve feedforward, the main problem is how to transmit the feedforward lists to PLC in accordance with EPICS driving mode. We remodify EPICS driving program developed by PSI laboratory. Targeting at RECORD DRIVER and DEVICE DRIVER, we add support of WAVEFORM data. In current, the transportation of big data array is achieved.

The previous power source doesn't have the function of CYCLE. Recently, the CYCLE function, used by the other power source of light source, is achieved by difficult and trivial DB. Therefore, reuse classical SNL language to achieve and test CYCLE function aiming at 19 unit curved iron power source, and then meet the requirement of physics group by testing.

6 SXFEL experimental apparatus and DCLS control system

SXFEL control system finishes research report and preliminary design report, identifies the total design plan: 1. Based on system design of EPICS distributed architecture, 2. Based on control system project objective of completely open-source software.

In accordance with the initial design report, we improve the budget of SXFEL control system, identify the device control plan of magnet power source, vacuum and various movement control, safety interlock system plan, accelerator master timing system design plan, create electrical construction diagram of SXFEL control system, count the control signal of power source, vacuum supervision, modulator, undulator, BBA, timing system.

Options for control system key device: based on the safety interlock system of OMRON PLC, based on the accelerator master-timing system of BNC high-precision digital delay timer, based on the IOC controller of embedded controller, based on the running environment of NIS and NFS control system, based on the physical counting platform of Python. We point at key device IOC for software integration development and testing, furthermore, we can use one type of IOC controller to meet the goal of all the device-control requirement.

DCLS control system has the same plan with SXFEL control system, including technology plan, equipment selection and control software.

In the technology design report, it completes Chinese and English version of control system. DCLS timing sequence contact sheet comes into being after the discussion with synchronization, beam measurement, microwave and power source. MPS interlock logical form and vacuum protection logical form come into being after the request analysis of DCLS safety interlock system. It uses server, work station and DA662 IOC to set up the physical development application platform, and establishes virtual PV channel of DCLS main accelerator containing power supply, modulator with high voltage and phase to serve beam tuning software development. It also identifies DCLS control network, network address allocation of bottom-layer device communication.

According to the requirement of assignment book, we finish sample machine research of control system project, including physical beam tuning software, running environment of control system, upper-layer OPI operation interface, device control IOC control software, etc. Moreover, we finish the development of device control project sample machine of Timing, modulator, vacuum, power supply, undulator and BBA Mover according to the project plan.

Comprehensive design of FEL operation interface: edm interface+WebOPI, two plans totally. edm uses lateral Global+ physical segmentation, graphical integration interface plan (Fig. 4) of vertical device controlling submenu options. WebOPI is used in access based on Internet Browser. In the research of sample machine, WebOPI interface achieves technology development taking undulator and BBA electric displacement platform as examples, and having access test to PC, IPAD and cellphone.

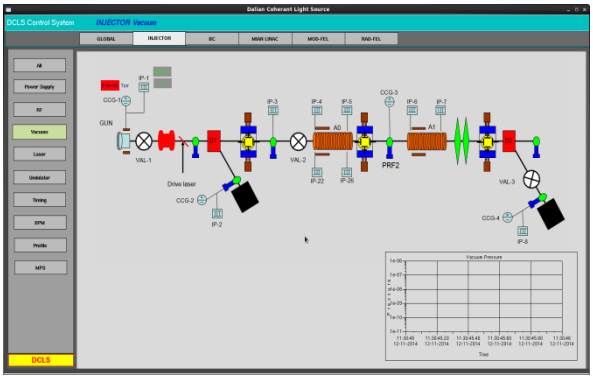

Fig.4 FEL interface design

7 Brazil SIRIUS light source linear accelerator control system

The control system of Brazil SIRIUS light source linear accelerator project starts from the middle of 2013, ends up in the end of the year 2013. This control system are all based on network device (Fig.5), which coincides with EPICS regulation.

The research of sample machines start from the beginning of 2014, on the light source control system, dramatically upgrade and revise the device driving program, add control technique such as system regulation software. In the end of 2014 we generally finish the research and testing of sample machine, in the meantime, the main devices are purchased and a portion of them start to be installed and debugged.

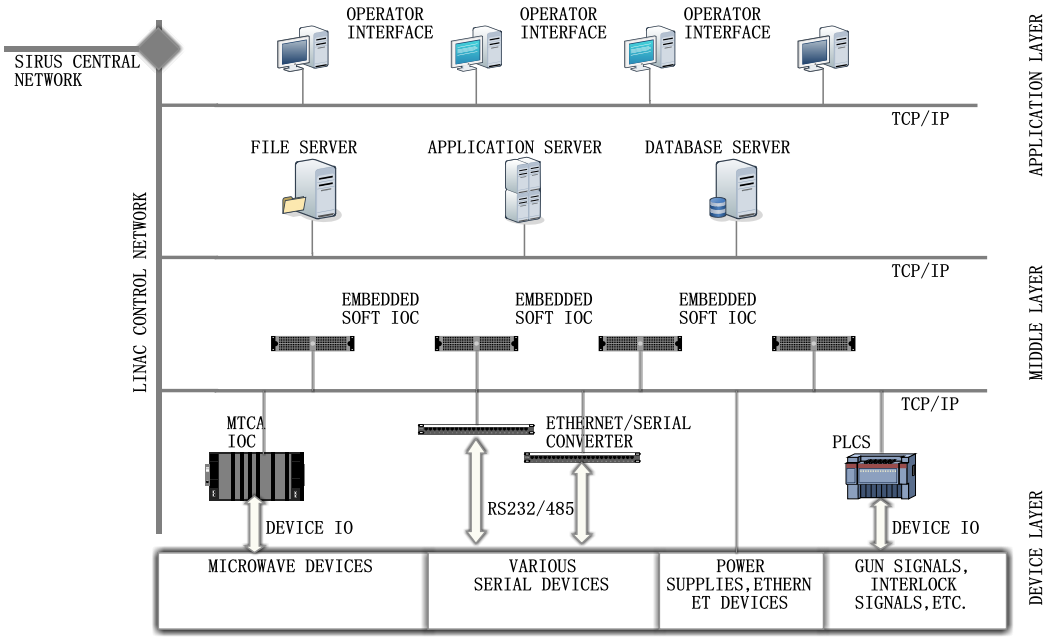

Fig.5 The design of Brazil SIRIUS light source linear accelerator control system

8 Proton therapy apparatus control system

Proton therapy apparatus control system further refines the design plan and the interface file based on numerous research work from 2013 to 2014. Ultimately ascertain the technology route and scheme, accomplish the script of the system design report, network project report and server system project report. Initially conducting the study of part of sample machine with partial system such as vacuum, power supply. Editing and debugging control system software such as driver, server regulation, GUI required by various proton therapy.

9 Research project of medical electronic linear accelerator control system

We finish the control system research of the first CMAX machine and pass the third-party inspection of SPDA. Currently it is in the hospital clinic stage. We also finish the control system research and debugging of IGRT (image guide radiotherapy) model, containing the first domestic multi-leaf collimator (MLC) research and IGRT interface based on FPGA, normally accessing program library for the invocation of IGRT program and arbitration administration of device controlling, sharing database interface and completing connection with TPS (therapy plan system).

束线机械组的研究进展（2013–2014）

束线机械工程技术部　机械组

束线机械组主要承担“上海光源”已建线站光束线机械系统的运行维护和新建线站机械系统的工程建设任务。已建线站光束线机械系统运行稳定，设备可靠性不断完善，有力支持了线站总体的稳定运行。工程建设方面，完成了“梦之线”光束线机械系统、蛋白质 5 线 6 站光束线机械系统的工程建设任务，主要包括三台液氮冷却单色器机械性能测试，标定，安装准直，7 台压弯聚焦镜的到货验收、LTP 检测、镜箱安装上线、镜子安装上线、姿态准直和运动测试等，一台水冷单色器的组装，测试验收以及安装准直，完成了 canted 双线偏转镜系统组装调试，镜箱安装上线、镜子安装上线、姿态准直和运动测试等，完成了蛋白设施 4 条光束线的系统集成，所有光束线以及关键部件的机械性能基本满足要求，光束线顺利通光。“梦之线”国内研制关键设备的安装调试，包括前置镜箱系统，偏转镜箱系统、ARPES 主线 KB 镜箱系统和 PEEM 支线 KB 镜箱系统，两套在线电离室、两套 YAG 晶体测光斑实验腔、热修正系统机械调节部件、两套杂光光阑，完成梦之线光束线机械系统系统集成。

单色器是当代同步辐射装置发展成熟起来的最重要光束线设备之一，目前主要的冷却方式分为水冷和液氮冷却两种。其中液氮冷却单色器多用于高热负载的插入件线站，而水冷单色器多用于弯铁线站。

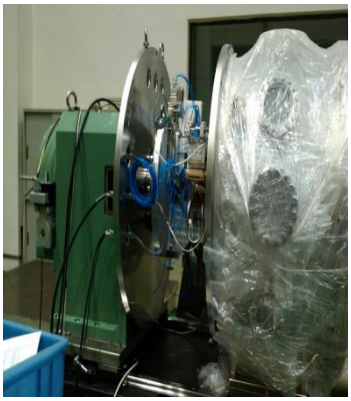

图 1　水冷单色器

高通量蛋白质晶体学光束线单色器距离光源 24.0 m，光束在单色器入口位置的横截面尺寸为 36 mm(H)×2.1 mm(V)。单色器的第一晶体为水冷平晶，最大接收功率是 30 W，最大的接收功率密度是 0.17 W/mm^3。单色器的能量范围为 5~20 keV，能量分辨率为≤2×10^{-4}。

国内首次建设了两条共直线节的插入件 undulator 光束线，简称 canted 光束线—复合物晶体结构光束线(BL19U1)和生物小角散射光束线(BL19U2)。canted 光束线最大的挑战就在于两条光束线距离很近，空间布局非常紧张。为了使两条光束线能分开足够的距离，在单色器下游加入了一台水平双偏转镜。

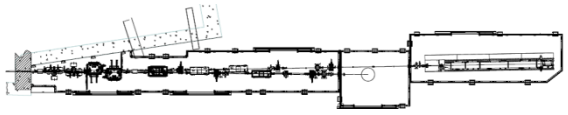

图 2　蛋白设施 canted 光束线总图

双线共用的偏转镜系统要求在超高真空环境中工作。偏转镜系统主要由平面镜、镜子底座、镜体调节机构、镜箱支撑调节机构、真空系统、控制系统等组成。镜体运动调节机构包括投角及 X 方向运动，但是要求滚角安装精度要好于 0.1 °。

图 3　偏转镜镜体

复合物晶体结构光束线(BL19U1)和生物小角散射光束线(BL19U2)目前已完成调光及指标优化，即将面向用户开放。上海光源二期规划中将建设多条 canted 光束线，蛋白设施 canted 双光束线的建成为二期 canted 光束线的设计、布局、调试等方面积累了丰富的实践经验。

Research development of beamline mechanics groups duration 2013−2014

Department of Beamline mechanics Engineering

Our group is responsible for the mechanical system operation and maintenance of constructed beamlines, and mechanical system engineering construction tasks of new beamlines at SSRF. The stable mechanical system operation of constructed beamlines and the continuously improvement of the equipment reliability were the strong support for the stable operation of the whole beamline system. Our group has completed the mechanical systems installation of the dream line and NFPS, which mainly include mechanical test, installation and on site alignment of 3 sets of cryo cooling DCM, 1 set of water cooling DCM, 7 sets of mirror bender system and 1 set of deflection mirror system for canted beamline. The mechanical system integration of non-standard equipment for 4 beamlines of NFPS has been completed. All the beamlines and key equipments meet the requirements, have been completed beam tuning and parameter optimization. The installation and commissioning of main equipments supplied by domestic manufacturers has been completed, including mirror systems, KB mirror systems for ARPES and PEEM, 2 sets of YAG monitor, adjustment mechanism of thermal correction system, 2 sets of stray light aperture and the mechanical system integration of non-standard equipments.

Monochromator is one of the most important beamline equipment, it is mainly divided into water cooling and cryo cooling two kinds according to the cooling temperature. Cryo cooling monochromator usually is used to insert device beamlines, and the water cooling monochromator usually is used to bending magnet beamlines.

Fig.1 Water cooling monochromator

A water cooled double crystal monochromator for the High Throughput Beamline will be placed at 24 m from the source. The maximum incoming beam size will be 36 mm wide by 2.1 mm high, and the maximum heat load density will be 0.17 W/mm^2. The DCM will be used at an energy range between 5~20 keV, the energy resolution will be less than 2×10^{-4}.

Two beamlines have been constructed at SSRF, they are named canted beamlines, which are complex crystallography beamline (BL19U1) and biology X-ray small angel scattering beamline (BL19U2), because they are originating from the same undulator source. The greatest challenge for designing the canted beamlines is setting up optical components at very limited space between two beamlines. To separate sufficient space between two beamlines, two reflecting mirrors which are mounted in one chamber are set up downstream of DCM respectively.

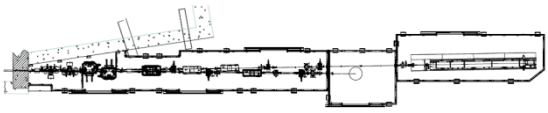

Fig.2 Layout of the canted beamlines

The deflection mirror system shared of two beam-lines works in the ultra high vacuum. Deflection Mirror system consists of plane mirror, mirror set, adjustment mechanism of mirror, support system, vacuum system, control system, etc. Adjustment Mechanism of Mirror contains the motion of pitch and X direction, and the installment accuracy of roll is less than 0.1 °.

Fig.3 Adjustment mechanism of mirrors

Complex Crystallography beamline (BL19U1) and BioSAXS (BL19U2) has been completed beam tuning and parameter optimization, and it will be opened to users. Multiple canted beamlines will be built in the two phase of SSRF. We have accumulated a wealth experience from the achievement of the canted beamlines for protein science which will contribute to the design and commissioning for canted beamlines during SSRF II.

束线工艺组工作进展（2013–2014）

束线机械工程技术部，束线工艺组

本组完成了蛋白质项目5线6站和梦之线项目的相关设备安装、前端调试和束线调光，完成了5线6站和“梦之线”冷却水、配电、压缩空气、棚屋排风和液氮输送等公用设施系统全部设备安装、系统测试、验收工作;配合各光束线站，完成各线站通光调试工作；配合完成5线6站和“梦之线”辐射防护棚屋通光辐射泄漏测试，配合完成各线站棚屋通光调试；在线辐射泄漏测试结果表明，棚屋的设计、加工与安装满足工艺要求。

配合完成蛋白质项目5线6站和“梦之线”项目专家组测试、工程验收；完成蛋白质项目5线6站和“梦之线”项目公用设施系统档案整理与归档；编制完成线站公用设施系统档案文件目录6份（21页），线站公用设施系统技术总结书6份，提交技术文档77份，设计图纸115份（549张）。

本组在微系统所项目，目前已完成弯铁前端区冷却水、配电、压缩空气工艺设计，完成前端区水、气、电系统设备明细表和材料清单;进行了光束线站冷却水、配电、压缩空气工艺设计，以及线站公用设施系统工程设计报告。

完成微系统所弯铁光束线和插入件前端区公用设施系统的工程设计、设计评审、施工设计、设备安装招标、签订加工与安装合同；微系统所弯铁光束线站公用设施系统设备安装工程，按计划完成80%的安装工作量；编制完成“微系统所弯铁线站公用设施系统工程设计报告”（20页）、“线站公用设施系统工程设计说明书（46 页）”，完成设计图纸46张。

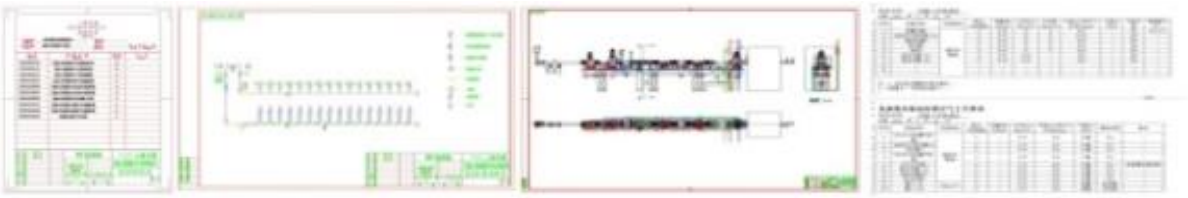

图 1　微系统所插入件线站前端区水、气系统工艺设计图

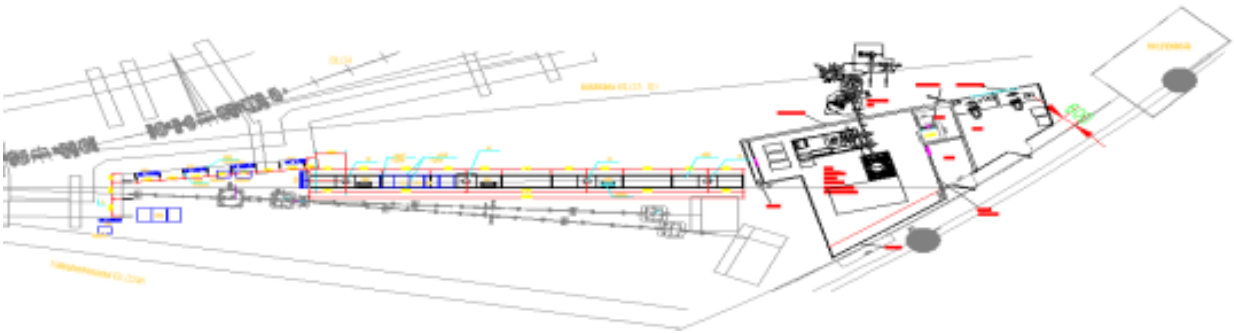

图 2　微系统所弯铁线站水、电、气公用设施系统布局图

本组完成了 X 光学测试光束线前端区公用设施系统的工程设计、设计评审、施工设计、设备安装招标、签订加工与安装合同;编制完成“X 光学测试光束线站前端区公用设施系统工程设计说明书（23页）”，完成设计图纸10张；设备安装工作计划在2015年寒假和暑假进行。

完成中石化三条线站棚屋防护和公用设施系统的初步设计报告、系统运行费估算；配合中石化完成线站公用设施部分基础设计报告。

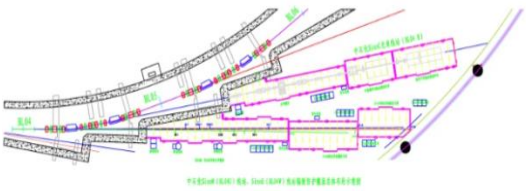

图 3　中石化线站辐射防护棚屋总体布局示意图

完成九院线站公用设施系统和棚屋防护系统的经费预算、运行费估算、线站公用设施和棚屋系统初步设计报告，制订工程实施的 CPM 计划。

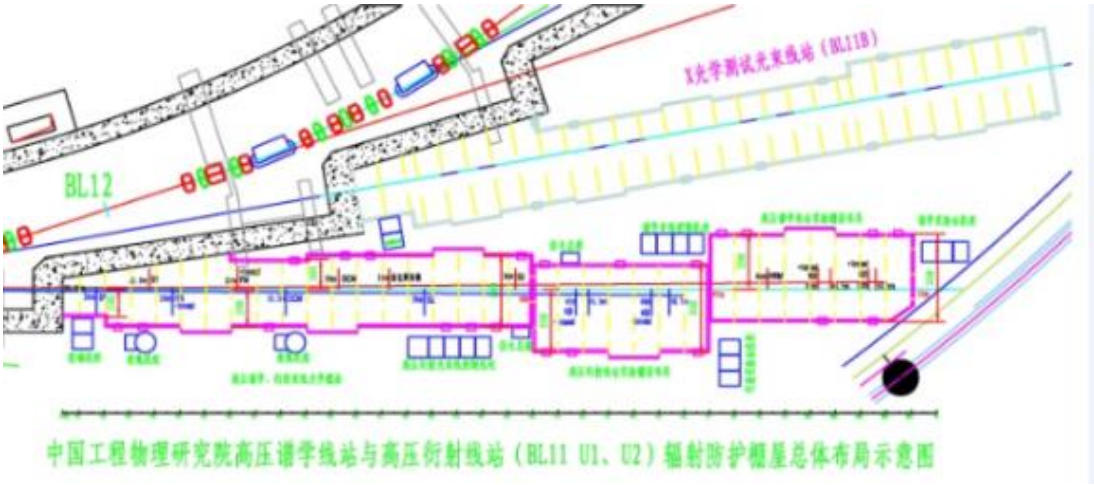

图 4 九院线站辐射防护棚屋总体布局示意图

参考文献

1. 苏东，刘运．微系统所弯铁和插入件线站前端区公用设施系统的工程设计说明书.
2. 苏东，杨东. X 光学测试光束线站前端区公用设施系统工程设计说明书.
3. 苏东，刘运．微系统所弯铁线站和插入件线站公用设施系统工程设计报告.

The progress of beam line process group (2013-2014)

Beam Line Mechanical Engineering Technology Department　Beam Line Technology Group

Our group completedthe related equipment installation、front-end debugging and beam line calibration for the protein project "Five Lines With Six Stations" and the "Dreamline" project of SSRF; completed installation for equipment, system testing and acceptance work of the water system, electricity system, gas system, hut exhaust and liquid nitrogen delivery of the 5-line 6-station and " Dreamline"; cooperated with each beam line station to complete the light debugging; cooperated to complete the optical radiation leakage test of radiation protection hut of the 5-line 6-station and "Dreamline", and cooperated with the completion of beam line calibration of all line stations. The results of online radiation leak test show that the design, processing and installation of the hut could meet the technological requirements.

Cooperated to complete test and project acceptance of 5-line 6-station and "Dreamline" project with the expert group; Completed the file arrangement and archiving of 5 line 6 station and "Dreamliner" utility system; Compiled and completed 6 copies of public utility system archive files of the line station, 6 copies of the technical summary of the utility system of the line station, 77 technical documents, 115 design drawings and 549 drawings.

Our group has completed the design of water, gas and electric design of the bend magnet front-end area, and completed the detailed list and material list of water, gas and electrical system equipment the front-end area for SIMIT's project. And completed the water, electricity and gas design of the beam line station, as well as the design report of the utility system of the line station were carried out.

Completed the engineering design, design review, construction design, equipment installation and bidding, signing processing and installation contract of the public utility system of the SIMIT's bend magnet beam line and insertion device front-end area; The installation project of the utility system equipment for bend magnet of SIMIT, with the planned completion of 80% of the installation work as planned; Compiled "the utility system engineering design report of the bend magnet beam line for SIMIT " page (20), "the engineering design instruction of the line station utilities systems (46 pages)", completed the design 46 drawings.

Fig.1　The design drawing of water and gas system of SIMIT's insertion device front-end area

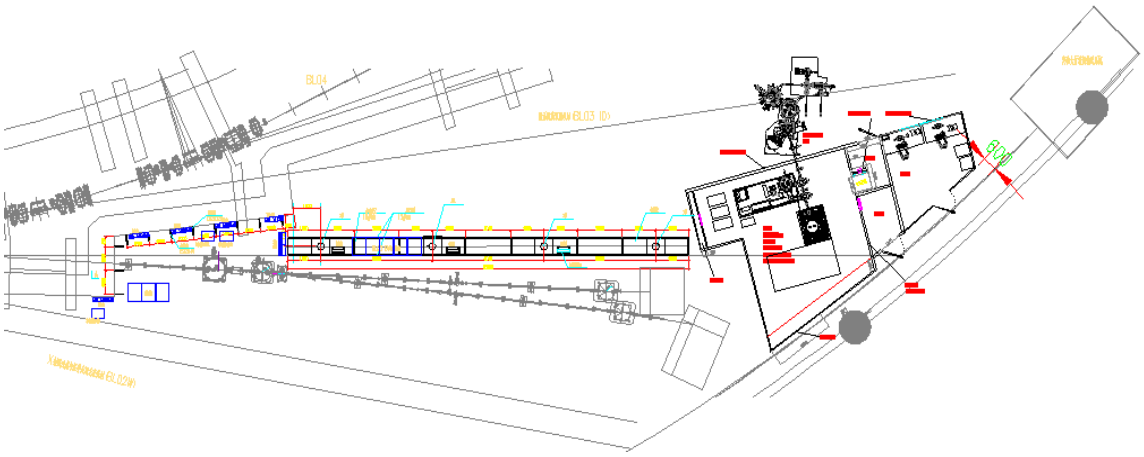

Fig.2　The layout of water, electricity and gas utility system for SIMIT's bend magnet beam line

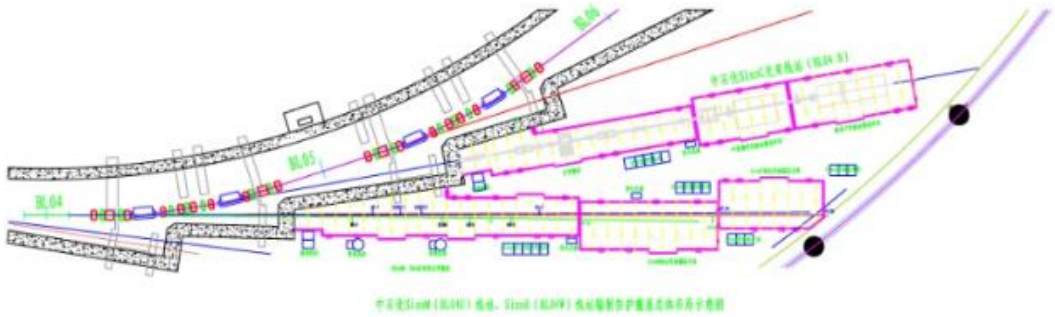

Fig.3 Schematic diagram of general layout of radiation protection hut of Sinopec line station.

Our group has completed the engineering design, design review, construction design, equipment installation and bidding, signing processing and installation contract of the public utility system of the front-end area of X-ray optical test beam line. Completed "the engineering design specification of the public utility system of the front-end area of the X optical test beam line station (23 pages)", completed the design drawings 10 pages; The equipment installation work is going to bein the winter vacation and summer vacation of 2015.

Completed the preliminary design report and system operation cost estimation of the hut protection and utility system of the three line stations for Sinopec; Cooperate with Sinopec to complete the basic design report of public facilities of the beam line station.

Completed the budget of the utility system and the hut protection system of the beam line station, estimate the operating cost, the preliminary design report of the line station public facilities and the hut system, and made the CPM plan for the implementation of the project.

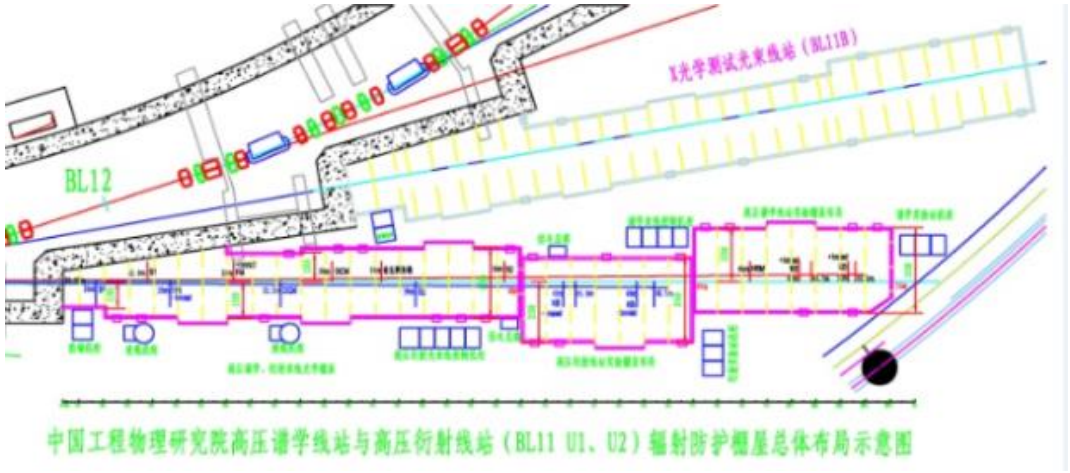

Fig.4 Schematic diagram of general layout of radiation protection hut of the beam line station.

电子学与探测器组的研究进展（2013–2014）

束线光学工程技术部　电子学与探测器组

本组完成了蛋白质项目五线六站和梦之线项目的相关设备安装、前端调试和束线调光，并成功实现了上海光源第一条 Canted 光束线站和红外线站的联锁控制和光束位置监测，且各条光束线站的性能测试达到设计指标。前端调试是对完成安装任务的各条光束线前端的所有设备进行功能性测试，以检查其是否符合光路的设计要求和能否承受 X 光的照射，同时标定和测试各前端 XBPM 探测器；束线调光是指继续检测除前端区以外的光路设计和设备安装的正确与否，包括光束线站基本指标参数的测试等。

蛋白质项目和梦之线的光束线前端的功能测试，主要包括前端束流的热负载测量、轨道调节与 XBPM 光束中心位置测量和辐射剂量测量三项，各项的测试结果均与预期的相同。前端束流的热负载测量主要是通过各个关键部件的温度变化来进行，其温度除了与束流的大小有关外，还与电子束的轨道相关联，不同的轨道会使得各部件受光照的位置不一样，进而其温度的变化也不同。测试结果表明，各个前端的关键部件温度在束流 200 mA 以下变化时的温升不大，都在设计的允许范围内；其最大的温升发生在 BL18U 的 PS2 闭合时，有 12.6 ℃，但其温度值不高(29.6 ℃)，也在设计的温度范围内。

轨道调节与 XBPM 光束中心位置测量的目的是为了检验各个 XBPM 的响应灵敏度，由于不方便精准调节，且 XBPM 的读数依赖于其对应的插入件 Gap 大小等多种原因，使得此项测试没有完全达到预想的效果，但实验数据还是能够粗略反映其相对应的变化规律。表 1 所示为改变轨道频率来调节轨道的水平方向偏移，测量其相应变化的实验结果，BL17B 是弯铁光源，其 XBPM 的读数几乎不变；图 1 的记录曲线更能说明其变化趋势。

表 1　轨道水平方向调节时各个 XBPM 的测量结果（测量单位：mm）

轨道变 化	19U1_XBPM(X,Y)		19U2_XBPM(X,Y)		18U1_XBPM(X,Y)		17B_XBPM1(Y)	17B_XBPM2(Y)
0	0.576	-1.454	-0.669	-1.478	0.084	0.524	0.109	0.221
外扩 50 μm	0.563	-1.455	-0.703	-1.471	0.058	0.524	0.109	0.221
内缩 50 μm	0.598	-1.456	-0.616	-1.475	0.116	0.524	0.109	0.221
外扩 100 μm	0.532	-1.451	-0.751	-1.470	0.023	0.525	0.110	0.221
内缩 100 μm	0.612	-1.457	-0.571	-1.478	0.141	0.525	0.108	0.221

当束流为 200 mA 时，分别调节 Canted 前端两个插入件的 Gap：一个至 8 mm，另一个拉开至 15 mm 的情况下，测量其前端及其棚屋附近的辐射防护剂量值。测量结果表明：都在规定的安全范围内，其中伽玛剂量为 93~171 nSv/h，中子剂量为 4.1~22 nSv/h。

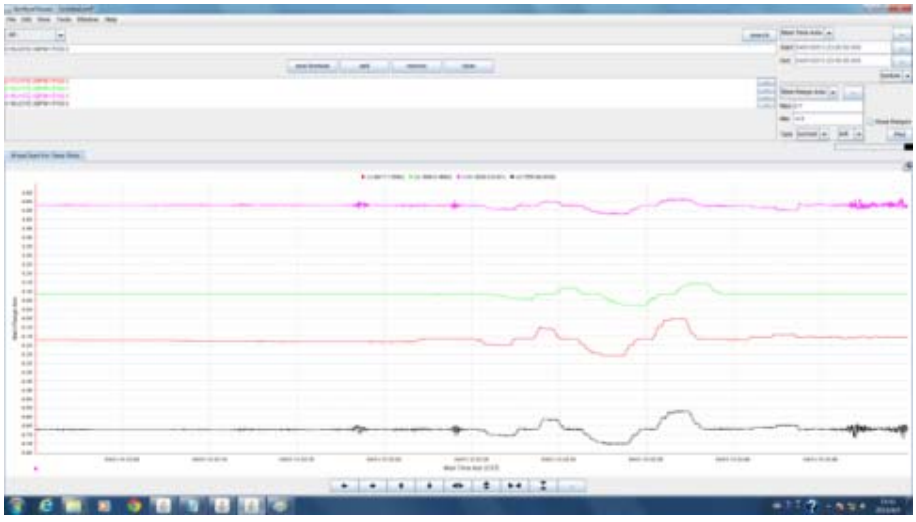

注：BL17U1 的显示是为了比较以前运行线站的测量结果

图 1　X 方向位置变化的测量曲线（BL19U1(粉红)、BL18U1(绿)、BL17U1(红)、BL19U2(黑)）

光束线站的运行维护是一项十分重要的任务，保证各条光束线站的正常运行和性能提升是能取得好的实验结果的前提。在暑期检修期间完成了BLl4W、BL15U、BL14B 和 BL16B 的前端 XBPM 探测器的升级改造任务，更换了电子学读出设备等；同时与美国 APS 光源的专家开展了 XBPM 探测器的合作研究；继 BLl7U 之后，其光斑位置的测量精度也达到了 1 μm 的水平，为实现光斑的进一步稳定控制创造了条件。

参考文献

1. 朱周侠, 等. 上海光源 Canted 光束线安全联锁系统设计[J], 核技术, 2014, **37**(9): 090102.
2. 张永立, 等. 上海光源红外光束线主动反馈控制器的设计[J]，核技术, 2014, **37**(1): 010102.
3. 刘占军，龚培荣．Libera Photon 处理器在上海光源 XBPM 中的应用研究，核技术, 2014, **37**(5): 050102.

Research development of electronics and detector groups duration 2013−2014

Department of Beamline Optics Engineering　Electronics and Detector Group

Our group has completed the equipment installation, front-end testing and adjusting the x-ray position for beamlines of NFPS (Nations Facilities of Protein System), and successfully realized the safety interlock control and X-ray position monitoring of first CANTED beamline and IR beamline at SSRF. The result of test shows that the performance of each beamline is in well accordance with the design target. The front-end testing means testing the performance of equipment of each beamline, finding if they meet the design requirements of the optical path and the ability to withstand x-ray irradiation, and calibrating the XBPM detector. And further check and test the basic parameters of the beamline.

Functional testing of the front-end of the beamline of the Protein project mainly include thermal load measurement of the front end, the relationship of orbital adjustment and XBPM beam center position measurement and radiation dose measurement. The test results are the same as expected. The thermal load measurement of the front end is mainly carried out by monitoring the temperature change of the key components. The temperature is not only related to beam current, but also the tracks of the electron beam. The exposed point of x-ray is different, and the change of temperature is also different under different orbitals. Test results show that temperature raise of the critical component of front-end is within the allowable range of design under 200 mA beam current. The maximum temperature rise occurred at 12.6 degrees centigrade when the PS2 of BL18U was closed, but the temperature was not high (29.6 degrees C), and it was also within the temperature range of the design.

To test the response sensitivity of each XBPM, we did the orbital adjustment and XBPM beam center position measurement. Because it is difficult to adjust orbital and the readout of XBPM is depending on its corresponding ID Gap size, the test did not achieve the desired results. But the experimental data can also reflect the corresponding change rule roughly. We measured the readout change of the XBPM by adjusting the horizontal deviation of the track. The measurement result is shown in table1. The readout of BL17B is almost constant due to BL17B is from the bending magnet. The recording curve of figure 1 can more markedly show the trend of change.

Table1　The readout change of the XBPM by adjusting the horizontal deviation of the track

Change of track	19U1_XBPM(X,Y)		19U2_XBPM(X,Y)		18U1_XBPM(X,Y)		17B_XBPM1(Y)	17B_XBPM2(Y)
0	0.576	-1.454	-0.669	-1.478	0.084	0.524	0.109	0.221
External 50 μm	0.563	-1.455	-0.703	-1.471	0.058	0.524	0.109	0.221
Indentation 50 μm	0.598	-1.456	-0.616	-1.475	0.116	0.524	0.109	0.221
External 100 μm	0.532	-1.451	-0.751	-1.470	0.023	0.525	0.110	0.221
Indentation 100 μm	0.612	-1.457	-0.571	-1.478	0.141	0.525	0.108	0.221

When the size of gaps for CANTED front-end are set as 8mm and 15 mm in current 200 mA, we measure the radiation dose near its front end and its hutch. The result shows the radiation dose is in the safe range. The Gamma dose is 93~171 nSv/h, and the neutron dose is 4.1~22 nSv/h.

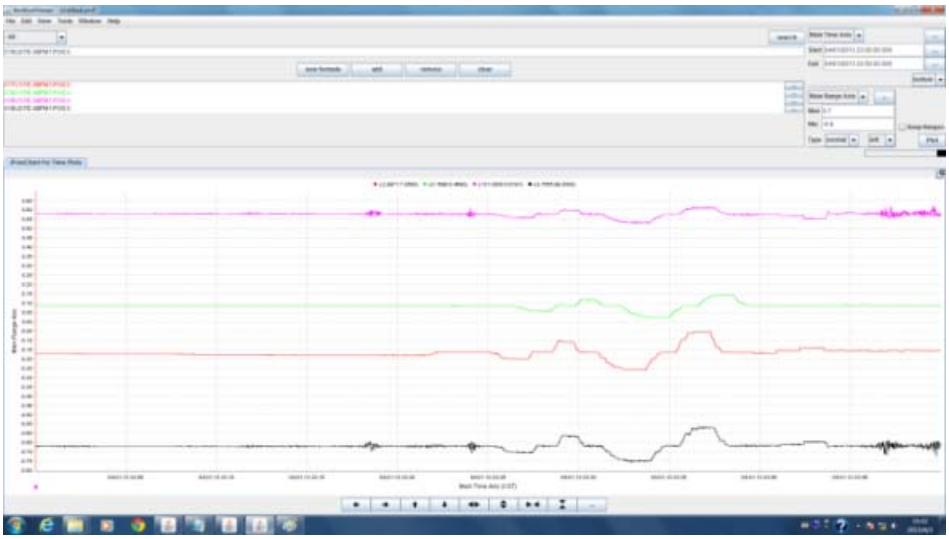

Note: display of BL17U1 is to compare the measurement results of the previous beamline.

Fig.1　The recording curve of XBPM in X direction (BL19U1(pink), BL18U1(green), BL17U1(red), BL19U2(black))

The operation and maintenance of beamline is a very important task. To ensure the normal operation and performance improvement of each beamline is the premise of good experimental results. During the summer overhaul, we completed the upgrade tasks of BLl4W, BL15U, BL14B and BL16B's front-end XBPM detectors, and replaced the electronics readout equipment. Meanwhile a collaborative study of the XBPM detector is also carried out with experts from APS in the United States. After BL17U, the measuring accuracy for spot position have been achieved the level of 1 micron, which created the condition for realizing further stable control of spot.

Reference

1. Zhou Zhouxia, *et al*. Design of the Canted beamline interlock system at SSRF. Nuclear Techniques (Chinese). 2014, **37**(9): 090102.
2. Zhang Yongli, *et al*. Design of active feedback controller used in the infrared beam line of SSRF. Nuclear Techniques (Chinese). 2014, **37** (1): 010102.
3. Liu Zhanjun, Peirong Gong, *et al*. Research on application of Libera Photon processor for XBPM in SSRF. Nuclear Techniques (Chinese). 2014, **37**(5): 050102.

“梦之线”热修正 BPM 探测器

束线光学工程技术部

“梦之线”热修正 BPM 探测器是用扫描方式测量平面光栅单色器后 0 级光的光斑尺寸的一种装置。光学镜面通常会因光照受热而产生变形，在这里，镜面热形变的最大影响就是改变光栅的物距，使聚焦条件不成立，狭缝处光斑垂直尺寸增大。因不同能量的光在通过光栅衍射后散开，可供使用的+1 级衍射光在狭缝处垂直方向上为连续分布，故可采用测量镜面热变形对 0 级光传输的影响来推算出对+1 级衍射光的影响。该装置的设计就是通过一个丝扫描 BPM 测量 0 级光斑尺寸的变化，计算出单色仪中的平面镜热变形的曲率半径，从而得出 Cff 需要改变的值，来修正热变形对能量分辨率的影响。

热修正 BPM 有平行的 7 根扫描丝，为防止丝之间的信号干扰，在每个丝之间用挡板隔开。BPM 前面设计了一个具有荧光靶性质的挡光器，其作用是保护 BPM 的扫描丝不会被光长时间照射而影响使用寿命。热修正 BPM 工作时，挡光器要先退出光路，让 BPM 的扫描丝受光照而产生电流信号输出，通过扫描测量来计算其光斑的中心位置和尺寸大小。

BPM 扫描丝选用的是直径 10 μm 的镀金钨丝，7 根丝信号在腔体内部通过编排后接线引出，部分丝两两相接，只需 4 根导线引出信号，再接入 I-V 转换器组成的电子学读出系统。电子学系统包含了数据采集和运动控制，使用 LabVIEW 软件来实现步进电机运动控制和数据采集的同步进行，并记录光栅尺的回读值；软件还需实现测量数据拟合的功能，在数据采集完成以后点击运算按钮即可得到光斑的尺寸。图 1 为热修正 BPM 的外形照片。

图 1　热修正 BPM 外形照

“梦之线”热修正 BPM 系统于 2013 年 8 月上线安装，9 月份完成在线测试。测试的结果如图 2 所示，图示尺寸是 0.431 4 mm，相对应的理论计算的光斑尺寸为 0.420 0 mm，通过测试对比即可得到光斑大小的微米量级的变化。

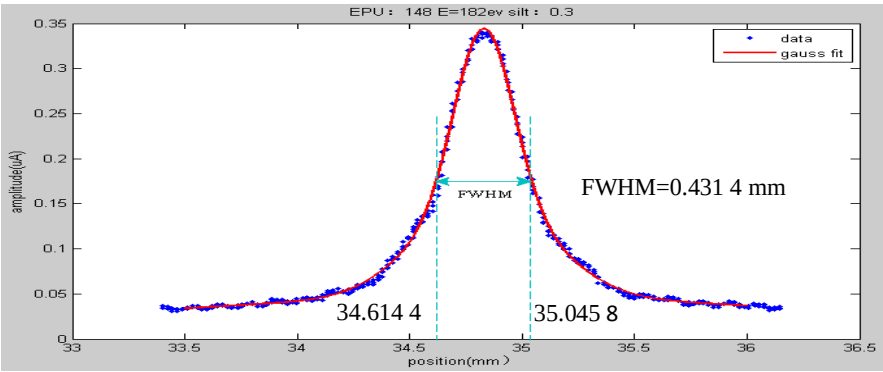

图 2　热修正 BPM 测试曲线

A detector for measuring changes of spot size of X-ray due to thermal deformation

Department of Beamline Optics Engineering

The x-ray detector with seven wires is used to measure the X-ray spot size of 0 diffraction order after the plane grating monochromator by scanning. The maximum effect of the thermal deformation of the mirror change the focusing conditions of the VLS grating, and change the object distance of the grating, so that the focusing conditions are not established. The grating is a dispersive element, the X-ray of different energy is scattered through the grating diffraction, and the required +1 x-ray is continuously distributed in the vertical direction of the slit. Therefore, the effect of the thermal deformation of the mirror on the X-ray transmission is calculated to predict the effect of the +1 X-ray diffraction. After measuring the change of 0 X-ray size, the effect of thermal deformation on energy resolution is corrected by changing the Cff value.

The BPM detector is composed of parallel 7 wires, and each wire is separated by a shield to prevent the signal interference between wires. A shutter is designed in front of detector to protect the detector filaments from being irradiated by X-ray. A light barrier with a fluorescent target is designed to protect the filament of the BPM detector, which is not affected by the long life. When the detector works, the light barrier is to exit the X-ray path.

The wire of BPM detector is a gold-plated tungsten wire with a diameter of 10 μm, and the seven wires are connected by the arrangement of internal wiring, and only four terminals are required. Four channels signal is connected to I-V converter and then to the electronics system. The electronics system includes data acquisition and motion control. The LabVIEW is used to achieve the motor cntrol by stepper motor and data acquisition synchronization, and records the return value of the coder. The software is also include the function of data waveform fitting, and just click on the operation button to get the size of the X-ray after the data acquisition is completed. Fig.1 is the photo of the X-ray BPM detector located at beamline.

Fig.1 The photo of the BPM detector

The X-ray BPM detector was installed in August 2013 and was tested online in September 2013. The X-ray size of the theoretical calculation is 0.420 0 mm, and the test result of the detector is 0.431 4 mm, and tested curve is shown in Fig.2. Through the test comparison, we believe that changes in micron magnitude of spot size can be measured.

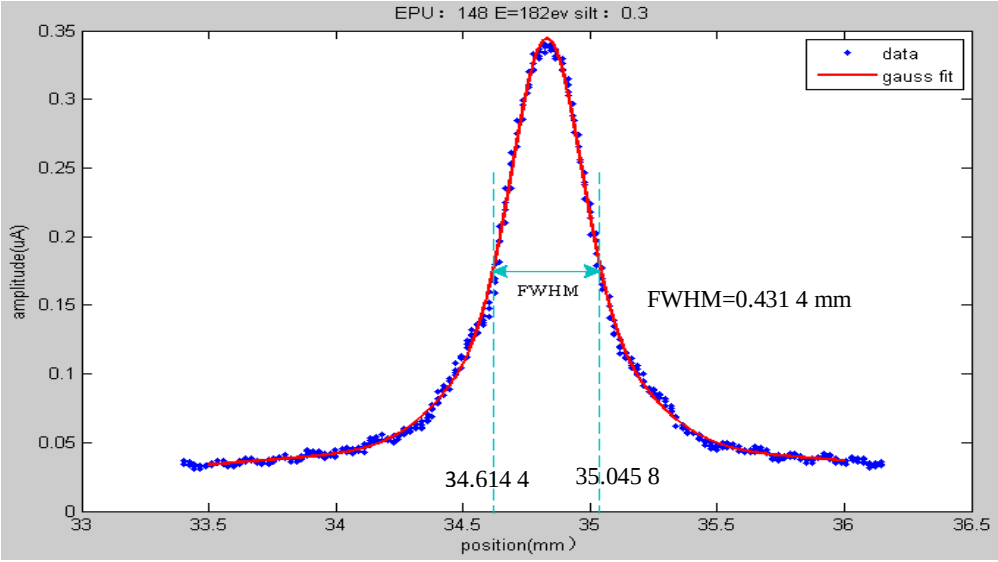

Fig.2 Tested curve of X-ray spot size by the BPM detector

束线控制组研究进展

束线光学工程技术部　束线控制组

束线控制组主要承担“上海光源”已建线站光束线控制系统的运行维护和新建线站控制系统的工程建设任务。已建线站光束线控制系统运行稳定，软硬件功能不断完善，有力支持了线站总体的稳定运行。工程建设方面，完成了“梦之线”光束线控制系统、蛋白质 5 线 6 站光束线控制系统的工程建设任务。2013−2014 年度，本组共发表 4 篇研究论文，编写技术文档 21 篇。线站维护方面，完成了 SAXS 线和 XRD 线两台国产单色器控制的软硬件改造、完善了 XBPM 的自动扫描和数据采集程序、改进了 XIL 线的自动曝光系统的程序结构、完成了新版控制 CPU 的 vxWorks 软件的开发、升级了 OPI 界面软件、更换了首批老旧的 OPI 电脑、更新了首批 EPICS SoftIOC 服务器。

除负责运行维护和工程建设外，本组还负责完成了部分实验站控制系统的改造任务、参加并完成了部分 973 课题的研究任务、完成了基于网口的便携式运动控制器的软硬件研制。另外，完成了微系统所新建线站前端运动控制系统的建设任务，完成了上海光源二期工程中光束线控制系统和实验站控制系统的可行性研究报告和初步设计报告的编写工作。

为发展基于 EPICS 软件平台的实验站控制技术，本组参与并负责完成了 14W1 XAFS 实验站的控制和数据获取系统的改造工作。将实验站电机的控制进行了标准化和统一化，统一采用基于 VME 机箱、MV5500 CPU、MAXv-8000 控制器、本组自行研制的 SMD 系统驱动器的硬件结构和基于 EPICS motor 模块的软件结构。将实验站电离室、32 元固探等探测器的控制和数据采集统一用 EPICS 实现。将自动配气系统等原位环境的控制也纳入到了 EPICS 环境下。在此基础上用 EPICS 的 SSCAN 机制和 Sequencer 机制，结合 Python 脚本语言和 CSS[1]图形化界面软件，在 EPICS 环境下实现了 XAFS 谱的采集和存储程序。

为了便于设备离线测试，开发了便携式的运动控制器，该控制器基于美国 galil 公司的 OME 模块，通过设计必须的硬件电路，开发并完成了相关的电路板模块。设计的硬件接口可以无缝连接到本组标准的步进电机驱动器系统。控制软件在 EPICS 下开发完成，基于国际上已经存在的驱动模板，结合本地应用环境的实际情况，经过二次开发，构建了完整的控制软件。完成了严格的软硬件测试，已经在部分光束线上开始试用。

本组承担并完成的 973 子课题《时间分辨 X 射线激发发光光谱实验系统的研制 XEOL(X Ray Excited Optical luminescence)》，在国内同步辐射装置上首次实现了纳秒时间分辨 X 射线激发发光光谱(Time-Resolved XEOL)实验方法[2−3]。上海光源是第三代同步辐射光源，其高亮度、储存环电子束团的脉冲时间结构以及同步辐射 X 射线能量连续可调等特点，为 TRXEOL 实验技术的实现提供了良好的基础。整套 TRXEOL 实验装置由定时系统、光谱仪系统和核电子学系统三部分组成。TRXEOL 实验技术是利用同步辐射 X 射线脉冲激发样品，在其后 200 ns 左右的时间间隔内测量、记录并分析样品发光衰减过程。该技术，通过调节同步辐射 X 射线的能量，选择性地激发样品中不同的元素，进而可以确定样品的发光中心，与发光产额的 XAFS 方法相结合，可以进一步确定发光材料中发光体的局域结构，为深入理解发光材料的发光行为提供重要的研究手段，特别是对研究具有复杂结构的发光材料，例如：纳米半导体材料、稀土闪烁材料、有机电致发光材料(OLED)、分子指示剂（生物研究中的光学标记和其他的软物质）等发光材料的发光机理，具有非常强大有效的作用。这些材料在光电器件、传感、平板显示、医学标记等很多领域都有广泛的应用。

为了实现纳秒量级时间分辨率的 TRXEOL 技术，解决了两个关键问题：其一，储存环电子束团实现了混合填充模式。加速器物理组在有限的机器研究时间内，经过紧张调试，实现了一种混合填充模式[4](5 mA 单束团和 225 mA 多束团，单束团前后的时间间隔约 220 ns)，该模式已经达到基本实验要求。既能够提供满足要求的单束团及其前后的时间间隔，束流强度又能够保证其它光束线站正常运行；其二，标定了储存环的时间结构以及精确地确定了样品的发光时间，定时系统是上海光源主定时系统在光束线站的延伸，提供的同步触发脉冲信号与单束团产生的 X 射线脉冲通过延时在样品点

同步，同步精度可达 6 ps[5]。

参考文献

1. http://controlsystemstudio.org.
2. 张招红, 姜政, 薛松, 等. 上海光源 XAFS 线站时间分辨 X 射线激发发光谱实验系统[J]. 光谱学与光谱分析, 2015, **35**(8): 2324-2328.
3. 张招红, 姜政, 薛松, 等. Time structure measurement of the SSRF storage ring using TRXEOL method[J]. 核技术(英文版), 2015, **26**(4).
4. 张文志, 刘桂民, 赵黎颖,等. 上海同步光源定时系统物理设计[C]//全国粒子加速器技术学术交流会. 2007, 109-111.
5. 赵黎颖. SSRF 主定时系统研究[D]. 中国科学院上海应用物理研究所, 2008.

Research development of beamline control group

Beamline Control Group Department of Beamline Optical Engineering

The beamline control group is mainly responsible for the operation and maintenance of the beam line control system and the project construction tasks of the control system for the new proposed Beamlines. The beamline control system has been running steadily and the functions of hardware and software have been continuously improved, effectively supporting the overall stable operation of the Facility. The completed work about engineering construction includes: the Dreamline beamline control system and the protein projetct 5 lines 6 stations beamline control system. In 2013−2014, a total of 4 research papers were published and 21 technical papers were prepared. The work about the operation maintenance includes: the update of the control system for the two domestic-made monochromators at the SAXS beam line and the XRD beam line , the optimization of the XBPM automatic scanning and data acquisition program to improve the XIL automatic exposure system efficiency, the development of a new version of the vxWorks software , the upgrade of the OPI interface software, the replacement of the first batch old OPI computer, the update of the old EPICS SoftIOC servers.

In addition to the operation, maintenance and construction, this group was also responsible for the control system transformation tasks for some experimental station. A 973 program sub project was achieved. A portable motion controller hardware and software was developed. In addition, the front-end motion control system was completed for the newly built beamline by the Shanghai Institute of Microsystem and Information Technology, and the feasibility study report and preliminary design report of the beamline control system and experimental station control system in the SSRF Phase II Project were completed.

In order to develop experimental station control technology based on EPICS software platform, the group participated in and completed the transformation of the control and data acquisition system at the 14W1 XAFS experimental station. The experimental station motion control was standardized and unified. The hardware includes VME chassis, MV5500CPU, MAXv-8000 controller and the group-developed SMD driver units. The motion software is based on EPICS motor module. The control and DAQ for ionization chamber, the 32-element solid detector etc. was re-done with EPICS. The control of the in-situ environment such as the automatic gas distribution system is also done in the EPICS environment. On this basis, EPICS SSCAN mechanism and EPICS Sequencer mechanism, combined with the Python scripting language and CSS[1] graphical interface software was used to develop the XAFS spectrum acquisition and the data storage.

In order to facilitate the off-line testing of the equipment, a portable motion controller was developed based on the OME module from Galil Corporation in the United States. The relevant circuit board module was developed. The designed hardware interface can be seamlessly connected to the standard stepper motor drive units. The control software was developed under EPICS. Based on the existing international driving template, combined with the actual situation of the local application environment, after secondary development, the complete control software was constructed. A rigorous hardware and software testing has been done. The controller has been used on some beam line.

The group undertook and has completed one 973 sub-project, developing the time-resolved X Ray Excited Optical Luminescence setup. A time-resolved X-ray excitation luminescence spectroscopy system was developed for the first time in China[2,3]. SSRF is the third generation synchrotron radiation light source, its high brightness, the pulse time structure of the stored-ring electorn beam and the continuous adjustable X-ray energy of synchrotron radiation. Technology to provide a good foundation for the TRXEOL experimental consists of timing system, spectrometer system and nuclear electronics system. The TRXEOL experimental technology uses the synchrotron radiation X-ray pulse to excite samples, during the following 200ns time interval to measure、record and analyze the sample luminescence decay process. This technology, by adjusting the energy of synchrotron radiation X-ray, selectively excited different elements in the sample, which can determine the luminescence center of the sample, combined with the luminous yield XAFS method, the local structure of the luminophore in the luminescent material can be further ascertained for better understanding luminescent behavior of samples. TRXEOL provides an important research method, especially for the study of luminescent materials with complex structures, such as nanometer semiconductor materials, rare earth scintillation materials, organic electroluminescent materials (OLEDs), molecular indicators (optics Markers and other soft substances) and other luminescent materials, such as light-emitting mechanism, has a very powerful and effective role in these materials in optoelectronic devices, sensing, flat panel display, medical marking and other fields have a wide range of applications.

In order to achieve TRXEOL technology with time resolution of nanoseconds, two key problems are solved. First, the storage ring electron bunches achieve a hybrid fill pattern. The Accelerator Physics team achieved a mixed-fill mode[4] (5 mA single beam and 225 mA multi-bunch, around 220 ns before and after single bundle) after intensive testing within a limited machine study time. The invention can not only provide the single bunch and the time interval before and after the excitation, but also can ensure the normal operation of other beamline stations. Second, the time structure of the storage ring is calibrated and the luminescence time of the sample is accurately determined. The timing system is an extension of Shanghai Light Source Master Timing System at the beamline station. The synchronization triggering pulse signal provided by the system is synchronized with the X-ray pulse generated by a single beam at the sample point. The synchronous precision is less than 6 ps[5].

Reference

1. http://controlsystemstudio.org.
2. ZHANG Zhao, JIANG Zheng, XUE Song, *et al*. Experimental system of time-resolved X-ray excitation emission spectrum of Shanghai Light Source XAFS Station[J] .Chinese Journal of Spectroscopy and Spectral Analysis, 2015, **35**(8): 2324-2328.
3. Zhang Zhao, Jiang Zheng, Xue Song *et al*. Time structure measurement of the SSRF storage ring using TRXEOL method[J]. Nuclear Techniques (English Edition), 2015, **26** (4).
4. ZHANG Wenzhi, LIU Guimin, ZHAO Liying, *et al*. Physical Design of Shanghai Synchrotron Light Source Timing System[C] // National Conference on Particle Acceleration Technology 2007: 109-111.
5. ZHAO Liying. Research on SSRF Main Timing System[D]. Shanghai Institute of Applied Physics, Chinese Academy of Sciences, 2008.

生物大分子晶体学研究进展(2013−2014)

生物大分子晶体学组

生物大分子晶体学组主要承担“上海光源”首批线站“生物大分子晶体学光束线站(BL17U1)”的运行维护与用户实验支持工作。该线站在2013−2014年度高效、低故障率运行，累计总供光机时10 906.8 h，其中提供用户机时9 274 h，执行用户课题598次。用户共发表文章368篇，其中Cell、Nature及Science顶级期刊文章21篇，用户解析结构总数连续两年名列世界第一。

本研究组在保证光束线安全高效运行的同时，开展了光束线站新方法和新技术的研究及发展：采用复合透镜(CRL)和pinhole相结合的方法，对BL17U1的光斑尺寸进行控制，可实现ϕ5 μm、10 μm、20 μm、50 μm及100 μm的光斑尺寸切换（图1）；为了实时监测BL17U1光束线的光斑变化，包括位置和强度信息，光束线站工作人员自行设计和研发了一套具有位置灵敏的X射线强度探测器[1]，图2给出了该套设备在BL17U1实验站测量数据和精度信息；为了配合生物大分子晶体自动化筛选及处理技术，BL17U1光束线工作人员结合国外先进经验，开发出适用于BL17U1实验站系统的Raster自动定位微小晶体技术。

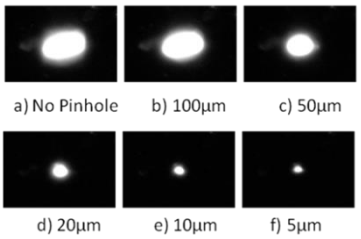

图1 利用CRL得到的聚焦点光斑尺

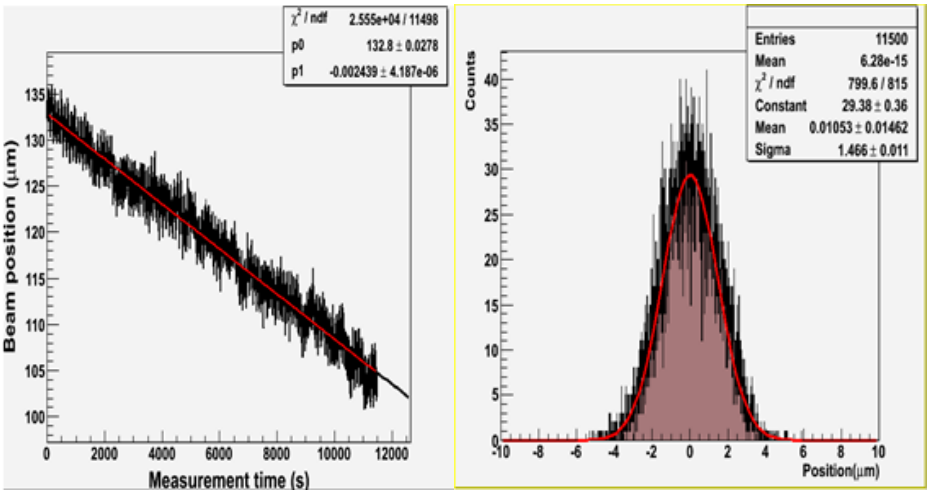

图2 位置灵敏探测器安装及测量结果

除负责上海光源一期生物大分子晶体学光束线站的日常运行维护及用户实验支撑外，本组还负责上海光源线站工程两条新建晶体学线站及一个用户辅助实验室的设计和建设工作。2013−2014年，课题组负责完成了“P2防护蛋白质晶体学线站”和“高性能膜蛋白晶体学线站”两条晶体学线站的物理设计，通过国际专家评审；完成了生物与医学辅助实验室项建书及可研报告撰写，通过专家评审。

本组在生物大分子晶体学实验方法学研究及重要蛋白质结构与功能研究方面也进行了不断的研究和探索。研究人员用氙(Xe)作为重原子用于天花粉蛋白结构的相位解析，并结合天花粉蛋白在云母表面的晶体外延生长特性，可以将天花粉蛋白发展为一种“全能型”的融合标签蛋白，用来帮助解析结构未知蛋白的三维晶体结构[2]。此外本课题组还解析了细胞色素P450酶TxtE及人源GDP岩藻糖合成酶的晶体结构[3−4]（图3）。

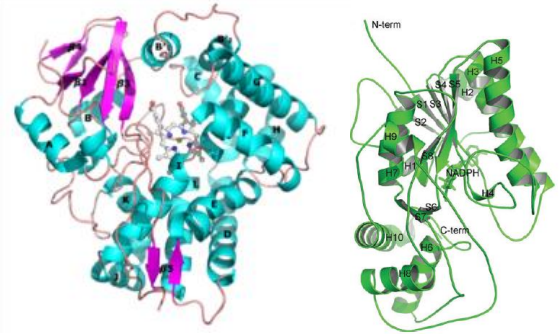

图3 TxtE(左)及人源GDP岩藻糖合成酶(右)晶体结构

2013−2014 年度，本课题组在研项目主要有：国家自然科学基金“cblC 型甲基丙二酸尿症和同型半胱氨酸尿症相关蛋白 MMACHC 的结构与分子机制研究”、“人源高尔基体蛋白 GRASP55 的结构与功能研究”和“生物大分子晶体样品自动筛选方法研究”；与上海交通大学合作研究的国家自然科学基金面上项目“古菌 RecJ-like 核酸酶参与校正 RNA 引物 3'末端错配核糖核苷酸的分子机制研究”等。

参考文献

1. Pan Q Y, Wang Q S, Wang Z J, *et al*. An active beamstop for accurate measurement of high intensity X-ray beams[J]. Nuclear Instruments and Methods in Physics Research A, 2014, **735**: 84–586.
2. Chen Y X, Li M J, Yu F, *et al*.Using Xe as a heavy atom forphase determination of protein trichosanthin structure[J]. Nuclear Science and Techniques, 2014: **25**(3).
3. Yu F, Li M J, Xu C Y, *et al*, Structural Insights into the Mechanism for Recognizing Substrate of the Cytochrome P450 Enzyme TxtE[J]. Plos One, 2013, **8**(11): e81526.
4. Zhou H, Sun L H, Li J, *et al*, The crystal structure of human GDP-L-fucose synthase[J]. Acta Biochim Biophys Sin, 2013, **25**(9): 720-72.

Research development of macromolecular crystallography group

Macromolecular Crystallography Group

Macromolecular Crystallography Group (MX group) is mainly in charge of operation and user support of the Macromolecular Crystallography Beamline (BL17U1). During 2013−2014, BL17U1 provided 10 906.8 h beam time, of which 9 274 h were allocated to 598 research projects. 368 papers including 21 top ones in the journals of "Cell, Nature and Science" were published by users during this period. The number of structures deposited in the Protein Data Bank by BL17U1 users in these two years ranked first in the world.

In order to ensure the safe and efficient operation of the beam line, research and development of the new method and technology of the beamline and the experiment station were also carried out. Using the method of combination compound refractive lenses (CRL) with pinhole, the spot size of ϕ 5 μm, 10 μm, 20 μm, 50 μm and 100 μm can be achieved in BL17U1 (Fig.1). A position sensitive X ray intensity detector was designed and developed to monitor the changes of BL17U1 beam size in real-time, including the information of the position and intensity of the focus spots[1]. Fig.2 shows the experiment results and accuracy of the equipment measured at BL17U1. In order to improve the automatic screening and processing technology of biological macromolecule crystals, combining with foreign advanced experience, the BL17U1 beamline staff developed the Raster technique to position micro crystals automatically suitable for BL17U1 experiment station system.

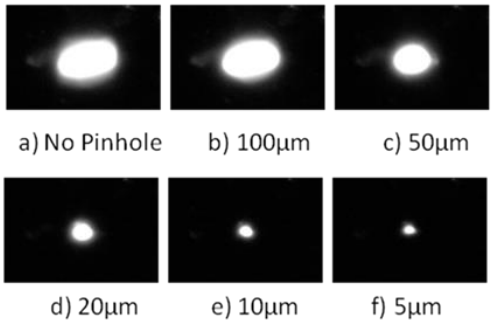

Fig.1 Focus spots obtained by using CRL

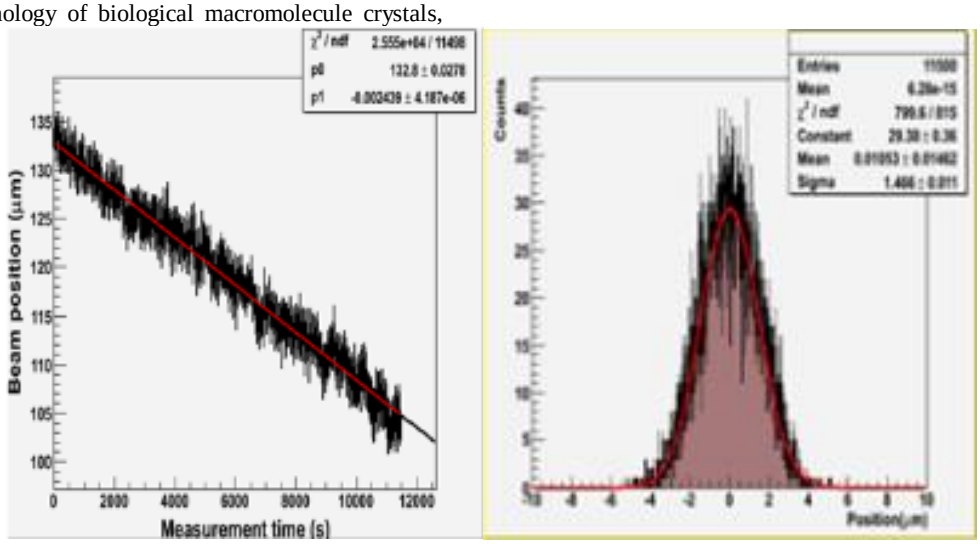

Fig.2 Position sensitive detector installation and measurement results

In addition to the daily operation and maintenance of the BL17U1, MX group is also responsible for the design and construction of two new macromolecular crystallography beamlines and a user laboratory in the PASEII beamline project. In the year of 2013−2014, MX group finished the physical design of the Biosafety P2 Macromolecular Crystallography Beamline and the High Performance Membrane Protein Crystallography beamline station two. The design reports were also evaluated by international experts. We also finished the proposal and feasibility study report of the biological and medical auxiliary laboratory project, which were then reviewed by the experts.

MX group has also carried out a continuous study and exploration in the structure and function of important proteins. Xenon (Xe) was used as a heavy atom for the phase analysis of TCS structure. The trichosanthin protein can be developed to be a "universal" fusion protein tag to cryatallize and solve the structures of unknown proteins by using its special character of the epitaxial crystal growth on mica surface[2]. In addition, the crystal structures of cytochrome P450 enzyme TxtE and human GDP fucose synthetase (Fig.3) [3-4] were also solved by the MX group.

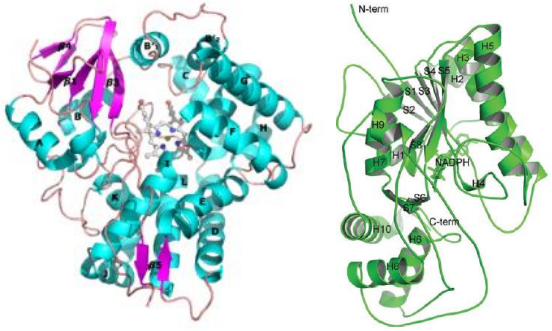

Fig.3 Crystal structures of TxtE (left) and human GDP fucose synthetase (right)

In 2013−2014, MX group also undertook some major research projects, including the National Natural Science Foundation "Structure and molecular mechanism study of cblC type methylmalonic aciduria and homocystinuria associated protein MMACHC", "The structure and function study of human Golgi protein GRASP55", "The study of automatic screening method of biological macromolecular crystals in macromolecular crystallography beamline" and “The molecular mechanism study of Archaeal RecJ-like nuclease involved in the correction of RNA 3'-end of the primer mismatch ribonucleotides" (in cooperation with Shanghai Jiaotong University).

Reference

1. Pan Q Y, Wang Q S, Wang Z J, *et al*. An active beamstop for accurate measurement of high intensity X-ray beams[J]. Nuclear Instruments and Methods in Physics Research A, 2014, **735**: 84–586.
2. Chen Y X, Li M J, Yu F, *et al*. Using Xe as a heavy atom forphase determination of protein trichosanthin structure[J]. Nuclear Science and Techniques, 2014: **25**(3).
3. Yu F, Li M J, Xu C Y, *et al*. Structural Insights into the Mechanism for Recognizing Substrate of the Cytochrome P450 Enzyme TxtE[J]. Plos One, 2013, **8**(11): e81526.
4. Zhou H, Sun L H, Li J, *et al*, The crystal structure of human GDP-L-fucose synthase[J]. Acta Biochim Biophys Sin, 2013, **25**(9): 720-72.

光电子组研究进展

光电子组

光电子组主要承担上海光源 “超高分辨宽能段光电子实验系统”（梦之线）线站的建设、调试及运行工作，以及线站工程中 S^2 线、E-line 软线和原位环境支撑实验室的建设。

梦之线 2014 年 5 月通过了院里组织的初测，10 月进行了院里组织的工艺验收测试，以全部指标达到或超过验收指标的优异成绩，通过了该测试。2014 年 11−12 月开始进入试运行。本组负责的建设任务主要包括光束线站核心设备-SX700 型平面光栅（变线间距）单色仪的物理指标的核定，招投标及采购和验收。针对光束线调试过程中单色器出现的相关技术问题，负责组织了所牵涉到的厂家和工程部技术人员的技术协商与问题解决。

本组负责了上海光源二期纳米自旋与磁学线站-S^2 线站的设计工作。做了光束线设计、磁学实验站设计，完成可研报告。负责了上海光源二期 E-line 光束线站的软线分支物理设计，包括了光束线设计、发射谱实验站设计，并撰写了该线站项目建议书及可行性研究报告。负责了上海光源二期辅助实验室中原位条件实验室的建设工作，通过参考国内外实验室建设方案，了解各光束线站不同用户的原位实验需求，调研各种原位实验设备，走访专家用户，撰写了二期原位环境实验室可研报告。

在梦之线上结合束线的调试，对高能量分辨率的束线性能进行了研究：①利用自主设计建造的 MCP 在线电离室，通过气体吸收谱对束线能量进行了标定，以及对低于两万以下的能量分辨率进行了测定，在氮吸收边测得了接近两万的能量分辨率（逼近所用光栅的设计指标）；②首次揭示了气体吸收谱对于高能量分辨率的测试极限；③首次发现了对于高分辨率的光束线，镜面碳污染不仅影响束线通量，而且会影响能量分辨率；④根据光电子 ARPES 实验站测试能量分辨率所需的金属费米边处光电离截面的特点，建议用铜替代金来测试，将测试时间一下缩短五倍，使得指标测试不仅切实可而且缩短了束线强通量照射下碳污染的时间。

在研项目主要有：973 项目“同步辐射手段表征纳米材料”子课题——软线 SXEOL 方法在软 X 射线线站的建立及其应用；国家自然科学基金“同步辐射光束线中的相干传输研究”[1]；国家自然科学基金“活体细胞的软 X 射线三维成像实验方法的研制”(11305254)；国家自然科学青年基金“结合会聚束电子衍射和 X 射线全散射对无铅压电材料局域结构的研究”(11104306)[2]；上海市青年科技英才扬帆计划项目(14YF1407500)，对量子点电子空穴复合机理的研究[3-4]。

在下一年度的工作中，抓好梦之线站运行工作，配合用户在 2015 年能发表一批高质量的文章；继续精调梦之线的指标，拓展偏振态能量区间；做好 E-line 软线、原位条件实验室、S^2 线站可研报告的国内评审及国际评审，进一步细化技术指标，将可研报告落实为初步设计报告。

参考文献

1. 孟祥雨，郭春磊，王勇，等.光学学报，2013, **33**: 0734001.
2. Cao J F, Guo C, Zou H M. Acta Crystallographica Section B. 2013, **69**: 556–562.
3. Chen Z H, Peng W, Zhang K, *et al*. Mater Chem A, 2014, **2**: 7004-7014.
4. Chen Z H, Li H, Tang Y B, *et al*. Material Research Express, 2014, **1:** 015034.

Research development of photoelectron group

Photoelectron Group

Photoelectron group (PE group) is mainly in charge of commission, operation and user support of the DREAMLINE beamline (High Energy Resolution and Broad Energy Range Photoelectron Experimental System) and, for the PHASE-II Beamline Projects, developing two beamlines, including S^2-line, E-line soft-branch, plus one user-supporting laboratory–in-situ instrumentation lab.

For its final acceptance, the DREAMLINE beamline passed a preliminary test in May and the final test in October 2014, both organized by CAS, with all specs achieved or surpassed. From November on, the beamline has entered the test-running phase. Our group has been responsible for ratifying physical specifications of the key device of the beamline–a SX700-type plane grating monochromator (VLS), for preparing bidding documents and for its final acceptance. Technical negotiations and fault diagnosis were organized by the PE group among the manufacturer and SSRF engineering staff.

Among the PHASEII beamline projects, the nanospin and magnetics beamline (S^2-line) has been designed by our group. The design work undertaken includes those for the beamline, magnetic station, and the feasibility report has been completed. For the E-line soft branch, the physical design for the entire beamline and experiment stations was concluded, and summarized in the feasibility report. For the user-supporting laboratory (in-situ instrumentation lab), the feasibility report was resulted from consulting domestic and overseas labs' plans, inquiring various in-situ experiment needs from SSRF beamlines, surveying on numerous in-situ commercial devices, interviewing with experienced users etc.

For the DREAMLINE beamlines, to pursue a good performance of high energy resolution, researches have been carried out in the aspect of: i. Beamline energy calibration via a home-made MCP online ionization chamber through gas absorption spectra, direct measurement of beamline energy resolving power (@N_2 K-edge approaching 20 000); ii. Reveal of the detection limit of energy resolution through gas absorption method; iii. Discovery of the deterioration of energy resolution, in addition to flux reduction, caused by carbon contamination on mirrors; iv. Use of copper Fermi edge as an alternative for gold Fermi edge based on a larger cross section in photoionization to enhance the signal intensity for a very high energy resolution detection.

The ongoing projects include the National Basic Research Program of China (973 Program) "Soft x-ray XEOL method and its application"; two projects supported by the National Natural Science Foundation of China, "Study on the coherent beam propagation in SR beamlines"[1] and "Soft X-ray 3D imaging on living cells" (11305254), one project supported by National Natural Science Youth Funds "Local structure study of lead-free piezoelectric material by convergent beam electron diffraction and X-ray total scattering technique" (11104306)[2], one project supported by Shanghai Youth Foundation (14YF1407500) "Study on the charge recombination mechanism of quantum dots" [3-4]

In 2015, besides the beamline operation and user experiments support for the DREAMLINE, its performance will be further explored and broader energy range with polarizations other than linear horizontal will be made available for users. Development work at involved PHASEII beamline projects will proceed, to be ready for domestic and international reviews for E-line soft branch, S^2-line and in-situ instrumentation lab, to refine beamline(lab) technical specifications as to transform their feasibility reports into preliminary design reports.

Reference

1. Meng X Y, Guo C L, Wang Y, *et al*. Acta Optica Sinica 2013, **33**: 0734001.
2. Cao J F, Guo C, Zou H M. Acta Crystallographica Section B. 2013, **69**: 556-562.
3. Chen Z H, Peng W, Zhang K, *et al*. Mater Chem A, 2014, **2**: 7004-7014.
4. Chen Z H, Li H, Tang Y B, *et al*. Material Research Express, 2014, **1**: 015034.

软 X 射线组研究进展

软 X 射线组

软 X 射线组主要承担上海光源软 X 射线谱学显微光束线站和干涉光刻(XIL)分支线站的运行维护与用户实验支持工作。该线站在 2013−2014 年度高效低故障运行，总供光机时 10 875 h，总故障率 0.5%。累计提供用户机时 8 046 h。接待用户实验人员 756 人次，执行用户课题 239 个，用户涵盖环境科学、材料科学、生物医学和物理学等领域。共发表包括 *Phys. Rev. Lett.*, *Journal of Hazardous Materials*, *Biomaterials*, *Environmental Science & Technology*, *J. Mater. Chem. A*, *Nanoscale* 等一区在内用户文章 66 篇，其中一区文章 16 篇。线站维护方面开展了 STXM 单色器的带光碳污染清洗工作，在镜箱中充入微量氧气，X 射线的照射下污染物和氧气反应转化为 CO、CO_2，达到的清洗目的，清洗后通量提高一倍。

XIL 分支线站 2013 年正式对用户开放。除负责上海光源一期软 X 射线谱学显微光束线站和 XIL 分支线站的日常运行维护及用户实验支持外，本组还负责上海光源线站工程 1 条新建线站“中能谱学线站”的初步设计；完成国家重大科研仪器设备研制专项 SiP·ME^2 项目弯铁软 X 射线光束线(02B)的初步设计；参与了 X 射线自由电子激光试验装置诊断光束线的部分设计和建设任务。

为满足不同学科领域用户研究的需求，发展了以下实验站方法学：①本组 2013−2014 年度实现了基于 STXM 的扫描 CDI 成像，对标准样品的成像分辨率优于 30 nm[1,2]；②在上海光源 BL08U1A 线站搭建了软 X 射线激发光学发光(XEOL)探测平台。与 TEY 技术结合，该技术具有元素，化学态及位点特异性等优势。③搭建了基于 STXM 的常温纳米 CT 平台，2014 年正式对用户开放，二维分辨率最高可以达到 50 nm，三维空间分辨率可达 200 nm；④设计了一套新的谱学测量系统。可获得比原来高一倍的光通量，能提供荧光、XEOL、TEY 等多种谱学测量方法，能实现样品的三维运动和沿竖直轴的转动，并在样品处提供低温、磁场等原位环境。2014 年度完成该系统的设计和各项采购。⑤XIL 分支线站在成功运行的基础上，与中科院化学所杨国强课题组合作研制 EUV 光刻胶放气检测装置，使 XIL 线站成为检测 EUV 光刻胶的完备系统。⑥XIL 线站发展了离线 OSA-mask 对准技术并进行了大面积拼接曝光，获得了大面积的曝光图形，在此基础上利用微量高次谐波，发展了可在线观测调节的 OSA 装置；⑦XIL 线站利用高空间相干性，进行了宽带 CDI 实验，取得了初步结果。

应用研究方面：①利用软 X 射线谱学显微技术首次研究了纳米气泡，利用原子力显微技术给出了单个纳米气泡的硬度信息[3,4]；②开展激光光子关联谱实验研究，在 $BaTiO_3$ 极化团簇弛豫特性研究取得进展[5]；③提出并理论验证了精确聚焦 VUV 单色器的概念，解决了 VUV 束线设计中的长期困难[6]。

本课题组承担的在研科研项目：国家自然科学基金面上项目“基于新型宽带相干光学技术的软 X 射线干涉光刻”；国家自然基金大科学装置联合项目“纳米气泡的同步辐射研究”；国家自然科学基金青年基金项目“多孔石墨烯分离膜的粒子束制备及其性能的理论研究”、“X 射线散斑和双光子关联谱法在极化团簇动力学研究中的应用”、“基于同步辐射研究纳米气泡的电化学方法的发展”；“同步辐射软 X 射线光束线位置无损在线监测技术的研究及其在纳米 CT 与透射扫描成像中的应用”；国家自然基金重大项目子课题“水科学先进实验技术研究”；973 项目子课题“弛豫铁电单晶多尺度微结构研究和巨压电性的起源”；上海市自然科学基金项目“碳纳米管材料在核电池辐射场中的损伤与修复机制研究”。

2015 年，软 X 射线组主要任务为：完成软 X 射线谱学显微和干涉光刻线站的运行维护；开展中能谱学线站的设计；完成 SiP·ME^2 项目弯铁软 X 射线光束线的束线安装；发展 STXM 和 XIL 相关的束线方法学，更好地为用户服务。

参考文献

1. Liu H G, Xu Z J, Zhang X Z, *et al*. Applied Optics, 2013, **52**: 2416.
2. Liu H G, Xu Z J, Zhang X Z, *et al*, Acta Physica Sinica, 2013, **62**: 150702.
3. Zhang L J, Zhao, B Y, Xue, L, *et al*. J. Synchrotron Rad, 2013, **20**, 413.
4. Zhao B Y, Song Y, Wang S, *et al*., Soft Matter, 2013, **9**: 8837.
5. 张明俊，郭智，郜仁忠，等. 铁电体中极化长程涨落的光子关联谱实验研究[J]. 物理学报, 2015, **64**: 147801.
6. Xue C F, Wu Y Q, Zou Y, J. Synchrotron Rad., 2015, **22**: 328

Research progress in soft X-ray group

Soft X-ray Group

Soft X-ray group is mainly in charge of operation and user support of soft X-ray scanning microscopy (STXM) beamline and soft X-ray interference lithography (XIL) branch beamline. During 2013−2014, this beamline has supported beam time of 10 875 h with a low fault rate of 0.5%. There were 8 046 h provided for 756 users from the 239 proposals, whose research fields covering environmental science, material science, biomedicine, physics and so on. During this time 66 user papers have been published on academic journals，including Phys. Rev. Lett., Journal of Hazardous Materials, Biomaterials, Environmental Science & Technology, J. Mater. Chem. A, Nanoscale etc. 16 papers were publiched on the top journals (SCI-I). As for the beamline maintance, the on-site carbon contamination clearance of STXM monochromator has been implemented, Oxygen gas is leaked into the chamber. The chemical reaction occurred between the cataminated material and oxygen, rendering the residual gas of CO_2 and CO. The photon flux can be doubled by means of the on-site carbon contamination clearance setup.

Besides the maintenance user suport work on STXM and XIL stations, soft X-ray group takes charge of the physical designing of Medium energy spectroscopy beamline; the physical designing of Bending magnetic soft X-ray beamline (02B) of National Major Scientific Instruments and Equipment Development of NSFC (SiP ME2). The group has anticipated in the partial designing and construction of Diagnostic beamline of XFEL Testing equipment.

In order to fulfill the requirements for user researches in multiple areas. Sevleral experimental methods have been developed: 1) The scanning coherent diffraction imaging based on STXM has been achieved during 2013−2014 period, the spatial resolution for standard sample is better than 30 nm[1,2]; 2) The soft X-ray excitation optical luminense(XEOL) detecting platform has been developed. In combination with TEY method, this method has the priorities of analyzing elements, chemical state etc. 3) Nano-CT platform at normal temperature based on STXM has been installed, and it has been opened to users from 2014, with the 2-D spatial resolution of 50 nm and 3-D resolution of 200 nm. 4) A new soft X-ray spectroscopy measuring system has been designed. The photon flux can be doubled. And The spectroscopy methods of fluorescence, XEOL, TEY etc. can be conducted. The 3-D motion and rotation along vertical axis can be achieved. The in situ environment of low temperature and magnetization can be supplied on sample position. The designing and purchasing of this system has been completed in 2014. 5) A device was designed and assembled on the XIL endstation to analyze the outgassing of photoresists under EUV exposure. The XIL station, integrated with this device, become a complete system for EUV resists testing; 6) Large-area exposure pattern is obtained by applying an off-line OSA-mask aligning technique developed by the XIL beamline. On this basis, an in-situ OSA-mask aligning system is developed by using trace high-order-harmonics from the undulator; 7) Based on high spatial coherent beam, broad-bandwidth CDI was done in XIL station, with successful preliminary results.

There are some progresses in application researches: 1) The imaging of nanobubbles was obtained using STXM techniques for the first time and gave the stiffness of single nanobubbles by atomic force microscopy techniques[3,4]; 2) The photon correlation spectroscopy based on laser has been implemented, inprovements of the relaxation characteristic of $BaTiO_3$ has achieved[5]; 3) The concept of extra-focus monochromator for VUV range was proposed and verified, which solves a long-term difficulty in the design of VUV beamline[6].

The ongoing projects include the Project of National Natural Science Foundation of China, “Soft X-ray inteference lithography based on new coherence optics”; The joint funding key projects for large scientific facility, “study on nanobubbles by synchrotron radiation”; The projects of the National Science Foundation for Young Scientists of China, “Theoretical research on the ion-beam fabrication and property of porous graphene membranes”, “Application of X-ray speckle and photon correlation spectroscopy on the dynamics research of PNRs”, “Developmentof electrochemical method for nanobubbles based on synchrotron radiation”; “ The study of detection technology for online non-invasive beam position monitoring of soft X-ray beamline and its application in nano-CT and STXM”; National natural funding major project-sub-project, “study on advanced experimental tech-niques for water science”; Subproject of the National Basic Research Program of China (973 Program),“Origin research for the multi-dimensional microstructure and ultrahigh piezoelectricity of relaxor ferroelectrics”; Project of Natural Science Foundation of Shanghai, “The damage and recovery mechanism of carbon nanotubes material in the radiation field of nuclear batteries”.

In 2015, there are the following tasks of Soft X-ray group: operation and maintenance of STXM and XIL endstation; design of medium energy spectroscopy beamline; construction of Bending magnetic soft X-ray beamline (02B) in Si.ME^2 project; development of methodology in STXM and XIL endstation, for better user support.

Reference

1. Liu H G, Xu Z J, Zhang X Z, *et al*. Applied Optics, 2013, **52**: 2416.
2. Liu H G, Xu Z J, Zhang X Z, *et al*, Acta Physica Sinica, 2013, **62**: 150702.
3. Zhang L J, Zhao B Y, Xue L, *et al*. J. Synchrotron Rad., 2013, **20**: 413.
4. Zhao B Y, Song Y, Wang S, *et al*. Soft Matter, 2013, **9**: 8837.
5. Experimental study of photon correlation spectroscopy for the long-range fluctuation of polarization in ferroelectrics[J] Acta Physica Sinica, 2015, **64**: 147801.
6. Xue C F, Wu Y Q, Zou Y, J. Synchrotron Rad., 2015, **22**: 328.

X 射线衍射组研究进展

X 射线衍射组

X 射线衍射组主要承担“上海光源”首批线站“X 射线衍射光束线站”的运行维护与用户实验支持工作。该线站在 2013–2014 年度高效、低故障率运行，总供光机时 11 001.9 h，总故障率为 1.4%。累计提供用户机时 8 968 h，接待用户实验人员 888 人次，执行用户课题 315 个，用户研究涵盖材料科学、化学、凝聚态物理、高分子科学、环境与地质等众多学科领域，共发表用户成果 122 篇，其中一区及以上 35 篇。线站维护方面，完成了光束线水冷弧矢单色器 Bragg 轴、单色器一晶、CCD 与控制电脑之间的通讯光纤的更换以及衍射仪控制和电缆维护等。

除负责上海光源一期 X 射线衍射线站的日常运行维护及用户实验支持外，本组还负责上海光源线站工程两条新建线站“白光劳厄衍射线站”和“表面衍射线站”、“工程材料分支线站”以及材料样品辅助实验室的设计工作，本年度负责完成了上述相关线站物理设计及项目建议书的撰写。

为满足不同学科领域用户研究的需求，本组在 X 射线衍射方法学研究及相关应用研究方面进行了不断的研究和探索，共发表论文 9 篇[1–9]，其中 SCI 收录 6 篇，获授权专利 4 项。线站工作人员致力于提升实验水平、发展新实验方法以及设计和研制新型原位设备。除了继续发展原有设备和方法（如低温电场薄膜衍射方法、PDF 方法等），初步开展了共振散射方法的研究，并新增了 20 K 低温原位实验平台、Mythen1K/Mythen6K 线形探测器、三轴高分辨衍射系统、无散射狭缝以及其他原位设备及装置。同时，对线站设备进行了调试和发展，如对 Mythen 1 K 探测器进行了校准、标定以及相关控制和数据处理软件的调试等工作。此外，在锂离子电池的构效关系[4]、薄膜表面结构研究、原子对分布函数的应用[5]以及有机太阳能电池[6]等诸多领域都有所进展。

在研项目主要有：（1）中国科学院百人计划项目；（2）国家自然科学基金面上项目“基于同步辐射 X 射线干涉光刻及原子层沉积技术制备可应用于生物医学等领域的高质量纳米容器及其特性的研究“和”新型配体金纳米粒子 X 射线探测器”；（3）国家自然科学基金大科学装置联合项目“利用同步辐射发展原子对分布函数在材料研究中的应用”、“填充方钴矿的结构及其填充原子局域振动行为研究”。

新申请获批项目 5 项：（1）国家自然科学基金大科学装置联合项目（重点）“一些钙钛矿氧化物多层膜界面微结构与物理性能的同步辐射研究”；（2）国家自然科学基金大科学装置联合项目“利用同步辐射二维掠入射 X 射线衍射实时表征共轭聚合物薄膜微结构变化的测试平台的搭建与相关方法学研究”；（3）国家自然科学基金青年基金“关联体系的同步辐射原位研究平台及在电子铁电材料中的应用”、“掺杂 $BiFeO_3$ 锂离子电池电极材料的同步辐射原位构效关系研究”；（4）中国科学院知识创新工程新锐计划项目“同步辐射黄昆漫散射平台的建立及其在 p 型透明导电 SnO_2 薄膜内部缺陷研究中的应用”。

本年度本组除了衍射线站的运行维护和用户实验支持、新建相关线站和实验室的设计以及上述科研项目外，将继续发展相关实验方法及各种原位设备，以满足相关领域用户的需求，包括发展单晶衍射系统、焊接原位装置以及配套的探测器等的软硬件调试和在线测试。另外，在 2015 年寒假停机期间，将对光束线进行升级改造、拓展光束线应用领域。还将在石墨烯负载二维材料、高分辨粉末衍射、有机半导体薄膜、多铁材料构效关系以及锂/钠电池电极材料等方面继续进行深入研究。

参考文献

1. Song B, Sun Q, Gao X Y, *et al.* Angew Chem Int Ed, 2014, **53**(25): 6358.
2. Cao L, Wang Y Z, Gao X Y, *et al.* J Phys Chem C, 2013, **117**(48): 25636.
3. Geng D P, Yang Y G, Gao X Y, *et al.* Chin Phys C, 2014, **38**(11): 118202.
4. Liu M, Lin C, Wen W, *et al.* J Phys Chem C, 2014, **118**(27): 14711-14722.
5. Wang L, Wang L J, Lin H, *et al.* J Solid State Chem, 2014, **212**: 128-133.
6. Yang Y G, Zheng G H J, Gao X Y, *et al.* Nucl Sci Tech, 2014, **37**: 020201.
7. Liu Y, Zhou P, Nucl Electr Detec Technol, 2014, **34**(3): 96-39.
8. Lu Y L, Liu Y, Wang L W, *et al.* Philos Mag, 2013, **93**(15): 1827-1842.
9. Su R, Li L, Nie Z H, *et al.* Appl Phys Lett, 2014, **105**(22): 221907(1-5).

Research development of X-ray diffraction group

X-ray Diffraction Group

X-ray diffraction (XRD) group is mainly in charge of operation and user support at X-ray diffraction beamline. In 2013−2014, this beamline provided 11 001.9 h beam time with a fault rate of 1.4%. There are 8 968 h allocated for 888 users from 315 proposals, whose research fields covered material science, chemistry, condensed matter physics, macromolecule science, environmental and geological sciences. 122 papers including 35 premium ones were published by users during this period. The completed beamline maintenance work included: the replacement of the Bragg axis for the water-cooled sagittal focusing monochromator, the replacement of the first crystal for the monochromator, the replacement of the communication cable between the CCD and the control computer, as well as the maintenance for the diffractometer control system.

Besides the routine beamline maintenance and user technical support, XRD group took charge of designing two new beamlines (white beam Laue diffraction and surface diffraction), the engineering material end station, and the sample preparation laboratory for material science in the second phase beamline project. In 2013−2014, the corresponding physical designs and reports were finished.

In order to meet users demands from different research disciplines, XRD group was dedicated to X ray diffraction methodology developments and their applications with 9 publications[1−9] (including 6 SCI-cited) and 4 authorized patents. The group members were committed to improve the experimental skills, develop new experimental methods, design and develop new type of in-situ instrumentations. In addition, to further develop the existed instrumentation and methods (such as low temperature diffraction method of thin films under electrical field and PDF method), XRD group worked on resonance scattering method, the new 20 K in-situ low temperature sample environment device, the integration of the Mythen1K/Mythen6K linear detector, three axis high resolution diffraction system, as well as the integration of non-scattering slit, other instrumentations, and other in-situ devices. The current equipments have been further debugged and developed. For example, Mythen 1K detector was calibrated and its control/calibration/data processing software were accomplished. Moreover, research progresses were made in the fields of structure-reactivity relationship of lithium ion battery[4], surface structure of thin films, application of atomic pair distribution function[5] and organic solar cells[6].

The on-going projects were as following: (1) Hundred-Talent Program (Chinese Academy of Sciences); (2) National Science Foundation of China: “The study on the preparation of high quality nanometer containers and their characteristics in biomedical and other fields based on synchrotron radiation X-ray interference lithography and atomic layer deposition techniques” and “Novel Coordinating Ligands Au Nano-particle X-ray Detector; 3) Joint Funds of the National Science Foundation of China: “The development and application of synchrotron radiation PDF in the study of materials” and “The study of the structure of the filled cobalt ore and its filling atomic area vibration behavior”.

The group also has 5 new grants approved. (1) The State Key program of the National Science Foundation of China: Study of the microstructure and the physical properties of some perovskite oxide multilayer membrane interfaces using synchrotron radiation; 2) Joint Funds of the National Science Foundation of China: Construction of test platform for the real-time characterization of the microstructural changes of conjugated polymer films using synchrotron radiation two dimensional grazing incidence X-ray diffraction; (3) National Science Foundation for Young Scientists of China: “Synchrotron radiation in situ structure-activity relationship studies of doping $BiFeO_3$ lithium ion battery electrode materials”, “The synchrotron radiation in situ research platform of the associated system and its application in electronic ferroelectric materials; (4) The Knowledge Innovation Program of Chinese Academy of Sciences.

In next two years, besides the beamline operation, user experimental support, the construction of new beamline and materials sample preparation laboratory for material science, as well as the above research projects, the group will continue to develop new experimental methods and in-situ equipment to satisfy different user’s demands, which includes single crystal diffraction system and in-situ welding equipment with its detector, debugging and online test software. In 2015 spring, the group will upgrade and reform the X-ray diffraction beamline. About the in-house research, XRD group will focus on high resolution powder diffraction, organic semiconducting films, structure-reactivity relationship of multi-ferroic materials, two dimensional graphene supporting materials, and Lithium/sodium battery electrode materials.

Reference

1. Song B, Sun Q, Gao X Y, *et al.* Angew Chem Int Ed, 2014, **53**(25): 6358.
2. Cao L, Wang Y Z, Gao X Y, *et al.* J Phys Chem C, 2013, **117**(48): 25636.
3. Geng D P, Yang Y G, Gao X Y, *et al.* Chin Phys C, 2014, **38**(11): 118202.
4. Liu M, Lin C, Wen W, *et al.* J Phys Chem C, 2014, **118**(27): 14711-14722.
5. Wang L, Wang L J, Lin H, *et al.* J Solid State Chem, 2014, **212**: 128-133.
6. Yang Y G, Zheng G H J, Gao X Y, *et al.* Nucl Sci Tech, 2014, **37**: 020201.
7. Liu Y, Zhou P, Nucl Electr Detec Technol, 2014, **34**(3): 96-39.
8. Lu Y L, Liu Y, Wang L W, *et al.* Philos Mag, 2013, **93**(15): 1827-1842.
9. Su R, Li L, Nie Z H, *et al.* Appl Phys Lett, 2014, **105**(22): 221907(1-5)

硬 X 射线谱学组研究进展

硬 X 射线谱学组

硬 X 射线谱学组主要承担上海光源首批线站“X 射线吸收精细结构光束线站(BL14W1)”的运行维护与用户实验支持工作。该线站在 2013–2014 年度高效运行，共为用户提供机时约 8 504 h，束线研究机时约 2 160 h。共完成了 346 个研究课题，用户发表文章 230 篇，其中 SCI-I 区文章 73 篇，占文章总数的 31.7%。用户研究涵盖化学、材料、物理学、环境地质等众多学科领域。

2013–2014 年度，BL14W1 线站在原有基础上，积极开展新实验技术和方法的研究，丰富了 XAFS 实验条件，拓展了研究范围。本组成员在 XAFS 方法发展及应用方面进行不断的研究和探索，共发表 SCI 论文 10 篇。

BL14W1 线站于 2013 年安装调试了 K-B 镜系统，通过 K-B 镜对实验站样品点的光斑进行重新聚焦，将样品处光斑成功聚焦到了 50 μm 以下，可实现 30 GPa 以上的压力条件，配合精密的五维样品台，实现了高压 EXAFS 方法。已经有毛河光、蒋建中等一批国内用户利用该方法开展了高压 XAFS 研究，并取得了较好的实验结果。继而，线站于 2014 年进一步发展了毛细管透镜聚焦的实验方法，该系统相比于 K-B 镜有两个突出优点：1) 由于毛细管接收角度大，光通量传输效率高，一般能达到 20%以上；2) 由于聚焦光的发散角很大，可以有效消除衍射峰带来的影响，有利于高压 EXAFS 获得较好的实验数据。

BL14W1 线站发展了高分辨发射谱方法，通过对水平 Rowland 圆谱仪的调试，实现了高能量分辨、高信噪比的良好谱仪性能[1–2]。硬 X 射线发射谱是常规 XAFS 方法研究电子结构的有力补充，在电子自旋、分子轨道、配体分辨等方面的研究有独特优势，是国际上前沿的同步辐射研究方法，发展该项实验技术，填补了国内在该领域的研究空白，可望大大提高国内用户的研究能力。

BL14W1 线站和束线控制组、加速器物理组紧密合作，解决了储存环电子束团实现了混合填充模式和储存环的时间结构和样品发光时间的精确标定两个关键难题，从而在国内同步辐射装置上首次实现了这种纳秒时间分辨的 XEOL 实验方法[3–4]。这种方法为深入理解发光材料的发光行为提供重要的研究手段，特别是对研究具有复杂结构的发光材料的发光机理，具有非常强大有效的作用。

为了进一步提高 XAFS 实验数据质量，BL14W1 线站采取了一系列措施：1) 发展了自动配气系统，确保电离室的气体配比满足 XAFS 实验最佳信噪比的要求；2) 发展了 VF 数据采集系统，大大提高了电离室计数的稳定性；3) 调试了高通量电离室，解决了高光通量下计数的线性问题；4) 对固体探测器设计合适的 Soller 狭缝，有效避免了散射信号的干扰。通过以上工作，使 XAFS 实验数据的质量有了较大提升。此外，由于稳定性的提升，采集速度也有了较大提高，整体实验效率提高了 10%~15%。

组内在研项目 28 项，共承担科研经费¥1 700 万元+$20 万元。

参考文献

1. Gao Xing, Gu Songqi, Gao Qian, *et al*. A high-resolution X-ray fluorescence spectrometer and its application at SSRF[J]. X-Ray Spectrom, 2013, **42**: 502–507.
2. GAO Xing, SHENG GuoDong, HUANG YuYing. Mechanism and microstructure of Eu(III) interaction with γ-MnOOH by a combination of batch and high resolution EXAFS investigation[J]. Science China Chemistry, 2013, **56**(11): 1658-1666.
3. ZHANG Zhaohong, JIANG Zheng, XUE Song, *et al*. Time structure measurement of the SSRF storage ring using TRXEOL method[J]. Nuclear Science And Techniques, 2015, **26**: 040202.
4. 张招红, 姜政, 薛松, 等. 上海光源 XAFS 线站时间分辨 X 射线激发发光谱实验系统[J]. 光谱学与光谱分析, 2015, **35**(8): 2324-2328.

Research development of XAFS group

XAFS Group

XAFS group is mainly in charge of operation and user support of X-ray Absorption Fine Structure Spectroscopy beamline (BL14W1). During 2013–2014, this beamline has supported beam time of 8 504 h for users and 2 160 h for in-house research. Users from all over the country have finished 346 proposals, whose research fields covering chemistry, material science, physics, environmental science and son on. 230 papers have been published by users during this 2 years, 73 in which were published on SCI-I journals.

A series of work has been carried out at BL14W1 to provide the optimal experimental conditions for users.

High-pressure is one of the important research fields in synchrotron radiation. At the beginning of the SSRF construction, there is no effective EXAFS technique for the investigations on local structures of sample at high pressures. The typical spot size of 300 μm×300 μm at BL14W1 limited further increase on pressure. Recently, Kirkpatrick-Baez optics based focusing technique has been used at BL14W1 to reduce the spot size at sample to less than 50 μm×50 μm. Now, pressure above 30 GPa can be reached for the related EXAFS study. Several groups have carried out their high-pressure experiments at BL14W1 with fairly good results.

X-ray emission spectroscopy (XES) utilizes high-index surface of crystals to achieve high energy resolution. It is an effective and powerful tool to provide valuable information with respect to the electronic structure as well as the ligand's environments for 3d transition metals. BL14W1 is a multi-pole wiggler beamline with the photon flux at sample position up to 10^{13} photons per second. Such high flux is good for XES. At BL14W1 beamline, the XES instrument based on horizontal Rowland geometry has been set up. The diameter of Rowland cycle can be adjusted between 1 m and 182 mm for high resolution and high counts, respectively. For manganese compounds, good performance with high quality and high resolution was achieved.

Cooperating with other groups, time-resolved X-ray excited optical luminescence (TRXEOL) method is implemented to measure time structure of the storage ring, and the measurements performed on BL14W1. This method provides an important research tool for in-depth understanding of the luminescent behavior of luminescent materials, especially for studying the luminescent mechanism of light-emitting materials with complex structure, it plays a very strong and effective role.

A series of work has been carried out at BL14W1 to provide the optimal experimental conditions for users. The detailed steps are: developing the automatic gas distribution system; developing a new ion chamber system, which is effective for the high-flux conditions; designing a set of Soller slits for the solid state detector to reduce the background. After the 2 year efforts, the data quality has been significantly improved, and various auxiliary methods and equipments have been developed to meet the users' requirements.

Our group are responsible for 28 ongoing projects, and take on funds of 17 million yuan +200 thousand dollars.

Reference

1. Gao Xing,GuSongqi, Gao Qian, *et al*. A high-resolution X-ray fluorescence spectrometer and its application at SSRF. X-Ray Spectrom. 2013, **42**: 502–507.
2. GAO Xing, SHENG GuoDong, HUANG YuYing. Mechanism and microstructure of Eu(III) interaction with γ-MnOOH by a combination of batch and high resolution EXAFS investigation. SCIENCE CHINA Chemistry.2013,**56**(11): 1658-1666.
3. ZHANG Zhaohong, JIANG Zheng, XUE Song, *et al*. Time structure measurement of the SSRF storage ring using TRXEOL method. NUCLEAR SCIENCE AND TECHNIQUES.2015,**26**: 040202.
4. ZHANG Zhaohong, JIANG Zheng, XUE Song, *et al*. TimeResolved XEOL Experiment System on BL 14W1 at SSRF. Spectroscopy and Spectral Analysis. 2015, **35**(8): 2324-2328.

X 射线小角散射组研究进展

生命科学部　散射组

1　BL16B1 线站开放运行及用户工作

2013−2014 年，BL16B1 线站共为用户提供机时约 9 182 h，束线研究机时约 1 965 h。共完成 303 个研究课题，用户发表文章 113 篇，其中 SCI-I 区文章 32 篇，占文章总数的 28%。

2　实验技术和方法学发展

2013−2014 年，BL16B1 线站将垂直聚焦镜更换为超环面镜，有效提高了光束线的光通量，完成光束线改造的验收工作；开展了新实验技术和方法学研究，发展了反常小角散射(ASAXS)技术，进行了溶液样品蠕动装置的原位测试。在实验站改造方面，完成小角相机偏心改造，实现 SAXS-WAXS 散射矢量连续测量的方法学研究；完成了原位变温冷热 GISAXS 平台的搭建(−100℃~500 ℃)，并且已经对用户开放。完成实验站控制软件的更新改进，升级改造后的控制系统操控更加便于各系统间的通信，更加便于操控。

2.1　反常小角散射(ASAXS)技术

在 BL16B1 线站发展了反常小角散射(ASAXS)方法学研究。利用 ASAXS 技术对 Al 合金样品进行测试（图 1），研究结果表明，Al 合金中有着 Zn 元素的析出，结果也得到 TEM 测试结果的支持。

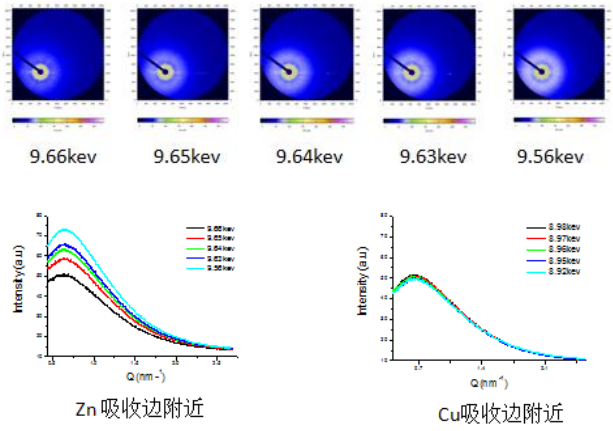

图 1　Al 合金的 ASAXS 测试结果

2.2　SAXS-WAXS 散射矢量连续测量

通过开展小角相机偏心改造（图 2），实现了 SAXS 区域和 WAXS 区域的无缝连接。改造后偏心小角相机 SAXS 区域探测 q 值范围为 0.06~3.50 nm^{-1}，SAXS-WAXS 联用可实现 0.06~34.8 nm^{-1} 的连续散射矢量测量（图 3）。

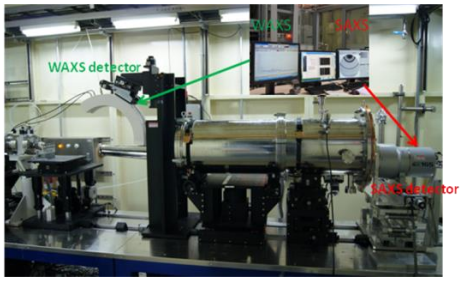

图 2　偏心改造后的 SAXS-WAXS 相机系统

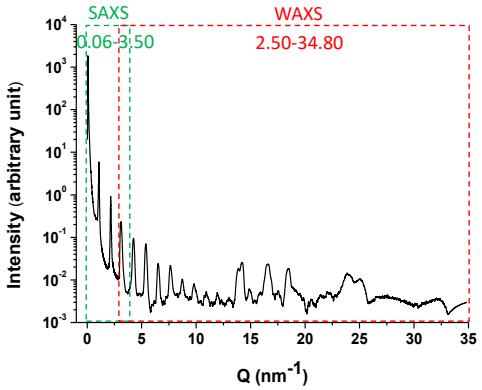

图 3　1D SAXS-WAXS 连续散射矢量测量数据

2.3　原位变温冷热 GISAXS 实验平台

完成原位变温冷热 GISAXS 实验平台的搭建(−100~500 ℃)，已经对用户开放（图 4）。

图 4 原位变温冷热 GISAXS 实验装置

3 科研工作

2013−2014 年度散射组成员积极利用束研机时在高分子材料、高性能纤维制备及结构表征等领域开展了相关的 In-house 研究[1−4]，取得了一系列丰硕的研究成果，共发表 SCI 文章 16 篇。

参考文献

1. In Situ Small Angle X-ray Scattering Study on Structural Evolution of Crosslinked Polytetrafluoro--ethylene During Deformation[J]. Appl Polym Sci, 2014, (131): 39883.
2. A general model for estimating the ordering of mesoporous film by grazing incidence small angle X-ray scattering[J]. Appl Phys, 2014, (115): 204311.
3. Three-dimensional and time-ordered surface-enhanced raman scattering hotspot matrix, J. Am. Chem. Soc. 2014, (136): 5332−5341
4. First-principles study of solute–vacancy binding in Cu, Journal of Alloys and Compounds, 2014, **608**: 334-337.

Progresses in research of X-ray scattering group

Department of Life Sciences X-ray scattering Group

1 Operation status and user results of BL16B1 beamline

In the two years of 2013 and 2014, BL16B1 provided about 9 182 h user beamtime, and about 1 965 h for beamline study. At the beamline, 303 user subjects have been finished in 2013 and 2014; the users have published 113 papers (SCI indexed) based on the research results of the beamline, in which 32 papers published on top 5% journals.

2 Beamline upgrading and Developing in Experimental techniques and methodologies

In 2013 and 2014，BL16B1 beamline performed the focusing mirror upgrading. The vertical focusing mirror was replaced into Toroidal mirror. The upgrading effectively enhances the beamline flux. In developing experimental techniques and methodologies, Anomalous SAXS technique and in-situ solution peristaltic device are developed. At the endstation upgrading, the SAXS camera system performed eccentricity setting, and developed the q continuous measurement technique by combining SAXS and WAXS; at the endstation, in-situ GISAXS device (temperature: −100℃~500 ℃) was developed and has opened to users; the endstation also has upgraded the control system in the two years.

2.1 ASAXS technique

At BL16B1, Anomalous SAXS (ASAXS) technique was developed. Based on ASAXS, Al alloy samples was measured (Fig.1). The results showed there was Zn element precipitation in Al alloy, which was coincident with TEM results.

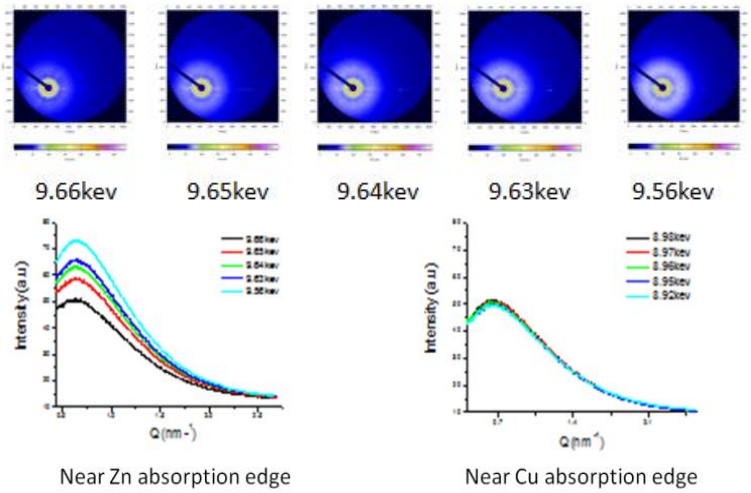

Fig.1 ASAXS measurements of Al alloy

2.2 Scattering vector continuous measurement by combining SAXS and WAXS

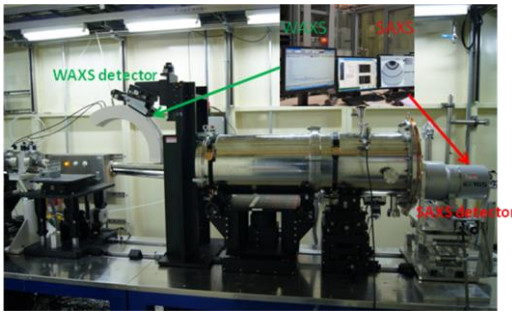

Fig.2 Eccentricity setting SAXS camera system

By eccentricity setting SAXS camera system (Fig.2), *q* seamless connection was performed. Combined SAXS and WAXS Synchronous measurement, the scattering vector *q* can continuously cover 0.06~34.8 nm^{-1} (Fig.3).

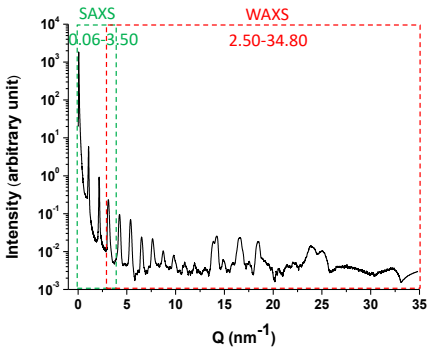

Fig.3 1D q continuous measurement data by combining SAXS and WAXS

2.3 in-situ GISAXS device

At SAXS endstation, in-situ GISAXS device (temperature: −100~500℃) was developed and has opened to users(Fig.4).

Fig.3 In-situ GISAXS device

3 Research activities

In the two years of 2013 and 2014, In-house study has been developed at BL16B1 in the field of high-perfomance fibers and polymers[1−4]. The X-ray scattering group has published 16 papers (SCI indexed) in the two years.

Reference

1. In Situ Small Angle X-ray Scattering Study on Structural Evolution of Crosslinked Polytetrafluoro- -ethylene During Deformation[J]. Appl Polym Sci, 2014, (131): 39883.
2. A general model for estimating the ordering of mesoporous film by grazing incidence small angle X-ray scattering[J]. Appl Phys, 2014, (115): 204311.
3. Three-dimensional and time-ordered surface-enhanced raman scattering hotspot matrix, J. Am. Chem. Soc. 2014, (136): 5332−5341
4. First-principles study of solute–vacancy binding in Cu, Journal of Alloys and Compounds, 2014, **608**: 334-337.

蛋白设施 canted 光束线建设

束线工程部机械组

国家蛋白设施（上海）中心基于上海光源(SSRF)建设了两条共直线节的插入件 undulator 光束线，简称 canted 光束线——复合物晶体结构光束线(BL19U1)和生物小角散射光束线(BL19U2)。canted 光束线最大的挑战就在于两条光束线距离很近，空间布局非常紧张。为了使两条光束线能分开足够的距离，在单色器下游加入了一台水平双偏转镜。BL19U1 光束线基本光学设置：液氮冷却双晶单色器位于距光源点 22.5 m 处，水平偏转镜位于 25.75 m 处，超环面镜位于 33.1 m 处，样品点位于 40.8 m 处。BL19U2 光束线基本光学设置：液氮冷却双晶单色器位于距光源点 23.6 m，水平偏转镜位于 28.2 m，水平聚焦镜位于 31.2 m，垂直聚焦镜位于 34 m，样品点位于 56 m。

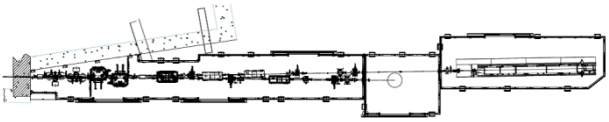

图 1 蛋白设施 canted 光束线总图

BL19U1 和 BL19U2 的单色器布局如图 2 所示，在 BL19U2、BL19U1 的第一晶体处的间距分别为 134 mm 和 143 mm。两台单色器均使用 Si(111)晶体无色散排列，能量范围 5~18 keV，其光学性能和各技术参数一致。单色器的调节机构参数如表 1 所示。

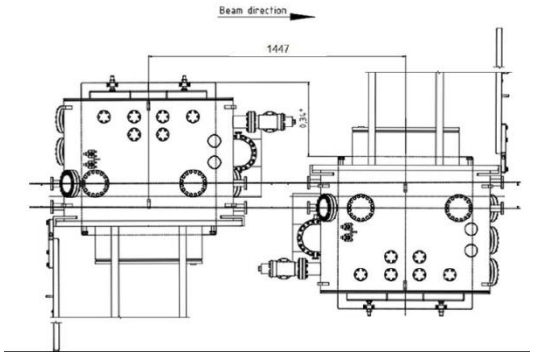

图 2 蛋白设施 canted 光束线单色器布局图

双线共用的偏转镜系统要求在超高真空环境中工作。偏转镜系统主要由平面镜、镜子底座、镜体调节机构、镜箱支撑调节机构、真空系统、控制系统等组成。镜体运动调节机构包括投角及 X 方向运动，但是要求滚角安装精度要好于 0.1°。偏转镜镜体调节机构如图 3，调节机构主要参数如表 2 所示。

表 1 单色器调节机构主要参数

运动	范围	精度	分辨率
Bragg 角	-5°~40°	0.36”（全步）	<1”
带编码器		0.05”	<0.2”
Roll 1st	±1°	<0.5”	<1”
T2	10-30 mm	<0.5 μm	<1 μm
Pitch 2nd	±1°	<1”	<2”
Piezo	100”	<0.05”	<0.2”

图 3 偏转镜镜体

表 2 偏转镜调节机构参数要求

运动	参数	生物小角散射	复合物
投角	调节范围	±0.5°	±0.5°
	步长	0.2″	0.2″
	重复性	≤±1″	≤±1″
滚角	安装精度	≤± 0.1°	
X 方向	调节范围	±5 mm	±5 mm
	步长	5 μm	2 μm
	重复性	≤±10 μm	≤±10 μm

复合物晶体结构光束线(BL19U1)和生物小角散射光束线(BL19U2)目前已完成调光及指标优化，即将面向用户开放。上海光源二期规划中将建设多条 canted 光束线，蛋白设施 canted 双光束线的建成为二期 canted 光束线的设计、布局、调试等方面积累了丰富的实践经验。

Construction of canted beamlines for protein science at SSRF

Mechanical group Department of beamline engineering

Two beamlines for protein science have been constructed at Shanghai Synchrotron Radiation Facility (SSRF) which are funded by National Facility for Protein Science. They are named canted beamlines, which are complex crystallography beamline (BL19U1) and biology X-ray small angel scattering beamline (BL19U2), because they are originating from the same undulator source. The greatest challenge for designing the canted beamlines is setting up optical components at very limited space between two beamlines. To separate sufficient space between two beamlines, two reflecting mirrors which are mounted in one chamber are set up downstream of double crystal monochromator (DCM) respectively. The layout for BL19U1 beamline is, DCM, horizontal reflecting mirror, toroidal mirror and sample point are located 22.5 m, 22.75 m, 33.1 m and 40.8 m from the center of the 2nd undulator source respectively. The layout for BL19U2 beamline is, DCM, horizontal reflecting mirror, horizontal focusing mirror, vertical focusing mirror and sample point are located 23.6 m, 28.2 m, 31.2 m, 34 m and 56m from the center of the 1st undulator source respectively. This is illustrated in Fig.1.

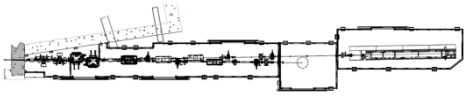

Fig.1 Layout of the canted beamlines

The layout of two DCMs for canted beamlines are illustrated in Fig.2. The distance between two beams is 134 mm at the center of the first crystal of the DCM (left) and 143 mm for the DCM (right) respectively. A pair of Si(111) are adapted for both DCMs which energy range are the same, from 5 keV to 18 keV. Specifications of DCM adjustments are shown in Table 1.

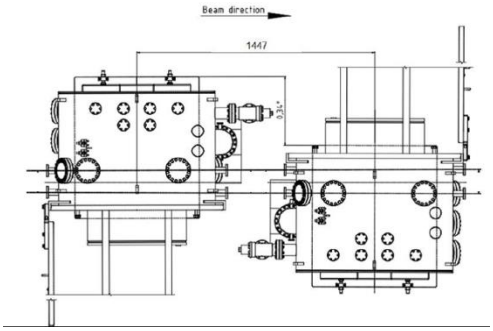

Fig.2 Layout of the two DCMs for canted beamlines

The deflection Mirror system shared of two beam-lines works in the ultra high vacuum. Deflection Mirror system consists of plane mirror, mirror set, adjustment mechanism of mirror, support system, vacuum system, control system, etc. Adjustment Mechanism of Mirror contains the motion of pitch and X direction, and the installment accuracy of roll is less than 0.1 °.

Table 1 Adjustment specifications for DCMs

Adjustment	Range	Accuracy	Resolution
Bragg With encoder	−5 °~40 °	0.36”(per full step)	<1”
		0.05”	<0.2”
Roll 1st	±1 °	<0.5”	<1”
T2	10~30 mm	<0.5 μm	<1 μm
Pitch 2nd	±1 °	<1”	<2”
Piezo	100”	<0.05”	<0.2”

The deflection mirror adjustment mechanism as shown in Fig.3. Parameters of deflection mirror adjustment are specified in Table 2.

Fig.3 Adjustment Mechanism of Mirrors

Table 2 Parameters of deflection mirror adjustment

Motion	Parameter	BioSAXS	Complex Crystallography
Pitch	Range	±0.5 °	±0.5 °
	Step	0.2″	0.2″
	Repeatability	⩽±1″	⩽±1″
Roll	Installation Accuracy	⩽± 0.1 °	
Horizontal (X)	Range	±5 mm	±5 mm
	Step	5 μm	2 μm
	Repeatability	⩽±10 μm	⩽±10 μm

Complex crystallography beamline (BL19U1) and BioSAXS (BL19U2) has been completed beam tuning and parameter optimization, and it will be opened to users. Multiple canted beamlines will be built in the two phase of SSRF. We have accumulated a wealth experience from the achievement of the canted beamlines for protein science which will contribute to the design and commissioning for canted beamlines during SSRF II.

X 射线成像组研究进展

X 射线成像组

X 射线成像组主要承担“上海光源”首批线站“X 射线成像及生物医学应用光束线站”的运行维护与用户实验支持工作。该线站在 2013–2014 年度高效低故障率运行，总供光机时 11150.3 h，总故障率为 0.5%。累计提供用户机时 9143.6 h，执行用户课题 332 个，用户研究涵盖生物医学、材料科学、地质考古学等众多学科领域，共发表用户成果 106 篇，其中 SCI 一区文章 6 篇，SCI 二区及以上文章 34 篇。在线站维护方面，完成了安全光闸和单色光狭缝处的波纹管更换、滤波器维护、更换了单色器 Si(111) 的二晶、更换了光束线末端铍窗、更换了 Kohzu 样品台等。在线站性能的提升方面，升级了成像探测器、开发了基于电离室反馈提升单色器稳定性的软件等。

除负责上海光源一期 X 射线成像及生物医学应用线站的日常运行维护及用户实验支持外，本组还负责上海光源线站工程 2 条新建线站“快速 X 光成像线站”和“纳米三维成像线站”，2013–2014 年度本组负责并完成了上述相关线站可行性研究报告的撰写。

为满足不同学科领域用户研究的需求，本组在 X 射线成像方法学研究及相关应用研究方面进行了不断的研究和探索，共发表论文 24 篇，获授权专利一项，在线站方法发展[1-2]、X 射线荧光 CT[3.4]、局部 CT[5,6]、纳米成像[7]、光栅成像[8]、图像处理[9]、纳米聚焦元件设计[10] 、X 射线成像探测器[11]等方法学研究方面取得了一系列的成果。应用研究方面，开展了中药材显微特征结构研究、木竹材无损检测研究、胶体颗粒研究[12-15]等。

X 射线成像组 13-14 年在研项目有：国家重点基础研究发展计划(973 课题)“同步辐射 X 射线医学影像新型成像方法及关键技术研究”、中国科学院对外合作重点项目“依托上海光源的 X 射线医学成像新方法及其应用国际合作计划”、国家自然科学基金 “中药材特征结构的 X 射线相衬显微 CT 研究”和“硅酸钙/玉米蛋白多孔活性支架及其在体骨修复评价中的研究”； 新增资助项目：CAS-CSIRO 合作研究项目“基于同步辐射显微 CT 的肿瘤血管三维结构定量分析”（项目批准号：GJHZ1303）、国家自然科学基金面上项目“基于“飞行”扫描与 OSEM 加速 X 射线荧光 CT 成像”（项目批准号：11275257）和“毫秒级动态定量显微 CT 研究” （项目批准号：11375257）、联合基金重点项目“小动物缺血性脑卒中模型的原位活体动态研究” （项目批准号：U1232205）、国家林业公益性行业专项“基于 X 射线成像的木竹材无损检测技术研究”（项目批准号：201304513）。

2015 年度本组除了进行成像线站的运行维护和用户实验支持、新建相关线站的设计以及执行上述科研项目外，还将成像与多种实验方法组合，发展小角散射 CT、衍射 CT、荧光 CT 等方法，以及开展中药材显微鉴别、木材无损检测等应用研究。

参考文献

1. Xie Honglan, *et al*. X-ray biomedical imaging beamline at SSRF[J]. Journal of Instrumentation, 2013，**8**: C08003
2. Chen R, *et al*. X-ray imaging for non-destructive microstructure analysis at SSRF[J]. Advanced Materials, 2014, **26**(46): 7688-7691.
3. Qun Yang, *et al*. X-ray fluorescence computed tomography with absorption correction for biomedical samples[J]. X-Ray Spectrometry. 2014, **43**: 278-285.
4. Deng Biao, *et al*. The progress of X-ray fluorescence computed tomography at SSRF[J]. Nuclear Instruments and Methods in Physics Research Section B，2013, **305**: 5-8.
5. Chen Wen Hao, *et al*. A synchrotron-based local computed tomography combined with data-constrained modelling approach for quantitative analysis of anthracite coal microstructure[J]. Journal of Synchrotron Radiation. 2014, S1600: 5775-14002793.
6. Chen Wenhao, *et al*. Pseudo-global tomography for local micro-CT with high brightness synchrotron X-rays[J]. Chinese Optics Letters, 2014, **12**(2): 023401.
7. Biao Deng, *et al*. Full field X-ray nano-imaging at SSRF，Proc. SPIE 2013, 88511D.
8. 戚俊成, 等. 第三代同步辐射光源 X 射线相干性测量研究[J]. 物理学报, 2014, **63** (10): 104202.
9. 梁传晖, 等. 同步辐射 X 射线图像对比度增强算法研究[J]. 光学学报, 2015, 35.
10. Chen Zhi, *et al*. Towards one nanometer X-ray focusing: a complex refractive lens design，Chinese Optics Letters, 2014, **12**(12).
11. 张永兴, 等. 基于透镜耦合的 X 射线成像探测器闪烁体厚度对成像质量的影响研究，核技术，2014，**7**: 7-12.
12. Peng Guanyun, *et al*. Detection of complex vascular system in bamboo node by X-ray μCT imaging technique[J]. Holzforschung. 2013, 0018-3830.
13. 彭冠云, 等. 基于同步辐射 X 射线相衬显微 CT 技术的竹木复合材料胶合界面特征研究[J]. 光谱学与光谱分析, 2013, **33**(3): 829-833.
14. Fu YN, *et al*. Three-dimensional structure of polystyrene colloidal crystal by synchrotron radiation X-ray phase-contrast computed tomography[J]. Applied Physics A, 2014, **115**(3): 781-790.
15. 叶琳琳, 等. 种子类中药材的三维显微结构的原位研究[J]. 中国中药杂志, 2014, **39**(14): 2619-2623.

Research development of X-ray imaging group

X-ray Imaging Group

X-ray imaging group is mainly in charge of operation and user support of X-ray imaging and biomedical applications beamline. During 2013–2014, this beamline has supported beam time of 11150.3h with a low fault rate of 0.5%. There are 9143.6 hours provided for 332 user proposals covering biomedicine, material science, archeology paleontology and so on. And 106 user papers have been published. The beamline maintenance includes: replacement of bellows between mono-beam slit and the safety shutter, maintenance of the filters, replacement of 2nd crystal of the monochromator, replacement of the beryllium window and the sample stage. The detector was upgraded and the stability of the exit beam from the monochromator was enhanced based on beam intensity feedback system.

In addition, the feasibility report of two new beamlines have been completed which are “Fast X-ray imaging beamline” and “Nano 3D imaging beamline”.

In order to meet the demands of users for different samples, many X-ray imaging methodologies have also been developed and explored. 24 papers have been published including beamline method development[1-2], X-ray fluorescence micro-CT[3,4], local CT[5,6], nano imaging[7], grating imaging[8], image processing[9], optics design for nanofocus[10] and detector development[11]. Some application researches have also been carried out, including microscopic identification of Chinese herbal medicine, nondestructive testing of bamboo structure, polystyrene colloidal crystal [12-15].

The ongoing projects include the National Basic Research Program of China (973 Program) “The Novel X-ray Medical Imaging Methodology and Key technology based Synchrotron Radiation”, The key international Cooperation Program of Chinese Academy of Sciences “The International Cooperation Program on the Novel X-ray Medical Imaging Methodology and its Applications at Shanghai Synchrotron Radiation Facility”; The projects supported by the National Natural Science Foundation of China including “3D X-ray fluorescence CT based SR”, “The X-ray phase contrast microscope CT research on structure of traditional Chinese medicine” and “Study of porous scaffolds made by Calcium silicate/corn protein in bone repair”.

In 2013-2014, some new projects have been approved including the CAS-CSIRO cooperative research project “Automated Quantitative Analysis of 3D Angiogenesis for Early Diagnosis of Tumors using Synchrotron Radiation X-Ray Microtomography” (No. GJHZ1303), the National Natural Science Foundation of China “Accelerating X-ray fluorescence CT based fast scanning and OSEM” (No. 11275257)，"Study on millisecond dynamic quantitative microscopic CT " (No. 11375257)，Joint fund key projects" In vivo and in vivo dynamic study of ischemic stroke in small animals" (No. U1232205), National forestry public welfare industry special project" Nondestructive testing technology of wood and bamboo based on X ray imaging"(No. 201304513).

In 2015, besides the beamline operation and user experiments support, design of new beamlines and perform the above research projects, the group will focus on the combination of imaging and multiple experimental methods including SAXS CT, diffraction CT, fluorescence CT and further study on related applications.

Reference

1. Xie Honglan, *et al*. X-ray biomedical imaging beamline at SSRF[J]. Journal of Instrumentation, 2013，**8**: C08003
2. Chen R, *et al*. X-ray imaging for non-destructive microstructure analysis at SSRF[J]. Advanced Materials, 2014, **26**(46): 7688-7691.
3. Qun Yang, *et al*. X-ray fluorescence computed tomography with absorption correction for biomedical samples[J]. X-Ray Spectrometry. 2014, **43**: 278-285.
4. Deng Biao, *et al*. The progress of X-ray fluorescence computed tomography at SSRF[J]. Nuclear Instruments and Methods in Physics Research Section B，2013, **305**: 5-8.
5. Chen Wen Hao, *et al*. A synchrotron-based local computed tomography combined with data-constrained modelling approach for quantitative analysis of anthracite coal microstructure[J]. Journal of Synchrotron Radiation. 2014, S1600: 5775-14002793.
6. Chen Wenhao, *et al*. Pseudo-global tomography for local micro-CT with high brightness synchrotron X-rays[J]. Chinese Optics Letters, 2014, **12**(2): 023401.
7. Biao Deng, *et al*. Full field X-ray nano-imaging at SSRF，Proc. SPIE 2013, 88511D.Qi J C, et al，Acta Physica Sinica, 2014, 63 (10): 104202.
8. Qi J C, *et al*, Acta Physica Sinica, 2014, **63** (10): 104202.
9. Liang C H, *et al*. Acta Optica Sinica, 2015, 35.
10. Chen Zhi, *et al*. Towards one nanometer X-ray focusing: a complex refractive lens design，Chinese Optics Letters, 2014, **12**(12).
11. Zhang R X, *et al*.Nuclear technique, 2014, **7**: 7-12.
12. Peng Guanyun, *et al*. Holzforschung. 2013, 0018-3830.
13. Peng G Y, *et al*. Spectroscopy and Spectral Analysis, 2013, **33**(3),829-833.
14. Fu Y N, *et al*.Applied Physics A-Materials Science & Processing,2014,115(3)781-790,2014
15. Ye L L, *et al*. China Journal of Chinese materia medica, 2014, **39**(14): 2619-2623

X 射线自由电子激光装置（SXFEL）进入工程全面实施阶段

自由电子激光部

国家重大科技基础设施 X 射线自由电子激光装置（SXFEL）进入全面工程实施阶段。X 射线自由电子激光试验装置由光阴极注入器、主加速器、两级高增益谐波放大波荡器系统，以及加速器隧道、速调管长廊、中央控制室和公用工程配套设施等组成。装置总长 300 m，是我国目前最大的激光器。SXFEL 的建设将分两步进行：第一步为建设一台试验装置，用于开展外种子型 FEL 的原理研究；第二步为将试验装置进一步升级为一台用户装置。SXFEL 试验装置建在上海光源装置旁边，其目标是基于 840 MeV 的直线加速器产生 8.8 nm 的全相干软 X 射线辐射，并验证级联回声型自由电子激光等先进的运行机制。SXFEL 试验装置于 2014 年 12 月开工，2015 年，全部的地基打桩、7 000 m^2 的基建和混凝土隧道已经完成。2016 年 4 月，SXFEL 试验装置隧道和速调管走廊基建全部完成并立即启动了设备安装工作。2016 年底，SXFEL 试验装置的加速器、波荡器及相关设备已全部安装完成 2016 年底，电子束通过 SXFEL 试验装置加速器及波荡器并产生了第一束辐射光。同时，SXFEL 用户装置的基建已于 2016 年 11 月正式开工。

The Shanghai soft x-ray FEL facility start construction

Free-Electron

The Shanghai Soft x-ray FEL facility enters into the construction phase. The Shanghai soft X-ray Free-Electron Laser facility (SXFEL) is being developed in two steps: the SXFEL test facility (SXFEL-TF) and the SXFEL user facility (SXFEL-UF). The SXFEL-TF is a critical development step towards the construction a soft X-ray FEL user facility in China, and is under commissioning at the Shanghai Synchrotron Radiation Facility (SSRF) campus. The test facility is going to generate 8.8 nm FEL radiation using an 840 MeV electron linac passing through the two-stage cascaded HGHG-HGHG or EEHG-HGHG (high-gain harmonic generation, echo-enabled harmonic generation) scheme. The construction of the SXFEL-TF started at the end of 2014. One year later, 547 pile foundations, a total area of about 7 000 m^2 of civil construction, and a concrete tunnel were completed. Its accelerator tunnel and klystron gallery were ready for equipment installation in April 2016, and the installation of the SXFEL-TF linac and radiator undulators were completed by the end of 2016. In the meantime, the SXFEL-UF, with a designated wavelength in the water window region, began construction in November 2016. This was based on upgrading the linac energy to 1.5 GeV, and the building of a second undulator line and five experimental end-stations.

CW 倍加型高压技术和 X 射线转换技术的应用

应用加速器研究室

高压发生器技术和电子束 X 射线转换技术是辐照加速器研制中的关键技术。2013–2014 年我们继续对工频驱动的 Cockcroft-Walton (CW) 型高压电源技术展开研究并研制了 800 kV/30 mA 加速器，在电子束 X 射线转换技术方面研制了 5 MV/20 mA 电子束 X 射线转换靶，并实现了 Ta-Cu 复合靶片的制造技术及工艺。

1 CW 倍加型高压加速器技术的研究

高压发生器可靠稳定的输出是加速器正常工作的重要保证。我们研究了工频驱动的 Cockcroft-Walton (CW) 型高压电源技术[1]并研制了三台输出分别为 1.2 MV/50mA, 300 kV/60 mA, 800 kV/30 mA 的辐照加速器，其中最新研发的 800 kV/30 mA 加速器具有结构简单，建造成本低和维护容易的优点。

(a) (b)

图 1 800 kV/30 mA 加速器及电源结构[2]. (a) 加速器，(b) 电源内部结构.

1 表 1 50 Hz 驱动的 CW 型高压电源

Performance	Type	Volt. ripple(%)	Stage number	Application field
1.2 MV/50 mA	Symmetrical	<= 10%	3	Flue gas treatment
300 kV/60 mA	Asymmetrical	<= 5%	1	Rubber vulcanization/Surface curing
800 kV/30 mA	Symmetrical	<= 5%	3	Wire and cable processing

2 电子束 X 射线转换技术的研究

由于电子束穿透能力有限，对不能采用电子束辐照处理的产品可以采用电子束 X 射线转换技术，该技术可以用于医用产品的灭菌和食品消毒领域。

采用优化的钽靶设计，X 射线的转换效率理论上对 5 MeV 有 8%–9%。我们设计了 100 kW 转靶，如下图 2 所示，采用 1 mm 钽，1 mm 铜，4 mm 水层和 4 mm 铝的复合型结构。

图 2 转换靶样机

研制的转换靶样机采用了复合型的靶板，克服了焊接和成型的多种工艺并申报了 5 项发明专利技术。靶片的测试表明，其热学能优异。实际的工作状态也表明其散热能力极佳。[3]

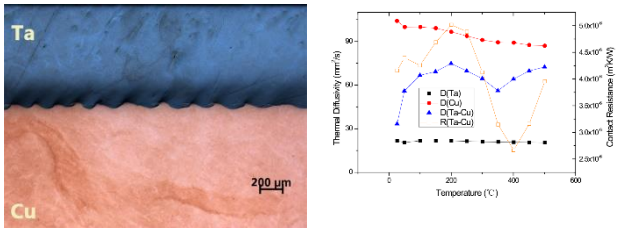

(a) (b)

图 **3** 靶片测试结果

参考文献

1. He Z F, Zhang J L, Liu Y H, *et al*. Characteristics of a symmetrical Cockcroft-Walton power supply of 50 Hz 1.2 MV/50 mA[J]. Review of Scientific Instruments, 2011 **82**(5): 055116-055117.
2. He Z F, Li D M, Liu Y H, *et al*. CW-type HV power supply of 50 Hz and its applications in accelerator power supply[J]. IPAC, 2013, 699-701.
3. He Z F, Li D M, Huang J M, *et al*. The design study of an ultra-high power EB/X-ray conversion facility[J]. Journal of Electron Spectroscopy and Related Phenomena, 2014, **196**: 152-155, 2014.

Application of CW-type HV power supply and EB/X-Ray conversion

Department of Applied Accelerator

High-voltage generator technology and electron beam X-ray (EB/X-ray) conversion technology are the key technologies in the development of accelerator for irradiation processing. In 2013–2014, we continued to study on the Cockcroft-Walton (CW) type of high-voltage power supply and developed the 800 kV/30 mA accelerator, we also made an EB/X-ray convertor for 5 MV/20 mA accelerator and realize the fabrication of the Ta-Cu composite target sheet.

1 Research on CW type of high-voltage accelerator technology

The high-voltage power supply is an integral part of accelerator technology, as its stable and reliable output is an important guarantee for accelerator properly working. We have studied the CW type HV generator driven by 50 Hz[1] and developed three accelerators with output of 1.2 MV/50 mA, 300 kV/60 mA and 800 kV/30 mA. The newly developed 800 kV/30 mA accelerator has the advantages of simple structure, low construction cost and easy maintenance.

(a) (b)

Fig.1 800 kV/30 mA accelerator and its structure[2]. (a) Accelerator. (b) Structure of the power supply.

Table 1 Power supplies of CW type driven by 50 Hz.

Performance	Type	Volt. ripple(%)	Stage number	Application field
1.2 MV/50 mA	Symmetrical	<= 10%	3	Flue gas treatment
300 kV/60 mA	Asymmetrical	<= 5%	1	Rubber vulcanization/Surface curing
800 kV/30 mA	Symmetrical	<= 5%	3	Wire and cable processing

2 Research on EB/X-Ray conversion technology

X-ray conversion is frequent need for irradiating the products that cannot be processed by electron beams, due to their limited penetration capacity in materials, in radiation sterilization of disposable healthcare products and food irradiation.

The X-ray conversion efficiency, i.e. ratio of the total X-ray power to the incident electron-beam power, is 8%–9% at 5 MeV. The 100 kW converter we designed is shown in FIG. 2, with composite structure of Ta (1 mm), Cu (1 mm), water (4 mm) and Al (4 mm).

Fig. 2 Prototype of EB/X-ray converter

The target prototype using a composite sheet. We have overcome the welding and forming processes and declared 5 patents for inventions. The test of the target sheet shows that its thermal properties are excellent[3] and its heat dissipation is very well in the actual working condition.

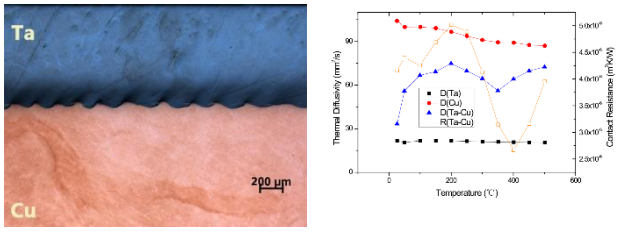

(a) (b)

Fig.3 Test result of the target sheet

Reference

1. He Z F, Zhang J L, Liu Y H, *et al*. Characteristics of a symmetrical Cockcroft-Walton power supply of 50 Hz 1.2 MV/50 mA[J]. Review of Scientific Instruments, 2011 **82**(5): 055116-055117.
2. He Z F, Li D M, Liu Y H, *et al*. CW-type HV power supply of 50 Hz and its applications in accelerator power supply[J]. IPAC, 2013, 699-701.
3. He ZF, Li D M, Huang J M, *et al*. The design study of an ultra-high power EB/X-ray conversion facility[J]. Journal of Electron Spectroscopy and Related Phenomena, 2014, **196**: 152-155, 2014.

TMSR

熔盐堆物理研究

反应堆物理部

背景

本课题基于钍基熔盐堆核能系统战略先导专项关于熔盐堆研发的“实验堆—示范堆—商用堆”总体技术路线，以完成系列熔盐实验堆物理设计为核心目标，在熔盐堆中子物理、热工水力学方面开展物理研究，同时展开 10 MW 固态燃料熔盐实验堆、2 MW 液态燃料熔盐实验堆、大功率球床熔盐堆的设计分析工作。

10 MW(th)固态燃料熔盐实验堆设计方面，先后完成了概念设计、初步物理分析，中子物理和热工水力设计的深度达到初步设计深度。

2 MW(th)液态燃料熔盐实验堆设计方面，先后完成了概念设计和中子物理初步设计。

大功率球床熔盐堆设计方面，先后完成了 100 MW(th)、600 MW(th)流动球床氟盐冷却高温堆初步物理设计。

此外，课题面向熔盐堆热工水力学需求，先后开展了熔盐管内对流换热系数和数据分析评估、球床堆堆芯流场模型研制和测量等基础研究工作。

10 MW(th)固态燃料熔盐实验堆设计

10 MW(th)固态燃料熔盐实验堆(TMSR-SF1)将是 TMSR 专项的首个实验堆，也是世界上首个有明确建造计划的氟盐冷却高温堆。

TMSR-SF1 的总体方案和参数包括：1) 总热功率为 10 MW，初装堆和满装堆预装燃料球 10 800 个和 14 650 个，分三批添加燃料，满功率运行 250 d；2) 使用 TRISO 包覆颗粒燃料球，直径 6 cm；3) 一回路冷却剂为 $2LiF\text{-}BeF_2$ 熔盐，Li-7 丰度约为 99.99%，二回路冷却剂为 FliNaK 熔盐；4) 堆芯包括燃料区及其外围的反射层，燃料区中燃料球为随机排列，堆芯冷却剂出入口温度为 628 ºC/600 ºC；5) 采用控制棒实现温度调节、功率调节、燃耗补偿和停堆等反应性控制功能；6) 堆本体由内向外分布为堆芯活性区、反射层、堆芯围筒、堆芯冷却剂下降环腔与上下腔室、反应堆主容器、氩气层、反应堆保护容器、热屏蔽层和隔热层。反应堆容器内最大压力小于 5 atm。7) 回路系统包括一回路、二回路、气路和熔盐检测设施等；8) 正常余热排出利用回路；失流事故情况下的余热排出由非能动堆外壳散热实现；9) 从堆芯正下方通道依靠熔盐浮力进球，采用逐球装载方式；从堆芯正上方通道卸球；10) 堆容器、堆内结构和回路材料主要为哈氏-N 合金，反射层材料为核石墨，控制棒套管采用 SiC/SiC 复合材料或者 C/C 复合材料；11) 安全设施包括包容体、非能动反应堆容器外壳散热系统等设施。TMSR-SF1 的物理方案如图 1 所示。

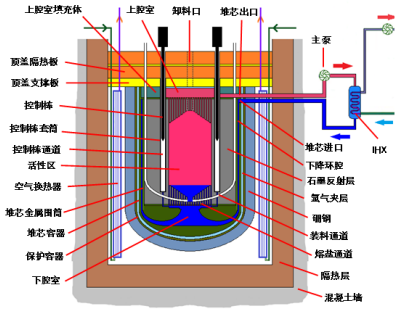

图 1 10 MW(th)固态燃料熔盐实验堆(TMSR-SF1)物理方案

2 MW(th)液态燃料熔盐实验堆设计

2 MW(th)液态燃料熔盐实验堆(TMSR-LF1)是继美国橡树岭国家实验室 MSRE 项目结束 50 年之后，人类重拾液态燃料熔盐堆技术的首堆。

TMSR-LF1 基本参数主要包括：1) ^{235}U 富集度低于 20%；2) 熔盐燃料为 $LiF\text{-}BeF_2\text{-}ThF_4\text{-}UF_4$，摩尔比为 70.2%-26.8%-0.073%-2.927%，其中 Li-7 丰度为 99.95%；3) 限制初始剩余反应性为 2000 pcm；4) 熔盐燃料中需含少量 Th，以验证钍铀转换；5) 反应性控制采用控制棒实现，设计停堆深度 3$。此外，对测量、监测及实验需求，设置了 4 个合金套管的孔道（图 6 右图），分别用于中子源、物理启动、功率监测以及辐照实验。TMSR-LF1 的物理方案如图 2 所示。

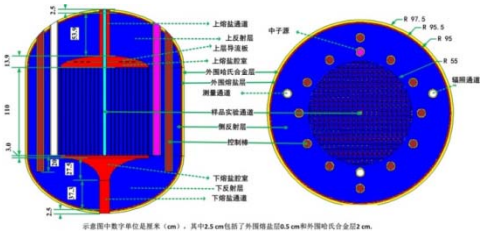

图 2 2 MW(th)液态燃料熔盐实验堆(TMSR-LF1)物理方案

大功率球床熔盐堆设计研究

大功率球床熔盐堆是 TMSR 专项框架内连接实验堆与商用堆的过渡环节，以示范氟盐冷却高温堆的安全性、经济性、可持续发展等先进性能为长远目标。

100 MW 氟盐冷却高温堆的主要目标包括：1) 进行氟盐冷却高温堆的经济性示范，实现高效发电与高温制氢综合应用；2) Th 资源在氟盐冷却高温堆中的利用示范；3) 实现工业规模球床氟盐冷却高温堆技术的集成与应用，进行商业应用推广示范，并为 GW 级 TMSR 研发奠定坚实基础。

100 MW 氟盐冷却高温堆由核岛部分和常规岛部分组成。核岛包括堆本体、冷却剂系统、相关辅助设施等，主要功能是利用核裂变能产生热量并传输到常规岛。常规岛主要包括汽轮机发电机组、高温制氢系统及配套设施，主要功能用于实现核热应用。

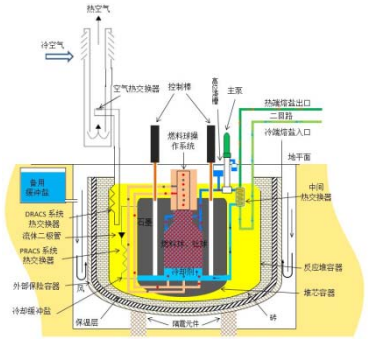

图 3 100 MW 氟盐冷却高温堆堆本体方案

2014 年，开展了 600 MW(th)固态燃料流动球床堆 TMSR-SF2 的概念设计工作。600 MW(th) TMSR-SF2 堆芯采用环形结构，中心石墨柱（即内反射层）中布置了控制棒孔道，其堆芯物理模型如图 4 所示，其中紫红色表示燃料区，黄色为冷却剂，灰黑色为石墨。

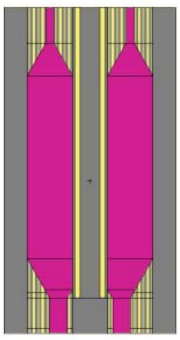

图 4 TMSR-SF2 纵截面示意图

熔盐堆热工水力学基础研究

课题依托硝酸盐回路(HTS)完成了光管内强迫对流换热系数测量，结果介于美国橡树岭国家实验室（ORNL）和北京工业大学测量结果之间，如图 5 所示。在此基础上，课题对熔盐管内对流换热系数进行了评估。

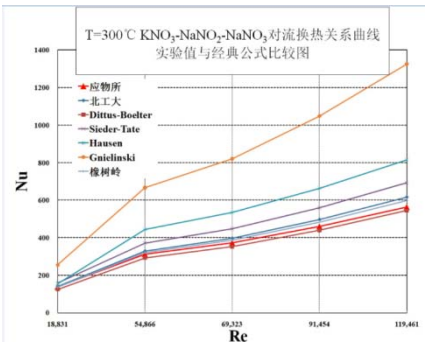

图 5 HTS 回路光管内强迫对流换热系数

课题建立了基于 PIV 的球床成像系统，制作了比例模化模型，以开展堆芯复杂几何区域的流场实验测量，模化模型燃料球间流场的测量结果及数据重构如图 6 所示。

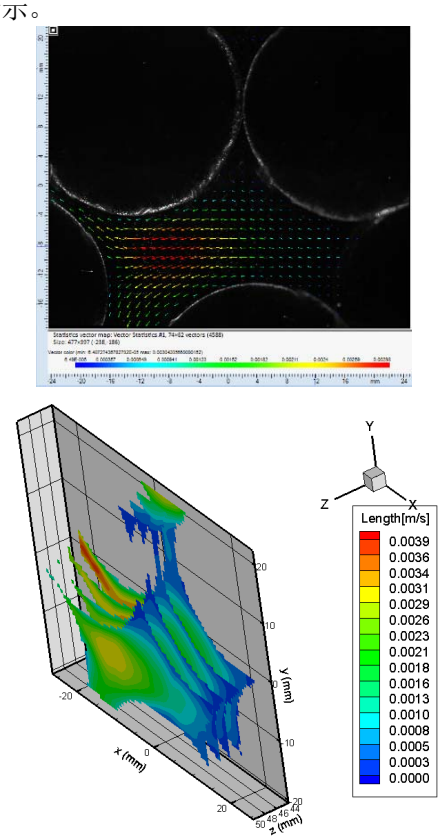

图 6 燃料球间流场测量结果（上）与数据重构（下）

Progress in reactor physics

Reactor Physics Division

Background

This project is based on the general technical route "Technology of Experimental Reactor-Demonstration Reactor -Commercial Reactor", which is planed by the center for Thorium Molten Salt Reactor system (TMSR）for the research and development of Molten Salt Reactor (MSR) nuclear energy system. This project is aimed to complete the physical design of a series of molten salt experimental reactors and research in neutron physics and thermal hydraulics in MSR. Meanwhile, 10 MW solid fuel molten salt experimental reactor (TMSR-SF1), 2 MW liquid fuel molten salt experimental reactor (TMSR-LF1), and high-power molten salt cooled pebble bed reactors are designed and analyzed.

For the design of 10 MW(th) solid fuel molten salt reactor, conceptual design and preliminary physical analysis were completed and the design ofneutron physics and thermal hydraulic reached a preliminary design level.

For the 2 MW(th) liquid fuel molten salt experimental reactor design, the conceptual nuclear design was completed.

For the design of high-power molten salt cooled pebble bed reactors, the concept design of 100 MW(th) pebble bed reactor and 600 MW(th) random arranged pebble bed fluoride salt cooled high temperature reactor were completed.

In addition, in order to meet the requirements of the thermal-hydraulic in molten salt reactors, basic researches such as the convective heat transfer coefficient in molten salt pipes, data analysis and assessment, and flow field measurement of pebble bed reactor cores have been carried out.

Desigh of 10 MW(th) solid fuel fluoride salt experimental reactor

The 10 MW(th) solid fuel experimental reactor (TMSR-SF1) will be the first experimental reactor for the TMSR project and also be the first fluoride-cooled high-temperature reactor in the world with a well-constructed plan.

The overall scheme and parameters of TMSR-SF1 are as fllowes. 1) The rated thermal power is 10 MW. 10 800 fuel pebbles are used respectively in the initial stack and full stack are 14 650 fuel pebbles. The fuel is loaded in three batches, and the equivalent full power operation is 250 days. 2) TRISO coated fuel is used, the diameter of fuel pebbles is 6 cm. 3) Primary coolant is 2LiF-BeF_2, abundance of Li-7 is approximately 99.99%, the secondary coolant is FliNaK. 4) The core include fuel zone and the reflector in its periphery. Fuel pebbles in the fuel zone are randomly arranged. The inlet/outlet temperatures of core coolant are 628 ºC/600 °C. 5) Control rods are used to achieve reactive control functions such as: temperature regulation, power regulation, fuel consumption compensation and shut down. 6) From inner to outer, the reactor consists: core active zone, the reflector layer, the core barrel, the down comer and the upper and lower chambers, the reactor vessel, the argon layer, the reactor container, heat shield and insulation layer. The maximum pressure in the reactor vessel is less than 5 atm. 7) The loop system includes the primary loop, secondary loop, gas loop and molten salt detection facilities and so on. 8) The decay heat is discharged by the passive decay heat removal system when the loop cannot work normally. It is discharged by the loop system under other conditions. 9) The pebbles are loaded in turn by the buoyancy of molten salt and are discharged from the channel directly above the core. 10) The materials of container, inner structure and circuit are mainly Hastelloy-N alloys. The reflector is nuclear-grade graphite, the control rod sleeves are SiC/SiC composites or C/C composites; 11) The safety facilities include containment bodies, passive decay heat removal system and other facilities. The physical scheme of TMSR-LF1 is shown in Fig.1.

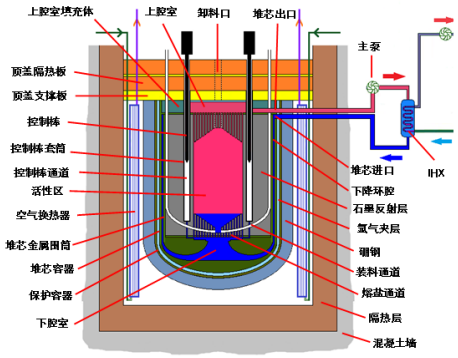

Fig.1 Physical solution of 10 MW(th) solid fuel molten salt experimental reactor (TMSR-SF1)

The design of 2 MW(th) liquid fuel molten salt ex-perimental reactor

The 2 MW(th) liquid fuel molten salt experimental reactor (TMSR-LF1) is the first reactor in 50 years after the end of the MSRE project at the Oak Ridge National Laboratory in the United States.

The basic parameters of TMSR-LF1 mainly include: 1) the ^{235}U enrichment is less than 20 wt%; 2) the molten salt fuel is LiF-BeF_2-ThF_4-UF_4, and the molar ratio is 70.2%-26.8%-0.073%-2.927%, in which the Li-7 abundance is 99.95%; 3) the initial residual reactivity is 2 000 pcm; 4) the molten salt fuel contains a small amount of Th to verify the thorium-uranium conversion; 5) the control of reactivity is achieved by using a control rod, shut-down margin at a depth of 3$. In addition, for the measurement, monitoring, and experimental needs, four Hastelloy sleeve channels (see Fig.2 right) were used for neutron sources, physical startup, power monitoring, and irradiation experiments, respectively. The physical scheme of TMSR-LF1 is shown in Fig.2.

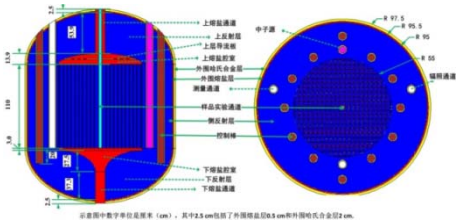

Fig.2 Physical scheme of 2 MW(th) liquid fuel molten salt experimental reactor (TMSR-SF1)

Design of high-power molten salt cooled pebble bed reactor

High-Power Molten Salt Cooled Pebble Bed Reactor, which is aimed to demonstrate the safety, economy, sustainable development of fluoride salt cooled high temperature reactor in the long-term goal, is an important part of the TMSR project to achive the transition from test reactor to commercial reactor. It inculds two kinds of reactor designes according to the reactor core: 100 MW(th) and 600 MW(th) flowing packed pebble bed.

The main goals of the 100 MW flowing pebble bed reacor include: 1) To demonstrate the economical efficiency of fluoride salt cooled high temperature reactor and to realize the integrated application of efficient power and high temperature hydrogen production; 2) To demonstrate the utilization of Th resources in fluoride salt cooled high temperature reactor; 3) To implement the integration and application of the technology of the industrial scaled fluoride salt cooled pebble bed reactorto demonstrate promotion for commercial application, and lay a solid foundation for the research and deveopment of GW level TMSR.

The nuclear power system of the 100 MW flowing packed pebble bed reacorconsists of nuclear island and conventional island. Nuclear island includes reactor proper, coolant system and related ancillary facilities, the main function are to generate heat and transfer it to the conventional island. Conventional is land mainly includs steam turbine generator set, high temperature hydrogen production system and the supporting facilities, the main function is to implement the application of the nuclear thermal.

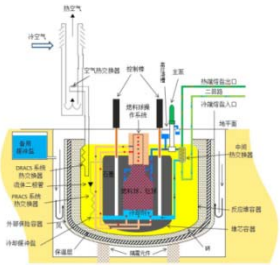

Fig.3 Schematic diagram of the reactor proper of the flowing packed pebble bed reacor

In 2014, TMSR designed a 600 MW(th) flowing pebble-bed flouride cooled high temperature reactor, named TMSR-SF2. Core of TMSR-SF2 adopts the ring structure with control rod channel arranged in the middle graphite reflector (inner reflector). The physical model of the reacorcore is shown in Fig.4. in which the purple refers to fuel, yellow for the coolant and grey for graphite.

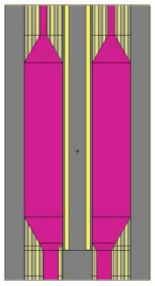

Fig.4 Longitudinal section sketch of the reactor core of TMSR-SF2

Basic research on thermal hydraulics in molten salt reactor

The measurement of the forced convective heat transfer coefficient in the smooth tube was completed based on the nitrate loop (HTS); the result is between the results of the ORNL measurements and Beijing University of Technology, as shown in Fig.5. Meanwhile, the convective heat transfer coefficient in pipe with molten salt was evaluated.

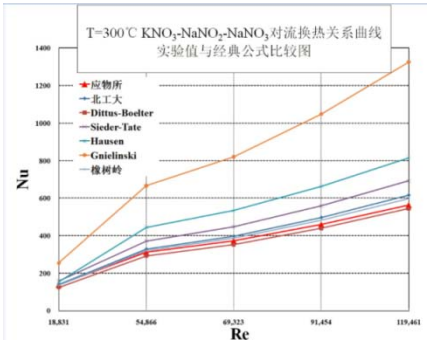

Fig.5 The forced convective heat transfer coefficient in the light tube based on HTS

A flow field measurement system was estabilished based on the Particle Image Velocimetry(PIV). The scaled model was devised according to TMSR-SF1. Experiments were conducted to investigate the flow field in the complex geometry area of the core. The flow field among the fuel pebbles and the reconstruction data are shown in Fig.6.

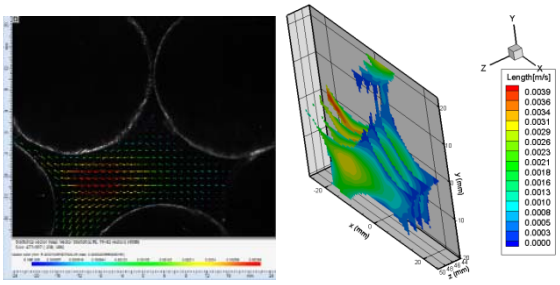

Fig.6 The flow field among the fuel pebbles and the reconstruction data

钍铀循环物理研究

反应堆物理部

背景

本课题基于钍基熔盐堆核能系统先导专项关于钍资源利用的基本战略方向，以优化熔盐堆钍资源利用性能为核心目标，从钍铀核能利用分析、钍铀核数据、加速器驱动中子物理实验装置等几个方面开展了研究。

在钍铀核能利用分析方面，首先对钍铀核燃料循环物理分析软件平台进行了完善，改善了固态熔盐堆燃料管理模式（批次换料）、燃耗计算方法，以及液态熔盐堆的在线添料、换料、后处理等燃料管理模式等。基于上述软件平台，进行了熔盐堆两种主要堆型的性能研究，包括固态燃料熔盐堆(TMSR-SF)不同燃料类型的中子学特性、液态燃料熔盐热堆(TMSR-LF)的温度反应性系数及 Th-U 增殖性能以及液态燃料熔盐快堆(MSFR-LF)的次锕系核素(MA)嬗变性能研究；同时开展了部分其他先进堆型燃料循环研究，如固态燃料气冷快堆 EM2 的 Th-U 核燃料循环、CANDLE 燃烧模式的行波堆启堆方案等，以便熔盐堆借鉴。

在钍铀核数据研究方面，根据钍铀核燃料循环分析需求，完成了 TMSR 专用工作库的规划及研究方案。根据该方案，建立了初版 CENDL-TMSR 工作子库。该工作子库中包含了初步完成的液态熔盐 FLiBe 的热中子散射数据，并以此库为基础初步完成了 TMSR 液态堆的不确定度分析及基于 ACE 和 WIMS 格式数据库的基准检验。此外，基于 ENDF/B-VII.0 评价数据库，完成了 SAND-II642 群数据库的研制。

在加速器驱动中子物理实验装置方面，完成了 15 MeV 电子加速器、中子产生靶装置、中子实验终端的建设、安装、联调和测试。

钍铀核燃料循环物理软件

钍铀核燃料循环物理软件方面，课题完成了基于 MCNP 和 ORIGEN 软件耦合的 MOCBurnup 燃耗分析平台的搭建以及基于 SCALE6 的熔盐堆后处理程序的开发工作。

MOCBurnup 燃耗分析平台在 MATLAB 平台上通过文件交互方式耦合了用于临界计算的 MCNP 程序以及用于燃耗计算的 ORIGEN 程序，可以充分借重 MATLAB 强大的数据处理能力与仿真能力进行相关的钍铀核燃料循环分析，包括 k_{eff}、中子通量分布、功率分布、核反应截面、核素演化、燃耗、放射性活度等参数的计算。

既有的 SCALE6 软件无法处理连续添料和连续后处理，因而无法进行熔盐堆后处理计算。本课题为 SCALE6 设计了一套后处理计算流程，实现了熔盐堆的连续添料、连续后处理和分批后处理功能。在程序计算过程中维持堆内锕系核质量守恒以及反应堆临界。计算流程如图 1 所示，计算参量包括临界值、中子通量密度、中子能谱、增殖比或转换比、核素随时间演化、寿期末锕系核放射性毒性演化等。

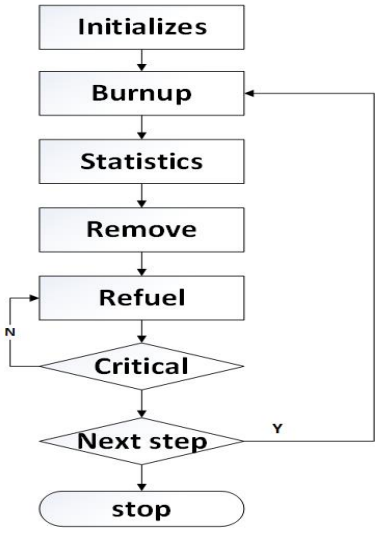

图 1 基于 SCALE6 的熔盐堆核燃料循环模拟流程

钍铀核燃料循环物理分析

基于上述两个主要软件平台，课题针对固态燃料熔盐堆、液态燃料熔盐堆以及部分新概念反应堆开展了钍铀核燃料循环物理分析。

课题以大功率(1 GW(th))氟盐冷却球床高温堆(FHR)为基准模型，分析了三种不同驱动燃料(U-233、U-235 和 Pu-239)情况下，钍基核燃料的能谱、温度反应性系数、燃耗演化和放射性毒性等中子学特性；同时比较分析了上述三种驱动燃料下钍基核燃料的相应中子学特性。图 2 为 6 个核燃料循环模式（采用三种不同驱动燃料的 Th-U 循环及

U-Pu 循环）下的能谱（上）和 k_{eff} 随时间演化（下）；图 3 为停堆后的总放射性毒性演化。

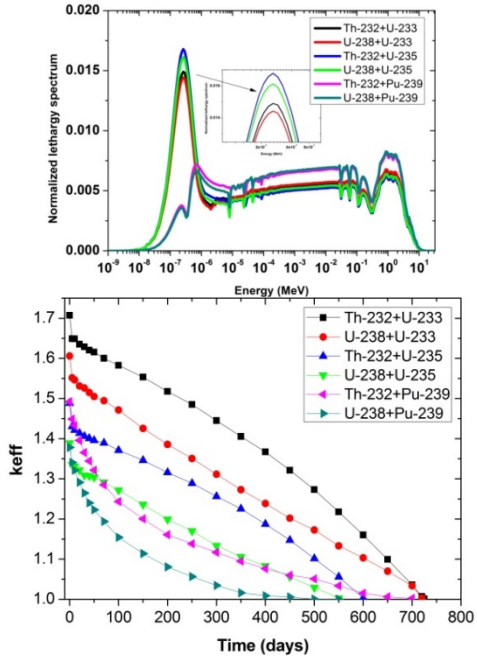

图 2 六个核燃料循环模式下，FHR 的能谱（上）及 k_{eff} 演化（下）

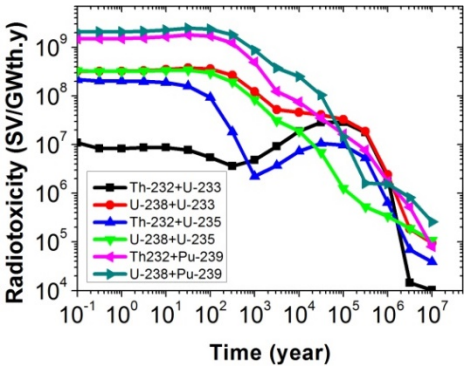

图 3 停堆后的总放射性毒性演化

核燃料增殖性能是液态燃料钍基熔盐热堆最主要的核燃料循环性能，课题以大功率(1 GW(th))液态燃料钍基熔盐堆（TMSR-LF）为基准模型，分析了增殖比、中子能谱、温度反应性系数等中子学特性随熔盐石墨比的变化。图 4 为不同慢化比下熔盐热堆的温度反应性系数（左）及增殖比（右）。

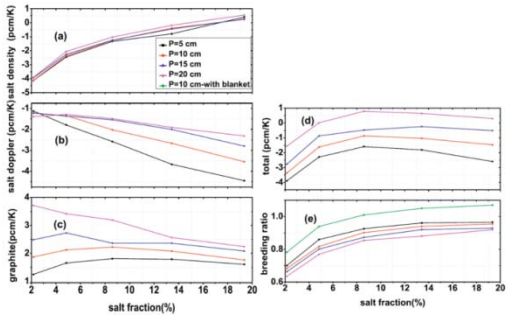

图 4 不同慢化比下熔盐热堆的温度反应性系数（左）及增殖比（右）

超铀核废料的安全处置问题是限制核能发展的一个重要问题。熔盐快堆在嬗变超铀核废料方面具有明显的优势，如高的嬗变效率、大的温度负反馈、在线添料和在线后处理等。因此，课题开展了基于熔盐快堆的次锕系核(MA)嬗变研究。图 5 为不同 MA 初装量条件下的嬗变效率随时间的演化。结果表明，各种 MA 初装量条件下 MSFR 都有足够大的温度负反馈维持堆的稳定运行，其中最大的 MA 装料(18.17%)情况下 50 年的嬗变量为 5 620 kg。

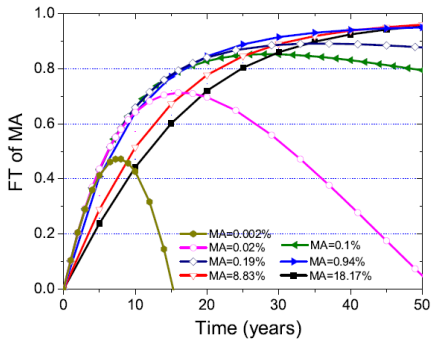

图 5 不同 MA 初装量条件下的嬗变效率随时间演化

课题跟踪国际进展，开展了 EM2 的 Th-U 核燃料循环、行波堆启堆方案等研究工作，以备将来在钍基熔盐堆燃料循环设计方面作参考。

EM2 是一种固态燃料气冷快堆，包含一个燃烧区和一个增殖区。课题分析了 EM2 中的 Th-U 核燃料循环性能，并与 U-Pu 核燃料循环进行了比较，两类核燃料循环下重要核素对 k_{eff} 的贡献如图 6 所示。

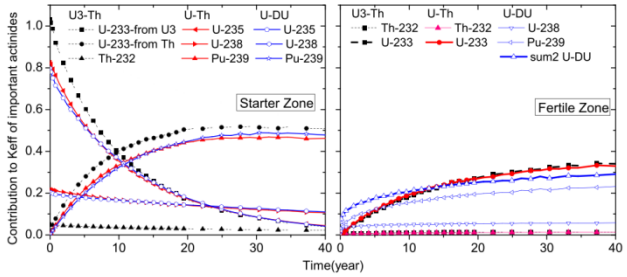

图 6 重要核素对 EM2 临界性能的影响

行波堆可达到非常高的燃耗，可采用一次通过式燃料循环模式，在保证核燃料高利用率及能源远期供给的基础上，保证了防核扩散需求。分析表明，行波堆的点火区结构和燃料成分分布优化可以显著降低堆芯初始的后备反应性，并且大幅降低堆芯寿期初的反应性波动，使行波堆更易于实现平稳运行，如图 7 所示。

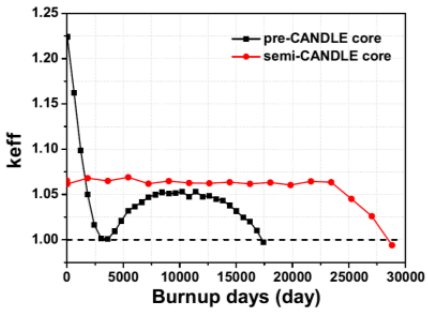

图 7　优化前后行波堆堆芯的 k_{eff} 演化图

钍铀核数据研究

以 U-235 为燃料的反应堆的核数据发展了近几十年，比较完备和精确。相对于 U-Pu 循环来说，Th-U 循环的核数据存在缺少或者误差比较大的问题。为此，课题对钍基熔盐堆专用核数据工作库(CENDL-TMSR)进行了规划，CENDL-TMSR-V1 将包括现有国际五大核数据库中较好的评价数据、新增 TMSR 特需的固液态 FLiBe 热中子散射数据和 TMSR 灵敏度高的 35 种重点核素。

基于 ENDF/B-VII.1 评价库，研制了 SAND-II 642 群数据库，包括 51 个核素、4 个温度点(30 °C、550 °C、600 °C 和 650 °C)和 84 个反应道。为了更快捷的研制数据库，建立了 TMSR-SAND-II 截面加工系统，加工流程如图 8 所示。

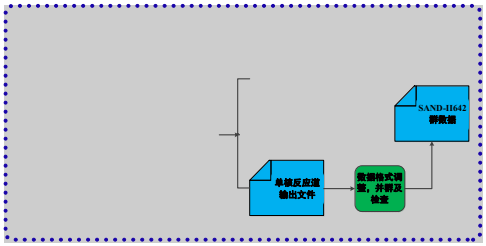

图 8　TMSR-SAND-II 截面加工流程

此外，课题完成了 CENDL- TMSR- WIMS 69 群数据库的宏观检验、CENDL- TMSR- ACE 格式数据库的宏观检验、MCNP 光核数据库加工流程和 ThO_2 中子泄漏谱测量。

加速器驱动中子物理实验装置

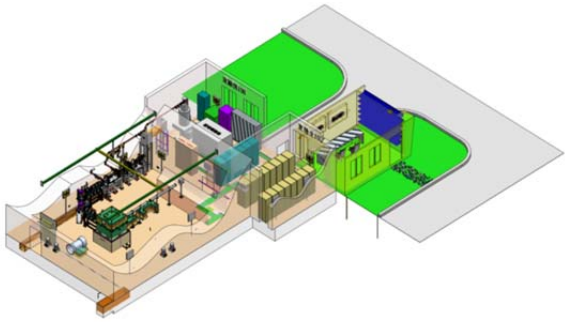

图 9　加速器驱动中子物理实验装置布局

2013 年完成了中子实验厅的改造施工，安装了 15 MeV 电子加速器、中子产生靶装置和中子实验终端设备，完成了中子/伽马监控探测器的测试和刻度；2014 年进行了加速器和中子实验终端的联合调试，完成了束流功率为 10~500 W 及脉冲宽度为 5 ns、50 ns、1.5 μs 等不同条件下的中子产额测量，实现了用 VME 和 Flash ADC (Digitizer)两种方法进行飞行时间法(TOF)中子数据获取系统的测试；同时开展了多单元中子探测器和伽玛阵列探测器的分组测试和组合搭建工作。

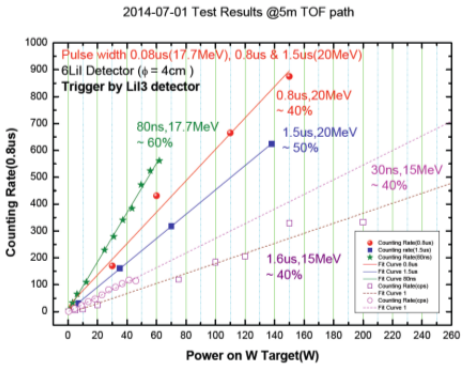

图 10　加速器功率与中子产额的关系曲线

Research on thorium-uranium fuel cycle

Reactor Physics Department

Background

This research is under the framework of the TMSR strategic pioneer science and technology project of CAS, aiming at the optimization of thorium utilization in molten salt reactors (MSRs). Several aspects of thorium-uranium fuel cycle research have been carried out, such as thorium uranium fuel cycle analysis, thorium uranium nuclear data research and accelerator driven neutron physics experiments.

The software platform has been improved especially in the field of solid fuel management (batch feeding), burn-up calculation optimization, on-line feeding, and pyro-processing process of liquid-fuel MSR etc. Based on the platform, two kinds of MSR including the solid-fueled molten salt reactor (TMSR-SF) and liquid-fueled molten salt reactor (TMSR-LF) were analyzed. The neutronic characteristics including neutron spectrum, effective multiplicity factor (k_{eff}), and temperature coefficient of reactivity (TCR), breeding ratio, transmutation behavior and burnup have been studied. Furthermore, the Th-U fuel cycle for some new conceptual reactors like EM2 and CANDLE has also been analyzed.

The special nuclear data library has been established based on the analysis requirements of Th-U fuel cycle. The CENDL-TMSR Library has been developed with the thermal neutron scattering data for FLiBe. Furthermore, the uncertainty analysis and database benchmarking of ACE and WIMS have been completed based on the CENDL-TMSR library. Besides, SAND-II642 has been developed based on ENDF/B-VII.0.

Besides, a 15 MeV electron linac-driven neutron source was constructed for key nuclear data measurements of Thorium Molten Salt Reactor (TMSR) project.

Thorium uranium fuel cycle physical analysis software

The coupling software MOCBurnup based on MCNP and Origen has been completed and the post-processing software based on SCALE6 has been developed.

MOCBurnup is a criticality and burnup calculation software compiled with MATLAB. The powerful data processing ability and simulation ability of MATLAB can be used to analyze thorium uranium fuel cycle, including k_{eff}, neutron flux distribution, power distribution, the nuclear reaction cross section, nuclide evolution, burnup, and radio-toxicities etc.

The existing SCALE6 software cannot handle the simulation for continuous feeding and on-line reprocessing in MSR. Therefore, a processing program has been developed based on SCALE6. This software can maintain minor actinides (MAs) mass conservation and reactor criticality during operation. The flowchart is shown in Fig.1. The calculated parameters include k_{eff}, neutron flux, neutron spectrum, breeding ratio, nuclide evolution and radio-toxicity etc.

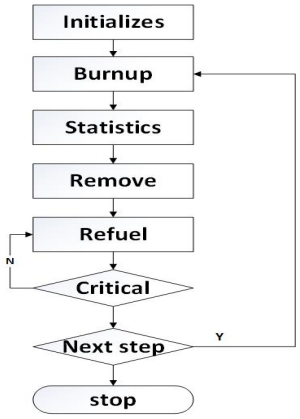

Fig.1 Flowchart of fuel cycle analysis software

Physical analysis of thorium uranium fuel cycle

Based on the above two softwares, the physical analysis of solid-fueled MSR, liquid-fueled MSR and new concept reactor were carried out.

In order to utilize thorium in Fluoride salt-cooled High-temperature Reactor (FHR), neutronics analysis for thorium based fuels (^{233}U+Th, ^{235}U+Th and ^{239}Pu+Th) was carried out in a whole-core model of pebble bed FHR. Uranium (^{238}U) based fuels with the above three fissile nuclides were also analyzed for comparison. Neutron characteristics including neutron spectrum, effective multiplicity factor (k_{eff}), temperature coefficient of reactivity (TCR), conversion ratio (CR) and burnup for the six fuel options were discussed. Results are shown in Fig.2 and Fig.3.

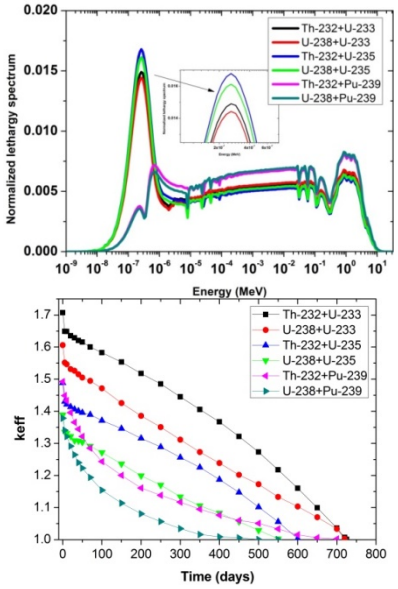

Fig. 2 Neutron spectra (top) and k_{eff} (bottom) of FHR for the studied fuel options

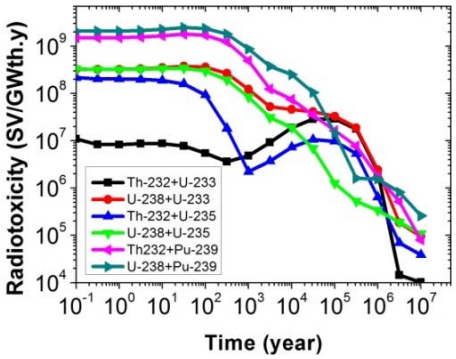

Fig.3 Radio-toxicities of the six fuels after shutdown

Breeding capacity is one of the most important characters of TMSR. The feedback coefficient and the breeding ratio are optimized based on the fuel-to-graphite ratio variation for a thorium based MSR (TMSR). A certain thermal core with negative feedback coefficient and relative high initial breeding ratio is chosen for the reprocessing scheme analysis. Results can are shown in Fig.4.

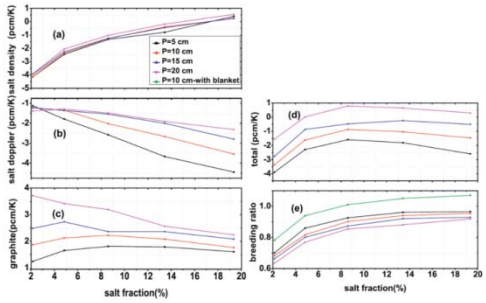

Fig. 4 Temperature feedback coefficient and initial breeding ratio with different moderation ratios.

Effective transmutation of minor actinides (MA) could be achieved in this kind of fast reactor, which is of importance in the future closed nuclear fuel cycle scenario. The reactivity, the fuel temperature coefficient, the effective delayed neutron fraction, the ^{233}U depletion and the MA transmutation capability were analyzed for different MA loadings. The result in Fig.5 shows that for all the operating powers the depletion ratio of MA to HN increases with time and reaches a maximum value. And additional MA should be fed into the fuel salt before the MA depletion ratio reaches the peak value to improve its transmutation capability. The net mass of the transmuted MA during the 50 years operation for 500 MW(th) is 5 620 kg which is very close to that for 1 000 MW(th).

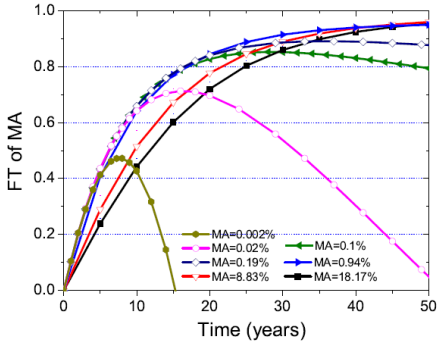

Fig.5 Time evolutions of FT for different MA loadings

The Energy Multiplier Module (EM2) is a compact gas-cooled fast reactor as one of candidates of the Generation-IV nuclear energy systems. Th-U fuel cycle has been analyzed in EM2 and can be used as reference for the design of TMSR.

EM2 core includes the starter zone, the fertile zone, the inner Be_2C and the outer graphite reflectors. The analysis gives an insight into the pros and cons of U-Pu and Th-U fuel cycles in terms of the breeding capability and the discharged radio-toxicity. The contribution to k_{eff} from key important actinides can be seen in Fig.6.

The semi-CANDLE is able to reach high burnup with once-through fuel cycle. This implies that the self-organizing nuclear burning regime, i.e. the equilibrium state of the semi-CANDLE core can be achieved after a time span of transition. In this state the shape of neutron flux, nuclide density and power density keep almost constant but move with a velocity proportionate to operating power. And a very high heavy metal utilization of ~50% can be achieved. It proves that constructing the ignition scheme with refer to an ideal equilibrium CANDLE is an effective way for building the startup of a CANDLE reactor. The results are shown Fig.7.

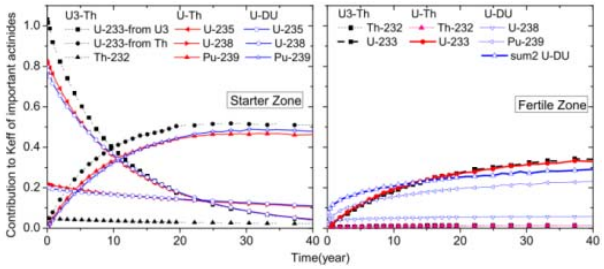

Fig.6 Contribution to k_{eff} from important actinides.

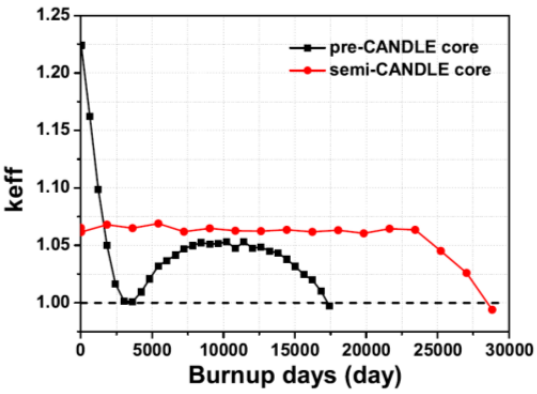

Fig.7 Symbolic k_{eff} versus burnup of the pre-CA (square point line) and the semi-CANDLE (circle point line).

Thorium-uranium nuclear data research

Nuclear data of U-235 has been developed for decades, which are relatively complete and accurate compared to the data of Th-U fuel cycle. In order to solve the problems of lack or error of Th-U nuclear data, a special nuclear data library of TMSR has been developed which is called CENDL-TMSR. CENDL-TMSR includes the preferable evaluated data of the five international databases, and the FLiBe thermal neutron

scattering data for TMSR, and 35 key nuclides with high sensitivity.

SAND-II 642 has been developed based on ENDF/B-VII.1 which includes 51 nuclides, 4 temperature points (30 ℃, 550 ℃, 600 ℃ and 650 ℃) and 84 reaction channels. The cross section processing has been established as shown in Fig.8 for faster manufacture of databases.

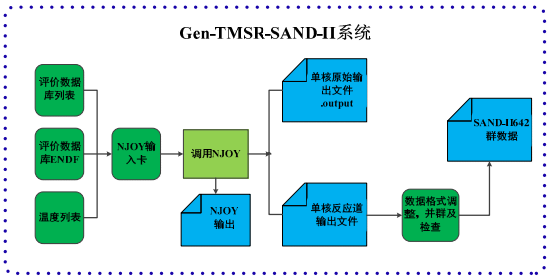

Fig.8 TMSR-SAND-II cross section processing

Besides, the macroscopic examination of CENDL-TMSR-WIMS and CENDL-TMSR-ACE with 69-group has been completed. And the processing of MCNP photon nuclear database and the measurement of ThO_2 leakage spectrum have been carried out.

Photo-neutron Source Driven by 15 MeV Electron Linac

An electron linac-driven neutron source was constructed at the Shanghai Institute of Applied Physics, Chinese Academy of Sciences (SINAP-CAS), as shown in Fig.9. The neutron source was designed for key nuclear data measurements for the TMSR project. The linac delivers an electron beam of 15 MeV, with a beam current of 0.1 mA, and avariable repetition rate from 1 to 266 Hz. The neutron yields under average electron beam powers from 10 W to 500 W, with beam pulse width of 5 ns, 50 ns, and 1.5 μs, were measured, as shown in Fig.10. The ToF spectrometer was constructed with several kinds of neutron detectors combined with Flash ADC digitizer and VME electronics systems.

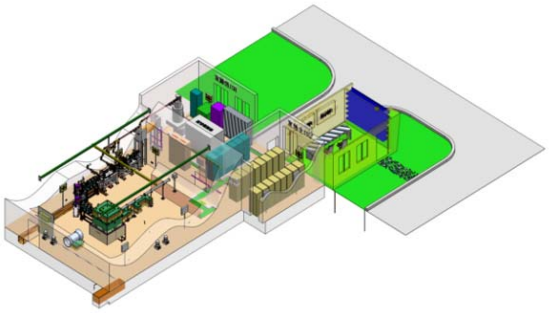

Fig.9 Layout of the Photo-neutron Source

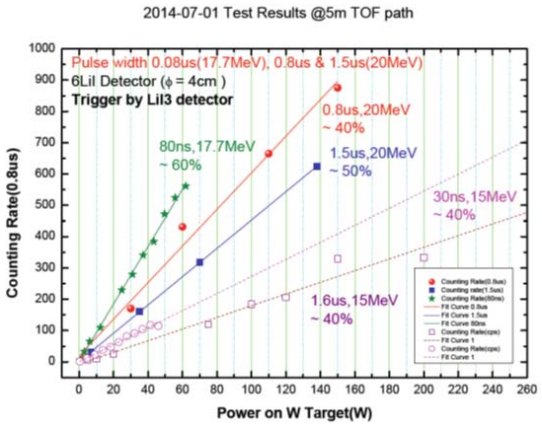

Fig. 10 The neutron yields with the Linac average power and beam pulse width.

反应堆物理部

本课题以熔盐堆关键工程技术研发与设备研制、完成熔盐实验堆工程设计为核心目标，主要包括固态熔盐堆的堆本体结构设计与结构力学评定、控制系统设计与研制、测量系统设计与研制。

固态熔盐堆的堆本体结构设计方面，跟随物理设计方案，完成了从 2 MW 有序堆积无中心石墨柱、10 MW 有序堆积到 10 MW 无序堆积的设计演变，并研制建造了堆芯石墨构件样机。

固态熔盐堆的堆本体结构力学评定方面，完成包括石墨构件、压力容器、控制棒、熔盐泵和管道等的力学分析。

熔盐堆控制系统设计与研制方面，完成了仪控系统的架构设计、控制系统软件结构设计、控制系统核心软件包的功能开发、保护系统及高温步进电机样机的研制。

熔盐堆测量系统设计与研制方面，完成了中子注量率测量方案设计、高温超声波流量计标定平台方案设计、以及 TMSR-SF1 反应性仪样机的研制以及热工参数测量仪表样机的研制。

固态熔盐堆的堆本体结构设计

固态燃料熔盐实验堆(TMSR-SF1)方案历经 2 MW 有序堆积无中心石墨柱、10 MW 有序堆积到 10 MW 无序堆积的设计演变，相应地，堆本体结构设计也跟随物理设计方案进行变更。

完成了 TMSR-SF1 堆本体机械结构、控制棒驱动机构结构、燃料球装卸机构以及堆内跑兔装置等结构的工程设计，完成了石墨堆芯、控制棒驱动机构单项研究、燃料球装卸机构、能谱测量跑兔机构等原理样机的研制和实验工作。目前，TMSR-SF1 的堆本体工程设计方案如图 1 所示，堆本体主要包括以下设备：反应堆堆芯、堆内构件、压力容器、控制棒及其驱动机构、监测样品管道系统、堆芯测量仪表系统等。堆芯主要由堆芯活性区和石墨反射层组件组成；堆内构件主要由石墨结构、堆芯围筒、压紧装置、堆内上部构件以及其它附属的结构组成；压力容器是冷却剂压力边界，主要用来装载反应堆堆芯、堆内构件和高温、高腐蚀反应堆冷却剂，包容放射性物质；控制棒驱动机构采用链轮链条型和直线电机型两种形式，控制棒则均采用单节棒体结构。加入几句话对堆本体工程设计方案的具体描述。图 2 为 TMSR-SF1 石墨堆芯 1/4 样机结构，主要用于测试石墨构件加工制造工艺、测试石墨构件与石墨销键和 T 型键的间隙，以确定合理的间隙值、测试石墨构件吊装工装设计是否合理等。

图 3 是 TMSR-SF1 控制棒驱动机构单项样机，在结构设计上引入了离心摩擦限速阻尼器，使控制棒驱动机构具有较好的速度跟随性，并采用了陶瓷球轴承和干膜润滑等设计。样机研制主要用于验证离心摩擦限速器的功能是否满足要求，并验证样机在常温环境下各设计指标是否满足要求，长期运行的可靠性是否满足要求等。

图 4 是 TMSR-SF1 燃料球装卸机构样机，用于模拟固态熔盐堆的燃料球操作与储存系统，同时考虑堆芯径向分区实验要求，实现燃料球卸载、装载、传输与检测分离等相关功能。

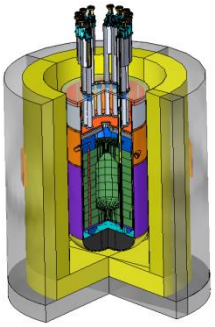

图 1 TMSR-SF1 的堆本体工程设计方案

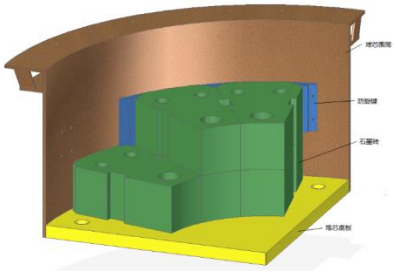

图 2 TMSR-SF1 石墨堆芯 1/4 样机结构

图 3 TMSR-SF1 控制棒驱动机构单项样机

图 4　TMSR-SF1 燃料球装卸机构样机

固态熔盐堆的堆本体结构力学评定

对于目前的 TMSR-SF1 设计版本，已完成包括石墨构件、压力容器、控制棒、熔盐泵和管道等设备或部件的的结构力学评定工作。其中，石墨辐照应力分析中考虑了石墨热导率的辐照效应和石墨辐照蠕变效应，并对不同辐照、不同应变和不同位置的应力进行了比较和优化，堆芯径向反射层砌块在辐照下的应力如图 5 所示；根据 ASME-NH 卷，采用弹性分析法对压力容器进行了应力评定，采用非弹性分析的方法，对压力容器进行了应变评定，压力容器应力分布云图如图 6 所示；将 ASME-NH 标准应用于高温熔盐泵的结构分析与评定，给出了高温熔盐泵的应力分析方法和评定标准，熔盐泵的应力分布云图如图 7 所示。

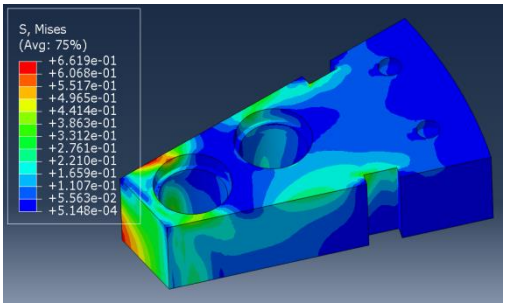

图 5　TMSR-SF1 堆芯径向反射层砌块在辐照下的应力云图

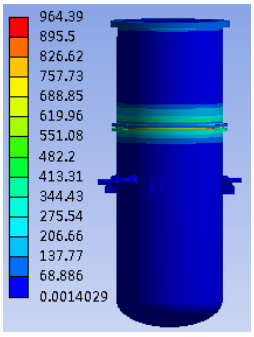

图 6　TMSR-SF1 压力容器应力分布云图

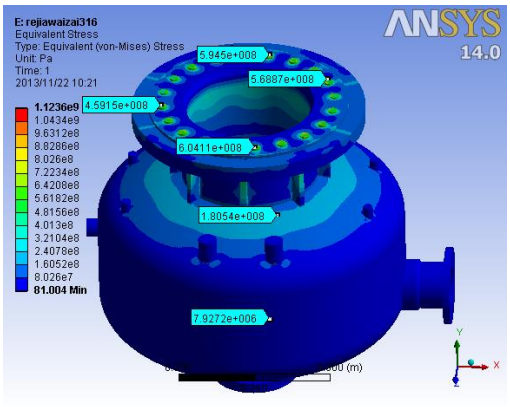

图 7　TMSR-SF1 压力容器应力分布云图

熔盐堆控制系统设计与研制

围绕 TMSR-SF1 概念设计完成了仪控系统的架构设计、控制系统软件结构设计、控制系统核心软件包的功能开发、保护系统及高温步进电机样机的研制。

整个仪控系统采用数字化的分布式控制系统架构并采用标准的监督控制层、网络层、过程控制层以及现场设备层四层设计。控制系统软件由核心软件包、人机界面软件、数据库软件、组态配置软件四部分组成。

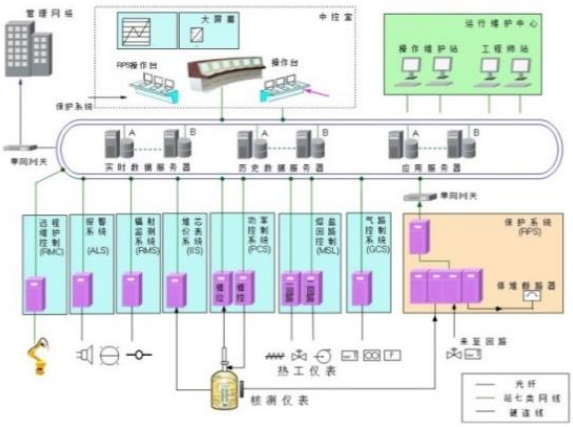

图 8　TMSR-SF1 仪控系统整体架构

控制系统软件开发主要内容是 EPICS 核心软件开发，包括基于 RT-Linux 的嵌入式 IOC 的设备驱动程序开发、控制系统人机界面软件开发、基于 Oracle 数据库的应用开发等。

保护系统原理样机主要解决基于 FPGA 的保护系统关键技术问题，验证方案可行性，重点在于实现原理功能，并结合样机开展关键技术研究。目前已完成样机研制和大部分关键技术研究，样机逻辑功能测试符合设计要求，保护系统原理样机如图 9 所示。

图 9　TMSR-SF1 保护系统原理样机

熔盐堆测量系统设计与研制

完成了中子注量率测量方案设计及相应的反应性仪电子学样机研制。

堆外中子测量系统初步方案如图 10 所示，由三个独立的序列组成，每个序列包含一个源量程、一个中间量程、一个功率量程探测器，三个量程相互重叠，实现反应堆从启堆到满功率运行的核功率测量。探测器信号被电子学仪表处理后，送入保护系统中，作为反应堆重要的保护变量，同时也作为反应堆功率控制的信号来源。

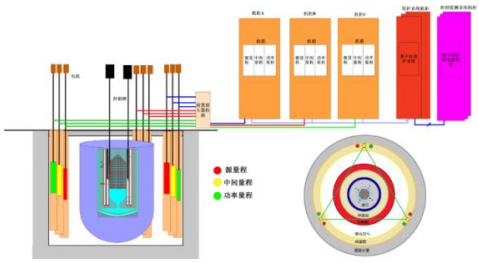

图 10　TMSR-SF1 堆外中子测量系统初步方案

完成了 TMSR-SF1 熔盐回路热工仪表的改进研制及标定平台的方案，标定平台将集成改进型的压力计、加热式热电偶液位传感器、电极液位开关等先进技术，系统构成如图 11 所示。

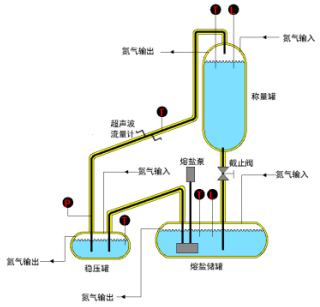

图 11　TMSR-SF1 流量标定系统

完成了反应性测量仪原理样机方案的设计和评审，采用便携式系统设计，由中子探测器、探测器电子学系统、信号采集模块、笔记本电脑组成，反应堆中子注量率信号通过探测器采集，电子学系统处理后，送入笔记本电脑中分析计算。通过逆动态法和周期法，实时计算给出反应性值。完成反应性测量系统的软件开发和系统测试，并在原子能院低微堆临界装置上对样机的功能和算法进行验证，实际测量结果如图 12 所示，在反应堆升功率过程中，反应性为定值，测量结果也反应了这个过程，所测量的反应性波动很小；另一方面随着控制棒的移动，会引入反应性，这一过程也被正确测量出来。表明系统能够正确处理脉冲及电流信号，并得到反应性。

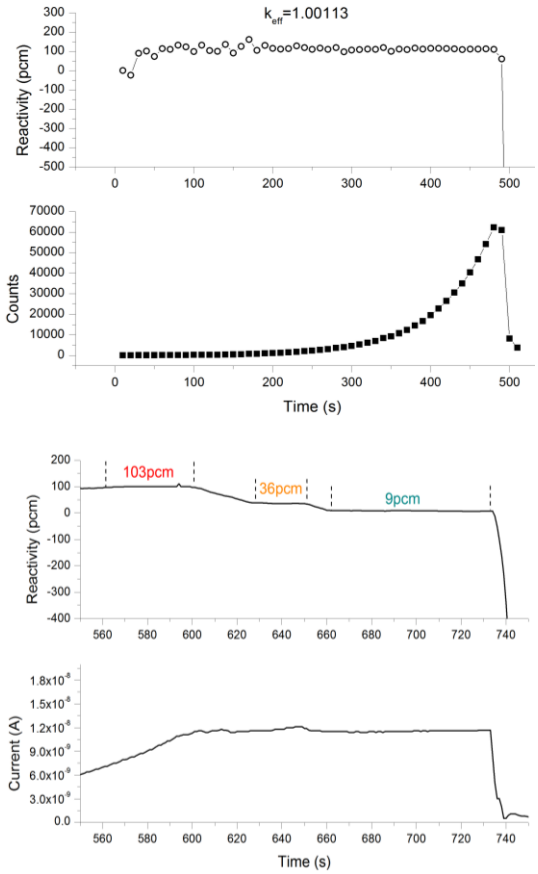

图 12　TMSR-SF1 反应性测量仪原理样机实验测量结果，上图为升功率过程，下图为控制棒跟随过程。

The research of reactor engineering technology

Reactor Physics Department

This project focused on the research and development of molten salt reactor's key engineering technology and equipment, as well as the engineering design of molten salt experimental reactor. The progress of this subject mainly included solid reactor design, structural mechanics evaluation, instrumentation and control system design and development.

Following the reactor physics design plan, The design evolvement from orderly accumulation of 2 MW to 10 MW, 10 MW orderly stacking to 10 MW random stacking was completed, and a core graphite component prototype was developed.

The structural mechanics group completed the mechanical analysis of graphite components, pressure vessels, control rods, molten salt pumps and pipes.

For the design and development of the molten salt reactor control system, the architecture design of the I&C system, the software structural design of the control system, the functional development of the core software package, the protection system, and the development of the high temperature stepper motor prototype were completed.

In the design and development of the molten salt reactor instrumentation system, the neutron flux measurement program design, high-temperature ultrasonic flowmeter calibration platform design, and the development of the TMSR-SF1 reactive instrument prototype, and the development of the thermo-parameter measurement instrument prototype were completed.

Reactor body structure design of solid molten salt re-actor

The TMSR-SF1 has undergone a design evolution of 2 MW ordered stacked with non-centered graphite col-umns, 10 MW ordered stacking to 10 MW disordered stacking. The design of the reactor body structure has also been changed following the physical design.

We had completed the engineering design of SF1 reactor body structure, control rod drive mechanism structure, fuel ball loading and unloading mechanism, and the rabbit running device inside the reactor. We had also completed the graphite core design, single structure reach of control rod drive mechanism, fuel ball loading and unloading mechanism, spectral measurement, such as running rabbit mechanism, what belong to prototype development and experimental work.

At present, the TMSR-SF1 reactor body engineering design scheme is shown in Fig.1. The reactor body mainly includes the following equipment: reactor core, reactor internals, pressure vessel, control rod and its drive mechanism, monitoring sample pipeline system, and core measurement instrumentation system, etc.

The core is mainly composed of an active core region and a graphite reflective layer assembly; the internal components are mainly composed of graphite structure, core surrounding cylinder, pressing device, upper inner member of the reactor, and other subsidiary structures;

The pressure vessel is the coolant pressure boundary and it is mainly used to load the reactor core, the internals and the coolant, which is high temperature and high corrosion. And it is also used to contain radioactive sub-stances;

The control rod drive mechanism has two types: the sprocket-chain control rod drive mechanism and the line- ar-motor control rod drive mechanism. The control rods adopt the single rod structure.

The 1/4 graphite core prototype of SF1 structure, shown in Fig.2, is mainly used to test the manufacturing process of graphite components, and used to test the gap between graphite components, graphite pin and T-key gap. Those results can used to determine a reason-able clearance value, and also make sure the designs of graphite components lifting tools are reasonable.

The single structure reach of control rod drive mechanism is shown in Fig.3. A centrifugal friction and speed limiting damper was introduced in the structural design to enable the control rod drive mechanism to have better speed following. It also use the design of ceramic ball bearings and dry film lubrication, etc.

The prototype is mainly used to make sure whether the function of the centrifugal friction and speed limiting damper can meets the requirements of design, and whether the design specifications of the prototype can meet the requirements in the normal temperature environment, and whether the long-term operation reliability can meets the requirements.

Fuel ball loading and unloading mechanism of SF1 is shown in Fig.4. It can used to simulate the fuel ball operation and storage system of solid-state molten salt reactors. It also considers the radial core partitioning experimental requirements to achieve fuel ball unloading, loading, transmission and detection and separation.

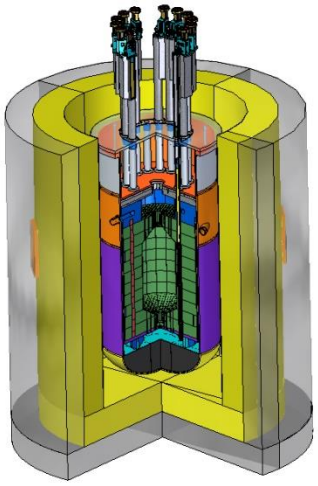

Fig.1 Reactor body structure design of TMSR-SF1

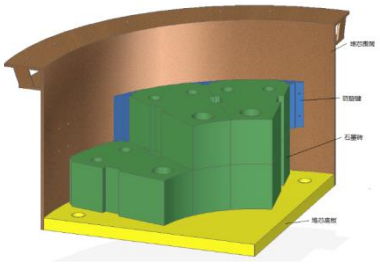

Fig.2 The 1/4 Graphite core prototype of TMSR-SF1

Fig.3 The single structure reach of control rod drive mechanism of TMSR

Fig.4 The fuel ball loading and unloading mechanism of TMSR-SF1

Structure evaluation of TMSR-SF1 reactor

Based on the current design version of TMSR-SF1, the safety assessment of equipment structures has been completed, including the graphite core components, reactor vessel, control rod, molten salt pump and loop piping, etc. The effect of neutron irradiation on thermal conductivity and irradiation induced creep are considered in the stress analysis of graphite core components. Fig.5 shows the von-Mises distribution in an irradiated graphite core component. The value of stresses at different positon with different irradiation fluence and different strain are compared and optimized. According to ASME-NH code, the load-controlled stress in pressure vessel is evaluated by using elastic analysis, while the strain and deformation of pressure vessel is evaluated by using simplified inelastic analysis. The contours of stress distribution in pressure vessel is shown in Fig.6. In addition, the stress in molted salt pump is analyzed and evaluated based on ASME-NH code. The contours of stress distribution in molten salt pump is shown in Fig.7.

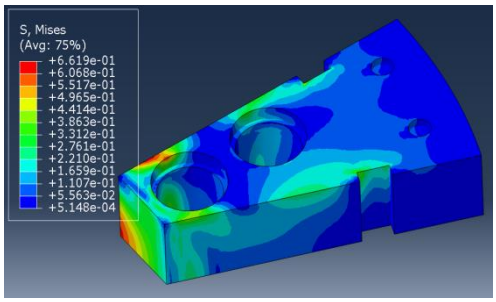

Fig.5 Contours of stress distribution in an irradiated graphite core component of TMSR-SF1

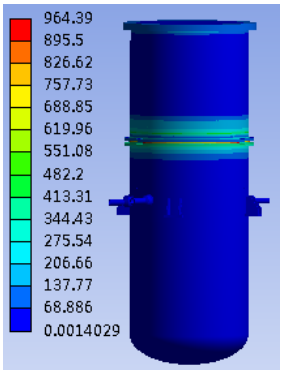

Fig.6 Contours of stress distribution in pressure vessel of TMSR-SF1

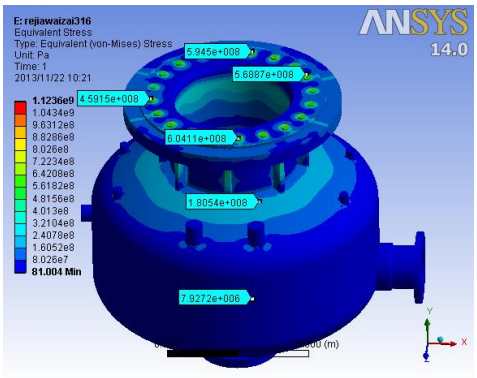

Fig.7 Contours of stress distribution in molten salt pump of TMSR-SF1

Design and development of the molten salt reactor control system

According to the conceptual design of the TMSR-SF1, the architecture design of the I&C system, the software structural design of the control system, the functional development of the control system core software package, the protection system, and the development of the high-temperature stepper motor prototype were completed.

The entire I&C system adopts a digital distributed control system architecture and adopts a standard four-layer design, including supervisory control layer, network layer, process control layer, and field device layer. The control system software consists of four parts: core software package, human-machine interface software, database software and configuration software.

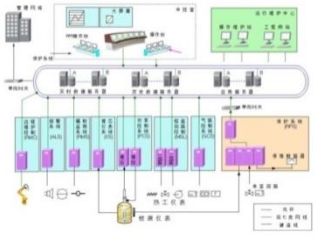

Fig.8 TMSR-SF1 I&C system overall architecture

The main development content of the control system software is the development of the EPICS core software, including device driver development based on RT-Linux embedded IOC, human-machine interface software development of control system, and application development based on Oracle database.

The protection system principle prototype mainly solves the key technical problems of the FPGA-based protection system, verifies the feasibility of the solution, focuses on the realization of the principle and functions, and combines the prototype to carry out key technology research. At present, prototype development and most of the key technologies have been completed. Prototype logic function tests meet the design requirements. The prototype of the protection system is shown in Fig.9.

Fig.9 TMSR-SF1 protection system principle prototype

Design and development of the molten salt reactor instrumentation system

The design of neutron flux instrumentation and the electronic prototype development of corresponding reactivity were completed.

The preliminary scheme of external neutron measurement system for the reactor is shown as Fig.10. It is composed of three separate sequence, each sequence contains a source detector, an intermediate detector, a power detector. The three ranges overlap, and the nuclear power measurement from start to full power is realized. The detector signal is processed by the electronic instrument, and it is sent to the protection system as an important protection variable and a signal source of the power control for the reactor.

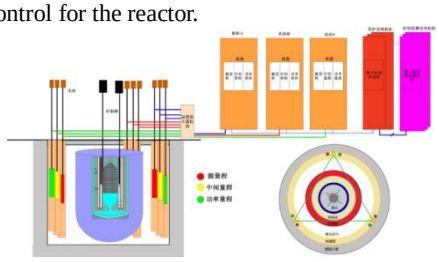

Fig.10 The preliminary scheme of the external neutron measurement system for TMSR-SF1

The conceptual design of thermal instrument and calibration of the platform for molten salt loop of TMSR were completed. The calibration platform integrated advanced technology such as pressure gauge, heating thermocouple liquid level sensor and electrode liquid level switch, etc. The system composition is shown as Fig.11.

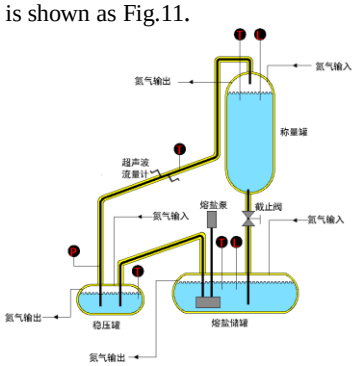

Fig.11 Flow calibration system for TMSR-SF1.

The design and review of the principle prototype of reactivity meter is completed. It adopts portable system design, which consists of neutron detector, electronics system, signal acquisition module and notebook computer. The neutron flux rate signal of the reactor is collected by the detector, processed by electronic system, and then sent to the laptop for analysis and calculation. The reactivity value is calculated by inverse dynamic method and periodic method. Related equipment purchases have been completed. The software development and test of the reactivity measurement system were completed, and the function and algorithm of the prototype were verified on the low-enriched micro-reactor critical device of the atomic energy institute. The actual measurement results are shown as Fig.12. In the process of rising power, the reactivity is determined, and the measurement results also reflect this process. When the control rods move, the reactivity is introduced, and the process is measured correctly. It shows that the system can handle pulse and current signal correctly ,and then get reactivity.

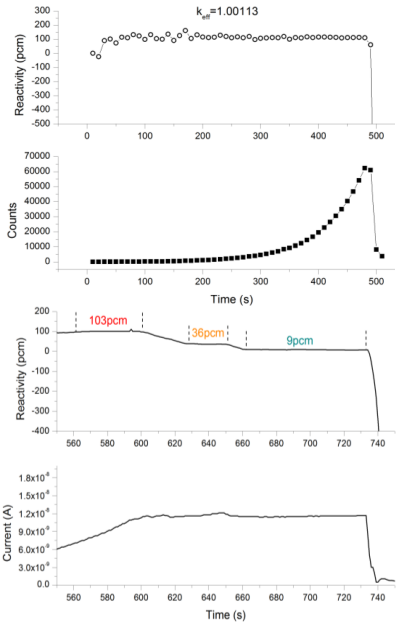

Fig.12 The actual measurement results of the reactivity measurement system for TMSR-SF1. T**he process of rising power (above); the process of control rods moving (under)**

核安全是核能发展的生命线，熔盐堆作为第四代先进反应堆，其本身具有良好的固有安全性。固态燃料钍基熔盐实验堆(TMSR-SF1)作为世界范围内同类堆型的首堆，在核安全工作上存在挑战；液态燃料钍基熔盐实验堆(TMSR- LF1)在放射性全封闭和辐射防护上更具挑战。自日本福岛核事故以来，公众和国家监管部门对于核安全的要求提升到了前所未有的高度。

钍铀核安全与工程项目作为钍基熔盐堆核能系统(TMSR)的重要组成，项目的总体目标是保障两个实验堆及其附属设施全寿期的核与辐射安全，通过国家核安全监管部门在全寿期各个阶段组织的技术审查和监督，获得必要的许可证。项目的主要工作包括钍基熔盐核能系统核安全、钍基熔盐核能系统辐射安全、钍铀放射性三废处理以及钍铀职业健康与环境影响等课题。

2013−2014 年度，本项目在厂址选择、安全系统设计、安全分析、安全设计准则与安全标准、辐射安全与放射性三废处理几个方面均取得了显著进展，同时熔盐堆安全标准和其它安全规范建立工作也取得了重要进展，为熔盐堆从实验向示范、商用的长远发展，建立了良好的开局。

厂址选择以及软土地基上建堆技术问题的解决

厂址选择工作以获得国家核安全监管部门颁发的厂址选择审查意见书为目标，分为区域调查、厂址普选和详细调查三个阶段。本项目先后建立了固态堆厂址评价准则和厂址审评原则，并完成了国家核安全监管部门组织的专家意见征询，为第三阶段工作（包括进场勘察）奠定了基础。

本项目成功解决了研究堆在软土地基上的抗震设计要求问题，使实验堆在大丰厂址的建造成为可能。我国目前已建、在建和计划建造的核动力厂为满足抗震的要求，均建造在基岩上，现有的研究堆（实验堆）厂址也都参考了核动力厂的选址标准。国内设计单位尚无在软土地基上开展反应堆设计的经验。本项目经过深入的研究，提出了 II 类研究堆（熔盐堆建议归为 II 类研究堆）可“按民用建筑抗震设计规范进行抗震设计，地震力按本地区基本地震作用加 1 度取值，按本地区基本烈度加 1 度采取抗震措施”的建议，并通过了国家核安全监管部门组织的专家论证。这一成果使熔盐堆在大丰厂址软土地基上的建造成为可能。熔盐堆在软土地基上的建造将开创我国民用反应堆的先例，在这一方向上的深入研究有望扩大可建造核动力设施的地区。

安全系统设计

安全系统设计工作分为概念设计、初步设计和详细设计三个阶段。2014 年已完成了概念设计，正与设计院合作开展初步设计。安全系统的设计工作严格按照专项的进度要求完成，保证了实验堆设计的整体进度。在进行大丰园区实验堆设计的同时，本项目还完成了嘉定园区辐射屏蔽与监测系统和放射性废物处理系统的设计、改造和建设，极大地提升了园区能力：一方面为专项开展钍铀燃料循环放射化学分离、钍铀核数据测量、材料辐照等关键研究创造了必要条件；另一方面也为实验堆的安全系统设计积累了宝贵的实践经验。

熔盐堆的安全分析是为了申请建造许可证而开展的，其安全分析报告要通过国家核安全局的审评。固态堆是同类堆型的首堆，熔盐堆在安全分析方面与其它堆型主要的不同，在于熔盐冷却剂在球床堆芯中的流动和换热特性，熔盐冷却剂特殊的物理化学性质，放射性物质在熔盐系统中的迁移规律等，熔融氟盐的防冻问题也需要重点关注。本项目在现有的计算方法基础上加入了熔盐堆特殊模型（植入保守的适用于球床堆芯的对流换热公式，且换热公式偏保守，符合安全分析中应使用保守模型的安全要求）。本项目已经开始撰写初步安全分析报告，安全分析计算工作已在进行中，安全分析的方法、安全分析报告的框架与美国 ORNL、UC-Berkeley 等单位的专家进行了讨论，也与国家核安全监管部门，以及国内的环保部核与辐射安全中心、苏州热工院核安全中心等国家核安全监管部门的技术支持单位进行了讨论，为申请建造许可证和安全审评奠定了基础。

本项目在安全分析软件上取得了重要进展，通过完成 RELAP5 程序的适应性修改，解决了固态堆系统安全分析无适用软件的问题，保证了安全分

析工作的进度。项目在熔盐自然循环排热实验上也取得了重要进展，完成了硝酸盐自然循环实验回路的设计与建造（图 1），同时已开展了涡流二极管的实验。自然循环回路和涡流二极管是大功率熔盐堆非能动衰变热排除系统的关键设备，未来大功率熔盐堆可以真正实现无水冷却，并可以彻底避免类似于福岛事故的严重事故的发生。

图 1 熔盐自然循环实验回路

安全分析

安全分析工作分为四个阶段：第一阶段确定安全分析报告框架和内容；第二阶段进行初步安全分析并撰写完成初步安全分析报告，初步建立安全分析方法，并提出试验验证计划；第三阶段开展试验验证并撰写最终安全分析报告；第四阶段，根据运行经验和堆上试验结果，修正、完善安全分析法。安全分析的工作严格按照专项总体进度要求完成。2014 年已完成第一阶段工作，第二阶段已完成了安全分析方法的初步提出，对固态堆概念设计进行了初步安全分析并完成了第一稿的初步安全分析报告。

安全设计准则和安全标准

安全设计准则核安全标准相关工作可以分为安全设计准则的建立、审评原则的起草和安全标准的建立三个部分。目前已基本建立安全设计准则，并由国家核安全监管部门的技术支持单位进行了评审，将会同各工艺系统的设计准则报国家核安全监管部门。目前正着手开展审评原则的起草工作。在安全标准方面，与美国知名研究机构、公司和政府部门，包括 ORNL、INL、SNL、MIT、UC-Berkeley、Westinghouse、NRC 等，以及中国环保部核与辐射安全中心建立了联合工作组，启动了氟盐冷却高温堆（中方称固态燃料熔盐堆）安全标准的研究制定工作。计划已获得美国核学会(Nuclear Facilities Standards Committee, NFSC) 批准，标准编号 ANSI/ANS-20.1，预计用五年左右的时间完成，完成之后将成为美国国家标准。

通过与美方合作开展熔盐堆的安全标准研究工作，我们进入了固态堆安全研究的核心俱乐部。在熔盐堆核安全理念、研究方法和技术路线上做到了与国际最先进水平同步。这一标准研究工作的阶段性成果和其最终建立，将为解决固态堆在我国的建造和运行中的安全问题提供较为系统的方法。

嘉定园区辐射监测系统

本项目在嘉定园区在项目的建设过程中，按照国家辐射监测相关的标准规范，基于实验物理及工业控制系统(EPICS)统，采用网络化技术实现了对实验室工作场所、流出物排放口及园区环境等不同监测位置以及对半导体区域γ监测仪、电离室区域γ监测仪、区域中子监测仪、环境γ监测仪、个人剂量报警仪、放射性气溶胶监测仪、工艺γ辐射监测仪、手足衣物表面污染监测仪、小物品监测仪等不同探测器类型的系统化集成监测，扩展性比较强，具有广泛的应用发展前景，实现了设计的合理性与先进性。

(a) 环境γ监测仪

(b) 放射性废液监测仪

(c)放化实验室出入控制

(d) 辐射监测系统监控软件

图 2 嘉定园区辐射监测设备及软件

嘉定园区放废处理设施改造

嘉定园区放射性废物处理设施改造的目的是满足未来 20 年我所嘉定园区开展 TMSR 钍铀核燃料循环研究实验的放射性废物处理需求，改造工程内容包括 104 废水处理车间、106 固体废物暂存库以及嘉定园区低放废液转运和贮存系统。低放废水处理满足《污水综合排放标准》(DB31/199-1997)，总 α 小于 1 Bq/L，总 β 小于 10 Bq/L，实现达标排放，低放废水处理工艺流程如图 3 所示。废水处理中产生的絮凝沉淀、蒸残液和废树脂进行水泥固化。压缩固体废物减容以及固体废物的暂存。改造完成后，该设施为华东地区核技术利用单位中工艺较先进、规模最大、功能最齐全的在役放射性三废处理设施。

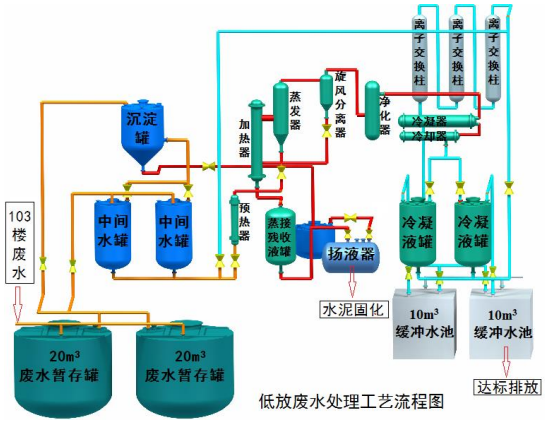

图 3 低放废水处理工艺流程图

Thorium-uranium nuclear safety and engineering

Nuclear Safety and Engineering

Nuclear safety is the lifeline of nuclear energy development. As one of the Generation IV reactor, MSR has a favourable inherent safety. Thorium-based Molten Salt Experiment Reactor with Solid Fuel (TMSR-SF1), which shall be the first kind of FHR around the world, will face unknow nuclear safety challenge; Also Thorium-based Molten Salt Experiment Reactor with Liquid Fuel (TMSR-LF1) will pay more attention on the radiation containment and protection. After Fukushima nuclear accident, the public and Government regulators have raised the requirement of nuclear safety to an unprecedented level.

Thorium-Uranium Nuclear Safety and Engineering is a vital component of TMSR. The goal of this project is to guarantee the nuclear and radiation safety of above two molten salt experiment reactors in the whole life, and pass the technical review and supervision from National Nuclear Safety Regulatory Authority (NNSRA) in each phase to obtain necessary licenses. In order this project is devided into TMSR Nuclear Safety, TMSR Radiation Safety, Thoirum- Uranium Radioactive Waste Disposal and Thoirum-Uranium Environmental and Occupational Health four tasks.

During the year from 2013−2014, many remarkable progresses such as site selection, the safety system design and analysis, safety design criteria and standard, radiation safety and radioactive waste disposal have been made. All work of nuclear and radiation safety, licenses application for reactor construction is compeleted on the schedule. Moreover, safety standard and other safety specification of molten salt reactor have pushed ahead, which shows a good start from experiment to demonstration and commercialization of MSR.

Site Selection and soft soil foundation

The work of site selection is to obtain the site selection review submissions issued by NNSRA in three phases of regional survey, site census and detail probe. We have successively established site evaluation criteria and site review principle of TMSR-SF1, and finished experts's consulation organized by NNSRA. It will lay the foundation for the third phase, including field investigation.

We successfully address the aseismatic design issue of research reactor on the soft soil foundation, making it possible for building the experiment reactor in the site of Dafeng. At present, the nuclear plants in our country have built and been building on the bedrock to satisfy the seismic requirement, and all research reactors refer to this standard. None domestic design institutes has experiences to design reactors on soft soil foundation. After a comprehensive investigation, we proposed the suggestion that the seismic design of II class reactor (molten salt experiment reactor is classified as II class reactor) can be carried out in the current aseismic design code for civil buildings, seismic force is set as basic earthquake action plus 1 in the region, anti-seismic measures is set as basic seismic intensity plus 1 in the region. It has passed the experts's argumentation organized by NNSRA, which makes it possible to build molten salt experiment reactor in the site of Dafeng. The investigation will expand buildable area of domestic nuclear power facility.

Safety System Design

Safety system design can be devided into three stages, as for concept design, preliminary design and detailed design. We have finished concept design in 2014, and preliminary design is under way by cooperating with domestic design insititute. The work strictly follows the schedule of TMSR, and ensures the design progress of molten salt experiment reactor. During the desing of Dafeng campus, we aslo finished the design, reform and construction of radiation shield and monitoring system, radioactive waste disposal system in Jiading campus, which improved the ability of radioactive management. On one hand, it has created necessary conditions for the key researches such as radiochemical separation of thorium-uranium fuel cycle, data measurement of thorium and uranium nucleus, and material irradiation. On the other hand, it has accumulated many valuable experiences for the safety system of MSR.

The safety analysis of MSR is Carried out

for the construction permit, and the safety analysis report calls for the review of National Nuclear Safety Administration. The safety analysis of solid fuel molten salt reactor is different with the other types of reactor, such as the flow and heat transfer characteristics of the coolant which lies in the pebble bed reactor core, the special physical and chemical properties of molten salt coolant, the law of migration for radioactive material in the molten salt system. The antifreezed fluoride molten salt also needs to be focused on. The initial development of the safety analysis method has been able to adapt to the needs of the preliminary safety analysis. Based on the existing calculation methods, the project added a special model of molten salt reactor (implanted a conservative convective heat transfer formula which is suitable for the core of the pebble bed reactor, and the heat transfer formula is conservative, which accords with the safety requirement of the conservative model in safety analysis). The project has prepared a preliminary safety analysis report, and the safety analysis and calculation work is in progress. The method of safety analysis, the framework of security analysis report, both has been dissussed by the national nuclear safety regulatory authorities, as well as the technical support units of the national nuclear safety, such as the national nuclear and radiation safety center, the nuclear safety center of Suzhou thermal engineering center, and other organizitions, as the experts of ORNL, UC-Berkeley, and so on which laid the foundation for the application for the construction of license and the security review.

Fig.1 Experimental loop of natural circulation for molten salt

The project has made important progress in the safety analysis software, by completing the adaptive modification of RELAP5 program, the problem of non-applicable software in solid fuel reactor system safety analysis is assloved, and the progress of safety analysis is ensured. The project has also made important progress in the following aspects: 1) the experiments of heat transfer in molten salt natural circulation; 2) The finishment of design and construction of the experimental loop of nitrate natural circulation (Fig.1); 3) The undergoing experiment of the eddy current diode. Natural circulation circuit and eddy current diode are the key equipments of passive decay heat elimination system for high-powered molten salt reactor. In the future, the anhydrous cooling can really be achived in high-power molten salt reactor, and serious accidents which similar to Fukushima can be completely avoided.

Safety analysis

The Safety analysis can be divided into four stages. The first stage is, the safety analysis report frame and the contents to be determined; the second stage is, the preliminary safety analysis report to be completed, the preliminary safety analysis method to be established, and the test-verify plan to be put forward; the third stage is, the experimental verification and the final safety analysis report to be carried out; the fourth stage is, according to the reactor test results the operation experience, the safety analysis method to be revised and perfected. The safety analysis is completed strictly in accordance with the requirements of the global progress. In 2014, the first stage has been completed, the preliminary safety analysis method has been promoted, the preliminary safety analysis has been made for the conceptual design of solid fuel molten salt reactor, and the first draft of safety analysis report has been completed.

Safety design criteria and safety standards

The related work of safety design criteria and nuclear safety standards can be divided into three parts: the establishment of safety design criteria, the drafting of review principles and the establishment of safety standards. At present, safety design guidelines have been basically established and evaluated by the technical support units of the national nuclear safety supervision department, and the design guidelines of all the process systems will be reported to the national nuclear safety supervision department. The drafting of the review principles is now being carried out. At the aspect of security standards, study on safety standards work for the fluoride salt cooled high-temperature reactor (which called as solid fuel in molten salt reactor by China) has been lauched by a joint working group, combined with the well-known research institutions、companies and government departments in the United States, including ORNL, INL, SNL, MIT, UC-Berkeley, Westinghouse, NRC, and national nuclear and radiation safety center in China. The plan has been approved by the Nuclear Facilities Standards Committee (NFSC) of the US nuclear society, and the standard number ANSI/ANS-20.1 is expected to be completed in about five years. After completion, it will become the national standard of the United States.

Through the cooperation with the United States for the developed safety standards of the molten salt reactor, we have entered the core club of the safety research of the solid fuel molten salt reactor. It has been synchronized with the most advanced international level in the safety concept、the research method、the technical route of the nuclear molten salt reactor. The phased achievement of this standard research work and its final establishment will provide a systematic solution for solving the safety problems of solid fuel moten salt reactor construction and operation in China.

Radiation monitoring system of Jiading Park

The project is basically built in Jiading Park, which is a real-time monitoring system for the rearch of thorium-uranium fuel cycle. It provides the monitoring means for long-term radiation safety in Jiading park.

During the construction of the project, the characteristics of radionuclides which involes thorium-uranium fuel cycle, In accordance with the national standards which related to radiation monitoring, based on physics experiment and industrial control system (EPICS), used of network technology, The system integration monitoring of different detector types is realized, such as the laboratory work, effluent discharge and park environment, and gamma monitor for semiconductor regions, gamma monitor for ionization chamber area, neutron regional monitor, gamma monitor for environmental, alarm system of personal dose meter, radioactive aerosol monitor, process gamma radiation monitor, hand foot clothing surface contamination monitor and small object monitor, which has strong expansibility and wide application prospect for development, and realizes the reasonable and advanced of the design.

(a) Environmental gamma monitor

(b) Radioactive waste liquid monitor

(c) Entry and exit control for the Radiochemistry Lab

(d) Monitoring software for radiation system

Fig.2 Radiation monitoring equipment and software in Jiading Park

Renovation of waste disposal facilities in Jiading Park

The popurse for radioactive waste treatment facilities renovation in Jiading Park is to meet the needs of radioactive waste treatment for TMSR Th-U nuclear fuel cycle experiment which to be carried out in the next 20 years. The renovation project includes the wastewater treatment plant in 104 building, the solid waste impoundments in 106 building, and the transport and storage system for low level liquid waste at Jiading park. The treatment of low level wastewater can meet the "comprehensive wastewater discharge standard" (DB31/ 199-1997).The total alpha radioactivity is less than 1 Bq/L, the total beta radioactivity is less than 10 Bq/L, and for effluent water to reache the standard, the treatment process of low level wastewater is shown in Fig.3. The flocculation, residue and waste resin produced in the treatment of waste water are fixed by cement. The functions of the waste bank include the reduction of compressible solid waste and the temporary storage of solid waste. After completion of the renovation, the facility is a more advanced, largest and most fully functioning radioactive waste disposal facility in the nuclear technology utilization unit of the east China.

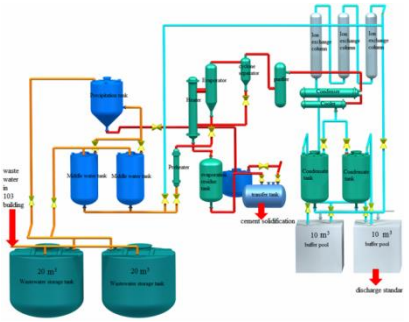

Fig.3 Process flow chart of low r adioactivity wastewater treatment

钍基熔盐堆设计平台

反应堆物理部

本课题面向钍基熔盐堆核能系统先导专项需求，建设 TMSR 设计计算分析能力，为系列钍基熔盐堆提供设计工具和平台。课题工作在设计平台硬件建设与运行、熔盐堆设计分析软件研发两个方面展开。

设计平台硬件建设与运行方面，TMSR 超算系统与 CAVE 系统先后建成投运，分别为专项提供高性能、大规模并行运算资源，以及全沉浸 3D 虚拟现实呈现平台与技术。

熔盐堆设计分析软件方面，先后完成了熔盐堆确定论分析软件框架以及部分计算方法、模块研发，并完成了固态燃料熔盐堆设计软件适用性分析研究。

TMSR 超算系统建设与运行

TMSR 超算系统采用 CPU-GPU 混合架构实现高性能运算，于 2011 年 5 月启动方案论证与单元测试，于 2012 年 12 月完成第一阶段建设，于 2013 年 8 月完成第二阶段建设，各建设阶段如图 1 所示。建成后，TMSR 超算系统核心硬件构成如图 2 所示；整个系统的单精度浮点运算能力达 204 Tflops。其中 33%运算能力来自 CPU，67%运算能力来自 GPU；存储网格裸容量 1.2 PB，其中 960 TB 为用户空间，276 TB 为备份空间，实现了聚合带宽高达 16 GB 的并行文件系统；系统内部高速互联基于全交换 40 G 高速 Infiniband 交换机，其延迟和带宽实测值均已超过预定指标。

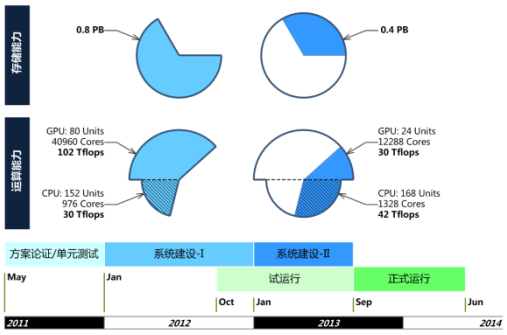

图 1 TMSR 超算系统建设阶段及各阶段的运算能力

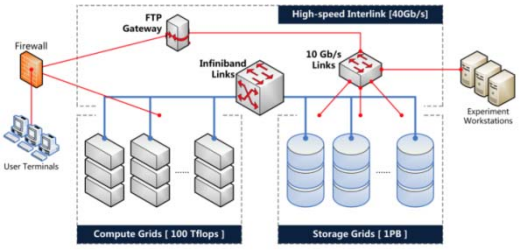

图 2 TMSR 超算系统核心硬件构成

TMSR 超算系统在完成第一阶段建设后即投入试运行，部署了反应堆中子学、热工水力学、辐射防护、材料科学等学科的计算分析软件。截至 2013 年底平台用户 150 余人，总共运行近 9 万个作业，总作业时间 310 万处理器小时；截至 2014 年底平台用户 173 人，总作业数 17 万条，总作业时间 1 100 万处理器小时。2014 年度超算系统作业时间及 CPU 资源利用率如图 3 所示。

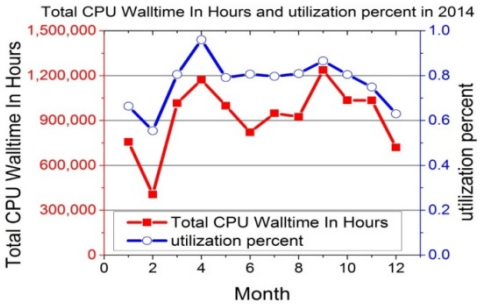

图 3 TMSR 超算系统 2014 年度作业时间及 CPU 资源利用率

CAVE 系统建设与运行

CAVE 系统采用 4 通道洞穴式沉浸环境、主动立体投影、人体定位与动作捕捉等先进虚拟现实技术，实现使用者与三维立体模型等数字内容之间的深度交互，获得身临其境的感受与认知。CAVE 系统于 2013 年 6 月完成建设，部署了液态熔盐堆系统概念演示数字内容；于 2014 年底从上海科学技术大学场地搬迁至我所嘉定园区。CAVE 系统设备平面布局如图 4 所示。

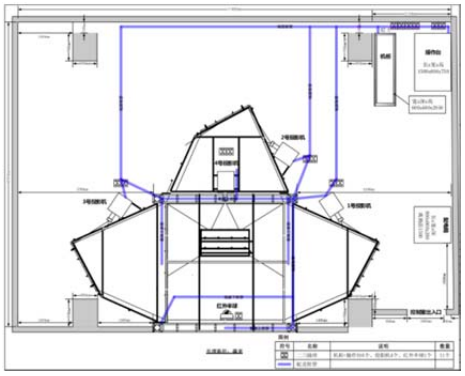

图 4　CAVE 系统设备布局平面图

熔盐堆确定论分析软件框架及部分计算方法、模块研发

熔盐堆确定论分析软件基于确定论方法，以实现对目标堆型及堆设计方案的安全分析为主要功能。熔盐堆确定论分析软件具有一个四层的零级架构，如图 5 所示。其中，公用动态数据负责整合整个软件的物理数据，一组功能模块负责实现软件的物理计算功能，一组通用模块负责实现与用户的人机交互以及功能模块间的相互匹配，主消息循环负责通过对各模块的调用来控制程序的运行。

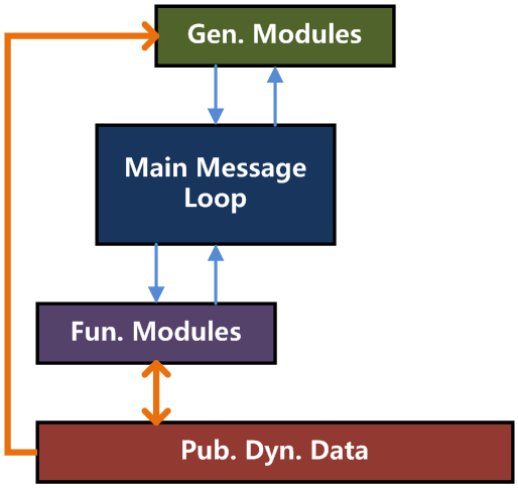

图 5　熔盐堆确定论分析软件零级架构

计算方法与模块研发包括堆中子物理与热工水力两个方面，包括：1）一维固态熔盐堆瞬态分析工具、2）二维球床熔盐堆瞬态分析程序、3）TRISO 燃料球宏观群常数加工栅元计算程序。

一维固态熔盐堆瞬态分析工具是在西安交通大学的点堆中子动力学程序模块基础上，参照清华高温气冷堆相关程序开发出的集总参数模型瞬态分析程序，其物理模型如图 6 所示。

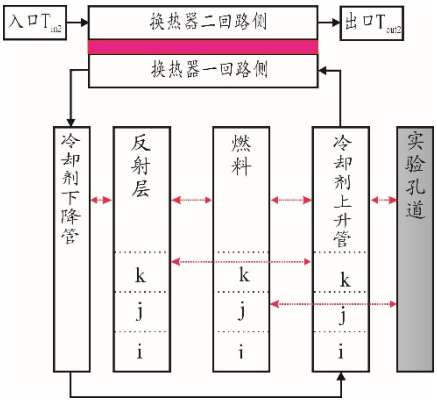

图 6　一维固态熔盐堆瞬态分析程序物理模型

二维球床熔盐堆瞬态分析程序满足瞬态分析需求，可对启堆、停堆、升功率、降功率等，以及部分超基准事故设计中的弹棒事故、紧急停堆等工况进行模拟计算，其物理模型如图 7 所示。

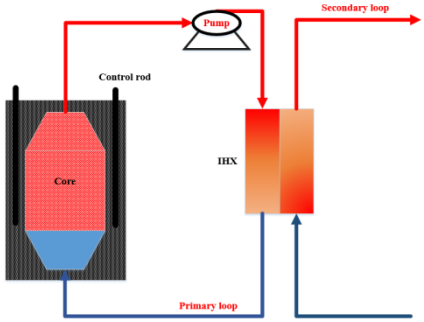

图 7　二维球床熔盐堆瞬态分析程序物理模型

宏观群常数计算程序分为栅元计算和组件计算两个模块，栅元计算模块先对燃料栅元和控制棒栅元进行均匀化计算，采用碰撞概率法，输出栅元多群宏观群常数；组件计算模块根据组件划分方案，在组件内建立输运方程，并采用穿透概率法求解。得到组件内各子区的通量谱后，再归并计算得到少群常数，以供扩散计算程序使用。课题完成了采用碰撞概率法的 TRISO 燃料球宏观群常数加工栅元计算程序开发，流程如图 8 所示。

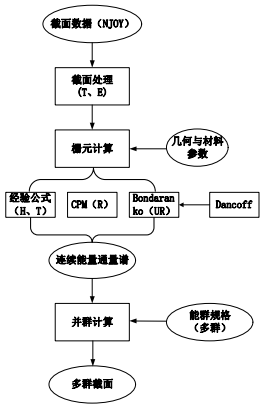

图 8　球床熔盐堆栅元计算流程

固态燃料熔盐堆设计软件适用性分析研究

课题在分别对某核动力厂初步安全分析报告、实验堆最终安全分析报告中的软件适用性说明进行充分调研后，与 4 个技术部的 6 个专业组合作完成了《10 MW 固态燃料钍基熔盐实验堆（TMSR-SF1）设计与安全分析软件适用性研究报告》。该报告从我国研究用反应堆设计安全相关的现行法规出发，归纳出研究堆的安全目标和主要特征，并对设计与安全分析软件适用性研究的总要求做了整理；介绍了固态燃料熔盐堆的基本概念和特征，概括了 TMSR-SF1 的总体设计，分析了固态燃料反应堆设计与安全分析对设计分析软件的共性需求，阐述了 TMSR-SF1 设计与安全分析的特别需求，并对当前 TMSR-SF1 设计分析软件体系的完备性进行了讨论；分别从堆物理设计及分析、热工水力设计及分析、结构力学计算与抗震分析、放射性源项与辐射计算、安全分析五个方面对 TMSR-SF1 的主要设计与安全分析程序的适用性进行了论述。

TMSR design platform

Department of Reactor Physics

The RMSR design platform sub-project has vision to provide design codes and tools for design & analysis of Molten Salt Reactors (MSR), as well as long-term ability build-up. The sub-project advances both in calculation infrastructure construction and in MSR design & analysis software development.

A super computer system and a CAVE system dedicated to TMSR project commissioned during last two years, providing large scale hybrid high performance computating resource and full-immersed 3D virtual reality display techniques respectively.

A framework of deterministic analysis code package for MSR has been established, as well as model, algorithm, codes and modules within the framework. Also, an investigation on the applicability of designing softwares for solid-fueld MSR has been conducted.

Construction of TMSR super computer system

The Super Computer System (SCS) of TMSR has a CPU-GPU hybrid architecture. The feasibility study and unit test of TMSR SCS started on May 2011, the first phase of construction was finished on December 2012 and the seconde phase of construction was finished on August 2013; those construction phases are shown as Fig.1. At the full commission of TMSR SCS, configuration of the core hardware system is shown as Fig.2; the single precision floating point performance can be as high as 204 TFLOPS, one third of the performance is proved by CPUs, the rest is proved by GPUs; the storage grid has a raw capacity of 1.2 PB, where the working domain has a volume of 960 TB, and the back-up domain has a volume of 276 TB, the combined parallel file system has a bandwidth as high as 16 GB; the high-speed internal linkage within the TMSR SCS is based on 40 GB Infiniband PBXs, both the measured delay and bandwidth has a beter performance than target values.

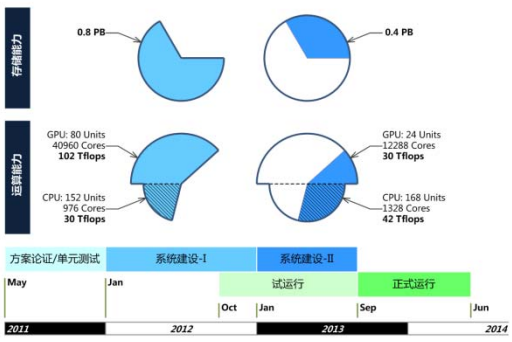

Fig.1 The construction phases of the TMSR SCS and performance accordingly

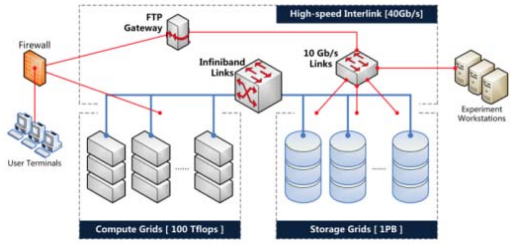

Fig.2 The core hardware configuration of the TMSR SCS

The trail operation of TMSR SCS started right after the construction phase-I, softwares and codes of reactor neutronics, thermal-hydraulics, shielding, and material scince are deployed. By the end of FY 2013, numbers of total user accounts on TMSR SCS reached 150, more than 90 000 computing jobs were executed, the overall walltime reached 3 100 000 processor hours; by the end of FY 2014, number of total user accounts on TMSR SCS reached 173, more than 170 000 computing jobs were executed, the overall walltime reached 11 000 000 processor hours. The walltime in hours and the CPU load ratio of TMSR SCS during FY 2014 are shown as Fig-3.

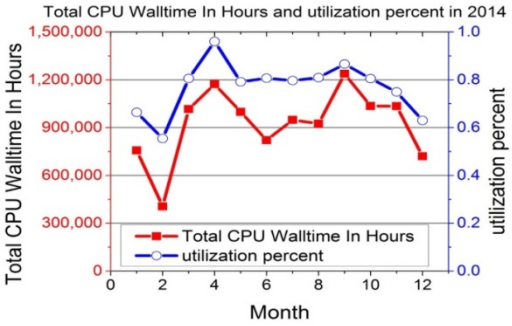

Fig.3 The walltime hours and the CPU load ratio of the TMSR SCS, FY 2014

Construction of TMSR CAVE System

The CAVE System (CS) of TMSR has advanced virtual reality technologies such as 4-channel cave-like full- immersed circumstances, active 3D projection, human positioning and motion capture, etc., to establish deep interactions between users and digital contents such as 3D solid models, through which users can experience vivid and immersive perception and cognition. The TMSR CS was built on June 2013 at the Shanghai University of Science and Technology, a digital content of liquid-fueld MSR conception was deployed on TMSR CS. The TMSR CS was relocated to SINAP JiaDing campus at the end of FY 2014. The equipment layout of TMSR CS is shown as Fig.4.

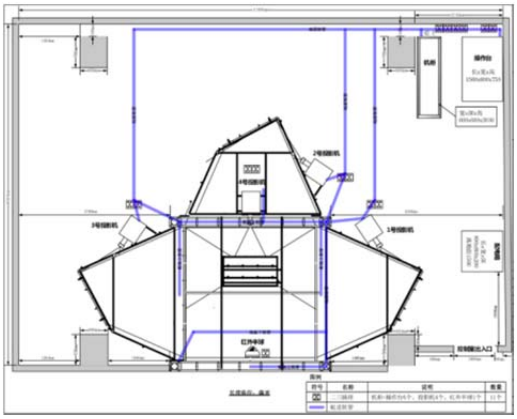

Fig.4 The equipment layout of TMSR CS

Research and development of the deterministic analysis code package for MSR

The Deterministic Analysis Code Package (DACP) for MSR has a long-term goal to accomplish determinis computer code for design analysis and safety assessment of target molten salt reactor types and models. One the level-0, The DCAP has a 4-layer architecture, as shown in Fig.5. Where the public dynamic data consolidates entire physical data within DCAP, a growing group of functional modules implement the demanded calculating and solving functions, a group of general modules conduct the function of user interfacing and match functions among functional modules, the main message loop controls the running procedure by calling those functional and/or general modules.

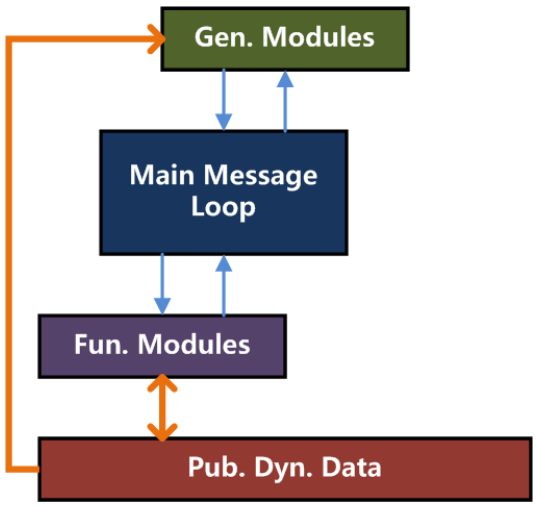

Fig.5 The level-0 architecture of DCAP-MSR

The R&D on model, algorithm, codes and modules of DCAP-MSR is unfolded in both reactor neutronics and thermal-hydraulics, including: 1) one-dimensional transient analysis code for solid-fueled MSR, 2) two- dimensional transient analysis code for pebble-bed MSR, 3) cell-level code of the macroscopic group-constants generator of TRISO-based pebble-bed reactor.

The one-dimensional transient analysis code for solid-fueled MSR is based on a point kinetics model developed by Xi'an JiaoTong University, integrated with a lumped parameter model used by High-Temperature Gas Reactor; the physical model is shown as Fig.6.

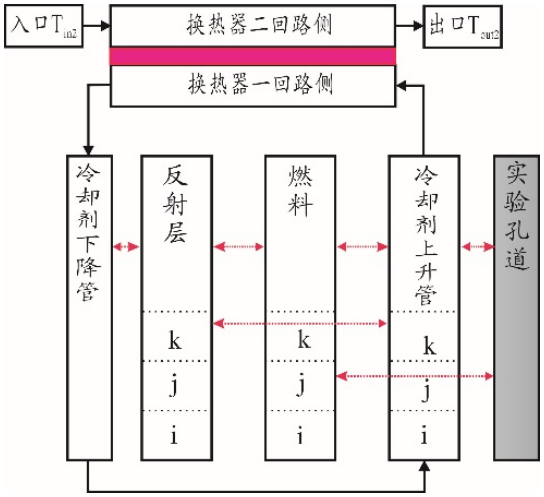

Fig.6 The physical model of one-dimensional transient analysis code for solid-fueled MSR

The two-dimensional transient analysis code for pebble-bed MSR can be used to simulate procedures such as reactor start-up, shut-down, power-up, power-down, and beyond design basis accidents (BDBA) like rod ejection, reactor scram; the physical model is shown as Fig.7.

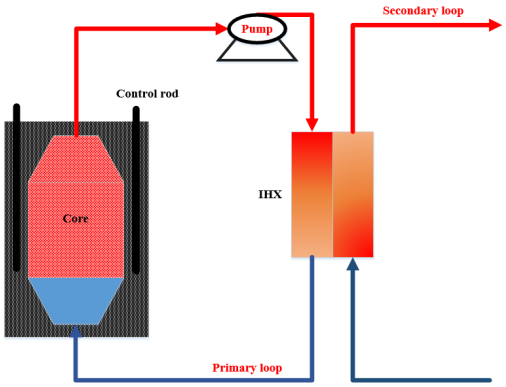

Fig.7 The physical model of two-dimensional transient analysis code for pebble-bed MSR

The macroscopic group-constants generator code of TRISO-based pebble-bed reactor is composed with two modules, cell-level module and assembly-level module. The cell-level module homogenizes the fuel cell and/or the poision cell by Collision Probability Method (CPM) and provide cell-homogenized macroscopic cross- section; the assembly-level module establish neutron transportation equation set within a fuel assembly, and slove the equation set using Transmission Probability Method (TPM). The few-group macroscopic cross- section calculated by the assembly-level module will be used in solving neutron diffusion equations for the reactor core. The cell-level code of the macroscopic group-constants generator of TRISO-based pebble is developed; the flow diagram is shown as Fig.8.

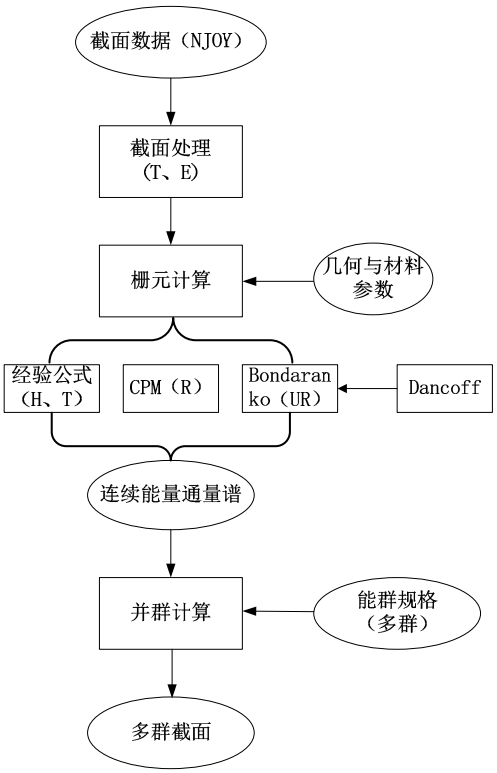

Fig.8 The flow diagram of the cell-level code of the macroscopic group-constants gener-ator of TRISO-based pebble

Investigation on the applicability of designing softwares for solid-fueld MSR

After a detaild survey of the required software applicability description in Preliminary Safety Analysis fow a given nuclear power plant, Final Safety Analysis for experimental reactor, an investigation on the applicability of designing softwares for solid-fueld MSR—“Assement report on the applicability of designing and safety analysis softwares for 10MW solid fueld Thorium- based Experimental Reactor (TMSR-SF1) ”— was done with collaboration from 4 departments, 6 groups. The report starts from investigations across the relevant existing legislation on design of safety for research reactor, the research reactor safety objectives and main features are generalized, requirements on applicability description for design and safety analysis softwares are summarized; basic concepts and characters of solid-fueled MSR are introduced, overall design of TMSR-SF1 was summarized; general demands of design and safety analysis software for solid fueled reactors are analyzed, specific demands for TMSR-SF1 design and safety analysis are stated, the completeness of TMSR-SF1 design and safety analysis tools are discussed; the applicability of major design and safety analysis tools for TMSR-SF1 are described, in such categories: reactor physics, thermal-hydaulics, structural mechanics and earthquake-resistant, radioactive source term and radiation calculation, safety analysis.

熔盐化学与工程技术部

熔盐回路是熔盐堆可靠和有效运行的保证，承担着为反应堆循环供给燃料和传递核裂变能（热能）等基本任务，对回路的安全密闭性能、耐高温性能、防腐蚀性能及运行可靠性等提出了极高的要求。熔盐回路技术的主要任务是研制适合高温耐腐蚀的熔盐回路关键设备，包括高温熔盐泵、冷冻阀、熔盐调节阀，冷冻法兰，双重密封法兰，伴热保温等，并建立相关试验台架进行性能测试，为熔盐回路安全可靠运行提供保障。

完成冷冻阀工程改进型设备研制和冷冻法兰工程改进型设备研制。完成管道双重密封法兰设计和高温气密封性能试验验证并完成常用密封件压缩机械性能试验。研制出主循环泵 304 不锈钢预样机，并完成水测试和热态试验等性能测试。在此试验数据的支持下，验证设计和计算方法，为后续核样泵的制造提供支撑。启动主循环泵哈氏合金样机设计。研制出适用氟盐介质压力计和差压计。研制出机械阀工程样机。完成熔盐泵熔盐试验台架设计，为主循环泵哈氏合金样机提供高温熔盐试验台架。研制设备及管道预热保温工程样机并完成性能测试。在 FLiNaK 回路基础上建立热工试验段并运行。

冷冻阀是熔盐堆关键设备之一，是连接反应堆和应急卸料罐之间的重要设备，主要用于熔盐存储系统截止阀，兼有过热安全排放阀功能。冷冻阀利用“非能动”设计理念，即利用流体自然对流、冷凝等原理来实现冷冻阀的开启与关闭。冷冻阀主要由阀体的扁平结构管段以及相应加热/冷却装置组成。正常工作状态下，冷冻阀的冷却装置开始工作，将阀体内的熔盐冷却凝固，起到阻断熔盐流动的作用。当意外发生时，或者关闭冷却装置时，冷冻阀体内的熔盐吸收热量，凝固的熔盐开始熔化，管路开始流通，使反应堆内的熔盐流到应急卸料罐中，减少了反应堆事故发生的概率，实现了反应堆的被动安全性。

设计 DN40 和 DN50 两种规格的工程试验型冷冻阀（图 1）。对加工完成的 DN50 冷冻法兰（图 2）在热分析试验台架上进行初步热分析测试，法兰盘面直径的二分之一处，温度比法兰中心温度降低了 100 ℃左右。将实验过程中的气体换成 FLiNaK 熔盐，熔盐熔点为 450 ℃，假如熔盐运行温度为 550 ℃，那法兰盘面直径二分之一处法兰空隙环面里的熔盐就会凝固形成凝固环面达到密封熔盐效果。

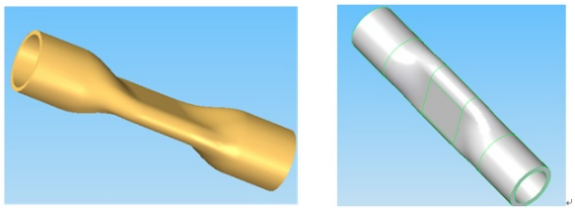

图 1 工程试验型冷冻阀三维结构图

2013 年 6 月完成 DN50 工程试验型冷冻法兰(Hastelloy C-276)加工验收，包括盘面带翅片的冷冻法兰，见图 2 所示。

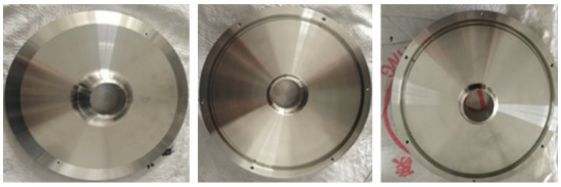

图 2 DN50 冷冻法兰加工完成照片

完成样泵 304 工艺样机的设计及零部件制造，该熔盐泵将在 FLiNaK 熔盐高温试验回路上运行。主要设计参数为：流量 5~15 m^3/h，扬程 20 m，运行温度 550~700 ℃。其特点为：泵罐内熔盐密封采用迷宫式气密封加干气密封的组合密封方式；轴承润滑油密封采用非接触式油密封装置，与传统的接触式机械密封相比较，使用寿命有较大的提高。在小流量泵的基础上，于 2013 年进行了大流量化工泵的工程放大研究，将流量由 15 m^3/h 放大到 300 m^3/h。总体结构见图 3。

于 2014 年 5–9 月进行了高温熔盐调节阀的方案设计，高温熔盐调节阀原理样机的设计参考 MSBE 调节阀结构，其运行工况与我方比较类似，该调节阀采用双重波纹管密封结构，总体结构设计参见图 4。

研制出适用氟盐介质压力计和差压计（图 5），最高工作温度 700 ℃，压力计量程 1 MPa，差压计量程 200 kPa，精度为满量程的 1%；正在尝试加工纯镍膜片和双重膜片的压力计和差压计。

研制了连接密封技术，如管道连接密封法兰

（图 6）、高温气密封性能。也研究了多种管道预热保温方式，如陶瓷加热器、电加热棒加热、电伴热带加热、高（中）频感应加热、远红外加热、强迫对流加热等。

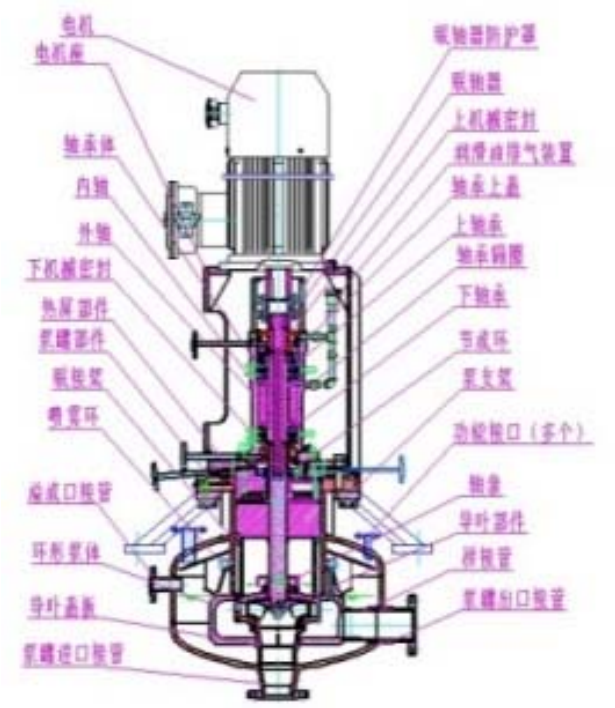

图 3 样泵总体结构示意图

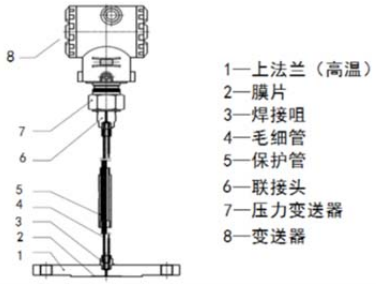

图 4 压力变送器加工图

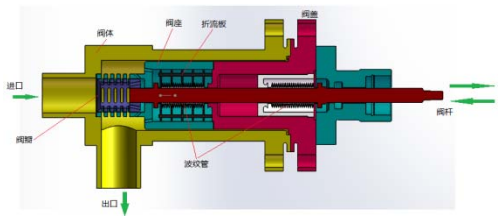

图 5 高温熔盐调节阀原理样机结构示意图

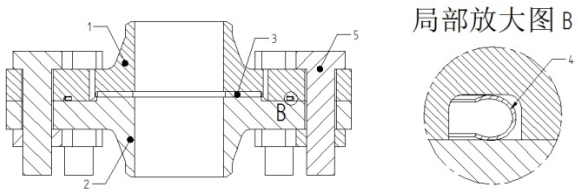

1 阴面法兰 2 阳面法兰 3 石墨缠绕垫片 4 金属 C 形密封圈 5 螺栓螺母

图 6 双重密封法兰结构示意图

完成主循环泵 304 不锈钢预样机设计、加工、安装、调试及冷、热态性能测试。启动主循环泵哈氏合金样机设计，完成初步设计并已订购哈氏合金。完成机械阀工程样机设计及计算分析，正在进行加工。完成工程改进型冷冻阀在不同运行温度下的开启关闭时间测试，分析了阀体加热冷却过程中的温度分布测试规律，完成冷冻法兰试验台架安装调试。完成熔盐泵熔盐试验台架设计工作，并启动台架及设备的加工制造工作。完成回路管道气加热及保温台架设计。对 FLiNaK 熔盐高温试验回路进行技术改造，实现系统运行。

Molten salt loop technology

Molten salt chemistry and engineering department

Molten salt loops are the assurances for reliable and effective operation of molten salt reactor, supply reactor with fuel and transfer nuclear fission (heat). That needs high requirements for safe sealing performance, high temperature resistant performance, corrosion resistant performance and reliability operation of the loop. The main task of the molten salt loop technology is developing the key equipments with high temperature corrosion resistant performance, including high temperature molten salt pump, freeze valve, molten salt regulating valve, freeze flange, double sealing flange, thermal insulation, etc., and establishing the related test loop to do performance test, which guarantees safe and reliable operation of the molten salt loop.

The developments of advanced freeze valve and freeze flange have been completed. The design of double sealing flange used in pipe and the test of high temperature gas seal performance test and the common seal compression mechanical properties have been completed. Primary circulation prototype pump of 304 stainless steel was developed, and completed the water test and hot performance test, to validate the pump structure design, calculation and simulation methods and offer the optimization direction and technology accumulation for subsequent pump used in Thorium-based Molten Salt Reactor. TMSR is developing primary circulation engineering prototype pump built with Hastelloy N. The fluoride salt pressure gauge and differential gauge have been developed. We have developed a mechanical valve engineering prototype. TMSR complete the pump test-bench design using molten salt, the primary circulation engineering prototype pump high temperature performance test conducted on the bench. We also developed the preheating insulation engineering prototype for the equipment and pipe and the performance test has been completed. The thermal test section has been built and run on the basis of FLiNaK loop.

Freeze valve is one of the key equipments for molten salt reactor. It is the important equipment for connecting between reactor and emergency drain tank, mainly used as globe valve in molten salt storage system, both used as overheat safety discharge valve. Freeze valve uses "passive" concept, namely natural convection and condensation principle to realize the valve open and closed. Freeze valve is mainly composed of flatten section of pipe and the heating, cooling equipments. Normally, the working cooling equipment makes the salt in valve frozen, which block the salt flow. When the accident occurred or cooling equipment closed, the frozen salt in valve absorbs heat and melt. The melt salt in valve can flow through the pipe, making the salt inside the reactor drain to the tank, which reduces the probability of reactor accident, realizes the passive safety of the reactor.

DN40 and DN50 of advanced freeze valves have been designed (Fig.1). The thermal performances of DN50 freeze flange have been tested on test bench. The result shows that the temperature on half the diameter was lower than the center temperature about 100 ℃. If replace the gas in the test with FLiNaK molten salt, which melting point is 450 ℃ and operating temperature is 550 ℃, the salt in the gap torus at the half the diameter of the flange is frozen, forming frozen salt seal.

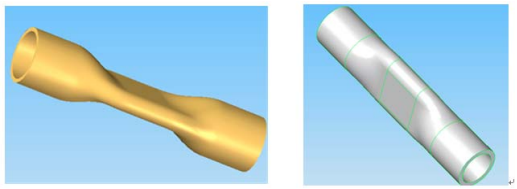

Fig.1 The structure diagram of freeze-valve

In June 2013, advance freeze flanges (Hastelloy C-276), including freeze flange with finned, as shown in figure 2, finished manufacture.

Fig.2 The figure of finished freeze flange

In 2012, TMSR developed the principle prototype pump. The pump has been successfully operated in FLiNaK molten salt high temperature test loop for more than 1 000 h. Its main design criterions criteria are:

Design temperature: 500~700 °C

Rate of flow: 5~15 m^3/h

Head: 20 m

Shaft seal assembly consists of dry gas seal, labyrinth seals and assisted seal of purge gas whose inlet is at pump adaptor flange. Bearing oil seal with non-contact oil sealing device, compared with the traditional contacting mechanical seal, the service life improved. Based on the principle prototype pump in 2013, TMSR developed chemical pump with large flow rate, amplified the flow consists of 15 m^3/h to 300 m^3/h. The overall structure is as shown in Fig.3.

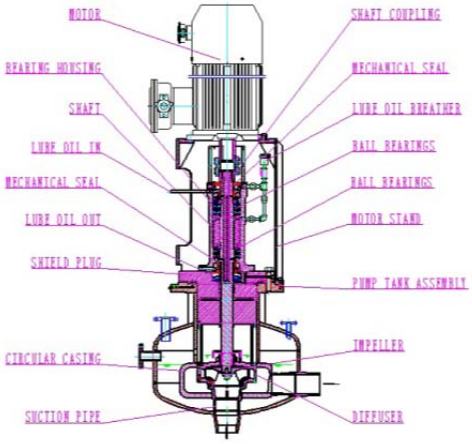

Fig.3 The structure diagram of pump

The high temperature molten salt throttle valve's design was carried out during 2014.5−2014.9, based on the structure of MSBE throttle valve. Its operating conditions are similar to ours. The overall structure design of valve with double bellows seal structure is showed on Fig.4.

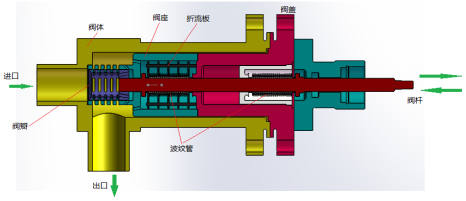

Fig.4 The structure diagram of pressure gauge

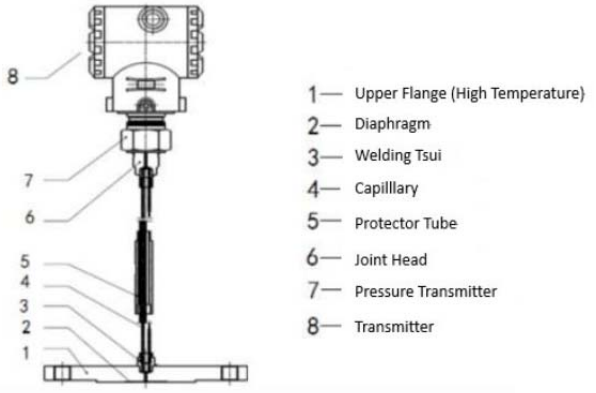

Fig.5 The structure diagram of high temperature molten salt throttle valve prototype

Develop the pressure gauge and the differential pressure gauge (Fig.5), applied to fluoride salt. The highest working temperature of two gauges is up to 700 ℃. The ranges of the pressure gauge and the differential pressure gauge are 1 MPa and 200 kPa respectively. The accuracy is 1% of the full range.

The pure nickel diaphragm and double diaphragm of pressure gauge and differential gauge are being tried to manufacture. The connecting seal technology is developed, such as pipe connecting sealing flange (Fig.6), high temperature gas seal performance. We also studied a variety of preheating insulation methods for pipe, such as ceramic heaters, electric heating rods, electric heating with tropical, high (medium) frequency induction heating, far infrared heating, forced convection heating.

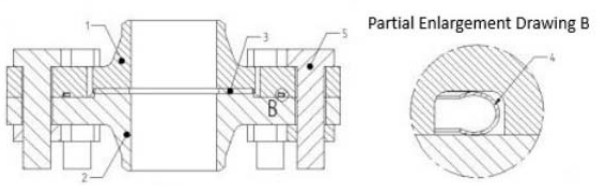

1. Female flange 2. Male flange 3.Graphite winding gasket 4.metal C ring seal 5.bolt and nut

Fig.6 The structure diagram of double sealing flange

TMSR complete primary circulation prototype pump of 304 stainless steel design, processing, installation, debugging, cold and hot state performance testing. The design of primary circulation engineering prototype pump built with Hastelloy N is completed. The design and analysis of mechanical valve engineering prototype has been completed, the manufacturing is being carried out. Complete the opening and closing performance test of advance freeze valve under different operating temperature test, analysis the rule of body temperature distribution in the process of cooling/heating .Complete frozen flange test-bed installation and debugging. The design of the pump test-bench using molten salt is completed, and start equipment manufacture of the bench .The loop gas heating and insulation device has been completed. Complete the FLiNaK high temperature molten salt test loop technical renovation, successfully operation.

熔盐回路试验平台

熔盐化学与工程技术部

建造熔盐回路试验平台，目的在于研究和解决熔盐回路及其相关设备的耐高温和耐氟盐性能，为开展大流量下高温氟盐流动特性（流速、压力损失）和传热特性（换热系数、换热面积、换热损失）研究和关键设备力学特性分析、气路设计能力验证、合金及石墨材料相容性试验以及控制、安全联锁、安全防护改进等提供研究平台。该试验平台还搭载了尾气处理系统，可为熔盐堆中氚控制系统的研制提供设备冷验证的平台，为氚监测系统的方案设计提供基础数据。2013−2014 年度，熔盐回路试验平台完成了对熔盐泵水力试验台架的升级改造、对 HTS 热工实验回路的维护改造，实现了 FLiNaK 熔盐高温试验回路的运行。依托两个回路组成的实验平台，取得了以下成果。

通过二年努力，建立高温熔盐工程试验回路（图 1），并顺利开展熔盐回路的长时间运行。积累熔盐操作和回路运行经验。同时，为大流量高温熔盐回路设备运行验证、热工和力学性能试验、控制与安全联锁系统改进等提供研究平台。根据试验回路的运行经验和实验结果，进行 TMSR-SF1 熔盐回路设计，设计过程充分考虑了腐蚀控制技术、预热与保温技术等。回路结构总体设计时需满足的设计准则，及所参考法规或标准包括但不限于：HAF201 研究堆设计安全规定；HAF202 研究堆运行安全规定；ASME-III核动力装置设备，第一册，NH 分卷，NC 分卷，NF 分卷；部分高温气冷堆与钠冷堆设计准则。系统示意图如下（图 2）：

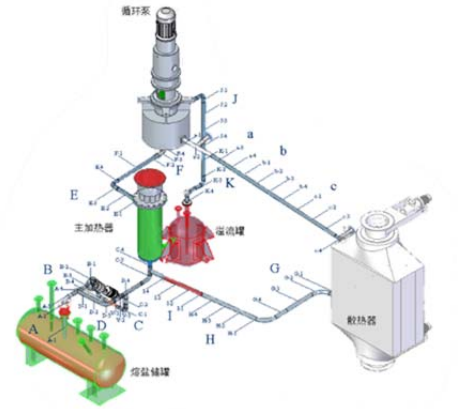

图 1　硝酸盐熔盐回路示意图

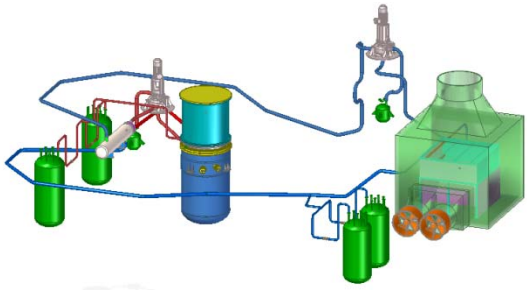

图 2　回路系统示意图

表 1　TMSR-SF1 10 MW 固态堆回路相关主要参数

	一回路	二回路
冷却剂(熔盐)种类	2LiF-BeF_2	FLiNaK
主泵质量流量调节范围 (kg/s)	45~150	161
主泵扬程 (×10^5Pa)	4	3
堆本体出入口压降 (×10^5Pa)	<1	
IHX 热交换器出/入口温度 (°C)	600/628	530/563
IXH 热交换器设计功率 (MW)	1~10 (低功率运行工况下为 0.02~0.2)	
主熔盐空气换热器设计热功率 (MW)	1~10 (低功率运行工况下为 0.01~0.1)	
主熔盐空气换热器空气出/入口空气温度 (°C)	260/40	

回路可以通过调节一、二回路主泵的流速以改变熔盐流量并进而改变换热功率。反应堆在 10 MW 功率下运行时，根据热工水力设计，一回路入口（接堆芯出口）温度为 628 ℃，出口（接堆

芯进口）温度为 600 ℃。二回路入口（IHX 二回路入口）温度为 530 ℃，出口（IHX 二回路出口）温度为 563 ℃。IHX 热交换器（双熔盐换热器）和主熔盐空气换热器的名义热功率均为 10 MW，以保证反应堆在 10 MW 功率下运行时将堆芯产生的 10 MW 热功率通过一、二回路最终传导至空气中。并综合考虑了一、二回路的系统安全功能，控制及安全联锁，测量等需求。

一回路由反应堆容器、主循环泵、熔盐-熔盐热交换器、溢流罐、管路和辅助系统组成。熔盐流过反应堆堆芯，通过与燃料球的热交换将裂变能带出反应堆堆芯，从堆芯出口流出的高温熔盐进入主循环泵罐，被主循环泵驱动进入熔盐-熔盐热交换器，与二回路冷却熔盐进行热交换，低温熔盐再流回反应堆堆芯入口，并进入反应堆堆芯与燃料球进行热交换及升温，完成一个循环。

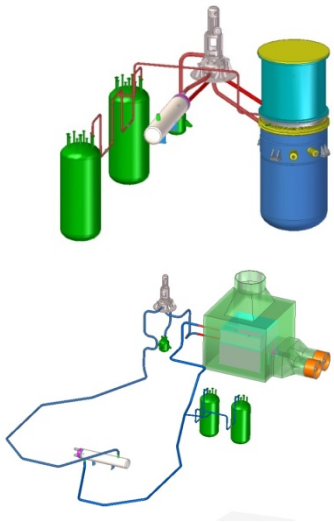

图 3　一回路熔盐装载及排放系统结构 二回路熔盐装载及排放系统结构

一回路熔盐装载及排放系统中采用阀门。当熔盐装载及排放完毕后，关闭阀门，隔离回路与加载及排放系统。该阀门设计为冷冻阀，无机械运动部件，提高了设备的运行可靠性。

二回路和一回路一样由循环泵、热交换器、溢流罐、管路和辅助系统等组成。所不同的是，二回路的热交换器是熔盐-空气换热器，通过该换热器将部分热量直接排放至空气中。二回路的熔盐在一、二回路间的双熔盐换热器中被一回路高温熔盐加热，被二回路循环泵抽出，驱动到二三回路间熔盐-空气换热器中与三回路热工介质空气进行热交换，加热三回路热工介质，同时二回路熔盐介质被热工介质冷却，冷却后的熔盐介质进入一、二回路间的换热器再次被一回路熔盐加热，完成一个循环。

在试验回路设计和运行经验的基础上，建成熔盐堆中不同形态氚的在线监测系统样机，氚在线测量系统原理图如图 4 所示。该在线监测系统能够实现总氚浓度的测量，并能够实现测量不同化学形态氚(HTO 和 HT)的活度，拥有惰性气体探测能力及 γ 补偿能力。

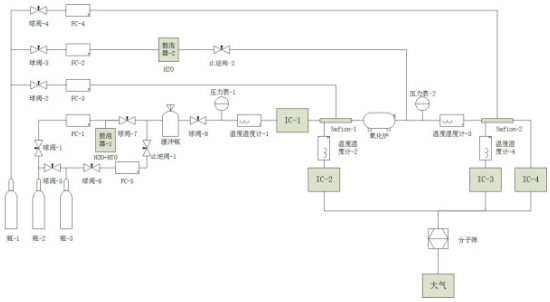

图 4　氚在线监测系统原理图

完成 TMSR-SF1 气路系统工艺原理设计。气路系统分为供气子系统、尾气处理子系统、气体加热子系统、气体稳压和超压保护子系统 4 个子系统。

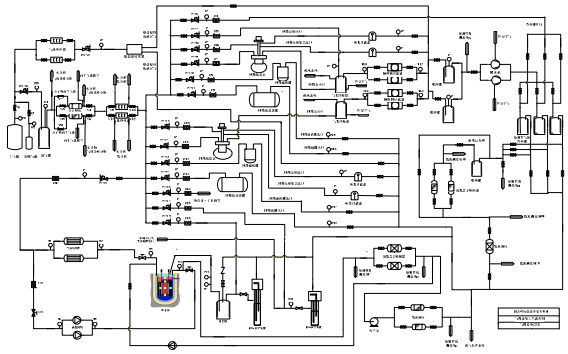

图 5　TMSR-SF1 气路系统工艺流程图

通过高温熔盐工程试验回路的运行，对熔盐泵的工作特性开展了大量研究。高温大流量熔盐泵研发取得阶段性进展，将小流量熔盐泵水力试验台架升级改造用于大流量熔盐泵水力试验，测试水介质下的大流量熔盐泵水力特性曲线及在线脱气功能，并观测流场分布情况。

Testing platform of molten salt loop

Department of Molten Salt Chemistry & Engineering

The purpose of construction of molten salt test loop platforms is to R&D the molten salt circuit system and its related equipment which is fluoride salt resistance and can perform well under high-temperature condition. It also serves as the platform for study of flow characteristics (flow rate, pressure loss) and heat transfer performances (coefficient of heat transfer, heat transfer area, heat loss) of fluoride salt under high temperature, research of mechanical characteristics of key equipment, verification of gas circuit design ability, test of materials compatibility of alloy and graphite, and study of control, safety interlocking and safety improvement, etc. A tail gas treatment system is also included in this test loop, the effect of which is to provide a cold state workbench for the development of tritium control system using in molten salt reactor and to support the scheme design of the tritium monitoring system by offering basic data.

A series of works have been done throughout 2013−2014. The hydraulic test-bed of molten salt pump was upgraded at first, then maintenance and upgrading of the HTS molten salt thermal test loop was finished. The FLiNaK high temperature molten salt test loop was successfully operated as well. The following results are obtained on basis of the HTS loop and the FLiNaK loop.

By the two years' efforts, the engineering-scale FLiNaK high temperature molten salt test loop, as shown in Fig.1, was firstly constructed, and has then been successfully running for a relatively long time. Experience about operation of molten salt and test loop was accumulated simultaneously. At the same time, it also provides a research platform for the operation and verification of key devices, thermal hydraulic and mechanical tests, and optimal design of control and safety interlocking system.

The TMSR-SF1 molten salt loop system design was carried out according to the operation experiences and experimental results of the above test loop, especially the corrosion control and the preheating and thermal insulation technologies. The design criteria and reference codes or standards that the loop structure design followed include but are not limited to: the HAF201 research reactor design safety regulations, the HAF202 research reactor operation safety regulations, the ASME-III rules for construction of nuclear facility components, specifically the subsection NH, NC, NF in division 1, and some design criteria of high temperature gas cooled reactor and sodium reactor. The schematic diagram of the system is shown in Fig.2.

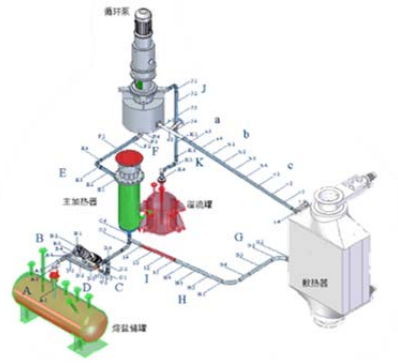

Fig.1 Schematic diagram of FLiNaK molten salt test loop

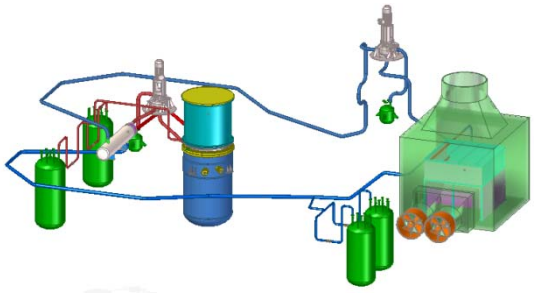

Fig.2 Schematic diagram of TMSR-SF1 loop design

Table 1 Major parameters of 10 MW TMSR-SF1 Loop

Contents	Primary Loop	Secondary Loop
Coolant (Molten Salt)	$2LiF\text{-}BeF_2$	FLiNaK
Range of primary pump mass flow (kg/s)	45~150	161
Head of primary pump	4	3
pressure drop between Core inward and outward ($\times10^5$Pa)	<1	
Temperature of IHX heat exchanger out/inlet (degree celsius)	600/628	530/563
Power of IHX heat exchanger (MW)	1~10 (low power operating condition at 0.02~0.2)	
Power of molten salt- Air heat exchanger(MW)	1~10 (low power operating condition at 0.01~0.1)	
Temperature of molten salt- Air heat exchanger out/inlet (°C)	260/40	

The heat transfer power of loop can be adjust by changing the flow of primary and secondary loop pump. When the reactor operates at the rated design condition 10 MW, according to the thermal hydraulic design, the primary loop inlet (the

core outlet) temperature is 628 °C, whilee the loop outlet (the core inlet) temperature is 600 °C. The secondary loop inlet (IHX inlet) temperature is 530 °C, and the outlet (IHX outlet) temperature is 563 °C. Both the rated thermal power of IHX heat exchanger and molten salt-Air heat exchanger are designed to be 10 MW, so as to assure that the maxium10MW heat can be finally transmitted from core to the air. The security functions of the loop system, control and safety interlocking, measurement requirements and so on were also fulfilled.

The primary loop system consists of reactor vessel, primary pump, molten salt heat exchanger, an overflow tank, piping and other auxiliary systems. When the molten salt flows through the reactor core, it would exchange heat with the fuel balls and takes the fission energy out. The heated molten salt will then be driven into the heat exchanger by the primary pump and transfers its heat to the secondary loop. After that the low temperature molten salt flows back to the reactor core and begins a new heat transfer circulation.

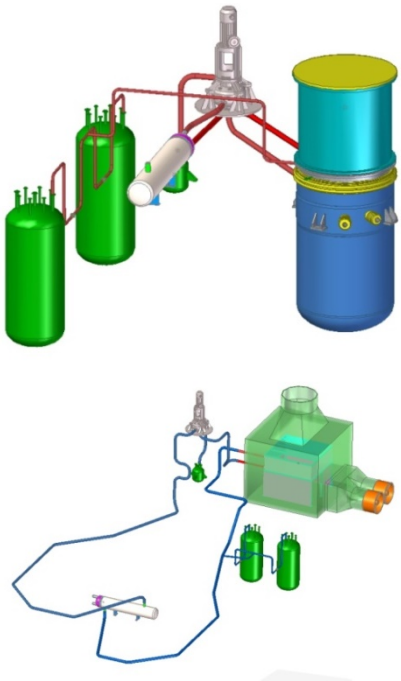

Fig.3 Mmolten salt loading and discharging system structure of the primary and secondary loops

Valves are used in the molten salt loading and discharge system of the primary loop. After molten salt is completely loaded or discharged, they are closed to isolate the loading and discharge system from circulating loops. The valves are called frozen ones since they have no mechanical moving components, which improves its operational reliability.

The secondary loop system composes of coolant pump, heat exchanger, overflow tank, piping and other auxiliary systems. The difference between these two loop systems is that the heat exchanger here is a salt-to-air one which transfers heat to environment. The molten salt of secondary loop is heated in the salt-to-salt heat exchanger firstly, and is then driven by the secondary coolant pump to the salt-to-air heat exchanger in which the heat will be exchanged to air. The cooled molten salt will be pumped back to the salt-to-salt heat exchanger to start a new heat transfer circulation.

Based on the succeeded design and operation of the testing loop, a prototype of tritium monitoring system which is able to determine different forms of tritium in molten salt reactor has been constructed. The principles of the online monitoring system are illustrated in Fig.4. The system is able to determine not only the total concentration of tritium but also the activities of different tritium pieces (such as HTO and HT). Furthermore the system has also the ability to detect the radioactive inert gas and to compensate for the gamma.

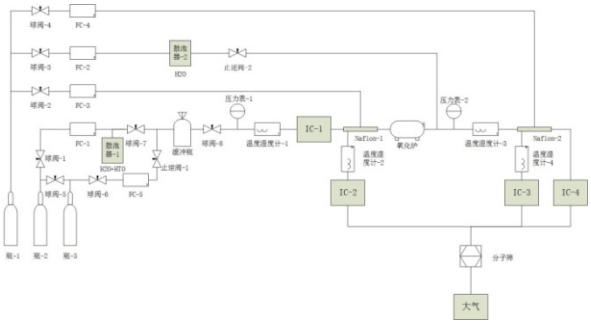

Fig.4 The principles of tritium online monitoring system

The design of the gas loop system for TMSR-SF1 has been completed. The process flowsheet of the gas loop is shown in Fig.5. The gas loop system consists of four subsystems, which are gas supply, off-gas treatment, gas heating and pressure stabilizing and overpressure protection subsystems.

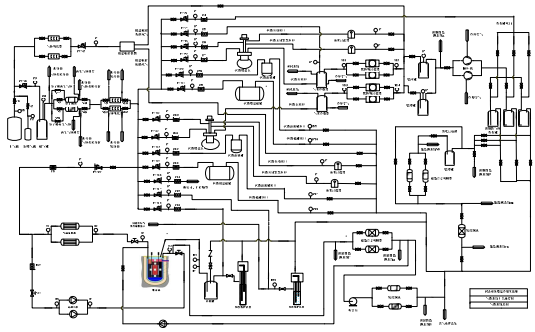

Fig.5 TMSR-SF1 Gas loop process flowsheet

Working characteristics of the molten salt pump have been extensively studied through the operation of the high temperature molten salt engineering test loop. By upgrading a small flow hydraulic test stand of the molten salt pump, research progress has been made in the R&D of large flow high temperature molten salt pump. The hydraulic characteristic curves and online degasification function were tested via water medium in this stand, in which the flow field distribution has also been observed.

熔盐化学研究平台

熔盐化学与工程技术部

为了满足熔盐堆设计、建造过程中对熔盐材料及相关技术、知识的需求，我们建立了熔盐化学研究平台。其主要任务是为熔盐堆建造提供合格的熔盐材料，同时为堆设计提供熔盐相关物理化学性质参数及化学安全知识。通过熔盐化学研究平台的建设，我们具有全面评估熔盐冷却剂各方面性能的能力，可以为熔盐堆冷却剂的选择及质量标准的制定提供建设性意见。2013−2014 年度，熔盐化学研究平台课题取得如下重要进展。

建立了完善的熔盐热物性测试平台。研制了样品制备炉、淬火炉、红外加热炉等样品制备与预处理设备，针对不同热物性参数测试的特点与要求，建立了相应的样品制备与预处理方法。通过旋转法实现了高温熔盐粘度的测试，测试范围 1.6~16 cP，测试精度小于 0.2 cP。通过激光闪光法实现了高温液态熔盐热扩散系数的测试，测试精度小于 10%。掌握了熔盐熔点、比热、热焓、接触角、表面张力、粘度、导热系数、密度、初晶温度、电导率等熔盐热物性参数的测试方法。在文献数据的基础上，完成 FLiBe 及 FKZr 熔盐体系热物性数据评估报告。掌握了通过二元系热力学数据库外推多元系相图的方法，利用该方法完成了 FLiBeThU 6 个二元系和 4 个三元系的数据库评估，初步建立了燃料盐热力学数据库。为满足涉铍废气处理的需要，研制了撞击流泡沫捕捉塔铍废气处理设备，能够有效的去除铍废气，同时不产生二次污染及设备维护导致的人员伤害。

表 1　FLiBe 熔盐体系数据

物理量	密度	粘度	比热	热导率	蒸汽压	表面张力	熔化热	电导率	熔点
单位	g/cm^3	cp	J/gK	W/mK	mmHg	N/m	J/g	ohm^{-1}cm^{-1}	Kelvin
数据	1.938	5.502	2.391	1.113	0.05056	0.179	444.898	2.850	733
温度	973K	973K	973K	973K	1173K	973K	733K	973K	
不确定度	±2.15%	±2%	±3%	±3%	——	±3%	——	±2%	± 10K

建立了以磷酸胆碱沉淀法测定锂、钠离子选择电极法测定钠、四苯硼钠重量法测定钾、硝酸镧电位滴定法测定氟的分析流程。明确了FLiBe和FKZr熔盐常量组分的分析方案。建立了熔盐中阴离子杂质的离子色谱定量分析方法。FLiNaK中常见阴离子Cl^-、NO_2^-、NO_3^-、SO_4^{2-}、PO_4^{3-}，测定加标回收率为98%~110%，相对标准偏差<1.0%，最小检出浓度<2 μg/g。

建立了固态 FLiNaK 熔盐 LIBS 半定量分析方法；与同步辐射结合，初步研制了适合硝酸盐、碳酸盐 XAFS 测试的液态样品测试原型装置。在充分考虑堆物理设计需求、熔盐材料相容性要求、化工净化工艺水平及分析检测水平等多方面因素的基础上，初步规定了进堆核纯熔盐的质量控制参数。

在先进熔盐分析检测技术方面，我们建立了熔盐光谱分析装置、熔盐浊度仪、熔盐电化学原位分析装置及方法等，并应用于熔盐热辐射吸收、熔盐浊度分析、氧化物沉淀行为等熔盐堆重点关注的熔盐物理化学行为研究中。

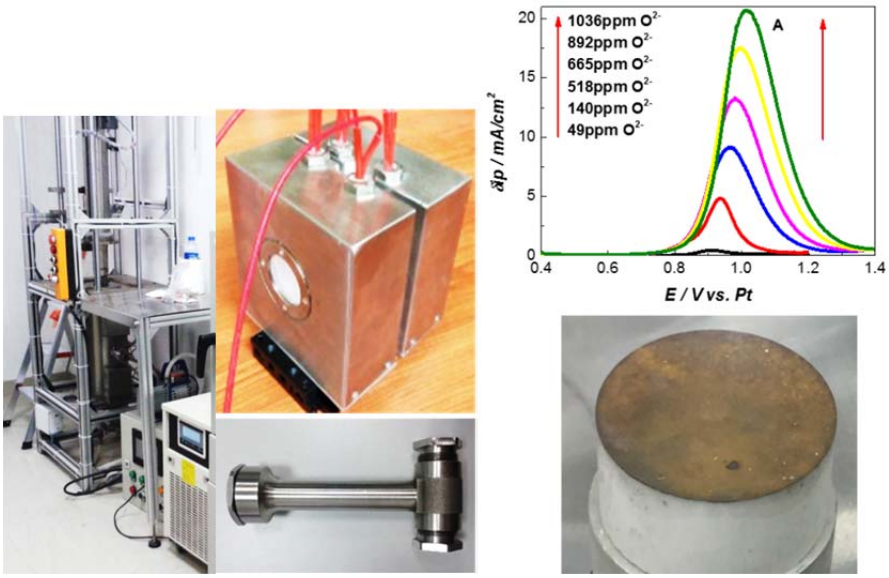

图 1　熔盐浊度仪（上），熔盐光谱池（中），熔盐电化学原位分析（下）

完成了 5 kg 级基于 HF-H_2 法的熔盐制备净化小试装置的设计和加工，并成功运行获得总氧低于 100 μg/g 的高纯 FLiNaK 产品。完成了 FLiNaK 高温试验回路运行所需的 1 030 kg 熔盐的转运装载任务。在此基础上设计了 TMSR-SF1 熔盐转运方案，并完成了其中关键设备熔盐转运阀的设计。设计加工了一套 TMSR-SF1 在线取样样机，并完成了设备的初步性能测试。

图 2　5 kg 级熔盐制备样机（上左）及 FLiNaK 熔盐产品照片（上右）在线取样样机 3D 设计图（下左）和熔盐转运阀设计图（下右）

核纯 FLiBe 制备纯化实现突破，纯化后的 FLiBe 熔盐优于 MSRE 水平，图 3 是我们制备的 FLiBe 熔盐与 MSRE 熔盐主要杂质含量的对比。

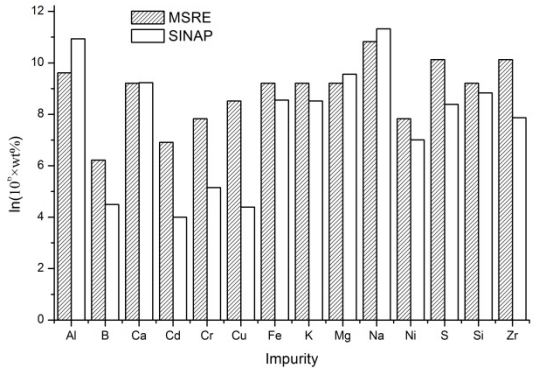

图 3　FLiBe 熔盐杂质含量对比

为满足涉铍废气处理的需要，研制了撞击流泡沫捕捉塔铍废气处理设备，能够有效的去除铍废气，同时不产生二次污染及设备维护导致的人员伤害。

涉铍安全防护的关键技术问题是含铍废气的处理。传统布袋除尘法，清灰困难，易产生二次扬尘，去除效率低，不满足项目要求；电极除尘法虽然可以增大电极以提高除尘效率，但是由于氟化盐的强腐蚀性，也无法适用；常规的洗涤法，由于废气排放带水量大，容易将溶解在水中的氟化盐尤其是氟化铍带入大气环境中造成污染，因此也无法适用，项目需要选择一种治理含氟化盐特别是氟化铍废气的有效方法。

2013−2014 年度，项目采用撞击流、泡沫捕捉的复合型原理，成功研制了超声波增湿-撞击流氟化铍净化器，经验证，空气中含铍浓度 4 μg/m^3 时，去除效率达 98%以上。车间空气总颗粒物浓度 0.12 μg/m^3 时，一次净化后废气的铍含量降为 0.08 μg/m^3，远优于国家规定的排放值(0.5 μg/m^3)，解决了含铍废气的处理技术难题。在此基础上，发展了处理能力为 10 000 m^3/h 的含铍废气处理系统。

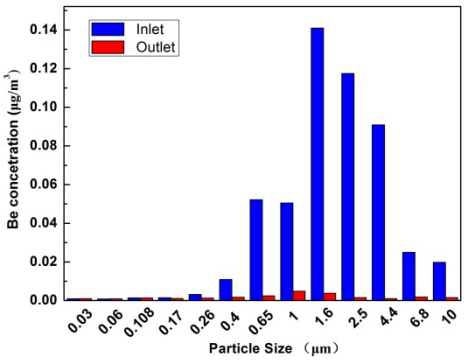

图 4　撞击流泡沫捕捉塔实验室空气净化器除尘效率

图 5　处理能力为 10 000 m^3/h 的含铍废气处理系统

Molten salt chemistry study platform

Department of Molten Salt Chemistry and Engineering

A molten salt chemistry study platform was built to meet the knowledge and technology demand of molten salt reactor design and construction. The main task of this study platform is to provide qualified molten salt for the experimental reactor along with various physical and chemical property data and chemical safety knowledges. These studies will help us have the ability to fully evaluate the performance of molten salt coolant, which can provide constructive suggestions for the selection of molten salt reactor coolant and the development of quality standards. In the year 2013−2014, we made following important progresses.

A perfect lab for testing thermophysical properties of molten salt is established. The sample preparation and pretreatment equipment such as sample preparation furnace, quenching furnace and infrared heating furnace were developed. Sample preparation and pretreatment methods were established according to the characteristics and requirements of different thermophysical parameters. The viscosity at high temperature of molten salt can be tested through the rotating method, the test range of 1.6~16 cP with the accuracy of less than 0.2 cP. By laser flash method, the thermal diffusivity of liquid molten salt can be determined, the test accuracy of less than 10%. The test methods for measuring the physical properties of molten salt such as melting point, specific heat capacity, enthalpy, contact angle, surface tension, viscosity, thermal conductivity, density, liquidus temperature and electrical conductivity were obtained. On the basis of the literature data, the thermophysical data assessment report of FLiBe and FKZr molten salt systems was completed. The method of extrapolating multivariate phase diagram through the thermodynamics database of the binary system was mastered. By this method, the six sub-binary systems and four sub-ternary systems of FLiBeThU was thermodynamically assessed, and the thermodynamic database of the fuel molten salt was established.

Table 1 FLiBe physical properties

	Density	Viscosity	Heat capacity	Thermo-ductivity	con-	Vapor pressure	Surface tension	Melting heat	Electro-ductivity	con-	Melt point
Unit	g/cm^3	cp	J/gK	W/mK		mmHg	N/m	J/g	$ohm^{-1}cm^{-1}$		Kelvin
Value	1.938	5.502	2.391	1.113		0.05056	0.179	444.898	2.850		733
Temp.	973K	973K	973K	973K		1173K	973K	733K	973K		
Uncertainty	±2.15%	±2%	±3%	±3%		——	±3%	——	±2%		± 10K

The process and method for quantitative analyzing four major components of FLiNaK was established. Gravimetric method was employed to determine the content of lithium and potassium with choline phosphate and sodium tetraphenylboron respectively. The percentage of sodium was measured with ion selective electrode method. Potentiometric titration with lanthanum nitrate was used for the analysis of fluorine ion. The protocol for the determination of main components of FLiBe and FKZr was also clarified. The method to analysis conventional anion in molten fluorides including Cl^-, NO_2^-, NO_3^-, SO_4^{2-} and PO_4^{3-} by ion chromatography was established with recovery rate 98%~110% and relative standard deviation less than 1%. The minimum detection concentration of anionic impurities was 2 μg/g. A semi-quantitative method for solid FLiNaK has been established with laser-induced breakdown spectroscopy (LIBS). A prototype sample compartment of synchrotron radiation-XAFS suitable for liquid nitrate and carbonate has been developed. The chemical specifications of coolant and fuel salt for TMSR were drawn based on the requirements of physical design, the compatibility between molten salt and structural materials, the technological level of purification and the detection limit of chemical analysis.

In the area of advanced analysis technique, UV-visible absorption spectrometer, turbid meter and in situ electrochemical device applied to molten salt were built and applied in the research on physical chemistry properties including thermal radiation absorption behavior, turbidity and oxide precipitation behavior in molten salt reactor.

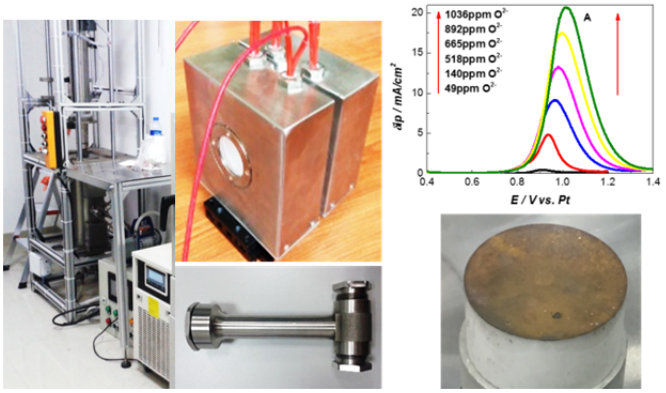

Fig.1 Molten salt turbid meter (left)，molten salt spectrum cell (middle)，in situ electrochemical analysis research (right)

A pilot plant with a capacity of 5 kg/batch was set up and test-operated to produce high quality FLiNaK by the classical H_2-HF process. Oxide content of the product was kept stable and lower than 100 μg/g. The knowledge obtained was then used for design of full-scale production systems and commercial products. 1 030 kg of FLiNaK was produced and transferred into a closed-loop pump-driven high temperature test equipment. Furthermore, in order to isolate FLiNaK from air during transferring or sampling, an interlinking valve between storage tank and test loop, as well as a sampler was newly designed and tested.

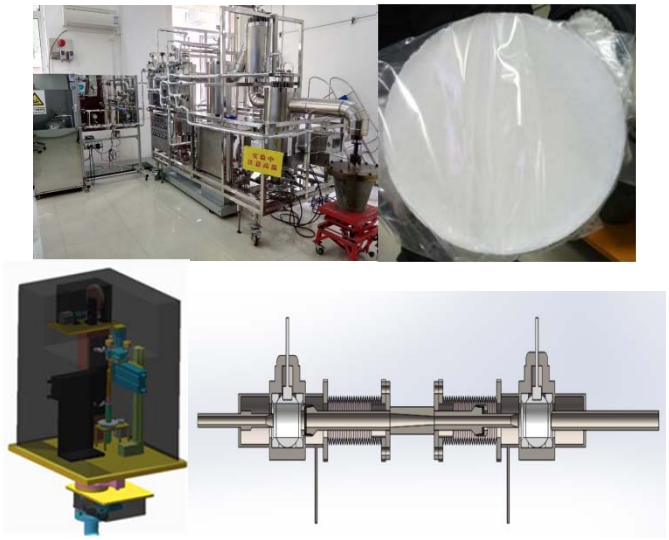

Fig.2 Pilot plant with a capacity of 5 kg FLiNaK per batch (up left), photograph of high quality FLiNaK (up right), 3 D models of of online sampler (down left) and transferring valve (down right)

Nuclear-grade FLiBe was successfully prepared. The contents of impurities in FLiBe after purification by us were less than those purified by MSRE. The specific data were compared in Fig.3.

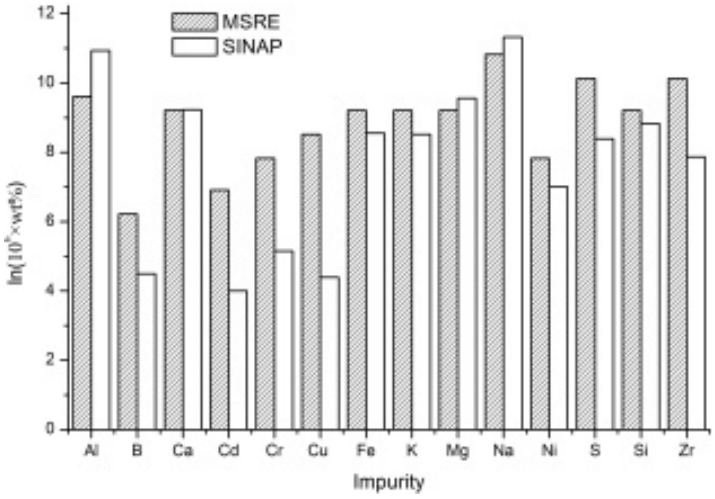

Fig.3 Comparison of contents of impurities in FLiBe after purification between

In order to meet the needs of disposal of beryllium-contained waste gas, a impinging stream bubble capture tower has been developed. This equipment can work effectively, produces no secondary pollution and has no personnel damage caused by maintenance.

The key problem of beryllium safety protection is beryllium-contained waste gas treatment. Traditional dust filtration with bag method has a lower dust removal efficiency and producing secondary waste when changing bag, which does not meet the requirements of this project. Although using large electrode could improve the electrode dust removal efficiency, it is unsuitable because of the strong causticity of fluoride salt. The conventional gas washing tower method is also inappropriate, as a result of waste water emission that containing beryllium fluoride, this method could take the fluoride salt especially beryllium fluoride dissolved in the water to the atmospheric environment and cause pollution. Therefore, an effective method should been chosen to disposal the waste gas beryllium fluoride.

The project developed a impinging stream bubble capture purifier of beryllium fluoride successfully during 2013 to 2014, that is combining impinging stream and bubble capture. It is verified that its total dust removal efficiency is more than 98% when the beryllium concentration in air is 4 μg/m^3. Meanwhile, when the concentration of total particulates is 0.12 μg/m^3 in the air of workshop, the beryllium concentration in waste gas decreases to 0.08 μg/m^3 after the first purification. This disposal result is far superior to the national emission standard (0.5 μg/m^3), It shows that this purifier can resolve the treatment problem of beryllium-contained waste gas. On the basis of the

research, a beryllium-contained waste gas disposal system has been developed with a processing capacity of 10 000 m^3/h.

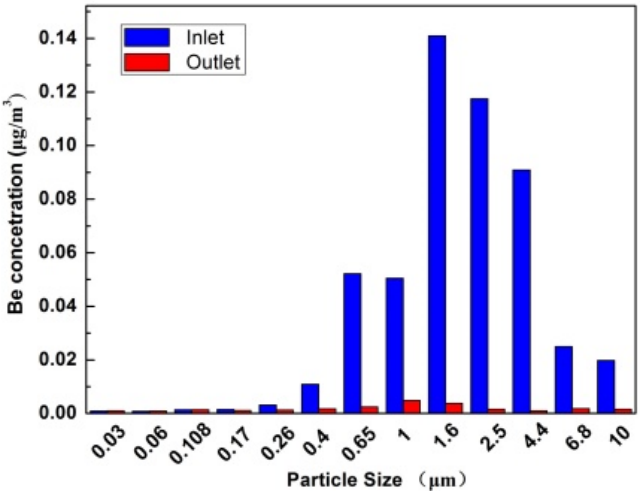

Fig.4 The dust removal efficiency of laboratory air purifier composed of impinging stream bubble capture tower.

Fig.5 The beryllium-contained waste gas disposal system with a processing capacity of 10 000 m^3/h

放射化学与工程技术部

2013−2014 年度，反应堆燃料技术研究课题组在前期工作的基础上，主要开展了如下工作：球形燃料元件破损率和裂变产物释放的理论分析；钍基球形燃料元件的研制，包括燃料核芯的制备、高温流化床反应装置的设计加工以及球形燃料元件压制研究，包括模具的设计加工和使用等工作；球形燃料元件的检测技术，以及钍基核燃料中痕量杂质的化学分析方法；海水提铀材料制备装置的设计和加工，以及海水提铀实验研究。

球形燃料元件的安全分析

建立了包覆颗粒燃料元件失效概率的分析方法，完成了 TMSR-SF1 燃料元件在正常运行和事故工况下的燃料破损率和裂变产物释放分析。现有的球形燃料元件设计在运行和事故工况下 Cs、Sr、I、Ag 等主要放射性核素释放份额低于 10^{-5}，满足反应堆设计要求（图 1）。

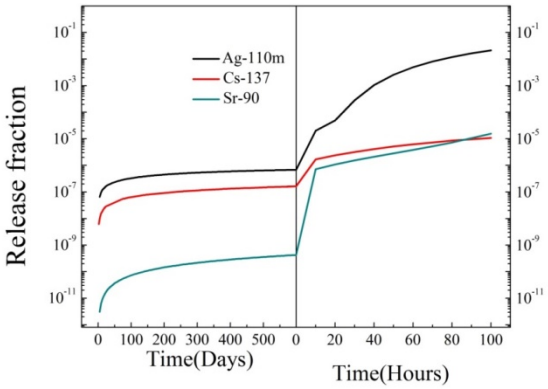

图 1 TMSR-SF1 正常运行（左）和事故工况（右）下 ^{137}Cs、^{110m}Ag 和 ^{90}Sr 的释放份额

球形燃料元件研制

建立了燃料元件研发实验室，用于开展新型球形燃料元件的制备；实验室面积总计 520 m^2，其中燃料制备实验室 300 m^2，分析检测实验室 220 m^2。搭建了氧化钍核芯制备装置，其规模为每批 100 g ThO_2 核芯颗粒。通过模拟实验，制得了表面光滑、球形度良好的 ZrO_2 烧结小球（模拟 ThO_2 燃料核芯）。开展了 ThO_2 燃料核芯制备的工艺研究，考察了内胶凝与外胶凝两种方法制备氧化钍核芯湿球的效果，通过对比确定采用外胶凝法工艺路线。通过研究优化了溶胶凝胶法工艺条件，得到了能获得具有较好质量的凝胶颗粒的工艺参数（图 2）。

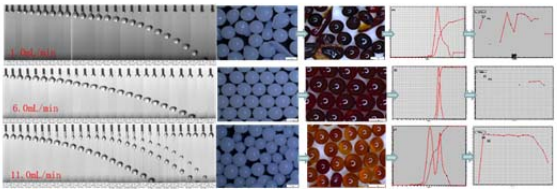

图 2 溶胶流速对球形度及尺寸分布的影响

开展了流化床冷态模拟实验，其结果用于优化高温流化床的设计；完成 FB-CVD 系统高温流化床反应炉和包覆气体供应系统、尾气处理系统的设计（图 3）。

采用冷（准）等静压方法制备球形燃料元件，图 4 显示了研制的硅胶模具，它由上模、中模和下模组成。利用研制的硅橡胶模具成功制备了直径 60 mm 的基体球。

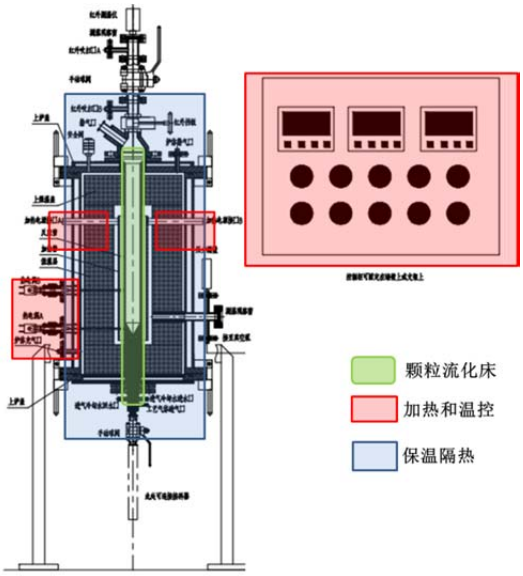

图 3 高温流化床气相沉积炉

图 4 硅橡胶模具设计效果图和实物照片

海水提铀

完成了 0.5 MeV 低能电子加速器的配套设备纤维传送系统和纤维接枝聚合装置、肟化装置的设计及采购。目前电子束辐照接枝试验线的相关设备已经进场，预计 2015 年 1 月底完成调试工作。完成了纤维接枝聚合装置和肟化装置的设计及采购工作，目前该套设备在厂家进行制造，预计安装验收时间为 2015 年 3 月。成功制备了 UHMWPE 纤维长丝吸附材料和 HDPE 纤维基吸附材料。实验室海水吸附装置正常运行，已完成约 50 个批次的吸附性能评估。评估显示一种偕胺肟基超高分子量聚乙烯(AO-UHMWPE)材料在模拟海水中(U 浓度 3.3×10^{-3} ppm)对 U 的吸附性能达 3.3‰。完成三处现场海水吸附场地调研，确立一个现场海水吸附试验点（图 1-5）。

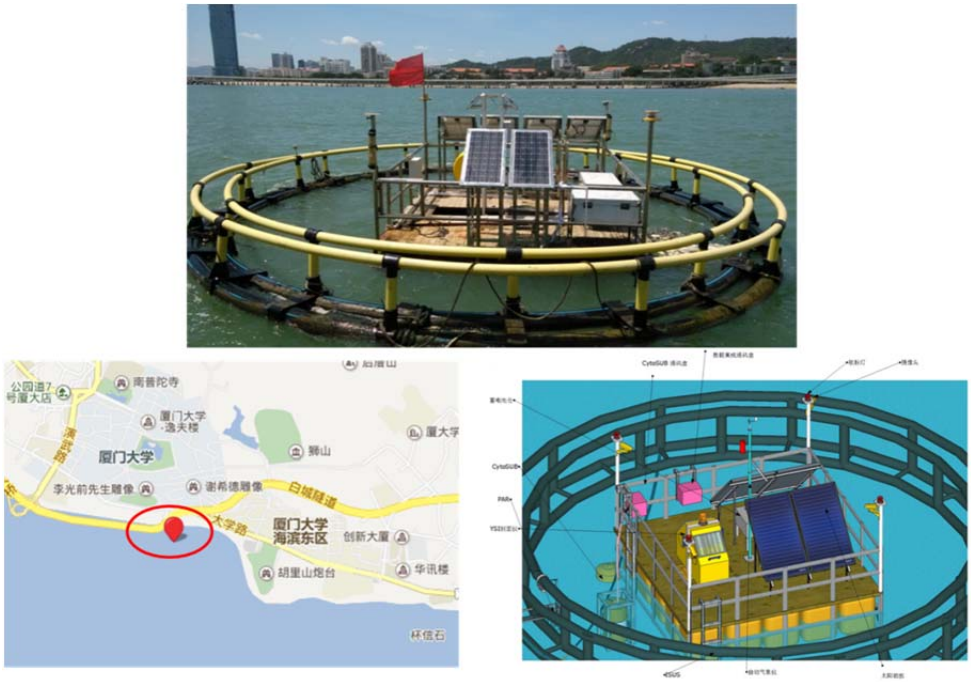

图 5 近海生态动力浮标检测平台

下一年度将在上述工作的基础上开展如下工作：改进钍基燃料核芯的制备工艺，得到合格的二氧化钍核芯烧结小球，开展高温流化床装置的加工和调试工作，开展球形燃料元件制备工艺研究；开展现场海水提铀吸附试验研究。

Reactor fuel technology research group

Department of Radiochemistry and Engineering

During 2013−2014, the reactor fuel technology research group carried out mainly the following work among others: the computational analysis of the broken rate and fission products release of the TRISO-coated particle fuel elements; the development of thorium-based fuel pebbles, including the preparation of thorium fuel kernels, the design and the manufacture of a Fluidized Bed-Chemical Vapor Deposition (FB-CVD) system; the pressing of spherical fuel elements employing specially designed compacting molds; the characterization methods of fuel pebbles, including the chemical analysis of impurities in thorium compounds; design and manufacture of fabrication facilities for uranium-adsorption materials, and the experimental study on the extraction of uranium from simulated and real seawaters.

Safety analysis of spherical fuel elements

A method for the probability analysis of the TRISO-coated particle fuel performance was established, and the broken rate analysis and the fission product release analysis of TMSR-SF1 fuel elements in normal operation and accident conditions was completed. The results (Fig.1, for example) showed that the release fractions of Cs, Sr, Ag, I and other important radionuclides from the spherical fuel elements, either in normal operation or in accident conditions, were all less than 10^{-5}, which satisfies the design requirements of the TMSR-SF1 reactor.

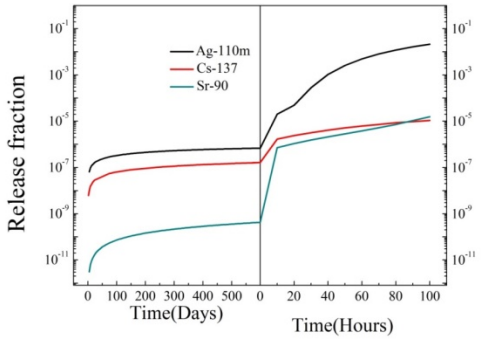

Fig.1 The release fractions of ^{137}Cs, ^{110m}Ag and ^{90}Sr under normal(left) and accident (right) conditions of TMSR-SF1

Fabrication of spherical fuel elements

A nuclear fuel R&D laboratory was established, with a total area of 520 m^2, 300 m^2 for fuel preparation and 220 m^2 for fuel characterization. Its main task is currently the development of new-type fuels for TMSRs. The thoria kernel preparation devices were built, with a capacity of 100 g ThO_2 kernels per batch. Using ZrO_2 as a modeling compound, good spherical sized ZrO_2 sintered particles with smooth surfaces were obtained. Then, the preparation of ThO_2 kernels was studied extensively. Both the external gelation method and the internal gelation method were studied, and finally the external gelation method was adopt for its operation convenience. The sol-gel process for preparing the gel particles was studied and the process parameters were optimized (Fig.2, for example). As a result, the gel balls we obtained have good appearance. However, in the heat treatment processes (especially calcination and sintering) much of them were cracked for reasons not identified.

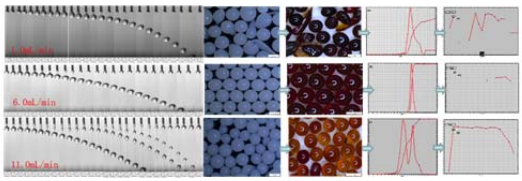

Fig.2 Effects of sol velocity on the spherical appearance and the size distribution of thoria gel balls

Simulation experiments were carried out upon a room temperature fluidized-bed device, and the results were used to optimize the design of high temperature FB-CVD. The design of the FB-CVD system was completed (Fig.3), including a high temperature fluidized bed reactor and its auxiliary devices for process controlling, gas supply and exhaust gas treatment, and so on. The whole system will be set up and tested in the next year.

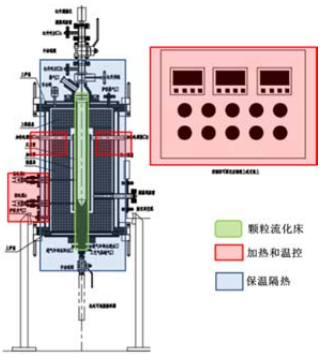

Fig.3 Fluidized bed-chemical vapor deposition system

Spherical fuel elements are prepared by a cold (quasi) isostatic pressing method. Fig.4 shows the developed silicone rubber mold, which consists of three parts: upper mold, middle mold and lower mold. Spherical matrix elements with 60 mm diameter were successfully pressed by using the developed silicone rubber mold.

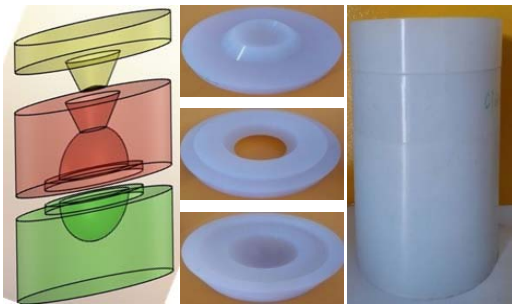

Fig.4 Design sketch and photos of Silicone Rubber mold

Uranium Extraction from seawater.

Fiber transmission system under beam of 0.5 MeV EB and the amidoximation equipment were designed and ordered. The EB irradiation equipment and associated equipment are in place, and the commissioning work will be finished in January 2015. The acceptance inspection of the grafting equipment and amidoximation equipment will be performed in March 2015. Amidoxime-based (AO) ultrahigh-molecular-weight polyethylene (UHMWPE) and high density polyethylene (HDPE) fibers were synthesized. Simulated seawater flow-through equipment was operated and 50 batches adsorption test were finished. Capacity from one type of the AO-UHMWPE fibers reached 3.3 mg U/g. Three places for natural coastal marine seawater adsorption were investigated and one of them was confirmed to carry out seawater adsorption test (Fig.5).

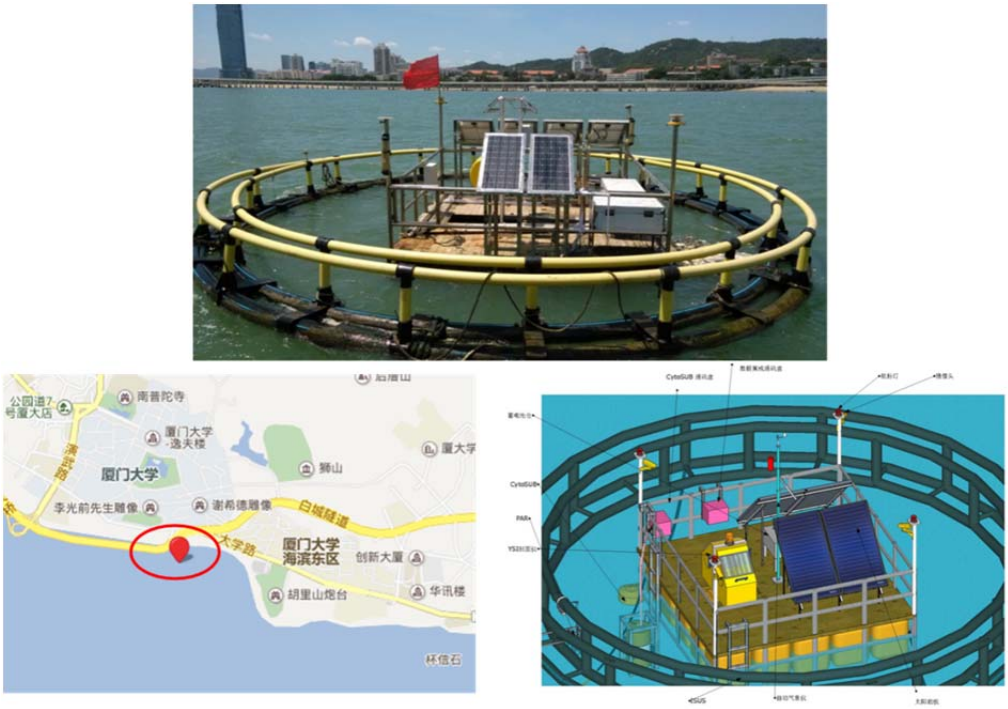

Fig.5 Ecological powered offshore floating detection platform

熔盐机械部和堆材料一部

在中国科学院战略先导专项《未来先进核裂变能-钍基熔盐核能系统》资助下，围绕国内首个熔盐堆材料的国产化和性能评估，开展了一些列的科学研究。熔盐堆材料主要包括合金结构材料和慢化剂石墨材料。国产化熔盐堆合金为 GH3535 镍基合金，国产化石墨为细颗粒石墨。

GH3535 合金研制中面临的主要难点包括：合金微量元素的控制、大锭型组织偏析问题、热加工开裂控制、热加工工件性能稳定性控制等。

熔盐堆用核级石墨目前采用超细颗粒骨料技术，在炭化阶段容易诱发材料的开裂，造成大规格国产核级石墨材料的成品率不高，性能不稳定，直接会增加核石墨材料的成本造价和制造周期，同时这类石墨也缺少相关熔盐和辐照的性能数据。

堆材料主要作为重要纽带，发现问题，分析问题，解决问题，促进工厂进行材料改进，性能得到保障，研发适合熔盐堆的材料，为熔盐堆安全服役提供有力保障。

合金结构材料

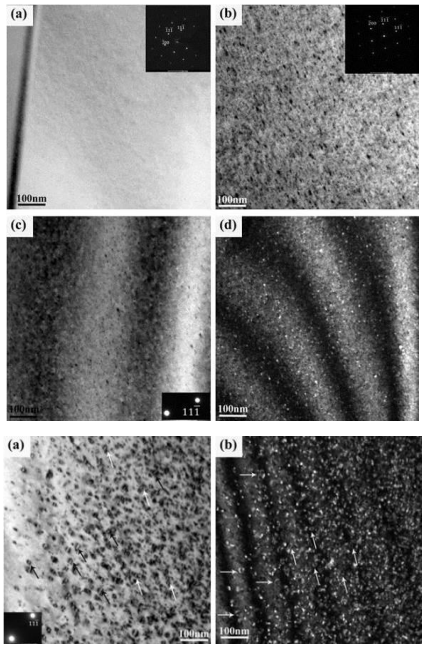

图 1　辐照前后 GH3535 样品的微结构

本实验表明，在低剂量辐照的样品中可以观察到纳米级的“黑斑”缺陷。以往的研究认为这些“黑斑”实质上是位错环，而且属于间隙型位错环(I-loops)。随着剂量的增加，“黑斑”逐渐演变为较大的位错环，并且位错环的密度和尺寸随着辐照剂量增加而增大。这些位错环可以吸收黑斑缺陷，随着剂量的增加，“黑斑”的密度减小，高剂量时反而观察不到明显的“黑斑”。

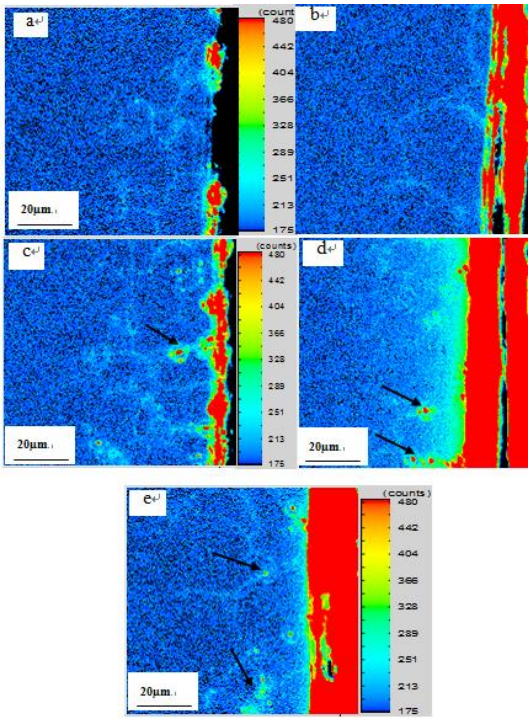

图 2　GH3535 合金在 700 ℃保温 100h 渗 Te 后裂变产物 Te 元素分布

GH3535 合金在 700 ℃保温 100 h 后，试样截面 Te 元素分布图电子探针结果。Te 在合金中的扩散方式主要为沿晶界扩散，且随 Te 含量升高，晶界处 Te 含量明显增大，出现如图中的黑色箭头所示 Te 的富集。

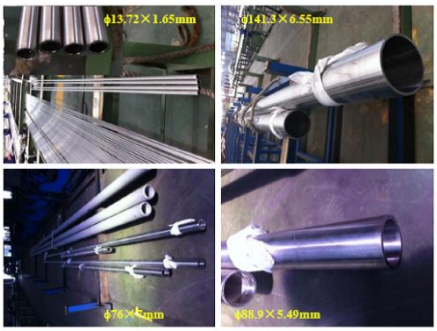

图 3　首次轧制成功的管材

轧制成功的各个规格的 GH3535 合金管材，该

管材经过拉伸性能、压扁性能、无损探伤等多种性能复验，完全满足预期性能指标。后续需要提高无缝管材的成材率。

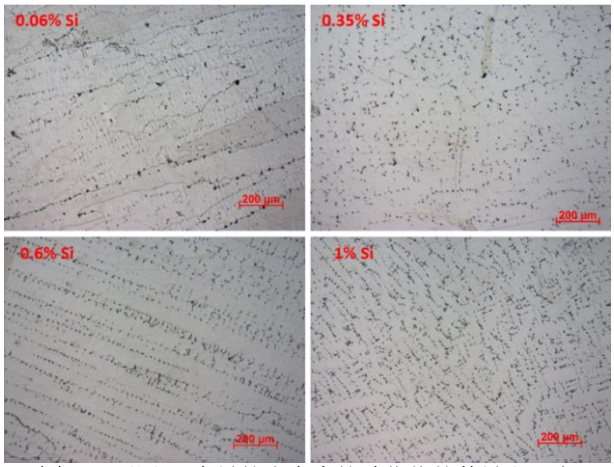

图 4　不同 Si 含量的合金中的碳化物的数量和形态

TEM-EDX 结果表明：Si 含量为 0.188%，0.319%和 0.562%合金中，碳化物的 Si 含量与合金总体 Si 含量成正比，Si 含量的富集程度最高达到 6 倍。正是由于 Si 在 M6C 中的富集导致碳化物热稳定性和形成能力的提高，从而改变了合金中碳化物的含量。值得注意的是，碳化物中的饱和 Si 含量约为 3.5%。

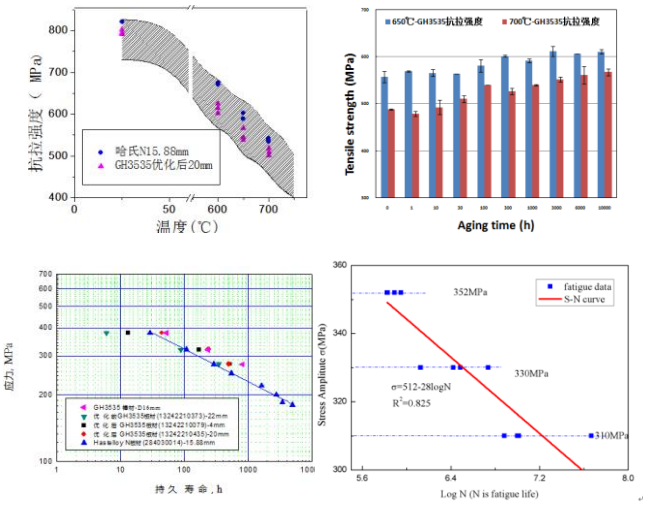

图 5　合金力学性能对比

进口 15.88 mm 板材和国产 20 mm 板材在力学性能上的差别，其中阴影部分为 ORNL 认为的材料验收标准。可以看出，优化后国产材料的抗拉强度比进口低 50 MPa 左右，屈服强度比进口材料低 30 MPa 左右。但延伸率在室温和 600 ℃与进口合金相当，在 650 ℃和 700 ℃要比进口合金高 5%~10%。但国产材料的数据点比较分散，说明材料的均匀性不及进口合金。GH3535 合金时效 10 000 h 的拉伸性能。650 ℃和 700 ℃，随着时效时间增加，GH3535 合金的屈服强度一直比较稳定，而抗拉强度呈缓慢增加趋势，延伸率和断面收缩率呈先增加（1 000 h 之前）后降低趋势（1 000 h 之后）。GH3535 合金材料优化后较优化前的 650 ℃高温持久性能有提高，且优化后（4 mm 板和 20 mm 板）持久性能均略高于进口 Hastelloy N 合金。高周疲劳方面，对优化后 GH3535 板材横向进行了室温高周疲劳测试。表 3 为不同应力水平下的循环寿命，图 5 则是依据 ASTM E739 绘制的 S-N 曲线。GH3535 室温屈服强度为 310 MPa，在该应力水平下材料仍具有接近一千万周的循环寿命，显示其在室温下具有良好的高周疲劳性能。

石墨材料

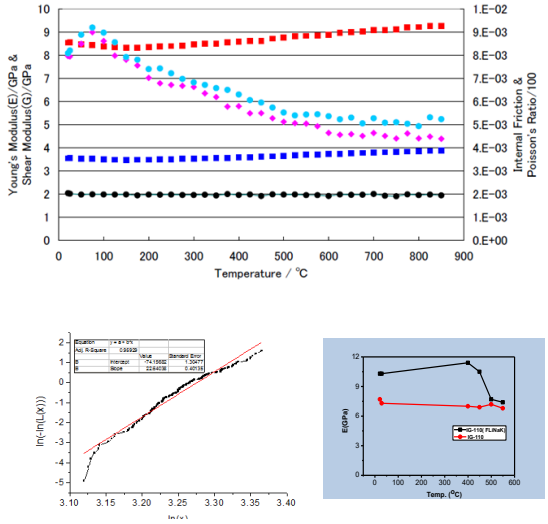

图 6　石墨性能测试

Weibull 分布是核石墨分散性重要的性能指标。根据德国 DIN 51914 抗拉强度测定标准，通过对尺寸为 400 mm×400 mm×600 mm 的石墨坯块进行取样，取样数量为 136 个样品，测定了 NG-CT-10 抗拉强度 Weibull 分布。核石墨 IG-110 弹性模量和剪切模量随温度升高缓慢上升，表明核石墨弹性模量随温度的变化趋势与强度一致。测定了熔盐对弹性模量和剪切模量的影响，熔盐熔点以前，浸渍熔盐试样弹性模量显著增加，浸渍熔盐后弹性模量显著降低到与未浸渍熔盐样弹性模量相等。浸渍熔盐后试验剪切模量显著大于未浸渍熔盐空白试样。

不同压力浸渗后三种炭/炭复合材料的断口 SEM 图像。在较低浸渗压力下，703 试样的熔盐浸渗量非常低。在 SEM 下基本观察不到熔盐浸渗痕迹。提高浸渗压力至 6×10^{-5} Pa 时，可以看出，熔盐沿纤维束间的孔隙浸渗入复合材料的内部。IMR 试样在 2×10^{-5} Pa 浸渗压力下即产生了 6.05%的熔

盐浸渗量。从其断口 SEM 图像中可以看出，熔盐在复合材料内部主要沿纤维束内的大孔、纤维束间孔浸渗。

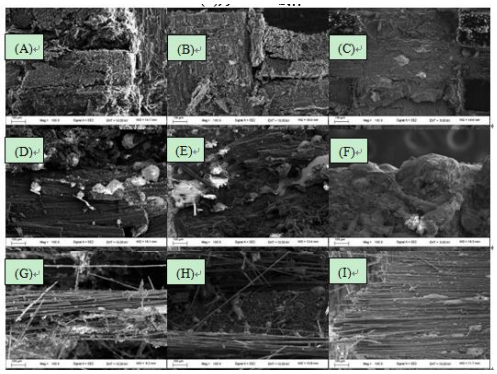

图 7 不同浸渗压力下三种炭/炭复合材料的断口形貌：(A), (B), (C)为 703 试样；(D), (E), (F)为 IMR 试样；(G), (H), (I)为 TOYO 试样

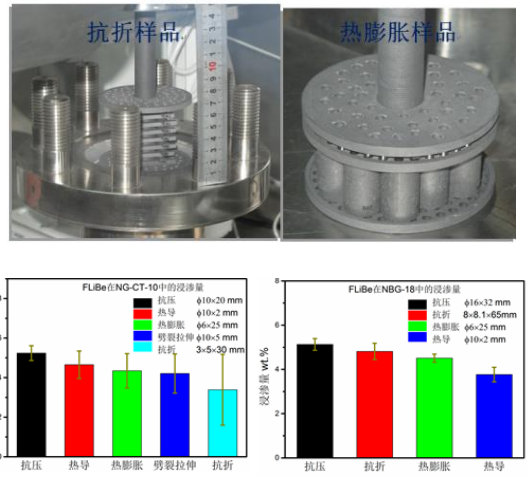

图 8 不同形状石墨的 FLiBe 盐浸渗实验

对比了 FLibe 盐不同形状及尺寸的石墨样品中的浸渗量。实验用大量的样品对比了形状及尺寸对 FLibe 盐浸渗量的影响。为进行该实验对设备的夹具进行了改进以适应不同形状样品的夹持以及保证实验结果的准备性。图 8 为不同形状样品的装样现场照片。对比不同尺寸及形状石墨的浸渗量表明对于 NG-CT-10 以及 NBG-18 样品，可以发现在 5×10^{-5} Pa 压强下，FLiBe 盐在 NG-CT-10 中的浸渗量与在 NBG-18 中的浸渗量相似，皆为 4%~5%。尺寸对浸渗量有一定的影响，但是差别很小。

研究了 10×10^{-5} Pa 熔盐浸渗后 NG-CT-10 以及 IG-110 与浸渗前的高温抗压强度。实验结果表明，熔盐浸渗后石墨的抗压强度有所降低，IG-110 的强度降低约 10%，而 NG-CT-10 的强度降低只有约 5%左右（图 9 左），这与盐在这两种石墨中的浸渗量是相关的，熔盐浸渗量越大则强度降低越多，这也可以从图 9 的右图中看出来。

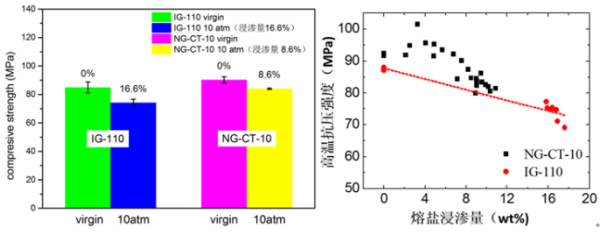

图 9 熔盐浸渗后石墨的力学性质变化

图 10 低孔径防熔盐浸渗细颗粒石墨材料Φ400×400 mm 工艺见证图片

石墨材料的规格尺寸由小到大的过程中，存在一定的放大效应，其中等静压包套成型工艺尤为凸显，本阶段工作通过数批次工艺试验，攻克了大规格样品包套一次成型的技术难关，为优化工艺前后生坯外形图片，成型生坯表面不规则会导致材料结构均匀性较差，内部应力和密度分布不均匀，影响最终石墨制品的热力学性能，甚至导致焙烧品开裂。

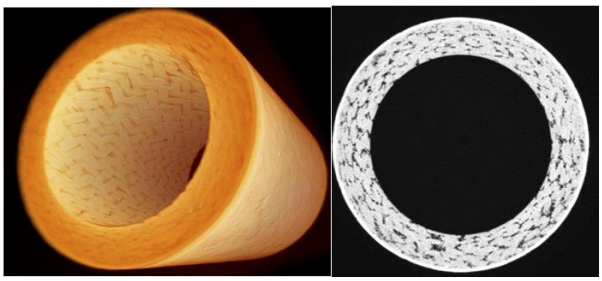

图 11 SiC/SiC 复合材料管的显微 CT

SiC/SiC 复合材料管的显微 CT，揭示 SiC/SiC 复合材料多孔。耐压实验检验表明 SiC/SiC 复合材料在 1×10^{-5} Pa Ar 气中 10 h 后泄漏了 10 kPa，经计算得出 SiC/SiC 复合材料在 1×10^{-5} Pa Ar 气中的泄漏率为 2.75×10^{-6} Pa·m^3/s。在 SiC/SiC 复合材料表面进行 CVD SiC 涂层后（约为 0.4 mm 厚），SiC/SiC 复合材料在 1×10^{-5} Pa Ar 气中 10 h 后泄漏了 0 kPa，在 5×10^{-4} Pa Ar 气中 10 h 后泄漏了 0 kPa，揭示表面 CVD SiC 涂层能提高复合材料的气密性，可能

有助于阻隔熔盐渗透。

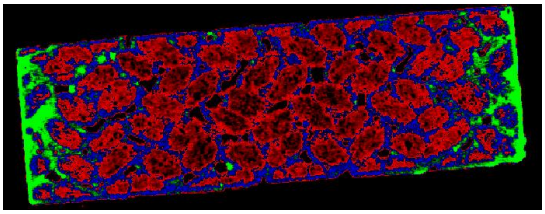

图 12 5×10^{-5} Pa 熔盐浸渗实验后 SiC/SiC 复合材料管的显微 CT (注：绿色代表熔盐，黑色代表孔洞，红色代表纤维束，蓝色代表基体)

在常压和 5×10^{-5} Pa 加压下，渗透进入 SiC/SiC 复合材料的 FLiNaK 熔盐<5%。图 12 是 5×10^{-5} Pa 盐浸渗后 SiC/SiC 复合材料的显微 CT，实验结果揭示熔盐仅渗透进入表面层。且 SEM 结果显示 SiC/SiC 复合材料表面孔洞已被 FLiNaK 熔盐填充。在常压和预充压熔盐实验中，复合材料内部孔洞中被常压和 1.5×10^{-5} Pa Ar 气填充，熔盐进入表面孔后使孔内形成较大气压，使熔盐无法渗透到内部孔中。

结论

1）完成了合金部分离子辐照实验，解释了辐照损伤原因；实现了 GH3535 管材挤压突破，制备出了大口径的无缝管；分析了合金中 Si 元素对碳化物富集度的影响规律，给出了合金中合适的 Si 含量；对比和国产化合金与进口合金性能，国产合金与进口合金性能相当。

2）评价了熔盐对石墨弹性模量、剪切模量和力学性能的影响，熔盐熔点以前，浸渍熔盐试样弹性模量显著增加，浸渍熔盐后弹性模量显著降低到与未浸渍熔盐样弹性模量相等；利用先进的 CT 成像技术，揭示了熔盐进入复合材料的机制。

Molten salt reactor structural materials

Departments of Molten salt Engineering and Reactor Materials

A series of studies have been conducted on the domestically fabrication and performance evaluation of structural materials for the first domestic molten salts reactor (MSR), supported by the Strategic Priority Research Program of the Chinese Academy of Sciences “Thorium-based Molten-Salt Reactor (TMSR) nuclear energy system”. The structural materials include alloy and nuclear graphite. The domestic-made alloy is named by GH3535 alloy, and the nuclear graphite is ultra-fine graphite.

The key challenges of R&D of GH3535 alloy include trace element control, precipitates in large-scale ingot, cracking control in hot working and stability of the product.

Reactor structural material division mainly serves as an important link between factories and design, to find, analyze and solved problems, which can improve the optimization of materials, ensure the material performance, develop suitable materials, and finally effectively guarantee the safety of MSR.

Alloy materials

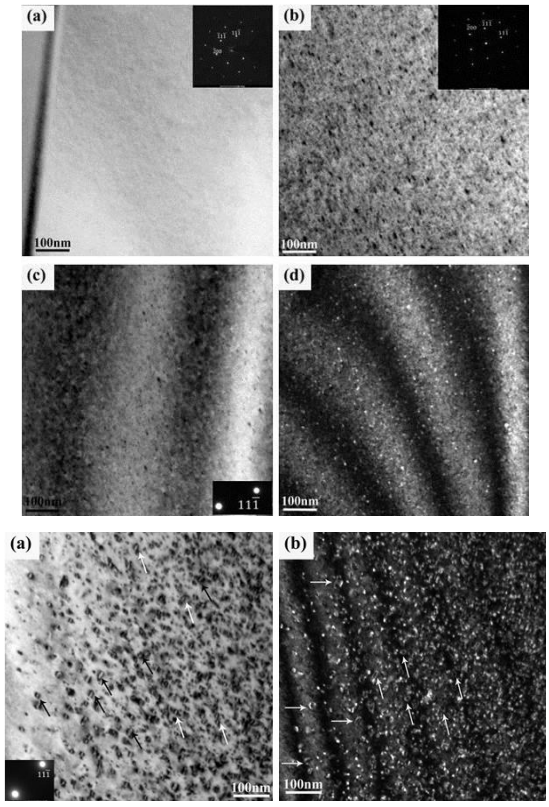

Fig.1 Microstructures of the GH3535 alloy sample before and after irradiation

Several nanoscale black-dot defects can be observed in the sample irradiated at low ion dose. According to the previous studies, these defects were believed to be some interstitial-type dislocation loops. It can be found that both the size and number density were increased with increasing ion dose.

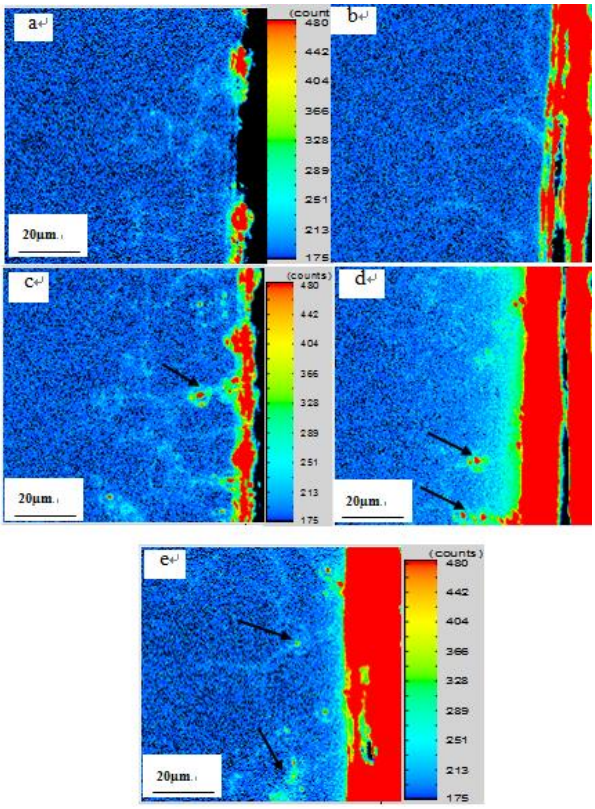

Fig.2 Te distribution of GH3535 alloy after corroding by Te at 700 ℃ for 100 h.

Fig.2 shows Te distribution of GH3535 alloy after corroding by Te at 700 ℃ for 100 h measured by EPMA. The diffusion type of Te in GH3535 alloy is intergranular diffusion. With the increase of Te content in the environment, the Te content in the grain boundary also increases, as the black arrows in Fig.2 shown.

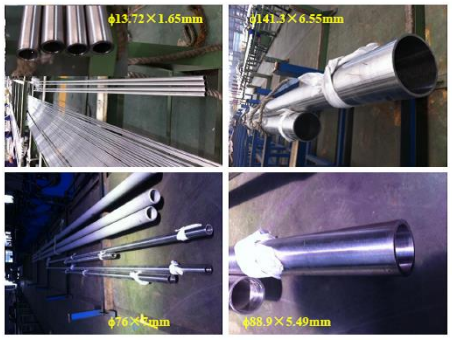

Fig.3 First successfully developed tube

The tube of GH3535 alloy with various sizes were successfully developed. After estimating their tensile and flattening properties, as well as nondestructive inspection, the tubes meet all the supposed performance index. The yield of the seamless tubes should be improved in the future.

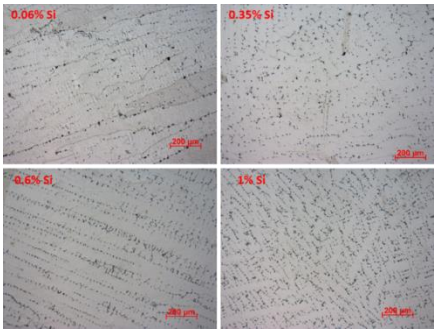

Fig.4 Densities and microstructures of carbides in the GH3535 alloy with different Si content.

TEM-EDX results show that in the GH3535 alloy with 0.188%, 0.319% and 0.562%，the Si content of carbides is in direct proportion to that of the matrix, and the maximum Si content of carbides reach 600% of that of matrix. Si can improve the stability and formation of the M6C carbides, leading to the change of densities of carbides. It should be noted that the saturation content of Si is 3.5%.

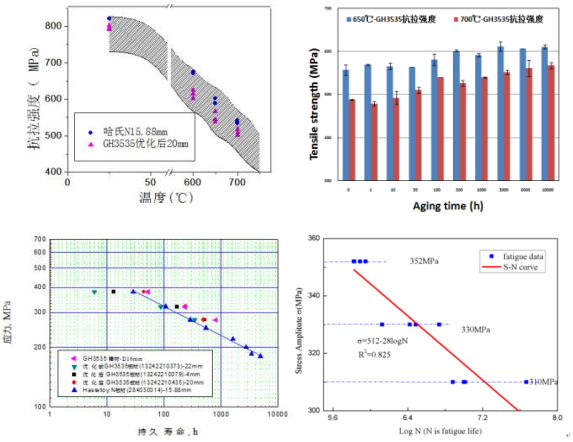

Fig.5 Mechanical performance of Hastelloy N and GH3535 alloy

Fig.5 shows the difference in mechanical performance of imported Hastelloy N plates with thickness of 15.88 mm and domestically made GH3535 plate with thickness of 20 mm, where the shadow part is the quality acceptance criteria of ORNL. It can be observed that the ultimate tensile strength (UTS) of GH3535 is 50MPa lower than that of Hastelloy N, while yield strength (YS) of GH3535 is 30 MPa lower than that of Hastelloy N. The elongation of GH3535 alloy is similar with that of Hastelloy N at room temperature and 600 ℃, which is 5%~10% exceeds that of Hastelloy N at 650 ℃ and 700 ℃. The scatter of the data of GH3535 alloy suggests the relative heterogeneity of the GH3535 alloy. at 650 ℃ and 700 ℃, with the aging time increasing, the YS of GH3535 keeps stable but the UTS of GH3535 slowly increases, while the elongation and section shrinkage increase in the first 1 000 h and then decrease. The creep rupture life of the improved GH3535 alloy (4 mm and 20 mm plate) at 650 ℃ increase a lot, which is slightly higher than that of imported Hastelloy N. As shown in Fig.5, the high-cycle fatigue measurement of improved GH3535 plate show the alloy has about 10 million cycles life at the stress 310 MPa (YS at room temperature), suggesting a good high-cycle fatigue performance at room temperature.

Nuclear Graphite

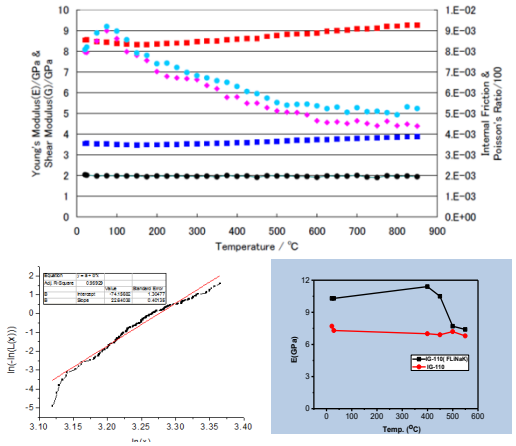

Fig.6 Graphite mechanical properties

Weibull distribution is an important indicator of nuclear graphite mechanical strength dispersion. According to German tensile strength measurement standards DIN 51914, 136 samples were taken from bulk graphiteNG-CT-10 (bulk size is 400 mm×400 mm×600 mm), the Weibull distribution of tensile strength of NG-CT-10 was measured. The elastic modulus and shear modulus of graphite IG-110increase slowly with the temperature, indicating that trend of elastic modulus and intensity with temperature is consistent. The effect of solid molten salt on the elastic modulus and shear modulus was determined. The results show that both of elastic modulus and shear modulus increased after molten salt infiltration.

Fig.7 shows the SEM images of three carbon / carbon composites after different pressure molten salt infiltration. The SEM image of 703 sample shows no molten salt infiltration were observed at lower infiltration pressure (Fig.7(a) and (b)), which means the infiltration capacity of 703 sample was very low. When the infiltration pressure increased to 6×10^{-5} Pa (as shown in Fig.7(c), molten salt impregnates the interior of the composite along the pores between the fiber bundles. However, IMR samples have been 6.05% impregnated when 2×10^{-5} Pa infiltration pressure (Fig.7(d-e)). Fig.7(g-I) show that the infiltration of molten salt inside the composites is mainly along the macropores in the fiber bundles, between the fiber bundles.

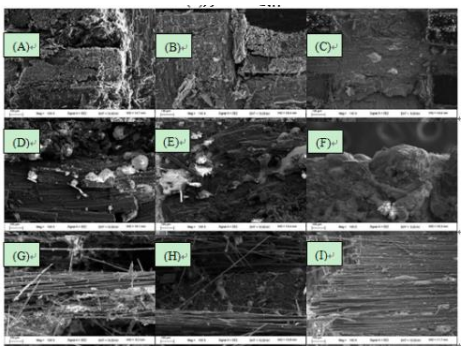

Fig.7 The the SEM images of three carbon / carbon composites after different pressure molten salt infiltration：(A), (B), (C) 703 samples；(D), (E), (F) IMR samples ； (G), (H), (I)TOYO samples

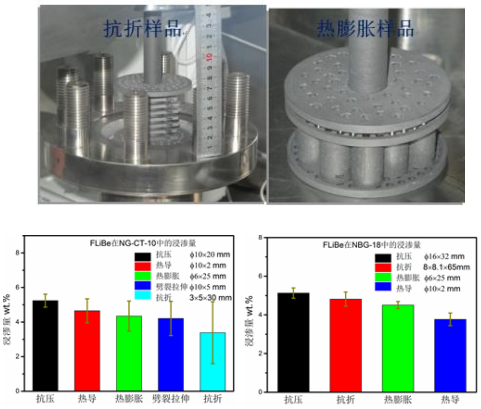

Fig.8 FLiBe salt infiltration experiment about different shapes of graphite

The infiltration capacity of FLiBe salt in graphite samples with different shapes and sizes was compared. A large number of samples are studied. Figure 8 shows the placement of samples of different shapes. The infiltration capacity of FLiBe salt in graphite NG-CT-10 is similar to that in the graphite NBG-18 at 5×10^{-5} Pa pressure, the infiltration capacity is 4%~5%. The size of infiltration has a certain impact, but the difference is small.

The high temperature compressive strength of NG-CT-10 and IG-110 after infiltration of 10×10^{-5} Pa molten salt was studied. The experimental results show that the compressive strength of graphite decreased after molten salt infiltration, the strength of IG-110 decreased ~10%, while the strength of NG-CT-10 decreased ~5% (Fig.9, left). The change of compressive strength is related to the infiltration of molten salt in graphite. The greater the infiltration of molten salt, the more serious the decrease of strength (as shown in Fig.9 right).

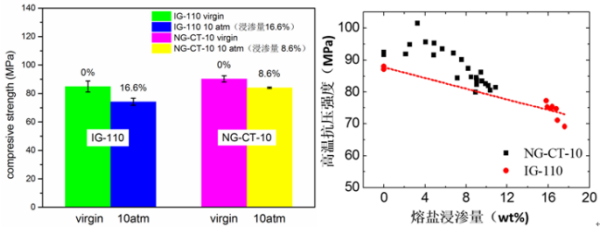

Fig.9 Mechanical properties of graphite after infiltration of molten salt

Fig.10 Anti-molten salt infiltration of fine graphite material Φ400×400 mmprocess witness picture

Properties such as the microstrcture homogeneity, stress, density of the graphite product change with the magnification of the graphite size specification, isostatic pressing process is particularly prominent. This year through several batches of process tests, capture a large sample size forming technology. If the surface of the graphite green body is irregular, it will lead to poor uniformity of the material structure, uneven distribution of internal stress and density, influence on the thermodynamic properties of the final graphite product, and even cracking of the baked product.

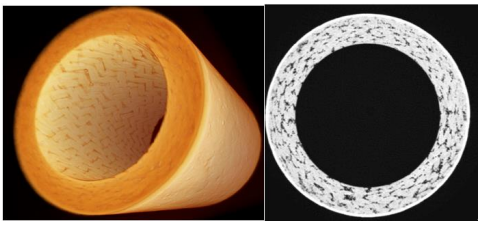

Fig.11 Micro-CT of SiC/SiC composite tubes

Micro-CT of SiC/SiC composite tube shows the porosity of SiC/SiC composite. The result of pressure-resistant test shows that the SiC/SiC composite material leaked 10 kPa in 1×10^{-5} Pa Ar gas for 10 h, and the leakage rate of SiC/SiC composite material in 1×10^{-5} Pa Ar gas is calculated to be 2.75×10^{-6} Pa·m^3/s. After CVD SiC coating on the SiC/SiC composite surface (~0.4 mm thick), the SiC/SiC composite leaked 0 kPa after 10 h in 1×10^{-5} Pa Ar gas and 0 kPa after 10 h in 5×10^{-5} Pa Ar gas, revealing Surface CVD SiC coatings improve the air-tightness of composites and may help to prevent penetration of molten salt.

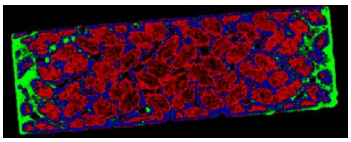

Fig.12 Micro-CT of SiC/SiC composite tube after molten salt infiltration experiment (Note: green represents molten salt, black represents hole, red represents fiber bundle, blue represents matrix)

The FLiNaK molten salt infiltrated into the SiC/SiC composite was <5% at atmospheric pressure and 5×10^{-5} Pa pressure. Figure 12 shows the microscopic CT of SiC/SiC composites after 5×10^{-5} Pa molten salt infiltration. The results show that the molten salt only infiltrated into the surface layer. The SEM results show that the surface pores of SiC/SiC composite have been filled with FLiNaK molten salt. In atmospheric pressure and pre-charged molten salt experiments, the composite material was filled with Ar gas at atmospheric pressure and 1.5×10^{-5} Pa. After the molten salt entered the surface pores, a larger pressure was formed in the pores, so that the molten salt could not penetrate into the internal pores.

Conclusion

1) Part of ion irradiation tests were completed and the alloy irradiation damage mechanism was explained; Process of tube extrusion was successfully developed and seamless tube with large diameter was fabricated; The relation between Si content and carbides was explored and the optimum Si content is obtained; The mechanical performance of imported Hastelloy N and domestically made GH3535 alloy is similar to each other.

2) The influence of molten salt on the elastic modulus, shear modulus and mechanical properties of graphite was evaluated. Both of elastic modulus and shear modulus increased after molten salt infiltration. Advanced CT imaging reveals the molten salt infiltration mechanism of the composite.

堆材料工程物理组对熔盐堆相关材料的辐照、腐蚀进行了测试分析及理论模拟研究。

对高温合金在熔融氟盐中的腐蚀机理和腐蚀过程有了系统全面的认识，为腐蚀测试的规范化以及腐蚀控制技术的研究奠定了基础。腐蚀对比测试表明：进口哈氏 N 合金与国产哈氏 N 合金的腐蚀抗力相当。初步探索了 316 不锈钢在 FLiNaK 熔盐中的腐蚀控制技术。

建立了材料辐照质保体系，完成合金样品堆内辐照试验，辐照温度达标；获取部分合金辐照数据；完成石墨样品准备及石墨条件辐照试验。开展了镍基合金、SiC 材料的离子束辐照研究，对比研究表明：第三代 SiC 纤维比国产纤维结晶度高，国产合金和进口合金在辐照后性能一致。

优化单质以及 Ni-Mo 二元合金的原子间相互作用势，通过模拟阐明单质和二元合金的辐照损伤规律，阐明氦原子和团簇在镍金属中的聚集和扩散规律，获得裂变产物在碳化硅晶界中的扩散方式和势垒。通过第一性原理拟合熔盐与石墨的相互作用势模型。系统研究了钢系氧化物、碳化物电子结构，缺陷结构与热力学性质，钢系材料表面性质、缺陷结构及其与包壳材料的相互作用。

材料腐蚀性能测试与评估

图 1　静态浸泡腐蚀流程

腐蚀抗力评估是哈氏 N 合金国产化研究的重要环节。本组的评估方案是采用静态条件下的加速腐蚀测试，对比国产哈氏 N 合金与进口哈氏 N 合金的腐蚀行为。具体方案如下。第一、建立标准的测试流程。由于熔融氟盐对环境极为敏感，腐蚀测试必须在极为严苛的条件下进行。为此，研制了专门的封装设备，包括手套箱（水含量保持在 1×10^{-6} 以下，氧含量保持在 10×10^{-6} 以下）、胶囊式反应釜，见图 1。第二、为配合国产哈氏 N 合金熔炼工艺的固化，需要在较短时间内获得其腐蚀抗力的初步结论。因此，采用适当的体系进行加速腐蚀测试。经综合考虑，最终选用三高石墨为容器，高纯 FLiNaK 熔盐为介质，进行等温浸泡。第三、对比方法：腐蚀特征对比，腐蚀程度对比。

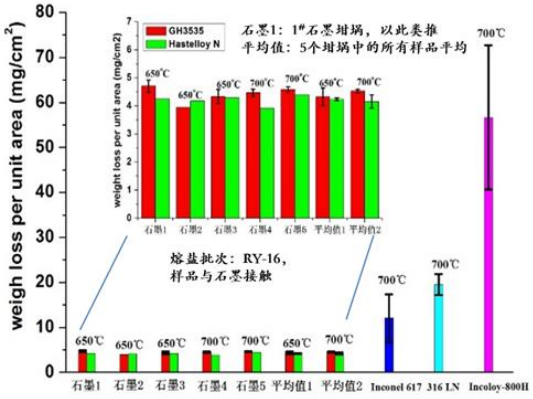

图 2　GH3535、进口哈氏 N 合金及几种参比合金的单位面积失重

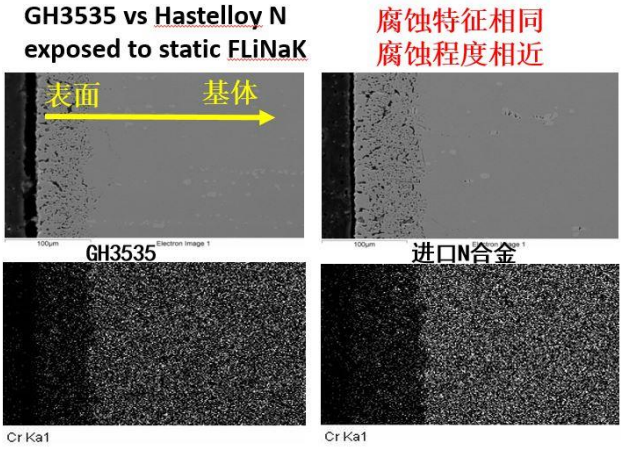

图 3　(GH3535)与进口哈氏 N 合金的腐蚀深度和腐蚀特征对比

经综合比对，确认国产哈氏 N 合金(GH3535)与进口哈氏 N 合金的腐蚀特征相同：均为铬元素溶出导致的均匀腐蚀；腐蚀程度相近：加速腐蚀状态下，两者的失重数据（图 2）和贫铬深度相近（图 3）。因此，GH3535 合金与进口哈氏 N 合金的腐蚀抗力相当。

材料辐照性能评价与测试

保体系和辐照方案

TMSR 堆材料部和质保组对于核动力研究设计院一所编制了质保大纲、过程质量计划、试验方案、试验大纲等文件进行了审查，并在过程质量计划中设置了控制点（H、W、R 点），以达到控制中子辐照试验质量的目的，并编写了试样传递操作细则，规定了试样传递流程和文件格式。

根据辐照要求，本试验选用核动力院的高通量工程试验堆的元件区 G7 辐照孔道进行石墨辐照试验，选择反射层区的 9#辐照孔道进行哈氏合金辐照试验，如图 4 所示。辐照试验段放置试验样品、中子探测器以及热电偶装置。合金辐照装置、两个石墨辐照装置的长度分别为：335 mm、330 mm、370 mm。通过计算，合金辐照装置和石墨辐照装置内的温度均可达到试验要求(650±50) ^{o}C。

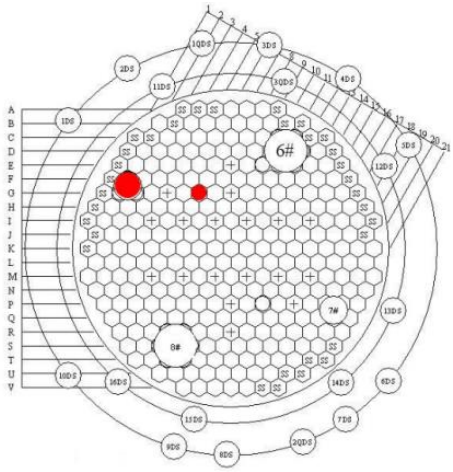

图 4 高通量工程试验堆辐照孔道示意图

合金辐照试验和辐照后测试

哈氏 N 合金辐照样品如图 5 所示。对辐照装置入堆前准备状态检查现场质量见证。现场检查了完工后的哈氏合金辐照装置，如图 6 所示。辐照装置实物与设计相符；对装置的保护恰当，吊装操作仔细。

核动力院一所于 2014 年 7 月 1−7 日开展了哈氏合金样品的条件试验。在此基础上，哈氏 N 合金辐照装置在 7 月 14 日入堆辐照。试验每两小时记录一次试验温度，通过温度控制系统调节试验温度，使满足试验要求（图 7）。辐照装置于 7 月 31 日出堆。合金样品的辐照后测试正在进行中。目前已开展尺寸、密度、硬度测试，室温拉伸测试，350 ^{o}C 以下的夏比冲击测试。

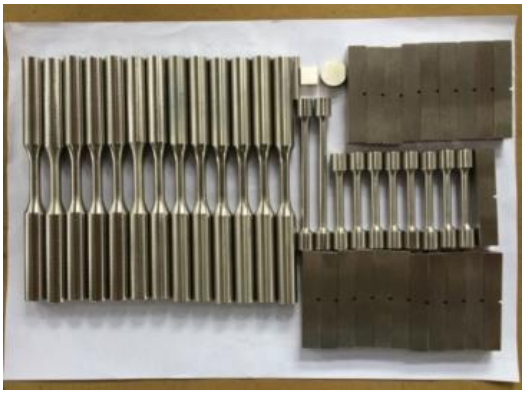

图 5 哈氏 N 合金辐照样品照片

图 6 辐照装置入堆操作

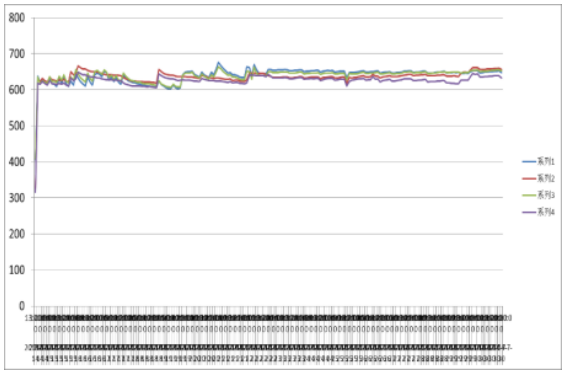

图 7 辐照过程中温度控制

石墨辐照试验

第一批核石墨样品和新材料样品已经准备完毕，如图 8 所示。样品加工后，进行了激光打标，尺寸检测、高温烘烤和封装。第二批熔盐浸渗石墨样品已经完成了激光打标、尺寸检测等工作，熔盐浸渗实验正在进行中，预计 2015 年 1 月份完成。核石墨的条件辐照试验于 2014 年 11 月底到 2014 年 12 月初进行。装置辐照后在热室中冷却。各项指标达到预期。

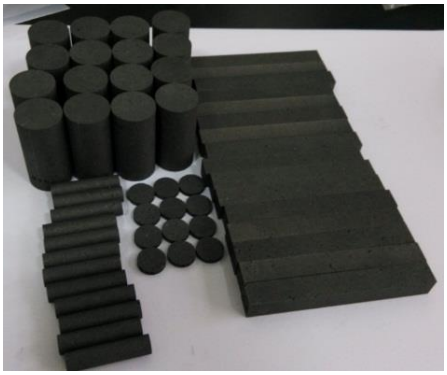

图 8　第一批 NBG-18 石墨样品

材料理论计算模拟与预测

镍基合金辐照损伤和氦脆效应

构建了精准的 Ni-Ni、Mo-Mo、Cr-Cr、Fe-Fe 以及 Ni-Mo 原子间相互作用势，采用分子动力学方法详细地模拟了金属单质 Ni、Mo、Cr、Fe 以及二元合金 Ni-Mo 体系受辐照初始阶段的级联碰撞过程。利用分子动力学方法模拟了氦在镍近表面的的聚集和和释放，结果表明氦泡的释放速度随着温度和压强的升高而加快（图 9）。通过模拟阐明了氦导致镍金属内部缺陷产生，以及氦与空位团簇、位错等缺陷相互作用的机制，获得氦和氦团簇的扩散系数。

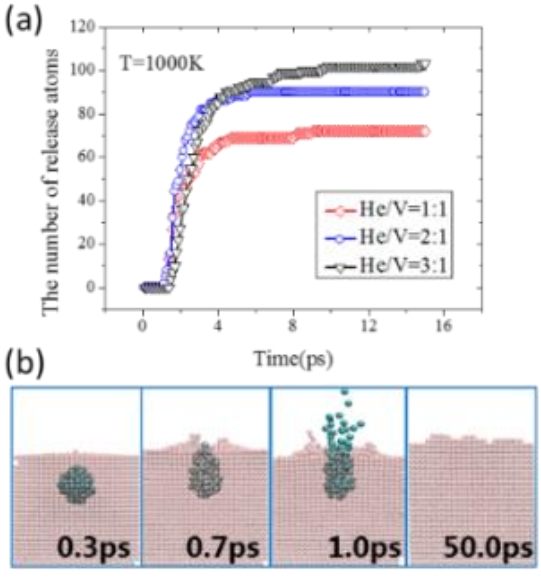

图 9　(a)不同浓度氦泡的释放过程；（b）氦释放过程

裂变产物-碳材料相互作用

TRISO 燃料球中裂变产物的泄露对反应堆回路造成污染，影响构件的服役寿命。因此，研究裂变产物在不同碳基材料中的扩散行为有助于理解裂变产物的堆内行为。采用密度泛函理论研究了 Cs、Xe 和 Ag 原子在 β 碳化硅的Σ9 倾斜晶界上的扩散情况。结果表明：Ag 扩散能垒低于 Cs 和 Xe。SiC 晶界的八圆环通道是裂变产物 Ag 通过 TRISO 球的 SiC 层的机制,如图 10 所示。

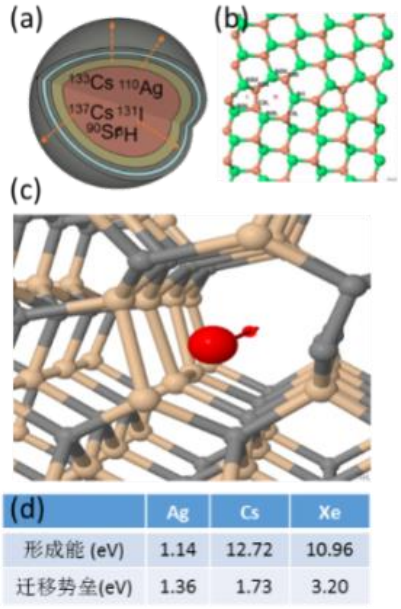

图 10　(a)裂变产物在 TRISO 燃料中示意图；(b)典型 SiC 晶界；(c)裂变产物在 SiC 中扩散示意图

锕系晶体性质研究

研究了裂变产物(He、Ne、Ar、Kr、Xe)在锕系氧化物晶体中的稳定性和扩散行为，研究结果表明不同惰性气体的肖特基缺陷最低能构型不同，构型的不同于惰性气体原子尺寸相关。研究了水分子在 ThO_2 表面的扩散和分解行为（图 11），解释了水分子在 ThO_2 表面扩散的机制，发现表面缺陷可以降低分解势垒和提高扩散势垒，从而使得 ThO_2 表面具有催化分解表面水的效应。

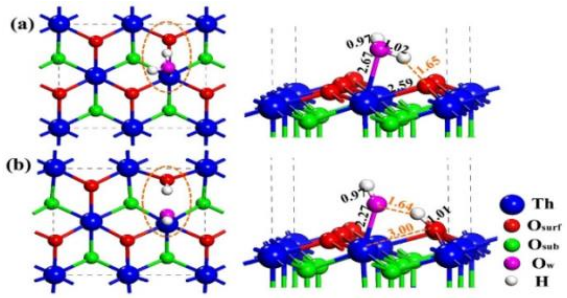

图 11　水分子在 ThO_2(111)表面吸附和分解

锕系分子性质研究

应用高精度从头算方法并包含自旋轨道(SO)效应研究了 UO_2F_2 及其水合物的配位结构和电子

光谱性质。水合物的几何参数与 EXAFS 实验结果相吻合。采用 DFT 计算的方法考察了液相中铀酰离子与胺基配体在不同 pH 条件下的络合过程。获得了络合物的稳定结构（图 12），电子结构以及热力学性质，对比了不同结构络合物的相对稳定性。相关结果有助于阐明胺基配体在海水提铀中起的作用。

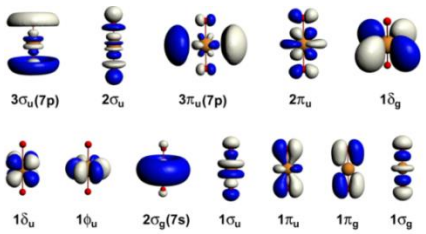

图 12 铀酰离子价轨道轮廓图

锕系元素熔盐的相互作用研究

采用第一性原理方法研究了 FLiBe 熔盐结构及性质，获得了其熔盐结构、熔盐原子间振动方式和声子谱性质，并且研究了锕系(Th、U)原子在熔盐中的络合结构及扩散行为，揭示了锕系元素在熔盐中的存在形态。用分子动力学方法获得了 ThF_4 分别在 LiF、FLiBe、FLiNaK 等熔盐中不同浓度及不同温度下的络合形态，并且预测了其动力学性质，如图 13 所示。

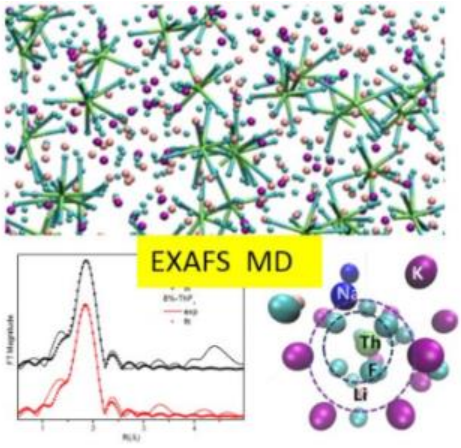

图 13 分子动力学方法获得了 Th4+和 Be2+在 FLiBe 熔盐的局域结构。

总结

本课题组按计划完成了材料腐蚀和辐照测试任务，开展了腐蚀、辐照、裂变产物、锕系材料性质等方面的理论模拟研究。这些工作为熔盐堆结构材料测试的规范化奠定了基础。下一年度将完善腐蚀测试规范、深化腐蚀控制技术、获取更多辐照数据。理论模拟方面进行更深入和更全面的研究。

Research on material engineering physics for TMSR

Division of Material Engineering and Technology

Group of reactor material engineering and physics conducted experimental and theoretical studies of irradiation effects and corrosion behavior of molten salt reactor materials.

A comprehensive understanding of corrosion mechanism and corrosion process of high-temperature alloys in molten fluoride salt is gotten, which lays a foundation for standardization of corrosion test and research on corrosion control technology. The comparison test shows that the corrosion resistance of the homemade Hastelloy N alloy is equivalent to that of the import Hastelloy N alloy. A corrosion control technology of 316 stainless steel in FLiNaK molten salt has been preliminarily explored.

Quality assurance system of material irradiation has been established. In-pile irradiation of alloy samples has been finished, and the temperature reached the designed value. Post-irradiation examination (PIE) is under way and part of the PIE results is achieved. Graphite samples' conditional irradiation test has been finished. Energetic ions have been used to study irradiation effects in alloys and SiC materials. It was showed that the third generation SiC fiber has much higher crystallinity than the second generation SiC fiber. Home-made alloy responds to irradiation in a way similar with the imported alloy.

The interatomic potentials are developed for metals e.g. Ni, Mo, Cr, Fe and binary alloy e.g. Ni-Mo. The cas-cade processes in the early stage of radiation damage are studied systematically by using molecular dynamic method; the aggregation and release processes of helium bubble at near-surface area of nickel are also clarified; the effective diffusion and corresponding energy barrier of fission products in grain boundaries of SiC are ob-tained. The electronic structure, defect and thermal dynamics properties of actinide oxide and carbide are systematically studied; the behaviors of water on the surface of actinide oxide, the microstructure and prop-erties of actinide molecule in water and molten salt environments are also studied.

Test and evaluation of material corrosion resistance

Fig.1 Static immersion corrosion procedure

The evaluation of corrosion resistance is an important link in the homemading of Hastelloy N alloy. Our evaluation roadmap is to use the accelerated corrosion test under static conditions to compare the corrosion behavior of the homemade Harris N alloy and the imported Harris N alloy. The detail process is as follows. Firstly, a standard test procedure should be established. Because the molten fluoride is very sensitive to the environment, the corrosion test must be carried out in extremely harsh conditions. For this reason, a special packaging equipment, including glove boxes (water content kept below 1×10^{-6}, oxygen content under 10×10^{-6}), capsule type reaction kettle, was set up (see Fig.1). Secondly, an appropriate system is used to accelerate corrosion testing, which is due to the reason as follow. A preliminary conclusion of corrosion resistance should be made in a relatively short time, in order to match the smelting process of the homemade Hastalloy N alloy. After comprehensive consideration, graphite (high in strength, purity and density) as the container, high pure FLiNaK molten salt as the medium, isothermal immersion were selected. The third is comparison contents including corrosion characteristics and corrosion degree.

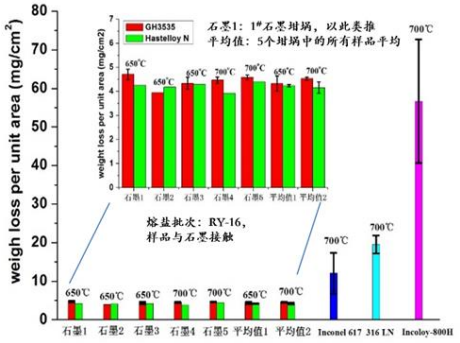

Fig.2 Weight loss per unit area of GH3535, imported N alloy and several reference alloys

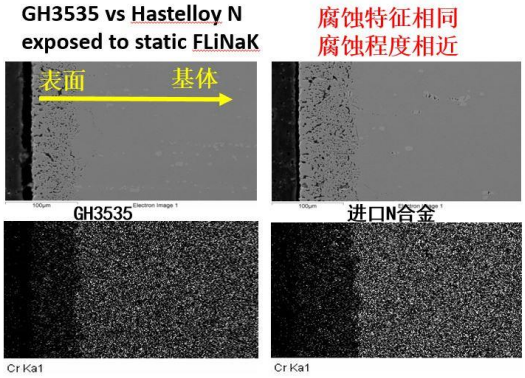

Fig.3 Comparison of corrosion depth and corrosion characteristics between GH3535 and imported Hastelloy N alloy

Through comprehensive comparison, it was confirmed that the corrosion characteristics of GH3535 and imported Hastelloy N alloy are the same. They are all uniform corrosion caused by dissolution of chromium. The corrosion degree is closed to each other. Under accelerated corrosion condition, the weight loss (Fig.2) and the chromium depletion depth (Fig.3) are equivalent. Therefore, the corrosion resistance of GH3535 alloy is equal to that of the imported Hastelloy N alloy.

Tests and evaluation of irradiation resistance of materials

Quality assurance system and irradiation program

Division of reactor materials and quality assurance group of TMSR investigated the quality assurance outline, process quality plan, test program and test outline that prepared by Nuclear Power Institute of China, and set up control points (H, W, R), aiming to control the quality of neutron irradiation tests. The group of material irradiation also prepared the rules of sample delivery, including the format of documents.

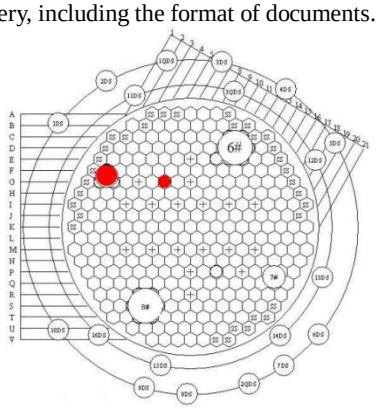

Fig.4 The irradiation channels in HFETR.

Based on the demand, the high flux engineering test reactor (HFETR) was chosen for material irradiation. the G7 channel was used for graphite irradiation, and the 9# channel in the reflector was used for alloy irradiation (Fig.4). Test section contained the samples, flux wires and thermocouples. The test sections of one alloy irradiation equipment and two graphite irradiation equipment have lengths of 335 mm, 330 mm and 370 mm, respectively. By calculation, the temperatures in alloy irradiation section and graphite irradiation section reached the design values (650±50) ^{o}C.

Alloy irradiation and post irradiation examination

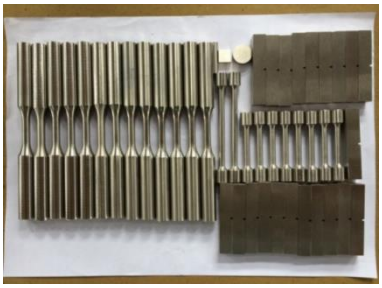

Fig.5 Alloy samples before in-pile irradiation

Fig.6 Inserting irradiation equipment into reactor.

Alloy samples are shown in Fig.5. The group of material irradiation examined the pre-irradiation conditions, and inspected the alloy irradiation equipment (Fig.6). The irradiation equipment met the design requirements. The irradiation equipment was protected and inserted into reactor carefully.

The condition test of alloy irradiation was started in July 1st 2014 and finished in July 7th 2014. Following the condition test, the alloy irradiation equipment was inserted into reactor in July 14th 2014. The temperature was maintained as request by using a temperature controlling system, and was recorded once in every two hours (Fig.7). The irradiation equipment was taken out of reactor in July 31st 2014. The post irradiation examination is underway. The measurements of dimensions, density and hardness, tensile test at room temperature, and Charpy impact test below 350 ^{o}C are finished.

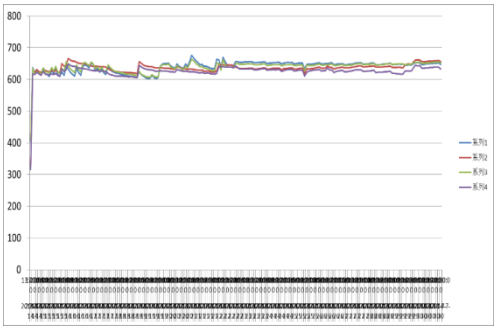

Fig.7 Temperature data recorded during irradiation.

Graphite irradiation test

The first batch of graphite samples and new materials samples were prepared (Fig.8). After machining, the samples were labeled by using the laser engraving method. The samples' sizes were measured before heating and package. The second batch samples were labeled by using laser engraving method. The sample sizes were measured. The salt infiltration experiment is underway and will be finished in January 2015. The condition test of graphite irradiation was started in the end of November, and finished in the beginning of December. The irradiated equipment for condition test is cooling down in hot cell. The temperature reached the desired values.

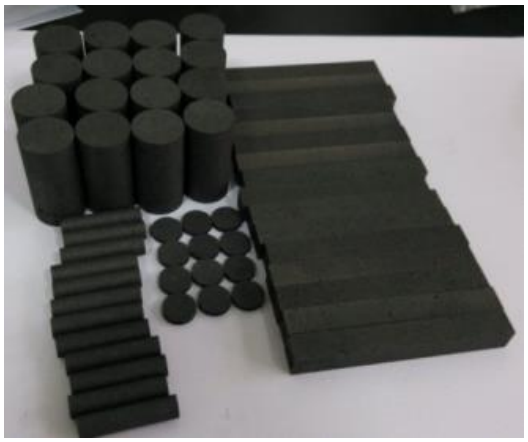

Fig.8 First batch of NBG-18 graphite.

Theoretical Simulation and Properties Prediction of Nuclear Materials

Radiation damage and Helium embrittlement of Nickel-based alloy

Precise interatomic potentials are established for metals such as Ni-Ni, Mo-Mo, Cr-Cr, Fe-Fe and Ni-Mo. The displacement cascade processes in the early stage of radiation damage are studied systematically for simple metals e.g. Ni, Mo, Cr, Fe and binary alloy, e.g. Ni-Mo by using molecular dynamics method based on the new developed potentials. The aggregation and release processes of helium bubble at near-surface area of nickel are also clarified (see Fig.9). It shows that release rates of helium bubble increase with the pressure and temperature of the bubble. The mechanism of defects creation induced by helium are studied by using MD simulation as well as the interaction mechanism between helium and vacancy clusters, or dislocations.

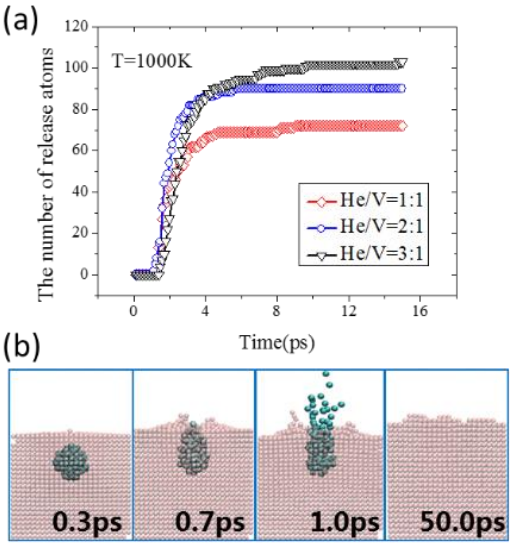

Fig.9 (a) The release processes of helium bubble with different pressure as function of release time; (b) Atomic configurations of helium bubble release processes.

The diffusion of fission products in SiC

The leakage of the fission products (FPs) in the TRISO fuel would cause pollution to the reactor loop and further affect the in-pile life of components. Therefore, the diffusion properties of FPs in carbon-based materials can help to understand their behaviors in the reactor. The diffusion processes of Cs, Xe and Ag atoms in Σ9 grain boundaries (GBs) of β-SiC are studied by using density functional theory (DFT) as shown in Fig.10. It shows that the diffusion energy barrier of Ag is lower than that of Cs and Xe. The 8-atom-ring structure of GB in SiC is a proper diffusion channel for Ag penetration through SiC layer in TRISO fuel.

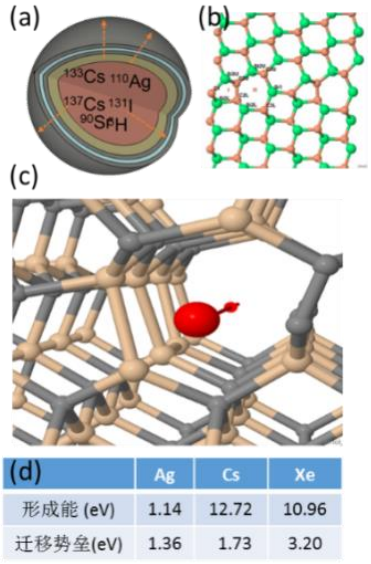

(d)	Ag	Cs	Xe
形成能 (eV)	1.14	12.72	10.96
迁移势垒(eV)	1.36	1.73	3.20

Fig.10 (a) Schematic diagram of TRISO fuel with typical fission products; (b) Typical SiC grain boundary; (c) Schematic diagram of the diffusion processes of FP in SiC.

Studies of Actinides Crystal

The stability and diffusion behaviors of fission products (He, Ne, Ar, Kr and Xe) in thorium dioxide are studied systematically. The results indicate that Schottky defect induced by different noble gas has different of lowest energy configuration depending on the size of noble gas atom. The diffusion and breakdown process of water molecules on the surface of ThO_2 are studied theoretically, as shown in Fig.12, to clarify the mechanism of surface diffusion of water molecule. It is found that surface defects can reduce the potential barriers of decomposing but raise the diffusion barrier. Such mechanism indicates that the surface of ThO_2 can be catalyst for water decomposing.

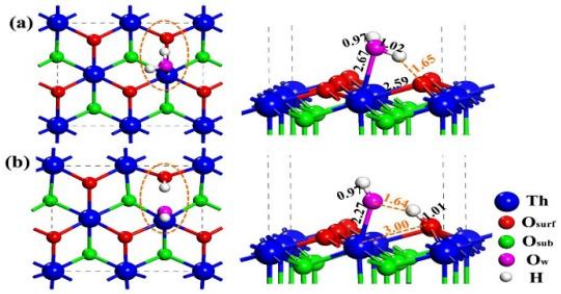

Fig.11 The adsorption and dissociation of H_2O on the ThO_2(111) surface.

Studies of Actinide molecules

The structures and electronic spectra properties of UO_2F_2 and its hydrate are studied by using spin-orbit ab initio calculations. The optimized geometrical parameters are consistent with the EXAFS results. The complexation of uranyl with amine ligands in aqueous solution under different pH levels are examined using density functional theory calculations. The geometries, relative stabilities of complexes, and changes in Gibbs free energies for different complexing reactions were

investigated. The results help to understand the role of amine ligands in the processes of extraction uranium from seawater.

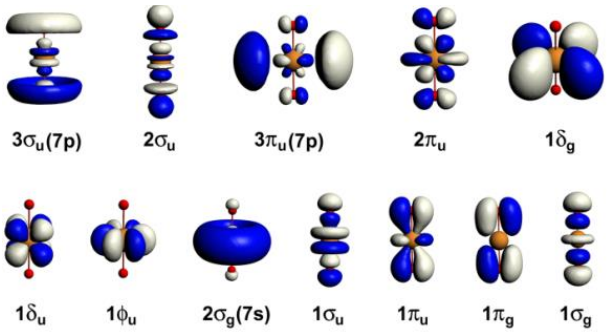

Fig.12 The orbit profile of uranyl ion.

Studies of the interaction between actinide and molten salts

The local structure and properties of LiF-BeF_2 molten salt have been studied by using the first principle method. The local structure, the vibration modes between the atoms and phonon spectra properties have been obtained. The local structure and the diffusion behavior of actinide (U) compounds molten salt have also been studied. It reveals that the existence of network structure in the contained actinide compounds molten salt. The local structure of ThF_4 in LiF, FLiBe, FLiNaK and other molten salts with different concentrations and temperatures were simulated by molecular dynamics simulation. And their dynamic properties (diffusion coefficient, viscosity) were predicted.

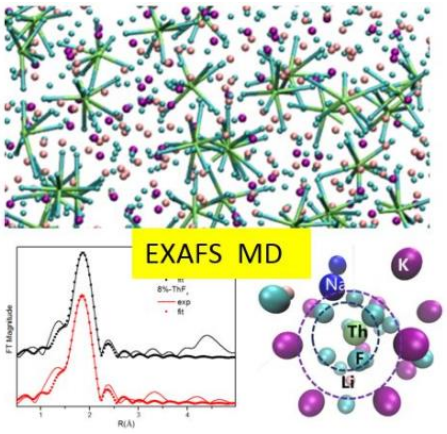

Fig.13 Local structures of Th_4+ and Be2+ in FLiBe molten salts.

Conclusion

According to the annual plan, the group completed the task of material corrosion and radiation testing, and conducted theoretical simulation research on corrosion, irradiation, fission products and properties of actinide materials. These work lays the foundation for the standardization of the test of the reactor structure materials. In the next year, the corrosion test specification will be improved, the corrosion control technology will be deepened, and more radiation data will be obtained. A more thorough and comprehensive study will be carried out in the theoretical simulation.

堆用聚合物材料研究进展

堆材料科学与工程二部

堆其它材料设三个子课题，分别开展高性能碳化硅纤维制备工艺研究、堆用聚合物研究和1.5 MeV 电子束辐照平台建设。

高性能 SiC 纤维制备工艺研究

1) 聚碳硅烷(PCS)纤维的辐射固化工艺研究。由于 PCS 原丝非常脆弱，首先解决了纤维的批量运输问题，然后优化了 PCS 纤维从生产厂家采购、辐照、后续烧结等步骤的技术对接问题，实现了批量纤维的辐照，完成了约 15 kg PCS 纤维的辐射固化（图 1）。对关键指标氧含量的检测结果显示，辐照固化 PCS 纤维和 SiC 纤维的氧含量均小于 3%，最小仅 0.7%，达到高性能 SiC 纤维的氧含量指标。

图 1 辐射固化 PCS 纤维

2) 碳化硅(SiC)纤维的烧结工艺研究。通过对辐射固化 PCS 纤维进行烧结，获得 SiC 纤维，本实验室重点开展两步烧结法工艺研究。结果显示，用辐射固化 PCS 纤维为原料，采用两步法烧结成功获得 SiC 纤维。通过优化烧结工艺，初步确定了两步法烧结的基本工艺参数，为后续大批量烧结奠定基础。

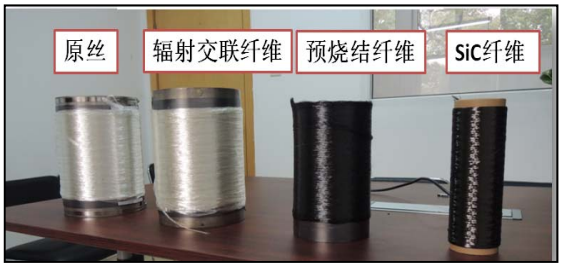

图 2 从 PCS 纤维到 SiC 纤维样品

3) 完成了 TMSR 新材料制备实验室的主要设备的采购和场地改造。设计加工制造了一整套 SiC 纤维的烧结实验线，目标是将辐射固化 PCS 纤维烧结制备 SiC 纤维，截至 2013 年烧结实验线的主要设备已经通过出厂验收改造工作。该线采用两步法烧结工艺，设计年加工 100 kg 第二代 SiC 纤维，也可以升级用于第三代纤维的烧结。实验室改造方面，根据实验线的安装条件进行总体设计和改造，从 2014 年 7 月开始施工，12 月初完成了场地改造工作，年底转入了 SiC 纤维烧结设备的安装、调试阶段。根据所内的分析测试条件，建立起了 SiC 纤维的性能分析检测平台，实现对纤维研制过程的质量控制。探索完成了一套性能测试方法，配合 SiC 纤维工艺研究，逐步建立起了过程控制和产品质量控制体系。

图 3 SiC 纤维烧结实验室

聚合物材料

堆用聚合物材料子课题主要开展常规（服役温度约为 90 ℃）、高温（服役温度约为 250 ℃）电缆料研制，2013−2014 年主要进展如下。

1) 完成了 60 a 使用寿命的核电电缆料热寿命评定，采用 60 a 使用寿命的电缆绝缘材料和护套材料制备的 3 mm×10 mm 额定电压 0.6/1 kV 及以下核电站用 1E 级 K1 类电力电缆，已由国家电线电缆质量监督检测中心(CT13-4973)进行 60 a 热寿命评定（150 ℃/2 376 h 老化），正在进行 1 500 kGy ^{60}Co γ 射线耐辐照试验。

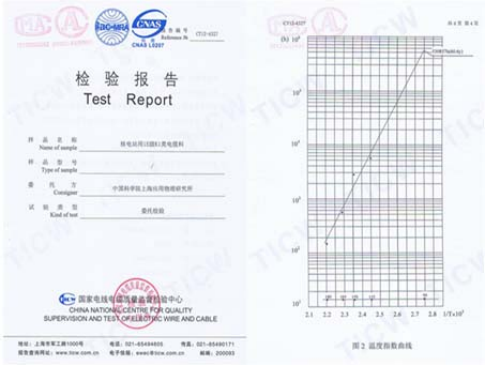

图 4 60 a 核电电缆料热寿命评定报告（部分）

2) 采用聚醚醚酮(PEEK)原料制备了高温（服役温度约为 250 ℃）电缆，已由国家电线电缆质量监督检验中心(CT14-2984)进行 250 ℃热寿命评定（280 ℃/168 h 老化）及耐辐照试验。

图 5 高温 PEEK 电缆耐辐照试验报告及样品

3) 完成了核电 K1 热收缩管全性能测试，制备了 60 a 使用寿命核电 K1 热收缩电缆附件。

表 1 60 a 核电 K1 热收缩材料性能

项目	单位	结果
抗张强度	MPa	11.2
断裂伸长率	%	272.8
180 ℃/150 h 热老化后性能		
断裂伸长率	%	152.1
180 ℃/150 h 老化后 γ 辐照试验 (10 kGy/h)		
500 kGy 断裂伸长率	%	119.0
1 000 kGy 断裂伸长率	%	71.2
180 ℃/150h 老化后 β 辐照试验(20 kGy/h)		
500 kGy 断裂伸长率	%	128.7
1 000 kGy 断裂伸长率	%	58.3

4) 完成了转矩流变仪、高温单/双螺杆挤出机及其配套设备的安装调试，使实验室具备高温电缆材料配方研究及高温电缆制备能力，同时联合已有的电子拉力机、熔融指数仪、氧指数测定仪、UL 老化烘箱等仪器，初步建立了一套核用电缆的加工测试平台。

图 6 核用高温电缆试验设备

1.5 MeV 电子束辐照平台建设

1) 完成了加速器机械、电器、控制系统安装以及相关配套的水电风、屏蔽系统、束下系统、安全连锁系统等工程，顺利完成 1.5 MeV 电子束辐照平台的建设。2013 年 7 月底，成功实现了设计能量、束流的稳定出束。同时经过一系列的剂量监测，在最高能量最高束流连续稳定出束的情况下，辐照平台周围环境辐射剂量低于设计目标剂量值，达到了防护设计要求。

图 7 1.5 MeV 电子束辐照平台

2) 在 1.5 MeV 电子束辐照平台上进行了一系列调试实验，通过遮蔽法或二次扫描法成功实现了低剂量率 β 射线辐照条件，在电子束束流能量为 1.2 MeV 情况下，使静态电子束辐照剂量率达到了 20 kGy/h，剂量率实验重现性良好，标志着 AP1000 三代核电站所要求的低剂量率 β 射线辐照检测工作在国内已具备检测条件。此外，进一步实现了 10 kGy/h、30 kGy/h、50 kGy/h、70kGy/h 等各种低剂量率 β 射线辐照条件。

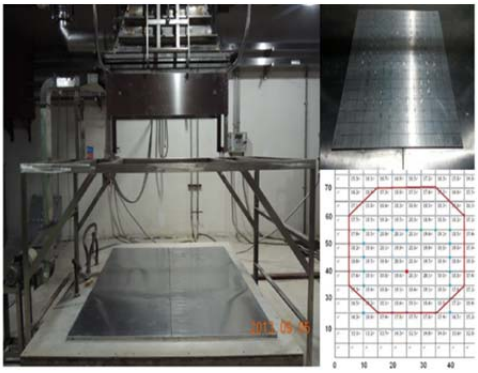

图 8 低剂量率 β 射线辐照考验实验

3) 建立了 ESR/丙氨酸剂量计剂量监测体系。利用丙氨酸剂量读出器和标准的丙氨酸剂量计，建立一套规范的操作程序和规章制度，形成射线辐照剂量测量的 ESR/丙氨酸剂量计剂量监测体系，获

得其中国计量科学研究院认证校准证书。

图 9 ESR/丙氨酸剂量计剂量监测体系及证书

4) 通过了 CNAS 实验室评审和能源局专家组验收。1.5 MeV 电子束辐照平台不仅能满足科研用 β 射线常规辐照要求，还通过自主研发，进一步实现了三代核电 β 射线低剂量率辐照考验条件要求，可为材料改性、科学试验等提供 β 射线辐照。同时起草了包含 1.5 MeV 电子束辐照平台和三套钴源为主体的辐照实验室相关人员、设备、物料、法规等技术资料文件，顺利通过了 CNAS 实验室评审，获得了相关资质。

2014 年 6 月 9 日国家能源局在上海主持召开了 β 辐照试验装置技术成果验收会。来自于中国科学技术大学、环保部核与辐射安全中心、上海核工程设计研究院、中国核电工程有限公司等多家单位的专家听取了装置的研制报告，审查了设计技术资料、验证试验报告等文件，见证了 β 辐照试验装置演示试验。建成的 β 辐照试验装置剂量率可调，功能可拓展，为开展相关技术领域科研试验创造了条件。同时在核电站设备鉴定 β 辐照试验领域填补了国内空白，相关技术达到国际领先水平，对推动我国核电事业的发展和核电设备国产化具有重要意义。

图 10 CNAS 实验室评审暨 β 辐照试验装置技术成果验收会

高性能碳化硅纤维的研制进展顺利，实验室已具备制备第二代碳化硅纤维的能力。堆用聚合物将继续在核用电缆加工测试平台上进一步研发常规和高温核用电缆，开展各项性能的测试和鉴定。1.5 MeV 电子束辐照平台提供 β 辐照鉴定试验后，将成为我国唯一一套专业针对核电材料和设备鉴定的 β 辐照试验装置，为我国核级电缆材料及相关设备的试验验证与质量鉴定提供有力的技术支持。

Progresses in developing other materials for the reactor

Reactor Materials Science and Engineering Division II

There are three subtopics in the other reactor materials for the reactor, the study on the high performance silicon carbide fiber, the polymer materials for the reactor and the 1.5 MeV electron beam irradiation platform construction.

Study on preparation technology of high performance SiC fiber

Study on radiation curing process of polycarbosilane (PCS) fiber. Because the PCS green fiber is very fragile, first the problem of transporting the fiber was solved, and then the technical docking problem of PCS fiber from the purchase, irradiation and subsequent sintering were optimized. The irradiation of bulk fiber was achieved and the radiation curing of PCS fiber was completed by about 15 kg. The results showed that the oxygen content of the irradiated PCS and SiC fibers was less than 3% and the minimum was only 0.7%, which achieved the oxygen content index of the high performance SiC fibers.

Fig.1 Radition cured PCS fiber

Study on sintering process of SiC fiber. SiC fiber was prepared by sintering the radition cured PCS fiber. The laboratory focuses on two-step sintering process. The results showed that the SiC fiber was successfully prepared by the two-step sintering process with radiation cured PCS fiber as raw material. By optimizing the sintering process, the basic process parameters of two-step sintering were preliminarily determined, which laied a foundation for subsequent mass sintering.

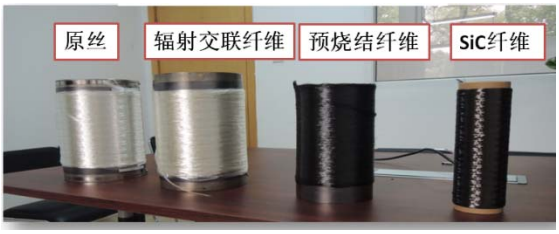

Fig.2 From PCS fiber to SiC fiber sample

The established of TMSR new material preparation laboratory. The sintering experiment line of SiC fiber was designed and fabricated. The goal is to prepare SiC fiber from the radiation cured PCS fiber, and the main equipment of the sintering experiment line has passed the factory acceptance. This line adopts two-step sintering process, which is designed to process 100 kg of second generation SiC fiber, and can also be upgraded for third-generation fiber sintering. In the laboratory reform, according to installation conditions the sintering experiment line was overall designed. Laboratory renovation started from July 2014, completed at the beginning of December. At the end of the year, the SiC fiber sintering equipment was installed. Based on the analysis and test conditions, the performance analysis and testing platform of SiC fiber was established, and used to quality control of fiber development process. The process control and product quality control system are established gradually with the development of SiC fiber process.

Fig.3 SiC Fiber sintering Laboratory

Polymer materials for the reactor

The main course of polymer materials for the reactor is the conventional (the service temperature is about 90 ºC) and the high temperature (the service temperature is about 250 ºC) nuclear power cable materials study and preparation. The main progress is as follows from 2013 to 2014.

Fig.4 60 years nuclear power cable material thermal life assessment report (partial)

The test has been completed for the 60 years hot life evaluation of the nuclear power cable material. the 3 mm× 10 mm 1E/K1 power cables for under 0.6/1 kV power prepared by cable insulation and covering materials with 60 years of service life have been evaluated thermal life test (150 ºC/ 2 376 h aging) by the national electric wire and cable quality

supervision and inspection center (CT13-4973). The 1 500 kGy ^{60}Co gamma-ray irradiation aging experiment was underway.

The high temperature nuclear power cable (the service temperature is about 250 ºC) prepared with PEEK materials has been evaluated the thermal life test (280 ºC/168 h aging) and the gamma-ray irradiation aging experiment by the national electric wire and cable quality supervision and inspection center (CT14-2984).

Fig.5 The PEEK high temperature nuclear power cable and the gamma-ray irradiation aging experiment

It has been tested for the full-peformance evaluation about the nuclear power K1 heat-shrinkable tube. The nuclear power K1 heat shrinkable cable accessories have been prepared with 60 years service life.

Table 1 The performance of 60 years snuclear power K1 heat shrinkable cable

Item	Unit	Result
Tensile strength	MPa	11.2
The break elongation	%	272.8
The performance after180 ℃/150 h thermal aging		
The break elongation	%	152.1
γ-ray irradiation test after 180 ℃/150 h thermal aging (10 kGy/h)		
500 kGyThe break elongation	%	119.0
1 000 kGyThe break elongation	%	71.2
β-ray irradiation test after 180 ℃/150 h thermal aging (20 kGy/h)		
500 kGy The break elongation	%	128.7
1 000 kGy The break elongation	%	58.3

It has been completed that the installation and debugging of torque rheometer, high temperature single/twin-screw extruder and its supporting equipments, which endues the laboratory with the ability of high temperature cable material formula research and high temperature cable preparation. Adding electronic tensile machine, melt index tester, oxygen index tester and UL-ageing oven, there is a set of processing and evaluation platform about nuclear power cable.

Fig.6 The experimental machine about high temperature nuclear power cable

1.5 MeV electron beam irradiation platform construction

1) It has been completed that the installation and debugging of the mechanical, electric, control system about the electron accelerator and its supporting water/air/electric system, shielding system, beam equipments system, safety interlock system, and so on, which signs that the construction of 1.5 MeV electron beam irradiation platform construction was over. In July, 2013, the stable beam current with designed energy and current have been achieved successfully. After a series of dose measurement and detection, the environmental radiation dose surrounding their radiation platform dose was lower than design value, which achieves the goal of protection design requirements.

Fig.7 1.5 MeV electron beam irradiation platform

2) After a series of debugging experiments, it has been achieved that the low dosage β-ray irradiation conditions by the shielding method or the second scaning technique when the electron energy is 1.2 MeV. The dosage experiment with good repeatability shows that 20 kGy/h can be obtained, which signs that the low dosage β-ray irradiation condition for third generation nuclear power plant, such as AP1000, can be carried out in our country. Moreover, other low dosage β-ray irradiation condition, 10 kGy/h, 30 kGy/h,50 kGy/h and 70 kGy/h, have been further achieved also.

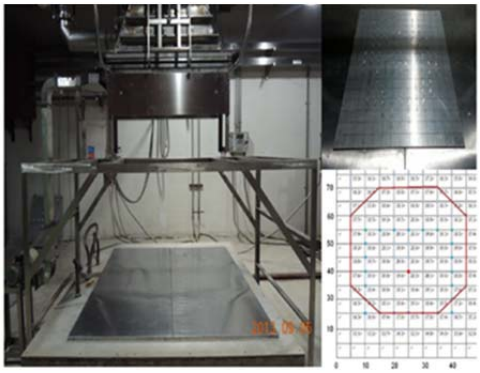

Fig.8 The low dosage β-ray irradiation experiment

3) The ESR/alanine dosimeter dosage monitoring system has been founded. The use of alanine dose reader and a standard alanine dosimeter established a set of standardized operating procedures, rules and regulations, formed ESR/ alanine dosimeter dose monitoring system for radiation dose measurement, which obtained calibration certificate from China national institute of metrology.

Fig.9 The ESR/alanine dosimeter dosage monitoring system and the certificate

4) Passed successfully the CNAS laboratory accreditation and obtained acceptance from China Energy Bureau expert group. 1.5 MeV electron beam irradiation platform not only can satisfy the common beta-ray irradiation requirements of scientific research, but also meet the beta low dose rate irradiation test conditions for the third generation of nuclear power plant through further independent research and development. The beta ray irradiation processing can be provided for material modification and scientific research experiment. It has been writed that the radiation laboratory technical data files about personnel, equipments, materials, regulations, and so on, involving 1.5 MeV electron beam irradiation platform and other three sets of cobalt source, which is helpful to pass the CNAS laboratory accreditation and obtain successfully the relevant qualification.

On June 9, 2014, the technological achievements verification meeting of beta irradiation testing device was organised by China Energy Bureau in Shanghai. the experts from University of Science and Technology of China, Nuclear and Radiation Safety Center, Shanghai Nuclear Engineering Research and Design Institute, China Nuclear Power Engineering Co., Ltd., and other units, listened to the device's research report, investigated the design technical data and validation test documents, witnessed the beta-gay irradiation demonstration test. The dosage rate of the beta irradiation test device can be adjusted and the function can be expanded, which can create good resolution for the scientific research experiment about the related technology field, at the same time fill the domestic blank in the field of nuclear power plant equipment appraisal about beta irradiation, and reach the international leading level. It is of great significance to promote the development of China's nuclear power plant and relevant domestic equipment.

Fig.10 The CNAS laboratory accreditation and the technological verification meeting of beta-ray irradiation testing device

The development of high performance SiC fiber is progressing well, the laboratory has the ability to prepare the second generation SiC fiber. The polymer materials for the reactor will continue to develop conventional and high- temperature nuclear cables using the nuclear power cable processing and evaluation platform and carry out testing and identification about various properties of nuclear power cable. After 1.5 MeV electron beam irradiation platform providing beta-ray low dose rate irradiation test, it will become the only beta-ray irradiation test facility for nuclear power plant materials and equipments, which will provide strong technical support for test verification and quality identification for nuclear cable materials and related equipments in our country.

材料评估测试平台

堆材料一部　上海光源

在中科院战略先导专项《未来先进核裂变能-钍基熔盐核能系统》资助下，围绕国内首个熔盐堆材料的性能评估及特殊工艺参数要求，开发研制/购置了一系列熔盐堆用材料测试设备，建立了堆材料评估测试平台。材料评估测试平台涵括：热学/力学测试平台、成分分析平台、微观结构分析平台、材料腐蚀性能测试平台、高温离子束辐照平台和同步辐射原位实验平台。平台现有仪器设备 100 余台（套），固定资产价值约 1 亿元。

材料评估测试平台可精确测定堆设计及堆安全评估所需的各类材料数据，具备了熔盐堆用镍基高温合金、高致密核石墨等材料的综合测试评估能力，实现了对堆材料批量评估、筛选的能力，为 TMSR 专项的顺利实施提供了有力支撑。

常规测试装置

(a) 电子探针　　(b) 扫描电镜

(c) 250 kN 万能试验机　　(d) X 射线荧光光谱仪

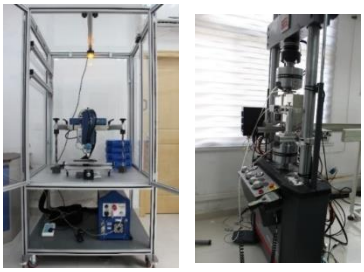

(e) 残余应力分析仪　　(f) 低周疲劳试验机

图 1　材料评估测试平台部分设备

建立了各种熔盐堆用材料的成分、组织、力学/物理/化学性能常规分析测试平台（图 1），其综合测试能力已达到国际先进水平。目前，利用该平台开展了合金及核石墨材料腐蚀及辐照前后的微观结构和性能测试，获取了微观组织、高温力学性能等重要信息，为核材料的研发、分析评估及服役提供了基础数据。

2013−2014 年度主要完成了电子探针、扫描电镜、250 kN 万能试验机、低周疲劳试验机、X 射线荧光光谱仪、温等静压机、复合材料裂纹检测仪、X 射线应力仪、真空高温万能试验机三坐标仪、线切割机、数控铣床、弯管机等设备的安装、调试、验收，验收性能达到预定指标。重复上述设备总体运行状态良好，部分设备如电子探针、扫描电镜、低周疲劳试验机使用率达 95%以上。提升了核材料力学性能测试、微结构分析以及材料加工、制备综合能力。

为了评估石墨材料的高温力学性能，2014 年 5 月完成真空高温万能试验机技术规格说明书编制，同年 8 月完成招标预审会，10 月完成招标，11 月合同签订,由于交货期较长，该设备将于 2015 年 8 月到货。因此，核能材料评估测试平台逐渐完善，由专人对设备进行日常使用及维护管理。力学、热学等主要相关测试设备每年定期年检，以确保测试数据的准确性。建立了一系列材料分析测试方法，部分已申请成为 ASTM 测试标准，并积极推进实验室 CNAS 认可工作。

材料熔盐相容性测试装置

基于熔盐堆材料腐蚀性能评估需求，建立了国内领先水平的堆材料与熔盐腐蚀实验室，成功研制了一套能够实时监测腐蚀失重和腐蚀产物浓度的装置——高温熔盐称重-电化学检测联动系统（图 2），制定了可形成企业规范的高温氟盐腐蚀测试规程，并形成了国内唯一的碳基材料熔盐相容性研究装置。

(a)　FLiNaK 熔盐腐蚀实验装置

(b) 涉铍腐蚀实验室

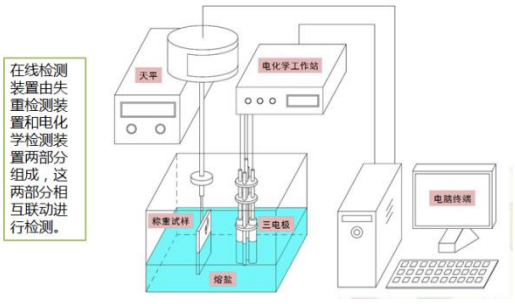

(c)熔盐腐蚀在线检测装置示意图

图 2 材料腐蚀性能测试平台

设计了自然对流腐蚀测试回路，通过温差实现熔盐在回路管道中的自然对流，模拟堆中材料在慢流速熔盐中的腐蚀行为，获得温差驱动质量迁移的定量腐蚀数据。

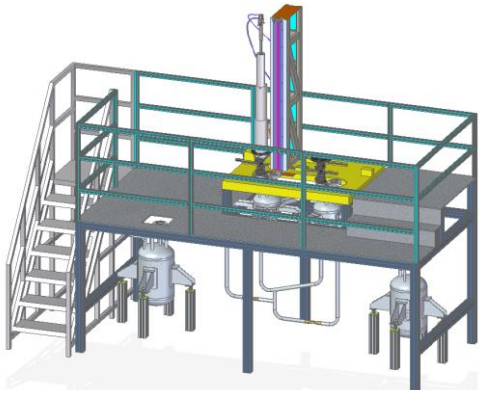

图 3 对流腐蚀回路示意图

图 3 是该回路的设备示意图，主要由回路主体结构、熔盐转运罐、中控系统、加热保温装置、气路真空系统、通风报警系统、液位计、设备支撑台架等组成。已完成各子系统合同签定，正在进行设备购置及非标加工。

成功研制了多套熔盐原位实验装置，以揭示核能材料在类熔盐环境下的各种性能。2014 年完成熔盐环境原位拉伸实验装置的加工、安装、调试，验收，已开展合金材料高温氩气下初步试验。设备实物图如图 4 所示。研制了熔盐环境下原位蠕变-疲劳设备，该装置主要用于测试金属材料在氟化熔盐环境中的高温蠕变性能和高温持久性能。原位蠕变-疲劳设备主要由拉伸单元、夹具、真空釜、加热炉、注盐罐、排盐罐、气体回路、真空机组和控制系统等组成。现已完成评审采购，进入制造阶段。

图 4 熔盐环境原位拉伸试验装置

材料辐照及测试装置

以 TMSR 堆材料的离子束辐照和分析需求为导向，对 4 MV 加速器进行了改造（表 1），研制了离子束辐照装置和离子束分析装置。该项目的顺利完成，使得 4 MV 加速器具有了离子束分析和离子束辐照两大功能，提升了离子束技术水平，为 TMSR 项目堆材料的研究提供了一个技术平台。

表 1 4 MV 加速器改造前后性能指标对比

主要功能指标	改造前	改造后
额定电压	3.0 MV	4.3 MV
电压稳定度	<±3 KV	<±2 KV
束流强度	H^+: 0.3MeV, 3μA,3.0 MeV, 3 μA; He^+: 3.0 MeV, 1 μA; Ar+: 3.0 MeV, 1.1 μA	H^+: 0.3 MeV, 8 μA, 3.0 MeV, 5 μA; He^+: 2.0 MeV, 2 μA; Ar+: 3.0 MeV, 2.0 μA; Xe+: 3.0 MeV, 1.0 μA
束流截面	<3 mm	3 mm
束流纹波	<±5%	<±5%
出束真空度	7×10^{-5} Pa	4×10^{-6} Pa
控制方式	机电	计算机，机电
束流诊断方式	法拉第筒	法拉第筒、束流剖面仪

顺利完成了 4 MeV 辐照装置的改造方案设计、安装和调试，改造后的加速器端电压达到 4.3 MV，束流品质（能量、流强、聚焦特性、稳定性等）得到了提升，可以满足堆材料的轻离子或重离子的离子束辐照需求，以及离子束分析需求。新建的离子束分析装置及其数据测量获取系统，可实现在高低温下（液氮温度到 700 ℃）进行卢瑟福背散射、质子激发 X 射线荧光、弹性反冲等分析。在国内首次研制成功了高低温（液氮温度到 950 ℃）离子束

辐照及在线换靶装置，整体达到国际同类设备先进水平，实现了堆材料的高温离子束辐照能力，可以开展熔盐堆材料的辐照效应机理研究和离子束材料分析研究。

建立了我国核电设备 β 射线辐照考验试验平台——TMSR-1.5 MeV 电子束辐照平台（图 5），成功实现了预定设计能量束流稳定出束，辐照平台周围剂量达到了防护设计要求，顺利通过国家能源局验收，获得我国核电设备 β 射线辐照能力 CNAS 认证。

图 5　1.5 MeV 电子束辐照平台

同步辐射原位实验装置

依托上海光源，研制了多套针对核能材料的同步辐射联用实验装置，完成了镍基高温合金装置、原位焊接装置、高温固液界面原位装置、原位分子振动光谱、非弹性散射等多种联合同步辐射原位测试装置的加工、安装、调试，陆续进入预验收和正式整体验收阶段。建立了材料基础研究所需的同步辐射实验方法，实现了部分材料的原位、在线、动态研究，具备了在熔盐环境下开展材料研究的能力。

穹顶高温镍基合金原位装置

图 6　穹顶铍窗高温热台

穹顶铍窗高温原位研究装置是联用装置中的典型代表，用于同步辐射、XAFS、XRD、成像和掠入射等方法高温下的原位动态测试，以分析合金/熔盐界面腐蚀机制、合金凝固机制、液态金属结构、析出相结构以及裂变产物 Te 与合金的相互作用等。该装置由穹顶高温真空室、夹持、微机温控系统、旋片式真空泵、涡轮分子泵、氦气供气装置、冷却水循环仪和六自由度电动样品定位台等组成，已于 2013 年完成了设计、评审和委托（美国 ADC 公司）定制加工合同，执行经费人民币 49 万元。该装置的核心——穹顶高温热台如图 6 所示。

高温熔盐原位研究样品池系统

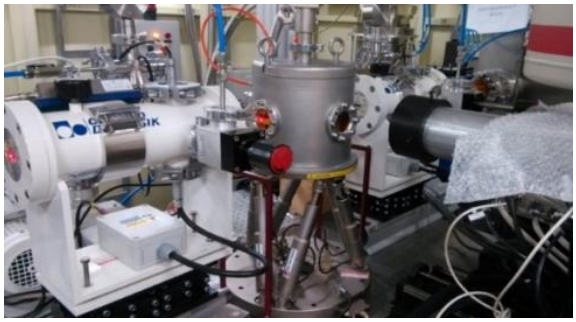

图 7　同步辐射高温熔盐原位装置在线调试

高温熔盐原位研究样品池系统已于 2013 年在上海光源完成安装调试（图 7），并利用 14 W 吸收谱线站进行在线测试，主要验收指标均已达标。利用 XAFS 和 X 射线小角散射等方法获取高温状态熔盐中金属离子种类、化学价态和近邻配位结构和熔体结构等信息。应用该装置探索了不同温度下 UF_4 在 FLiBe 熔盐中的局域结构变化，发现了熔盐中铀最近邻的 F 离子随温度升高发生的重新排列现象。

总结和展望

核能材料评估测试平台逐渐完善，材料的力学、热学、微结构分析测试能力不断增强。平台设备由专人负责运行维护，力学、热学等相关测试设备每年定期年检，以确保测试数据的准确性。

建立了国内领先水平的堆材料与熔盐腐蚀实验室。熔盐环境原位拉伸试验装置调试、验收，初步开展了合金材料高温试验；确定了自然对流腐蚀回路设计方案。多台同步辐射联用装置开始安装、调试，部分设备已整体验收，可以在上海光源上使用，实现部分核能材料的原位、动态、在线的研究。利用改造后 4 MV 加速器和离子束分析装置，开展了堆材料的高温离子束辐照研究。

材料评估测试平台基本具备了熔盐堆用镍基高温合金、高致密核石墨等材料的综合测试评估能力，为 TMSR 专项的顺利实施提供了有力支撑。

Material evaluation test platform

Department of nuclear materials SSRF

Supported by the strategic precursor project of the Chinese Academy of Sciences "Future Advanced Nuclear Fission Energy - Thorium-based Molten Salt Nuclear Energy System", based on the performance evaluation and special process parameters of material used in the first molten salt reactor in China, a series of material testing equipment for molten salt reactor were developed and purchased, and the material evaluation test platform was established.

The material evaluation test platform includes: thermal/mechanics test platform, component analysis platform, microstructure analysis platform, material corrosion performance test platform, high temperature ion beam irradiation platform and synchrotron radiation in situ experimental platform. The platform has more than 100 facilities, with fixed assets over 100 million RMB

The material evaluation test platform can accurately determine the various material data required for reactor design and safety assessment, including the ability of comprehensive analysis of nicle based super alloy and high-density graphite. The platform has the ability of batch assessment and screening of nuclear materials, and provides strong support for the implementation of TMSR.

General test equipment

(a) Electronic probe

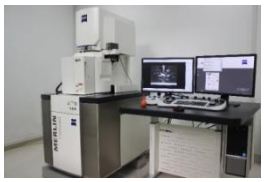

(b) Scanning electron microscope

(c) 250 kN Universal testing machine

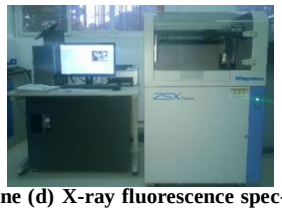

(d) X-ray fluorescence spectrometer

(e) Residual stress analyzer

(f) Low cycle fatigue testing machine

Fig.1 Typical equipment in material evaluation test platform

Conventional analysis and test platform for molten salt reactor materials composition, organization, mechanical / physical / chemical properties is established (Fig.1). The comprehensive testing capabilities have reached the international advanced level. At present, microstructure and properties of alloy and nucleated graphite before and after corrosion and irradiation were studied by using this platform. The microstructure and mechanical properties at high temperature were obtained, which provided the basic data for R & D, evaluation and service of nuclear materials.

In 2013 and 2014, the installation, commissioning and acceptance of a series equipments have been completed. These equipments include: electronic probe, scanning electron microscope, 250 kN universal testing machine, low cycle fatigue testing machine, X-ray fluorescence spectrometer, isostatic press, composite material crack detector, X-ray stress analyzer, universal vacuum high temperature testing machine and three coordinate measuring machine, wire cutting machine, CNC milling machine, pipe bender and other equipment.

Overall, all the equipment is working well. The usage of some instruments such as electronic probes, scanning electron microscopy, low cycle fatigue testing machine exceeds 95% every year. The comprehensive ability of nuclear material mechanical properties testing, microstructure analysis, material processing and preparation has been enhanced.

In order to evaluate the high-temperature mechanical properties of graphite materials, in May 2014, the technical specification of vacuum high-temperature universal testing machine was completed, the pre-bidding meeting was completed in August, the bidding was completed in October and the contract was signed in November. The device arrived in August 2015.

Therefore, the nuclear material evaluation test platform is gradually being improved. The daily use and maintenance management of each equipment is the responsibility of professionals. In order to ensure the accuracy of test data, mechanical, thermal and other major related test equipment regularly is calibrated every year. A series of material analysis and testing methods have been established, some of the testing standards have become ASTM standards, and the CNAS conformity work in the laboratory has been actively promoted.

Test equipment of materials-molten salt compatibility

A molten salt corrosion laboratory which is leading domestic level was established for reactor structures evaluation in corrosion resistance. A linkage device (Fig.2) capable of weighing and electrochemical detection was assembled. In this device, corrosion weight loss and corrosion product concentration in molten salt could be monitored in real-time. An enterprise specification for high temperature fluoride salt corrosion test was set.

(a) FLiNaK corrosion experimental equipment

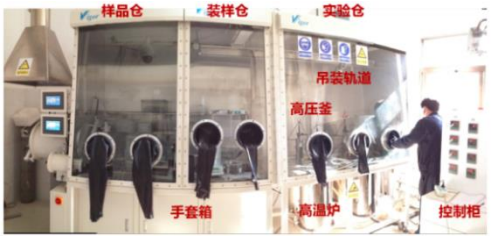

(b) FLibe corrosion laboratory

(c)

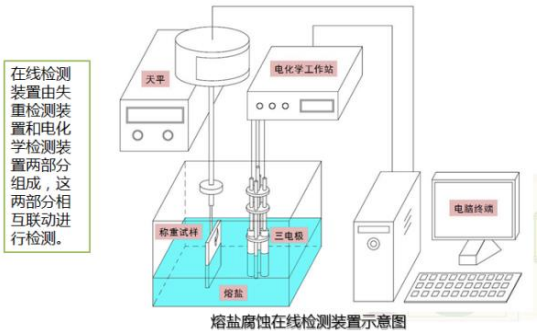

(c) Schematic diagram of an on-line detection device for molten salt corrosion

Fig.2 Testing platform for materials corrosion resistance

A natural convection corrosion test loop was designed. The convection of molten salt in the loop pipe is realized through temperature difference. Corrosion behavior of reactor material in slow flow molten salt was simulated, consequently quantitative corrosion data of temperature difference driven mass transfer could be obtained.

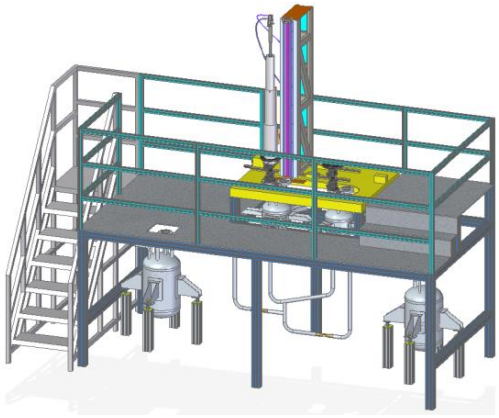

Fig.3 Schematic diagram of the convective corrosion loop

Fig.3 is the schematic diagram of the equipment in the loop, which is mainly composed of the main structure of the loop, molten salt transport tank, central control system, heating and insulation device, gas and vacuum system, ventilation alarm system, liquid level gauge and support platform. The contract signing of each subsystem has been completed, equipment purchase and custom-made processing are being carried out.

Several molten salt environment in-situ materials testers were developed in order to determine various properties of the materials under molten salt environment. During 2014, a molten salt environment in-situ materials tensile tester was fabricated, installed, adjusted, and met the requirements of acceptance. Preliminary tensile tests under argon atmosphere has started with the tester. The photo of the tensile tester is shown in Fig.4. A molten salt environment in-situ materials creep-fatigue tester was designed for testing the high temperature creep and rupture property of metallic materials in fluoride salts. The creep-fatigue tester consists of a loading unit, sample clamps, an autoclave, furnaces, tanks for injecting and dumping salts, gas path, a vacuum pump, and a control system. This tester has passed the design review and procurement process, it is now under fabrication.

Fig.4 Molten salt environment in-situ materials tensile tester

Material irradiation and test equipment

Because the TMSR reactor material needs the ion beam irradiation and ion beam analysis methods, the 4 MV accelerator was upgraded (Table 1). The ion beam irradiation device and the ion beam analysis device were developed. Now, the 4 MV accelerator Lab have two main functions: ion beam analysis and ion beam irradiation, and improved the level of ion beam application technology. So, it provided a platform for the research of the material in TMSR project.

The design, installation and commissioning of the 4 MeV irradiation device were successfully completed. The upgraded accelerator voltage reached 4.3 MV and the beam quality (beam energy, beam current, focusing characteristics, stability, etc.) was improved, and meet the requirements of light or heavy ions Ion beam irradiation, as well as ion beam analysis needs. The new developed ion beam analysis system and its data acquisition system can be used to Rutherford backscattering, proton-induced X-ray fluorescence and elastic recoil analysis at high and low temperatures (liquid nitrogen temperature to 700 ℃). In China, the ion beam irradiation device is the first time successful development at high and low temperature

(liquid nitrogen temperature to 950 ℃). The sample can be changed online without vacuum broken. The main function indicators of this device has reached same level of similar equipment in the world. The studying on TMSR material irradiation effect and Ion Beam Analysis can be carried on.

Table 1 4 MV accelerator performance indicators

The main function indicators	Before upgrade	After upgrade
Rated terminal voltage	3.0 MV	4.3 MV
Voltage stability	<±3 KV	<±2 KV
Beam current	H+: 0.3 MeV, 3 μA, 3.0 MeV, 3 μA; He+: 3.0 MeV, 1 μA; Ar+: 3.0 MeV, 1.1 μA	H+: 0.3 MeV, 8 μA, 3.0 MeV, 5 μA; He+: 2.0 MeV, 2 μA; Ar+: 3.0 MeV, 2.0 μA; Xe+: 3.0 MeV, 1.0 μA
Beam cross section	<3 mm	3mm
Beam current ripple	<±5%	<±5%
Vacuum (with beam)	7×10^{-5} Pa	4×10^{-6} Pa
Control mode	Electromechanical, analog control	Computer, electromechanical, digital control
Beam diagnosis method	Faraday cup	Faraday cup, beam integrator

The TMSR 1.5 MeV electron beam irradiation platform for the beta radiation test of nuclear power equipment in China (Fig.5) has been set up. The beam under the designed energy is stable, and the dose around the irradiation platform has reached the requirements of protection design. It has passed the acceptance of the national energy board successfully. The CNAS certification of beta radiation ability of nuclear power equipment in China is obtained.

Fig.5 1.5 MeV electron beam irradiation platform

In situ experimental devices with synchrotron radiation

Multiple sets of experimental devices coupled with multi-technology on synchrotron radiation was developed for the study of nuclear materials with the support of Shanghai Synchrotron Radiation Facility (SSRF), incuding a high temperature device for in-situ study on nickel base alloys, an in-situ welding device, a high temperature device for in situ studys of solid-liquid interface, an in situ molecular vibration spectrometer, an inelastic scattering spectrometer and so on. The processing, installation, and debugging of the devices have been completed. They entered the pre-acceptance and formal overall acceptance stage one after another. The experimental methods of synchrotron radiation required for material foundation research have been established. The in-situ, on-line and dynamic research of some nuclear materials has been realized, and the ability of research on materials in molten salt environment has been achieved.

High temperature device with a beryllium dome for in-situ study on nickel base alloys

Fig.6 High temperature beryllium dome hotstage

The high temperature beryllium dome device for in-situ study is a typical representative for the multi-technology combined devices. It is used for in-situ dynamic testing with synchrotron radiation at high temperature, such as XAFS, XRD, imaging and grazing incidence methods, to analyze the corrosion mechanism of alloy / molten salt interface, the solidification mechanism of alloys, the structure of liquid metals, the structure of precipitates, and interaction of fission product Te and alloys. The device is composed of a vacuum dome chamber of high temperature, sample holder, the microcomputer temperature control system, rotary vane vacuum pump, turbomolecular pump, helium gas supply unit, water cooler and six-dimensional motorized sample-positioning system and so on. The design, review, and consigned processing of the device have been completed in 2013, funded by RMB 490 000. The core of the device- the high temperature beryllium dome hotstage is shown in Fig.6.

Sample cell system for in situ study of high temperature molten salt

The sample cell system for in situ study of high temperature molten salt has been installed and debugged in Shanghai light source in 2013 (Fig.7). It has been tested online at the 14 W XAFS beamline of SSRF, and the design specifications have been reached. The species of the metal ions, chemical valence states, near neighbouring coordination structure and melt structure of molten salt in high temperature state molten salt can be measured in this device by using XAFS and small angle X-ray scattering. The change of the local structure of UF_4 in FLiBe molten salt at different temperatures was investigated using this device. The rearrangement phenomenon of F ion of the nearest neighbor of U was foundin the molten salt with increasing the temperature.

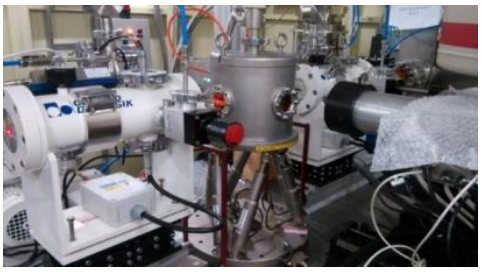

Fig.7 On-line debugging of high temperature device for in situ study of high temperature molten salt with synchrotron radiation

Conclusion and prospect

Nuclear energy material evaluation test platform is gradually improved and material mechanics, thermal, microstructure analysis and testing capabilities is constantly increase. Each device is run by someone responsible for the maintenance. In order to ensure the accuracy of the test data, each device is regularly calibrated every year.

The leading materials and molten salt corrosion laboratory is established in China. Debugging and acceptance for the molten salt environment in situ tensile device have been completed, and the alloy material test was initially carried out. Natural convection corrosion circuit design has been confirmed.

Several synchrotron radiation units are started to the installation and commissioning, some of which has been overall accepted, and put to use in SSRF. In situ on-line and dynamic studies of some nuclear materials have been carried out. The 4 MV accelerator and ion beam analyzer were upgraded; the high temperature ion beams irradiation of nuclear materials has been studied.

The material evaluation test platform basically possesses the capability of comprehensive testing and evaluation of materials such as nickel base superalloy and high density nuclear graphite, which provides a powerful support for the successful implementation of TMSR.

钍基熔盐干法在线处理

放射化学与工程技术部

钍基熔盐堆核能系统(TMSR)的首要科学目标是“钍基核能”，即实现钍基核燃料的循环利用。TMSR 实现钍基核燃料循环利用的技术路线是液态燃料钍基熔盐堆加燃料干法处理。“钍基熔盐干法在线处理”以建立适用于钍基熔盐核能系统的燃料盐干法处理流程为目标，开展氟化挥发、减压蒸馏、熔盐电化学等干法技术的工艺可行性研究，进行干法设备放大和工艺集成，并开展关键支持技术研发，重点解决氟化挥发和减压蒸馏技术从实验室走向工程应用的关键技术问题。并形成燃料盐干法处理流程设计能力，干法工艺设备设计、研发、调试和运行能力。2013−2014 年取得的进展如下：

1 TMSR 液态燃料处理流程

围绕 TMSR 钍基燃料循环利用的目标，充分考虑到燃料盐中裂变产物种类繁多、性质不一、各自含量低的特性，提出 TMSR 燃料处理流程的设计原则：1) 干法在线分离并循环有用的物质，即及时分离 U 和载体盐 ^{7}LiF-BeF$_2$ 并回堆循环；2) 干法尾料离堆冷却后，再分离 ^{233}U（^{233}Pa 衰变得到）和 Th，适时回堆循环；3) 尽可能使用成熟的技术；4) 用于 U 和载体盐分离的技术还需具备产物易重构、一定的可连续操作的特点。在上述原则指导下，选择了氟化挥发技术和减压蒸馏技术作为燃料盐在线处理的关键技术优先发展。同时发展干法尾料转化和再回收技术，选择包括高温水解技术和可用于钍铀共萃的 THOREX 工艺。目前初步确定 TMSR 燃料处理流程见图 1。该方案即缓解了燃料在线处理的强度和难度，又使得最有价值的燃料和载体盐及时循环使用，减少相应的临堆存量。

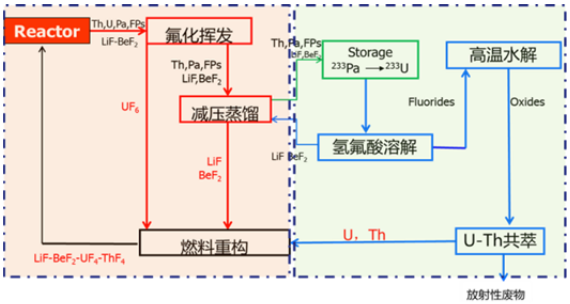

图 1 TMSR 液态燃料处理流程

2 干法关键技术

2.1 氟化挥发技术

在氟化挥发技术发展中，确定了铀氟化挥发过程红外在线分析监测和产物吸附纯化、UF_6 冷凝回收技术的技术路线（图 2），建立了高温氟化反应实验装置。利用 UF_4 和 F_2 的气-固氟化反应，建立梯度冷凝的产物收集技术，铀回收率超过 95%，并成功将红外光谱技术应用于铀的氟化挥发过程的在线监测。以 KF-ZrF4-UF_4 熔盐模拟燃料盐开展铀氟化挥发研究，红外在线监测能有效监测反应过程，U 的分离率超过 99%，UF_6 产物冷凝收率达到 95% 以上，挥发后熔盐中铀残留 10 ppm。确定了一种以 NaF 粉末、粘结剂和水为原料的 NaF 吸附剂制备工艺，所制得吸附剂孔隙率 40%~45%、平均孔径 3~4 μm、比表面积 0.4~0.6 m^2/g，静态吸附条件下最大吸附容量为 115 (mg MoF_6/g NaF)，基本满足氟化产物纯化需要。在此基础上，正在设计和研制适用 FLiBe 体系研究的氟化挥发反应实验装置。

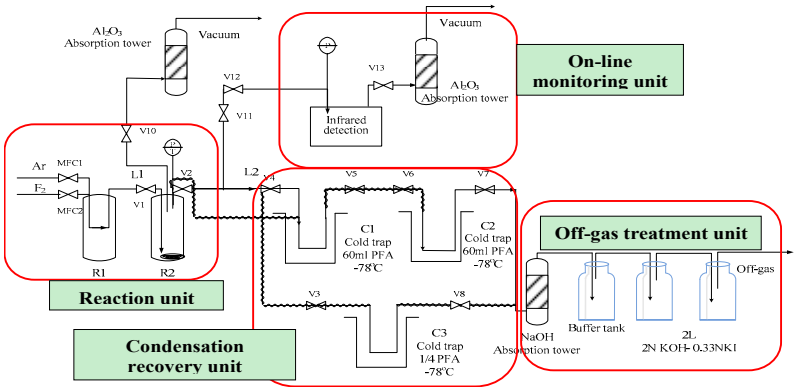

图 2 氟化挥发铀分离与纯化回收工艺流程图

2.2 冷冻壁技术

氟化挥发工艺中高温氟气和高温液态氟盐的“协同”作用，对可预知范围内的金属材料都会产生严重腐蚀。为了降低工艺过程对材质的腐蚀，借鉴化工和冶金行业中常用的冷却壁或冷冻壁技术，发展熔盐体系冷冻壁技术用于干法处理工艺，减轻器壁腐蚀，延长反应器服役期，从而减少次生放射性废物的产生。研制了一套硝酸盐体系的冷冻壁技术的实验研究装置（图 3），在冷冻壁实验装置上，通过控制温度观察了熔盐冷冻壁从静态形成到平衡的过程，图 3 右下角为形成的冷冻壁实物图。初步试验结果表明，通过控制热交换，可以有效形成并维持冷冻层，热电偶测温法能有效监测冷冻层的形成及厚度。后续将对此设备进行改造，使之具备开展氟盐体系研究的条件，重点研究冷冻壁形成对容器内壁的保护作用。

图 3 冷冻壁技术实验装置和形成的冷冻壁外观图

2.3 氟盐减压蒸馏技术

在减压蒸馏技术发展中，研制了克级热失重蒸发装置，初步获得了 FLiNaK 熔盐的蒸馏工艺条件和稀土氟盐的相对挥发度数据。还研制了百克级密闭式蒸馏装置，该装置可利用温度梯度驱动熔盐蒸发、冷凝、收集，获得了温度场对氟盐冷凝收集行为的影响，实现载体盐高回收率(98%)，回收盐中稀土氟化物去污因子高于 10^2。在氟盐蒸发、冷凝行为研究的基础上，设计、研制了千克级高蒸发面积的卧式减压蒸馏装置，在该装置上不但可进一步研究减压蒸馏技术分离载体氟盐的可行性，而且能够对前期研究中获得的蒸馏工艺进行验证和优化。目前在此装置开展千克级的 FLiNaK 蒸馏实验中，盐收集率可达 94%以上，蒸发速率约 1 kg/h。综上研究结果表明：减压蒸馏技术用于载体盐的纯化与回收是可行的，并研究确定了影响熔盐收集率和纯度的各种因素。后续将开展 FLiBe 体系的减压蒸馏工艺研究。图 4 为目前已研制的设备及主要功能。

图 4 减压蒸馏熔盐回收技术的研究与工艺装置（左：克量级研究装置；中：百克量级研究装置；右：千克级工艺研究装置）

2.4 氟化挥发和减压蒸馏工艺冷态贯通

用 FKZr 熔盐体系模拟熔盐堆载体盐，在冷态条件下贯通了氟化挥发和减压蒸馏两个工艺段，重点研究铀和裂变产物在工艺过程中的走向与分布。在贯通实验中，氟化挥发工艺确定了 550 ºC 的氟化反应温度，含有 UF_4 和模拟裂变产物氟化物的 KF-ZrF_4 (58-42 mol%)混合盐在 0.2 L/min 的 20% F_2/Ar 混合气作用下持续反应，气体产物通过保温管道，进入−60 ºC 的两级 PFA 冷阱中进行冷凝收集，氟化过程中利用红外光谱仪对气体产物组成进行在线取样分析。然后对经过氟化挥发的混合熔盐进行密闭式蒸馏，蒸发温度 1 000 ℃。结合仪器分析获得了工艺过程中裂变产物与铀的分布及产物中裂变产物的去污系数（图 5）。在工艺贯通实验中，U 回收率超过 95%，U 产品中裂变产物的去污大于 10^3，载体盐的回收率超过 98%，回收盐中稀土裂变产物的去污约为 10^2。

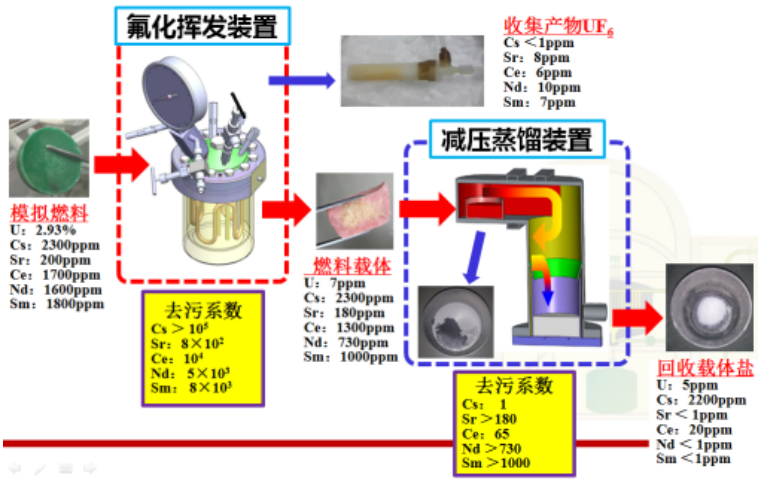

图 5　裂变产物和铀在分离工艺流程中的走向

2.5　氟盐体系电化学技术

在不同熔盐(FLiNaK, FLiBe, LiCl-KCl)中进行了铀电解分离实验研究，在 FLiBe 熔盐中铀分离率达 92%，LiCl-KCl 熔盐中铀分离率达 98%，在 FLiNaK 熔盐中分离率达 73%；在不同熔盐(FLiNaK, FLiBe, LiCl-KCl)中研究了铀的电化学性质并测定了基础参数；固化了 FLiNaK 熔盐参比电极和 LiCl-KCl 熔盐参比电极制作工艺，初步完成了 FLiBe 熔盐中参比电极的制备和工艺完善；阳极研究取得进展，FLiNaK 熔盐中石墨阳极的反应机理与产物表征表明石墨表面的阳极反应与电解条件密切相关。

表 1　不同熔盐中铀电解分离实验结果

熔盐	电解前 (U wt%)	电解后 (U wt%)	铀分离率 (%)
FLiBe	2.27	0.18	92.03
FLiNaK	7.68	2.02	73.70
LiCl-KCl	1.52	0.028	98.14

3　展望

针对 TMSR 燃料循环的需求，对可能适用于氟盐处理的技术或工艺进行了原理验证和筛选，确定了以氟化挥发分离铀和减压蒸馏纯化载体盐为优先发展技术、熔盐电化学技术作为备用技术的发展思路。就目前来说，所有的研究装置和研究主要是面向实验室级水平（百克级至千克级），离真正的实用化还有一段距离。除了实验量的差异，在可供热室内使用方面还有不少的功能未被实现，热室内实验装置的远程操控和过程监测一直是干法设备使用过程中的主要难点之一。

后续的工作重点用模拟燃料或真实燃料进行基本工艺单元的验证和优化，包括氟化挥发、减压蒸馏和熔盐电化学工艺单元。研发从冷态实验到示范实验的关键技术，重点研发可远程操控的干法分离设备。掌握不同输入条件下盐、An 和 FP 在各工艺单元中的轨迹或走向，废物类型与产生量，在此基础上进行干法分离全流程物质平衡动态模似，评估和优化 TMSR 燃料处理流程。

Pyroprocessing technologies for on-line treatment of TMSR fuel

Department of Radiochemistry and Engineering

The primary scientific goal of the Thorium-based Molten-Salt Reactor system (TMSR) is “thorium-based nuclear energy”, that is, the thorium-based fuel cycle. The technical route to realize the thorium-based fuel cycle in TMSR is liquid fueled TMSR coupled with pyroprocessing facility. This study has been devoted to establishing a fuel processing flowsheet suitable for TMSR system and to achieving the following purposes: 1) demonstration of process feasibility of pyroprocessing technologies, such as fluoride volatility, low pressure distillation, molten salt electrochemistry, etc; 2) the enlargement of process equipments and the integration of pyroprocessing technologies; 3) solution of the key technical problems in the industrialization of fluoride volatility and low pressure distillation; 4) qualification of the ability of designing TMSR process flowsheet and the R&D, commissioning and operation of pyroprocessing equipments.

The main progresses obtained in recent two years are listed as follows:

1 Fuel processing flowsheet for TMSR liquid fuel

Principles for designing TMSR fuel processing flowsheet based on the target to fulfil thorium based fuel cycle in TMSR and full consideration of the characteristics of fission products(FPs) have been proposed as follow: 1) separating and recycling the most valuable UF_4 and carrier salts on-line as soon as possible using pyroprocessing technologies; 2) separating ^{233}U (decay from ^{233}Pa) and Th from the residue after cooling for several months for recycling at a suitable time; 3) choosing relatively mature technologies as much as possible; 4) the technologies used for the separation of U and carrier salt should also be characterized by easy reconfiguration of the products and continuous operation. Under the guidance of the above principles, fluoride volatility and low pressure distillation technologies are selected as the key on-line processing technologies. Meanwhile, process tailings transformation and recycling technologies have been also under development, including pyrohydrolysis and Modified THOREX process for the co-extraction of uranium and thorium. The preliminary scheme of fuel processing flowsheet is shown in Fig.1. The scheme not only relieves the strength and difficulty of on-line processing, but also makes the most valuable fuel and carrier salt recycled in time and minimize the out-of-reactor inventory.

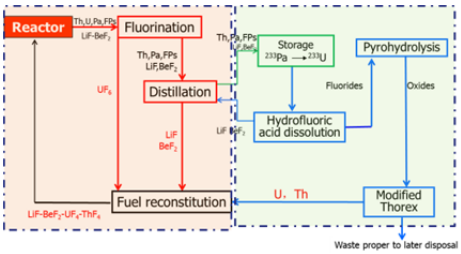

Fig.1 The preliminary processing flowsheet for TMSR liquid fuel

2 Key pyroprocessing technologies

2.1 The fluoride volatility technology

For the fluoride volatility technique, we have determined a pathway that includes IR spectroscopy to monitor the process, an adsorption method to purify the products, and gradient condensation to collect the volatilized UF_6. The equipment has been built, and the IR instrument and a technique for on-line monitoring of the fluoride volatility process have also been developed. A series experiments have proven that UF_6 can been recovered by using the fluoride volatility process from UF_4 powder or eutectic UF_4-FKZr, and the recovery ratio of U is over 95%. A method for preparing the NaF adsorbent from NaF powder, a binder, and water as raw materials has been developed. The adsorbent exhibits excellent properties, namely, a void fraction of 40%~45% and an average pore diameter of 3~4 μm. The maximum adsorption capacity for MoF_6 is 115 mg MoF_6/g NaF, which meets to the requirements of the purification procedure.

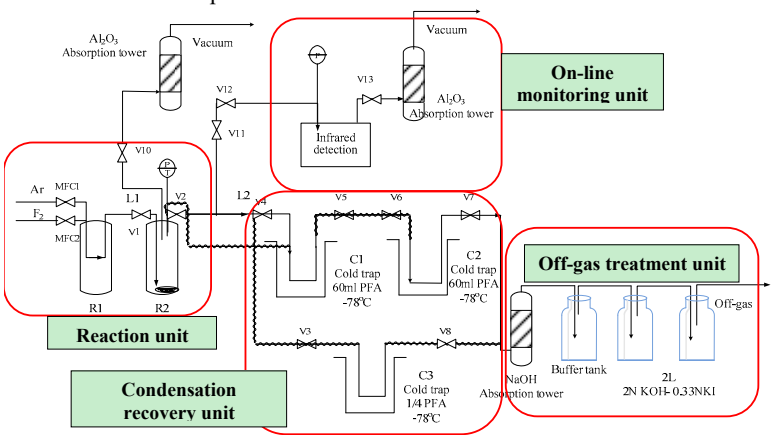

Fig.2 The process for uranium volatility, purification and recovery of UF_6

2.2 Frozen-wall technology

The coordination effects of fluorine and molten fluoride salts during the fluoride volatility process will cause severe corrosion of any known metal construct materials. To prevent such corrosion, we are planning to develop a technique called the “frozen-wall” which is extensively applied in the metallurgical industry. This technique will effectively prolong the lifetimes of the fluorinator and therefore decrease the volume of radioactive waste produced by the process. A research facility for investigating the nitrate system has been built, and the preliminary results indicate that a nitride salt frozen wall can be formed and maintained by controlling the heat exchange rate. The state of the frozen wall and its thicknesses can be measured by monitoring the temperature with thermocouples. Thus, the frozen wall could be an option for solving the challenges arising from corrosion. Subsequently, the equipment will be upgraded to provide conditions for operation of fluoride salt, it will focus on research of the protection effect of frozen-wall for the inner wall of fluorinator.

Fig.3 Picture of frozen-wall facility and image of the formed frozen wall

2.3 Low pressure distillation technology

A gram-scale vacuum thermogravimetric system has been developed, and the distillation rate of FLiNaK and the relative volatility of a series of RE fluorides have been determined experimentally using this system. We have developed a 100 gram-scale fully sealed distillation device in which the distillation, condensation, and collection of the molten salt are driven by the temperature gradient. The dependence of the collection efficiency on the temperature field was investigated in detail, and a recovery ratio of more than 98% with DF of REs more than 10^2 was obtained. Kilogram-scale distillation of FLiNaK was performed at a horizontal distillation facility with a large evaporation surface. The evaporation rate of FLiNaK reached 1 kg/h, and the collection efficiency was more than 94%. The above-mentioned results suggest that the application of low-pressure distillation for purification and recovery of the carrier fluoride salts is feasible. Furthermore, the factors that affect the collection efficiency and the purity of the recovered salt were also identified. Further work will focus on eutectic FLiBe, which is the real coolant or carrier salt for the MSR. Fig.4 shows the home-made distillation equipments.

Fig.4 The distillation equipment of fluoride melt (Left: gram-scale vacuum thermogravimetric system; Middle: 100 gram-scale fully sealed distillation device; Right: kg-scale horizontal distillation facility)

2.4 Process integration of fluoride volatility and distillation under cold condition

The process integration experiments of the fluoride volatility and distillation were carried out in KF-ZrF_4 (58-42 mol%) molten salt. The experiment focused on the behaviors and distribution of uranium and FPs in the processes. The process parameters of the fluoride volatility were as follow: the temperature of fluorination was 550 °C, gas flow of 20% F_2-Ar gas was 0.2 L/min, the temperature of cold traps was −60 °C. The FTIR was used to detect the product gas on-line. After the fluorination, the residue salt was transferred to the closed chamber distillation system and evaporated at 1 000 °C. The distribution of FPs and U and DF of FPs in process product were determined by element analysis. The results are shown in Fig.5. In process integration experiments, the recovery ratio of U was more than 95% and the DF of FPs was over 10^3, the recovery of carrier salt was up to 98% and the DF of REs was about 10^2.

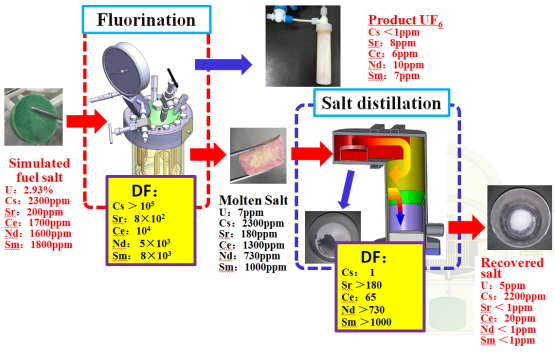

Fig.5 The distribution of FPs and U and DF of FPs in product in process integration experiments

2.5 Electrochemistry technology in fluorine salt system

The experimental researches of uranium electrolysis in different molten salts (FLiNaK, FLiBe, LiCl-KCl) have been carried out. The separation ratios of uranium in FLiBe, LiCl-KCl and FLiNaK molten salts reached 92%, 98% and 73%, respectively. The electrochemical properties of UF_4 were studied in different molten salts (FLiNaK, FLiBe, LiCl-KCl) and the foundation parameters were measured. The technology of reference electrode preparation used in FLiNaK and LiCl-KCl molten salt was established, and the preparation procedure of reference electrode in FLiBe molten salt was determined and the technology was preliminarily optimized. Considerable progress in anode research was achieved, and the reaction mechanism and product characterization of graphite anode in FLiNaK molten salt showed that the reactions on the graphite anode is closely related to the electrolysis conditions.

Table 1 Results of uranium electrolysis in different molten salts

Motlen salt	Before electrolysis (U wt%)	After electrolysis (U wt%)	Separation ratio of U(%)
FLiBe	2.27	0.18	92.03
FLiNaK	7.68	2.02	73.70
LiCl-KCl	1.52	0.028	98.14

3 Prospect

According to the demand of TMSR fuel cycle, the feasibility verification and screening of technologies and procedures that may be suitable for fluoride fuel salt treatment have been carried out. The fluoride volatility and low pressure distillation methods to separate uranium and carrier salt, respectively, have been determined as the priority technologies, while the electrochemical technology has been selected as alternative. Currently, all the researches and experiment devices are at laboratory scale (100 g to 1 kg), which is far away from the engineering application. In addition to the scale difference, many functions for the operation in hot cell still have not been realized, and the remote handling and process monitoring in hot cell are always the main challenges in the development of pyroprocessing equipments.

The later work will be focused on the verification and optimization of basic process units with simulated fuel or real fuel, including fluoride volatility, low pressure distillation and molten salt electrochemistry. The development of key technologies will be performed from cold experiment to demonstration experiment, focusing on developing remotely handling pyroprocessing equipments. A variety of parameters should be obtained in the process demonstration: the distribution and flow direction of salt, An and FPs in every process units under different conditions, and the waste type and amount. On this basis, the dynamic model of material balance in the pyroprocessing flowsheet will be established, and the TMSR fuel process flowsheet will also be evaluated and optimized.

钍基核燃料水法后处理方法研究

放射化学与工程技术部

核燃料后处理是闭式核燃料循环的关键组成部分。同铀钚燃料循环一样，在钍铀燃料循环中，针对于传统水堆 ThO_2 燃料，水法分离技术仍然是最成熟可靠的后处理方法。此外，对于钍基熔盐堆燃料的后处理而言，水法技术也能解决一些干法技术难以解决的问题。针对水法技术在钍铀燃料后处理中的应用，重点开展了铀提取流程研究、钍铀燃料处理新萃取剂研究及氟化物高温水解研究等工作。

如图 1 所示，铀提取流程可以批量快速的从辐照 ThO_2 中进行 ^{233}U 的分离提取。在混合澄清槽台架冷实验的基础上，以 ^{235}U 靶辐照产生的 FPs 作为示踪剂，在热室中进行了铀提取流程混合澄清槽台架示踪实验，结果表明设备在热室中能够平稳运行，总 γ、β 及 $^{89+90}Sr$ 去污系数分别为 3.34×10^4、2.57×10^4 及 6.71×10^6，钍铀分离系数及铀收率分别能达到 7.60×10^5 及 99.83%。与国内外已报道的同类流程相比，铀提取流程上述指标均达到或优于报道结果。其中，在钍铀分离系数这一指标上，较国外报道结果普遍高约一个数量级。而在裂变产物去污系数指标方面，在不采取额外去污措施情况下去污系数优于报道结果或相当。

考虑到 TBP 在处理钍铀燃料时的缺陷，例如钍萃取分配比及萃取容量低，容易出现“第三相”，钍铀分离系数不高等，对新萃取剂（P350）的辐照稳定性进行了初步研究，并提出了基于 P350 的钍铀回收流程，串级实验结果表明，P350 流程主要技术指标与使用 TBP 的 Thorex 流程基本上保持在同一水平，但由于 P350 流程使用较低的萃取剂流比，可以减少流程放射性有机废液的产生，同时 P350 流程在运行过程中不产生“第三相”，在钍铀燃料处理中具有较大的应用潜力。

为进一步通过水法分离技术回收经干法处理后钍基熔盐堆燃料中的有用材料，并避免强放射性氟化物废物的产生，开展了不同氟化物高温水解性质的研究，考察了单一氟盐如 ThF_4、UF_4、SmF_3 和 SrF_2 高温水解的热转化温度、反应时间，进行了转化产物结构表征和溶解实验。完成了一系列不同组份熔盐固熔体的制备、结构表征、高温水解转化产物结构表征和溶解实验。结果表明混合氟化物熔盐固熔体中的 ThF_4 在实验条件下可以实现到其氧化物的转化，加速剂如 Cr_2O_3、WO_3 等酸性氧化物能够实现难转化碱金属氟化物到其氧化物的转化。以上实验证明了利用高温水解技术实现氟化物至氧化物转化的可行性，进而可以通过水法技术进一步实现其中 Th、U 及 FPs 的分离。

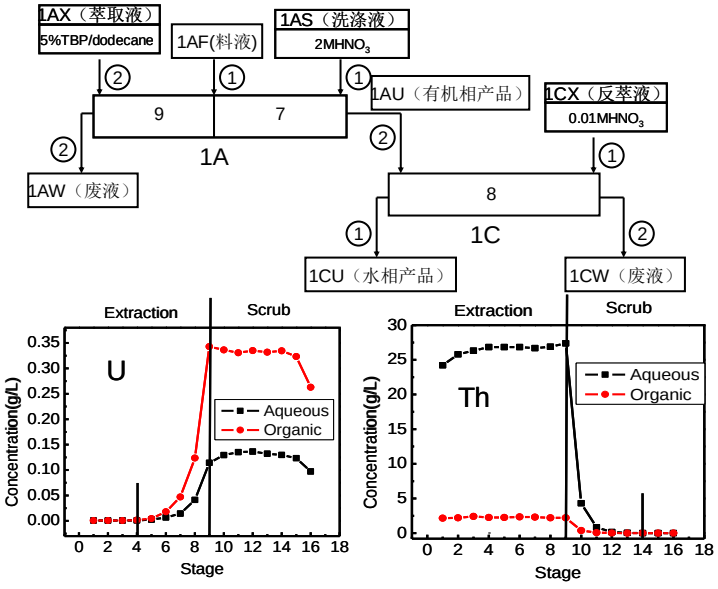

图 1 铀提取工艺流程图（上）及冷台架实验 1A 段钍、铀浓度分布（下）

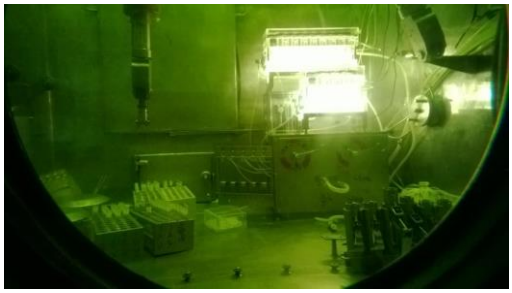

图 2　热室内运行中的 ^{233}U 提取示踪试验台架

图 3　高温水解实验装置

为掌握 ThO_2 燃料水法后处理关键技术，开展了 Th/U 萃取分离流程等研究工作。其中，铀提取流程混合澄清槽台架示踪实验结果表明，铀提取流程主要技术指标都达到或超过了国内外相似流程水平。筛选出了更适用于钍铀燃料处理的新萃取剂 P350，并提出了具有自主知识产权的基于 P350 的钍铀回收流程。此外，还开展了氟化物的高温水解研究工作，证明了其在钍基熔盐堆燃料干水结合工艺中使用的可行性，为钍基熔盐堆燃料处理提供了技术储备。

核燃料后处理技术研发对于闭式核燃料循环的最终实现具有重要意义。在钍铀燃料水法后处理中，后续研究中应重点考虑更适合钍基燃料处理萃取剂及相关流程的筛选及开发，掌握核心技术，切实提高水法后处理技术水平。另外，针对于钍基熔盐堆燃料等不同类型燃料的处理要求，还需开发不同的燃料处理技术及工艺，并通过一系列台架实验及热实验对相关工艺进行验证，以实现核燃料循环中资源的充分利用及废物的合理处置。

Aqueous reprocessing for thorium based nuclear fuel

Department of radiochemical Engineering and Technology

Spent fuel reprocessing is a vital component in "closed" nuclear fuel cycle. As the same as U-Pu fuel cycle, for conventional ThO_2 fuel used in Th-U fuel cycle, the aqueous separation technology is still the most mature and reliable reprocessing method. In addition, the aqueous separation technique also can solve some problems, which can't be solved by using pyrochemical method in the reprocessing of TMSR fuel. Thus, to develop the application of aqueous technology in Th-U fuel reprocessing, the uranium extraction process, new extractants for Th-U fuel reprocessing and pyrohydrolysis of fluorides were studied.

As shown in Fig.1, uranium extraction process can be used to separate and recover ^{233}U from irradiated ThO_2. Based on the "cold" bench experiments, the "trace" bench experiment for uranium extraction process by using radioactive FPs from irradiated ^{235}U and mixer-settler were performed. It is found the bench equipments ran well in the "hot" cell. The decontamination factor for total γ, β and $^{89+90}Sr$ are 3.34×10^4, 2.57×10^4 and 6.71×10^6, respectively. Furthermore, the separation factor for U/Th and recovery of U could also reach 7.60×10^5 and 99.83%, respectively. The main indices in uranium extraction process have reached or exceeded that in the domestic and foreign similar process. Especially, the separation factor for U/Th is one order of magnitude higher than that in domestic and foreign reports. The decontamination factor could also reach or exceed that in domestic and foreign reports in the absence of added decontamination step.

Considering the defects of TBP in Th-U fuel reprocessing, such as lower distribution coefficient and extraction capacity for Th, "third phase" formation, and lower separation factor for U/Th, the irradiation stability of P350, a new extractant for Th-U fuel reprocessing, was also studied, and a new process for the recovery of Th and U based P350 was proposed. The results of multistage countercurrent extraction experiment using batch simulation demonstrate that the main indices in P350 process are at the same level compared with that in Thorex process using TBP as extractant. However, a lower extractant flow ratio is used in the P350 process, and it could reduce the amount of generated radioactive organic waste liquid. Furthermore, the formation of "third phase" could also be prevented in the P350 process. Thus, the extractant of P350 possesses a high application potential in Th-U fuel reprocessing.

In order to further recycle useful materials in TMSR fuel after pyroprocessing and to avoid the generation of strong radioactive fluoride wastes, a study on pyrohydrolysis of different fluorides at high temperature was carried out. The pyrohydrolysis experiments of single fluoride such as ThF_4, UF_4, SmF_3, and SrF_2 at high temperature was conducted under different thermal conversion temperature and within different reaction time respectively, and the structural characterization of their conversion products, as well as the dissolving experiments, were performed too. Besides, a series of molten salts of different components were prepared, followed by their structural characterization, the structural characterization of conversion products and dissolving experiments. Results indicated that ThF_4 in mixed fluoride molten salts can be converted into its corresponding oxide under experimental conditions, and alkali metal fluoride which is difficult to be converted can be transformed into its oxide by use of accelerators such as Cr_2O_3, WO_3, and other acid oxides. The feasibility of pyrohydrolysis technology in the conversion of fluoride to oxide was confirmed by the above experiments, paving the way for its application in the separation of Th, U, and FPs.

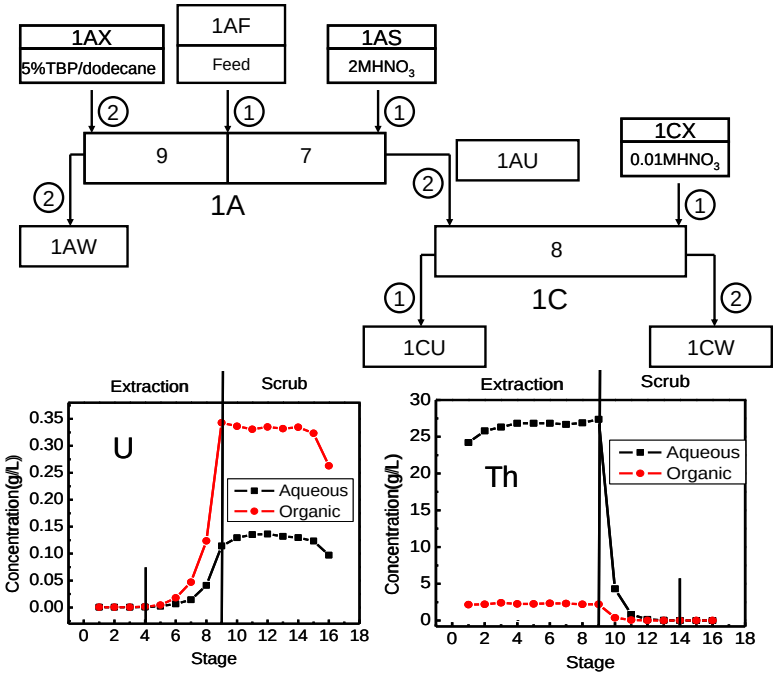

Fig.1 The flow sheet of uranium extraction process (up) and concentration profiles of Th, U in 1A cycle of "cold" bench experiment in uranium extraction process (down)

Fig.2 The “trace” bench experiment of uranium extraction process in “hot” cell

Fig.3 The experimental installation for pyrohydrolysis of fluorides

To master the key aqueous separation technology for ThO_2 fuel reprocessing, the Th/U extraction separation process was developed. The results of “trace” bench experiment for uranium extraction process using mixer-settler demonstrate that the main indices in uranium extraction process have reached or exceeded that in the domestic and foreign similar process. The P350 is more appropriate for the Th-U fuel reprocessing, and a new process with self-owned intellectual property for the recovery of Th and U based P350 was proposed. Furthermore, the pyrohydrolysis of fluorides were also studied, and the feasibility of using pyrohydrolysis in pyro-hydro-reprocessing for TMSR fuel was proved. All of these works could provide some technical reserves for the TMSR fuel reprocessing.

Research and development of nuclear fuel reprocessing technology is of great significance for the final realization of closed nuclear fuel cycle. The selection and development of new extractants and related processes for Th-U fuel reprocessing should be considered in the follow-up research to master the key technology and improve the technological level of aqueous reprocessing. In addition, for the different processing requirements of various types of Th-U fuel, different fuel treatment technologies and processes also should be developed and tested by using a series of bench and “hot” experiments to realize the full utilization of resources and the reasonable disposal of waste in the nuclear fuel cycle.

钍铀燃料循环研究平台

放射化学与工程技术部

钍铀燃料循环研究平台是开展 TMSR 燃料研发、干法分离技术研发以及钍铀燃料循环相关核化学与放射化学研究的基础实验设施。总体目标是建设先进放射化学分析测试平台及核化学与放射化学综合研究设施，形成一个较为完善的钍基核能系统放射化学研究基地。主要任务包括：放化分析测试平台建设与运行、103 放化实验室的改造、干法处理实验设施的设计等。2013−2014 年的工作进展如下：

1 放射化学分析测试平台

放射化学分析测试平台是为钍铀燃料循环研究相关放射化学分析测试提供由多种仪器设备构成的较为完备的分析测试平台。分析测试平台主要仪器（表 1）包括：1) 放射性分析测试仪器，包括 γ 谱仪四台、α 谱仪两台、液体闪烁计数仪一台。2) 化学分析测试仪器，包括 ICP-MS、ICP-AES、AAS、XRD、高温拉曼光谱仪、离子色谱、高效液相色谱等。2013−2014 年放射化学分析测试平台总体运行良好，较好地完成了 TMSR 相关研究的分析测试任务，为 TMSR 相关科研任务的完成提供了很好的技术支持。针对 TMSR 燃料处理工艺研究中的分析测试需求，开展了相关分析测试方法的研究，建立了以钍、铀、裂变产物分析为主的分析测试方法。

表 1 放射化学分析测试平台主要仪器设备

名　称	数 量	用　途
ICP-MS	1	稀土及重金属核素分析
ICP-AES	1	元素分析
原子吸收光谱	1	痕量元素分析
高温拉曼光谱	1	熔盐结构分析
阿尔法能谱	4	
伽玛能谱	6	放射性核素分析
液体闪烁计数器	1	
XRD（X 射线衍射光谱仪）	1	固态熔融盐及沉淀物等物相分析
高效液相色谱	2	有机化合物、大分子化合物等的分离纯化及定性、定量分析
离子色谱仪	1	无机阴阳离子的分离与定性定量分析 有机酸的定性定量分析
电化学工作站	3	电化学分析以及电解方法学研究

2 103 放化实验室改造

围绕嘉定园区 103 放化实验室恢复操作长寿命放射性核素和锕系核素能力的目标，对 103 放化实验室放化工艺设备进行了重新设计与研制，主要设备包括热室设备线一套、薄壁手套箱 14 套，其中热室设备线由 7 个热室、三个屏蔽手套箱以及放射性物料转运系统组成。热室的 γ 屏蔽能力为 1.85×10^{9} Bq（以 ^{137}Cs 计）；远程操作方式由剑式机械手升级为关节机械手，可完成复杂动作的操作；物料转运系统可实现热室室间放射性物料的自动转移；采用双盖密闭转运技术，有效地降低了放射性沾污的可能。目前放化工艺设备的加工与安装调试已经完成，热室、手套箱及放射性物料转运系统的泄漏率 T_f 均小于 2.5×10^{-3} h^{-1}，符合箱室设备密封性的要求，工艺设备其它各项技术指标也均满足设计要求。针对实验室年久失修、设备老化等问题，对实验室主要配套辅助系统进行了系统改造，包括放射性废气处理系统、放射性废液暂存系统、放射性废物暂存系统、工艺设备控制系统、集中供气系统等，目前主要系统、设备的加工与安装调试均已完成，各项技术指标均满足设计要求。103 放化实验室即将进入试运行阶段。

图 1 103 放化实验室主要工艺设备

3 干法处理实验设施设计

针对液态燃料钍基熔盐堆中燃料盐分离关键

技术研发和干法处理工艺热验证的需要，开展了干法处理实验设施的设计工作。2014 年完成了初步可行性研究报告的编制。确定了设施的功能、规模、主要工艺流程（图 2）、主要工艺系统和设备、主要配套辅助系统、总体布局等。热室系统包括两个主工艺热室（氩气氛和空气氛热室各一个）、两个分析热室、一个辅助热室和一个模拟热室，主工艺热室和辅助热室的辐射防护按 3.7×10^{15} Bq 进行设计。氩气热室是开展干法处理工艺热验证的核心设备，热室为长方体箱式结构，按 α-γ 型热室设计。内箱体长 15 m，深 6 m，高 6.5 m。双面操作，共设置 12 个操作工位。热室整体泄漏率(T_f)小于 $1\times10^{-5}\ h^{-1}$。热室内部气氛采用氩气保护气氛设计，压力为−200~−1 000 Pa，气氛中水含量小于 10mg/L、氧含量小于 30 mg/ L 为严格控制热室气氛内的水氧含量，配置专门的配套气氛控制系统（图 3），主要由供气单元、循环冷却单元、净化单元、压力保护及排气单元组成。

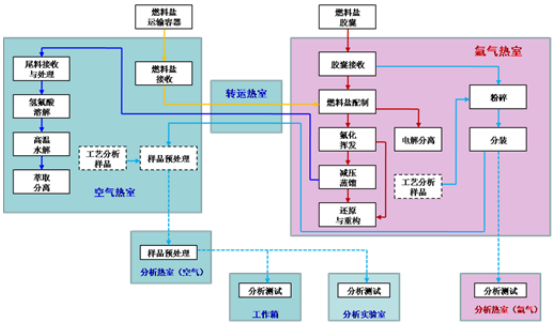

图 2　干法处理实验设施工艺流程

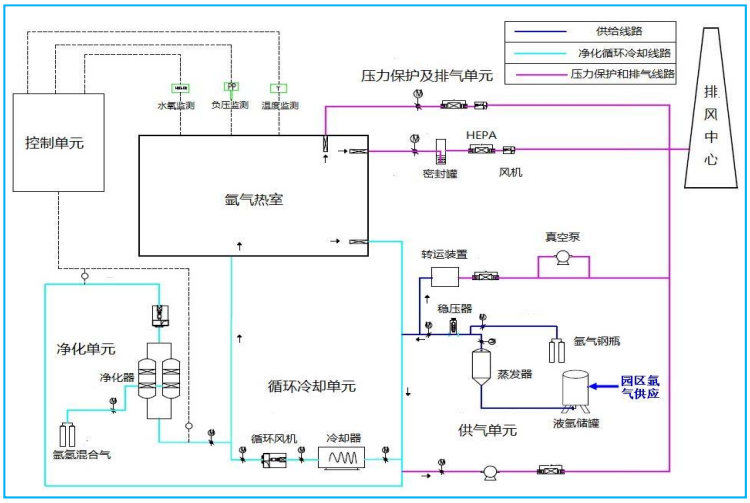

图 3　氩气热室气氛控制系统

4　小结与展望

放射化学分析测试平台运行良好，较好地完成了 TMSR 相关研究的分析测试任务。为提高分析测试能力与水平，后续将重点开展 CNAS 实验室认可申请工作。103 放化实验室已完成主要系统与设备的安装调试，即将进入试运行阶段，后续工作重点是建立并完善放化实验室各项管理规章制度，确保实验室的安全运行。完成了干法处理实验设施初步可行性研究报告的编制，后续将针对设计中的技术难点，开展氩气热室关键技术的研发，包括密封技术、气氛控制技术以及不同气氛下的物料转移技术等。

Research platform of thorium-uranium fuel cycle

Department of Radiochemical Engineering and Technology

The Research Platform of Thorium-Uranium Fuel Cycle is a basic experimental facility for research and development of TMSR fuel, pyroprocessing technology of depleted fuel, and other nuclear chemistry and radiochemistry for thorium-uranium fuel cycle. The main objective is to establish an advanced radiochemical analysis platform and thorium- uranium fuel cycle experiment facility, thus to build a complete research base for TMSR radiochemical research. The main tasks include construction and operation of the radiochemical analysis platform, reconstruction of radiochemical laboratory in building 103 and design of pyroprocessing experimental facilities.

The progress of the work during 2013 and 2014 are as follows:

1 Radiochemical analysis platform

The radiochemical analysis platform is a relatively complete analysis platform for thorium-uranium fuel cycle research, which contains a variety of relative instruments. The main instruments are shown in Table 1: 1) radioactive analysis instruments including 4 gamma spectrometers, 2 alpha spectrometers and 1 liquid scintillation counter. 2) chemical analysis instruments including ICP-MS, ICP-AES, AAS, XRD, high temperature Raman spectrum, IC, HPLC and so on. During 2013−2014, the radiochemical analysis platform has worked well, completed all the analysis tasks for TMSR related research, and provided excellent technical support for the TMSR related research. In order to meet the requirement of analysis in reprocessing technology of depleted fuel of TMSR, the platform has carried out researches for related analysis methods and built the analysis methods for thorium and uranium fission products analysis.

Table 1 The main instruments for radiochemical analysis platform

Instrument	Amount	Application
ICP-MS	1	Rare Earth and Heavy Metals Nuclide Analysis
ICP-OES	1	Elemental analysis
AAS	1	Trace element analysis
Raman	1	Molten salt structure analysis
Alpha spectrometer	2	
Gamma spectrometer	4	Radionuclide analysis
liquid scintillation counter	1	
XRD	1	phase analysis of molten salt and sediment
HPLC	2	Organic compounds, macromolecular compounds such as the separation and purification and qualitative and quantitative analysis
IC	1	Separation, Qualitative and Quantitative Analysis of Inorganic Cations and Anions Qualitative and quantitative analysis of organic acids
Electrochemical Workstation	3	Electrochemical Analysis and Electrolysis Methodology

2 Reconstruction of radiochemical laboratory in building 103

In order to recover the ability to operate with long life radioactive nuclides and actinide nuclide, the equipment of the radiochemical laboratory in building 103 are redesigned, the main equipments include hot cell systems (including 7 hot cells, 3 radiation shielding gloveboxes and radioactive material transfer system) and 14 gloveboxes. The γ shielding ability of hot cell is 1.85×10^{9} Bq (^{137}Cs).The remote handling equipment for hot cells has been upgraded from remote-handling tongs to articulated manipulator, which can complete complex operation. The radioactive material transfer system can transport the radioactive material between the hot cells automatically, which can reduce the possibility of radioactive contamination. So far by now, the manufacturing, installing and testing of radiochemical process equipment have been completed. The leak rate T_f of hot cell, glovebox and radioactive material transfer system is less than 2.5×10^{-3} h^{-1}, which is consistent with the requirements of sealing, and the other technical parameters of radiochemical process equipment also meet the requirement of design.

Due to long years out of repair and equipment aging, the auxiliary systems of the lab are also reconstructed, such as the radioactive waste gas treatment system, radioactive waste storage system, radioactive liquid storage system, control system for radiochemical processing equipments and centralized gas supply system. By now, the manufacturing, installing and testing of the main system and equipments are all completed and the technical parameters meet the requirement of design. The radiochemical laboratory in building 103 is about to enter the trial operation stage.

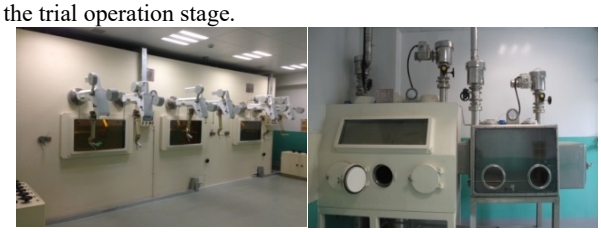

Fig.1 The main process equipment of radiochemical laboratory in building 103

3 Design of pyroprocessing experimental facilities

In order to meet the requirement of TMSR fuel salt separation key technology development and pyroprocessing technology development, the design of pyroreprocessing experimental facility has been carried out. The preliminary feasibility study report has been completed by 2014. The function, scale, the main process, equipments, auxiliary systems and overall layout are confirmed. The hot cell systems contains 2 main process hot cell (1 Ar atmosphere hot cell and 1 Air hot cell), 2 analysis hot cells, 1 auxiliary hot cell and 1 mockup cell. The designed radiation shielding ability is about 3.7×10^{15} Bq. The Ar atmosphere hot cell is the core equipment for the verification of pyroprocessing technology, the structure is cuboid and designed to be an α-γ hot cell. The inner cell is 15 m long, 6 m deep and 6.5 m high. It can be operated in two sides and have 12 operation positions. The leak rate Tf is less than 1×10^{-5} h^{-1}. The protect gas inside is Ar with the pressure between −200 Pa and −1 000 Pa, and the content of water is less than 10 mg/L and the oxygen less than 30 mg/L. The Ar atmosphere control system is used to control the content of water and oxygen, which contains gas supply unit, recycling-cooling unit, purification unit, pressure protection and off gas unit.

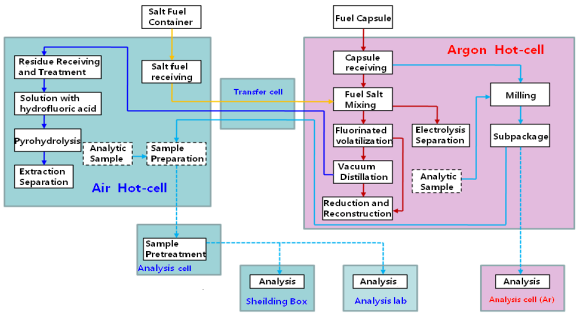

Fig.2 The process of pyroprocessing experimental facility

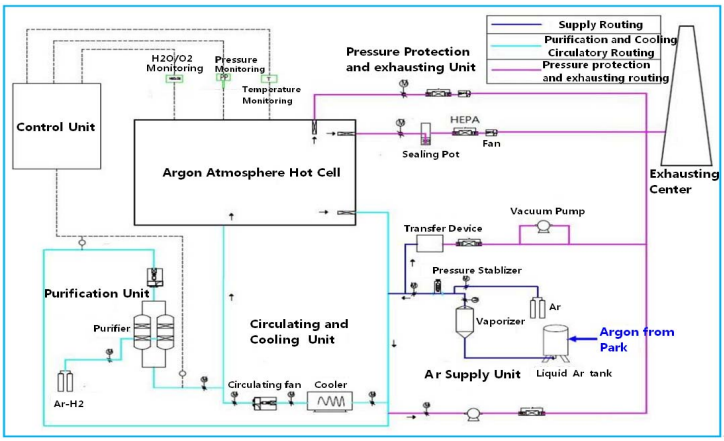

Fig.3 The Ar atmosphere control system for Ar hot cell

4 Summary and Prospect

The radiochemical analysis platform is running well and it has completed the analysis task for TMSR related research. In order to improve the ability and level of radiochemical analysis, the application of CNAS laboratory accreditation will be carried out. The manufacturing, installing and testing of the main systems and equipments of radiochemical laboratory in building 103 are all completed and will enter the trial operation stage, the subsequent main work is to establish and improve the management rules and regulations for the chemical laboratory to ensure the safe operation of the laboratory. The preliminary feasibility study report of pyroprocessing experimental facility has been completed, the subsequent work are development of key technologies of Ar atmosphere hot cell including sealing technology, atmosphere control technology and radioactive material transfer technology in different atmosphere.

基础与交叉

相对论重离子对撞物理研究

核物理研究室

位于美国布鲁克海汶国家实验室的相对论重离子对撞机上(RHIC)产生了类似于宇宙大爆炸早期的物质形态，是研究宇宙早期新物质形态的理想实验场所。2013−2014 年我们在 RHIC-STAR 上主要开展了双轻子产额的测量以及能量扫描实验中测量了正反粒子椭圆流差别，同时我们也在理论上利用唯象输运模型对相对论重离子对撞动力学进行研究。

1 RHIC-STAR 实验研究

我们利用 RHIC-STAR 实验探测器开展了多方面的实验研究。我们和 STAR 实验组其它单位合作，测量了 200 GeV 金核-金核对心碰撞中双轻子的产生，该工作对于理解高能重离子碰撞产生的 QGP 物质的性质具有十分重要的意义[1]。我们发现双轻子在 ρ 质量区间有明显的增加，这一现象不能用纯真空 ρ 介子来解释。同时，我们还利用 STAR 能量扫描实验研究了不同种类粒子的椭圆流[2]，发现随着碰撞能量的降低，正反粒子的椭圆流差别增大，并且在低能量区间，粒子不再符合单一的 NCQ 标度。

2 RHIC 物理唯象动力学研究

在理论方面，研究了质子-铅核碰撞和铅核-铅核碰撞中的椭圆流和三角流，发现在质子-铅核碰撞中的不同粒子的椭圆流满足质量排序而三角流不满足，并预言了质子-铅核碰撞中集体流的快度依赖性，和更高阶次集体流的横向动量依赖性[3]。研究了在质心系能量为 7 TeV 质子-质子和 5.02 TeV 的质子-铅核碰撞中的两粒子长程方位角关联分布，发现是由于末态部分子级联散射所产生的集体运动所带来的[4]。通过将初始的电荷四极分布引入多相粒子输运模型中，发现了正负电荷的 π 介子的椭圆流对电荷不对称因子的线性依赖的斜率可以由部分子级联过程产生并受到后续末态过程的影响[5]。通过光子-强子方位角关联避开了复杂的喷注重构过程，并在理论上研究了在质心系能量为 200 GeV 的金核-金核碰撞中发现直接光子触发的背向喷注中的软粒子由于和热密介质的相互作用，被激发到远离喷注轴的方向[6]。研究了在高能重离子碰撞中，相比于领头喷注，由于次领头喷注能量损失更大,所以导致次领头喷注的形状改变更大一些[7]。通过研究发现高能重离子碰撞中的喷注碎裂函数可以分解成为由喷注碎裂强子化和喷注组合强子化带来的两种贡献，这表明在不同的碰撞中心度和不同的动量分数区间存在着不同喷注强子化机制之间的竞争[8]。研究重构了 LHC 能量下铅核-铅核碰撞中光子喷注，研究了光子喷注的动量不对称度的中心度依赖性，发现这种不对称性质主要是喷注与部分子物质相互作用所造成[9]。通过研究 LHC 能量下铅核-铅核碰撞中双喷注的不对称性演化函数，揭示了这种不对称性的起源，发现是由初始不对称性和喷注的能量损失共同决定的[10]。

参考文献

1. Adamczyk L, Adkins J K, Agakishiev G, *et al*. (STAR Collaboration) Dilepton Mass Spectra from Au+Au Collisions at 200 GeV[J], Physical Review Letter 2014, **113**: 022301.
2. Adamczyk L, Adkins J K, G. Agakishiev *et al*. (STAR Collaboration) Observation of an Energy-Dependence Difference in Elliptic Flow between Particles and Antiparticles in Relativistic Heavy Ion Collisions[J]. Physical Review Letter, 2013, **110**: 142301.
3. Adam Bzdak, Ma G L. Elliptic and Triangular Flow in p-Pb and Peripheral Pb-Pb Collisions from Parton Scatterings[J]. Physical Review Letter, 2014, **113**: 252301.
4. Ma G L, Adam Bzdak. Long-range azimuthal correlations in proton-proton and proton-nucleus collisions from the incoherent scattering of partons[J], Physics Letter B, 2014, **739**: 209-213.
5. Ma G L. Final state effects on charge asymmetry of pion elliptic flow in high-energy heavy-ion collisions[J]. Physics Letter B, 2014, 735: 383-386.
6. Ma G L. Medium modifications of the photon-tagged jet fragmentation function in high-energy heavy-ion collisions[J], Physical Review C, 2014, **89**: 064909.
7. Ma G L. Medium modifications of jet shapes in Pb + Pb collisions at $\sqrt{S_{\rm NN}}$ =2.76 TeV within a multiphase transport model[J]. Physical Review C, 2014, **89**: 024902.
8. Ma G L. Decomposition of the jet fragmentation function in high-energy heavy-ion collisions[J], Physical Review C, 2013, 88: 021902(R).
9. Ma G L. Towards detailed tomography of high energy heavy-ion collisions by γ-jet[J]. Physics Letter B, 2013, **724**: 278-282.
10. Ma G L. Dijet asymmetry in Pb+Pb collisions at Phys $\sqrt{S_{\rm NN}}$ =2.76 TeV within a multiphase transport model [J]. Rev C, 2013, **87**: 064901.

The researches on relativistic heavy-ion collisions

Division of Nuclear Physics

The Relativistic Heavy-Ion Collider at Brookhaven National Laboratory created a condition similar to the early universe at a few microseconds just after the Big Bang, thus it is the ideal lab to understand the early state of the universe. During 2013 and 2014, our research focus on measurements of di-electron production and energy-dependent difference of elliptical flow between particles and antiparticles in Au+Au collisions at RHIC-STAR. Meanwhile, we use phenomenological models to study the partonic dynamics in relativistic heavy-ion collisions.

1 Experimental researches at RHIC-STAR

We measured dielectron (e+e−) production at midrapidity ($|\eta|<1$) in Au+Au collisions at $\sqrt{S_{\rm NN}}$ =200 GeV[1]. The dielectron yields in the ω and φ mass regions are well described by the hadronic cocktail model while yields at higher mass, 1~3 GeV/c^2, can be understood as mostly from decay leptons of charm pairs. In the 0.30~0.76 GeV/c^2 region, however, there exists a clear excess over the hadronic cocktail that cannot be explained by a pure vacuum ρ. This research is very important in understanding the properties of QGP created in relativistic heavy ion collisions. We also measured elliptic flow values for identified particles at midrapidity in Au+Au collisions in the beam energy scan at RHIC at $\sqrt{S_{\rm NN}}$ =7.7–62.4 GeV[2]. The difference in v_2 between particles and antiparticles increases with decreasing beam energy. At lower energies, particles and antiparticles are no longer consistent with the single NCQ scaling that was observed for data at $\sqrt{S_{\rm NN}}$ =200 GeV.

2 Phenomenological study on partonic dynamics in relativistic heavy-ion collisions

On theory study side, we studied the elliptic flow and triangular flow in p+Pb and Pb+Pb collisions[3]. The characteristic mass ordering of v_2 in p+Pb collision is reproduced, whereas for v_3, this is not observed. We also predicted the pseudorapidity dependence of v_2 and v_3 in p+Pb and observe that both are increasing when going from a proton side to a Pb-nucleus side. We further predicted the higher-order Fourier coefficients, v_4 and v_5 in p+Pb collisions. We studied the long-range azimuthal correlations in 7 TeV p+p collisions and 5.02 TeV p+Pb collisions, we found the correlations are from the incoherent scattering of partons[4]. We calculated the difference between the elliptic flow of positive and negative pions within AMPT model with imported initial electric quadrupole moment. The slope parameter r is found to be increased by the hadronization given by the coalescence[5]. We studied the medium modifications of prompt photon-tagged jet fragmentation function by comparing prompt photon-tagged hadron azimuthal correlation in Au+Au collisions (0%~40%) and in p+p collisions at $\sqrt{S_{\rm NN}}$ =200 GeV. We found a medium-modified jet shape in which the medium enhancement of soft particles is preferentially located far away from the jet axis[6]. We studied the medium modifications of jet shapes in Pb+Pb collisions at $\sqrt{S_{\rm NN}}$ = 2.76 TeV. We found that subleading jets display larger modifications than leading jets[7]. We studied the decomposition of jet fragmentation function, we found the measured jet fragmentation function ratio of Pb+Pb to p+p collision is decomposed into two parts, corresponding to two contributions of jet hadronization from fragmentation and coalescence, which suggest an existence of distinct competition between two jet hadronization mechanism[8]. We studied the transverse momentum imbalance between prompt photon and jet in Pb+Pb collisions at $\sqrt{S_{\rm NN}}$ = 2.76 TeV. We found jet loses more energy in more central collisions due to strong partonic interactions between parton shower and partonic matter[9]. We studied the dijet asymmetry in Pb+Pb collisions at $\sqrt{S_{\rm NN}}$ =2.76 TeV, and reveal the origin of this asymmetry. We found the asymmetry is driven by both initial asymmetry and partonic jet energy loss[10].

Reference

1. Adamczyk L, Adkins J K, Agakishiev G, *et al*. (STAR Collaboration) Dilepton Mass Spectra from Au+Au Collisions at 200 GeV[J], Physical Review Letter 2014, **113**: 022301.
2. Adamczyk L, Adkins J K, G. Agakishiev *et al*. (STAR Collaboration) Observation of an Energy-Dependence Difference in Elliptic Flow between Particles and Antiparticles in Relativistic Heavy Ion Collisions[J]. Physical Review Letter, 2013, **110**: 142301.
3. Adam Bzdak, Ma G L. Elliptic and Triangular Flow in p-Pb and Peripheral Pb-Pb Collisions from Parton Scatterings[J]. Physical Review Letter, 2014, **113**: 252301.
4. Ma G L, Adam Bzdak. Long-range azimuthal correlations in proton-proton and proton-nucleus collisions from the incoherent scattering of partons[J], Physics Letter B, 2014, **739**: 209-213.
5. Ma G L. Final state effects on charge asymmetry of pion elliptic flow in high-energy heavy-ion collisions[J]. Physics Letter B, 2014, **735**: 383-386.
6. Ma G L. Medium modifications of the photon-tagged jet fragmentation function in high-energy heavy-ion collisions[J], Physical Review C, 2014, **89**: 064909.
7. Ma G L. Medium modifications of jet shapes in Pb + Pb collisions at $\sqrt{S_{\rm NN}}$ =2.76 TeV within a multiphase transport model[J]. Physical Review C, 2014, **89**: 024902.
8. Ma G L. Decomposition of the jet fragmentation function in high-energy heavy-ion collisions[J], Physical Review C, 2013, **88**: 021902(R).
9. Ma G L. Towards detailed tomography of high energy heavy-ion collisions by γ-jet[J]. Physics Letter B, 2013, **724**: 278-282.
10. Ma G L. Dijet asymmetry in Pb+Pb collisions at Phys $\sqrt{S_{\rm NN}}$ =2.76 TeV within a multiphase transport model [J]. Rev C, 2013, **87**: 064901.

上海激光电子伽玛源（SLEGS）

核物理研究室

上海激光电子伽玛源(SLEGS)是基于激光康普顿散射原理建设的高质量γ光装置，γ光的能区为0.4~20 MeV。其科学目标如下：通过光核反应开展核天体物理、核结构、极化物理等领域中的基础物理研究，特别是解决核天体物理中具有重大科学价值的问题；此外，还开展与航天、国防、核能等战略需求相关的应用基础研究，如利用γ射线开展航天电子元器件空间辐射效应中的总剂量效应和抗辐射加固评估的研究，以及航天用γ探测器的精确定标[1]。2013–2014 年度，主要专注 SLEGS 的初步设计和关键设备的前期预制研究。取得的主要成果如下。

1 完成关键设备初步设计

发展了一套基于 Geant4 的激光康普顿散射过程蒙特卡罗程序。基于这套模拟程序，首先完成了 SLEGS γ光产生和传输过程的模拟（图 1），确定 SLEGS 能区、流强、束斑等关键参数。

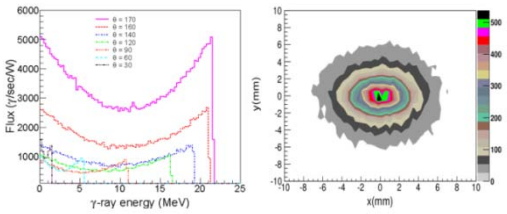

图 1 SLEGS 光源点处能谱和束斑

进而利用此程序模拟了影响 SLEGS γ性质的各种可能因素（图 2）。根据模拟结果并结合 SSRF 加速器相关参数确定了 SLEGS 碰撞点靶室等关键设备的设计参数[2]。

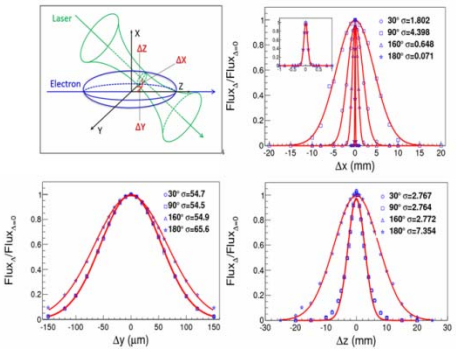

图 2 激光的位置偏差对通量的影响

在上述模拟的基础上，完成了 SLEGS 碰撞点靶室、多通组件、激光检测、准直器、衰减器等关键设备的初步设计。其中碰撞点靶室的初步设计如图 3 所示[2]。

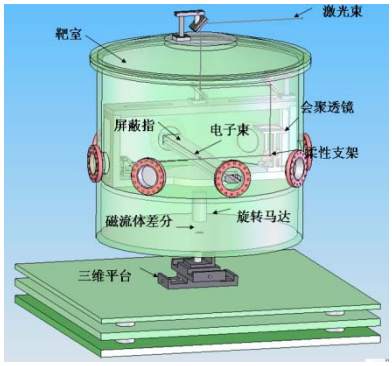

图 3 碰撞点靶室设计示意图

2 SLEGS 样机 III 建设

为 SLEGS 建设储备关键技术，建设 SLEGS 样机 III。SLEGS 样机 III 基于上海深紫外自由电子激光装置 150 MeV 电子直线加速器，利用 800 nm TW 激光，通过调节激光入射角产生的 X 射线能量为90~500 keV，通量可以达到10^5 photons/s。SLEGS 样机 III 的布局如图 4 所示。

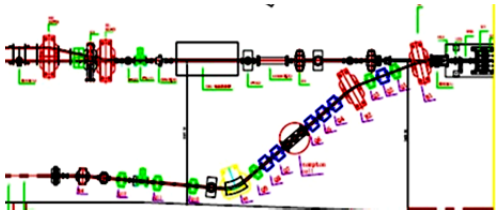

图 4 SLEGS 样机 III 布局

通过两年的工作，已经完成了样机 III 相互作用区靶室的设计和加工，激光系统关键部件购买，以及 X 射线测量系统的建设。

参考文献

1. 徐望，范功涛，等. 上海激光电子伽玛源(SLEGS)项目建设建议书，中国科学院上海应用物理研究所, 2012.
2. 徐望，范功涛，等. 上海激光电子伽玛源(SLEGS)线站设计报告，中国科学院上海应用物理研究所, 2013.

Shanghai laser electron gamma source (SLEGS)

Department of Nuclear Physics

Shanghai Laser Electron Gamma Source (SLEGS) is one of the high quality gamma sources based on Laser Compton Scattering (LCS). The energy region of SLEGS is 0.4~20 MeV. Based on the method of photon nuclear reaction, SLEGS aims at basic physics researches, such as nuclear astrophysics, nuclear physics, and polarization physics. In addition, SLEGS also tends to carry out applied research relating to aerospace, national defense, nuclear energy and other strategic demand of our country, such as space radiation effect research of the aerospace electronic components, and accurate calibration of the gamma detector for aerospace[1]. During 2013−2014, we mainly focus on the preliminary design of SLEGS and the pre-research of key equipment. The main results are as follows.

1 Preliminary design of key equipment

We developed a laser Compton scattering process Monte Carlo program based on Geant4. With this simulation program, we carefully simulated the gamma ray generation and transmission process of SLEGS (Fig.1). Then the key parameters of SLEGS such as energy region, intensity, and size of beam spot were determined.

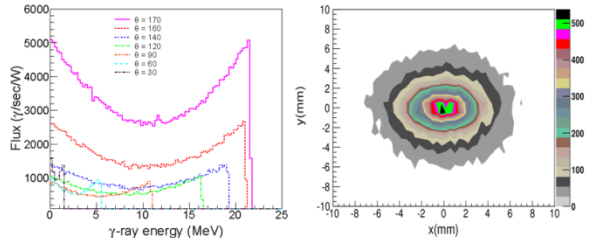

Fig.1 The energy spectrum and beam spot of SLEGS at collision point

We also used this program to calculate the various possible factors which might influence the gamma nature of SLEGS (Fig.2). Then the design parameters of key equipments, such as the target chamber at collision point, were determined according to the calculation results and the parameters of SSRF accelerator[2].

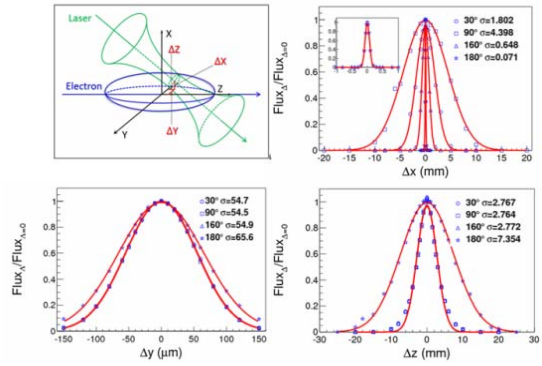

Fig.2 Relationship between position deviation of laser and gamma flux

Basis on the simulation, we have completed the preliminary design of the key equipments of SLEGS, such as LCS target chamber at collision point, mirror chamber at front end, laser detection, collimator and attenuator. The preliminary design of LCS chamber at collision point is shown in Fig.3[2].

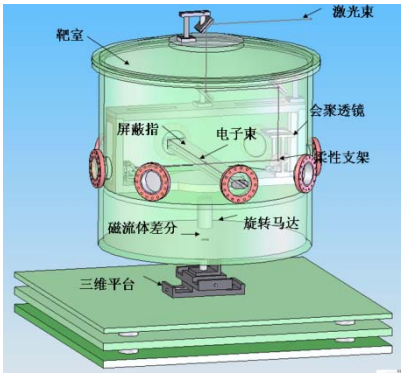

Fig.3 Preliminary design of LCS chamber

2 Construction of SLEGS prototypes III

In order to accumulate the key technology for SLEGS, we will carry out the SLEGS prototype III. prototype III will built at the 150 MeV electron linear accelerator of Shanghai Deep Ultraviolet-Free Electron Laser. Using 800 nm TW laser, prototype III can produce 90~500 keV X-ray with flux of 10^5 photons/s. The layout of SLEGS prototype III is shown in Fig.4.

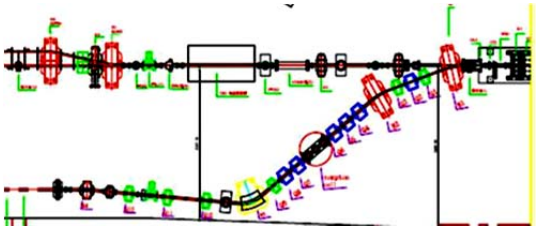

Fig.4 Layout of SLEGS prototype III

During the past two years, we have finished the design and built of the prototype III's LCS chamber at collision point, also finished the construction of the laser system and X-ray measuring system.

Reference

1. Xu W, Fan G T, *et al*. The proposal of shanghai Laser Electron Gamma Source(SLEGS), Shanghai Institute of Applied Physics, Chinese Academy of Science, 2012.
2. Xu W, Fan G T, *et al*. The design report of Shanghai Laser Electron Gamma Source(SLEGS), Shanghai Institute of Applied Physics, Chinese Academy of Science, 2013.

低中能重离子碰撞物理

核物理研究室

本研究方向主要在丰质子核的β缓发质子及双质子实验测量、中能重离子碰撞中的同位旋与自旋物理研究、原子核的集体激发与巨共振研究等方面开展了系列实验或理论研究。

1 丰质子核的β缓发质子与双质子实验测量

质子及双质子发射是质子滴线区原子核的奇特衰变方式，对其进行实验研究具有重要意义。我们在兰州重离子加速器装置的 RIBLL 束流线上开展了丰质子核 ^{23}Si、^{22}Al 等的β延迟质子与双质子发射实验测量。实验采用能量为 76*A* MeV 的 ^{28}Si 主束。产生的次级束被注入到放置在 T2 靶室后的薄硅微条探测器中，发生β衰变后布居到 ^{23}Al、^{22}Mg 等核的激发态。衰变发射的质子及双质子被注入探测器周围由硅微条加四分硅组成的望远镜系统探测。

2 中能重离子碰撞中的同位旋物理与自旋物理研究

中子和质子是核子的两种不同的同位旋态，同位旋物理则是研究中子与质子数不同体系(同位旋非对称体系)的特殊性质。核物质则是均匀核子构成的理想体系。同位旋非对称核物质体系的能量一般要比同位旋对称核物质体系的能量高，它们之间的差别称为对称能。π^-/π^+产额比作为高密度对称能实验探针，已受到实验与理论核物理学者的广泛关注，我们考虑了 π 介子同位旋依赖的 s 波和 p 波相互作用，发现其介质效应极大地影响着对称能的获取精度，尤其是在反应能量较低时[1]。一般认为，对称核物质中的液气相变是一级相变，非对称核物理中的液气相变是连续相变，我们利用弛豫时间近似方法发现核物质液气相变附近的约化粘滞系数有极小值，而最小值约为理论最低极限的 4~5 倍[2]。核反应中的氚核与 ^{3}He 的产额比以及丰中子原子核的中子皮厚度均可作为对称能的探针，我们发现可以通过实验上测量氚核与 ^{3}He 的产额比来获取炮弹核中子皮的厚度[3]。利用简单的范德瓦耳斯方程，我们建立了核物质状态方程甚至对称能与介质中核子散射截面的近似关系，并基于此发展出相关的波尔兹曼输运模型[4]。

另一方面，核子作为费米子，是自旋为 1/2 的粒子。不同自旋的粒子在外部自旋轨道耦合势下有不同的动力学，这是自旋霍尔效应的普遍原理。核力中也存在自旋轨道耦合，这对解释原子核壳结构十分重要。在非对心重离子碰撞中，由于核子自旋与垂直于反应平面角动量的耦合作用，会造成核子的有趣自旋动力学。我们首次将核自旋轨道相互作用引入波尔兹曼输运模型，发现核反应中不同自旋核子的横向流之差或可作为核自旋轨道力的有效探针[5–6]。

3 原子核的集体激发与巨共振研究

原子核有许多集体激发模式，比如沿半径方向的呼吸振动模式称为巨单极共振，偶极形变产生的振动模式称为巨偶极共振。如果中子与质子振动模式一致称为同位旋标量振动，如果中子与质子振动模式相反则称为同位旋矢量振动。我们用量子分子动力学模型分别研究了轻核到重核的各类原子核激发模式，及其与核物质状态方程的关系[7–8]。另一方面，对于轻原子核中是否存在 α 粒子结团是核物理界热门课题，我们发现可利用轻原子核的同位旋矢量巨偶极共振特征γ谱来推断内部 α 结团的构型[9]。在核反应中，也存在动力学同位旋矢量巨偶极振动，我们利用波尔兹曼输运模型对这一现象及其与对称能的对应关系进行了研究[10]。

参考文献

1. Xu J, Chen L W, Ko C M, *et al*. Energy dependence of pion in-medium effects on the pi(-)/pi(+) ratio in heavy-ion collisions[J]. Phys Rev C, 2013, **87**: 067601.
2. Xu J, Chen L W, Ko C M, *et al*. Shear viscosity of neutron-rich nucleonic matter near its liquid–gas phase transition[J]. Phys Lett B, 2013, **727**: 244.
3. Dai Z. T, Fang D Q, Ma Y G, *et al*. Triton/^{3}He ratio as an observable for neutron-skin thickness[J]. Phys Rev C, 2014, **89**: 014613.
4. Veselsky M and Ma Y G, *et al*. Symmetry energy and nucleon-nucleon cross sections[J]. Phys Rev C, 2013, **87**: 034615.
5. Xu J and Li B A. Probing in-medium spin–orbit interaction with intermediate-energy heavy-ion collisions[J]. Phys Lett B, 2013, **724**: 346.
6. Xia Y, Xu J, Li B A, *et al*. Spin-orbit coupling and the up-down differential transverse flow in intermediate-energy heavy-ion collision[J]. Phys Rev C, 2014, **89**:

064606.
7. Tao C, Ma Y G, Zhang G Q, *et al.* Pygmy and giant dipole resonances by Coulomb excitation using a quantum molecular dynamics model[J]. Phys Rev C, 2013, **87**: 014621.
8. Tao C, Ma Y G, Zhang G Q, *et al*. Isoscalar giant monopole resonance in Sn isotopes using a quantum molecular dynamics model[J]. Phys Rev C, 2013, **88**: 064615.
9. He W B, Ma Y G, Cao X G, *et al.* Giant Dipole Resonance as a Fingerprint of α Clustering Configurations in ^{12}C and ^{16}O[J] Phys Rev Lett, 2014, **113**: 032506.
10. Ye S Q, Cai X Z, Ma Y G, *et al*. Symmetry-energy dependence of the dynamical dipole mode in the Boltzmann-Uehling-Uhlenbeck model[J]. Phys Rev C, 2013, **88**: 047602.

Low and intermediate energy heavy ion collision physics

Division of Nuclear Physics

This research field focuses on the following subjects: β-delayed proton and two-proton emissions in proton-rich nuclei, isospin and spin physics in intermediate energy heavy-ion collisions, nucleus collective excitation and giant resonances.

1 Experimental study on β-delayed proton and two-proton emissions in proton-rich nuclei

One and two proton emissions are the exotic decay mode of the very proton-rich nuclei. It is significant to study these phenomena experimentally. The β-delayed 1p and 2p emissions from ^{23}Si and ^{22}Al were measured at the RIBLL in the Heavy Ion Research Facility in Lanzhou. Secondary beams were produced through the projectile fragmentation of an 76*A* MeV ^{28}Si primary beam bombing on a Be target at the target chamber (T0). The produced ions of ^{23}Si and ^{22}Al were injected into a thin silicon strip detector at T2. The excited states of ^{23}Al and ^{22}Mg were populated after the β-decay of ^{23}Si and ^{22}Al. A silicon box detector system was used to detect the emitted protons.

2 Isospin and spin physics in intermediate energy heavy-ion collisions

Neutrons and protons are two different isospin states of nucleons. Isospin physics studies special properties of systems with different numbers of neutrons and protons (isospin asymmetric systems). Nuclear matter is an ideal system composed of uniformly distributed nucleons. The energy of an isospin asymmetric nuclear matter is generally higher than that of an isospin symmetric one, and the energy difference is called the symmetry energy. As an experimental probe of the high-density symmetry energy, the π^-/π^+ ratio has attracted global attentions among experimental and theoretical nuclear physicists. We found the pion s-wave and p-wave interactions in nuclear medium significantly affect the accuracy of extracting the symmetry energy, especially in nuclear reactions at lower collision energies[1]. Generally, the liquid-gas phase transition in isospin symmetric matter is a first-order phase transition, while that in isospin asymmetric matter is a smooth one. Using a relaxation time approximation approach, we found that the specific shear viscosity has a minimum value near nuclear liquid-gas phase transition, and the smallest value is around 4~5 times of the theoretical lower limit[2]. The triton/^{3}H ratio in nuclear reactions and the neutron skin thickness of neutron-rich nuclei are both probe of the symmetry energy, and we found it is possible to measure experimentally the triton/^{3}H in order to extract the neutron skin thickness of the projectile nuclei[3]. Based on the simple Van der Waals equation of state, we have related approximately the nuclear equation of state or even the symmetry energy to the in-medium nucleon-nucleon scattering cross sections, and developed a corresponding Boltzmann transport model[4].

On the other hand, as fermions, nucleons have a spin of 1/2. Particles with different spins have their different dynamics in an external spin-orbit coupling potential, and this is the fundamental principle of the spin-hall effect. As a crucial component of nuclear force, the spin-orbit nuclear interaction is important in explaining the shell structure of finite nuclei. In non-central heavy-ion collisions, due to the coupling to the angular momentum perpendicular to the reaction plane, interesting spin dynamics for nucleons will occur. For the first time, we have incorporated the nuclear spin-orbit interaction into the Boltzmann transport model, and found that the difference in the transverse flow for nucleons with different spins can be a good probe of the nuclear spin-orbit interaction[5–6].

3 Studies on nucleus collective excitations and giant resonances

Nuclei have many collective excitation modes. For example, the breathing oscillation mode along the radial direction is called the giant monopole resonance, while that due to the dipole deformation is called the giant dipole resonance. It is called the isoscalar oscillation if neutrons and protons are moving in the same direction, and called the isovector oscillation if neutrons are moving against protons. Employing a quantum molecular dynamics model, we have studied the various excitation modes from light to heavy nuclei, as well as the relation to the nuclear equation of states[7–8]. On the other hand, whether there exist alpha clusters in light nuclei is a hot topic, and we found that it is possible to investigate the configuration of alpha clusters in light nuclei by using specific gamma spectra from isovector giant dipole resonances of those nuclei[9]. In nuclear reactions, there also exist dynamical isovector giant dipole oscillations, and we have studied this phenomenon as well as the corresponding relations to the symmetry energy using a Boltzmann transport model[10].

References

1. Xu J, Chen L W, Ko C M, *et al.* Energy dependence of pion in-medium effects on the pi(-)/pi(+) ratio in heavy-ion collisions[J]. Phys Rev C, 2013, **87**: 067601.
2. Xu J, Chen L W, Ko C M, *et al.* Shear viscosity of neutron-rich nucleonic matter near its liquid–gas phase transition[J]. Phys Lett B, 2013, **727**: 244.
3. Dai Z. T, Fang D Q, Ma Y G, *et al.* Triton/^{3}He ratio as an observable for neutron-skin thickness[J]. Phys Rev C, 2014, **89**: 014613.
4. Veselsky M and Ma Y G, *et al.* Symmetry energy and nucleon-nucleon cross sections[J]. Phys Rev C, 2013, **87**: 034615.
5. Xu J and Li B A. Probing in-medium spin–orbit interaction with intermediate-energy heavy-ion collisions[J]. Phys Lett B, 2013, **724**: 346.
6. Xia Y, Xu J, Li B A, *et al.* Spin-orbit coupling and the up-down differential transverse flow in intermediate-energy heavy-ion collision[J]. Phys Rev C, 2014, **89**: 064606.

7. Tao C, Ma Y G, Zhang G Q, *et al.* Pygmy and giant dipole resonances by Coulomb excitation using a quantum molecular dynamics model[J]. Phys Rev C, 2013, **87**: 014621.
8. Tao C, Ma Y G, Zhang G Q, *et al.* Isoscalar giant monopole resonance in Sn isotopes using a quantum molecular dynamics model[J]. Phys Rev C, 2013, **88**: 064615.
9. He W B, Ma Y G, Cao X G, *et al.* Giant Dipole Resonance as a Fingerprint of α Clustering Configurations in ^{12}C and ^{16}O[J] Phys Rev Lett, 2014, **113**: 032506.
10. Ye S Q, Cai X Z, Ma Y G, *et al*. Symmetry-energy dependence of the dynamical dipole mode in the Boltzmann-Uehling-Uhlenbeck model[J]. Phys Rev C, 2013, **88**: 047602.

CUORE 及 PandaX 合作实验

核物理研究室

本研究方向主要在超低本底深地实验室及非加速器物理前沿的无中微子双贝塔衰变测量(CUORE)和国内锦屏地下实验室暗物质直接探测实验(PandaX)合作两方面开展研究工作，围绕两个合作实验开展了一系列超低本底探测器研发和本底分析，在 CUORE 和 PandaX 两个大型国际合作实验中起到了重要的作用。

1 无中微子双贝塔衰变国际合作(CUORE)

CUORE (Cryogenic Underground Observatory for Rare Events)目前主要的研究目标是测量可能的极其稀有的 ^{130}Te 无中微子双贝塔衰变(0VDBD)事件，0VDBD 的测量对决定中微子绝对质量，中微子是 Majorana 粒子还是 Dirac 粒子以及轻子数违反等都具有决定性意义。核物理室 2008−2012 年成功高质量完成了 CUORE 所有晶体材料的纯度测量工作，并研制了低本底 γ 探测器和宇宙射线探测器。

CUORE-0 作为 CUORE 的第一个原型塔，完全采用和 CUORE 一样的生产、安装标准和流程，CUORE-0 塔包含 52 块 TeO_2 晶体，CUORE-0 塔所用铜支架表面进行了特殊的纯化处理以减少氡及其它污染源，于 2013 年 3 月开始在 CUORICINO 低温器中运行，取数据至 2013 年 8 月，2013 年 11 月又接着取数据[1]。

合作组成员曹喜光、邓先概分别于 2014 年 1 月 11 日至 3 月 12 日和 2014 年 11 月 15 日至 2015 年 1 月 23 日访问意大利核物理研究院 LNGS 国家地下实验室，参加 CUORE-0 实验低温器运行维护、数据在线获取及离线分析工作。在这两次访问中我们排查、克服了一系列困难，比如 CUORE-0 基线温度异常升高、线缆异常排查、主真空泵异常等，确保了 CUORE-0 数据获取高质量进行。

经过整个合作组紧张、细致的工作，CUORE 在 2014 年完成了整个 19 个 TeO_2 塔的组装，2014 年 9 月为 CUORE19 个塔定制建造的低温器试运行达到了低于 8 mK 的基线温度[1]。

2 暗物质直接测量(PandaX)

在 PandaX 合作方面，合作组成员曹喜光从 2013 年 9 月起承担了上海交通大学粒子物理与宇宙学开放课题“低本底快中子探测器符合测量”，开展探测器研发。本项目计划研制一套低本底快中子符合测量装置：在已有的高灵敏度 ^{3}He 管正比计数器的基础上，再增加 4 条长塑料闪烁体探测器+PMT，组成一个中子符合测量装置，用于锦屏山地下实验室的快中子本底测量。为此开展了三方面的研究工作：1) EJ301 液体闪烁体探测器的波形甄别和能量刻度；2) EJ339A 俘获门控中子探测器双脉冲特性；3) 利用 ^{3}He 管和 EJ301 开展对锦屏地下实验室中子本底的一系列实地测量。2014 年 6 月在锦屏地下实验室测量装置示意图如图 1 所示，^{3}He 正比计数器的直径为 5.08 cm，长度 1 m。

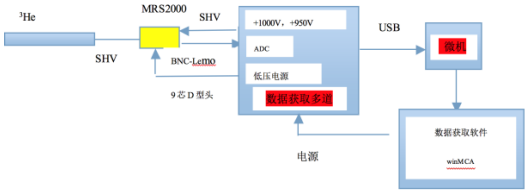

图 1 锦屏地下实验室快中子测量装置示意图

测量结果显示 ^{3}He 管工作状态受实验室电源波动影响非常大，另外 ^{3}He 管也需要静置一段时间才能达到稳定工作状态，否则会引起很大的噪声。仍需要进步一改变测量条件继续测量，确认计数率是否达到稳定。

PandaX 实验顺利完成第一期建造并运行、取数据[2]，于 2014 年发表了第一个暗物质测量结果[3]，37 kg Xe 17.4 d 有效测量没有发现暗物质候选粒子，否定了 DAMA/LIBRA 实验关于暗物质粒子第一个肯定的报道，此报道可以用质量 10~50 GeV/c^2 的 WIMP 来解释。PandaX-I 结果得出对于 49 GeV/c^2 的 WIMP 候选粒子，在 90%置信度下得出其和核子散射截面的上限为 3.7×10^{-44} cm^2，如图 2 所示。

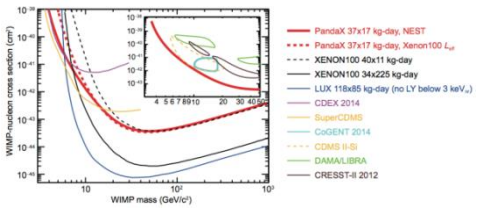

图 2 PandaX-I 结果以及和国际上别的实验组结果比较，取自文献[3]。

参考文献

1. https://wiki.wlab.yale.edu/cuore/.
2. Cao X G, *et al.* PandaX: a liquid xenon dark matter experiment at CJPL, Science China Physics[J]. Mechanics & Astronomy, 2014, **57**(8): 1476-1494.
3. Xiao M J, *et al.* First dark matter search results from the PandaX-I experiment[J].Science China Physics, Mechanics & Astronomy, 2014, **57**(11), 2024-2030.

CUORE and PandaX collaboration experiments

Nuclear Physics Division

This research field focuses on ultra low background deep underground laboratory and non-accelerator physics: neutrinoless double beta decay measurement (CUORE) and dark matter direct detection experiment (PandaX) in China Jinping underground laboratory (CJPL). We have carried out a series of R&D and background analysis of ultra low background detectors, which play an important role in the above two international cooperation experiments.

1 0VDBD experimental collaboration (CUORE)

The main goal of CUORE (Cryogenic Underground Observatory for Rare Events) is to measure possible extremely rare neutrinoless double neutrino beta decay (0VDBD) of ^{130}Te. The measurement of 0VDBD is crucial to determine the absolute mass of neutrinos, whether neutrinos are Majorana particles or Dirac particles, and the lepton number violation. The nuclear physics division successfully completed the measurement of purity of all CUORE crystal materials from 2008~2012, and developed low background gamma detectors and cosmic ray detectors.

CUORE-0, the first prototype tower of CUORE, uses the same manufacturing, assembly standards and processes as CUORE, contains 52 TeO_2 crystals, and the surface of the copper frame has been specially purified to reduce radon and other sources of pollution. CUORE-0 began to run in CUORICINO cryostat from March 2013, taking data till Augest 2013. It then continues to take data from Nov 2013[1].

Two members from our group visited LNGS national underground laboratory of Istituto Nazionale di Fisica Nucleare (INFN) Italy, from January 11, 2014 to March 12, 2014 and from November 15, 2014 to January 23, 2015, respectively, participated in the operation, maintenance of CUORE-0 cryostat, online data acquisition, and offline analysis work. During the two visits, we investigated and overcome a series of difficulties, such as the abnormal increasing of CUORE-0 baseline temperature, the abnormal cable inspection and the main vacuum pump anomalies, which ensure the high quality of CUORE-0 data acquisition.

The assembly of the 19 TeO_2 towers was finished in 2014. The custom cryostat for the 19 towers has commissioned and reached a baseline temperature lower than 8 mK[1].

2 Direct Measurement of Dark Matter (PandaX)

In PandaX collaboration, we undertook an open topic project of particle physics and cosmology laboratory of Shanghai Jiao Tong University: "Fast neutron coincidence detector measurement in low background" from September 2013. This project aims to develop a low background fast neutron coincidence measurement device based on existing high sensitivity ^{3}He proportional counter tube and 4 new long plastic scintillator detectors + PMTs. This research work has been carried out in three aspects: 1) waveform digitizer and energy calibration of EJ301 liquid scintillation detector; 2) dual pulse characteristics study of capture gated neutron detector of EJ339A; 3) a series of measurements using ^{3}He tube and EJ301 in Jinping underground laboratory. The schematic diagram of measurement device used in CJPL in Jun 2014 was shown in Fig.1, where the ^{3}He proportional counter has a diameter of 5.08 cm and a length of 1 meter.

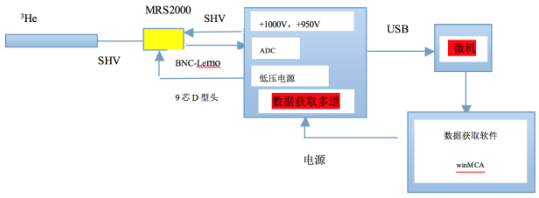

Fig.1 Schematic diagram of fast neutron measurement device used in CJPL.

The measurement results showed that the working state of the ^{3}He tube was greatly affected by the fluctuation of the power supply of the laboratory. In addition, the ^{3}He tube needed to be stationary for a period of time to achieve a stable working point, otherwise it will cause a lot of noise. There is still a need to change the measurement conditions, to confirm whether the counting rate is stable.

PandaX successfully completed the first phase of construction, operation and data taking[2], and the first dark matter (DM) measurement result was published in 2014[3]. In the 37-kg liquid xenon target with 17.4 live-days of exposure, no DM particle candidate event was found. This result disfavored the first reported positive observation from the DAMA/LIBRA experiment, which can be explained by WIMPs with masses around 10 or 50 GeV/c^2. The minimum upper limit, 3.7×10^{-44} cm^2, for the DM-nucleon scattering cross section, was obtained for a 49 GeV/c^2 DM-particle mass at 90% confidence level.

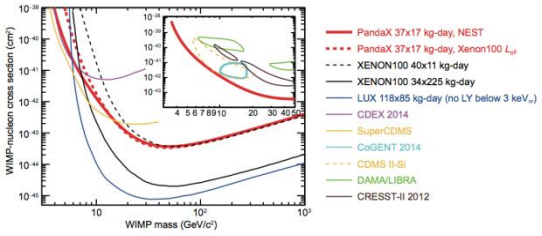

Fig.2 PandaX-I results, as well as the results of other experimental groups, taken from the reference[3].

Reference

1. https://wiki.wlab.yale.edu/cuore/
2. Cao X G, *et al.* PandaX: a liquid xenon dark matter experiment at CJPL, Science China Physics[J]. Mechanics & Astronomy, 2014, **57**(8): 1476-1494.
3. Xiao M J, *et al.* First dark matter search results from the PandaX-I experiment[J].Science China Physics, Mechanics & Astronomy, 2014, **57**(11), 2024-2030.

中子物理实验装置（白光中子源）

核物理研究室

中子物理实验装置（又称为光中子源，PNS），2013 年完成了 15 MeV 电子加速器驱动的白光中子源装置土建改造，加速器、靶屏蔽体，靶冷却系统和实验终端设备安装（图 1），开展 15 MeV 电子-白光中子源的联合调试；在韩国浦项 PNF 白光中子源装置上开展了 ^{19}F（AlF_3, Al 靶）总截面的初步测量，参加了 ^{232}Th 活化实验测量[1]，数据分析处理结果如图 2 所示；完成了多种中子/γ 探测器的测试，在脉冲反应堆上完成了 ^{6}LiI 热中子探测器，EJ401 闪烁体热中子探测器的刻度分析[2]；初步组建了多单元中子探测器和伽玛阵列探测器，采购了电子学系统；完成了中子产生能谱，中子输运真空管道的模拟计算，比较不同厚度铅屏蔽体对中子与光子的阻挡效应，中子在 AlF_3 和 Al 中的多重散射对中子截面影响，慢化体厚度优化分析以及 ^{6}LiI 晶体探测器中的中子、伽马能损分析[3]；调试完成了波形数字采样获取系统，VME 多参数获取系统（单机版和网络版）的调试[4]；完成了总截面，裂变截面，弹性截面，俘获截面等实验方案的调研分析[5−6]。

图 1　中子物理实验装置效果图及现场照片

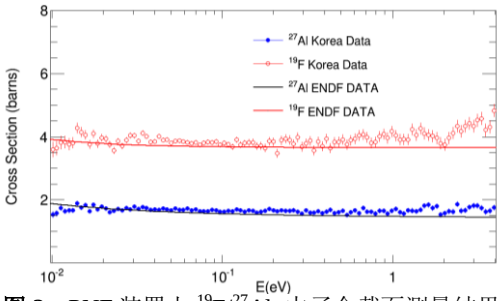

图 2　PNF 装置上 ^{19}F/^{27}Al 中子全截面测量结果

1　中子物理实验装置的试车调试

图 3 给出了试车调试的初步结果，在脉冲宽度 1.5 μs，电子能量 20 MeV 条件下，随着加速器功率的提升，5 m 处中子飞行时间探测器测量的计数率也随着增加，初步分析显示，热中子和慢中子产额符合设计要求。Cd/Ag/In 等刻度靶获得了 TOF 谱中中子吸收峰位置等结果。

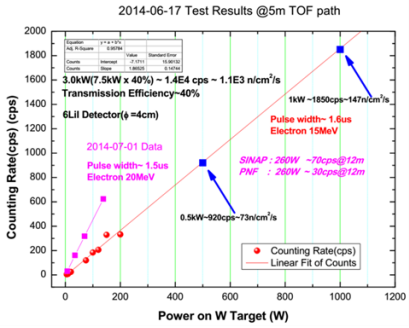

图 3　试车调试结果：中子产额与加速器功率

2　多单元中子探测器和 γ 探测器阵列设计

多单元中子探测器采用锂玻璃与塑料闪烁体组合的探测器结构，研制由 42 个 CsI(Tl)晶体组成的 γ 探测器阵列，探测器覆盖的空间立体角可以达到 95%以上。探测器的单元晶体已经加工到货 30 根，经过测试，能量分辨都在 10%以下。整体支架已经加工完成，2014 年将开始探测器的整体组装和单元性能的详细测试工作。

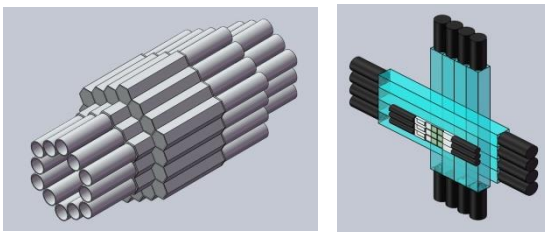

图 4　多单元伽马探测器和中子探测器设计

参考文献

1. 卢飞，张国强，王宏伟，等. 韩国 PNF 实验测量及初步数据分析[R]. 中国科学院上海应用物理研究所, 2013.
2. 杜龙，常乐，王玉廷，等. ^{6}LiI/(nat)LiI 闪烁体探测器效率的模拟计算及实验测量[J].核技术，2014，**37**(4): 040201.
3. 张松，王宏伟，张桂林，等，中子慢化和中子飞行管道限流系统的模拟研究[R]. 中国科学院上海应用物理研究所, 2013.
4. 王宏伟，曹喜光，张国强，等. 波形数字采样及液闪探测器研究[R]. 中国科学院上海应用物理研究所, 2013.
5. 王宏伟，张松，曹喜光，等. 总截面(n,Total) 测量方案设计[R]. 中国科学院上海应用物理研究所, 2013.
6. 李琛，蔡翔舟，陈金根，等. 俘获截面测量方案[R]. 中国科学院上海应用物理研究所, 2013.

Neutron physics experimental facility (White light neutron source)

Nuclear Physics Division

The neutron physics experimental facility, (also called as photo neutron source-PNS) the 15MeV electron LINAC driven white light neutron source was finished the building project, and accelerator, production target shielding, target cooling system and terminal devices installation (Fig.1), started the 15 MeV electron-neutron joint commissioning; Experimental measurement of ^{19}F (AlF_3 and Al target material) neutron total cross section and ^{232}Th radioactive experiment at PNF(Pohang Neutron Facility) of Korea, the final results shown in Fig.2, shows well agreement with ENDF/VII Library evaluated data; Finished the ^{6}LiI crystal and solid plastic scintillator calibration at pulsed reactor with thermal neutron beam; Build a multi gamma and neutron detector array with CsI(Tl) crystal and Li Glass combined with plastic scintillator, electronics system and so on; Simulation with GEANT4 for neutron production spectra, neutron transmission vacuum tube, compared the stopping effect of different thickness of Lean shield cell, and multi-scattering effect in AlF_3 and Al thick target, optimization analysis of PE and Boron loaded PE moderator and neutron gamma energy loss analysis in ^{6}LiI crystal. Finished the waveform and VME based DAQ system(single PC and network version), study the neutron total cross section, fission, elastic and inelastic, capture cross section measurement setup and detector's design.

Fig.1 Photo of neutron physics experimental facility

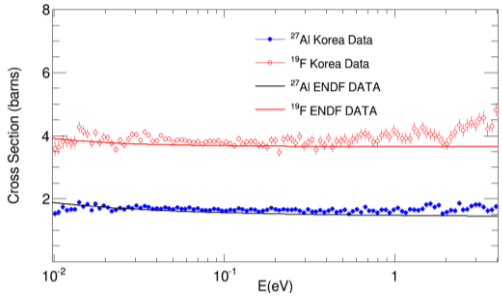

Fig.2 ^{19}F/ ^{27}Al neutron total cross section results and compared with ENDF/VII data at PNF Korea

1 Commissioning results of PNS

Fig.3 shows the relationship of neutron TOF detector's counting rate with the accelerator power, at the conditions of 1.5 μs pulse width and 20 MeV electron energy and 5m TOF path. The preliminary analysis indicated that the total thermal and quasi-thermal neutron yields was matched the designed results. The Cd/Ag/In film calibrated target get the absorption peak from the TOF spectra.

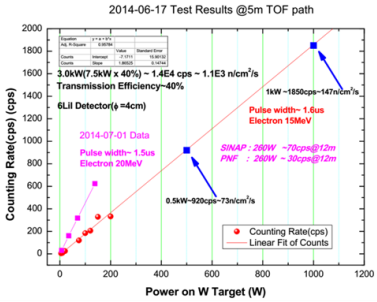

Fig.3 Commissioning results: relationship in neutron counting rate and accelerator power

2 Design of Multi-unit Detector Array

Designed with Li glass and plastic scintillator for neutron detector array and 42 CsI(Tl) crystal for gamma detector array of neutron capture reaction. The solid angle of detector array coverage about 95% of 4π angle. The unit detector has finished 30 pieces and energy resolution of CsI detector less then 10%, All detector array design will be finished at 2014, and then start the detail calibration work.

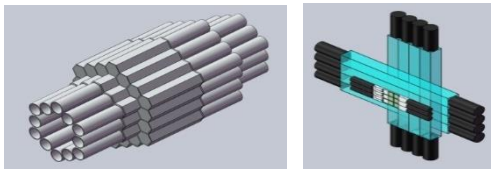

Fig.4 Multi-unit gamma and neutron detector array design

Reference

1. Lu F, Zhang G Q, Wang H W, *et al.* The PNF experimental measurement and primary data analysis[R]. Shanghai Institute of Applied Physics, Chinese Academy of Science, 2013.
2. Du L, Chang L, Wang Y T, *et al.* Detection efficiency simulation and measurement of 6LiI/natLiI scintillation detector[J]. Nuclear Science and Techniques, 2014, **37**: 040201.
3. Zhang S, Wang H W, Zhang G Q, *et al.* Neutron moderator and transmission tube of neutron current limiting system simulation[R]. Shanghai Institute of Applied Physics, Chinese Academy of Science, 2013.
4. Wang H W, Cao X G, Zhang G Q, *et al.* Waveform digitizer and Liquid scintillator detector study[R]. Shanghai Institute of Applied Physics, Chinese Academy of Science,, 2013.
5. Wang H W, Zhang S, Cao X G, *et al.* Design of experimental setup of neutron total cross section measurement[R]. Shanghai Institute of Applied Physics, Chinese Academy of Science, 2013.
6. Li C, Cai X Z, Chen J G, *et al.* Measurement setup of neutron capture[R]. Shanghai Institute of Applied Physics, Chinese Academy of Science, 2013.

应用理论物理研究

计算物理组

应用理论物理研究组从事理论物理学与生物学的交叉研究，主要是纳米生物学和纳米尺度界面水的特性研究。本组以上海光源和我所重要研究方向为导向，利用长期积累的微纳尺度界面水性质等研究基础，与相关实验组密切结合开展应用基础理论研究，并建设相关的模拟计算平台，为实验提供模拟计算支持。另外，与所内其他课题组合作，本年度取得了重要成果。

石墨烯和氧化石墨烯对细胞脂膜破坏作用研究

石墨烯作为一种新型材料不断受到关注，如何与生物分子（如蛋白质、细胞脂膜等）发生作用，是其生物相容性方面的重要问题之一。石墨烯以 sp^2 杂化的碳为主的成键方式，形成独特的二维结构，具有显著的疏水特征。细胞脂膜主要是由双亲的磷脂分子在水环境中自组装而成。上海应用物理研究所水科学与技术研究室方海平研究员与扬州大学涂育松教授合作，研究了石墨烯等纳米颗粒在水的环境中与生物膜的相互作用过程，发现在水介导下石墨烯可以破坏细菌细胞膜，为揭示石墨烯的细胞毒性提供了一种可能的分子机制：研究发现水分子会直接参与石墨烯对细胞膜的破坏过程，一方面水分子会促使石墨烯在热涨落的帮助下主动插入细胞膜，另一方面水分子会帮助石墨烯将磷脂分子抽离细胞膜。该分子机制为发展具有生物相容性的纳米材料、纳米器件提供了基础和借鉴。部分成果已发表在国际顶级学术期刊《自然 纳米科技》[1]。

氧化石墨烯表面氧化位点高度相关

石墨烯是一种新型的二维超薄纳米材料，它具有独特的结构、力学和电子性质，被认为有着广泛的应用前景。氧化石墨烯因其良好的水溶性特点，使得它在涉及到液相条件的相关实验中拥有比石墨烯更广泛的应用空间。中国科学院上海应用物理研究所水科学与技术研究室的博士生杨金荣、石国升博士、方海平研究员与扬州大学的涂育松教授合作，运用密度泛函理论计算和传统反应动力学理论相结合，首次阐述了酸性水溶液环境中石墨烯的氧化机制，揭示了氧化石墨烯表面氧化位点的高度相关特性，建立了全新的氧化石墨烯结构模型（图1）。相关研究工作以 VIP (Very important paper)形式发表于《德国应用化学》杂志[2]。

该氧化石墨烯结构模型为理解当前实验的观测结果提供了一个新视角，阐述了氧化石墨烯表面氧化区域和未氧化区域分布的内在关联性。同时，该模型给出了氧化石墨烯表面官能团的细节分布，将进一步拓展氧化石墨烯在分子动力学模拟方面的相关研究。

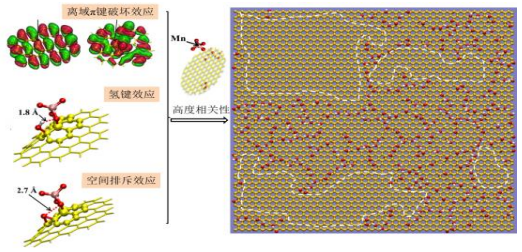

图 1 高度相关性的三种效应：离域 π 键破坏效应、氢键效应和空间排斥效应，高度相关性的氧化石墨烯结构模型，虚线区域代表未氧化区域。

纳米受限空间溶液中溶质在分散与聚集两态之间的自发双向转变

溶液中溶质的分散或聚集行为对于众多物理、化学和生物过程会产生重要影响。中国科学院上海应用物理研究所水科学与技术研究室的博士生赵亮、王春雷博士、方海平研究员等与上海大学的涂育松博士、英国雷丁大学的王作维博士合作，运用分子动力学模拟提出在纳米受限空间内的溶液中，溶质的溶解状态可以在分散与聚集之间双向转变。

在纳米尺度下，往往有着不同于宏观系统的物理现象。当溶质聚集到一定程度，由于纳米体系中总的溶质数目受限，聚集状态的颗粒团簇不能从溶液里获得更多溶质，颗粒数目达不到稳定状态的要求。在热扰动下，聚集颗粒会重新分散开来，从而溶质的溶解状态可以在分散态和聚集态之间进行双向转变。通过建立理论模型，发现分散态和聚集态分别对应于系统自由能曲线上的两个极小值，两个状态之间自由能垒的大小与热扰动保持在同一数量级上。这样，在热涨落环境中，系统会在两个状态之间发生自发地双向转变。正是因为这种双向转变，聚集成稳定颗粒团簇在纳米受限条件下则需要更多的溶质，进而提高临界成核浓度。纳米受限

溶液广泛分布于细胞液中大分子间，人造纳米器械，岩石孔洞及土壤缝隙中等，该研究从理论层次加深了对纳米受限条件下溶液中溶质行为的理解，也为解释一些常见的实际受限溶液环境中分子的溶解行为，比如药物分子的吸收、纳米材料的毒性、石油开采和土壤中碳元素的储存等问题有启示意义。相关研究工作已发表在《物理评论快报》[3]。

水分子与锐钛矿氧空位研究

二氧化钛作为一种重要的半导体材料，在有机物降解、水解制氢以及太阳能电池等方面有着广泛应用。由于大部分反应发生在水环境中，因此二氧化钛与水分子之间的相互作用一直是研究热点。中科院上海应用物理研究所水科学研究室硕士生李亚东在高嶷研究员指导下，利用密度泛函理论计算，发现了水与二氧化钛锐钛矿(101)亚表面氧空位相互的新机制。相关研究工作已发表在《物理评论快报》[4]。

二氧化钛表面的高反应活性一直以来被认为由其表面氧空位决定。近年来，科学家们在锐钛矿研究中发现亚表面以及体相氧空位比表面的氧空位更加稳定。当温度高于 200 K 时，表面的氧空位就会迁移到体相中去。这些发现为理解锐钛矿表面的高反应活性带来了困惑。李亚东和高嶷研究员通过计算模拟发现，水在锐钛矿表面的吸附可以造成表面氧空位与亚表面氧空位的相对稳定性发生反转，从而引发亚表面氧空位越过一个较低的能垒迁移到表面，形成表面氧空位。该表面氧空位进而可以诱导水分子分解，在锐钛矿表面上形成两个羟基。在另一条竞争路径中，水分子在亚表面氧空位上分解，也可诱导亚表面氧空位向表面的迁移。该机制说明锐钛矿表面的高反应活性不仅仅依赖于表面氧空位的多少，也同时决定于亚表面乃至体相氧缺陷的数量。这种新奇的基底与吸附质之间的相互作用一方面为理解锐钛矿(101)表面的高催化活性提供了新解释，另一方面也为理解其他金属氧化物表面的高反应活性提供了全新的视角。

铝离子结合在蛋白骨架上形成环状结构：理解铝的神经毒性的分子机理新视角

铝在日常生活中曾经得到广泛应用：铝锅、铝壶等餐具，油条、馒头、面条、膨化食品等等中含铝的食品添加剂[例如，明矾(硫酸铝钾)]。到 90 年代，人们确认了铝对人体有害，长期摄入，可能导致老年痴呆等神经系统的疾病，甚至影响儿童的生长、发育和智力。因此，不仅含铝餐具被限制使用，近期，在馒头、发糕等面制品中也不再允许使用含铝的食品添加剂。尽管如此，铝如何与蛋白作用，导致生物毒性的分子机理依然不清楚。这严重阻碍了相关疾病的预防和治疗。

中国科学院上海应用物理研究所宋波、高兴宇、方海平研究员与中国石油大学黄方教授等通过多方合作，采用量子计算、经典分子动力学模拟与同步辐射能谱和 X 射线光电子谱(XPS)、圆二色谱(CD)、核磁共振谱(NMR)等谱学实验相结合的方法，研究了铝对蛋白结构的影响，提出了一种铝对人体生物毒性的新分子机制（图 2）。相关研究结果作为首页插图发表于《德国应用化学》[5]。

图 2 A) 含铝的食品添加剂已经被禁止使用。B) 铝制餐具已经被限制使用。C)铝离子结合在蛋白骨架上形成环状结构及其对蛋白二级结构的破坏。左下：正常的蛋白结构；右上：铝离子结合在蛋白骨架上形成的环状结构；左上：该骨架环状结构对蛋白结构的破坏。

研究人员根据铝具有的离子键和共价键共存化学特性，提出：铝离子能同时与神经退行性疾病相关的蛋白的骨架上的氮原子、氧原子同时形成化学键，导致环状结构，进而破坏蛋白的二级结构，使蛋白产生不可逆的变性和积聚。

参考文献

1. Tu Y S, Lv M, Xiu Pen, *et al.* Destructive extraction of phospholipids from Escherichia colimembranes by graphene nanosheets[J]. Nature nanotechnology, 2013, **8**(8): 594-601.
2. Yang J, Shi G, Tu Y, *et al.* High Correlation between Oxidation Loci on Graphene Oxide[J], Angew. Chem. Int. Ed., 2014, **53**(38): 10190.
3. Zhao Liang, Wang Chunlei, Liu Jian, *et al.* Reversible State Transition in Nanoconfined Aqueous Solutions[J]. Phys. Rev. Lett., 2014, **112**(7): 0708301.
4. Li Yadong, Gao Yi. Interplay between Water and TiO_2 Anatase (101) Surface with Subsurface Oxygen Vacancy[J]. Phys Rev Lett, 2014, **115**(14): 149601.
5. Song Bo, Sun Qian, Li Haikuo, *et al.* Irreversible Denaturation of Proteins through Aluminum-Induced Formation of Backbone Ring Structures[J]. Angew. Chem. Int. Ed., 2014, **53**(25): 6358-6363.

Theoretical physics for nanobiology and interfacial water

Group of Computational Physics

The group is engaged in interdisciplinary studies on theoretical physics and nanobiology, focusing on molecular dynamics simulation and other computational studies on biomolecules and interfacial water. These provide theoretical assistance to synchrotron radiation studies and other experimental research programs at SINAP. Collaborating well with the experimental groups, the group has made remarkable progresses.

Destructive extraction of phospholipids from Escherichia coli membranes by graphene nanosheets

Graphene has attached more research attention in recent years, Thus, to understand how it interacts with macromolecules (such as proteins, cell membranes and so on) is crucial for its biomedical applications. Graphene is a two dimensional single-atom-thick nanomaterial with unique hydrophobicity. The cell membrane mainly consists of self- assembled amphiphiles in aqueous environment. Recently, Prof. Yusong Tu from Yangzhou University and Prof. Haiping Fang from the Shanghai Institute of Applied Physics, Chinese Academy of Sciences have shown that there are two types of molecular mechanism for the graphene-induced degradation of E. coli cell membranes: one by severe insertion and cutting, and the other by destructive extraction of lipid molecules. The direct extraction of phospholipids from lipid membranes was first observed in our computer simulations, and then validated by our TEM images. This strong attraction between graphene and membrane lipids is largely derived from graphene's unique two-dimensional structure with all sp2-carbons, which facilitates exceptionally strong dispersion interactions between graphene and lipid molecules. Cooperative movements of extracted lipid molecules were also observed on the two-dimensional graphene surface due to the redistribution of the hydrophobic tails to maximize hydrophobic interactions with the graphene surface. Our current findings might have implications in the design of novel antibiotics and other clinical applications. In particular, we envisage that graphene might become a new type of 'green' antibacterial material for everyday use, with little bacterial resistance due to its 'physical damage'- based bacterial killing mechanism. It might also stimulate the cytotoxicity studies of other nanomaterials in this emerging field of nanotoxicology. This work has been published on the journal of Nature Nanotechnology[1].

High Correlation between Oxidation Loci on Graphene Oxide

Graphene is a new type of two-dimensional ultra-thin materials, which is considered to have wide applications due to its unique structure, mechanical and electronic properties. In contrast to the hydrophobicity of graphene, graphene oxide (GO) has the vital advantage of water solubility. This results in that GO in related experiments has more extensive applications than graphene under liquid phase conditions. Combining density functional theory with conventional transition-state theory, Jinrong Yang, Dr. Guosheng Shi and Prof. Haiping Fang from SINAP collaboration with Prof. Yusong Tu from Yangzhou University firstly described the oxidation mechanism of graphene in acidic aqueous solution. This study a kinetic profile for graphene oxidation with high correlation between oxidation loci and built a new model of GO(Fig.1). This work was published in Angew. Chem. Int. Ed[2], which was selected as very important paper (VIP).

The study of the detailed atomic structure of GO not only provides new explanations for experimental observations and an extension of relevant molecular-dynamics studies, but also provides a more detailed description and understanding of the physical nature of the oxidized and unoxidized regions on GO.

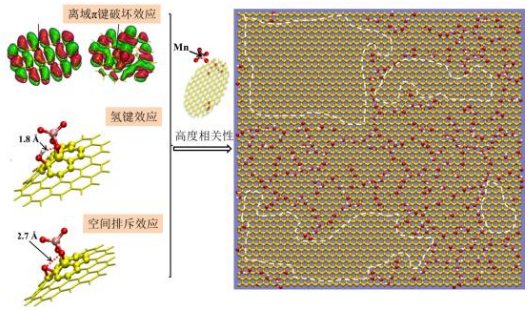

Fig.1 Three crucial effects on high correlation:1) breaking of delocalized π bonds; 2) steric hindrance; 3) hydrogen-bond formation.

Reversible State Transition in Nanoconfined Aqueous Solutions

Whether solute molecules are in the dissolved or aggregated states has fundamental importance in a large variety of physical and biological processes, including the reaction efficiency of chemical catalysis, the functions of proteins, and the possible toxicity of nanoparticles. Recently, Liang Zhao, Dr. Chunlei Wang, Prof. Haiping Fang and colleagues from the Shanghai Institute of Applied Physics, Chinese Academy of Sciences and Prof. Zuowei Wang from the Reading University in United Kingdom have observed the reversible state transition in the nano-confined aqueous solutions by MD simulations.

Systems at nanoscales usually display physical behavior qualitatively different from that of macroscale systems. In the reversible state, the system can switch between the dispersion state and the aggregation state as the time goes on. Besides, the confinement also leads to a significant increase of critical aggregation concentration. Based on the developed theoretical model, they found the reversible state transition was attributed to the low free energy barrier (of order kBT) comparable to the thermal fluctuation in between two energy minima corresponding to the dispersion and aggregation states, and the enhancement of the critical aggregation concentration resulted

from the fact that at lower concentrations the number of solute molecules was not large enough to allow the formation of a stable cluster in the confined systems. These findings enrich the theory of the association behavior of the solute molecules to the nanoscale and may give insights into the fields relevant to the dissolution property of material in confined aqueous environment, such as the drug absorption, toxicity of nanomaterial, oil extraction and restoration of carbon element in soil. This work has been published on the journal of Physical Review Letters[3].

Interplay between Water and oxygen vacancy on TiO_2 anatase

TiO_2 is an important semiconductor with applications in a wide range of areas, such as degradation of toxic organic pollutants, water splitting, and solar cells. Its interaction with water has brought a particular research interest because most of reactions take place at aqueous surroundings. Researchers at Shanghai Institute of Applied Physics, Chinese Academy of Science, recently discovered a novel intrplay between water and subsurface oxygen vacancy (Vo) on TiO_2 anatase (101) sureface. Their relevant research has been published on Physical Review Letters[4].

In contrast with rutile, the subsurface Vo is more stable than surface Vo, and the surface Vo's will diffuse to bulk site at temperature as low as 200 K. However, with the adsorbed water on the surface, the relative stability of surface and subsurface Vo will reverse because of the stronger adsorption of water over surface Vo. By utilizing density-functional calculation, we found a novel interplay between adsorbed water and subsurface Vo. The adsorbed water can induce subsurface Vo to bubble up to the surface layer, which further facilitate water dissociation. In another energetically competitive pathway, molecular water dissociates over subsurface Vo first, followed by barrierless Vo diffusion from subsurface to surface. This interplay may enrich our knowledge about molecule adsorption on metal oxide surface and also provide a new perspective way to understand the catalytic activity of anatase(101) surface.

Aluminum-induced formation of backbone ring structures: an innovative view for understanding molecular mechanism underlying the aluminum-induced neurotoxicity

Aluminum is widely used in antimicrobial coagulants, cookware, and even additives of food involving fried bread stick, steamed bun, noodle and puffed food. In the 90 s, it was confirmed that aluminum is harmful to human body. Long-term intake of aluminum, it can lead to diseases of the nervous system such as Alzheimer's, and even affects the growth, development and intelligence of children. Hence, cookware which contains aluminum has been limited to use. Likewise, the use of aluminum containing food additives is no longer permitted recently in products such as steamed buns and cakes. Despite this close relationship between aluminum and health, the mechanisms behind these aluminum-related diseases are poorly understood, especially on the molecular level, which limits efforts to prevent and treat these diseases.

Fig.2 a) Food additives containing aluminum have been banned. **b)** Aluminum tableware has been restricted. **c)** Aluminum ion combines with the protein skeleton to form the ring structure and its damage to the protein secondary structure. Left lower diagram shows normal structure of protein. Upper right diagram indicates the ring structure. Upper left diagram presents the destruction of protein structure.

Bo Song, Prof. Xingyu Gao, and Prof. Haiping Fang from the institute of applied physics of CAS cooperated with prof. Fang Huang from china university of petroleumto apply. They applied the combination of ab initio calculations, classical molecular dynamical simulations, circular dichroism, nuclear magnetic resonance, and X-ray photoelectron spectroscopy to investigate the effect of aluminum on the protein structure(Fig.2). The corresponding results were published as homepage illustration in the journal of Angew. Chem. Int. Ed[5].

According to the coexisting chemical properties of ionic bonds and covalent bonds, researchers proposed that aluminum ions have the ability to form chemical bonds simultaneously with both the amide nitrogen and carbonyl oxygen atoms on the peptide backbone of protein involving Neurodegenerative disease. It results in the formation of a ring structure. Thereby the secondary structure of the protein is destroyed, which causes the protein to produce irreversible degeneration and accumulation.

References

1. Tu Y S, Lv M, Xiu Pen, *et al.* Destructive extraction of phospholipids from Escherichia colimembranes by graphene nanosheets[J]. Nature nanotechnology, 2013, **8**(8): 594-601.
2. Yang J, Shi G, Tu Y, *et al.* High Correlation between Oxidation Loci on Graphene Oxide[J], Angew. Chem. Int. Ed., 2014, **53**(38): 10190.
3. Zhao Liang, Wang Chunlei, Liu Jian, *et al.* Reversible State Transition in Nanoconfined Aqueous Solutions[J]. Phys Rev Lett, 2014, **112**(7): 0708301.
4. Li Yadong, Gao Yi. Interplay between Water and TiO_2 Anatase (101) Surface with Subsurface Oxygen Vacancy[J]. Phys Rev Lett, 2014, **115**(14): 149601.
5. Song Bo, Sun Qian, Li Haikuo, *et al.* Irreversible Denaturation of Proteins through Aluminum-Induced Formation of Backbone Ring Structures[J]. Angew. Chem. Int. Ed., 2014, **53**(25): 6358-6363.

太赫兹技术及应用研究

水科学　太赫兹实验组

本组主要从事太赫兹技术及其应用基础研究工作。利用太赫兹光谱开展不同物质结构和弱相互作用探测研究，并结合量子化学理论计算对太赫兹光谱进行解析，揭示光谱信号与物质结构间的关系。

分子间弱相互作用探测

利用太赫兹光谱探测观察到在固态无溶剂条件下，尿嘧啶和尿素间能够通过氢键相互作用产生分子间相互识别，高效地形成共晶二聚体，并在太赫兹波段呈现指纹特征光谱[1](图 1)。研究结果对于理解尿素对核酸碱基相互作用机制有所帮助，提示太赫兹光谱对物质结构和弱相互作用敏感，该技术在生物无标记探测和医药的在线检测中具有重要的应用前景[2-3]。

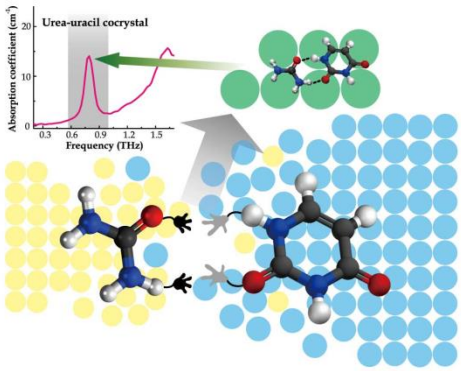

图 1　尿嘧啶与尿素在固态条件下的相互识别

太赫兹时域光谱系统研制

2013 年，在中国科学院仪器设备功能开发技术创新项目支持下，成功研制一套基于光电导天线技术的太赫兹时域光谱系统，包括透射及反射测试功能（图 2）。系统带宽 0.1~3.5 THz，动态范围>80 dB，频率分辨率<2 GHz，稳定度±0.13%@1 THz。采用 LabVIEW、MATLAB 等语言编写可视化界面，通过混合编程技术对有关程序进行集成和改进，提高数据处理效率。图 3 为用户利用该系统完成的相关实验[4]。

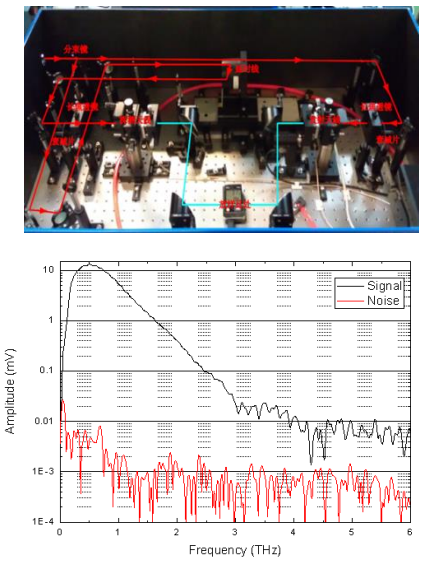

图 2　(a)太赫兹时域光谱系统实物图；(b) 系统带宽及信噪比测试结果

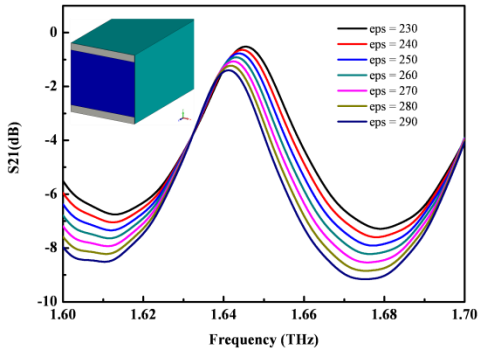

图 3　IDE 结构在 THz 下的透射谱

参考文献

1. Jingqi Yang, Shaoxian Li, Hongwei Zhao, *et al*. Molecular recognition and interaction between uracil and urea in solid-state studied by terahertz time-domain spectroscopy. [J]. The Journal of Physical Chemistry A, 2014, **118**: 10927.
2. Te Ji, Zengyan Zhang, Hongwei Zhao, *et al*. A THz-TDS measurement method for multiple samples. Optics Communications, 2014, **312**: 292.
3. Ji Te, Zhao Hongwei, Han Pengyu, *et al*. Terahertz identification and quantification of penicillamine enantiomers[J]. Nuclear Science and Techniques. 2013, **24**(1): 010201.
4. Bian, Y L, Wu C, Li H Q, *et al*. A tunable metamaterial dependent on electric field at terahertz with barium strontium titanate thin film[J]. Applied Physics Letters, 2014, **104**(4): 042906.

Terahertz technique and applications

THz Experimental Group

The group is engaged in the studies on terahertz (THz) technique and its applications. THz time-domain spectroscopy was applied to investigate the structure and interactions of molecules. Quantum chemistry calculation was adopted to analyze the relationship between the THz spectrum and the structural properties.

The detection of weak intermolecular interaction

Using terahertz (THz) time-domain spectroscopy technique, we observed that urea is able to recognize and interact with uracil efficiently even in the solid phase without involving water or solvents. A cocrystal configuration linked by a pair of hydrogen bonds between uracil and urea was formed and presents distinct THz fingerprint[1](Fig.1). The work enables in-depth understanding of recognition and interaction of urea with nucleobases and comprehension of the denaturation related to RNA. The study demonstrates that THz spectroscopy has high sensitivity to different molecules and interactions. It is an effective and alternative tool for label-free and online measurement in pharmaceutical and biochemical studies[2-4].

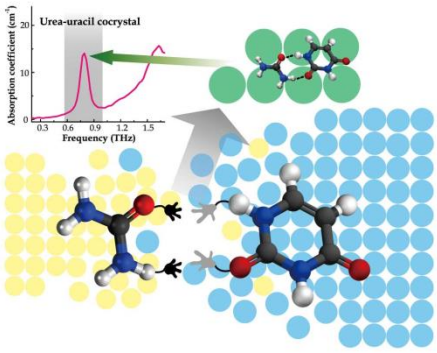

Fig.1 The recognition and interaction of uracil and urea under solid-state.

Development of terahertz time-domain spectroscopy system

In 2013, we developed a terahertz time-domain spectroscopy system based on the photoconductive antenna technology, including transmission and reflection testing functions supported by the instrument and equipment functional development and technical innovation project of the Chinese Academy of Sciences. The system possesses the bandwidth 0.1~3.5 THz, dynamic range >80 dB (Fig.2), frequency resolution <2 GHz, and stability ±0.13%@1 THz. We developed the visual interface by LabVIEW, MATLAB and other languages. The efficiency and convenience of the data processing have been improved through the integration and improvement of programs. Fig.3 shows an experimental result obtained by our user on this system[4].

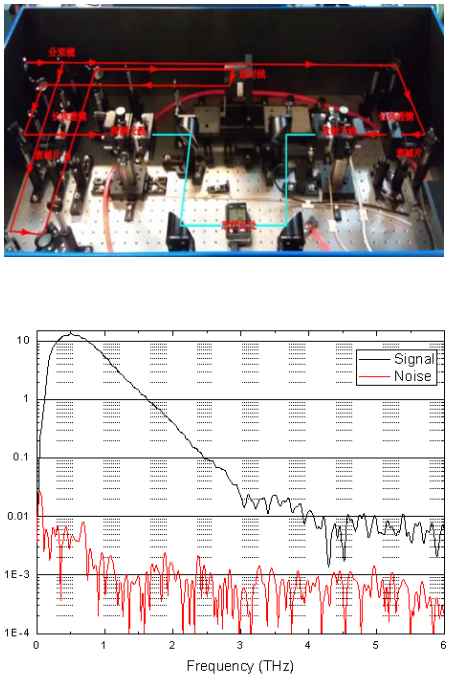

Fig.2 (a) Real object of the terahertz time-domain spectrum system; (b) System bandwidth and signal-to-noise ratio.

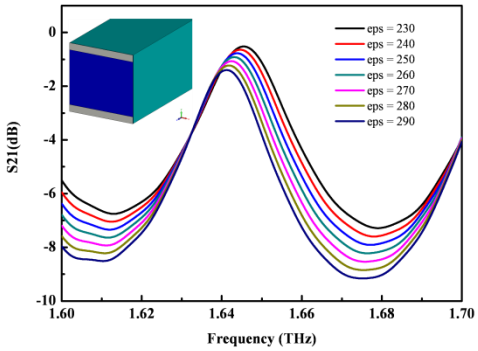

Fig.3 Transmission spectrum of IDE structure under THz

References

1. Jingqi Yang, Shaoxian Li, Hongwei Zhao, *et al*. Molecular recognition and interaction between uracil and urea in solid-state studied by terahertz time-domain spectroscopy. [J]. The Journal of Physical Chemistry A, 2014, **118**: 10927.
2. Te Ji, Zengyan Zhang, Hongwei Zhao, *et al*. A THz-TDS measurement method for multiple samples. Optics Communications, 2014, **312**: 292.
3. Ji Te, Zhao Hongwei, Han Pengyu, *et al*. Terahertz identification and quantification of penicillamine enantiomers[J]. Nuclear Science and Techniques. 2013, **24**(1): 010201.
4. Bian, Y L, Wu C, Li H Q, *et al*. A tunable metamaterial dependent on electric field at terahertz with barium strontium titanate thin film[J]. Applied Physics Letters, 2014, **104**(4): 042906.

工业应用界面水研究

水科学研究室 纳米材料实验组

本组长期从事糖类物质的辐射化学基础应用研究、生物材料及纳米材料的研制、高分子材料的辐射改性研究、过滤膜结构与性质研究等。主要研究：高分子材料改性及其在膜过滤技术及有机无机复合材料制备中的应用、同步辐射技术应用和水科学应用基础。

在聚偏氟乙烯(PVDF)溶液中均相辐射接枝 PVP 并制备微滤膜

在均相溶液中，我们通过共辐射接枝的方法在聚偏氟乙烯(PVDF)分子上成功地接枝上聚 N-乙烯基吡咯烷酮(PVP)，并得到接枝产物(PVDF-g-PVP)。首先对其辐照诱导的接枝聚合动力学进行了研究。全反射模式(ATR)的 FT-IR 光谱表明了产物中存在 PVP 的接枝链。然后，以 PVDF 和具有不同接枝率(DG)的 PVDF-g-PVP 为成膜材料采用相转化法制备微滤膜。我们测定了膜的接触角、吸水率、水过滤性能和防污性能，并利用原子力显微镜和扫描电镜对其形貌进行了研究。结果表明：随着接枝率(DG)的增加，膜的接触角变小，膜的吸水率、均方根粗糙度、水通量(图 1)、孔径和膜表面量增加。水通量的恢复表明 PVDF-g-PVP 膜具有有效的防污性能[1](图 2)。

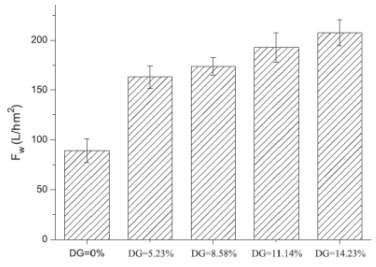

图 1 水通量与膜材料接枝率(DG)之间 的关系，从 PVDF 到 PVDF-g-PVP 接枝率 14.23%

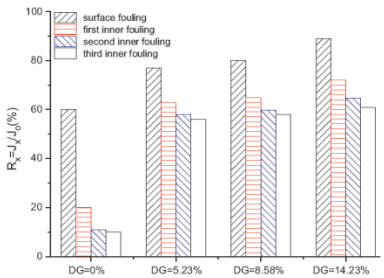

图 2 PVDF 和 PVDF-g-PVP 膜在被牛血清白蛋白溶液进行表面和内部污染后的水通量恢复百分比

预辐照诱导接枝聚合法合成 PVDF-g-PVP 粉体并制备防污微滤膜

本文使用预辐照诱导的接枝聚合技术对聚偏氟乙烯 (PVDF) 粉体接枝 N-乙烯基吡咯烷酮。考察了反应时间、 吸收的剂量、 单体浓度对接枝率的影响。并采用傅里叶变换红外光谱、 热重分析和差式扫描量热仪对接枝后的 PVDF 粉末进行了表征。以相转换方法将接枝后的 PVDF 粉末制备微滤膜并测定了其接触角和水吸收能力。采用扫描电镜表征膜的形貌，并测试了其水过滤性能(图 3)。膜的抗污染性能通过测定被牛血清白蛋白污染后膜的水通量恢复百分数进行表征。结果证实：聚（N-乙烯基吡咯烷酮）(PVP) 接枝链的存在改善改善了 PVDF-g-PVP 微滤膜的亲水性和抗污染性能[2]。

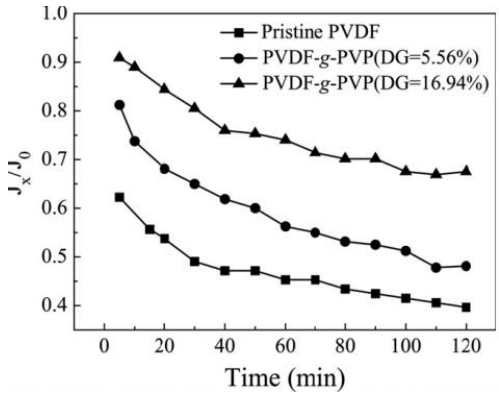

图 3 归一化的膜通量，膜材料为 PVDF 何 PVDF-g-PVP。过滤介质为 1 g/L 的牛血清白蛋白溶液

从界面微液滴通过表面活性剂介导制备聚合物微透镜

微纳透镜在光伏或发光器件中的抗反射层以及近场模式的超分辨成像中有着广泛的应用前景。一种能大批量制备聚合物微透镜的方法就是将在固液界面上形成的大量单体前驱体的微液滴进行聚合。微液滴通过溶剂交换法从其饱和的溶液中析出。在这项工作中，我们通过使用表面活性剂改良了此方法。在液相中添加一种阳离子表面活性剂来控制可聚合的微液滴和他们相应的微纳聚合物透镜（即聚合后的微纳液滴）的形成和形貌。结果表明，表面活性剂可以使溶剂交换技术在亲水的基底

上产生可聚合的微液滴，消除了基底润湿性能对制备微纳透镜的限制(图 4)。此外，微透镜的粒度分布和长宽比可以通过改变表面活性剂的浓度进行调节(图 5)[3]。

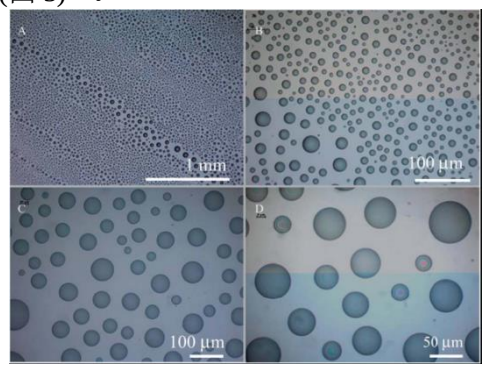

图 4 在亲水的硅基底上制备的微透镜的光学图像。制备微液滴时采用 CTAB 0.5 cmc 水溶液作为液相进行生产

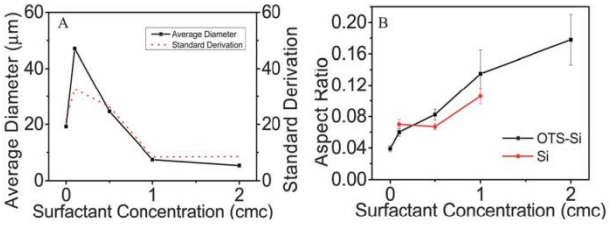

图 5 (A)在疏水 OTS-Si 基底上微透镜的平均直径和标准偏差， (B) 在疏水 OTS-Si 和亲水性 Si 基底表面上微透镜的纵横比随液相中表面活性剂浓度的变化曲线

力模式蘸笔纳米刻蚀技术的机制

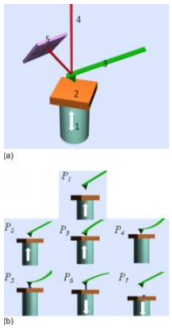

图 6 (a)实施 FMDPN 技术的原子力显微镜系统的示意图: (1) 扫描管、(2)基底、(3) AFM 针尖、(4)激光、(5)光电探测器; (b) 一系列表示 AFM 针尖与扫描管的相对位置和运动的示意图 (P1 到 P7)。扫描管沿箭头(P1、P2、P3、P6 和 P7)所示的方向移动。如果扫描管不懂，则没有箭头显示(P4 和 P5)

在这项工作中，力模式蘸笔纳米刻蚀技术(FMDPN) 的底层机制通过深入分析在实施 FMDPN 期间的力曲线、轻敲模式针尖偏折信号及“Z-扫描”电压变化等信息进行了研究。FMDPN 的操作参数，包括相对“触发阈值”和“表面延迟”参数对控制加载力和油墨沉积停顿时间至关重要。我们也提出了一个模型来模拟实施 FMDPN 过程中原子力显微镜针尖与软性基底之间的相互作用。(图 6)该模型可以很好地对实验数据拟合(图 7)[4]。

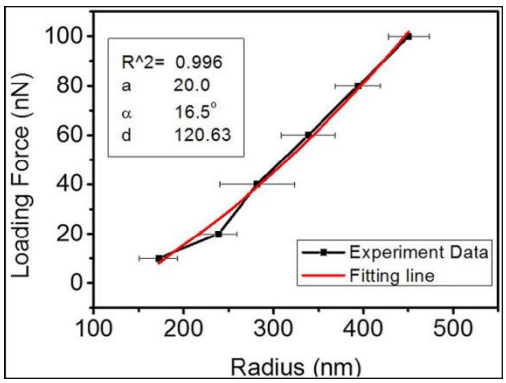

图 7 拟合实验数据与理论模型

Floading 是通过 AFM 针尖施加到基底上的加载力；rink 是是沉积的墨水点的半径；a 和 d 分别为半月板的厚度和墨水分子的扩散长度；是这个模型中基底形变的角度的一半。

参考文献

1. Qin Qiang, Hou Zhengchi, Lu Xiaofeng, *et al*. Microfiltration membranes prepared from poly (N-vinyl-2-pyrrolidone) grafted poly (vinylidene fluoride) synthesized by simultaneous irradiation [J]. Journal of Membrane Science, 2013, **427**: 303−310.
2. Chen Lifang, Hou Zhengchi, Lu Xiaofeng, *et al*. Antifouling microfiltration membranes prepared from poly(vinylidene fluoride)-graft-Poly(N- vinyl pyrrolidone) powders synthesized via pre-irradiation induced graft polymerization[J]. Journal of Applied Polymer Science, 2013, **128** (6): 3949–3956.
3. Yang Haijun, Peng Shuhua, Hao Xiaotao, *et al*. Surfactant-mediated formation of polymeric microlenses from interfacial microdroplets[J]. 2014, **10**(7): 957-964, (Feature Article).
4. Yang Haijun, Xie Hui, Wu Haixia, *et al*. Mechanism of force mode dip-pen nanolithography[J]. Appl Phys, 2014, **115**: 174314.

.

Industrial application of interfacial water research

Department of Water Science

Basic and applied research radiation chemistry of carbohydrates has long been engaged in this group, the development of biological materials and nano-materials, radiation modification of polymer materials, filtration membrane structure and properties research. The main research area includes as follows: modification of polymer materials and its application in filtration membrane technology and organic-inorganic composite materials, synchrotron radiation applications and scientific applications of water based technology.

Microfiltration membranes prepared from poly(N-vinyl-2-pyrrolidone) grafted poly(vinylidene fluoride) synthesized by simultaneous irradiation

Poly(N-vinyl-2-pyrrolidone) grafted poly(vinylidene fluoride) (PVDF-g-PVP) copolymers were synthesized by a simultaneous irradiation induced graft polymerization technique in a homogeneous system. The kinetics of the radiation induced graft polymerization was studied. Evidence for the existence of the graft chains in grafted PVDF was characterized by FT-IR spectroscopy in ATR mode. Then, membranes were cast from pristine PVDF and PVDF-g-PVP of different degree of grafting (DG) under phase inversion method. The contact angle, water uptake, water filtration and antifouling property of membranes were measured. The morphology was also studied with the use of AFM and SEM. The results showed that with the increasing DG, the contact angle became smaller, the water uptake, RMS roughness, water flux and pore size and amount of the membrane surface increased(Fig.1). The water flux recovery showed that membranes cast from PVDF-g-PVP also possessed an effective antifouling performance [1] (Fig.2).

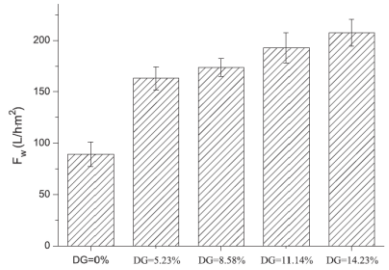

Fig.1 The relationship of water flux with DG of membranes cast from pristine PVDF and PVDF-g-PVP.

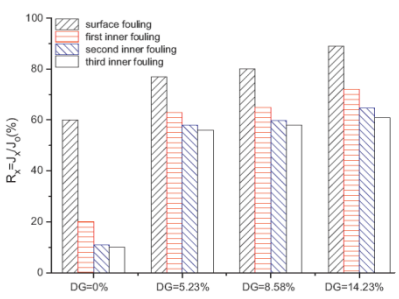

Fig.2 Water flux recovery percentage of membranes cast from PVDF and PVDF-g-PVP of different DGs after surface and inner fouling by BSA solution.

Antifouling Microfiltration Membranes Prepared from Poly(vinylidene fluoride)-graft-Poly(N-vinyl pyrrolidone) Powders Synthesized via Pre-Irradiation Induced Graft Polymerization

Poly(vinylidene fluoride) (PVDF) powders were grafted with N-vinyl pyrrolidone using the pre-irradiation induced graft polymerization technique. The effects of reaction time, absorbed dose, and monomer concentration on the degree of grafting were investigated, and the grafted PVDF powders were characterized by Fourier transform infrared spectroscopy, thermogravimetric analysis, and differential scanning calorimetry. The grafted PVDF powders were also cast into microfiltration (MF) membranes via the phase-inversion method. The contact angle and water uptake were measured. The membrane morphology was studied by scanning electron microscopy, and the water filtration properties of the membranes were tested(Fig.3). The antifouling properties were determined through measurements of the recovery percentage of pure water flux after the MF membranes were fouled with bovine serum albumin solution. The results confirmed that the existence of poly(N-vinyl pyrrolidone) (PVP) graft chains improved the hydrophilicity and antifouling properties of the MF membranes cast from PVDF-g-PVP powders[2].

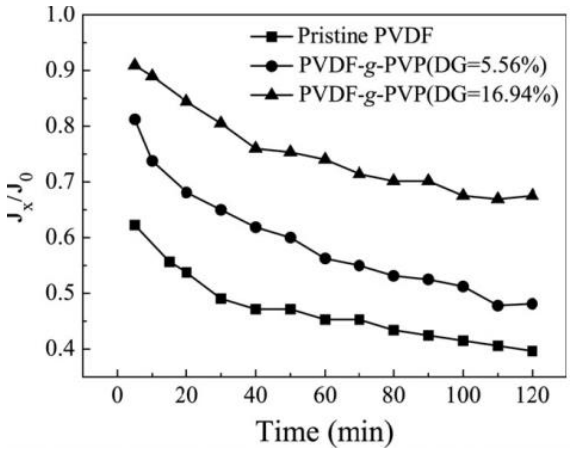

Fig.3 Normalized flux of MF membranes cast from pristine PVDF and PVDF-g-PVP powders at different DGs during filtration of 1 g/L BSA solution.

Surfactant-mediated formation of polymeric microlenses from interfacial microdroplets

Nano- and micro-scale lenses have a range of potential applications, such as in antireflective layers in photovoltaic or light emission devices, and in super resolution imaging in the near field modes. One of the protocols to mass produce polymeric microlenses is through the polymerization of microdroplets of a monomer precursor that are produced at solid–liquid interfaces by a solvent exchange technique. In this work, we have advanced this protocol by using surfactants. A cationic surfactant was added to the liquid phase for the control over the

formation and morphology of polymerisable microdroplets and their resultant microlenses (i.e. the polymerized microdroplets). The results demonstrate that the surfactant could enable the production of polymerizable microdroplets on hydrophilic substrates by the solvent exchange technique, and eliminate the restriction by the substrate wettability on the microlens fabrication(Fig.4). Furthermore, the size distribution and aspect ratio of microlenses could be tuned by the surfactant concentration[2](Fig.5).

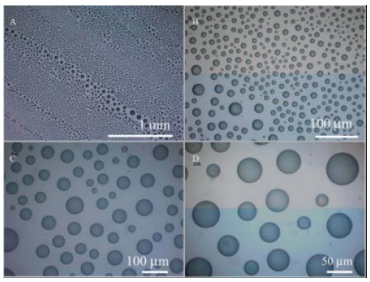

Fig.4 Optical images of microlenses produced on silicon. The microdroplets were produced by using 0.5 cmc CTAB aqueous solution as Solution B.

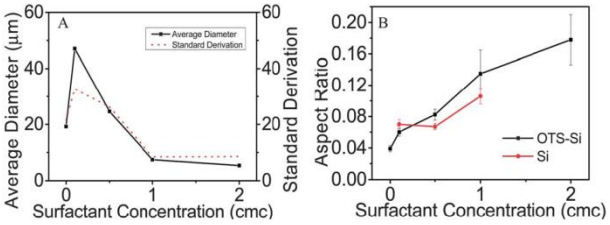

Fig.5 (A) Average diameter and standard derivation of microlenses on the hydrophobic OTS–Si substrate and (B) aspect ratio of microlenses on hydrophobic OTS–Si and hydrophilic Si substrate surfaces at different surfactant concentrations.

Mechanism of force mode dip-pen nanolithography

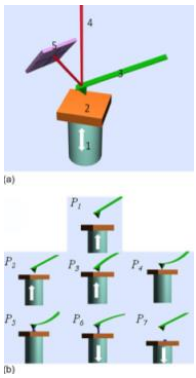

Fig.6 (A) A schematic AFM system for FMDPN: (1) piezo tube, (2) substrate, (3) AFM tip, (4) laser, (5) photodetector; (B) a serial of schemes represent the relative position and movement of the AFM tip and scanner at different feature points (P1 to P7). The piezo tube moves along the direction indicated by the arrow (P1, P2, P3, P6, and P7). If the piezo is stationary, no arrow is shown (P4 and P5).

In this work, the underlying mechanism of the force mode dip-pen nanolithography (FMDPN) is investigated in depth by analyzing force curves, tapping mode deflection signals, and "Z-scan" voltage variations during the FMDPN. The operation parameters including the relative "trigger threshold" and "surface delay" parameters are vital to control the loading force and dwell time for ink deposition during FMDPN. A model is also developed to simulate the interactions between the atomic force microscope tip and soft substrate during FMDPN(Fig.6), and verified by its good performance in fitting our experimental data[4] (Fig.7).

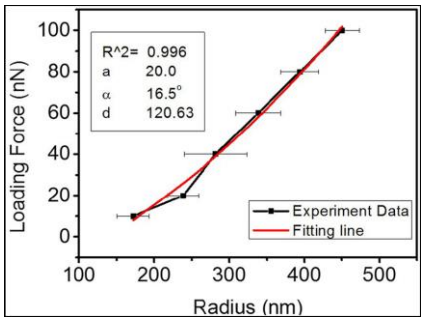

Fig.7 Fitting the experiment data to the theoretical model:

$$F_{loading}(r_{ink}) = 1.15 \times 10^{6} \tan\alpha (r_{ink} - a - d)^2 + 0.22(r_{ink} - d) - 0.18a$$,

Floading is the loading force exerted by the AFM tip onto the substrate; rink is the radius of the deposited ink dots after FMDPN; a and d are the thickness of the meniscus and the diffusion length of ink molecules during FMDPN, respectively; is the half angle of the substrate deformation in this model.

References

1. Qin Qiang, Hou Zhengchi, Lu Xiaofeng, *et al.* Microfiltration membranes prepared from poly (N-vinyl-2-pyrrolidone) grafted poly (vinylidene fluoride) synthesized by simultaneous irradiation [J]. Journal of Membrane Science, 2013, **427**: 303−310.
2. Chen Lifang, Hou Zhengchi, Lu Xiaofeng, *et al.* Antifouling microfiltration membranes prepared from poly(vinylidene fluoride)-graft-Poly(N- vinyl pyrrolidone) powders synthesized via pre-irradiation induced graft polymerization[J]. Journal of Applied Polymer Science, 2013, **128** (6): 3949–3956.
3. Yang Haijun, Peng Shuhua, Hao Xiaotao, *et al.* Surfactant-mediated formation of polymeric microlenses from interfacial microdroplets[J]. 2014, **10**(7): 957-964, (Feature Article).
4. Yang Haijun, Xie Hui, Wu Haixia, *et al*. Mechanism of force mode dip-pen nanolithography[J]. Appl Phys, 2014, **115**: 174314.

多肽自组装研究进展

物理生物学研究室

多肽自组装的研究具有重要意义。在淀粉样疾病的致病机制方面，界面辅助的多肽自组装受到了广泛关注，由多肽自组装产生的纳米生物材料也具有潜在应用价值。然而，长久以来多肽分子的自组装机制并没有在分子水平上得到很好的阐释。近年来，我们课题组在多肽自组装的分子机制、自组装结构控制方面取得了一些进展，在此作一个简单的介绍。

固液界面上多肽分子自组装结构和及其组装分子机制

我们与 IBM 沃森研究中心的周如鸿教授课题组合作，通过分子动力学模拟研究了一个被称为 GAV-9 的多肽在云母和石墨表面的自组装机制。结果显示，GAV-9 肽自组装受到基底上云母原子晶格的影响，肽分子通过带正电的 N 端与带负电（K^+ 空穴）的云母表面之间的静电吸引相互作用维持稳定，多肽分子形成平行的 β-sheet 结构。为了考察 GAV-9 肽是沿云母晶格的 a-方向（周期 0.48 nm）还是 b-方向（周期 0.92 nm）延伸，我们在云母表面上放置一个 7×7 的 GAV-9 肽“小岛”，在溶液中随机加入了 10 条 GAV-9 肽，考察这 10 条 GAV-9 肽吸附在小岛的哪个边缘。分子动力学模拟结果显示，GAV-9 肽分子通过疏水相互作用力沿云母晶格 b-方向延伸；与此同时，GAV-9 肽分子之间通过氢键结合在一起。在石墨表面，我们首先设定不同密度的 GAV-9 肽分子“站立”在表面，系统运行一段时间以后，肽分子由于其侧链和石墨的疏水相互作用，“躺在”了石墨表面上。

盐离子驱动多肽分子在固液界面的多层直立自组装

我们通过实验和理论相结合的方法，研究了 GAV-9 肽在固液界面上的自组装。在高盐浓度条件下，我们发现 GAV-9 肽可以自组装成高度有序的、多层次的纳米纤维。出人意料的是，多肽分子采用直立的排列方式。原子力显微镜(AFM)原位观察和基于 AFM 纳米操纵实验强有力地证明，调整溶液的离子强度可以控制 GAV-9 肽分子在垂直方向上直立堆叠形成多层的纳米结构。例如盐($MgCl_2$)浓度在 0 mM 时，GAV-9 肽会组装成单层的直立纳米结构；在 100 mM 时，GAV-9 肽主要组装成双层直立纳米结构；到 250 mM 时，GAV-9 肽会组装成双层、三层、四层和更多层的直立纳米结构。

分子动力学模拟揭示，由于各层多肽分子的微环境不同，GAV-9 肽自组装成的多层直立自组装结构的各层多肽分子采取不同的 β-sheet 排列方式，第一层多肽分子采取平行的 β-sheet 排列方式（N 端指向云母），而上层多肽分子采取反并行 β-sheets 排列方式，上层多肽分子通过和下层多肽分子的 C 端的 $CONH_2$ 基团形成氢键维持结构的稳定，多肽分子间疏水相互作用力也起到了非常重要的作用；同时发现过量的阳离子降低了云母的负电性，减少了 GAV-9 肽的吸附位点，从而驱动 GAV-9 肽在第一层的上面自组装第二层而不是重新自组装成一个单层的纳米细丝。

进一步的实验表明，GAV-9 肽在云母/水界面自组装成多层直立结构是一个普遍现象，不同种类的盐都可以控制 GAV-9 肽的直立自组装。与其它多肽或蛋白自组装成不确定的形貌相比，我们的 GAV-9 肽自组装的研究表明通过仔细的序列设计、衬底晶格匹配、离子强度的调控、纳米操纵等手段可以得到有序的和可控的纳米结构。

云母表面淀粉样多肽的分等级的有序化现象

淀粉样多肽分子积聚成纤维的现象与许多神经退行性疾病相关，而细胞膜和生物分子的表面被认为对淀粉样多肽分子的积聚发挥重要的调节作用。在生物体内，从分子水平上进行实验研究多肽纤维化是非常具有挑战性的，因此生物表面如何影响淀粉样多肽纤维的结构和积聚机制目前仍不清楚。我们以吸附在云母表面水膜中的胰岛素分子为模型体系，考察这个肽在不同条件下的聚集行为。AFM 研究表明，胰岛素纤维的结构和取向显著地受到云母晶格和胰岛素浓度的影响。在低肽浓度(~0.05 mg/mL)时，胰岛素积聚成为三维对称的、具有良好取向的、平均高度为 1.6 nm 的短纤维。将胰岛素的浓度增加到 0.2~2.0 mg/mL 时，出现了一种平均高度为 3.8 nm 的纤维。当胰岛素浓度高于 2.0 mg/mL，形成了二维液晶状组装体。这些结

果为我们更好地理解生物表面对淀粉样多肽纤维化的作用提供了崭新的信息。

参考文献

1. Dia B, Kang S G, Huynh T, *et al*. Proc. Natl. Acad. Sci. USA 2013, **110**: 8543-8548.
2. Zhou X F, Zhang Y Y, Zhang F, *et al*. Nanoscale 2013, **5**: 4816-4822.
3. Seung-gu Kang, Tien Huynh, Zhen Xia, *et al*. J. Am. Chem. Soc. 2013, **135**: 3150-3157.

Progresses in peptide self-assembly

Physical Biology Division

The study on the self-assembly of peptides is valuable since it has been recognized as an important approach to understanding the pathology of some diseases as well as exploring the applications in *de novo* nanodevice design and fabrication. However, the molecular level understanding of how the peptides assemble into ordered nanostructures still remains elusive. Herein, I introduce the progresses that we have made in the molecular mechnisms as well as molecular-level control on peptide self-assembly that have conducted in our group.

Self-assembled peptide nanostructures and its molecular mechnisms

By cooperating with Prof. Ruhong Zhou's group at IBM Thomas J. Watson Research Center, the molecular mechanism of epitaxial fibril formation has been investigated for GAV-9 (NH_3-VGGAVVAGV-$CONH_2$), an amyloid-like peptide extracted from a consensus sequence of amyloidogenic proteins. Using atomistic molecular dynamics simulations, we found that the surface polarity determines the global morphologies of GAV-9, "upright" on mica and "flat" on HOPG, even with relatively low surface peptide density. The lattice structure (i.e., a- and b-directions) of the mica surface are commensurate with the molecular dimension of the peptides, which induces a highly ordered β-stranded structure with synergies from both the backbone hydrogen bondings and the side-chain hydrophobic packings along the surface crystallographic a- and b-directions, respectively. On the assembly growth mechanism, the binding interaction between the 7×7 peptide island and the GAV-9 monomers ascertained the dominant role of the hydrophobic packings, thus suggesting the b-directional growth to be the longitudinal axis of the GAV- 9 epitaxy on mica. GAV-9 contains only hydrophobic side chains except for the charged N-terminus; thus, it would be energetically favorable to lie down on the hydrophobic HOPG surface to maximize the hydrophobic packing. Our simulations reveal both static structures and dynamic processes on the peptide self-assembly on highly ordered surfaces such as mica and HOPG with atomic details.

Salts drive controllable multilayered upright assembly of amyloid-like peptides at mica/water interface

We have investigated the formation of multilayered nanofilaments of the amyloidal peptide GAV-9 on the surface of mica under high-salt concentrations with both experimental and theoretical approaches. In situ AFM images and delicate nanomechanical manipulation experiments show that GAV-9 peptide exhibits a very strong tendency to assemble uniformly into a double-layered nanostructure with all-upright conformations in 100 mM $MgCl_2$ solutions. This layer-by-layer assembly of the upright-oriented peptides can be modulated by adjusting the salt concentration (i.e., the ionic strength). Our molecular dynamics simulations and PMF calculations suggest a parallel β-sheet conformation for the first layer but an antiparallel β-sheet for the second layer and beyond. The more stable antiparallel conformation for the second-layer peptide is a result of balanced complex interactions between peptide and peptide, peptide and water, and peptide and mica, which are also more consistent with the findings of the current AFM experiment as well as with the commonly observed antiparallel amyloid fibril structures. The different assembly patterns for the first and second layers also emphasize the importance of the microenvironment, such as template surfaces (i.e., on mica, on peptide surface) even under the same salt solution. Further studies with a variety of salt types (e.g., KCl, NaCl, $MgSO_4$) and a wide range of salt concentrations (0–250 mM) indicate that this is a common phenomenon, with an even higher number of well-ordered upright layers (three, four, or five layers) possible. Compared with previous selfassemblies of other peptides and proteins with indefinite morphologies, the current study with GAV-9 peptides indicates that highly ordered, controllable nanostructures can be achieved through careful sequence design, substrate lattice matching, and ionic strength tuning.

Hierarchical ordering of amyloid fibrils on the mica surface

The aggregation of amyloid peptides into ordered fibrils is closely associated with many neurodegenerative diseases. The surfaces of cell membranes and biomolecules are believed to play important roles in modulation of peptide aggregation under physiological conditions. Experimental studies of fibrillogenesis at the molecular level in vivo, however, are inherently challenging, and the molecular mechanisms of how surface affects the structure and ordering of amyloid fibrils still remain unclear.

We have investigated the aggregation behavior of insulin peptides within water films adsorbed on the mica surface. AFM measurements revealed that the structure and orientation of fibrils were significantly affected by the mica lattice and the peptide concentration. At low peptide concentration (0.05 mg/mL), there appeared a single layer of short and well oriented fibrils with a mean height of 1.6 nm. With an increase of concentration to a range of 0.2~2.0 mg/mL, a different type of fibrils with a mean height of 3.8 nm was present. Interestingly, when the concentration was above 2.0 mg/mL, the thicker fibrils exhibited two-dimensional liquid-crystal-like ordering probably caused by the combination of entropic and electrostatic forces. These results could help us gain better insight into the effects of the substrate on amyloid fibrillation.

Reference

1. Dia B, Kang S G, Huynh T, *et al*. Proc. Natl. Acad. Sci. USA 2013, **110**: 8543-8548.

2. Zhou X F, Zhang Y Y, Zhang F, *et al*. Nanoscale 2013, **5**: 4816-4822.

3. Seung-gu Kang, Tien Huynh, Zhen Xia, *et al*. J. Am. Chem. Soc. 2013, **135**: 3150-3157.

远场光学成像

物理生物学研究室

远场光学显微成像技术能够对细胞开展无损伤、三维、实时动态的活细胞观察，是揭示纷繁复杂的生命现象内在机制的重要技术手段，广泛应用于生物学，医学，纳米科学等领域。课题组主要从事远场光学成像的理论和技术，突破光学衍射极限的超高分辨率系统的研制等方面的研究，旨在发展可用于亚细胞结构及动态过程的精细观察，纳米材料的生物学效应和 DNA 纳米技术等方面高精度的检测与分析。

成像平台

成像平台旨在发展微观水平上探索复杂生物分子体系的结构与功能，从而为药物设计与研发、生物检测，疾病诊断等方面提供新的技术路线。2013 年购置的三台仪器——激光共聚焦扫描显微镜，活细胞工作站和小动物成像系统已经通过了技术验收，运行正常。这些设备可为相关学科领域的发展起到很好的推动作用。

图 1 激光共聚焦显微镜

突破光学衍射极限的超分辨系统研制

课题组利用商品化激光共聚焦显微系统的平台，对系统进行了分辨率升级，分别添加了连续光输出和白激光器脉冲光的损耗光模块，分别建立了连续光[1]和脉冲光的受激发射损耗显微镜，获得 70 nm 的突破光学衍射极限的超高分辨率（CW-STE1）系统，分辨能力是原共聚焦显微镜的 4 倍（图 2）。目前为止，我们的系统实现了在生物样品高分辨观察的应用。在对细胞微管的超分辨成像中，分辨率达到 75 nm，如图 3(b)所示。与普通共聚焦扫描成像（图 3(a)）相比，分辨能力是原系统的 2.5 倍。

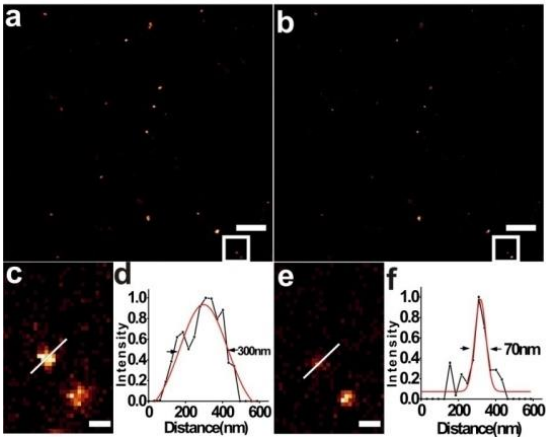

图 2 CW-STED 系统分辨率的测量。平铺在玻片上 DNA 四面体的普通共聚焦成像(a)与 CW-STED(b)成像比较。(c)和(e)分别对应为(a)和(b)的白色矩形中的放大图片。(d)和(f)给出的是(c)和(e)中沿着白线的归一化强度轮廓图。Scale bars: 5 μm in (a) and (b), 500 nm in (c) and (e)

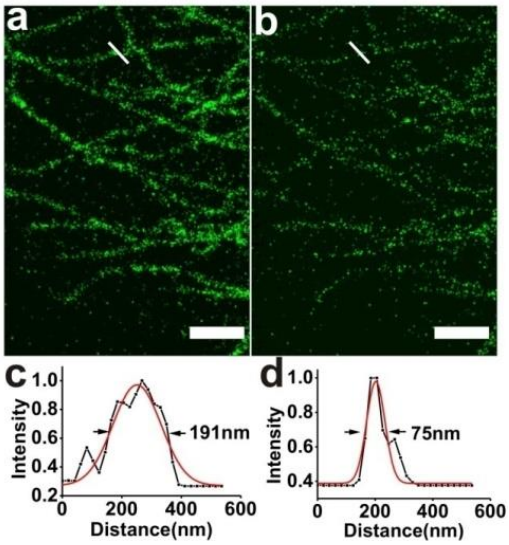

图 3 Chromeo 488 标记的 Hela 细胞微管的共聚焦(a)与 CW-STED 高分辨(b)的成像对比。(c)和(d)给出的是(a)和(b)中沿着白线的归一化强度轮廓图，数据显示 CW-STED 分辨率达到 75 nm。Scale bar: 2 μm

参考文献

1. DU J C, Deng S H, Hou S G, *et al*. Superresolution imaging of DNA tetrahedral nanostructures in cells by STED method with continuous wave lasers[J]. Chinese Optics Letters, 2014, **12**(4): 041101.

Progresses in developing far-field light microscopy

Division of Physical Biology

The far-field light microscope is a valuable sciectific instrument in life sciences for the noninvasive and time-resdved imaging of the interior of transparent objects, like cells in three dimensions and is widely applied in the research of biology, medical science and nanoscience. The Division is mainly to develop the theory and the technology of the far-field light microscopy and the methods of imaging with the diffraction barrier broken. These methods are hoped to describe the intracellular structure of the organelle and their dynmic processes, precisely analyze the biological effects of the nanomaterials and DNA nanotechnology with super-higer resolution.

Imaging platform

The imaging platform provides new imaging technologies to explore the complex biological systems at microscopic level and can be used in drug testing, biological detection and hoped to offer an in-depth understanding of complex genetic diseases. In the year of 2013, three equipments including the laser cofocal scanning microscope, live-work station and small animal imaging system were purchased. At present, these systems have passed the technical approval and work properly. These instruments are helpful to advance the developments of the related science.

Fig.1 The setup of the laser confocal scanning microscope.

Superresolution imaging with the diffraction limit broken

Based on the platform of the laser confocal scanning microscope, we improved the spatial resolution of this system. By building a module of the depletion beam of continuous wave beam[1] or a pulsed beam from the supercontinuum laer, the stimulated emission depletion (STED) microscopes with continuous wave laser or with the plused laer are established. A resolution of 70 nm was obtained and 4-fold increament of the resolution compared with that of the corresponding confocal system was demonstrated in Fig.2. Up to present, these superresolution systems have been applied in the imaging of the biological samples. The resolution of 75nm was demonstrated in the imaging of the samples of the microtubulins in the Hela cell, as shown in Fig.3(b). This resolution is increased 2.5 times over the confocal imaing in Fig.3(a).

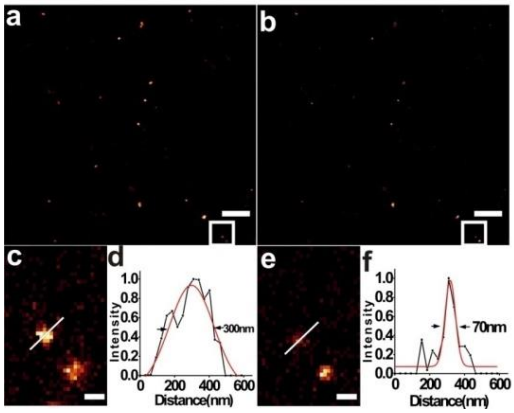

Fig.2 Confocal (a) and CW-STED (b) micrographs of tetrahedron marked by YoYo-1. (c) Confocal and (e) STED images in the white boxes in (a) and (b). Confocal (d) and STED (f) profiles of the bead indicated in (c) and (e) with a white line. Scale bar: 5μm in (a) and (b), 500 nm in (c) and (e)

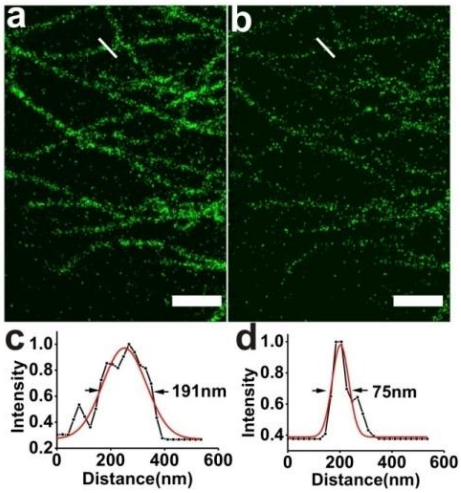

Fig.3 Comparison of confocal (a) and STED (b) images of the microtubule marked with Chromeo488. Confocal (c) and STED (d) profiles of the microtubule indicated in (a) and (b) with a white line. Scale bar: 2 μm

Reference

1. DU J C, Deng S H, Hou S G, *et al*. Superresolution imaging of DNA tetrahedral nanostructures in cells by STED method with continuous wave lasers[J]. Chinese Optics Letters, 2014, **12**(4): 041101.

纳米材料与细胞相互作用的研究进展

物理生物学研究室

在 2013−2014 年度，我们课题组围绕纳米材料的生物学效应、潜在应用和相关的细胞学机理开展了一系列的工作。主要工作可以归纳为以下几个方面：

1　多种纳米材料作为核酸载体的细胞学应用

纳米材料作为新型的药物载体具有广阔的应用前景。之前，我们课题组分别使用代表性的无机（纳米金颗粒）和有机（DNA 四面体结构）纳米材料作为载体，载带具有促炎效应的 CpG 单链寡核苷酸进入细胞，发挥了免疫刺激作用。在进一步的工作中，我们一方面就纳米材料的种类进行了扩展，尝试使用小尺寸的氧化石墨烯(sGO)和条形 DNA 结构作为新的 CpG 纳米载体，均得到了活性超越商用转染试剂的纳米复合物。另一方面，我们也针对材料合成、表面修饰、核酸链偶联等关键的技术环节进行了一系列的尝试和优化：例如，制备 CpG-纳米金复合物的经典方法使用了巯基修饰的 DNA 分子，我们尝试将不经化学修饰的 DNA 序列设计成双嵌段寡核苷酸，利用 polyA 序列与金纳米粒子之间的强吸附力，将 DNA 固定在金纳米粒子表面，而核心序列部分则用于进行蛋白受体的识别。这一新方法不仅可以有效地制备稳定的复合物，而且可以通过改变 A 碱基的长度来调控纳米金表面 CpG 的密度，在纳米尺度上精确控制核酸分子之间的距离，避免 CpG 分子之间的相互作用和空间构象阻碍，实现 CpG 序列的高识别活性和促免疫活性。这些体系将可能为 CpG 寡核苷酸药物的临床应用提供新的可能。这一系列工作分别发表于 ***Adv Mater***，***Small***，和 ***ACS Appl Mater Interfaces.*** 期刊（Ref.1-4）。

2　石墨烯抗菌的机制探讨与应用。

我们课题组于 2010 年首次报道了石墨烯的抗菌作用（ACS Nano，2010，4, 4317），该工作发表后立即引起了广泛兴趣，短短三年已有超过 50 篇石墨烯抗菌相关研究工作发表。然而，石墨烯如何通过与细菌细胞膜的相互作用而产生抗菌能力，一直缺乏明确的分子机制。近期，通过与方海平课题组和周如鸿课题组的合作，将计算机模拟与实验紧密结合起来，提出了石墨烯与细菌细胞膜相互作用的分子机制，即石墨烯不仅可以插入细胞膜进行切割，还可以对膜上的磷脂分子直接抽取，从而破坏细胞膜和杀死细菌。我们通过电镜实验，直接观察到了细菌细胞膜与氧化石墨烯作用后产生的大范围空腔结构，为理论计算结果提供了实验证据。该工作发表后立即得到了众多国际科学媒体的关注，ChemistryWorld, Before It's News, GrapheneWiki & News 等网站均进行了报导与评论。此外，我们也致力于拓展石墨烯抗菌的应用。例如，通过与李景烨课题组合作，成功制备了耐清洗和具有长时间抗菌能力的石墨烯棉布，是石墨烯纳米材料在抗菌方面的一个典型应用 。上述工作分别发表于 ***Nature Nanotechnol.***，***Adv. Healthc. Mater.***和 ***Sci. Rep.***等期刊 (Ref.5-7)。

3　纳米材料与细胞界面的相互作用。

近年来， DNA 纳米结构已被越来越广泛地应用于生物物理、药物载运、疾病诊断和治疗等领域。这些应用研究也促使研究者对于 DNA 纳米结构与人工或生命体系的相互作用过程和机制产生了浓厚的兴趣。特别是如何理解和调控 DNA 纳米结构的理化性质，以充分发挥 DNA 的独特优势，已成为该领域研究的一个重要问题。针对这一问题，我们课题组长期从事相关方面的研究，构建了一系列从一维到三维的 DNA 纳米结构，并系统研究了这些结构与无机材料的界面复合过程，以及在细胞界面上的作用机制，并在此基础上拓展和优化了 DNA 纳米材料的生物学应用。基于这些工作，我们近期受邀为权威化学综述杂志 ***Accounts of Chemical Research*** 撰写了相关综述论文[8]（Ref. 8）。为了更为直观地揭示 DNA 纳米结构与细胞的作用过程，我们重点研究了 DNA 纳米结构穿越细胞膜的过程和在细胞内的运动和命运：利用全内反射显微镜、单粒子示踪等细胞成像技术，实时观察到了 DNA 四面体结构在细胞膜上的小窝蛋白介导下产生内吞，随后，DNA 四面体结构通过由微管蛋白构成的细胞骨架系统进行运输，并最终到达溶酶体而被降解。有意思的是，载有核定位序列 NLS 的 DNA 四面体结构可以从溶酶体中逃逸出来而进

入细胞核内。该成果发表于 ***Angew Chem Int Ed*** (Ref. 9)。

另一方面，我们也针对一些经典的无机纳米材料干扰细胞学过程和调节生理功能的机制做了更为深入的研究。例如，我们发现，量子点对于细胞自噬水平的提高极大地增强了细胞对于镉离子毒性的敏感性，合理地解释了 CdTe 量子点与等量 $CdCl_2$ 的细胞学毒性差异所在，首次揭示了之前提出的量子点在细胞内发挥“纳米效应”的生物学本质。此外，我们也对于纳米金等无机粒子调节细胞和机体代谢的多方面机制进行了研究，相关成果分别发表于 ***Adv Healthc Mater*** 和 ***Small*** (Ref.10-11)。

参考文献

1. Li J, Fan C, Pei H, *et al*. Smart drug delivery nanocarriers with self-assembled DNA nanostructures[J]. Adv. Mater., 2016, **25**(7): 4386.
2. Ouyang X Y, Li J, Liu h J, *et al*. Rolling circle amplification-based DNA origami nanostructrures for intracellular delivery of immunostimulatory drugs[J]. Small, 2013, **9**: 3082.
3. Chen N, Wei M, Sun Y H, *et al*. Self-assembly of poly-adenine-tailed CpG oligonucleotide-gold nanoparticle nanoconjugates with immunostimulatory activity[J]. Small, 2014, **10**: 368.
4. Sun J, Chao J, Huang J, *et al*. Uniform small graphene oxide as an efficient cellular nanocarrier for immunostimulatory CpG oligonucleotides[J]. ACS Appl Mater Interfaces, 2014, **6**(10): 7926-32.
5. Tu Y SA, Lv M, Xiu P, *et al*. Destructive extraction of phospholipids from Escherichia coli membranes by graphene nanosheets[J]. Nature Nanotechnol, 2013, **8**: 594.
6. Zhao J M, Deng B, Lv M, *et al*. Graphene oxide-based antibacterial cotton fabrics[J]. Adv. Healthc. Mater., 2013, **2**: 1259.
7. Liu H Z, Lv M, Deng B, *et al*. Laundering durable antibacterial cotton fabrics grafted with pomegranate-shaped polymer wrapped in silver nanoparticle aggregations[J]. Sci Rep., 2014, **4**: 4920.
8. Chen N, Li J, Song H Y, *et al*. Physical and biochemical insights on DNA structures in artificial and living systems[J]. Acc. Chem. Res., 2014, **47**: 1720.
9. Liang L, Li J, Li Q, *et al*. Single-particle tracking and modulation of cell entry pathways of a tetrahedral DNA nanostructure in live cells[J], Angew. Chem. Int. Ed., 2014, **53**: 7745.
10. Li X M, Chen N, Su Y Y, *et al*. Autophagy-sensitized cytotoxicity of quantum dots in PC12 cells[J]. Adv. Healthc. Mater., 2014, **3**: 354.
11. Chen N, Wang H, Huang Q, *et al*. Long-term effects of nanoparticles on nutrition and metabolism[J]. Small, 2014, **10**: 3603-3611.

Progresses in the interaction between nanomaterials and cell

Division of Physical Biology

In 2013−2014, we continued our research on nano-biology and focused on the bio-effects and underlying mechanisms of both inorganic and DNA-based nanomaterials, as well as their potential applications. Some accomplishments were summarized in the following.

1 Application of nanomaterials as intracellular carriers of DNA

Nanomaterials (NMs) are promising candidate carriers of therapeutic DNAs in biomedical research. Previously, we have reported successful application of a popular inorganic NM (AuNPs) and DNA tetrahedral structure for the delivery of proinflammatory CpG ODN into mouse macrophages, respectively. Based on these findings, we further extended the variety of nanomaterials for CpG ODN delivery. We tried to utilize uniformed small graphene oxide (sGO) and RCA-based DNA Origami Nanostructures as novel intracellular carriers of CpG ODN. Both materials performed superior to commercial transfection reagents. On the other hand, we also put a lot of efforts to optimize the immunostimulatory activity of CpG ODN-NM conjugates. Attempts toward this goal include modification of physiochemical characteristics of NMs, as well as the method of conjugation. For example, the classical preparation method of AuNP-CpG nanocomposites need thiol modified DNA, which complicates the process and increases the cost. We found that non-thiolated, diblock ODNs containing a CpG motif and a poly-adenine (polyA) tail can readily self-assemble on the surface of AuNPs with controllable and tunable density. Such nanoconjugates are efficiently delivered into RAW264.7 cells and induce immune response. In addition, varying the length of the polyA tail can modulate the immunostimulatory activity of CpG-AuNPs. We also demonstrated the in vivo induction of immune responses in mice. These approaches may provide new potentials for the clinical application of CpG ODNs. These work were published in ***Adv. Mater.***, ***Small***, and ***ACS Appl Mater Interfaces.*** (Ref.1-4).

2 Mechanism and application of anti-bacterial effect of graphene

Our group is one of the earliest to report the antibacterial effect of graphene (Nano ACS, 2010, 4, 4317), which has attracted a broad range of interest. Over 50 publications on this topic have been published in last 3 years. However, a clear molecular mechanism to depict how the interaction between graphene and bacterial cell membrane induced its antibacterial has been lacking. Until recently, we proposed a novel molecular mechanism of the interaction between graphene and bacterial cell membrane. This project is carried out through cooperation with the Prof. Fang Haiping's group and Prof. Zhou Ruhong's group. We show experimentally and theoretically that pristine graphene and graphene oxide nanosheets can induce the degradation of the inner and outer cell membranes of *Escherichia coli*, and reduce their viability. Transmission electron microscopy shows three rough stages, and molecular dynamics simulations reveal the atomic details of the process. Graphene nanosheets can penetrate into and extract large amounts of phospholipids from the cell membranes because of the strong dispersion interactions between graphene and lipid molecules. This destructive extraction offers a novel mechanism for the molecular basis of graphene's cytotoxicity and antibacterial activity. Our finding attracted the attention of many scientific media, including Chemistry World, Before It's News, Graphene Wiki & News. In addition, we are also committed to expand the application of antibacterial ability of grapheme. For example, through collaboration with Prof. Li Jingye's group, we successfully prepared flexible, foldable, and re-usable GO-based antibacterial cotton fabrics as a type of new nano-engineered antibacterial materials, which has a wide range of applications. These work were published in ***Nature Nanotechnol***. ***Adv. Healthc. Mater.*** and ***Sci. Rep.*** (Ref.5-7).

3 Interfaces between cell and nanomaterials

Recently, DNA nanostructures have been more and more widely applied in biophysics, drug delivery, diagnosis and therapy of diseases. These studies have also caused a strong interest in explore the interaction between DNA nanostructures and artificial or life systems. In particular, how to understand and control the physical and chemical properties of DNA nanostructures to achieve best performance, is an important issue in the field. Toward this goal, our group has been engaged in the design, development and optimization of a series of DNA nanostructures, from one-dimensional to three-dimensional, for biological applications. We have studied the interface between DNA structures and inorganic materials, as well as cell interface. Based on these work, we were recently invited to write a review for ***Accounts of Chemical Research*** (Ref. 8). In order to more straightforwardly reveal the interaction between DNA nanostructures and cells, we investigated the endocytosis and subsequent intracellular transport of tetrahedral DNA nanostructures (TDNs) by mammalian cells through single-particle tracking. We found that TDNs were rapidly internalized through a caveolin-dependent pathway. After endocytosis, the TDNs were transported to the lysosomes in a highly ordered, microtubule-dependent manner. To modulate the cellular fate of the TDNs, we functionalized them with nuclear localization signals that directed their escape from the lysosomes and entry into the cellular nuclei. This study improves our understanding of the entry into cells and transport pathways of DNA nanostructures, and the results can be used as a basis for designing DNA- nanostructure-based drug delivery carriers for targeted therapy. These results were published in ***Angew. Chem. Int. Ed.*** (Ref. 9).

Besides, we have also explored certain widely used inorganic NMs for their interaction and interference on physiolog-

ical processes. For example, we identified autophagy as a novel cellular effect of QDs. QDs-induced autophagy greatly enhanced the sensitivity of cells to the toxicity cadmium ion, which explained well the different toxicity between CdTe QDs and CSS QDs. In addition, we have also studied the long-term effects on nutrition and metabolism of nanoparticles including AuNPs. These results were published in ***Adv Healthc Mater.*** and ***Small*** (Ref.10-11).

Reference

1. Li J, Fan C, Pei H, *et al.* Smart drug delivery nanocarriers with self-assembled DNA nanostructures[J]. Adv. Mater., 2016, **25**(7): 4386.
2. Ouyang X Y, Li J, Liu h J, *et al.* Rolling circle amplification-based DNA origami nanostructrures for intracellular delivery of immunostimulatory drugs[J]. Small, 2013, **9**: 3082.
3. Chen N, Wei M, Sun Y H, *et al.* Self-assembly of poly-adenine-tailed CpG oligonucleotide-gold nanoparticle nanoconjugates with immunostimulatory activity[J]. Small, 2014, **10**: 368.
4. Sun J, Chao J, Huang J, *et al.* Uniform small graphene oxide as an efficient cellular nanocarrier for immunostimulatory CpG oligonucleotides[J]. ACS Appl Mater Interfaces, 2014, **6**(10): 7926-32.
5. Tu Y SA, Lv M, Xiu P, *et al.* Destructive extraction of phospholipids from Escherichia coli membranes by graphene nanosheets[J]. Nature Nanotechnol, 2013, **8**: 594.
6. Zhao J M, Deng B, Lv M, *et al.* Graphene oxide-based antibacterial cotton fabrics[J]. Adv. Healthc. Mater., 2013, **2**: 1259.
7. Liu H Z, Lv M, Deng B, *et al.* Laundering durable antibacterial cotton fabrics grafted with pomegranate-shaped polymer wrapped in silver nanoparticle aggregations[J]. Sci. Rep., 2014, **4**: 4920
8. Chen N, Li J, Song H Y, *et al.* Physical and biochemical insights on DNA structures in artificial and living systems[J]. Acc. Chem. Res., 2014, **47**: 1720.
9. Liang L, Li J, Li Q, *et al.* Single-particle tracking and modulation of cell entry pathways of a tetrahedral DNA nanostructure in live cells[J]. Angew. Chem. Int. Ed, 2014, **53**: 7745.
10. Li X M, Chen N, Su Y Y, *et al*. Autophagy-sensitized cytotoxicity of quantum dots in PC12 cells[J]. Adv. Healthc. Mater, 2014, **3**: 354.
11. Chen N, Wang H, Huang Q, *et al.* Long-term effects of nanoparticles on nutrition and metabolism[J]. Small, 2014, **10**: 3603-3611.

同步辐射 X 射线显微技术在纳米生物成像中的应用

物理生物学研究室

纳米颗粒的小尺寸及独特的化学性质使纳米生物效应研究面临诸多挑战。同步辐射 X 射线显微成像技术，具有极高的空间分辨率和良好的元素识别特性，为纳米颗粒和生命系统的相互作用研究提供了全新的技术平台。近年来，我们课题组依托上海光源有利条件，在该领域开展了一系列研究，内容包括：纳米材料的细胞内分布；纳米材料-离子复合物的细胞生物效应；纳米 TiO_2 的体内生物效应。2014 年受邀分别为国际著名杂志《先进材料》和《纳米医学》撰写综述文章，介绍相关领域工作进展[1–2]。

纳米材料的细胞内分布

我们对 CdTe 量子点的亚细胞定位进行了精确成像，发现 CdTe 量子点在细胞内呈现不均一的分布，主要富集在核膜外围区域，为解释镉系量子点的细胞生物学效应提供了关键性证据，相关结果应邀以观点文章(Leading opinion paper)发表于生物材料领域的著名杂志《生物材料》[3]。观察了 TiO_2 纳米颗粒在细胞内的分布，证明该纳米材料主要分布在细胞膜上和细胞质中，细胞核中未见分布[4]。

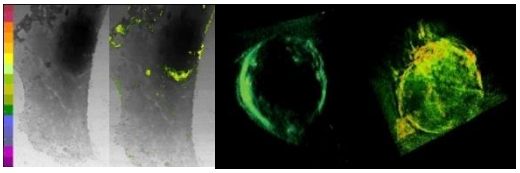

纳米材料的细胞内分布：量子点和纳米 TiO_2

纳米金刚石-离子复合物的细胞生物效应

研究了纳米金刚石-离子复合物和细胞的相互作用，发现纳米金刚石在无血清的培养液中吸附大量钠离子，并载带进入细胞，从而导致相应的细胞效应[5]。进一步地，我们还发现纳米金刚石能吸附并载带铜，镍等多种金属离子进入细胞，显示纳米金刚石是良好的细胞内离子输运载体[6]。

纳米 TiO_2 的体内生物效应

在体内实验中，发现气管滴注后，TiO_2 纳米颗粒主要滞留在小鼠肺中，且清除缓慢。TiO_2 在肺内的滞留导致肺内其他原生元素 K, Ca, Fe, Cu 和 Zn 等的自然分布也发生显著变化，为揭示纳米 TiO_2 毒性机理提供了证据[7]。

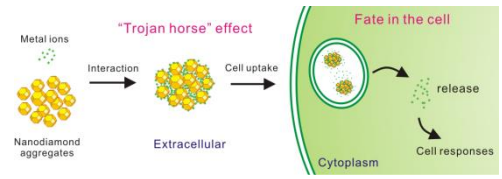

纳米金刚石-离子复合物的细胞生物效应

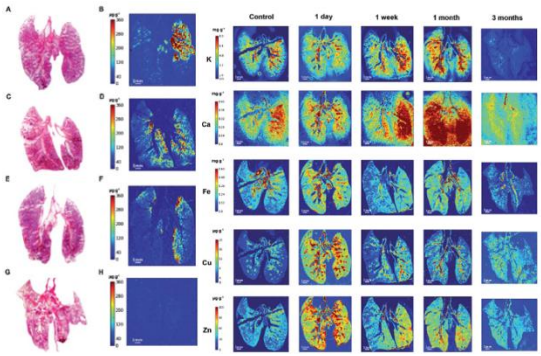

纳米 TiO_2 在小鼠体内的生物效应

参考文献

1. Zhu Y, Earnest T, Huang Q, *et al*. Adv. Mater., 2014, **26**: 7889-7895.
2. Zhu Y, Cai X Q, Li J, *et al*. Nanomed-Nanotechnol, 2014, **10**: 515-524.
3. Chen N, He Y, Su Y Y, *et al*. Biomaterials, 2012, **33**: 1238-1244.
4. Zhang J C, Cai X Q, Zhang Y, *et al*. Huang, Anal Methods-Uk, 2013, **5**: 6611-6616.
5. Zhu Y, Li W, Zhang Y, *et al*. Small, 2012, **8**: 1771-1779.
6. Zhu Y, Yu Z, Shi G S, *et al*. Part Fibre Toxicol, 2015, **12**: 2.
7. Zhang J, Li B, Zhang Y, *et al*. Analyst, 2013, **138**: 6511-6516.

Synchrotron-based X-ray microscocy for nanoscale bioimaging

Division of Physical Biology

There have been increasing interests in studying biological effects of nanomaterials, which are nevertheless faced up with many challenges due to their nanoscale dimensions and unique chemical properties. Synchrotron-based X-ray microscopy, an advanced imaging technology with high spatial resolution and excellent elemental specificity, provides a new platform for studying interactions between nanomaterials and living systems. Due to our outstanding achievements in this field, we have been invited to contribute two review papers in *Advanced Materials* and *Nanomedicine* in 2014[1–2].

Intracellular Distribution of Nanomaterials

By using STXM techniques, we found that quantum dots (QDs) non-uniformly distributed in the cell, mainly concentrated in the peripheral region of the nucleus membrane, which provides crucial evidence understanding the cell effects of QDs[3]. In another study, high-resolution TXM images showed that TiO_2 nanoparticles (NPs) were mainly distributed in the cell membrane surface[4].

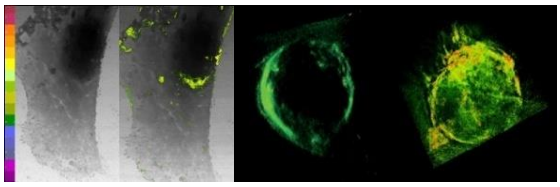

Intracellular distribution of nanomaterials

Cellular effects of nanodiamond-ion complexes

We found that large amount of sodium ions were adsorbed and delivered into the cell interior by nanodimonds (NDs) in serum-free medium, which led to obvious cell response[5]. In the follow-up work, we demonstrated other metal ions such as Cu^{2+}, Ni^{2+} could be adsorbed and delivered into the cell interior by NDs, illustrating the potential of NDs as vehicles for metal ion delivery[6].

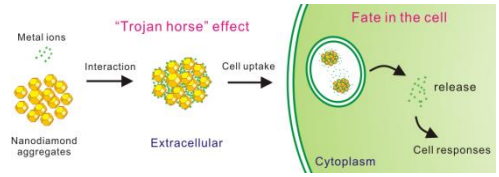

Cellular effects of nanodiamond-ion complexes

Bioeffects of nanoscale titanium dioxide in mice

We examined the *in vivo* distribution and pulmonary toxicity of TiO_2 NPs in mice after intratracheal instillation. XRF images showed that TiO_2 NPs were mainly retained in lung and slowly cleared. Moreover, TiO_2 NPs interfered with the natural distribution of K, Ca, Fe, Cu and Zn in lung, and the change in the level of these elements was closely related to the pulmonary toxicity resulted from TiO_2 NPs[7].

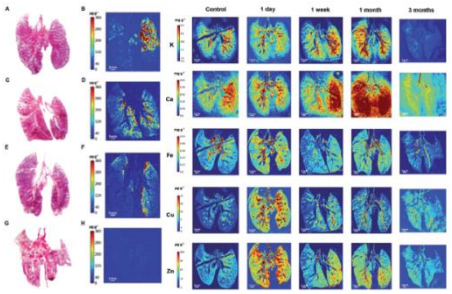

Bioeffects of nanoscale titanium dioxide in mice

Reference

1. Zhu Y, Earnest T, Huang Q, *et al*. Adv. Mater., 2014, **26**: 7889-7895.
2. Zhu Y, Cai X Q, Li J, *et al*. Nanomed-Nanotechnol, 2014, **10**: 515-524.
3. Chen N, He Y, Su Y Y, *et al*. Biomaterials, 2012, **33**: 1238-1244.
4. Zhang J C, Cai X Q, Zhang Y, *et al*. Huang, Anal Methods-Uk, 2013, **5**: 6611-6616.
5. Zhu Y, Li W, Zhang Y, *et al*. Small, 2012, **8**: 1771-1779.
6. Zhu Y, Yu Z, Shi G S, *et al*. Part Fibre Toxicol, 2015, **12**: 2.
7. Zhang J, Li B, Zhang Y, *et al*. Analyst, 2013, **138**: 6511-6516.

生物传感平台的建立及生物检测应用

物理生物学研究室

课题组依托上海光源和物理生物学研究室，围绕中国科学院“创新 2020”和研究所“一三五”规划，与其他相关课题组进行紧密合作，主要从事纳米生物传感界面、重大疾病的早期诊断、微流控芯片、DNA 纳米技术与分子机器等方面的研究，旨在发展可用于疾病诊断、食品安全、环境监测等重大国家需求领域的快速、便携、高灵敏、高特异的生物传感器与生物芯片。

生物传感界面的精确调控

生物分子探针在传感界面上的组装过程很大程度上决定了生物传感检测的性能。如何调控生物分子在界面上的密度和取向，减少生物分子与界面的非特异性吸附并避免界面分子间的侧向作用力则已成为该领域的挑战性问题之一。针对这一问题，课题组对 DNA 分子在宏观和纳米界面上的组装过程进行了系统研究。由于 DNA 是一种软物质，常规使用的一维单链探针容易产生链间纠缠而聚集。通过引入 DNA 纳米技术发展出刚性的三维结构 DNA 探针，实现了 DNA 探针之间距离的精确调控。这为构筑有序的生物分子界面提供了新的途径，提高了界面生物识别能力，进而显著提升了生物传感器的检测能力。在这一新型生物传感平台上深入研究了界面识别和电子传递等物理化学机制，并实现了核酸、抗原和小分子的超高灵敏检测[1–7]。

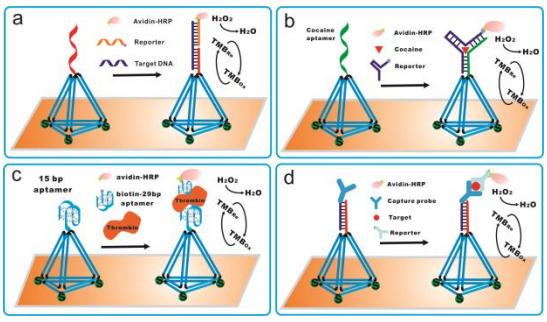

图 1 三维 DNA 纳米探针在生物检测中的应用

智能微型化电化学生物传感器

多功能集成、用户友好的便携式现场检测设备在低成本医疗和应对突发性传染病中发挥着重要作用。研究组发展了一种基于“气泡”介导的电化学生物传感器，解决了一步反应完成免疫分析的关键技术问题，并实现了多种重要疾病标志物的快速灵敏检测，有望为便携式现场生化检测提供新的手段[8]。

电化学生物传感器具有廉价、能耗低、响应快和易于微型化的优点，并可实现定量检测，非常适合于现场诊断(Point-of-care test, POCT)领域。基于电化学技术的血糖仪即是一个成功的范例。然而，核酸和蛋白质分子的检测方法往往涉及孵育、清洗等多个步骤，难以一步完成整个分析过程。针对这一挑战性问题，研究人员设计了一种便携式的智能微型化电化学生物传感器(Intelligent microscale electrochemical device, iMED)，利用气泡介导的原理可将反应所需的多种溶液自动、可控地输运到电极表面。研究表明，这种 iMED 传感器可在分钟量级对前列腺癌和禽流感(H1N1)相关的多种疾病标志物进行快速、灵敏的检测。这一技术解决了电化学生物传感器走向实际应用的一个瓶颈问题，为重大疾病快速筛查提供了新的契机。

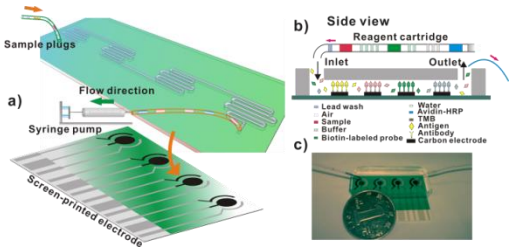

图 2 智能微型化电化学生物传感器实现“一步”检测

潜指纹表面等离子体成像及毒品检测

指纹，由于其终身不变性、唯一性和方便性，已作为生物特征识别的重要手段而广泛应用于日常生活中。与正指纹相对应的潜指纹，是指手指与其他基底无意识接触后，手指中的汗液，油脂等留在基底表面，形成的肉眼不可见指纹。对潜指纹成像及其化学成分进行分析检测，在身份鉴定的同时，还可发掘出更多有价值的生物学和医学信息。研究组发展了基于表面等离子体成像技术的新型潜指纹识别技术。研究发现金纳米粒子可以吸附在潜指

纹的油脂上，并发出很强的局域表面等离子体共振光散射(LSPRS)信号，利用暗场显微镜可以对潜指纹实现清晰成像。进一步，通过在金纳米粒子表面修饰可卡因核酸适配体，赋予其显影及分子识别双重功能后，该纳米光子学方法就可以对指纹中的可卡因进行灵敏检测。正常人指纹散射绿光，载带可卡因的指纹散射红光，该方法对指纹中的可卡应的检测限可达到 50 ng。这种方法可以解决吸毒人群中血清及尿液中毒品检测时效性差的问题，同时将毒品信息和个人身份信息（指纹）结合起来，有望在刑侦中用于吸毒、携毒人员的筛查[9]。

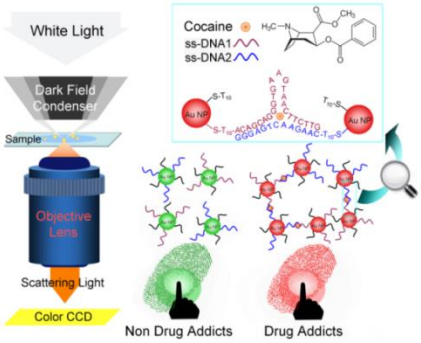

图 3　潜指纹表面等离子体成像及毒品检测

纳米颗粒表面的生物分子精确自组装

DNA-纳米颗粒的复合探针是一种常用的纳米生物材料，在生物检测、治疗乃至纳米光子学中具有广泛的应用。研究人员发展出一种制备高性能DNA-银纳米粒子复合探针的新方法。这种探针不仅避免了使用修饰 DNA 分子，而且能够精确调控银纳米粒子表面 DNA 分子的密度、取向和构型，显著提高了该探针的识别能力。制备 DNA-银纳米颗粒复合探针的经典方法是通过巯基修饰的 DNA 分子在纳米银颗粒表面的自组装得到的。这种方法中使用了化学修饰的 DNA 分子，成本较高且操作复杂。尽管多年来研究者已对这一体系进行了系统的优化，但是如何精确控制 DNA 分子在金纳米粒子表面的密度、取向和构型仍然是一个挑战性问题。研究人员直接采用天然的 DNA 序列设计成双嵌段寡核苷酸来解决这些问题。研究首先发现了连续的胞嘧啶碱基(polyC)与银纳米粒子之间存在很强的吸附力，因而将双嵌段序列设计成包含两部分，探针部分用于进行 DNA 识别，polyC 部分则将 DNA 固定在银纳米粒子上[10−11]。

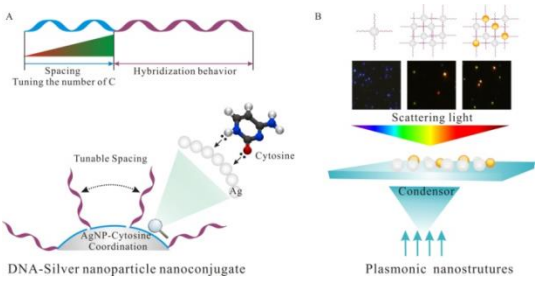

图 4　纳米银颗粒表面上的生物分子组装调控

研究表明，这一新方法不仅可以有效制备稳定的复合探针，而且可以通过改变 C 碱基的长度来调控纳米金表面上 DNA 密度，在纳米尺度上精确控制 DNA 分子之间的距离，从而可以避免 DNA 分子之间的相互作用，实现探针的高识别活性。通过这种方法制备的DNA-银纳米粒子复合探针具有很高的稳定性和识别活性，可以在短时间内实现对 DNA 分子的高灵敏快速检测。 由于 DNA-银纳米粒子复合探针已在纳米生物和医学研究中具有了广泛的应用，可以预期这种新型制备方法将为这些应用提供新的契机

参考文献

1. Abi A, Lin M H, Pei H, *et al*. Acs Appl Mater Inter, 2014, **6**: 8928.
2. Chen X Q, Zhou G B, Song P, *et al*. Anal Chem, 2014, **86**, 7337.
3. Ge Z L, Lin M H, Wang P, *et al*. Anal Chem, 2014, **86**: 2124.
4. Lin M H, Wen Y L, Li L Y, *et al*. Anal Chem, 2014, **86**: 2285.
5. Pei H, Zuo X L, Pan D. *et al*. Npg Asia Mater, 2013, **5**: e51.
6. Pei H, Zuo X L, Zhu D, *et al*. Accounts Chem Res 2014, **47**: 550.
7. Zhou G B, Lin M H, Song P, *et al*. Anal Chem, 2014, **86**: 7843.
8. Yang F, Zuo X L, Li Z H, *et al*. Adv Mater 2014, **26**: 4671.
9. Li K, Qin W W, Li F, *et al*. Angew Chem Int Edit, 2013: **52**, 11542.
10. Lin M H, Pei H, Yang F, *et al*. Adv Mater, 2013, **25**: 3490.
11. Zhu D, Chao J, Pei H, *et al*. Acs Appl Mater Inter, 2015, **7**: 11047.

Progresses in developing biosensor platform and the biodetection applications

Division of Physical Biology

Relying on the Shanghai Synchrotron Radiation Facility and Division of Physical Biology, our research group is mainly engaged in the research of nano-biosensing interface, early diagnostics of diseases, microfluidic biochip, DNA nanotechnology and molecular machine. Our research is aimed at developing next generation sensors to meet China's requirements for disease diagnostics, environmental monitoring and food safety. The next generation biosensors are meant to have high sensitivity and selectivity, and to be cost-effective with short detection time and capable of further devising into portable chips.

Precise regulation of biosensing interface

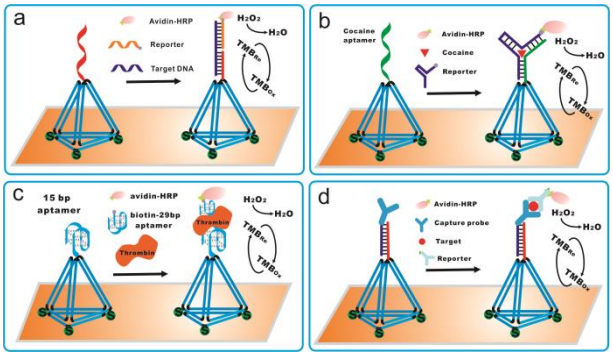

Fig.1 Three-dimensional DNA nanoprobes for biodetection applications

Understanding the physical structure of a DNA probe immobilized on a surface is critical in applications using DNA as a molecular recognition element. The properties of the DNA molecular recognition layer (such as selectivity, sensitivity and reproducibility) highly depend on the structure of the self-assembled DNA film. Constructing a reproducible DNA recognition layer with these properties is a critical challenge owing to unexpected surface adsorptions, disordered conformations, inconsistencies in grafting density and the flexibility of probe molecules. Tetrahedral DNA nanostructures with thiol modifications can be self-assembled at the gold surface with high reproducibility. Since DNA tetrahedra are highly rigid and well-defined structures with atomic precision and versatile functionality, they provide scaffolds for anchoring of a variety of biomolecular probes (DNA, aptamers, peptides, and proteins) for biosensing. Significantly, this DNA nanostructure-based biosensing platform greatly increases target accessibility and improves the sensitivity for various types of molecular targets (DNA, RNA, proteins, and small molecules) by several orders of magnitude[1–7].

Intelligent Microscale Electrochemical Device

The requirements for integrated, user-friendly point-of-care test (POCT) devices for the rapid and sensitive detection of biomarkers in resource-limited settings, e.g., the detection of emerging diseases are very demanding. Our group reported the design of a low-cost, portable intelligent microscale electrochemical device (iMED) that can automatically deliver multiple reagents in a controlled manner to the electrochemical sensor surface. We demonstrated that this fully integrated iMED sensor is a rapid and sensitive detector of multiple biomarkers for infectious diseases (H1N1) and cancers and performs single-step assays within minutes[8].

Electrochemical biosensors possess many attractive features that are required for POCTs (e.g., low costs, rapid response times, and ease of miniaturisation). Moreover, the quantitative nature of electrochemistry makes these sensors ideal candidates for quantitative POCTs where widely used colorimetric assays are not feasible. Indeed, glucose meters that employ electrochemical detectors and inexpensive screen-printed electrodes (SPEs) have proven to be a legendary marketing success. However, unlike the detection of glucose, which involves only single-step enzymatic catalysis, the detection of nucleic acids and proteins is usually a multi-step and complex process. Although microfl uidic devices provide a potentially feasible solution, the development of a one-step assay with a fully integrated and automated device without a complex microchannel design and extensive user intervention remains a challenge. Our iMED employs a low-cost “plug-in-cartridge” technology, which relies on air bubbles to separate multiple plugs with reagents to deliver the reagents to the SPE surface for electrochemical biosensing.

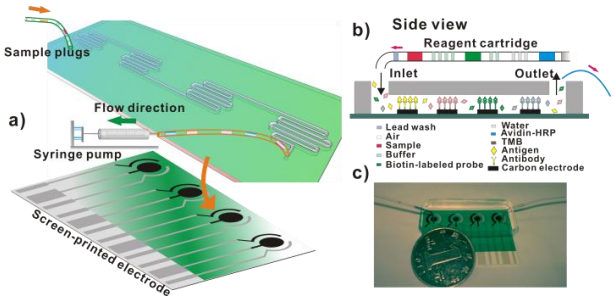

Fig.2 Intelligent microscale electrochemical device for the “single step” detection

Nanoplasmonic Imaging of Latent Fingerprints and Identification of Cocaine

Fingerprints are impressions of the friction ridges of all or any part of a human finger. When a finger touches a surface, eccrine sweat, together with oily substances picked up by the finger, forms an impression of the fingers ridge pattern. Such an impression is known as a latent fingerprint (LFP) for its invisibility to the naked eye. The uniqueness and invariableness of an individual’s fingerprint have long been recognized as important physical personal identification, and is hence widely used in individual credentials, access control, and forensic investigation. On the other hand, researchers have realized that fingerprints carry more biological information about individuals than just their identity. We have demonstrated a nanoplas-

monic method to visualize LFPs by exploiting the localized surface plasmon

resonance (LSPR) property of aptamer-bound AuNPs. The level 2 and level 3 characteristic details of sebaceous LFPs could be clearly observed by dark-field microscopy (DFM). Moreover, the cocaine-induced aggregation of AuNPs results in true green-to-red color change of the scattering in the darkfield image, thus providing a quasi-quantative method to identify cocaine loadings in LFPs[9].

Fig.3 Nanoplasmonic imaging of latent fingerprints and identfication of cocaine

Precise regulation biomolacular assembly on nanoparticles

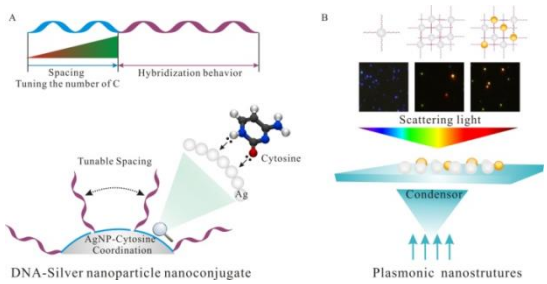

Fig.4 Cytosine-Ag coordination based DNA regulation on silver nanoparticles

DNA-decorated nanoparticles have become popular tools in a variety of areas including bioelectronics, biosensors, bioimaging and drug delivery. Whereas there have been several methods to prepare DNA-AgNP conjugates with sophisticated protocols, e.g., the use of DNA with special modifications of disulfide, thioctic acid or cyclic disulfide, it remains a hurdle to facilely and controllably assemble DNA on AgNPs. We devised a highly programmable strategy to synthesize DNA-AgNP conjugates by exploiting the specific silver-cytosine (Ag-C) coordination[10-11].

When the thiol-based method is used to assemble DNA on AgNPs, the resulting thiolated DNA-AgNP nanoconjugates exhibited limited stability and poor bioactivity, which hampered the applications of AgNPs in plasmonics. We have demonstrated a silver-cytosine coordination-mediated self-assembly of DNA-AgNP conjugates with fully retained hybridization behavior of DNA, faster hybridization kinetics, controlled DNA density and enhanced stability. The DNA-Ag nanoconjugates exhibit excellent plasmonic property with larger plasmonic peak shift (3 times larger than that of DNA-AuNP nanoconjugates). The Au-Ag hybrid nanostructures exhibit interesting anisotropic plasmonic scattering.

Reference

1. Abi A, Lin M H, Pei H, *et al*. Acs Appl Mater Inter, 2014, **6**: 8928.
2. Chen X Q, Zhou G B, Song P, *et al.* Anal Chem, 2014, **86**, 7337.
3. Ge Z L, Lin M H, Wang P, *et al.* Anal Chem, 2014, **86**: 2124.
4. Lin M H, Wen Y L, Li L Y, *et al.* Anal Chem, 2014, **86**: 2285.
5. Pei H, Zuo X L, Pan D. *et al.* Npg Asia Mater, 2013, **5**: e51.
6. Pei H, Zuo X L, Zhu D, *et al.* Accounts Chem Res, 2014, **47**: 550.
7. Zhou G B, Lin M H, Song P, *et al.* Anal Chem, 2014, **86**: 7843.
8. Yang F, Zuo X L, Li Z H, *et al.* Adv Mater 2014, **26**: 4671.
9. Li K, Qin W W, Li F, *et al.* Angew Chem Int Edit, 2013: **52**, 11542.
10. Lin M H, Pei H, Yang F, *et al.* Adv Mater, 2013, **25**: 3490.
11. Zhu D, Chao J, Pei H, *et al*. Acs Appl Mater Inter, 2015, **7**: 11047.

附录 1

2013-2014 年上海应用物理所博士、硕士学位授予一览表

PhD & MD Programs Completed at SINAP IN 2013-2014

2013

No.	学位	学生	专业	导师	论文题目	研究方向
1	博士	任秀平	粒子物理与原子核物理	胡钧	纳米受限空间内醇水溶液去浸润现象的理论研究	纳米尺度的去浸润
2	博士	刘中华	核技术及应用	李勇平	图像分类算法及同步辐射散射图像处理技术应用研究	计算机图像处理
3	博士	张俊强	核技术及应用	赵明华	上海光源直线加速器次谐波聚束器的幅相控制	加速器低电平技术
4	博士	姚剑	核技术及应用	刘卫	上海市大气细颗粒物的预警和能见度的分析研究	大气科学
5	博士	李海霞	无机化学	王文锋	加替沙星和二氟沙星光化学性质及光敏损伤研究	快速反应动力学
6	博士	周铖龙	粒子物理与原子核物理	马余刚	中低能重离子碰撞中热力学及输运性质的研究	相对论重离子碰撞
7	博士	曾建荣	粒子物理与原子核物理	李燕	海盐颗粒物理化特征及其对上海市大气环境的影响	核科学技术在环境科学中的应用
8	博士	王广华	粒子物理与原子核物理	刘卫	上海市大气含碳颗粒物的研究	大气科学
9	博士	杨朝霞	核技术及应用	李德明	质子治疗装置治疗头束流调制与传输的模拟计算研究	质子治疗装置
10	博士	马静远	核技术及应用	黄宇营	室温离子液体的 X 射线吸收精细结构谱学（XAFS）方法研究	同步辐射光束线技术及应用
11	博士	刘海岗	核技术及应用	邰仁忠	软 X 射线相干衍射成像研究	相干衍射成像
12	博士	周欢	无机化学	何建华	人源 GDP-岩藻糖合成酶结构解析与火球菌 8-氧鸟嘌呤 DNA 糖苷酶功能研究	蛋白质结构与功能
13	博士	姜伯玮	无机化学	樊春海	功能化磁性纳米材料的设计合成及其生物学应用	纳米生物传感
14	博士	赵杰	粒子物理与原子核物理	马余刚	相对论重离子碰撞(RHIC)实验中双轻子的产生	高能核物理
15	博士	张萌	粒子物理与原子核物理	方海平	氮气纳米气泡成核浓度及纳米颗粒与生物分子的相互作用研究	分子动力学模拟
16	博士	张金金	粒子物理与原子核物理	胡钧	非接触调频模式 AFM 的研制及其对生物样品的高分辨成像应用	非接触调频模式原子力显微镜的研制及其对生物样品的高分辨成像应用

17	博士	张琛	粒子物理与原子核物理	胡钧	基于原子力显微镜分子操纵技术的机械力诱导的单分子 DNA 突变研究	单分子生物物理
18	博士	王琴	粒子物理与原子核物理	方海平	固体表面的润湿性对表面单层水的蒸发性质的影响	纳米尺度水的理论研究
19	博士	李永江	粒子物理与原子核物理	徐望	超高精度 d(γ,n)p 强子间弱作用实验的前期研究	粒子物理与原子核物理
20	博士	闻炳海	粒子物理与原子核物理	方海平	用晶格 Boltzmann 方法研究界面动力	计算物理学
21	博士	邢哲	无机化学	吴国忠	超高分子量聚乙烯纤维辐射接枝改性及性能研究	高分子材料辐射改性
22	博士	刘亚芬	核能科学与工程	蔡翔舟	钍基熔盐堆增殖物理特性的研究	反应堆物理
23	博士	韩立欣	粒子物理与原子核物理	马余刚	相对论重离子碰撞中初始涨落对集体流影响的研究	相对论重粒子碰撞
24	博士	陶城	粒子物理与原子核物理	马余刚	应用量子分子动力学研究丰中子原子核系统的共振模式	中低能重离子碰撞
25	博士	朱逾卉	粒子物理与原子核物理	马余刚	相对论重离子碰撞(RHIC)实验下超氚核的产生及寿命测量	相对论重离子对撞物理
26	博士	梅龙伟	粒子物理与原子核物理	蔡翔舟	熔盐堆中 FLiBe 热中子散射效应研究	反应堆物理
27	博士	刘艳成	无机化学	王文锋	环丙沙星、帕珠沙星对生物分子光敏损伤的动力学研究	氟喹诺酮类抗菌素光敏损伤生物分子的动力学研究
28	博士	代彬	无机化学	胡钧	固液界面上淀粉样多肽的多层直立自组装及纳米纤维机械性能研究	多肽自组装
29	博士	张一	无机化学	黄庆	无机纳米材料在细胞内的抗凋亡机制和模拟酶效应	纳米生物学
30	博士	葛志磊	无机化学	樊春海	基于 DNA 纳米技术的生物传感研究和应用	DNA 纳米和生物传感
31	博士	李晓明	无机化学	黄庆	镉系量子点引发的细胞学毒性及其机制研究	纳米材料的生物学效应
32	博士	魏敏	无机化学	黄庆	基于自组装的 CpG ODN-金纳米粒子多价免疫激活纳米制剂的生物学效应	纳米生物学效应
33	博士	毛秀海	无机化学	樊春海	基于 DNA 的功能化纳米材料的设计及其性质研究	DNA 纳米技术
34	博士	刘敏	核技术及应用	周兴泰	熔盐反应堆结构材料 Hastelloy N 合金的腐蚀及辐照性能研究	核分析科学与技术
35	博士	申月	核技术及应用	胡钧	单层还原态氧化石墨烯的充放电性质及电荷迁移行为研究	纳米科术
36	博士	盛尹祥子	核技术及应用	夏晓彬	基于辐射防护目的的中国女性参考人体素模型的开发和应用	辐射剂量学

37	博士	张兴民	核技术及应用	周兴泰	纳米材料的同步辐射 X 射线衍射表征	纳米材料的同步辐射表征技术
38	博士	李小芸	核技术及应用	王劼	X 射线散射实验方法及在高分子与纤维微观结构的应用研究	同步辐射小角散射
39	博士	冯超	核技术及应用	赵振堂	高增益自由电子激光新运行机制的理论与实验研究	自由电子激光
40	博士	林作康	核技术及应用	戴志敏	电子加速器驱动钍基次临界系统及实验中子靶装置的研究	先进反应堆
41	博士	王娟	核技术及应用	余笑寒	直接硼氢化钠燃料电池中 Co/N/C 阴极催化剂催化机理的同步辐射研究	同步辐射束线技术及应用
42	博士	王宝鹏	核技术及应用	冷用斌	腔式 BPM 信号处理技术研究	高速数据采集与信号处理
43	博士	张彤	核技术及应用	王东	全相干自由电子激光若干物理问题研究	自由电子激光
44	博士	滑文强	核技术及应用	王劼	相干 X 射线传输特性研究	相干 X 射线传输特性研究
45	硕士	邱敬科	核技术及应用	余笑寒	同步辐射微束 X 射线荧光 CT 三维元素成像方法研究	同步辐射 X 射线 CT 成像
46	硕士	郭策	信号与信息处理	王东	SDUV-FEL 光学系统控制改进	加速器控制
47	硕士	秦强	高分子化学与物理	陆晓峰	PVDF 均相共辐照接枝 NVP 的研究及滤膜的制备、表征	高分子辐射改性及滤膜制备
48	硕士	杨敏	无机化学	何建华	Hsp90N-抑制剂复合物晶体结构解析及火球菌 RecJ 蛋白初步晶体学研究	蛋白质晶体生长
49	硕士	沈建磊	无机化学	李迪	DNA 调控复杂金属纳米结构的合成及其 SERS 效应研究	功能纳米材料合成
50	硕士	刘西艳	高分子化学与物理	王敏	偕胺肟基材料对铀酰离子的吸附性能研究	高分子材料吸附行为
51	硕士	王海伟	核能科学与工程	蔡翔舟	熔盐堆钍铀增殖循环研究	熔盐堆钍铀转换循环研究
52	硕士	陈立宏	信号与信息处理	李勇平	基于 MURA 准直器核辐射成像系统研究	核辐射成像系统
53	硕士	李开湖	信号与信息处理	李德明	超低电流纹波检测及纹波抑制方法研究	电流纹波检测及抑制
54	硕士	王佳	粒子物理与原子核物理	沈文庆	1.5GeV/A 以下的 Au+Au 碰撞中初始涨落对集体流的影响	中能重离子碰撞
55	硕士	王晓攀	核能科学与工程	陈金根	0.1-20 MeV n+232Th 核反应数据的计算和分析	核数据评价
56	硕士	郭春磊	光学工程	吴衍青	相干光束线的空间相干性分析及优化设计	同步辐射光学与光学器件

57	硕士	刘永芳	信号与信息处理	谷鸣	高功率调制器脉冲幅度精密监测和稳定度控制	脉冲信号检测与处理
58	硕士	李锋	信号与信息处理	陈志豪	高功率固态脉冲调制器技术研究	脉冲信号检测与处理
59	硕士	叶泽文	高分子化学与物理	吴国忠	辐射固化 PCS 纤维制备陶瓷纤维及其性能研究	高分子材料的改性与加工
60	硕士	何亚星	核技术及应用	吴国忠	负载于微/纳米材料表面的咪唑类离子液体的相行为和结构研究	离子液体
61	硕士	孙旭东	信号与信息处理	冷用斌	基于统计学习的束流诊断设备建模与加速器数据异常检测	软件无线电与数据挖掘
62	硕士	余盛辉	光学工程	薛松	弧矢聚焦双晶单色器晶面扭曲问题研究	精密机械与精密仪器
63	硕士	刘畅	信号与信息处理	冷用斌	基于 Cerenkov 原理的光纤束损探测系统关键技术的研究	分布式数据采集系统
64	硕士	邹欣	核能科学与工程	戴志敏	高温熔盐试验回路电磁感应加热的数值模拟	反应堆热工水力
65	硕士	刘邃庆	核技术及应用	刘卫	活性炭对氪和氙的吸附特性研究	活性炭对氪和氙的吸附特性研究
66	硕士	孟祥雨	光学工程	王勇	同步辐射光束线中部分相干光的传播研究	同步辐射光学
67	硕士	李国强	信号与信息处理	余笑寒	上海光源 BL15U 线站光束位置的反馈控制	信号与信息处理，自动控制
68	硕士	刘立兴	核技术及应用	夏晓彬	先进同步辐射装置辐射场的实验研究	辐射防护
69	硕士	胡雪	信号与信息处理	赵明华	行波电子直线加速器自动频率控制（AFC）系统的研制	核技术及应用
70	硕士	程甲一	光学工程	邰仁忠	纳米 CT 样品漂移在线自动校正及其等角度扫描初步研究	同步辐射光学

2014

No.	学位	学生	专业	导师	论文题目	研究方向
1	博士	周雪梅	核技术及应用	刘桂民	钍基熔盐堆中子能谱测量方法的研究	反应堆测量技术
2	博士	盛楠	粒子物理与原子核物理	方海平	有限时间尺度内分子指向相关的不对称自由扩散	纳米科学
3	博士	高星	核技术及应用	黄宇营	上海光源 BL14W1 线站高分辨 XAFS 方法的实现及其应用研究	同步辐射束线技术及应用
4	博士	赵彬	核技术及应用	樊春海	多功能纳米生物探针的制备及其在生物分析中的应用	生物传感器与生物芯片

5	博士	贾彦彦	核技术及应用	徐洪杰	碲在镍中的扩散行为及晶间脆化机理的研究	熔盐堆结构材料
6	博士	胡正	核技术及应用	黎忠	上海光源光束线运行数据存档系统的研究及应用	计算机网络及数据库
7	博士	张继超	核技术及应用	余笑寒	微束X射线荧光成像方法及其在纳米材料生物学效应研究中的应用	同步辐射束线技术及应用
8	博士	赵国璧	核技术及应用	冷用斌	纽扣电极型束流探头信号检测、传输技术研究	核技术及应用
9	博士	叶琳琳	核技术及应用	肖体乔	中药材显微特征结构的原位三维定量研究	X射线成像对中药材应用研究
10	博士	徐加强	核技术及应用	夏晓彬	上海光源光束线站的屏蔽设计研究	核技术及应用
11	博士	蔡军	核技术及应用	夏晓彬	熔盐堆反应性引入事件初步分析	反应堆核与辐射安全
12	博士	叶绍强	粒子物理与原子核物理	沈文庆	利用同位旋相关的BUU模型研究重离子核反应中的动力学偶极模式	重离子碰撞
13	博士	戚俊成	核技术及应用	肖体乔	同步辐射X射线光栅成像及其在相干性测量中的应用研究	X射线光栅成像
14	博士	蔡晓鹭	粒子物理与原子核物理	徐望	奇异核（12, 14Be、8B）核物质密度分布的提取及其应用	原子核物理
15	博士	龙时磊	粒子物理与原子核物理	李燕	上海地区灰霾过程中的主要物理和化学问题研究	同步辐射技术和核技术在环境科学中的应用
16	博士	王松	粒子物理与原子核物理	朱志远	石墨烯缺陷结构与氟及乙炔等小分子相互作用的理论研究	放射性核束物理与重离子物理
17	博士	巩文斌	核技术及应用	朱志远	碳/金属复合纳米结构性质调控及其能量转化的理论研究	核分析科学与技术
18	博士	王廷栋	粒子物理与原子核物理	怀平	半导体量子线中载流子多体相互作用及其光谱学效应	半导体光谱学
19	博士	陈之初	核技术及应用	冷用斌	储存环全局数据关联分析的研究	束流诊断
20	博士	陈文豪	核技术及应用	肖体乔	X射线局部显微CT伪全局算法及其应用研究	局部CT算法及应用
21	博士	李凡	无机化学	樊春海	基于无机纳米材料和DNA纳米结构的研究及应用	纳米材料的研究及其应用
22	博士	李吉豪	无机化学	李景烨	还原自组装法制备功能化石墨烯材料及其性能研究	高分子辐射化学
23	博士	李荣	无机化学	王文锋	磺化PP无纺布血液相容性与吸附低密度脂蛋白性能研究	医用高分子材料
24	博士	李昆	无机化学	樊春海	纳米等离子体激元结构的构建及其在生物检测和纳米催化中的应用	纳米光子学

25	博士	李海浪	无机化学	吴国忠	壳聚糖衍生物的制备及其在药物载体中的应用研究	高分子材料药物载体
26	博士	冯尚蕾	核技术及应用	周兴泰	核石墨热解炭涂层的辐照损伤及熔盐浸渗特性的研究	核能碳基材料的研究
27	博士	谷端	核技术及应用	赵明华	基于束流的准直技术研究	基于束流的准直技术研究
28	博士	申利国	无机化学	陆晓峰	聚醚砜（PES）膜改性及抗污染性能研究	膜科学与技术
29	博士	鲍洪亮	无机化学	黄宇营	双金属纳米粒子 X 射线吸收精细结构谱研究	同步辐射光学与技术
30	博士	程进辉	核技术及应用	黎忠	传蓄热熔盐的热物性研究	反应堆技术及应用
31	博士	梁乐	无机化学	黄庆	功能 DNA 纳米结构在生物成像中的应用	纳米材料研究及其应用
32	博士	林建波	核技术及应用	余笑寒	Hastelloy N 合金的离子辐照损伤及辐照后熔盐腐蚀机理研究	熔盐堆结构材料
33	博士	刘文冠	核技术及应用	徐洪杰	基于第一性原理的镍基合金晶界脆化机理的理论研究	合金材料的模拟计算
34	博士	张欢	无机化学	黄庆	纳米材料尺寸依赖的生物学效应及应用研究	物理生物学
35	博士	贾思思	无机化学	樊春海	DNA 折纸术模板构建金属纳米图案及其表面等离子体性质的研究	生物传感器
36	博士	刘汉洲	无机化学	李景烨	辐射法制备含配位基团功能材料及其与重金属离子相互作用研究	高分子辐射化学
37	博士	张宏陆	无机化学	樊春海	DNA 自组装技术及其在基因分型中的应用	物理生物学
38	博士	王东方	无机化学	宋世平	基于功能化纳米材料的生物传感器设计及在生物医学中的应用	生物传感器
39	博士	程懋松	核能科学与工程	戴志敏	钍基熔盐快堆多物理耦合研究	熔盐堆多物理耦合
40	博士	贾丽娜	无机化学	张岚	基于点击化学的分子影像探针制备研究	放射性药物与分子影像探针
41	博士	王光磊	粒子物理与原子核物理	王东	自由电子激光噪声和运行新机制的研究	自由电子激光和加速器物理
42	硕士	周彬	粒子物理与原子核物理	朱志远	螺旋型碳纳米管在碳离子辐照下的结构损伤模拟研究	碳纳米材料的离子辐照模拟计算
43	硕士	黄灿	粒子物理与原子核物理	朱智勇	辐照法制备太赫兹波发射晶体的机理研究	太赫兹发射晶体的制备
44	硕士	张永兴	光学工程	谢红兰	闪烁体厚度对 X 射线成像探测器成像质量影响的研究	X 射线成像探测器

45	硕士	钟逸	电磁场与微波技术	周巧根	霍尔探头低温标定装置的热分析研究	电磁场与微波技术
46	硕士	江勇	电磁场与微波技术	许皆平	制冷机直接冷却式小型超导磁体测试装置研制及实验	低温与超导技术应用
47	硕士	崔金星	信号与信息处理	郑丽芳	基于 DSP 的运动控制器的研究与实现	光束线站控制
48	硕士	杨静怡	信号与信息处理	怀平	C/C 复合材料离子束辐照的微观结构表征	碳/碳复合材料的离子束辐照效应
49	硕士	杜龙	核技术及应用	王宏伟	基于6Li 中子探测器的蒙特卡洛模拟及实验测量	探测器模拟、实验测试
50	硕士	宋洋	生物物理学	胡钧	固液界面纳米气泡与原子力显微镜探针的相互作用研究	固液界面纳米气泡与原子力显微镜探针的相互作用研究
51	硕士	余良波	核技术及应用	王劼	黄麻纤维素纳米晶的制备及 SR-SAXS/WAXS 表征研究	同步辐射小角 X 射线散射及应用
52	硕士	童金	信号与信息处理	谷鸣	基于 FPGA 和 DDS 的质子同步加速器共振慢引出信号源研制	嵌入式系统设计与信号处理
53	硕士	王亚星	核技术及应用	吴国忠	离子液体在二氧化硅纳米受限空间内的微观结构与相行为研究	离子液体
54	硕士	刘占军	信号与信息处理	龚培荣	用于 XBPM 的嵌入式数据采集分析系统	数据采集分析
55	硕士	迟洪影	高分子化学与物理	王敏	胺基材料吸附脱附铀酰离子性能研究	高分子化学
56	硕士	潘玲	高分子化学与物理	陆晓峰	聚合物辅助超滤技术处理模拟低放射性废水中的铈和锶	放射化学与辐射化学
57	硕士	陈亚星	生物物理学	何建华	火球菌 RecJ-like 核酸酶结构与功能及以氙为重原子解析天花粉蛋白结构的研究	蛋白质结构与功能
58	硕士	李达	粒子物理与原子核物理	赵振堂	光阴极微波电子枪研究	低发射度光阴极微波电子枪理论与实验
59	硕士	戴悦来	核技术及应用	戴志敏	PRACS 涡流二极管设计研究	反应堆热工水力
60	硕士	邵士靖	粒子物理与原子核物理	方海平	极化表面有序水的结构、能量和氢键弛豫时间	纳米和分子尺度的水分子结构和功能研究
61	硕士	李健	核能科学与工程	戴志敏	2MW 熔盐实验堆的系统模拟及其跟随负载的瞬态分析	反应堆物理
62	硕士	李凌	核技术及应用	周兴泰	Ti3SiC2、Ti3AlC2 在 LiF-NaF-KF 熔盐中的腐蚀行为研究	MAX 相材料在熔融氟盐中的腐蚀行为研究
63	硕士	耿东平	光学工程	高兴宇	用于反光电子谱仪的高效单色电子源设计	反光电子谱仪
64	硕士	尹文静	粒子物理与原子核物理	朱智勇	TRISO 包覆燃料颗粒放射性核素的产生及安全性分析	核燃料模拟计算

65	硕士	王飞	信号与信息处理	李勇平	数字式时差法超声流量计的设计与实现	超声流量测量
66	硕士	唐正博	电磁场与微波技术	刘建飞	超导腔的预调谐技术研究	电磁场与微波
67	硕士	郭鑫	信号与信息处理	李德明	基于分布式控制的束流路径校正和远程监测研究	加速器控制技术
68	硕士	王奇	生物工程	李宾	基于DNA折纸的DNA复制的原子力显微术研究	纳米生物学
69	硕士	牛强	核能与核技术工程	蔡翔舟	熔盐冷却球床堆堆芯热工水力特性数值分析	反应堆物理
70	硕士	冯新康	光学工程	王纳秀	直接冷却单色器晶体加工方法及其工艺的研究	晶体加工与检测
71	硕士	陈怀灿	核能与核技术工程	周兴泰	锆基非晶合金离子束辐照的结构性能研究	非晶合金的辐照研究
72	硕士	马明超	电子与通信工程	陈建锋	基于实时以太网的分布式IO系统	实时以太网通信
73	硕士	杨迎国	生物工程	高兴宇	有机太阳能电池的同步辐射XRD表征及其性能研究	有机薄膜制备与同步表征

附录 2

2013 年度论文发表一览表

Papers Published in 2013-2014

2013

No.	论文名称	期刊名称	作者	卷	页
1	Sealing nuclear graphite with pyrolytic carbon	Journal of Nuclear Materials	周兴泰	441	449
2	Imaging cellular uptake and intracellular distribution of TiO_2 nanoparticles	Analytical Methods	黄庆	2013	6611
3	Investigation on corrosion behavior of Ni-based alloys in molten fluoride salt using synchrotron radiation techniques	Journal of Nuclear Materials	周兴泰	440	124
4	Generation of multifocal spherical spots with Bessel-Gaussian radially polarized beam modulated with diffractive optical element	量子电子学报	刘海港	30	385
5	Corrosion characteristics of Hastelloy N alloy after He^+ ion irradiation	Journal of Nuclear Science and Technology	何上明		
6	Protection of nuclear graphite toward liquid fluoride salt by isotropic pyrolytic carbon coating	Journal of Nuclear Materials	夏汇浩	442	306
7	Investigation on Corrosion Behavior of Ni-Based Alloys in Molten Fluoride Salt Using Synchrotron Radiation Techniques	Journal of Nuclear Materials	周兴泰	440	124
8	Microstructure and properties of ultrasonic assisted copper coated graphite foams	Materials Science and Technology	夏汇浩	29	1389
9	长期时效对 C276 合金组织和力学性能的影响	金属学报	周兴泰	49	763
10	高温 He 离子辐照引起的 Hastelloy N 合金微结构变化研究	核技术	周兴泰、陆燕玲	36	050205（1）
11	长期时效对 C276 合金组织和力学性能的影响	金属学报	周兴泰	49	763
12	Sealing nuclear graphite with pyrolytic carbon	Journal of Nuclear Materials	周兴泰，白朔，杨新梅	441	449
13	Three-dimensional finite element analysis of temperature and stress distributions for in-service welding process	Materials & Design	黎超文	52	1052
14	沙尘暴对上海大气颗粒物中 S、Cl、Ca 化学种态的影响	核技术	李燕	36	100101
16	Effect of temperature on diffusion behavior of Te into nickel	Journal of Nuclear Materials	徐洪杰，邹杨，李志军	441	372
17	Ni-Te 系统的扩散激活能和扩散系数研究	上海金属	徐洪杰，李志军	35	1

18	化学成分以及辐照条件对压力容器钢中子辐照损伤的影响	材料导报	黄鹤飞	27	106
19	The Experimental Study of Lanthanum Bromide Detector in the Gamma	Applied Mechanics and Materials	赵翠兰	336	373
20	Study of Control rod worth in the TMSR	Nuclear Science and Techniques	周雪梅	24	1
21	Study on neutron energy spectrum in the TMSR	Applied Mechanics and Materials	周雪梅	239	287
22	Seismic analysis of the molten salt pump for TMSR	ANSYS 中国用户大会	毛文玉		1
23	The Structural Design and Dynamic Buckling Simulation of the Control Rod Buffer	2013 ANSYS 中国用户大会优秀论文	王晓艳		1
24	非晶铁磁纤维应力阻抗效应的理论分析	中国科学: 物理学 力学 天文学	苏飞	43	874
25	The Application of Improved EDM in the Thermal Loop Control System of Molten Salt Reactor	核电子学与探测技术	郭冰	33	675
26	Research and implementation of Control System Studio for TMSR	核技术	郭冰	36	110602-1
27	The conceptual design of electron-accelerator-driven subcritical thorium molten salt system	Energy Procedia	林作康		267
28	Investigation of thermal neutron scattering data for BeF_2 and LiF crystals	Journal of Nuclear Science and Technology	蔡翔舟	50	419
29	The investigation of thermal neutron scattering data for molten salt Flibe	Journal of Nuclear Science and Technology	蔡翔舟	50	682
30	熔盐堆堆芯分区结构对钍燃料增殖性能的影响	核技术	蔡翔舟	36	90601-1
31	燃料球体积填充率对 2MW 先进高温堆物理特性的影响	核技术	陈金根	36	73
32	$^{n+}$Th-232 核反应光学模型势的计算	核技术	王晓攀	36	060603-1
33	Fluorine-18 labeling by click chemistry: Multiple probes in one pot	Applied Radiation and Isotopes	张岚 程登峰	75	64
34	点击化学在 ^{18}F 标记 PET 药物中的应用	核化学与放射化学	张岚	35	193
35	Electron transfer in N-butylpyridinium tetrafluoroborate ionic liquid by pulse radiolysis	Chinese Science Bulletin	付海英	58	1882
36	离子液体[bmim][PF_6]对氧杂蒽酮光化学及反应动力学的影响	光谱学与光谱分析	付海英	33	1744
37	Study on The Electrochemical Extraction of Rare Earth Elements From Flinak	Global 2013	龙德武		411
38	THz Wave Emission of GaAs induced by He^+ Ion Implantation	Nuclear Instruments and Methods in Physics Research B	朱智勇	307	199
39	Research of organic carbon components in MSW	环境科学与技术	李燕	36	95
40	Fuel Strategy for 2MW SF-TMSR	Global 2013	朱智勇		1097

41	Compression of ionic liquid when confined in porous silica nanoparticles	RSC Advances	吴国忠	0	9618
42	The Influence of Silica Nanoparticles on Ionic Liquid Behavior: A Clear Difference between Adsorption and Confinement	International Journal of Molecular sciences	吴国忠	14	21045
43	Property variation of ionic liquid [Bmim][$AuCl_4$] immobilized on carboxylated polystyrene submicrospheres with a small surface area	Chinses science bulletin	吴国忠	58	2950
44	Crystal structure and mechanical properties of UHMWPE-g-PMA fiber prepared by radiation grafting	Radiation Physics and Chemistry	吴国忠	86	84
45	Preparation of microcellular polystyrene/polyethylene alloy foams by supercritical CO_2 foaming and analysis by X-ray microtomography	Journal of Supercritical Fluids	吴国忠	82	50
46	Properties and evaluation of amidoxime-based UHMWPE fibrous adsorbent for extraction of uranium from seawater	Science China Chemistry	吴国忠	56	1504
47	Radiation oxidation and subsequent thermal curing of polyacrylonitrile fiber	Radiation Physics and Chemistry	吴国忠	94	9
48	Building up Graphene-Based Conductive Polymer Composite Thin Films Using Reduced Graphene Oxide Prepared by γ-Ray Irradiation	The Scientific World Journal	李景烨	2013	1
49	Self-healing of the superhydrophobicity by ironing for the abrasion durable superhydrophobic cotton fabrics	Scientific Reports	李景烨	3	1
50	Laundering Durability of Photocatalyzed Self-Cleaning Cotton Fabric with TiO_2 Nanoparticles Covalently Immobilized	ACS Applied Materials & Interfaces	李景烨	5	3697
51	Graphene Oxide-Based Antibacterial Cotton Fabrics	Advanced Healthcare Materials	李景烨 黄庆 樊春海	2	1259
52	A Novel Avenue to Gold Nanostructured Microtubes Using	ACS Applied Materials & Interfaces	李景烨	17	8761
53	辐射接枝改性对 UHMWPE 纤维性能的影响	高分子材料科学与工程	吴国忠	29	36
54	Criticality Safety Analyses For Solid Fuel Thorium Molten Salt Reactor (TMSR-SF) Core Replacement	ANS NCSD 2013 - Criticality Safety in the Modern Era: Raising the Bar	陈堃		1
55	The Analysis of Tritium Production in the Sold Fuel Thorium Molten Salt Reactor	ANS National Meeting-2013 Winter Meeting and Technology Expo	陈堃		1

56	Reactivity Initiated Transient Analysis of Molten Salt Reactor	Proceedings of the 2013 21st International Conference on Nuclear Engineering	夏晓彬		1
57	NEUTRON STARS WITH KAON CONDENSATION IN RELATIVISTIC EFFECTIVE MODEL	INT J MOD PHYS E	吴琛	22	1350026-1
58	Strange baryonic matter and hypernuclei in the improved quark mass density-dependent model	J PHYS G NUCL PARTIC	吴琛		075107-1
59	Towards detailed tomography of high energy heavy-ion collisions by γ -jet	PHYS LETT B	马国亮		278
60	Dijet asymmetry in Pb+Pb collisions at √ sNN=2.76 TeV within a multiphase transport model	PHYS REV C	马国亮	6	64091-1
61	Decomposition of the jet fragmentation function in high-energy heavy-ion collisions	PHYS REV C	马国亮		21902-1
62	Dihadron, γ -hadron and γ +jet correlations in relativistic heavy-ion collisions	AIP Conference Proceedings	马国亮	1533	51
63	Thermodynamic properties and shear viscosity over entropy-density ratio of the nuclear fireball in a quantum-molecular dynamics model	PHYS REV C	马余刚		024604-1
64	Energy dependence of pion in-medium effects on the π？/π+ ratio in heavy-ion collisions	PHYSICAL REVIEW C	徐骏		067601-1
65	Shear viscosity of neutron-rich nucleonic matternearits liquid－gasphase transition	PHYS LETT B	马余刚		244
66	Probingin-mediumspin－orbitinteractionwithintermediate-energyheavy-ioncollisions	PHYS LETT B	徐骏		346
67	Shear viscosity of nuclear matter	Nuclear Science and Techniques	徐骏		050514-1
68	Elliptic flow of identified hadrons in Au+Au collisions at √ sNN = 7.7－62.4 GeV	PHYS REV C	STAR COLLABORATION		014902-1
69	Observation of an Energy Dependent Difference in Elliptic Flow between Particles and Antiparticles in Relativistic Heavy Ion Collisions	PHYSICAL REVIEW LETTERS	STAR		142301-1
70	Experimental studies of di-jets in Au+Au collisions using angular correlations with respect to back-to-back leading hadrons	PHYS REV C	STAR		044903-1
71	J/ψ production at high transverse momenta in p + p and Au + Au collisions √ sNN = 200 GeV	PHYS LETT B	STAR		55

72	Measurement of J=c Azimuthal Anisotropy in AutAu Collisions at √ SNN=200GEV	PHYS REV LETT	STAR		052301-1
73	Freeze-out dynamics via charged kaon femtoscopy in √ sNN = 200 GeV central Au+Au collisions	PHYS REV C	STAR		034906-1
74	Third harmonic flow of charged particles in Au+ Au collisions at √ sNN = 200 GeV	PHYS REV C	STAR		014904-1
75	Observation of antimatter nuclei at RHIC-STAR	Journal of Physics: Conference Series	马余刚		12036-1
76	Symmetry-energy dependence of the dynamical dipole mode in the Boltzmann-Uehling-Uhlenbeck model	PHYS REV C	马余刚		047602-1
77	Influence of the symmetry energy on isospin ratios from projectile and target fragmentations in intermediate-energy heavy-ion collisions	PHYS REV C	马余刚		047603-1
78	Hunting Antimatter Nuclei in Ultrarelativistic Heavy-Ion Collisions	Nuclear Physics News	马余刚	23	10
79	Role of neutrons to protons ratio in determining the symmetry energy at sub and supra-saturation densities	Journal of Physics: Conference Series	Sanjeev Kumar		1
80	Shear viscosity to entropy density ratio of nuclear matter by transport model	Journal of Physics: Conference Series	方德清		012083-1
81	Search for 14.4 keV solar axions from M1 transition of 57Fe with CUORE crystals	J COSMOL ASTROPART P	CUORE		007-1
82	A simulationpackagetostudythefeasibilityofanexperiment tosearchforparityviolationin d γ ; nTp	Nuclear Instruments and Methods	徐望		67
83	System-size dependence of transverse momentum correlations at √ sNN = 62.4 and 200 GeV at the BNL Relativistic Heavy Ion Collider	PHYS REV C	STAR		064902-1
84	Single spin asymmetry AN in polarized proton − proton elastic scattering √ s = 200 GeV	PHYS LETT B	STAR		62
85	Extraction of dihadron-jet correlations with rigorous flow-background subtraction in a multiphase transport model	PHYS REV C	马余刚		024904-1
86	Initial fluctuation effect on elliptic flow in Au+Au collision at 1 GeV/A	Nuclear Science and Techniques	马余刚		030501-1

87	Symmetry energy dependence of the pygmy and giant dipole resonances in an isospin dependent quantum moleculardynamics model	Nuclear Science and Techniques	马余刚		30502-1
88	Pygmy and giant dipole resonances by Coulomb excitation using a quantum molecular dynamics model	PHYS REV C	马余刚		014621-1
89	Investigation of compressibilities using neutron-rich projectile’s fragmentation at intermediate energy	Nuclear Physics A	马余刚		59
90	Design of a Superconducting Undulater Magnet Prototype for SSRF	4th International Particle Accelerator Conference (IPAC'13)	许皆平	1	2205
91	Inhomogeneity of external magnetic field for permanent magnet	物理学报	何永周	62	084105-1
92	Research on magnetic properties of magnet for cryogenic undulator of shanghai synchrotron radiation facility	物理学报	何永周	62	044106-1
93	Experimental research on the residual magnetization of a rare-earth permanent magnet for a cryogenic undulator	Chin. Phys. B	何永周	22	074101-1
94	Design and test of superconducting wiggler test coils	低温与超导	江勇	41	22
95	Inhomogeneity of external magnetic field for permanent magnet	物理学报	何永周	62	217502-1
96	THE MAGNETIC PERFORMANCE OF A DOUBLE ELLIPTICALLY POLARIZED UNDULATOR	Proceedings of IPAC2013	周巧根	1	2208
97	Undulator Chamber R&D for SXFEL	Proceedings of IPAC2013	胡晓	1	2193
98	APPLICATION OF MAGNETIC FIELD INTEGRAL MEASUREMENT OF MAGNET MODULE TO RESEARCH ALTERABLE GAP UNDULATOR	Proceedings of IPAC2013	王宏飞	1	3549
99	MEASUREMENT AND RESEARCH ON CRYOGENIC REMANENCE OF CHUNKS PM FOR CRYOGENIC UNDULATOR	Proceedings of IPAC2013	何永周	1	2190
100	DESIGN OF A TEST CRYOMODULE FOR IMP ADS-INJECTOR II	Proceedings of IPAC2013	王莉	1	3546
101	DESIGN OF THE COLD MASS SUPPORT ASSEMBLY OF TEST CRYOMODULE FOR IMP ADS-INJECTOR II	Proceedings of IPAC2013	刘以勇		3543
102	The Magnetic Performance of Two Undulators for HLS	Proceedings of IPAC2013	张伟	1	2202

103	A NEW HARMONIC COIL BENCH AT SINAP FOR THE ALS COMBINED FUNCTION SEXTUPOLE MAGNETS	Proceedings of IPAC2013	Jidong Zhang		3662
104	MECHANICAL DESIGN OF SHIFT DRIVING SYSTEM FOR DEPU AT SSRF	Proceedings of IPAC2013	邓荣兵		2187
105	The Research Progress of Corrosion Behavior of Materials for Molten Salt Reactors in High Temperature Molten Fluorides	化学通报	汪洋	76	307
106	Specific properties improvement of polycarbonate induced by irradiation at elevated particular temperature	Radiation Physics and Chemistry	唐忠锋	96	171
107	Modification of calcium carbonate by using coupling agent and the influence to the mechanical properties of SBS	材料科学与工艺	程国君	21	49
108	An active beamstop for accurate measurement of high intensity X-ray beams	Nuclear Instruments and Methods in Physics Research A	潘强岩		584
109	Confinement effects on glass transition temperature, transition， breadth, and linear expansivity: An ultraslow X-ray reflectivity study on supported ultrathin polystyrene films	THE EUROPEAN PHYSICAL JOURNAL E	杨春明，Isao Takahashi	36	1
110	Structural Insights into the Mechanism for Recognizing Substrate of the Cytochrome P450 Enzyme TxtE	PLOS One	郁峰、何建华	8	e81526
111	Co-axial electrospun polystyrene/polyurethane fibers for oil collection from water surface	Nanoscale	丁斌	5	2745
112	Impact of Temperature Inversion Layer on Accumulation Process	环境科学与技术	李燕	36	104
113	The crystal structure of human GDP-L-fucose synthase	Acta Biochim Biophys Sin	何建华	45	720
114	Beam Instrumentation System Optimization for Top-up Operation in SSRF	Proceedings of IPAC2013	冷用斌		589
115	Point Spread Function Study of X-ray Pinhole Camera in SSRF	Proceedings of IPAC2013	冷用斌		592
116	Bunch-by-bunch Beam Position and Charge Monitor based on Broadband Scope in SSRF	Proceedings of IPAC2013	冷用斌		595
117	Beam Diagnostics System for a Photo-Neutron Source Driven by 15MeV Electron Linac	Proceedings of IBIC2013	冷用斌		57
118	Bunch Length Measurement With Streak Camera At SSRF Storage Ring	Proceedings of IBIC2013	冷用斌		478

119	Phase Space Measurement using X-ray Pinhole Camera at SSRF	Proceedings of IBIC2013	冷用斌		539
120	Bunch By Bunch Transverse Beam Position Observation and Analyze During Injection at SSRF	Proceedings of IBIC2013	冷用斌		746
121	Beam Signal Stretch Method Based on Square Process	Applied Mechanics and Materials	冷用斌		584
122	数字束流位置信号处理算法优化	强激光与粒子束	冷用斌	25	109
123	腔式束流位置探头初步束流实验与参数仿真	核技术	冷用斌	36	050102-1
124	Study of algorithms of phase advance measurement between BPMs and its application in SSRF	Nuclear Science and Techniques	冷用斌	24	010102-1
125	SDUV-FEL 实验装置中的电源控制系统	核技术	赵欢	36	080410-1
126	Development of Cavity Beam Position Monitor System	Proceedings of IPAC2013	冷用斌		586
127	MATLAB Simulation of DBPM Digital Down Conversion	Applied Mechanics and Materials	冷用斌		680
128	Cavity Beam Position Monitor Test System Based on Virtual Instrument	Applied Mechanics and Materials	冷用斌	333	2354
129	嵌入式上海光源 EPICS 插入件控制系统	强激光与粒子束	蒋舸扬	25	1001
130	Design and test of SX-FEL cavity BPM	Chinese Physics C	袁任贤	37	118001-1
131	Subpicosecond beam length measurement study based on the TM010 mode	Phys. Rev. ST Accel. Beams	袁任贤	16	072801-1
132	Design and measurement of signal processing system for cavity beam position monitor	Nuclear Science and Techniques	冷用斌	24	020101-1
133	基于切伦科夫原理的光纤束损探测系统研制	核技术	冷用斌	36	080102-1
134	Out gassing Characteristic of Graphite Sheet in Shanghai	真空与科学技术学报	薛松	33	661
135	Study on twist problem of sagittally bent crystal	核技术	薛松	36	070101-1
136	Study on cooling for optical parts with high heat loads at the SSRF	Journal of Physics	徐中民	425	1
137	MOTION CONTROL OF THE MIRROR CHAMBER	Proceedings of IPAC2013	郑丽芳		2998
138	EPICS-based control system in the water cooled DCM	核电子学与探测技术	郑丽芳	33	945
139	Ice or water: thermal properties of monolayer water adsorbed on a substrate	Journal of Statistical Mechanics: Theory and Experiment	陈济舸	13	P06009-1

140	Aggregated Gas Molecules: Toxic to Protein?	scientific reports	方海平、高嶷		1
141	“ Ligand Effects of Thiolate-Protected Au^{102} Nanoclusters.“	J. Phys. Chem. C	高嶷		8983
142	STATUS OF NON-DESTRUCTIVE BUNCH LENGTH MEASUREMENT BASED ON COHERENT CHERENKOV RADIATION	Proceedings of IPAC2013	邓海啸		583
143	Low Frequency Response of Biomolecule Probed by Terahertz Time-Domain Spectroscopy	第八届全国光生物学学术会议	赵红卫		1
144	Ethanol promotes dewetting transition at low concentrations	Soft Matter	Haiping Fang,*Jun Hu*Ruhong Zhou*		1
145	Interaction of Graphene-on-Al(111) Composite with D ？ Glucopyranose and Its Application in Biodetection	J. Phys. Chem. C	宋波		7967
146	Anisotropic Dielectric Relaxation of the Water Confined in Nanotubes for Terahertz Spectroscopy Studied by Molecular Dynamics Simulations	J. Phys. Chem. B	方海平、宋波		7967
147	Lateral Migration and Nonuniform Rotation of Biconcave Particle Suspended in Poiseuille Flow	CHIN. PHYS. LETT	张超英		064701-1
148	水的潜热：凝结，大气运动和冰啤酒	物理	陈济舸	42	281
149	Ion Enrichment on the Hydrophobic Carbon-based Surface in Aqueous Salt Solutions due to Cation- π Interactions	Scientific Reports	方海平		1
150	The dehydration processes of biological tissues investigated by terahertz time-domain spectroscopy	红外与毫米波学报	赵红卫		1
151	The ice-like water monolayer near the wall makes inner water shells diffuse faster inside a charged nanotube	J. Chem. Phys.	Hangjun Lu		204710-1
152	Diagnosis of schistosomiasis japonica with interfacial co-assembly-based multi-channel electrochemical immunosensor arrays	Scientific reports	Wei Hu, Shiping Song, Zheng Feng		1
153	Programmed self-assembly of DNA origami nanoblocks into anisotropic higher-order nanopatterns	Chinese Science Bulletin	LIU HuaJie， FAN ChunHai		2646
154	Smart Drug Delivery Nanocarriers with Self-Assembled DNA Nanostructures	Advanced Materials	Chunhai Fan ， Qing Huang		4386

155	A power-free microfluidic chip for SNP genotyping using graphene oxide and a DNA intercalating dye	Chem Commun	Lihua Wang,Rui Liu	3125
156	Applications of Gold Nanoparticles in the Detection and Identifi cation of Infectious Diseases and Biothreats	Advanced Materials	Chunhai Fan , Xiaolei Zuo	3490
157	Real Time in Vitro Regulation of DNA Methylation Using a 5？Fluorouracil Conjugated DNA-Based Stimuli-Responsive Platform	ACS Appl. Mater. Interfaces	Jimin Gao，Chunhai Fan	2604
158	Rolling Circle Amplifi cation-Based DNA Origami Nanostructrures for Intracellular Delivery of Immunostimulatory Drugs	Small	Jie Chao , Chunhai Fan	1
159	Scaffolded biosensors with designed DNA nanostructures	NPG Asia Materials	Chunhai Fan	1
160	DNA Nanostructure-based Interfacial engineering for PCR-free ultrasensitive electrochemical analysis of microRNA	Scientific reports	Chunhai Fan	1
161	Highly sensitive and selective detection of silver(I) in aqueous solution with silver(I)-specific DNA and Sybr green I?	Analyst	Hui Xu，Linsheng Tang	2057
162	Carbon Nanotubes Multifunctionalized by Rolling Circle Amplifi cation and Their Application for Highly Sensitive Detection of Cancer Markers	Small	Shiping Song	2595
163	Single-Step Rapid Assembly of DNA Origami Nanostructures for Addressable Nanoscale Bioreactors	J. Am. Chem. Soc.	liuhuajie,Fan Chunhai	696
164	Synchrotron-based X-ray microscopic studies for bioeffects of nanomaterials.	Nanomedicine	Zengtao Zhong, Chunhai Fan	0
165	Self-assembly of DNA-based drug delivery nanocarriers with rolling circle amplification	Methods	Chunhai Fan, Jie Chao	0
166	Nanoplasmonic Imaging of Latent Fingerprints and Identification of Cocaine	Angew Chem Int Edit	Chunhai Fan, Di Li	11542
167	Biodistribution and pulmonary toxicity of intratracheally instilled graphene oxide in mice	NPG Asia Materials	Qing Huang，Chunhai Fan1	1
168	Uniform Ultrasmall Graphene Oxide Nanosheets with Low Cytotoxicity and High Cellular Uptake	ACS Appl. Mater. Interfaces	Rui Liu，Qing Huang	1761
169	Conjugation of Dexamethasone to C^{60} for the Design of an Anti-Inflammatory Nanomedicine with Reduced Cellular Apoptosis	ACS Appl. Mater. Interfaces	Yanhong Sun，Zengtao Zhong	5291

170	Bias controlled capacitive driven cantilever oscillation for high resolution dynamic force microscopy	Applied Physics Letters	Daniel M. Czajkowsky，Zhifeng Shao	1
171	Dendrime-folate-copper conjugates as bioprobes for synchrotron X-ray fluorescence imaging？	Chem Commun	Yanhong Sun, Qing Huang	10388
172	Synchrotron radiation X-ray fluorescence analysis of biodistribution and pulmonary toxicity of nanoscale titanium dioxide in mice	Analyst	Bo Li, Xiaohan Yu, Xiaoqing Cai	6511
173	Encapsulation of curcumin within poly(amidoamine) dendrimers for delivery to cancer cells	J Mater Sci Mater Med	Yanhong Sun	2137
174	Self-Assembly of Poly-Adenine-Tailed CpG Oligonucleotide-Gold Nanoparticle Nanoconjugates with Immunostimulatory Activity	Small	Chunhai Fan, Qing Huang	1
175	Charge transfer between reduced graphene oxide sheets on insulating substrates	Applied Physics Letters	Yi Zhang	1
176	Salts drive controllable multilayered upright assembly of amyloid-like peptides at mica/water interface	Proc. Natl. Acad. Sci. , USA	Yi Zhang, Ruhong Zhou	8543
177	Molecular Threading and Tunable Molecular Recognition on DNA Origami Nanostructures	J. Am. Chem. Soc.	Jun Hu,Bin Li, and Chunhai Fan	12172
178	Gold nanoparticle-assisted primer walking for closing the human chromosomal gap	Analytical Methods	Junhong LU,Runsheng Chen and Jun Hu	4746
179	A Novel Electromagnetic Apparatus for Rapid Multiplex Single Molecule Force Spectroscopy	JOURNAL OF NANOSCIENCE AND NANOTECHNOLOGY	Shao, Zhifeng	1232
180	Mechanical force-induced DNA damage during AFM single-molecule manipulation	Nuclear Science and Techniques	HU Jun	030504-1
181	Autophagy-Sensitized Cytotoxicity of Quantum Dots in PC12 Cells	Adv Healthc Mater	Nan Chen, Chunhai Fan, Qing Huang	1
182	Graphene oxide-based antibacterial cotton fabrics	Adv Healthc Mater	Qing Huang, Chunhai Fan	1259
183	Pattern Recognition Analysis of Proteins Using DNA-Decorated Catalytic Gold Nanoparticles	Small	Qing Huang	2844
184	溶液环境中利用声学、磁力、光热和静电力驱动微悬臂的动力学分析比较	核技术	胡钧	070501-1
185	基于原子力显微镜操纵构建纳米颗粒杂合结构	电子显微学报	张益	101
186	利用AFM探针施加的正偏压提高单个DNA分子的分离效率	电子显微学报	胡钧	139

187	基于原子力显微镜对多肽自组装结构的纳米操纵研究	电子显微学报	张益		30
188	HOPG/水界面纳米气泡与纳米气层的原子力显微技术研究	电子显微学报	胡钧		122
189	振动模式扫描极化力显微镜对氧化石墨烯热还原过程的实时原位监控	电子显微学报	胡钧		95
190	An in situ XAFS study—the formation mechanism of gold nanoparticles from X-ray-irradiated ionic liquid	Physical Chemistry Chemical Physics	Yuying Huang	15	11904
191	Effect of the Ratio between Ionic Liquids [BMIM]Br and [BMIM][BF_4] on the Charge Transfer of Br-	物理化学学报(Acta Phys. -Chim. Sin.)	黄宇营	29	1618
192	Structure of PtnNi Nanoparticles Electrocatalysts Investigated by X-ray Absorption Spectroscopy	J. Phys. Chem. C	黄宇营，孙公权，王建强	117	20584
193	Applicability study of the structure-factor phase method for determining the polarity of binary semiconductors	Acta Crystallographica Section B	曹杰峰		556
194	中心挡板对扫描相干 X 射线衍射成像的影响	物理学报	许子健，邰仁忠		150702-1
195	同步辐射光束线中部分相干光的传播研究	光学学报	王勇	33	318
196	Imaging interfacial micro- and nano-bubbles by scanning transmission soft X-ray microscopy	J. Synchrotron Rad.	张立娟，邰仁忠，胡钧		413
197	Mechanical mapping of nanobubbles by PeakForce atomic force microscopy	Soft Matter	张立娟，吕军鸿，胡钧	9	8837
198	Fate of Arsenate Adsorbed on Nano-TiO_2 in the Presence of Sulfate Reducing Bacteria	Enviromental Science & Technology	景传勇	47	10939
199	Effects of missing low-frequency information on ptychographic and plane-wave coherent diffraction imaging	APPLIED OPTICS	许子健，邰仁忠	52	2416
200	Determination of Zn istribution and speciation in basic oxygen furnace sludge by synchrotron radiation induced u-XRF and u-XANES microspectroscopy	X-ray Spectrometry	黄宇营	42	423
201	Zn distribution and speciation in zinc-containing steelmaking wastes by synchrotron radiation induced μ-XRF and μ-XANES spectroscopy	Journal of Physics: Conference Series	黄宇营	430	12097-1
202	Mechanism and microstructure of Eu(III) interaction with γ-MnOOH by a combination of batch and high resolution EXAFS investigation	Science China Chemistry	黄宇营	56	1658

203	A high-resolution X-ray fluorescence spectrometer and its application at SSRF	X-Ray Spectrometry	黄宇营	42	502
204	Comparison of single distance phase retrieval algorithms by considering different object composition and the effect of statistical and structural noise	Optics Express	Rongchang Chen	21	7384
205	Three-dimensional morphology of the Sinocyclocheilus hyalinus (Cypriniformes：Cyprinidae) horn based on synchrotron X-ray microtomography	Zoological Research	You He	34	128
206	Application of synchrotron hard X-ray based imaging on small animal’s cerebral vasculature and function studies	生命科学	HE You	25	803
207	X-ray imaging and its biomedical applications at SSRF	生命科学	肖体乔	25	762
208	X-ray biomedical imaging beamline at SSRF	Journal of Instrumentation	Tiqiao Xiao	8	0800301
209	Application of X-ray phase contrast micro-tomography to the identification of traditional Chinese medicines	Journal of Instrumentation	Tiqiao Xiao	8	0700600
210	Terahertz identification and quantification of penicillamine enantiomers	Nuclear Science and Technology	CHEN Min	24	01010101
211	Detection of complex vascular system in bamboo node by X-ray μ CT imaging technique	Holzforschung	Guanyun Peng	67	008001
212	Investigation of Characteric Microstructures of Adhesive Interface in wood/bamboo composite material by synchrotron radiation X-ray phase contrast microscopy	光谱学与光谱分析	王玉荣，肖体乔	33	829
213	Far-Infrared Characteristics of NaCl and Alkali Halide	Proceedings of SPIE	CHEN Min		8909001
214	Multiple Contrast Micro-Computed Tomography System Based on X-ray Grating Imaging	光学学报	肖体乔	33	103400101
215	X-Ray Phase Contrast Micro-Tomography and Its Application in Quantitative 3D Imaging Study of Ginseng Charateristic Structure	光学学报	肖体乔	33	123400201
216	CW-type HV Power Supply of 50 Hz and its Application in Accelerator Power Supply	Proceedings of 4th International Particle Accelerator Conference	Zi-Feng He(何子锋)		699
217	An 800kV 30mA Line-Frequency Cockcroft-Walton Dc Generator Using Gas Insulated Transformer for Radiation Application	Proceedings of 4th International Particle Accelerator Conference	Y.H. Liu(刘永好)		3675

218	Studies of Density Distribution and Emittance Measurement for High Current Electronic Beam	Proceedings of 4th International Particle Accelerator Conference	D.M. Li(李德明)		3672
219	Research on Modeling of the High-density Current Electron Gun System Based on T-S Fuzzy Model	Proceedings of 4th International Particle Accelerator Conference	Deming Li(李德明)		3678
220	Novel design of a micro-pulse electron gun	10.1016/j.nima.2013.07.064.	赵明华	729	381
221	Multipacting analysis in micro-pulse electron gun	10.1088/1674-1137/37/11/117004.	赵明华	37	117004-1
222	Seed laser transmission and injection system for the Shanghai Deep ultraviolet FEL test facility		王兴涛	36	050103-1
223	Demonstration of a widely-tunable and fully-coherent high-gain harmonic-generation free-electron laser	10.1103/PhysRevSTAB.16.020704	赵振堂	16	020704-1
224	Harmonic lasing of X-ray free electron laser: on the way to smaller and cheaper	10.1088/1674-1137/37/10/102001	邓海啸	37	102001-1
225	FEL polarization control studies on Dalian coherent light source	10.1088/1674-1137/37/11/118101	邓海啸	37	118101-1
226	Using Off-Resonance Laser Modulation for Beam-Energy-Spread Cooling in Generation of Short-Wavelength Radiation	10.1103/PhysRevLett.111.084801	邓海啸	111	084801-1
227	Chirped pulse amplification in a seeded free-electron laser for generating high-power ultra-short radiation	10.1016/j.nima.2013.01.063	赵振堂	712	113
228	Slippage effect on energy modulation in seeded free-electron lasers	10.1103/PhysRevSTAB.16.060705	赵振堂	16	060705-1
229	Novel design of a micro-pulse electron gun	10.1016/j.nima.2013.07.064.	邓海啸	729	381
230	Study on the seed laser phase error multiplication in seeded free electron lasers	10.1016/j.nima.2013.11.020	邓海啸	737	237
231	Transverse Instabilities of Two Twisted Beams in a Storage Ring	IPAC2013	姜伯承		172
232	Double-Mini-Betay Optics for the SSRF Storage Ring	IPAC2013	田顺强		1943
233	Effects Estimation of Superconducting Wiggler in SSRF	IPAC2013	张庆磊		1946
234	Conceptual Design of a Superfluid Superconducting Third Harmonic RF System for the SSRF Storage Ring	IPAC2013	侯洪涛		2381
235	上海光源储存环恒流注入束流安全性模拟	强激光与粒子束	姜伯承	25	985

2014

No.	论文名称	期刊名称	作者	卷	页
1	Morphology, microstructure and chemical composition of single inhalable particles in Shanghai, China	ENVIRONMENTAL MONITORING AND ASSESSMENT	Akram, Waheed; Madhuku, Morgan; Ahmad, Ishaq	186	8587
2	Generation of energy bands in the electron beam with an asymmetric chicane-type emittance exchange beamline	NUCLEAR INSTRUMENTS & METHODS IN PHYSICS RESEARCH SECTION A-ACCELERATORS SPECTROMETERS DETECTORS AND ASSOCIATED EQUIPMENT	Jiang, Bo-Cheng; Zhao, Zhen-tang; Feng, Chao	764	48
3	Efficient Hydrogenation of Alkyl Formate to Methanol over Nanocomposite Copper/Alumina Catalysts	CHEMCATCHEM	Du, Xian-Long; Sun, Xue-Ping; Jin, Chan	6	3075
4	Lattice dynamics and lattice thermal conductivity of thorium dicarbide	JOURNAL OF NUCLEAR MATERIALS	Liao, Zongmeng; Huai, Ping; Qiu, Wujie	454	142
5	TEM, XRD and nanoindentation characterization of Xenon ion irradiation damage in austenitic stainless steels	JOURNAL OF NUCLEAR MATERIALS	Huang, H. F.; Li, J. J.; Li, D. H.	454	168
6	Evolution of amorphization and nanohardness in SiC under Xe ion irradiation	JOURNAL OF NUCLEAR MATERIALS	Li, Jianjian; Huang, Hefei; Lei, Guanhong	454	173
7	Molecular-scale Hydrophilicity Induced by Solute: Molecular-thick Charged Pancakes of Aqueous Salt Solution on Hydrophobic Carbon-based Surfaces	SCIENTIFIC REPORTS	Shi, Guosheng; Shen, Yue; Liu, Jian	4	6793
8	DNA Nanostructure-Based Universal Microarray Platform for High-Efficiency Multiplex Bioanalysis in Biofluids	ACS APPLIED MATERIALS & INTERFACES	Li, Zhenhua; Zhao, Bin; Wang, Dongfang	6	17944
9	Coherent photon beam based diagnostics for a seeded extreme ultraviolet free-electron laser	PHYSICAL REVIEW SPECIAL TOPICS-ACCELERATORS AND BEAMS	Feng, Chao; Deng, Haixiao; Dai, Zhimin	17	100702
10	Charge separation with fluctuating domains in relativistic heavy-ion collisions	PHYSICAL REVIEW C	Shou, Qi-Ye; Ma, Guo-Liang; Ma, Yu-Gang	90	47901
11	Intrinsic Autocorrelation Time of Picoseconds for Thermal Noise in Water	JOURNAL OF PHYSICAL CHEMISTRY A	Zhu, Zhi; Sheng, Nan; Wan, Rongzheng	118	8936
12	Direct electrochemistry of glucose oxidase and a biosensor for glucose based on a glass carbon electrode modified with MoS_2 nanosheets decorated with gold nanoparticles	MICROCHIMICA ACTA	Su, Shao; Sun, Haofan; Xu, Fei	181	1497

13	Preparation and characterization of the antifouling porous membranes from poly(vinylidene fluoride)-graft-poly(N-vinyl pyrrolidone) powders	NUCLEAR SCIENCE AND TECHNIQUES	Chen Li-Fang; Bian Xiao-Kai; Hou Zheng-Chi	25	50303
14	The effect of Nb additive on Te-induced stress corrosion cracking in Ni alloy: a first-principles calculation	NUCLEAR SCIENCE AND TECHNIQUES	Liu Wen-Guan; Han Han; Ren Cui-Lan	25	50603
15	Dose rate distribution of photoneutrons in an ID beamline of SSRF: simulations and measurements	NUCLEAR SCIENCE AND TECHNIQUES	Xu Jia-Qiang; Xia Xiao-Bin; Sheng Yin-Xiang-Zi	25	50101
16	TEMPERATURE EFFECT OF Xe ION IRRADIATION TO 316 AUSTENITIC STAINLESS STEEL	ACTA METALLURGICA SINICA	Huang Hefei; Li Jianjian; Liu Renduo	50	1189
17	Crystal size shrinking in radiation-induced crosslinking of polytetrafluoroethylene: Synchrotron small angle X-ray scattering and scanning electron microscopy analysis	EUROPEAN POLYMER JOURNAL	Tang, Zhongfeng; Wang, Mouhua; Tian, Feng	59	156
18	Characterization of the effects of 3-MeV proton irradiation on fine-grained isotropic nuclear graphite	CARBON	Zhang, Baoliang; Xia, Huihao; He, Xiujie	77	311
19	Water dispersible polytetrafluoroethylene microparticles prepared by grafting of poly(acrylic acid)	RADIATION PHYSICS AND CHEMISTRY	Yang, Changqiao; Xu, Lu; Zeng, Hongyan	103	103
20	Long-Term Effects of Nanoparticles on Nutrition and Metabolism	SMALL	Chen, Nan; Wang, Hui; Huang, Qing	10	3603
21	Study on the Cr deposition and poisoning phenomenon at $(La_{0.6}Sr_{0.4})(Co_{0.2}Fe_{0.8})O_3$-delta electrode of solid oxide fuel cells by transmission X-ray microscopy	INTERNATIONAL JOURNAL OF HYDROGEN ENERGY	Chen, Xinbing; Jin, Chan; Zhao, Ling	39	15728
22	High Correlation between Oxidation Loci on Graphene Oxide	ANGEWANDTE CHEMIE-INTERNATIONAL EDITION	Yang, Jinrong; Shi, Guosheng; Tu, Yusong	53	10190
23	Surface functionalization of coal powder with different coupling agents for potential applications in organic materials	APPLIED SURFACE SCIENCE	Cheng, Guojun; Tong, Bin; Tang, Zhongfeng	313	954
24	Echo-enabled tunable terahertz radiation generation with a laser-modulated relativistic electron beam	PHYSICAL REVIEW SPECIAL TOPICS-ACCELERATORS AND BEAMS	Wang, Zhen; Huang, Dazhang; Gu, Qiang	17	90701
25	Characteristics evaluation of calcium carbonate particles modified by surface functionalization	ADVANCED POWDER TECHNOLOGY	Tang, Zhongfeng; Cheng, Guojun; Chen, Youshuang	25	1618
26	X-ray fluorescence computed tomography with absorption correction for biomedical samples	X-RAY SPECTROMETRY	Yang, Qun; Deng, Biao; Du, Guohao	43	278
27	Effects of rare earth yttrium on microstructure and properties of Ni-16Mo-7Cr-4Fe nickel-based superalloy	MATERIALS CHARACTERIZATION	Li, X. L.; He, S. M.; Zhou, X. T.	95	171
28	Anisotropic nanocrystallization of a Zr-based metallic glass induced by Xe ion irradiation	INTERMETALLICS	Chen, H. C.; Yan, L.; Liu, R. D.	52	15
29	Cellulose nanofibrils aerogels generated from jute fibers	CARBOHYDRATE POLYMERS	Lin, Jinyou; Yu, Liangbo; Tian, Feng	109	35
30	Synthesis of Few-Layer Reduced Graphene Oxide for Lithium-Ion Battery Electrode Materials	INDUSTRIAL & ENGINEERING	Li, Jihao; Li, Linfan; Zhang, Bowu	53	13348

		CHEMISTRY RESEARCH			
31	Orbital Effect-Induced Anomalous Anion-p Interactions between Electron-Rich Aromatic Hydrocarbons and Fluoride	CHEMPHYSCHEM	Shi, Guosheng; Yang, Jinrong; Ding, Yihong	15	2588
32	GInR Negatively Regulates the Transcription of the Alanine Dehydrogenase Encoding Gene ald in Amycolatopsis mediterranei U^{32} under Nitrogen Limited Conditions *via* Specific Binding to Its Major Transcription Initiation Site	PLOS ONE	Wang, Ying; Li, Chen; Duan, Na	9	104811
33	Efficient orange-red phosphorescent organic light-emitting diodes using an in situ synthesized copper(I) complex as the emitter	JOURNAL OF MATERIALS CHEMISTRY C	Wei, Feng; Qiu, Jacky; Liu, Xiaochen	2	6333
34	Molecular Insights into the Electric Double Layers of Ionic Liquids on Au(100) Electrodes	ACS APPLIED MATERIALS & INTERFACES	Sha, Maolin; Dou, Qiang; Luo, Fabao	6	12556
35	Recent Development of Sandwich Assay Based on the Nanobiotechnologies for Proteins, Nucleic Acids, Small Molecules, and Ions	CHEMICAL REVIEWS	Shen, Juwen; Li, Yuebin; Gu, Haoshuang	114	7631
36	Ultrasensitive Electrochemical Detection of Prostate-Specific Antigen by Using Antibodies Anchored on a DNA Nanostructural Scaffold	ANALYTICAL CHEMISTRY	Chen, Xiaoqing; Zhou, Guobao; Song, Ping	86	7337
37	Multivalent Capture and Detection of Cancer Cells with DNA Nanostructured Biosensors and Multibranched Hybridization Chain Reaction Amplification	ANALYTICAL CHEMISTRY	Zhou, Guobao; Lin, Meihua; Song, Ping	86	7843
38	Dynamic and Quantitative Control of the DNA-Mediated Growth of Gold Plasmonic Nanostructures	ANGEWANDTE CHEMIE-INTERNATIONAL EDITION	Shen, Jianlei; Xu, Lifeng; Wang, Chunpeng	53	8338
39	Nanostructure Variations and Their Effects on Mechanical Strength of Ni-17Mo-7Cr Alloy under Xenon Ion Irradiation	MATERIALS TRANSACTIONS	Huang, H. F.; Li, D. H.; Li, J. J.	55	1243
40	Simulation studies on two-frequency RF gun	NUCLEAR SCIENCE AND TECHNIQUES	Li Da; Fang Wen-Cheng; Gu Qiang	25	40101
41	Apparatus for determining permeability of hydrogen isotopes in molten-salt	NUCLEAR SCIENCE AND TECHNIQUES	Zeng You-Shi; Wu Sheng-Wei; Qian Yuan	25	40602
42	Structural changes of Rh-Mn nanoparticles inside carbon nanotubes studied by X-ray absorption spectroscopy	CHINESE JOURNAL OF CATALYSIS	Bao, Hongliang; Sun, Xueping; Jiang, Zheng	35	1418
43	Laundering durable antibacterial cotton fabrics grafted with pomegranate-shaped polymer wrapped in silver nanoparticle aggregations	SCIENTIFIC REPORTS	Liu, Hanzhou; Lv, Ming; Deng, Bo	4	5920
44	Final state effects on charge asymmetry of pion elliptic flow in high-energy heavy-ion collisions	PHYSICS LETTERS B	Ma, Guo-Liang;;	735	383
45	Azimuthal anisotropies of reconstructed jets in Pb plus Pb collisions at root S-NN=2.76 TeV in a multiphase transport model	PHYSICAL REVIEW C	Nie, Mao-Wu; Ma, Guo-Liang;	90	14907
46	Single-Particle Tracking and Modulation of Cell Entry Pathways of a Tetrahedral DNA Nanostructure in Live Cells	ANGEWANDTE CHEMIE-INTERNATIO	Liang, Le; Li, Jiang; Li, Qian	53	7745

		NAL EDITION			
47	Excited States and Luminescent Properties of UO_2F_2 and Its Solvated Complexes in Aqueous Solution	INORGANIC CHEMISTRY	Su, Jing; Wang, Zheming; Pan, Duoqiang	53	7340
48	Influence of neutron-skin thickness on the pi(-)/pi(+) ratio in Pb plus Pb collisions	PHYSICAL REVIEW C	Wei, Gao-Feng; Li, Bao-An; Xu, Jun	90	14610
49	Beam energy chirp effects in seeded free-electron lasers	NUCLEAR INSTRUMENTS & METHODS IN PHYSICS RESEARCH SECTION A-ACCELERATORS SPECTROMETERS DETECTORS AND ASSOCIATED EQUIPMENT	Wang, Guanglei; Feng, Chao; Deng, Haixiao	753	56
50	Enhanced Permeation of a Hydrophobic Fluid through Particles with Hydrophobic and Hydrophilic Patterned Surfaces	SCIENTIFIC REPORTS	Zhang, Renliang; Xu, Yousheng; Wen, Binghai	4	5738
51	Giant Dipole Resonance as a Fingerprint of a Clustering Configurations in C-12 and O-16	PHYSICAL REVIEW LETTERS	He, W. B.; Ma, Y. G.; Cao, X. G.	113	32506
52	A Bubble-Mediated Intelligent Microscale Electrochemical Device for Single-Step Quantitative Bioassays	ADVANCED MATERIALS	Yang, Fan; Zuo, Xiaolei; Li, Zhenhua	26	4671
53	Planar and Channel Waveguide Structures in CdS Crystals at 633 and 1539 nm	JOURNAL OF LIGHTWAVE TECHNOLOGY	Liu, Tao; Liu, Peng; Zhang, Lian	32	
54	Metal Ion-Mediated Assembly of DNA Nanostructures for Cascade Fluorescence Resonance Energy Transfer-Based Fingerprint Analysis	ANALYTICAL CHEMISTRY	Xia, Jiaoyun; Lin, Meihua; Zuo, Xiaolei	86	7084
55	Oxygen Reduction Contributing to Charge Transfer during the First Discharge of the CeO_2-$Bi_2Fe_4O_9$-Li Battery: In Situ X-ray Diffraction and X-ray Absorption Near-Edge Structure Investigation	JOURNAL OF PHYSICAL CHEMISTRY C	Liu, Min; Lin, Chuan; Gu, Yueliang	118	14711
56	Effect of Defects Induced by C-12(+) Ion Irradiation on the Fluorination of Pyrolytic Carbon Coating in Flinak Salt	ADVANCED ENGINEERING MATERIALS	Feng, Shanglei; Li, Li; Yang, Xinmei	16	897
57	Performance evaluation of BPM system in SSRF using PCA method	CHINESE PHYSICS C	Chen Zhi-Chu; Leng Yong-Bin; Yan Ying-Bing	38	77004
58	Experimental study using Touschek lifetime as machine status flag in SSRF	CHINESE PHYSICS C	Chen Zhi-Chu; Leng Yong-Bin; Yuan Ren-Xian	38	77005
59	Terahertz study of L-asparagine and its monohydrate	ACTA PHYSICA SINICA	Yang Jing-Qi; Li Shao-Xian; Zhao Hong-Wei	63	133203
60	Synthesis and evaluation of (18) F-labeled bile acid compound: A potential PET imaging agent for FXR-related diseases	NUCLEAR MEDICINE AND BIOLOGY	Jia, Lina; Jiang, Dawei; Hu, Pengcheng	41	495
61	Sample-charged mode scanning polarization force microscopy for characterizing reduced graphene oxide sheets	JOURNAL OF APPLIED PHYSICS	Shen, Yue; Wang, Ying; Zhang, Jinjin	115	244302

62	Surface Structural Reconstruction for Optical Response in Iodine-Modified TiO2 Photocatalyst System	JOURNAL OF PHYSICAL CHEMISTRY C	Zhang, Linjuan; Zhou, Jing; Li, Jiong	118	13726
63	Hydrogen-Bonded Polymers with Bent-Shaped Side Chains and Poly(4-vinylpridine) Backbone: Phase Behavior and Thin Film Morphologies	MACROMOLECULES	Liu, Xiaoshan; Chen, Xiaofang; Wang, Jingkui	47	3917
64	Medium modifications of the photon-tagged jet fragmentation function in high-energy heavy-ion collisions	PHYSICAL REVIEW C	Ma, Guo-Liang;;	89	64909
65	An improved DNA force field for ssDNA interactions with gold nanoparticles	JOURNAL OF CHEMICAL PHYSICS	Jiang, Xiankai; Gao, Jun; Huynh, Tien	140	234102
66	Spin-orbit coupling and the up-down differential transverse flow in intermediate-energy heavy-ion collisions	PHYSICAL REVIEW C	Xia, Yin; Xu, Jun; Li, Bao-An	89	64606
67	A rapid preparation of acicular Ni impregnated anode with enhanced conductivity and operational stability	JOURNAL OF POWER SOURCES	Zhu, Xingbao; Guan, Chengzhi; Lue, Zhe	256	424
68	Electrochemical Switching with 3D DNA Tetrahedral Nanostructures Self-Assembled at Gold Electrodes	ACS APPLIED MATERIALS & INTERFACES	Abi, Alireza; Lin, Meihua; Pei, Hao	6	8928
69	Compensating the electron beam energy spread by the natural transverse gradient of laser undulator in all-optical x-ray light sources	OPTICS EXPRESS	Zhang, Tong; Feng, Chao; Deng, Haixiao	22	13880
70	Nuclear modification factor in intermediate-energy heavy-ion collisions	PHYSICS LETTERS B	Lv, M.; Ma, Y. G.; Zhang, G. Q.	733	105
71	Analysis on reactivity initiated transient from control rod failure events of a molten salt reactor	NUCLEAR SCIENCE AND TECHNIQUES	Cai Jun; Xia Xiao-Bin; Chen Kun	25	30602
72	Using Xe as a heavy atom for phase determination of protein trichosanthin structure	NUCLEAR SCIENCE AND TECHNIQUES	Chen Ya-Xing; Li Min-Jun; Yu Feng	25	30502
73	Frequency control and pre-tuning of a large aperture 500 MHz 5-cell superconducting RF cavity	NUCLEAR SCIENCE AND TECHNIQUES	Tang Zheng-Bo; Ma Zhen-Yu; Hou Hong-Tao	25	30102
74	Double-mini-beta(y) optics design in the SSRF storage ring	NUCLEAR SCIENCE AND TECHNIQUES	Tian Shun-Qiang; Jiang Bo-Cheng; Leng Yong-Bin	25	30101
75	Systematic study of dynamical dipole mode *via* the isospin-dependent Boltzmann-Uehling-Uhlenbeck model	NUCLEAR SCIENCE AND TECHNIQUES	Ye Shao-Qiang; Cai Xiang-Zhou; Fang De-Qing	25	30501
76	Efficient Ternary CdSSe Quantum-Dot-Sensitized Solar Cells based on MgO-coated TiO_2 Nanoparticles	ENERGY TECHNOLOGY	Li, Hui; Xiao, Ran; Li, Zhe	2	526
77	Physical and Biochemical Insights on DNA Structures in Artificial and Living Systems	ACCOUNTS OF CHEMICAL RESEARCH	Chen, Nan; Li, Jiang; Song, Haiyun	47	1720
78	Absolute surface metrology by rotational averaging in oblique incidence interferometry	APPLIED OPTICS	Lin, Weihao; He, Yumei; Song, Li	53	3370
79	Irreversible Denaturation of Proteins through Aluminum-Induced Formation of Backbone Ring Structures	ANGEWANDTE CHEMIE-INTERNATIONAL EDITION	Song, Bo; Sun, Qian; Li, Haikuo	53	6357
80	Three-dimensional structure of polystyrene colloidal crystal by synchrotron radiation X-ray phase-contrast computed	APPLIED PHYSICS A-MATERIALS	Fu, Yanan; Xie, Honglan; Deng, Biao	115	781

	tomography	SCIENCE & PROCESSING			
81	Identification of a new series of potent diphenol HSP90 inhibitors by fragment merging and structure-based optimization	BIOORGANIC & MEDICINAL CHEMISTRY LETTERS	Ren, Jing; Li, Jian; Wang, Yueqin	24	2525
82	Galilean invariant fluid-solid interfacial dynamics in lattice Boltzmann simulations	JOURNAL OF COMPUTATIONAL PHYSICS	Wen, Binghai; Zhang, Chaoying; Tu, Yusong	266	161
83	Development of a Cryogenic Calorimeter for Investigating Beam-Based Heat Load of Superconducting Undulators	IEEE TRANSACTIONS ON APPLIED SUPERCONDUCTIVITY	Cui, J.; Xu, J. P.; Li, W.	24	503604
84	Design and Test of a Superconducting Undulator Mock-Up Coil at SSRF	IEEE TRANSACTIONS ON APPLIED SUPERCONDUCTIVITY	Zhang, Zhengchen; Xu, Jieping; Cui, Jian	24	4101503
85	A comparative first-principles study of the electronic, mechanical, defect and acoustic properties of Ti2AlC and Ti3AlC	JOURNAL OF PHYSICS D-APPLIED PHYSICS	Tan, Jie; Han, Han; Wickramaratne, Darshana	47	215301
86	A general model for estimating the ordering of mesoporous film by grazing incidence small angle X-ray scattering	JOURNAL OF APPLIED PHYSICS	Zhao, Nie; Yang, Chunming; Zhang, Qian	115	206101
87	Uniform Small Graphene Oxide as an Efficient Cellular Nanocarrier for Immunostimulatory CpG Oligonucleotides	ACS APPLIED MATERIALS & INTERFACES	Sun, Jinli; Chao, Jie; Huang, Jing	6	7926
88	CMOS-Compatible Silicon Nanowire Field-Effect Transistors for Ultrasensitive and Label-Free MicroRNAs Sensing	SMALL	Lu, Na; Gao, Anran; Dai, Pengfei	10	2022
89	Interplay between Water and TiO2 Anatase (101) Surface with Subsurface Oxygen Vacancy	PHYSICAL REVIEW LETTERS	Li, Yadong; Gao, Yi;	112	
90	Self-assembly of DNA-based drug delivery nanocarriers with rolling circle amplification	METHODS	Ouyang, Xiangyuan; Li, Jiang; Liu, Huajie	67	198
91	Mechanism of force mode dip-pen nanolithography	JOURNAL OF APPLIED PHYSICS	Yang, Haijun; Xie, Hui; Wu, Haixia	115	174314
92	Coherence of X-ray in the third synchrotron radiation source	ACTA PHYSICA SINICA	Qi Jun-Cheng; Ye Lin-Lin; Chen Rong-Chang	63	104202
93	DNA Origami Nanoreactors	PROGRESS IN CHEMISTRY	Jia Sisi; Chao Jie; Fan Chunhai	26	695
94	SiC coating: An alternative for the protection of nuclear graphite from liquid fluoride salt	JOURNAL OF NUCLEAR MATERIALS	He, Xiujie; Song, Jinliang; Tan, Jie	448	1
95	Characteristics of secondary inorganic aerosol and sulfate species in size-fractionated aerosol particles in Shanghai	JOURNAL OF ENVIRONMENTAL SCIENCES-CHINA	Long, Shilei; Zeng, Jianrong; Li, Yan	26	1040
96	A synchrotron-based local computed tomography combined with data-constrained modelling approach for quantitative	JOURNAL OF SYNCHROTRON	Chen, Wen Hao; Yang, Sam Y. S.; Xiao, Ti Qiao	21	586

	analysis of anthracite coal microstructure	RADIATION SCIENCE			
97	Recent advances on ordered water monolayer that does not completely wet water" at room temperature	CHINA-PHYSICS MECHANICS & ASTRONOMY	Wang ChunLei; Yang YiZhou; Fang HaiPing	57	802
98	Morphology Change and Detachment of Lipid Bilayers from the Mica Substrate Driven by Graphene Oxide Sheets	LANGMUIR	Lei, Haozhi; Zhou, Xuejiao; Wu, Haixia	30	4678
99	Shear viscosity of hot nuclear matter by the mean free path method	PHYSICAL REVIEW C	Fang, D. Q.; Ma, Y. G.; Zhou, C. L.	89	47601
100	Morphological effect of oscillating magnetic nanoparticles in killing tumor cells	NANOSCALE RESEARCH LETTERS	Cheng, Dengfeng; Li, Xiao; Zhang, Guoxin	9	195
101	Phase-merging enhanced harmonic generation free-electron laser	NEW JOURNAL OF PHYSICS	Feng, Chao; Deng, Haixiao; Wang, Dong	16	43021
102	Transverse multibunch instabilities for two bunch trains on separated orbits	PHYSICAL REVIEW SPECIAL TOPICS-ACCELERATORS AND BEAMS	Jiang, B. C.; Xia, G. X.; Zhang, M. Z.	17	40703
103	Size-Dependent Programming of the Dynamic Range of Graphene Oxide-DNA Interaction-Based Ion Sensors	ANALYTICAL CHEMISTRY	Zhang, Huan; Jia, Sisi; Lv, Min	86	4047
104	A methylation-blocked cascade amplification strategy for label-free colorimetric detection of DNA methyltransferase activity	BIOSENSORS & BIOELECTRONICS	Zhao, Yongxi; Chen, Feng; Lin, Manli	54	565
105	Superresolution imaging of DNA tetrahedral nanostructures in cells by STED method with continuous wave lasers	CHINESE OPTICS LETTERS	Du, Jiancong; Deng, Suhui; Hou, Shangguo	12	41101
106	Integrated analytical techniques with high sensitivity for studying brain translocation and potential impairment induced by intranasally instilled copper nanoparticles	TOXICOLOGY LETTERS	Bai, Ru; Zhang, Lili; Liu, Ying	226	70
107	A method for determination of the s orbital component of Be-12 ground state	NUCLEAR SCIENCE AND TECHNIQUES	Cai Xiao-Lu; Fan Guang-Wei; Xu Hang-hua	25	20501
108	Beam position monitor troubleshooting by using principal component analysis in Shanghai Synchrotron Radiation Facility	NUCLEAR SCIENCE AND TECHNIQUES	Chen Zhi-Chu; Leng Yong-Bin; Yuan Ren-Xian	25	20102
109	EPICS data archiver at SSRF beamlines	NUCLEAR SCIENCE AND TECHNIQUES	Hu Zheng; Mi Qing-Ru; Zhen Li-Fang	25	20103
110	Ordered water monolayer on ionic model substrates studied by molecular dynamics simulations	NUCLEAR SCIENCE AND TECHNIQUES	Shao Shi-Jing; Guo Pan; Zhao Liang	25	20502
111	Implementation and integration of a systematic DBPM calibration with PLL frequency synthesis and FPGA	NUCLEAR SCIENCE AND TECHNIQUES	Sun Xu-Dong; Leng Yong-Bin;	25	20401
112	Design and study of a C-band pulse compressor for the SXFEL linac	NUCLEAR SCIENCE AND TECHNIQUES	Wang Chao-Peng; Fang Wen-Cheng; Tong De-Chun	25	20101
113	Magnetic properties of bulk polycrystalline Pr1-xNdx(x=0, 0.8)FeB permanent magnets	CHINESE PHYSICS B	He Yong-Zhou; Wu Hong-Ping; Zou Zhi-Qiang	23	47501
114	Synchrotron-based X-ray microscopic studies for bioeffects of nanomaterials	NANOMEDICINE-NANOTECHNOLOGY BIOLOGY AND	Zhu, Ying; Cai, Xiaoqing; Li, Jiang	10	515

		MEDICINE			
115	The investigation of order-disorder transition process of ZSM-5 induced by spark plasma sintering	JOURNAL OF SOLID STATE CHEMISTRY	Wang, Liang; Wang, Lianjun; Jiang, Wan	212	128
116	Dynamic correlation of photo-excited electrons: Anomalous levels induced by light-matter coupling	PHYSICA B-CONDENSED MATTER	Jiang, Xiankai; Huai, Ping; Song, Bo	438	109
117	Production and ratio of pi, K, p, and Lambda in Pb plus Pb collisions at root s(NN)=2.76 TeV	PHYSICAL REVIEW C	Zhang, S.; Han, L. X.; Ma, Y. G.	89	34918
118	Effect of a Room-Temperature Ionic Liquid on the Structure and Properties of Electrospun Poly(vinylidene fluoride) Nanofibers	ACS APPLIED MATERIALS & INTERFACES	Xing, Chenyang; Guan, Jipeng; Li, Yongjin	6	4447
119	DNA-Gold Nanoparticle Conjugates-Based Nanoplasmonic Probe for Specific Differentiation of Cell Types	ANALYTICAL CHEMISTRY	Yang, Xiafeng; Li, Jiang; Pei, Hao	86	3227
120	Squared form factors of vibronic excitations in 12-13.3 eV of nitrogen studied by high-resolution inelastic x-ray scattering	PHYSICAL REVIEW A	Peng, Yi-Geng; Kang, Xu; Yang, Ke	89	32512
121	Target-Responsive, DNA Nanostructure-Based E-DNA Sensor for microRNA Analysis	ANALYTICAL CHEMISTRY	Lin, Meihua; Wen, Yanli; Li, Lanying	86	2285
122	Folate-polyethylene glycol conjugated carboxymethyl chitosan for tumor-targeted delivery of 5-fluorouracil	MOLECULAR MEDICINE REPORTS	Li, Hai-Lang; He, Ya-Xing; Gao, Qian-Hong	9	786
123	Autophagy-Sensitized Cytotoxicity of Quantum Dots in PC12 Cells	ADVANCED HEALTHCARE MATERIALS	Li, Xiaoming; Chen, Nan; Su, Yuanyuan	3	354
124	Effects of pH and polarity on the excited states of norfloxacin and its 4'-N-acetyl derivative: A steady-state and time-resolved study	SCIENCE CHINA-CHEMISTRY	Zhang Peng; Li HaiXia; Yao SiDe	57	409
125	Specific properties improvement of polycarbonate induced by irradiation at elevated particular temperature	RADIATION PHYSICS AND CHEMISTRY	Tang, Zhongfeng; Chen Youshuang; Wang Mouhua	96	171
126	The Origin of the "Snap-In" in the Force Curve between AFM Probe and the Water/Gas Interface of Nanobubbles	CHEMPHYSCHEM	Song, Yang; Zhao, Binyu; Zhang, Lijuan	15	492
127	Reversible State Transition in Nanoconfined Aqueous Solutions	PHYSICAL REVIEW LETTERS	Zhao, Liang; Wang, Chunlei; Liu, Jian	112	78301
128	Polarization switching demonstration using crossed-planar undulators in a seeded free-electron laser	PHYSICAL REVIEW SPECIAL TOPICS-ACCELERATORS AND BEAMS	Deng, Haixiao; Zhang, Tong; Feng, Lie	17	20704
129	Functional DNA Nanostructures for Theranostic Applications	ACCOUNTS OF CHEMICAL RESEARCH	Pei, Hao; Zuo, Xiaolei; Zhu, Dan	47	550
130	Molecular Logic Gates on DNA Origami Nanostructures for MicroRNA Diagnostics	ANALYTICAL CHEMISTRY	Wang, Dongfang; Fu, Yanming; Yan, Juan	86	1932
131	Hybridization Chain Reaction Amplification of MicroRNA Detection with a Tetrahedral DNA Nanostructure-Based Electrochemical Biosensor	ANALYTICAL CHEMISTRY	Ge, Zhilei; Lin, Meihua; Wang, Ping	86	2124
132	In Situ Small Angle X-ray Scattering Study on Structural	JOURNAL OF	Li, Xiaoyun; Tian, Feng;	131	39883

	Evolution of Crosslinked Polytetrafluoroethylene During Deformation	APPLIED POLYMER SCIENCE	Yang, Chunming		
133	$Pt_2Cl_8^{2-}$ Dimer Formation of [Bmim](2)$PtCl_4$ Ionic Liquid When Confined in Silica Nanopores	JOURNAL OF PHYSICAL CHEMISTRY C	Li, Cheng; Wang, Yaxing; Guo, Xiaojing	118	3140
134	Study on the seed laser phase error multiplication in seeded free electron lasers	NUCLEAR INSTRUMENTS & METHODS IN PHYSICS RESEARCH SECTION A-ACCELERATORS SPECTROMETERS DETECTORS AND ASSOCIATED EQUIPMENT	Wang, Guanglei; Feng, Chao; Zhang, Tong	737	237
135	Pseudo-global tomography for local micro-computed tomography with high-brightness synchrotron X-rays	CHINESE OPTICS LETTERS	Chen, Wenhao; Wang, Yudan; Liu, Huiqiang	12	23401
136	AB INITIO INVESTIGATIONS OF THE MAGNETISM IN DILUTED MAGNETIC SEMICONDUCTOR Fe-DOPED GaN	MODERN PHYSICS LETTERS B	Cheng, Jie; Zhou, Jing; Xu, Wei	28	1450031
137	Medium modifications of jet shapes in Pb plus Pb collisions at root S-NN=2.76 TeV within a multiphase transport model	PHYSICAL REVIEW C	Ma, Guo-Liang;;	89	24902
138	Development of a three dimension multi-physics code for molten salt fast reactor	NUCLEAR SCIENCE AND TECHNIQUES	Cheng Mao-Song; Dai Zhi-Min;	25	10601
139	Adsorption behavior of uranyl ions onto amino-type adsorbents prepared by radiation-induced graft copolymerization	NUCLEAR SCIENCE AND TECHNIQUES	Chi Hong-Ying; Liu Xi-Yan; Ma Hong-Juan	25	10302
140	Feasibility study on optical vortex generation at Shanghai deep ultraviolet free-electron laser	NUCLEAR SCIENCE AND TECHNIQUES	Deng Hai-Xiao;;	25	10101
141	Lattice design and optimization of the SSRF storage ring with super-bends	NUCLEAR SCIENCE AND TECHNIQUES	Tian Shun-Qiang; Jiang Bo-Cheng; Zhou Qiao-Gen	25	10102
142	Temperature and carrier-density dependent excitonic absorption spectra of semiconductor quantum wires	NUCLEAR SCIENCE AND TECHNIQUES	Wang Ting-Dong; Huai Ping;	25	10201
143	Using activation method to measure neutron spectrum in an irradiation chamber of a research reactor	NUCLEAR SCIENCE AND TECHNIQUES	Zhou Xue-Mei; Liu Gui-Min; Li Da	25	10603
144	Bromate formation in bromide-containing waters irradiated by gamma rays	NUCLEAR SCIENCE AND TECHNIQUES	Zhou Yan; Cao Chang-Qing; Wang Min	25	10301
145	Self-assembly of DNA Origami Using Rolling Circle Amplification Based DNA Nanoribbons	CHINESE JOURNAL OF CHEMISTRY	Liu, Bing; Ouyang, Xiangyuan; Chao, Jie	32	137
146	Detection of complex vascular system in bamboo node by X-ray mu CT imaging technique	HOLZFORSCHUNG	Peng, Guanyun; Jiang, Zehui; Liu, Xing'e	68	223
147	Simulation studies on laser pulse stability for Dalian coherent light source	CHINESE PHYSICS C	Deng Hai-Xiao; Zhang Meng; Gu Duan	38	28101
148	A THz-TDS measurement method for multiple samples	OPTICS COMMUNICATIONS	Ji, Te; Zhang, Zengyan; Zhao, Hongwei	312	292

149	High Accuracy Sample Positioning System for Hard X-Ray Microprobe	SPECTROSCOPY AND SPECTRAL ANALYSIS	Zhang Ji-chao; Liang Dong-xu; He Yan	34	557
150	TEM Investigation on the Microstructural Evolution of Hastelloy N Induced by Ar+ Ion Irradiation	MICROSCOPY RESEARCH AND TECHNIQUE	Liu, Min; Lu, Yanling; Liu, Renduo	77	161
151	Corrosion characteristics of Hastelloy N alloy after He^{+} ion irradiation	JOURNAL OF NUCLEAR SCIENCE AND TECHNOLOGY	Lin, Jianbo; Li, Aiguo; Yu, Xiaohan	51	175
152	Upright or Flat Orientations of the Ethanol Molecules on a Surface with Charge Dipoles and the Implication for Wetting Behavior	JOURNAL OF PHYSICAL CHEMISTRY C	Wang, Chunlei; Zhao, Liang; Zhang, Donghua	118	1873
153	Interaction between O^{-2} and neutral/charged Au-n (n=1-3) clusters: A comparative study between density-functional theory and coupled cluster calculations	CHEMICAL PHYSICS LETTERS	Zhao, Yu; Khetrapal, Navneet Singh; Li, Hui	592	127
154	Self-Assembly of Poly-Adenine-Tailed CpG Oligonucleotide-Gold Nanoparticle Nanoconjugates with Immunostimulatory Activity	SMALL	Chen, Nan; Wei, Min; Sun, Yanhong	10	368
155	Determination of the electronic structure of atoms and molecules in the ground state: Measurement of molecular hydrogen by high-resolution x-ray scattering	PHYSICAL REVIEW A	Liu, Ya-Wei; Mei, Xiao-Xun; Kang, Xu	89	14502
156	First-principles study of the effect of phosphorus on nickel grain boundary	JOURNAL OF APPLIED PHYSICS	Liu, Wenguan; Ren, Cuilan; Han, Han	115	43706
157	Triton/He-3 ratio as an observable for neutron-skin thickness	PHYSICAL REVIEW C	Dai, Z. T.; Fang, D. Q.; Ma, Y. G.	89	14613
158	An active beamstop for accurate measurement of high intensity X-ray beams	NUCLEAR INSTRUMENTS & METHODS IN PHYSICS RESEARCH SECTION A-ACCELERATORS SPECTROMETERS DETECTORS AND ASSOCIATED EQUIPMENT	Pan, Qiangyan; Wang, Qisheng; Wang, Zhijun	735	584
159	Template-Free Synthesis of Hematite Photoanodes with Nanostructured ATO Conductive Underlayer for PEC Water Splitting	ACS APPLIED MATERIALS & INTERFACES	Wang, Degao; Zhang, Yuying; Wang, Jianqiang	6	36
160	Elliptic Flow Splitting as a Probe of the QCD Phase Structure at Finite Baryon Chemical Potential	PHYSICAL REVIEW LETTERS	Xu, Jun; Song, Taesoo; Ko, Che Ming	112	12301
161	Gold nanostructures encoded by non-fluorescent small molecules in polyA-mediated nanogaps as universal SERS nanotags for recognizing various bioactive molecules	CHEMICAL SCIENCE	Zhao, Bin; Shen, Jianlei; Chen, Shixing	5	4460
162	Influence of polyethylene glycol coating on biodistribution and toxicity of nanoscale graphene oxide in mice after intravenous	INTERNATIONAL JOURNAL OF	Li, Bo; Zhang, Xiao-Yong; Yang, Jian-Zhong	9	4697

	injection	NANOMEDICINE			
163		INPC 2013 - INTERNATIONAL NUCLEAR PHYSICS CONFERENCE, VOL. 2	Ma, Yu-Gang;;	66	4020
164	Detecting the anti-hypertriton and anti-helium-4 from the RHIC Aerosol inhalation exposure study of respiratory toxicity induced by 20 nm anatase titanium dioxide nanoparticles	TOXICOLOGY RESEARCH	Yin, Jilei; Kang, Cheng; Li, Yufeng	3	367
165	Pore Scale Thermal Hydraulics Investigations of Molten Salt Cooled Pebble Bed High Temperature Reactor with BCC and FCC Configurations	SCIENCE AND TECHNOLOGY OF NUCLEAR INSTALLATIONS	Song, Shixiong; Cai, Xiangzhou; Liu, Yafen		589895
166		14TH INTERNATIONAL CONFERENCE ON STRANGENESS IN QUARK MATTER (SQM2013)	Ma, Guo-Liang;;	509	12074
	Tomography of QGP with jet asymmetries				
167	First-principles study of intergranular embrittlement induced by Te in the Ni Sigma 5 grain boundary	COMPUTATIONAL MATERIALS SCIENCE	Liu, Wenguan; Han, Han; Ren, Cuilan	88	22
168	Built-up superhydrophobic composite membrane with carbon nanotubes for water desalination	RSC ADVANCES	Zhang, Bowu; Liu, Lixia; Xie, Siyuan	4	16561
169	Flexible graphene fibers prepared by chemical reduction-induced self-assembly	JOURNAL OF MATERIALS CHEMISTRY A	Li, Jihao; Li, Jingye; Li, Linfan	2	6359
170	Cellulose nanofibrils generated from jute fibers with tunable polymorphs and crystallinity	JOURNAL OF MATERIALS CHEMISTRY A	Yu, Liangbo; Lin, Jinyou; Tian, Feng	2	6402
171	Designs of fullerene-based frameworks for hydrogen storage	JOURNAL OF MATERIALS CHEMISTRY A	Gao, Yi; Wu, Xiaojun; Zeng, Xiao Cheng	2	5910
172	Nanoscale optical probes for cellular imaging	CHEMICAL SOCIETY REVIEWS	Xu, Hui; Li, Qian; Wang, Lihua	43	2650
173	Ultra-light, compressible and fire-resistant graphene aerogel as a highly efficient and recyclable absorbent for organic liquids	JOURNAL OF MATERIALS CHEMISTRY A	Li, Jihao; Li, Jingye; Meng, Hu	2	2934
174	Functional nanoprobes for ultrasensitive detection of biomolecules: an update	CHEMICAL SOCIETY REVIEWS	Xu, Jing-Juan; Zhao, Wei-Wei; Song, Shiping	43	1601
175	Theoretical advances of the structures and catalytic activities of small-sized gold nanoclusters	CHINESE SCIENCE BULLETIN	Li, Yadong; Gao, Yi;	59	239
176	Thermal Conductivity of the Partly Covered Inner Tube in a Double-Walled Carbon Nanotube with Varied Coverage Ratios	CHINESE PHYSICS LETTERS	Pan Rui-Qin; Xu Zi-Jian; Dai Cui-Xia	31	16501
177	Simulation of energy scan of pion interferometry in central Au plus Au collisions at relativistic energies	CHINESE PHYSICS C	Zhang Zheng-Qiao; Zhang Song; Ma Yu-Gang	38	14102
178	Optimization of a multilayer Laue lens system for a hard x-ray	JOURNAL OF OPTICS	Jiang, Hui; Wang, Hua;	16	15002

	nanoprobe		Mao, Chengwen		
179	Design of an ultrahigh-energy-resolution and wide-energy-range soft X-ray beamline	JOURNAL OF SYNCHROTRON RADIATION	Xue, L.; Reininger, R.; Wu, Y. -Q.	21	273
180	Nanoprobes for super-resolution fluorescence imaging at the nanoscale	SCIENCE CHINA-CHEMISTRY	Hou ShangGuo; Liang Le; Deng SuHui	57	100
181	Radiation oxidation and subsequent thermal curing of polyacrylonitrile fiber	RADIATION PHYSICS AND CHEMISTRY	Liu, Weihua; Wang, Mouhua; Xing, Zhe	94	9
182	gamma-ray irradiation effects on graphene oxide in an ethylenediamine aqueous solution	RADIATION PHYSICS AND CHEMISTRY	Li, Jihao; Zhang, Bowu; Li, Linfan	94	80
183	Pre-irradiation induced emulsion co-graft polymerization of acrylonitrile and acrylic acid onto a polyethylene nonwoven fabric	RADIATION PHYSICS AND CHEMISTRY	Liu, Hanzhou; Yu, Ming; Ma, Hongjuan	94	129
184	EFFECTS OF CARBON NANOTUBES ON RAT LIVER AND BRAIN	NANO	Wang, Fu-De; Cao, Ling-Ling; Jin, Chan	9	1450083
185	Beam Energy Dependence of Moments of the Net-Charge Multiplicity Distributions in Au plus Au Collisions at RHIC	PHYSICAL REVIEW LETTERS	Adamczyk, L.; Adkins, J. K.; Agakishiev, G.	113	92301
186	Improving B-cell epitope prediction and its application to global antibody-antigen docking	BIOINFORMATICS	Krawczyk, Konrad; Liu, Xiaofeng; Baker, Terry	30	2288
187	Measurement of Longitudinal Spin Asymmetries for Weak Boson Production in Polarized Proton-Proton Collisions at RHIC	PHYSICAL REVIEW LETTERS	Adamczyk, L.; Adkins, J. K.; Agakishiev, G.	113	72301
188	J/psi production at low p(T) in Au plus Au and Cu plus Cu collisions at root s(NN)=200 GeV with the STAR detector	PHYSICAL REVIEW C	Adamczyk, L.; Adkins, J. K.; Agakishiev, G.	90	24906
189	Initial performance of the CUORE-0 experiment	EUROPEAN PHYSICAL JOURNAL C	Artusa, D. R.; Avignone, F. T., III; Azzolini, O.	74	2956
190	Beam-Energy Dependence of Charge Separation along the Magnetic Field in Au plus Au Collisions at RHIC	PHYSICAL REVIEW LETTERS	Adamczyk, L.; Adkins, J. K.; Agakishiev, G.	113	52302
191	Suppression of Upsilon production in d plus Au and Au plus Au collisions at root S-NN=200 GeV	PHYSICS LETTERS B	Adamczyk, L.; Adkins, J. K.; Agakishiev, G.	735	127
192	Dielectron Mass Spectra from Au plus Au Collisions at root s(NN)=200 Ge V	PHYSICAL REVIEW LETTERS	Adamczyk, L.; Adkins, J. K.; Agakishiev, G.	113	22301
193	Distribution of Graphene Oxide and TiO2-Graphene Oxide Composite in A^{549} Cells	BIOLOGICAL TRACE ELEMENT RESEARCH	Jin, Chan; Wang, Fude; Tang, Ying	159	393
194	Beam-Energy Dependence of the Directed Flow of Protons, Antiprotons, and Pions in Au plus Au Collisions	PHYSICAL REVIEW LETTERS	Adamczyk, L.; Adkins, J. K.; Agakishiev, G.	112	162301
195	Measurement of charge multiplicity asymmetry correlations in high-energy nucleus-nucleus collisions at root S-NN=200 GeV	PHYSICAL REVIEW C	Adamczyk, L.; Adkins, J. K.; Agakishiev, G.	89	44908
196	Event-plane-dependent dihadron correlations with harmonic *v*(n) subtraction in Au plus Au collisions at v root sNN=200 GeV	PHYSICAL REVIEW C	Agakishiev, H.; Aggarwal, M. M.; Ahammed, Z.	89	41901
197	Charge-changing cross sections of Ne-30, Na-32,Na-33 with a proton target	PHYSICAL REVIEW C	Ozawa, A.; Moriguchi, T.; Ohtsubo, T.	89	44602

198	Jet-Hadron Correlations in root s(NN)=200 GeV p plus p and Central Au plus Au Collisions	PHYSICAL REVIEW LETTERS	Adamczyk, L.; Adkins, J. K.; Agakishiev, G.	112	122301
199	Determination of the electronic structure of atoms and molecules in the ground state: Measurement of molecular hydrogen by high-resolution x-ray scattering	PHYSICAL REVIEW A	Liu, Ya-Wei; Mei, Xiao-Xun; Kang, Xu	89	14502
200	Energy Dependence of Moments of Net-Proton Multiplicity Distributions at RHIC	PHYSICAL REVIEW LETTERS	Adamczyk, L.; Adkins, J. K.; Agakishiev, G.	112	32302
201	Cooling for SC Devices of Test Cryomodule for ADS Injector II at IMP	ADVANCES IN CRYOGENIC ENGINEERING	Wang, L.; Wang, S. Y.; Sun, S.	1573	1333
202	Cryogenic System with GM Cryocooler for Krypton, Xenon Separation from Hydrogen-Helium Purge Gas	ADVANCES IN CRYOGENIC ENGINEERING	Chu, X. X.; Zhang, M. M.; Zhang, D. X.	1573	1638
203	Giant dipole resonance as a fingerprint of α clustering configurations in C^{12} and O^{16}	Physical Review Letters	He, W.B.; Ma, Y.G.; Cao, X.G.	113	3
204	Jet-hadron correlations in sNN =200GeV p+p and central Au+Au collisions	Physical Review Letters	STAR	112	12
205	Observation of D0 meson nuclear modifications in Au+Au collisions at sNN =200 GeV	Physical Review Letters	STAR	113	14
206	Dielectron mass spectra from Au+Au collisions at sNN =200 GeV	Physical Review Letters	STAR	113	2
207	Beam energy dependence of moments of the net-charge multiplicity distributions in Au+Au collisions at RHIC	Physical Review Letters	STAR	113	9
208	Beam-energy dependence of the directed flow of protons, antiprotons, and pions in au+au collisions	Physical Review Letters	STAR	121	16
209	Beam-energy dependence of charge separation along the magnetic field in Au+Au collisions at RHIC	Physical Review Letters	STAR	113	5
210	Oxygen vacancy-induced room-temperature ferromagnetism in D-D neutron irradiated single-crystal TiO_2 (001) rutile	Chinese Physics B	Xu, Nan-Nan; Li, Gong-Ping; Pan, Xiao-Dong	23	
211	Effect of flibe molten salt on cell-homogenized group cross-section in PB-FHR	Yuanzineng Kexue Jishu/Atomic Energy Science and Technology	Qin, Wei; Mei, Long-Wei; Wang, Xiao-He	48	673
212	Electronic decay and fragmentation dynamics of iodomethane, multiply core-ionized by photoabsorption of intense XFEL pulses	Journal of Physics: Conference Series	Motomura, K.; Kukk, E.; Wada, S.	488	
213	Charge migration and molecular dissociation following multiphoton multiple ionization of iodine-substitute molecules by X-Ray free-electron laser pulses from SACLA	Optics InfoBase Conference Papers	Motomura, K.; Kukk, E.; Nagaya, K.		
214	Study on the Cr deposition and poisoning phenomenon at $(La_{0.6}Sr_{0.4})(Co_{0.2}Fe_{0.8})O^{3-\delta}$ electrode of solid oxide fuel cells by transmission X-ray microscopy	International Journal of Hydrogen Energy	Chen, Xinbing; Jin, Chan; Zhao, Ling	39	15728
215	Turbulent transport effect of delayed neutron precursor in molten salt fast reactor	Yuanzineng Kexue Jishu/Atomic Energy	Cheng, Mao-Song; Dai, Zhi-Min;	48	131

216	Corrugated pipe as beam energy stabilizer	Science and Technology Qiangjiguang Yu Lizishu/High Power Laser and Particle Beams	Zhang, Meng; Li, Xuan; Deng, Haixiao	26	
217	Magnetic properties of bulk polycrystalline Pr1-xNdx (x = 0, 0.8)FeB permanent magnets	Chinese Physics B	He, Yong-Zhou; Wu, Hong-Ping; Zou, Zhi-Qiang	23	
218	The design study of an ultra-high power EB/X-ray conversion facility	Journal of Electron Spectroscopy and Related Phenomena	He, Zi-Feng; Li, Deming; Huang, Jian-Ming	196	152
219	Pt_2Cl_8 2- dimer formation of [Bmim] 2$PtCl_4$ ionic liquid when confined in silica nanopores	Journal of Physical Chemistry C	Li, Cheng; Wang, Yaxing; Guo, Xiaojing	118	3140
220	Synchronous measurement of beam orbit and relative environment parameters	Qiangjiguang Yu Lizishu/High Power Laser and Particle Beams	Lai, Longwei; Zhou, Weimin; Leng, Yongbin	26	
221	Spectrum of multi-bunch beam position model and parameter acquisition algorithm	Qiangjiguang Yu Lizishu/High Power Laser and Particle Beams	Yang, Yong; Leng, Yongbin; Wang, Baopeng	26	
222	Application of model independent analysis-based method to accelerator bunch-by-bunch research	Qiangjiguang Yu Lizishu/High Power Laser and Particle Beams	Zhang, Ning; Yang, Yong; Leng, Yongbin	26	
223	Atomic structure of $Pd_{81}Si_{19}$ glassy alloy under high pressure	Acta Materialia	Lou, H.B.; Xiong, L.H.; Ahmad, A.S.	81	420
224	Highly selective hydrogenation of phenol and derivatives over Pd catalysts supported on SiO_2 and γ -Al_2O_3 in aqueous media	Catalysis Communications	Cheng, Ling; Dai, Qiguang; Li, Hua	57	23
225	Highly selective hydrogenation of phenol and derivatives over Pd catalysts supported on SiO_2 and γ -Al_2O_3 in aqueous media	Catalysis Communications	Cheng, Ling; Dai, Qiguang; Li, Hua	57	23
226	Investigation on performance of gas separators in gas removal system for MSR	Hedongli Gongcheng/Nuclear Power Engineering	Zhang, Nana; Yan, Changqi; Sun, Licheng	35	137
227	SSRF Radiation dose interlock PLC system with error records	Yuanzineng Kexue Jishu/Atomic Energy Science and Technology	Guo, Chun-Long; Xu, Xun-Jiang; Shen, Wei-Zu	48	175
228	Ambiguous proximity distribution	Lecture Notes in Computer Science (including subseries Lecture Notes in Artificial Intelligence and Lecture Notes in Bioinformatics)	Wang, Quanquan; Li, Yongping;	8589 LNAI	409
229	Characteristic of bubble breakup in venturi-type bubble generator	Yuanzineng Kexue Jishu/Atomic Energy Science and Technology	Tang, Wen-Cai; Yan, Chang-Qi; Sun, Li-Cheng	48	844
230	Detection of complex vascular system in bamboo node by X-ray μ CT imaging technique	Holzforschung	Peng, Guanyun; Jiang, Zehui; Liu, Xing'e	68	223

231	Overview of organically bound tritium in plant for atmospheric release of tritium from nuclear installation	Yuanzineng Kexue Jishu/Atomic Energy Science and Technology	Shen, Hui-Fang; Qian, Yuan; Du, Lin	48	1766
232	First-principles study of intergranular embrittlement induced by Te in the Ni Σ 5 grain boundary	Computational Materials Science	Liu, Wenguan; Han, Han; Ren, Cuilan	88	22
233	Dynamic covalent diblock copolymers: Instructed coupling, micellation and redox responsiveness	Macromolecules	Yang, Qinglai; Bai, Ling; Zhang, Yuanqing	47	7431
234	Charge asymmetry dependency of π /K anisotropic flow in U+U SNN = 193 GeV and Au+Au SNN = 200 GeV collisions at STAR	Journal of Physics: Conference Series	Shou, Qi-Ye;;	509	
235	High performance Pt monolayer catalysts produced via core-catalyzed coating in ethanol	ACS Catalysis	Zhang, Yu; Hsieh, Yu-Chi; Volkov, Vyacheslav	4	738
236	Effect of 110 keV electrons on the deformation mechanisms of low density polyethylene	Polymer Degradation and Stability	Rui, Erming; Yang, Jianqun; Li, Xingji	109	59
237	Role of wave packet width in quantum molecular dynamics in fusion reactions near barrier	Journal of Physics: Conference Series	Cao, X.G.; Ma, Y.G.; Zhang, G.Q.	515	
238	Astrophysics studies relevant to stellar x-ray bursts	AIP Conference Proceedings	He, J.J.; Hu, J.; Zhang, L.Y.	1594	176
239	Design and fabrication of cascaded X-ray planar parabolic compound refractive lens	Wuli Xuebao/Acta Physica Sinica	Fu, Ming-Lei; Le, Zi-Chun; Zhou, Han-Qing	63	
240	Flexible and wire-shaped micro-supercapacitor based on Ni(OH) 2-nanowire and ordered mesoporous carbon electrodes	Advanced Functional Materials	Dong, Xiaoli; Guo, Ziyang; Song, Yanfang	24	3405
241	Graphite intercalation compounds (GICs): A new type of promising anode material for lithium-ion batteries	Advanced Energy Materials	Wang, Fei; Yi, Jin; Wang, Yonggang	4	
242	Comparison between air-cooled and water-cooled schemes for the passive residual heat removal system of molten salt reactor	Hedongli Gongcheng/Nuclear Power Engineering	Sun, Lu; Sun, Licheng; Yan, Changqi	35	18
243	X-ray absorption spectroscopy study on the thermal and hydrazine reduction of graphene oxide	Journal of Electron Spectroscopy and Related Phenomena	Liang, Xianqing; Wang, Yu; Zheng, Huiyuan	196	89
244	Photoinduced electron transfer between 2-methylanthraquinone and triethylamine in an ionic liquid: Time-resolved EPR and transient absorption spectroscopy study	Spectrochimica Acta - Part A: Molecular and Biomolecular Spectroscopy	Zhu, Guanglai; Wang, Yu; Fu, Haiying	137	148
245	Colloidal processing of $Mg(OH)_2$ aqueous suspensions using sodium polyacrylate as dispersant	Industrial and Engineering Chemistry Research	Tong, Kefeng; Song, Xingfu; Xiao, Guoping	53	4755
246	In situ synchrotron X-ray imaging on morphological evolution of dendrites in SnBi hypoeutectic alloy under electric currents	Applied Physics A: Materials Science and Processing	Wang, Tongmin; Zhu, Jing; Kang, Huijun	117	1059
247	The application of multiscale quasi 4D CT to the study of $SrCrO_4$ distributions and the development of porous networks in epoxy-based primer coatings	Progress in Organic Coatings	Hughes, A.E.; Trinchi, A.; Chen, F.F.	77	1946
248	Progresses of X-ray imaging methodology and its applications	Guangxue Xuebao/Acta	Xiao, Tiqiao; Xie, Honglan;	34	

	at Shanghai synchrotron radiation facility	Optica Sinica	Deng, Biao		
249	Elliptic flow difference between particles and antiparticles and the EoS of baryon-rich matter	Acta Physica Polonica B, Proceedings Supplement	Ko, Che Ming; Chen, Lie-Wen; Greco, Vincenzo	7	183
250	Substitutional carbon doping of hexagonal multi-walled boron nitride nanotubes (h-MWBNNTs) via ion implantation	Journal of Nanoparticle Research	Ahmad, Ishaq; Usman, M.; Rabab Naqvi, S.	16	
251	Benchmark data of squared form factors for various atoms and molecules by inelastic x-ray scattering method	Journal of Physics: Conference Series	Kang, Xu; Yang, Ke; Zhu, Lin-Fan	488	
252	Surface double-layer structure in (110) oriented $BiFeO_3$ thin film	Applied Physics Letters	Yang, Tieying; Wang, Can; Zhang, Xingmin	105	
253	Simulation study of all optical-FEL based on the laser wakefield accelerator	Zhongguo Jiguang/Chinese Journal of Lasers	Wang, Guanglei; Yao, Haifeng; Zhang, Tong	41	
254	Optimization design of photo-injector using genetic algorithm	Qiangjiguang Yu Lizishu/High Power Laser and Particle Beams	Zhang, Meng; Liao, Lang;	26	
255	Three dimensional visualization of engineered bone and soft tissue by combined x-ray micro-diffraction and phase contrast tomography	Physics in Medicine and Biology	Cedola, Alessia; Campi, Gaetano; Pelliccia, Daniele	59	189
256	Highly efficient $Sr_3Y_2(Si_3O_9)_2:Ce^{3+},Tb^{3+}/Mn^{2+}/Eu^{2+}$phosphors for white LEDs: Structure refinement, color tuning and energy transfer	RSC Advances	Zhang, Mengfei; Liang, Yujun; Tang, Rui	4	40626
257	The study of electron energy loss spectroscopy of Ni-4.8at%Ti alloy	Applied Mechanics and Materials	Yang, Wei Guo; Li, De Hui; Cai, Hong Jin	446	8

附录 3

2013-2014 年专利授权一览表

Patents in 2013-2014

2013

No.	专利名称	申请号	申请日	授权日	类型	发明人
1	一种质子交换膜及其制备方法	200910052176.0	2009/5/27	2013/3/20	发明	李景烨 李林繁 邓波 谢雷东 虞鸣 吉玉玲 于洋
2	一种高分子滤膜的亲水性改性方法及所得产品	200910194727.7	2009/8/28	2013/7/3	发明	李景烨 邓波 于洋 李林繁 虞鸣 杨璇璇 张伯武
3	一种织物或非织造布的亲水性改性方法及所得产品	200910194726.2	2009/8/28	2013/3/20	发明	李景烨 邓波 虞鸣 于洋 李林繁
4	一种聚偏氟乙烯接枝甲基丙烯酸缩水甘油酯的方法	200910195300.9	2009/9/8	2013/11/6	发明	王敏 张敬 马红娟 李景烨 邓波 虞鸣
5	锝标记雌二醇类衍生物及其参照化合物及其制备方法、应用和其中间体	200910196336.9	2009/9/24	2013/2/20	发明	沈玉梅 黄立梁 朱华
6	一种含氟接枝聚合物的接枝率的测定方法	200910196785.3	2009/9/29	2013/11/6	发明	李景烨 邓波 李林繁 谢雷东 虞鸣 于洋 张伯武 杨璇璇
7	一种接枝改性高分子材料及其制备方法	200910197597.2	2009/10/23	2013/11/6	发明	李景烨 樊春海 虞鸣 张伯武 裴昊 邓波 李林繁
8	一种提高单个 DNA 分子 AFM 图像对比度的方法	200910197713.0	2009/10/27	2013/5/8	发明	李宾 胡钧
9	超疏水织物或无纺布及其制备方法	201010200425.9	2010/6/12	2013/12/4	发明	李景烨 邓波 蔡仁 于洋 李林繁 虞鸣
10	一种 99mTc 配合物、其制备方法、中间体及其应用	201010230680.8	2010/7/20	2013/7/3	发明	沈玉梅 许晓平 张元庆 朱华 王旭东
11	一种纳米金-氧化石墨烯纳米复合材料的制备方法	201010515131.5	2010/10/21	2013/7/3	发明	张玉杰 耿马可 张欢 李江 樊春海 黄庆
12	数字信号的自动增益控制方法	201010521856.5	2010/10/27	2013/1/16	发明	赖龙伟 冷用斌 韩扣兄 张宁
13	超疏水织物或超疏水无纺布,及其制备方法	201010619389.X	2010/12/30	2013/1/16	发明	李景烨 邓波 李林繁 虞鸣 蒋海青 于洋
14	单个生物分子反应实时原位表征方法	201110069865.X	2011/3/22	2013/7/3	发明	吴娜 李宾 胡钧
15	靶向分子受体检测方法、聚酰胺-氨衍生物及其制备方法	201110152831.7	2011/6/8	2013/4/17	发明	孙艳红 张元庆 许晓平 沈玉梅 林俊 郭智 王华 崔巍 杨光
16	同步辐射原位在线纤维纺丝设备	201110173600.4	2011/6/24	2013/4/17	发明	李秀宏 边风刚 柳义 李志军 王玉柱 周平 王劼
17	接枝改性高分子材料及其制备方法和应用	201110255378.2	2011/8/22	2013/12/18	发明	李景烨 李林繁 邓波 虞鸣
18	一种还原氧化石墨烯及其制备方法	201110243292.8	2011/8/23	2013/7/24	发明	李景烨 张伯武 黄庆 于洋 李林繁 邓波 虞鸣

19	预辐照 PVDF 接枝 NVP 的制备方法和所制得的共聚物	201110346202.8	2011/11/4	2013/8/28	发明	侯铮迟 陈利芳 陆晓峰
20	一种碳纳米材料-棉纤维复合导电材料及其制备方法和用途	201110360286.0	2011/11/15	2013/11/6	发明	李景烨 邓波 张伯武 王自强 李林繁 虞鸣 蒋海青
21	一种改性超高分子量聚乙烯纤维及其制备方法	201110388139.4	2011/11/29	2013/12/18	发明	王谋华 吴国忠 邢哲 刘伟华
22	一种涉及 DNA 折纸的方法及其结构和应用	201110451573.2	2011/12/27	2013/12/18	发明	吴娜 李宾 胡钧
23	熔盐电化学实验装置	201210003346.8	2012/1/6	2013/12/18	发明	左勇 黄鹤 李晓云 王敏
24	一种高温同步辐射原位研究装置	201210014460.0	2012/1/17	2013/8/14	发明	何上明 李爱国 闫帅 李晓丽 林建波 邹杨 余笑寒
25	加热装置	201210034327.1	2012/2/15	2013/8/28	发明	何上明 李爱国 闫帅 李晓丽 林建波 邹杨 余笑寒
26	一种海水提铀用螯合纤维吸附剂及其制备方法	201210076705.2	2012/3/21	2013/12/18	发明	王谋华 吴国忠 邢哲 刘伟华 张文礼
27	一种控制系统网络架构	201220143366.0	2012/4/6	2013/1/23	实用新型	蔡浩军 沈立人 陈建锋 缪海峰 丁建国 蒋舸扬 万天敏 胡守明
28	一种低温液氮远距离输送管道	201220165870.0	2012/4/18	2013/1/23	实用新型	苏东 朱卫华 郑永培 杨建萍 杨东
29	一种荧光靶探测器	201220198995.3	2012/5/3	2013/3/13	实用新型	徐慧超 周剑英 龚培荣 刘昕 张永立 蒋建国 朱周侠
30	PVDF-g-PVP 接枝共聚物的制备方法及所得的接枝共聚物	201210151999.0	2012/5/15	2013/12/4	发明	侯铮迟 秦强
31	组合式辐射防护棚屋	201220235837.0	2012/5/22	2013/6/12	实用新型	朱卫华 杨东 黄正国 刘小栋 乌振亮
32	箱式电源的状态监控系统	201220235808.4	2012/5/22	2013/3/13	实用新型	吴盈锋 胡纯
33	液体样品池	201220238306.7	2012/5/23	2013/3/13	实用新型	赵红卫 张建兵 武宇亭 杨航 李晴暖
34	紧凑型双向兼用条带激励电极	201220260246.9	2012/6/4	2013/1/23	实用新型	袁任贤 俞路阳 周伟民 阎映炳 陈杰 陈之初 叶恺容 冷用斌
35	液体样品池	201220417598.0	2012/8/21	2013/3/13	实用新型	赵红卫 杨航 张建兵 亓文鹏
36	一种抑制信号振铃的滤波器	201220524955.3	2012/10/12	2013/3/27	实用新型	周伟民 冷用斌 叶恺容 俞路阳 袁任贤
37	高温熔盐泵轴密封装置	201220581425.2	2012/11/6	2013/5/8	实用新型	黎忠 傅远 谢雷东 唐忠锋
38	一种高温介质泵热屏蔽装置	201220656612.2	2012/12/3	2013/7/3	实用新型	黎忠 傅远 黄建平 张健宇 林良程 毛文玉 王纳秀 王晓 李波 陆世瑞
39	一种采用碲化镉量子点清除帕金森模式细胞中产生的α-核突触蛋白的方法及其应用	201210586127.7	2012/12/28	2013/12/18	发明	黄庆 陈楠 李晓明 魏敏 樊春海
40	电解槽	201320023881.X	2013/1/16	2013/7/24	实用新型	龙德武 黄卫 蒋锋 李晴暖

41	一种双重密封法兰	201320025684.1	2013/1/17	2013/7/24	实用新型	傅远 张钦华 黎忠 谢雷东 唐忠锋 杨新梅 孔祥波 朱海华
42	一种高频感应流体加热器	201320025427.8	2013/1/17	2013/7/24	实用新型	黎忠 谢雷东 傅远 封自强 张钦华 唐忠锋 杨新梅 李岩 解明强 邹欣
43	反应器及包括其的反应系统	201320049949.1	2013/1/29	2013/7/24	实用新型	周金豪 张焕琦 程治强 李杨娟 戴建兴 李晴暖 吴国忠
44	一种多通道印刷电极阵列芯片	201320185459.4	2013/4/12	2013/11/6	实用新型	樊春海 宋世平 邓王平 李建永
45	一种溶液样品蠕动实验装置	201320203183.8	2013/4/19	2013/11/6	实用新型	边风刚 李怡雯 王劼
46	一种大气中不同形态氚的采样设备	201320454218.5	2013/7/29	2013/12/18	实用新型	刘卫 包广粮 吴勐 钱渊 刘京 张东勋 黄豫 楚鑫新 杜林

2014

No.	专利名称	申请号	申请日	授权日	类型	发明人
1	氧化石墨烯的应用	201010546630.0	2010/11/16	2014/8/27	发明	米丽娟 张益 郭守武 胡钧
2	对功能分子进行 18F 标记的方法	201110152843.X	2011/6/8	2014/7/16	发明	张岚 施玲丽 李剑波 王成 周伟
3	一种防烫伤纺织品及其制备方法	201110303495.1	2011/10/10	2014/7/16	发明	李景烨 于洋 邓波 李林繁 虞鸣 蒋海青
4	一种多通道电路不对称性的校准方法	201210044556.1	2012/2/24	2014/7/24	发明	易星 冷用斌
5	偕胺肟基螯合聚丙烯腈纤维及其制备方法和应用	201210048187.3	2012/2/28	2014/7/16	发明	吴国忠 王谋华 张文礼 刘伟华 邢哲 叶泽文 何亚星
6	一种光强探测电离室	201210058796.7	2012/3/7	2014/11/26	发明	边风刚 王劼 李秀宏 王玉柱 田丰 周平
7	同步辐射红外显微镜的数值孔径匹配装置	201210096476.0	2012/4/1	2014/3/5	发明	佟亚军 陈敏 吉特 张增艳 肖体乔
8	一种对化合物进行[18F]标记的方法	201210103511.7	2012/4/10	2014/11/19	发明	张岚 贾丽娜 李剑波 施玲丽
9	实现单色器与谱学显微镜通信的接口系统和方法	201210163250.8	2012/5/22	2014/7/23	发明	刘平 王勇 郑丽芳
10	多维调整平台	201210174581.1	2012/5/30	2014/7/16	发明	姜政 李丽娜 黄宇营 魏向军 张硕 高倩
11	核用电缆无卤阻燃护套料、电缆护套，制备方法和应用	201210352803.4	2012/9/20	2014/7/16	发明	张聪 李景烨 李林繁 蒋海青 黄卫兵 张阔
12	无卤无红磷阻燃热收缩材料、热收缩管，制备方法和应用	201210356195.4	2012/9/20	2014/11/19	发明	张聪 李景烨 李林繁 蒋海青 黄卫兵 张阔

13	核用电缆无卤阻燃绝缘料、电缆绝缘层，制备方法和应用	201210356203.5	2012/9/20	2014/8/27	发明	张聪 李景烨 李林繁 蒋海青 黄卫兵 张阔
14	一种水性的聚四氟乙烯材料及其制备方法和用途	201210356207.3	2012/9/20	2014/11/19	发明	吴国忠 杨常桥 钟磊 王谋华 刘伟华 邢哲
15	高温熔盐泵轴密封装置	201210437444.2	2012/11/6	2014/11/19	发明	黎忠 傅远 谢雷东 唐忠锋
16	一种基于 DNA 三维纳米结构探针的电化学 miRNA 检测方法	201210445958.2	2012/11/9	2014/7/16	发明	樊春海 闻艳丽 林美华
17	一种高频感应流体加热器	201310017801.4	2013/1/17	2014/11/26	发明	黎忠 谢雷东 傅远 封自强 张钦华 唐忠锋 杨新梅 李岩 解明强 邹欣
18	反应器及包括其的反应系统和其内衬的制造方法	201310034098.8	2013/1/29	2014/12/24	发明	周金豪 张焕琦 程治强 李杨娟 戴建兴 李晴暖 吴国忠
19	蒸馏装置	201310050642.8	2013/2/7	2014/12/24	发明	付海英 窦强 杨洋 王子豪 周金豪 李晴暖
20	一种用于低能重离子的束团参数测量系统，以及一种频率谐振选能能量测量方法	201310161430.7	2013/5/3	2014/12/24	发明	袁任贤 周伟民 冷用斌 陈之初 陈杰 叶恺容 俞路阳 阎映炳
21	^{3}H 和 ^{14}C 的采样设备	201320436819.3	2013/7/22	2014/3/5	实用新型	刘卫 吴勐 钱渊 包广粮 杜林 曾友石 皮力
22	一种有机氚的氧化取样设备	201320457002.4	2013/7/29	2014/3/5	实用新型	刘卫 钱渊 朱海云 杜林 吴勐 吴胜伟 黄悟真 李华 董墨 刘邃庆
23	一种电子束低温发热测量系统	201320811554.0	2013/12/10	2014/7/16	实用新型	崔剑 许皆平 张正臣 李明 徐俊杰 郁静芳 樊勇 季现凯 江勇
24	一种溶液样品蠕动实验系统	201420051207.7	2014/1/26	2014/12/3	实用新型	边风刚 李怡雯 洪春霞 王劼
25	一种用于单胞超导腔内表面化学抛光的磁搅拌装置	201420233937.9	2014/5/8	2014/11/19	实用新型	马震宇 刘建飞 侯洪涛 封自强 毛冬青 罗琛
26	一种用于超导腔内表面化学抛光的封闭式循环系统	201420234405.7	2014/5/8	2014/11/19	实用新型	马震宇 刘建飞 侯洪涛 封自强 毛冬青 罗琛
27	一种用于产生类三角波励磁电流的扫描电源	201420343827.8	2014/6/25	2014/11/26	实用新型	李瑞 郁亚男 黄毛毛 胡志敏 武万锋
28	一种交直流电流传感器	201420413079.6	2014/7/24	2014/12/24	实用新型	王东兴 卢宋林 李瑞 朱燕燕 胡志敏 黄毛毛 刘洪 武万锋 谭松清 郭春龙 许瑞年

附录 4

2013-2014 国际学术会议报告表

Presentations by SINAP Scientists at International Scientific Meetings in 2013-2014

2013

No.	会议全称	报告名称	报告人	报告类别	报告学科领域	时间	地点
1	第 28 届国际辐射化学 Miller 会议	Successful grafting of acrylonitrile onto ultra-high molecular weight polyethylene fiber and its application in uranium extraction from seawater	吴国忠	大会报告	核技术在工、农业和医学中的应用	2013-03-13	以色列
2	第 28 届国际辐射化学 Miller 会议	Preparation of polymer decorated graphene oxide by γ -ray induced graft polymerization	张伯武	展板报告	核技术在工、农业和医学中的应用	2013-03-13	以色列
3	第 28 届国际辐射化学 Miller 会议	Super-hydrophobic cotton fabrics prepared by radiation induced graft polymerization technique	李景烨	展板报告	核技术在工、农业和医学中的应用	2013-03-13	以色列
4	第 25 届固体中原子碰撞国际会议	Harvesting and Stroing Laser Irradiation Energy with Graphene-Cu Compound Structure	巩文斌	展板报告	能源	2012-10-20	日本
5	先进同步辐射光和材料科学国际研讨会	The introduce of Shanghai Synchrotron Radiation Faciality	邰仁忠	大会报告	同步辐射技术及其应用	2013-03-12	日本
6	第二届中国-南非核物理联合论坛	Explore the limit of exotic nuclear structure by heavy ion collision at intermediate energy	曹喜光	大会报告	核物理	2012-12-02	南非
7	2012 年国际束测设备会议	上海光源轨道反馈进展	姜伯承	分会报告	束测	2012-10-01	日本
8	2013 年度低温工程/国际低温材料会议	Cryogenic system with GM cryocooler for krypton, xenon separation from hydrogen-helium purge gas	楚鑫新	展板报告	制冷	2013-06-16	美国
9	CSIRO 计算与模拟科学及 e-研究年会及研讨会	上海光源 X 射线成像中的图像重构及定量分析现状	肖体乔	大会报告	计算模拟方法与应用	2013-03-19	澳大利亚
10	第 3 届国际生物传感技术大会	Gold nanaopaticle-based DNA detection technology	宋世平	分会报告	生物物理化学	2013-05-11	西班牙
11	ARW2013 国际会议	ACCELERATORS and RELIABILITY AT SINAP	殷立新	大会报告	束流物理与加速器技术	2013-04-13	澳大利亚

12	ARW2013 国际会议	Improvement in stability and reliability for the storage ring RF operation of SSRF	赵申杰	大会报告	束流物理与加速器技术	2013-04-13	澳大利亚
13	美国 2013 物理学会会议并访问加州大学	Understanding the quark-gluon plasma via phi-meson analysis and the discovery of antihypertriton	陈金辉	大会报告	核物理	2013-04-12	美国
14	钍基熔盐堆国际技术研讨会	钍基熔盐堆核能系统系统（TMSR）研发现状	徐洪杰	大会报告	核技术及其应用	2013-04-15	日本
15	中美能源科学合作第二届协调委员会会议	上海光源工程和美方合作情况及未来合作计划	赵振堂	大会报告	束流物理与加速器技术	2013-05-05	美国
16	第 142 届 TMS（矿物、金属和材料协会）2013 年会	Introduction of Shanghai Synchrotron Radiation Facility and One Scientific Case Focused on Deformation Behavior of Nanostructured Cu/Ag Multilayered Films at Beamline 14B1	李丽	分会报告	金属材料的形变与损伤	2013-03-02	美国
17	访问加利福利亚大学并参加 ACS 全国第 245 次会议暨展览会	Gold nanoparticle-based DNA detection technology	樊春海	分会报告	生物无机化学	2013-04-03	美国
18	访问加利福利亚大学并参加 ACS 全国第 245 次会议暨展览会	Quantum dots-based cellular interractions and effects	黄庆	分会报告	生物无机化学	2013-04-03	美国
19	第二十届放射性药物国际研讨会	18F-Labeling of small molecules: Multi-click in one pot	贾丽娜	展板报告	放射性药物和标记化合物	2013-05-12	韩国
20	第二十届放射性药物国际研讨会	Synthesis, radiolabeling and sidtribution studies of varisized nano graphene oxide sheets	江大卫	展板报告	放射性药物和标记化合物	2013-05-12	韩国
21	第十七届泛美同步辐射装置会议	Stress-induced phase transition in cubic Gd2O3	蒋升	展板报告	同步辐射技术及其应用	2013-06-16	美国
22	第十七届泛美同步辐射装置会议	Recent progresses of high pressure techniques at bl15u1 of SSRF	杨科	分会报告	同步辐射技术及其应用	2013-06-16	美国
23	第七届材料工程国际学术会议	Effect of Poly[bis(phenoxy)phosphazene] Content in Magnesium Hydroxide/low-density Polyethylene Blends on Electron Beam Irradiation and Flame Resistance	张聪	展板报告	特殊与极端环境下的高分子材料	2013-06-30	新加坡
24	17 届美同步辐射装置会议及高压国际研讨会	上海光源在高压科学研究的中的应用	肖体乔	大会报告	同步辐射技术及其应用	2013-06-16	美国

25	“基于钍铀循环的熔盐堆发展”国际研讨会议	TMSR 项目基于熔盐堆的钍能利用研究	余笑寒	大会报告	反应堆物理与技术	2013-01-28	韩国
26	“基于钍铀循环的熔盐堆发展”国际研讨会议	TMSR 项目基于熔盐堆的钍能利用研究	蔡翔舟	大会报告	反应堆物理与技术	2013-01-28	韩国
27	钍基核能的挑战和未来国际研讨会	Current Status and Future of Development of Thorium Molten Salt Reactor in China	徐洪杰	大会报告	核技术及其应用	2013-05-16	日本
28	第七届国际先进材料国际会议	Water Promotion for CO Oxidation on Small-sized Gold Clusters	高嶷	大会报告	金属材料的微观结构	2013-06-29	新加坡
29	美国氟盐冷却高温核反应堆热和流体验证实验研讨会	HTS 自然循环回路仿真设计	袁晓凤	分会报告	实验流体力学	2013-04-27	美国
30	美国氟盐冷却高温核反应堆热和流体验证实验研讨会	熔盐泵	黎忠	分会报告	实验流体力学	2013-04-27	美国
31	美国氟盐冷却高温核反应堆热和流体验证实验研讨会	HTS 自然循环实验回路验证	陈堃	分会报告	实验流体力学	2013-04-27	美国
32	美国氟盐冷却高温核反应堆热和流体验证实验研讨会	TMSR 热工实验验证	王纳秀	分会报告	实验流体力学	2013-04-27	美国
33	美国氟盐冷却高温核反应堆热和流体验证实验研讨会	TMSR 回路装置	傅远	分会报告	实验流体力学	2013-04-27	美国
34	25 届国际核物理大会	相对论重离子碰撞中的反物质原子核和奇特超核”（ Antinuclei and exotic hypernuclei in relativistic Heavy-lon collisions）	马余刚	大会报告	核物理	2013-06-01	意大利
35	第五届微束团不稳定性国际研讨会	上海软 X 射线自由电子激光装置中的微束团不稳定性研究	黄大章	大会报告	束流物理与加速器技术	2013-05-07	韩国
36	第 23 届磁铁技术国际会议	Status of Cryogenic Calorimeter for Simulation the Heat Load of Superconducting Undulator	崔剑	展板报告	束流物理与加速器技术	2013-07-13	美国
37	第 23 届磁铁技术国际会议	Design of Superconducting Dipole Magnets for SSRF Upgrade Project	许皆平	展板报告	束流物理与加速器技术	2013-07-13	美国
38	第 23 届磁铁技术国际会议	Design and Tests of a Superconducting NbTi Undulator Magnet for SSRF	张正臣	展板报告	束流物理与加速器技术	2013-07-13	美国
39	第 17 届国际辐照效应及	The structure of hdpe	闫隆	展板报告	金属结构材料	2013-06-29	芬兰

	绝缘会议	irradiated with swift Fe ions					
40	第 17 届国际辐照效应及绝缘会议	Stability of coiled carbon nanostructure under ion irradiation	张伟	展板报告	金属结构材料	2013-06-29	芬兰
41	第 17 届国际辐照效应及绝缘会议	The effect of temperature on primary defect formation in Ni-Fe alloy	王呈斌	展板报告	金属结构材料	2013-06-29	芬兰
42	核动力学与热力学国际会议	中能重离子碰撞中的自旋效应 (Spin effects in intermediate-energy heavy-ion collisions)	徐骏	大会报告	核物理	2013-08-17	美国
43	2013 高梯度技术国际研讨会	The status of the C band system at SINAP	顾强	大会报告	核技术及其应用	2013-06-02	意大利
44	2013 年度材料研究合作会议	Nanomesh to epitaxial graphene	高兴宇	分会报告	同步辐射技术及其应用	2013-06-23	韩国
45	第八届先进材料与加工泛太平洋国际会议	Effect of Long Time Thermal Exposure on Microstructure and Mechanical properties of C276 Superalloy	陆燕玲	分会报告	金属结构材料	2013-08-03	美国
46	第八届先进材料与加工泛太平洋国际会议	The Effect of Silicon Addition on the Thermal Stability and Morphology of Carbides in a Ni-Mo-Cr Superalloy	蒋力	分会报告	金属结构材料	2013-08-03	美国
47	第十四届核石墨国际会议及核石墨小样测试会议	熔盐堆中石墨的应力分析	曾广礼	大会报告	力学中的基本问题和方法	2013-09-13	美国
48	2013 年度国际核碎裂反应大会	Hypernuclear physics at RHIC	马余刚	大会报告	核物理	2013-09-28	土耳其
49	2013 年度国际核碎裂反应大会	Shear viscosity to entropy density ratio of nuclear matter by transport model	方德清	大会报告	核物理	2013-09-28	土耳其
50	2013 年度 SPIE 光学工程和应用国际研讨会	Conceptual design for the hard x-ray nanoprobe beamline at the SSRF	李爱国	展板报告	同步辐射技术及其应用	2013-08-24	美国
51	2013 年度 SPIE 光学工程和应用国际研讨会	Conceptual design for the hard x-ray nanoprobe beamline at the SSRF	蒋晖	展板报告	同步辐射技术及其应用	2013-08-24	美国
52	第三届创新核能系统结构材料国际研讨会	Temperature effect on primary defect formation in Ni-Fe alloy	任翠兰	展板报告	极端条件下使用的金属材料	2013-10-06	美国
53	第三届创新核能系统结构材料国际研讨会	Evolution of microstructure and nanohardness in Hastelloy N alloy after Xe26+ ion	黄鹤飞	展板报告	极端条件下使用的金属材料	2013-10-06	美国

		irradiation					
54	第八届国际非弹性 X 射线散射会议和顺访斯坦福大学同福辐射实验室	A High-resolution X-ray Spectrometer and its application at SSRF	黄宇营	展板报告	同步辐射技术及其应用	2013-08-10	美国
55	第十六届均相和多相催化国际研讨会	Nanocatalysis and advanced sychrotron technique in SSRF	王建强	展板报告	物理无机化学	2013-08-03	日本
56	第三届低发射度储存环研讨会	Low emittance study in SSRF Phase II project	冷用斌	大会报告	束流物理与加速器技术	2013-07-07	英国
57	2013 年锕系元素国际会议	First-principle calculation of intrinsic and defective properties of UO2 and ThO2	程诚	展板报告	反应堆物理与技术	2013-07-20	德国
58	第 35 届国际自由电子激光大会并与 SLAC 进行自由电子激光物理与技术交流	The laser system of Shanghai Deep-Ultraviolet Free Electron Laser test facility (SDUV-FEL)	王兴涛	展板报告	自由电子激光原理和技术	2013-08-24	美国
59	第 35 届国际自由电子激光大会并与 SLAC 进行自由电子激光物理与技术交流	Evolvement of the laser and synchronization system for the Shanghai DUV-FEL Test Facility	刘波	展板报告	自由电子激光原理和技术	2013-08-24	美国
60	第 35 届国际自由电子激光大会并与 SLAC 进行自由电子激光物理与技术交流	Simulation studies on laser pulse stability for Dalian Coherent Light Source	邓海啸	展板报告	自由电子激光原理和技术	2013-08-24	美国
61	第 35 届国际自由电子激光大会并与 SLAC 进行自由电子激光物理与技术交流	Slippage effect on laser phase error amplification in seeded harmonic generation free-electron lasers	冯超	展板报告	自由电子激光原理和技术	2013-08-24	美国
62	第 35 届国际自由电子激光大会并与 SLAC 进行自由电子激光物理与技术交流	Optical synchronization system for the Shanghai Soft X-ray Free-Electron Laser facility	兰太和	展板报告	自由电子激光原理和技术	2013-08-24	美国
63	第 35 届国际自由电子激光大会并与 SLAC 进行自由电子激光物理与技术交流	A ring-based high gain FEL in soft x-ray regime	王东	展板报告	自由电子激光原理和技术	2013-08-24	美国
64	国际光奇异性与拓扑结构研讨会与 FERMI-FEL 实验	X-rays carrying orbital angular momentum at the SXFEL	陈建辉	展板报告	自由电子激光原理和技术	2013-07-06	意大利
65	第六届国际低电平会议（LLRF13）	RF system operation and LLRF system upgrade in SSRF	赵玉彬	展板报告	束流物理与加速器技术	2013-09-30	美国

66	2013 夸克物质中的奇异性国际会议	Tomography of high energy heavy-ion collisions with asymmetries of photon-jet and di-jet。	马国亮	大会报告	核物理	2013-07-21	英国
67	杜克大学高强度伽马光源二期研讨会并访问杜克大学	A pilot-study for the d(γ,n)p PV experiment	许杭华	分会报告	核物理	2013-06-02	美国
68	杜克大学高强度伽马光源二期研讨会并访问杜克大学	12C(α,γ)16O 天体物理 S 因子	安振东	分会报告	核物理	2013-06-02	美国
69	Global2013 年国际核燃料循环会议	Fuel Strategy for 2MW SF-TMSR	朱智勇	分会报告	中高能核物理	2013-09-28	美国
70	Global2013 年国际核燃料循环会议	Study on the electrochemical extraction of REs from FLINAK	龙德武	分会报告	中高能核物理	2013-09-28	美国
71	Global2013 年国际核燃料循环会议	A？Preliminary？Study？on？Low？Pressure？Distillation？Behavior？of？Fluoride？Salts	窦强	分会报告	中高能核物理	2013-09-28	美国
72	Global2013 年国际核燃料循环会议	A 233U extraction process for providing ignition fuel for TMSR	李峥	展板报告	中高能核物理	2013-09-28	美国
73	2013 年 ISTROS 核物理国际会议	Investigations on hyper-nuclei	马余刚	大会报告	核物理	2013-09-22	斯洛伐克共和国
74	2013 年 ISTROS 核物理国际会议	Experimental investigations on the exotic structure of proton rich nuclei	方德清	大会报告	核物理	2013-09-22	斯洛伐克共和国
75	美国核学会核临界安全分会	CRITICALITY SAFETY ANALYSES FOR SOLID FUEL THORIUM MOLTEN SALT REACTOR (SF-TMSR) CORE REPLACEMENT	陈堃	分会报告	核技术及其应用	2013-09-28	美国
76	第四届国际物理学前沿会议	Special Session on Synchrotron Light Source	何建华	大会报告	同步辐射技术及其应用	2013-08-26	马来西亚
77	2013 年国际低温工程暨低温材料大会	Conceptual Design of a Multiple-function Cryogenic System for Superconducting Devices in SSRF Upgrade 和 Cooling for SC Devices of Test Cryomodule for ADS Injector II at IMP	王莉	展板报告	制冷	2013-06-16	美国
78	第五届亚太地区放射化学会议	Study on electrochemical behaviors of rare earth elements in FLINAK eutectic	田丽芳	展板报告	核放射化学	2013-09-22	日本

		salt.					
79	第五届亚太地区放射化学会议	Thorium based Molten Salt Fuel Cycle	李晴暖	展板报告	核放射化学	2013-09-22	日本
80	15 届亚洲化学会议	Nanometer-thick Charged Pancakes of Aqueous Salt Solution on the Hydrophobic Carbon-based Surfaces via Cation-π Interactions	方海平	分会报告	溶液化学	2013-08-19	新加坡
81	第 14 届加速器与大型实验物理控制系统国际会议	新型定时系统研究状况	刘鸣	大会报告	核技术及其应用	2013-10-05	美国
82	第八届物理化学及生物界面水的国际会议	Time duration required for a molecule reaching a solid surface	郭盼	展板报告	统计物理学与复杂系统	2013-10-20	保加利亚
83	纳米谱学显微国际会议	STXM beamline at the Shanghai Synchrotron Radiation Facility	王勇	大会报告	同步辐射技术及其应用	2013-10-23	韩国
84	东盟 2013：生物传感器生物诊断和生物芯片的第二次区域研讨会	Self-assembled DNA nanostructures for biomedical applications	樊春海	大会报告	生物化学	2013-12-10	泰国
85	美国材料研究学会 2013 年秋季会议	Active Sites of Gold-Ceria Catalysts for Water-Gas Shift Reaction: In-Situ Combined XAFS/DRIFTS under Transient Conditions	司锐	分会报告	无机材料化学	2013-12-01	美国
86	第 224 次电化学会会议	Bismuth Ferrites As Electrodes for Lithium Batteries: An in Situ XRD and XANES Investigation	文闻	分会报告	电化学	2013-10-26	美国
87	2013 年度美洲粒子加速器国际会议	Overview of Seeded FELs and Harmonic Generation	赵振堂	大会报告	非加速器粒子物理	2013-09-28	美国
88	第四届亚洲配位化学国际会议	Theoretical Studies on the Electronic Structure and Chemical Bonding of Uranyl Halide Complexes	苏静	展板报告	配位化学	2013-11-03	韩国
89	美国能源部和中科院共同组织的第二届执委会和工作小组会议	Uranium from Sea Water	吴国忠	大会报告	核技术及其应用	2013-10-23	美国
90	美国能源部和中科院共同组织的第二届执委会和工作小组会议	Conceptual Design of the TMSR-SF1 Experimental Reactor	戴志敏	大会报告	核技术及其应用	2013-10-23	美国

91	美国能源部和中科院共同组织的第二届执委会和工作小组会议	Safety Analyses of the TMSR-SF1 Reactor	陈堃	大会报告	核技术及其应用	2013-10-23	美国
92	美国能源部和中科院共同组织的第二届执委会和工作小组会议	Radiation Protection of the TMSR-SF1 Reactor	夏晓彬	大会报告	核技术及其应用	2013-10-23	美国
93	电子化学和表面催化领域研究—国际研究和教育合作团队年度会议	Designing nanomaterials for biosensors	樊春海	大会报告	生物化学	2013-12-15	美国
94	第 14 届国际加速器和大型实验物理控制系统国际会议	The Control System of the Water-cooled DCM in SSRF	贾文红	展板报告	束流物理与加速器技术	2013-10-05	美国
95	第 14 届国际加速器和大型实验物理控制系统国际会议	The Openration Environment of SSRF Beamline Control System	米清茹	展板报告	束流物理与加速器技术	2013-10-05	美国
96	第 14 届国际加速器和大型实验物理控制系统国际会议	Preliminary design of the SXFEL control system	丁建国	展板报告	束流物理与加速器技术	2013-10-05	美国
97	第十一届国际生物学与同步辐射会议	Macromolecular Crystallography Beamlines at SSRF	何建华	大会报告	同步辐射技术及其应用	2013-09-07	德国
98	SPIEX 射线纳米成像仪器与方法国际会议	Full-field x-ray nano-imaging at SSRF	邓彪	展板报告	X 射线、红外、THz 物理	2013-08-24	美国
99	阿姆斯特丹 TECHNART2013 国际会议及国家博物馆文物分析技术研讨会	Technical Study of a Painted Wallpaper from the Forbidden City with Synchrotron Radiation X-ray Fluorescence and X-ray Absorption Spectroscopy	魏向军	大会报告	同步辐射技术及其应用	2013-09-22	荷兰
100	阿姆斯特丹 TECHNART2013 国际会议及国家博物馆文物分析技术研讨会	Technical Study of a Painted Wallpaper from the Forbidden City with Synchrotron Radiation X-ray Fluorescence and X-ray Absorption Spectroscopy	魏向军	大会报告	同步辐射技术及其应用	2013-09-22	德国
101	2013 年自由电子激光国际会议并访问美国布鲁克海文国家实验室	Experimental Studies of Echo-enabled HG FEL	赵振堂	大会报告	束流物理与加速器技术	2013-08-25	美国
102	美国能源部和中科院共同组织的第二届执委会和工作小组会议	Reactor Physics of the TMSR-SF1 Reactor	余笑寒	大会报告	核技术及其应用	2013-10-23	美国
103	美国能源部和中科院共同组织的第二届执委会和工作小组会议	Fluoride Salt Production and Chemical Control	谢雷东	大会报告	核技术及其应用	2013-10-23	美国

104	美国能源部和中科院共同组织的第二届执委会和工作小组会议	TMSR-SF1 Materials Considerations	周兴泰	大会报告	核技术及其应用	2013-10-23	美国
105	美国能源部和中科院共同组织的第二届执委会和工作小组会议	Current Status of the CAS TMSR project	徐洪杰	大会报告	核技术及其应用	2013-10-23	美国
106	第 7 届亚太同步辐射论坛和论坛培训班	Facilities’ Projects in China	徐洪杰	大会报告	同步辐射技术及其应用	2013-09-21	日本
107	第 34 届中美高能物理合作委员会会议	上海应物所 2012-2013 年度中美高能物理合作情况	赵振堂	大会报告	束流物理与加速器技术	2013-10-30	美国
108	2013 年国际束流测量会议	Bunch length measurement with streak camera at SSRF Storage Ring	陈杰	展板报告	束流物理与加速器技术	2013-09-15	英国
109	2013 年国际束流测量会议	Image Analysis for Pepper Pot Emittance Measurement	叶恺容	展板报告	束流物理与加速器技术	2013-09-15	英国
110	2013 年国际束流测量会议	Beam Diagnostics System for a Photo-Neutron Source Driven by 15MeV Electron Linac	阎映炳	展板报告	束流物理与加速器技术	2013-09-15	英国
111	2013 年国际束流测量会议	bunch by bunch Transverse beam position observation and analyze during injection at ssrf	冷用斌	展板报告	束流物理与加速器技术	2013-09-15	英国
112	第 56 届日本辐射化学年会	Photocatalyzed Self-Cleaning Cotton Fabric with TiO2 Nanoparticles Covalently Immobilized by Radiation Induced Graft Polymerization	李景烨	大会报告	核技术在工、农业和医学中的应用	2013-09-27	日本
113	东盟 2013：生物传感器生物诊断和生物芯片的第二次区域研讨会	Portable immunosensors with disposable screen-printed electrodes based on nano-assembly for sensitive and rapid biodetection	宋世平	大会报告	生化分析及生物传感	2013-12-10	泰国
114	2013 日中科学技术研讨会	厌氧膜生物反应器处理食品废水报告	陆晓峰	大会报告	水污染化学	2013-11-28	日本
115	上海应物所-上海光源 SSRF 与西班牙 ALBA 光源双边研讨会	上海光源二期线站建设工作总体情况	赵振堂	大会报告	束流物理与加速器技术	2013-12-15	西班牙
116	上海光源-西班牙 ALBA 光源双边交流会议	Machine operation and studies at SSRF	张文志	大会报告	同步辐射技术及其应用	2013-12-15	西班牙
117	上海光源-西班牙 ALBA 光源双边交流会议	Dreamline and an overview of soft X-ray beamlines at SSRF	王勇	大会报告	同步辐射技术及其应用	2013-12-15	西班牙
118	上海光源-西班牙 ALBA 光源双边交流会议	Beamline control and data acquisition system at SSRF	张招红	大会报告	同步辐射技术及其应用	2013-12-15	西班牙
119	上海光源-西班牙 ALBA 光源双边交流会议	SiP and ME2 beamilines at SSRF	郭智	大会报告	同步辐射技术及其应用	2013-12-15	西班牙

120	2013 年度钍能源国际会议	Thorium Energy R&D in China	蔡翔舟	大会报告	反应堆物理与技术	2013-10-26	瑞士
121	ALBA-SSRF 双边学术交流会	IDs and ID developments at SSRF	周巧根	大会报告	同步辐射光源原理和技术	2013-12-15	西班牙
122	美国核学会 2013 年冬季年会	The Analysis of Tritium Production in the Solid Fuel Thorium Molten Salt Reactor	陈堃	展板报告	核技术及其应用	2013-11-08	美国
123	Proceedings of the 2013 21st International Conference on Nuclear Engineering,ICONE21	Preliminary Analysis of Self-breeding and Radiotoxicity on TMSR	蔡翔舟	分会报告	Next Generation Reactors and Advanced Reactors	2013.7. 29 - 8. 2	中国
124	Colloids and Energy 2013, 3rd International Colloids Conference	Water Promotion for CO Oxidation on Small-Sized Gold Clusters.	高嶷	墙报	化学	2013.4.22	中国
125	International Symposium on Organic Reaction Mechanisms	Water Promotion for CO Oxidation on Small-Sized Gold Clusters.	高嶷	墙报	化学	2013.5.8	中国
126	6th International Conference on Computational Nanoscience and New Energy Materials	Introduction of Gold Clusters and Gold Nanocatalysts	高嶷	大会报告	纳米材料	2013.6.21	中国
127	International Symposium on Nanostructures and Their Applications in Renewable Energy.	The Theoretical Study of Gold Nanocatalysts in Renewable Energy	高嶷	大会报告	纳米材料	2013.10.27	中国
128	2013 China-Europe International Workshop on Alloy Nanoparticles	Theoretical Design of Alloyed Clusters and Their Applications	高嶷	大会报告	纳米材料	2013.11.20	中国
129	QCD vacuum and matter under strong magnetic field	Final state dynamics of charge separation in a transport model	马国亮	大会报告	核物理	2013.4.29-30	中国
130	10th Workshop on QCD Phase Transition and Relativistic Heavy-ion Physics	Transport view of probing QGP medium with reconstructed jets	马国亮	大会报告	核物理	2013.8.8-10	中国
131	The 2nd Workshop on Initial Fluctuations and Final Correlations	Reconstructed-jet correlations in AMPT	马国亮	大会报告	核物理	2013.8.11-14	中国
132	STAR Regional meeting	γ-jet correlations with AMPT model	马国亮	大会报告	核物理	2013.9.9-11	中国
133	International Conference on Nanoscience and Technology	Asymmetrical free diffusion with orientation-dependence of molecules in finite timescales	盛楠	分会报告	纳米科学	2013.9.5-9.7	中国

134	2nd China-Japan Academic Symposium on Nuclear Fuel Cycle ASNFC 2013	Theoretical Studies of the Electronic Structure and Chemical Bonding in Uranium Penta-halide Complexes	苏静	分会报告	理论放射化学	2013.11.27-11.30	中国
135	8th International Conference on High Temperature Ceramic Matrix Composites	The Influence of Molten Fluoride Salt (LiF-NaF-KF) Penetration on the Properties of C/C Composites	张东升	分会报告	材料学	2013.9.22-9.26	中国
136	International workshop on ion interactions with materials at nano/micrometer scale	Ion irradiation damage of carbon nanotubes	张伟	分会报告	材料辐照效应	2013.7.16-7.18	中国
137	Clustering Aspects in Nuclei/KITPC	The cluster dynamics induced by clustering nuclei collisions at low energy	曹喜光	大会	核物理	2013.4.1-4.26	中国
138	21st International Conference on Nuclear Engineering	Primary Shielding Design for an Optimized Molten Salt Reactor	张志宏	分会报告	辐射防护	2013.7.29-2013.8.02	中国
139	21st International Conference on Nuclear Engineering	STABILITY ANALYSIS OF THE MSBR	程懋松	分会报告	NEXT GENERATION REACTORS AND ADVANCED REACTORS	2013.7.29-2013.8.02	中国
140	21st International Conference on Nuclear Engineering	THE IMPACT OF DIFFERENT CARRIER SALTS ON THE PHYSICAL CHARACTERISTICS OF THE MSFR	程懋松	分会报告	NEXT GENERATION REACTORS AND ADVANCED REACTORS	2013.7.29-2013.8.02	中国
141	IWA Symposium on Environmental Nanotechnology 2013	Submicroscopic Gas Bubbles investigated by STXM	张立娟	分会报告	环境科学	2013.4.24-4.27	中国
142	4th International Particle Accelerator Conference (IPAC'13)	Bunch-by-bunch Beam Position and Charge Monitor based on Broadband Scope in SSRF	杨勇	墙报	束流测量	2013.5.12 – 5.17	中国
143	4th International Particle Accelerator Conference (IPAC'13)	Point Spread Function Study of X-ray Pinhole Camera in SSRF	陈之初	墙报	束流测量	2013.5.12 – 5.17	中国
144	4th International Particle Accelerator Conference (IPAC'13)	Development of Cavity Beam Position Monitor System	王宝鹏	墙报	束流测量	2013.5.12 – 5.17	中国
145	4th International Particle Accelerator Conference (IPAC'13)	Beam Instrumentation System Optimization for Top-up Operation in SSRF	阎映炳	墙报	束流测量	2013.5.12 – 5.17	中国

146	4th International Particle Accelerator Conference (IPAC'13)	Development Status of SINAP Timing System	殷重先	墙报	核技术	2013.5.12-5.17	中国
147	4th International Particle Accelerator Conference (IPAC'13)	Status of SSRF Fast Orbit Feedback System	刘鸣	墙报	核技术	2013.5.12-5.17	中国
148	4th International Particle Accelerator Conference (IPAC'13)	The Magnetic Performance of Two Undulators for HLS	张伟	墙报	加速器	2013.5.10	中国
149	4th International Particle Accelerator Conference (IPAC'13)	Mechanical Design of Shift Driving System for Depu at AT SSRF	邓荣兵	墙报	加速器	2013.5.12-5.17	中国
150	4th International Particle Accelerator Conference (IPAC'13)	Design of a Superconducting Undulator Magnet	张正臣	墙报	加速器技术	2013.05.12-05.17	中国
151	4th International Particle Accelerator Conference (IPAC'13)	An Overview of Light Source Development in Asia	王东	大会报告	加速器	2013.5.12-2013.5.17	中国
152	4th International Particle Accelerator Conference (IPAC'13)	Generating Polarization Controllable FELs at Dalian Coherent Light Source	张彤	大会报告	加速器	2013.5.12-2013.5.17	中国
153	4th International Particle Accelerator Conference (IPAC'13)	Status of Non-destructive Bunch Length Measurement based on Coherent Cherenkov Radiation	张建兵	墙报	加速器	2013.5.12-2013.5.17	中国
154	4th International Particle Accelerator Conference (IPAC'13)	High Brightness and Fully Coherent X-ray Pulses from XFELO Seeded High-gain FEL Schemes	邓海啸	墙报	加速器	2013.5.12-2013.5.17	中国
155	4th International Particle Accelerator Conference (IPAC'13)	Linac Design for Dalian Coherent Light Source	张猛	墙报	加速器	2013.5.12-2013.5.17	中国
156	4th International Particle Accelerator Conference (IPAC'13)	Linac Design for Nuclear Data Measurement Facility	张猛	墙报	加速器	2013.5.12-2013.5.17	中国
157	4th International Particle Accelerator Conference (IPAC'13)	R&D of New C-band Accelerating Structure for SXFEL Facility	方文程	墙报	加速器	2013.5.12-2013.5.17	中国
158	4th International Particle Accelerator Conference (IPAC'13)	New X-band Deflecting Cavity Design for Ultra-short Bunch Length Measure of FEL at SINAP	谭健豪	墙报	加速器	2013.5.12-2013.5.17	中国
159	4th International Particle Accelerator Conference	R&D of C-band Pulse Compression for Soft X-ray	王超鹏	墙报	加速器	2013.5.12-2013.5.17	中国

	(IPAC'13)	FEL at SINAP

2014

No.	会议全称	报告名称	报告人	报告类别	报告学科领域	时间	地点
1	第 58 届美国生物物理学会年会	Tunable binding reaction on DNA origami nanostructures	李宾	分会报告	生物物理、生物化学与分子生物学研究的新方法与新技术	2014-02-14	美国
2	第六届亚洲核物理组织研讨会	“相对论重离子碰撞中的反物质原子核探测”	马余刚	大会报告	核物理	2014-02-17	印度
3	2014 年 X 射线相衬成像生物医学应用国际研讨会	A low dose and fast micro-CT system based on equally sloped tomography at SSRF	周光照	墙报报告	X 射线与 CT、电子与离子束、放射诊断与质量控制	2014-01-20	德国
4	2014 年 X 射线相衬成像生物医学应用国际研讨会	Mouse brain imaging by X-ray in-line phase contrast tomography	任玉琦	墙报报告	X 射线与 CT、电子与离子束、放射诊断与质量控制	2014-01-20	德国
5	软物质物理的前沿会议	Asymmetrical Free Diffusion with Orientation-dependence of molecules in Finite Timescales	方海平	分会报告	统计物理学与复杂系统	2014-01-12	香港
6	软物质物理的前沿会议	Unexpect hydrophilicity on the hydrophobic carbon-based surfaces due to the cation-pi interaction	石国升	分会报告	统计物理学与复杂系统	2014-01-12	香港
7	软物质物理的前沿会议	Unexpected hydrophobicity and hydrophilicity due to the surface morphology	王春雷	分会报告	统计物理学与复杂系统	2014-01-12	香港
8	生物/纳米接口领域前沿科技研讨会	Designing nanomaterials for biosensors	樊春海	大会报告	生物化学	2014-01-23	香港
9	参加 2014 戈登学术会议:可再生能源:太阳能	Yygy@661215	高嶷	墙报报告	统计物理学与复杂系统	2014-01-18	美国
10	2014 年美国化学会年会胶体与界面化学分会	In situ XAFS technique for nanomaterial in catalysis reactions	王建强	分会报告	物理无机化学	2014-03-15	美国
11	2015 年国际粒子加速器大会程序委员会及组委会第一次会议	Overview of IPAC2013	冷用斌	大会报告	束流物理与加速器技术	2014-01-07	美国
12	第四届 ACAS WORKSHOP 和第五届 AFAD 国际会议	FEL Activities at SINAP	王东	大会报告	束流物理与加速器技术	2014-01-13	澳大利亚
13	第五届 AFAD 论坛和第四届 ACAS 讨论会	Emittance Minimisation in Light Source Storage Rings	田顺强	大会报告	束流物理与加速器技术	2014-01-13	澳大利亚

14	访问加州大学圣地亚哥分校生物工程系;ACS 全国第 247 次会议暨展览会	Gold nanoparticle-based DNA detection technology	樊春海	分会报告	生物无机化学	2014-03-09	美国
15	访问加州大学圣地亚哥分校生物工程系;ACS 全国第 247 次会议暨展览会	Quantum dots-based cellular interractions and effects	黄庆	分会报告	生物无机化学	2014-03-09	美国
16	第六届 HOPE 会议	中能重离子碰撞中椭圆流与约化粘滞系数的关联	周铖龙	大会报告	中高能核物理	2014-03-10	日本
17	第七届国际纳米毒理学会议	The Biocompatibility of Nanodiamonds and Their Application in Drug Delivery Systems	诸颖	分会报告	生物无机化学	2014-04-22	土耳其
18	2014 先进核电厂国际会议	A Preliminary Experimental Design Study on the Friction Coefficient of an Ordered Pebble Bed Core of the TMSR-SF1 Reactor	曲世祥	分会报告	核技术及其应用	2014-04-05	美国
19	超导波荡器研讨会	SSRF 超导波荡器模型机冷却系统设计	王莉	大会报告	同步辐射光源原理和技术	2014-04-26	英国
20	超导波荡器研讨会	SSRF 超导波荡器模型机磁体设计	张正臣	大会报告	同步辐射光源原理和技术	2014-04-26	英国
21	2014 年第 12 届 ASME/NRC 泵、阀、在役检查和新反应堆研讨会	Preliminary study of freeze-valve for a passive shutdown system in molten salt reactors(MSRs)	李启明	分会报告	核技术及其应用	2014-06-21	美国
22	2014 年第 12 届 ASME/NRC 泵、阀、在役检查和新反应堆研讨会	Design and test for a high temperature molten salt pump	林良程	分会报告	核技术及其应用	2014-06-21	美国
23	2014 年 MRS 春季会议	An In-Situ Synchrotron X-Ray Diffraction Study of Micromechanical Behavior of Cu/Ag Nanostructured Multilayered Films	李丽	分会报告	同步辐射技术及其应用	2014-04-21	美国
24	2014 年 IEEE 铁电材料应用会议	lectric field control of metallic insulator transition in charge-ordered Fe_2OBO_3	李晓龙	墙报报告	凝聚态物理中的新效应及其他问题	2014-05-11	美国
25	第 17 届放射化学国际会议	Thorium based Molten Salt Fuel Cycle	李晴暖	分会报告	核放射化学	2014-05-10	捷克共和国
26	第 17 届放射化学国际会议	Uranium extraction from seawater using radiation-grafted UHMWPE fiber: from	吴国忠	分会报告	核放射化学	2014-05-10	捷克共和国

		laboratory to pilot scale					
27	第 17 届放射化学国际会议	Electrochemical Behaviors of Europium(III)/Europium(II) in LiF-NaF-KF Molten Salt	黄卫	分会报告	核放射化学	2014-05-10	捷克共和国
28	第 17 届放射化学国际会议	Preliminary Research on MonitoringUranium Fluoride Volatility Process by Fourier Transform Infrared Spectroscopy	孙理鑫	分会报告	核放射化学	2014-05-10	捷克共和国
29	2014 年欧洲材料学会春季会议	Adsorption and diffusion of Thorium and Uranium adatoms on graphene nanoribbons: A first principle study	程诚	墙报报告	块体材料的电子态	2014-05-25	法国
30	第九届界面接触角浸润及黏附国际会议	Unexpect hydrophilicity on the hydrophobic carbon-based surfaces due to the cation-pi interaction	石国升	大会报告	统计物理学与复杂系统	2014-06-15	美国
31	第九届界面接触角浸润及黏附国际会议	Unexpected hydrophobicity and hydrophilicity due to the surface morphology	王春雷	大会报告	统计物理学与复杂系统	2014-06-15	美国
32	24 届国际超相对论核核碰撞“夸克物质 2014”会议	Transport model studies on reconstructed jets in a hot partonic medium	马国亮	大会报告	核物理	2014-05-18	德国
33	“生物传感器 2014”国际会议	DNA-mediated gold-silver nanoprobes with SERS-active nanogaps for multiplex DNA biosensing	宋世平	分会报告	生物物理、生物化学与分子生物学研究的新方法与新技术	2014-05-26	澳大利亚
34	“2014 欧洲核会议—核技术议题、应用及挑战论坛”	Mechanism study of freeze-valve for molten salt reactor (MSR)	张钦华	墙报报告	核技术及其应用	2014-05-09	法国
35	2014 第六届新材料国际研讨会	Evolution of nanohardness and microstructure in Hastelloy N alloy under Xe ion irradiation	黄鹤飞	分会报告	离子束与物质相互作用和辐照损伤	2014-06-14	意大利
36	参加 2014 夸克物质会议	Quark deconfinement phase transition in nuclear matter for improved quark mass density-dependent model	吴琛	大会报告	核物理	2014-05-18	德国
37	材料研究合作会议 2014	Monochromatic photoemission from alkane-ligated Au nanoparticles	高兴宇	分会报告	光电子显示材料、器件及技术	2014-06-22	韩国
38	第四届 Asian Core Workshop	New FEL Facilities at SINAP	刘波	大会报告	束流物理与加速器技术	2014-05-07	韩国

39	第四届 Asian Core Workshop	Instant phase matching broadband non-collinear optical parametric amplification: a candidate front-end for the future laser wake-field accelerator	沈磊	大会报告	束流物理与加速器技术	2014-05-07	韩国
40	第四届 Asian Core Workshop	Crossed-planar undulator experiment at SDUV-FEL	邓海啸	大会报告	束流物理与加速器技术	2014-05-07	韩国
41	第四届 Asian Core Workshop	Ion related multi-bunch instability in SSRF storage ring	姜伯承	大会报告	束流物理与加速器技术	2014-05-07	韩国
42	第四届 Asian Core Workshop	Investigation of the possibility to reduce horizontal emittance using a Robinson wiggler in SSRF	张庆磊	大会报告	束流物理与加速器技术	2014-05-07	韩国
43	第 16 届辐射成像探测器会议(iWorid-2014)	Imaging and its detector status at SSRF	肖体乔	大会报告	探测与成像系统	2014-06-21	意大利
44	第 16 届辐射成像探测器会议(iWorid-2014)	Factors related to image quality in the lens-coupled X-ray detector	杜国浩	墙报报告	探测与成像系统	2014-06-21	意大利
45	第 16 届辐射成像探测器会议(iWorid-2014)	Program status on the dynamic tomography at sub-second time scale	陈荣昌	墙报报告	探测与成像系统	2014-06-21	意大利
46	第 26 届 ESB2014 国际会议	Study on calcium silicate / zein scaffold implanted *in vivo* by synchrotron radiation-based X-ray imaging	郭瀚	墙报报告	生物材料	2014-08-30	英国
47	QuarkMatter 国际学术会议并做分会报告	STAR 实验中手征磁波和电荷不对称性依赖的研究	寿齐烨	分会报告	核物理	2014-05-13	德国
48	2014 应用超导国际会议	Design of Cold Mass Supports for a Superconducting Undulator Prototype at SINAP	刘以勇	墙报报告	束流物理与加速器技术	2014-08-09	美国
49	中俄 BLTP/JINR-SKLTP/CAS 双边研讨会	核团簇与巨偶极共振研究进展	马余刚	大会报告	核物理	2014-07-13	俄罗斯
50	参加第 23 届流体力学离散模拟学术研讨会	Numerical investigation on the performance of a bubble rotary turbine separator	李华	墙报报告	计算流体力学	2014-07-27	法国
51	“第 23 届国际晶体学大会”	Remote Access of the beamline BL17U at Shanghai Synchrotron Radiation Facility	汪启胜	墙报报告	同步辐射技术及其应用	2014-08-04	加拿大
52	“第 23 届国际晶体学大会”	The crystal structure of the cytochrome P450 enzyme TxtE	徐春艳	墙报报告	同步辐射技术及其应用	2014-08-04	加拿大
53	第五届国际粒子加速器会议	2013 年 IPAC 会议召开情况总结	赵振堂	1	束流物理与加速器技术	2014-06-14	德国

54	2014 年国际生物物理学大会	The crystal structure of the cytochrome P450 enzyme TxtE	何建华	墙报报告	结构生物物理化学	2014-08-02	澳大利亚
55	2014 年国际生物物理学大会	Using noble gas xenon as a heavy atom for phase determination of protein trichosanthin structure	李敏军	墙报报告	结构生物物理化学	2014-08-02	澳大利亚
56	2014 年度美国核学会年会	Application of RELAP5/MOD4.0 Code in a Fluoride Salt-Cooled High-Temperature Test Reactor	陈堃	大会报告	核技术及其应用	2014-06-14	美国
57	第五届国际粒子加速器会议	Development of Digital Low Level Radio Frequency Controller at SSRF	赵玉彬	墙报报告	束流物理与加速器技术	2014-06-14	德国
58	第五届国际粒子加速器会议	Development of Digital Power Supply Controller Based on FPGA at SSRF	李瑞	墙报报告	束流物理与加速器技术	2014-06-14	德国
59	2014 应用超导国际会议	Design and test results of a Model Superconducting Undulator	许皆平	墙报报告	束流物理与加速器技术	2014-08-10	美国
60	2014 应用超导国际会议	Experimental Study of Beam-based Heat Load Using Cryogenic Calorimeter	崔剑	墙报报告	束流物理与加速器技术	2014-08-10	美国
61	2014 年国际高温后处理研究会议	Current progress in R&D on pyroprocess technology for TMSR in SINAP 上海应用物理研究所 TMSR 中心干法技术研发的进展报告	李晴暖	大会报告	核化学与核燃料化学	2014-10-19	美国
62	2014 年国际高温后处理研究会议	Electrochemical behavior of U, Th in fluoride molten salt 铀、钍在氟化熔盐中的电化学行为	龙德武	大会报告	核化学与核燃料化学	2014-10-19	美国
63	2014 国际统计物理会议	Asymmetrical Free Diffusion With Orientation-Dependence Of Molecules In Finite Timescales_	盛楠	大会报告	高分子理论计算与模拟	2014-07-06	希腊
64	第 27 届直线加速器国际会议	基于 pi 模的双枪微脉冲电子枪	赵明华	墙报报告	束流物理与加速器技术	2014-08-30	瑞士
65	第 27 届直线加速器国际会议	基于电子直线加速器太赫兹辐射源的研究	黄大章	墙报报告	束流物理与加速器技术	2014-08-30	瑞士
66	参加第 5 届亚洲三方重离子会议	Nucleon-nucleon correlation in heavy ion collision	方德清	大会报告	核物理	2014-08-04	日本
67	第 5 届亚洲三方重离子会议	Collectivity in p+p, p+A and A+A collisions from parton scatterings	马国亮	大会报告	核物理	2014-08-04	日本

68	2014 年度国际自由电子激光会议	Beam energy chirp effects in seeded free electron lasers	王东	墙报报告	自由电子激光原理和技术	2014-08-24	瑞士
69	2014 年度国际自由电子激光会议	Evolvement of the laser and synchronization system for the Shanghai DUV-FEL test facility	刘波	墙报报告	自由电子激光原理和技术	2014-08-24	瑞士
70	2014 年度国际自由电子激光会议	Using Off-Resonance Laser Modulation for Beam-Energy-Spread Cooling in Generation of Short-Wavelength Radiation	邓海啸	大会报告	自由电子激光原理和技术	2014-08-24	瑞士
71	2014 年度国际自由电子激光会议	Experimental study of the chirped pulse amplification in a seeded FEL	冯超	墙报报告	自由电子激光原理和技术	2014-08-24	瑞士
72	2014 年度国际自由电子激光会议	Division-of-amplitude photo-polarimeter for single-shot measurement of free electron laser at SDUV-FEL	冯冽	墙报报告	自由电子激光原理和技术	2014-08-24	瑞士
73	ASME 锅炉和压力容器委员会会议	ASME 完全评定方法中的失效概率分析	曾广礼	大会报告	力学中的基本问题和方法	2014-08-17	美国
74	第五届亚太辐射化学国际会议	Radiation grafting of acrylonitrile to UHMWPE fiber and its application for uranium extraction from seawater	吴国忠	大会报告	辐射化学	2014-09-07	日本
75	第五届亚太辐射化学国际会议	Radiation effect on polyacrylonitrile fiber and application of radiation technology in carbon fiber production	王谋华	分会报告	辐射化学	2014-09-07	日本
76	第五届亚太辐射化学国际会议	New avenues to the immobilization of nanoparticles onto polymers by radiation grafting	虞鸣	分会报告	辐射化学	2014-09-07	日本
77	第五届亚太辐射化学国际会议	Selective adsorption, reduction and separation of Au (III) from aqueous solution by amine-type adsorbent prepared from radiation induced graft polymerization	马红娟	分会报告	辐射化学	2014-09-07	日本
78	“第八届纳米结构高聚物和纳米复合物 ECNP 国际会议”	Nanoscale Control on the Assembly of Amyloid-like Peptides at Solid/Water Interfaces	张益	墙报报告	生物物理化学	2014-09-15	德国

79	2014 低发射度储存环国际研讨会和考察 INFN 实验室 DAfNE 加速器	On axis injection scheme for ultimate storage ring with double RF systems	姜伯承	大会报告	束流物理与加速器技术	2014-09-16	意大利
80	第四届美国、日本物理学会核物理分会联合会议	STAR 在超核及反超核物理的研究进展	陈金辉	大会报告	核物理	2014-10-06	美国
81	2014 年度第三届核燃料循环研讨会	Tactical-Level Implementation Assessment of Molten-Salt Reactor Technologies	蔡翔舟	大会报告	核化学与核燃料化学	2014-07-21	美国
82	第三届有机氚国际研讨会	Study of OBT Concentration in crops Acutely Exposed to Atmospheric HTO at Different Daytime	钱渊	墙报报告	核技术及其应用	2014-09-14	加拿大
83	IBIC 2014 国际会议	BUNCH BY BUNCH DBPM PROCESSOR DEVELOPMENT AND PRELIMINARY EXPERIMENT IN SSRF	冷用斌	大会报告	束流物理与加速器技术	2014-09-13	美国
84	IBIC 2014 国际会议	A Self-trigger Abnormal Beam Operation Monitor	赖龙伟	墙报报告	束流物理与加速器技术	2014-09-13	美国
85	IBIC 2014 国际会议	Beam Based Injector Measurement in SSRF	陈之初	墙报报告	束流物理与加速器技术	2014-09-13	美国
86	2014 年度核材料国际会议	Enhanced molten salt corrosion in Hastelloy N by dissimilar material interactions at high temperature	侯娟	分会报告	金属高温腐蚀与防护	2014-10-25	美国
87	2014 年度反应堆物理国际会议	Reactivity-insertion-transient Analysis of a Fluoride Salt Cooled High Temperature Reactor	杨洋	分会报告	核技术及其应用	2014-09-27	日本
88	PCaPAC 2014 国际会议	Beam data logging system base on NoSQL database at SSRF	阎映炳	墙报报告	束流物理与加速器技术	2014-10-13	德国
89	参加 2014 年度 XRM 国际会议	X - RAY MiCROSCOPY RELATED STUDIES IN SSRF: THE CURRENT AND THE FUTURE	邰仁忠	墙报报告	同步辐射技术及其应用	2014-10-25	澳大利亚
90	2014 年度 XRM 国际会议	Conceptual Design for the Hard X-ray Nanoprobe Beamline at the SSRF	李爱国	墙报报告	同步辐射技术及其应用	2014-10-25	澳大利亚
91	2014 年度 XRM 国际会议	PTYCHOGRAPHIC COHERENT DIFFRACTION IMAGING AT STXM BEAMLINE OF THE SSRF	许子健	墙报报告	同步辐射技术及其应用	2014-10-25	澳大利亚

92	2014 年度 XRM 国际会议	Potential Applications on Environmental Science by Medium Energy Micro-probe Technique Proposed in SSRF Phase-II Beamlines Project	李丽娜	墙报报告	同步辐射技术及其应用	2014-10-25	澳大利亚
93	电离辐射和高分子论坛（IRaP2014）国际会议	Uranium collection from seawater using radiation-grafting technology: fiber adsorbent fabrication and adsorption test	吴国忠	大会报告	核技术在工、农业和医学中的应用	2014-10-04	韩国
94	电离辐射和高分子论坛（IRaP2014）国际会议	Fabric modification by radiation methods	李景烨	大会报告	核技术在工、农业和医学中的应用	2014-10-04	韩国
95	电离辐射和高分子论坛（IRaP2014）国际会议	Preparation and characterization of novel cellulose fibers organic-inorganic hybrid	胡江涛	墙报报告	核技术在工、农业和医学中的应用	2014-10-04	韩国
96	电离辐射和高分子论坛（IRaP2014）国际会议	Fabrication of soluble multi-walled carbon nanotubes by gamma-ray irradiation	张伯武	墙报报告	核技术在工、农业和医学中的应用	2014-10-04	韩国
97	2014 年度 X 射线显微国际会议和大数据研讨会	X-Ray Fluorescence Computed Tomography at SSRF	邓彪	分会报告	同步辐射技术及其应用	2014-10-24	澳大利亚
98	2014 年度 X 射线显微国际会议和大数据研讨会	BIG DATA FOR X-RAY IMAGING AT SSRF	王玉丹	墙报报告	同步辐射技术及其应用	2014-10-24	澳大利亚
99	2014 同步辐射装置设备与仪器机械工程设计大会	A MECHANICAL INSTALLATION PROTOTYPE FOR THE DCLS RADIATOR SECTION	殷立新	大会报告	同步辐射技术及其应用	2014-10-18	澳大利亚
100	2014 同步辐射装置设备与仪器机械工程设计大会	Mechanical Stability Monitoring for Storage Ring Key Components at SSRF	邓荣兵	大会报告	同步辐射技术及其应用	2014-10-18	澳大利亚
101	2014 同步辐射装置设备与仪器机械工程设计大会	Vacuum Chamber R&D for SXFEL Undulator	胡晓	大会报告	同步辐射技术及其应用	2014-10-18	澳大利亚
102	国际加速器运行会议	Operation progress and upgrade in SSRF	张庆磊	分会报告	束流物理与加速器技术	2014-10-25	德国
103	2014 锕系元素谱学中的先进技术国际研讨会	A Joint Photoelectron Spectroscopy and Theoretical Study on Uranium Halide Complexes	苏静	分会报告	核化学与核燃料化学	2014-11-02	德国
104	电子储存环激光康普顿伽马射线源国际研讨会	Laser-Compton Scattering activities at SINAP	陈建辉	大会报告	束流物理与加速器技术	2014-11-06	加拿大

105	访问罗马尼亚 ICIT 研究所并参加“低温与同位素分离进展 2014”国际会议	Diffusion characterization of hydrogen isotopes in GH3535 alloy for the application of molten salt reactors	张东勋	墙报报告	核技术在环境科学、地学和考古中的应用	2014-10-20	罗马尼亚
106	2014 锕系元素谱学中的先进技术国际研讨会	Probing the Electronic Structures of Uranyl Halides Using Anion Photoelectron Spectroscopy	刘洪涛	墙报报告	核化学与核燃料化学	2014-11-02	德国
107	2014 年核学会冬季年会和核能技术博览会，并访问 NuScale Power 公司	An Overview of the Thorium Program of the Chinese Academy of Sciences	徐洪杰	大会报告	反应堆物理与技术	2014-11-08	美国
108	第 6 届原子力显微镜生物医学国际会议	Investigating the Impact of Antigen Density on Antigen-antibody Binding Efficiency with AFM	李宾	墙报报告	生物物理化学	2014-12-12	美国
109	2014 不稳定核束物理国际研讨会(ISPUN14)及亚洲核物理协会（ANPhA）2014 理事会	Giant dipole resonance as a fingerprint of alpha clustering configura4ons of light nuclei	马余刚	大会报告	核物理	2014-11-02	越南
110	2014 年韩国核协会秋季学术会议	Overview of Thorium Utilization Strategy of TMSR	戴志敏	大会报告	反应堆物理与技术	2014-10-28	韩国
111	美国材料研究学会 2014 年秋季会议	Soft Engineering of Biosensing Interfaces with Self-Assembled DNA Nanostructures	樊春海	大会报告	无机材料化学	2014-11-30	美国
112	2014 年计算科学与工程国际探讨会	Dynamics of Surface of Metal Oxides	高嶷	大会报告	理论和计算化学	2014-12-12	香港
113	ASME 锅炉和压力容器委员会议	Tensile strength test for small graphite samples	曾广礼	大会报告	分析力学	2014-11-14	美国
114	高能核碰撞的“初始阶段”国际会议	Collective flow in small systems from parton scatterings	马国亮	大会报告	核物理	2014-12-02	美国
115	美国材料研究学会 2014 年秋季会议	Nano-bioeffects and Nanoscale Cellular Imaging	黄庆	大会报告	生物化学	2014-11-30	美国
116	2014 International Actinide Coordination Chemistry Symposium(2014 IACCS)	Theoretical Studies on Coordination Structures and Electronic Spectra of Actinyl Complexes	苏静	墙贴报告	锕系理论化学	2014.10.24	苏州大学
117	第三届两岸同步辐射学术研讨会	上海光源高能量分辨技术	王勇	口头报告	同步辐射技术	2014/9/21	上海
118	SSRF 国际评审	STXM and XIL beamline at SSRF	王勇	口头报告	同步辐射技术	2014/4/24	上海

119	International Conference on Water Science	Interfacial Nanobubbles investigated by Synchrotron Radiation Techniques	张立娟	口头报告	界面科学	2014.4.14	北京大学
120	Conference on Nanobubbles, Gas-filled Micropancakes and their Applications	Nanobubbles Investigated by Synchrotron Radiation Techniques	张立娟	口头报告	界面科学	2014.10.21	上海光源
121	Conference on Nanobubbles, Gas-filled Micropancakes and their Applications	Exploration on Mechanism of Anesthesia of Gas	张立娟	口头报告	界面科学	2014.10.21	上海光源
122	AMF-AMEC2014(亚洲铁电-电瓷国际会议)	Dual Relaxation Dynamics for the long range correlation of polarization clusters in ferroelectrics by Photo Correlation Spectroscopy（报告编号：I08-5B-A669）	郭智	邀请报告	材料，光学	2014.10.26	上海国际会议中心
123	AOFSRR2014	A new extra-focus monochromator designed for high-performance VUV beamlines	吴衍青	展板报告	同步辐射束线技术	2014.9.15	台湾新竹
124	14th ISE Topical Meeting	Immunosensors Based on SPE and Nano-assembly for Rapid Biodetection	宋世平	Oral presentation	电化学	2014.3.29	南京
125	EPICS Collaboration meeting 2014	Development Status of SINAP Timing Syatem	赵黎颖	口头报告	加速器控制系统	2014.5.19	兰州
126	EPICS Collaboration meeting 2014	The Status of Machine Interlock System Co-designed by Cosylab and SINAP	赵黎颖	口头报告	加速器控制系统	2014.5.19	兰州
127	EPICS Collaboration meeting 2014	Development Status of SINAP Timing Syatem	蒋舸扬	口头报告	加速器控制系统	2014.5.19	兰州
128	EPICS Collaboration meeting 2014	The Status of Machine Interlock System Co-designed by Cosylab and SINAP	蒋舸扬	口头报告	加速器控制系统	2014.5.19	兰州
129	International workshop on Cluster structure of unstable nuclei and its decay	Alpha-clustering and its effect on GDR in a QMD-based model	马余刚	大会报告	核物理	2014.12	南京

130	PKU - CUSTIPEN Nuclear Reaction Workshop “Reactions and Spectroscopy of Unstable Nuclei"	How alpha-Cluster Configuration Affects Giant Dipole Resonance,	马余刚	大会报告	核物理	2014.8.10	北京
131	A STAR Regional Meeting & a workshop on “high temperature and high density nuclear matter study”	Low energy correspondences on nuclear modification factor and shear viscosity in HIC	马余刚	大会报告	核物理	2014.8.19	威海
132	Facilities, activities, and plans for HIC in China	International Workshop on Simulations of Low and Intermediate Energy Heavy Ion Collisions (Transport 2014)	马余刚	大会报告	核物理	2014.1.8	上海
133	The 4th International Workshop on Nuclear Dynamics in Heavy-Ion Reactions (IWND2014)	How Exotic Cluster Configuration Affects the Collective Motion in Nuclei	曹喜光	大会报告	核物理	2014.8.15	兰州
134	international Workshop on simulations of low and intermediate energy heavy ion collisions	Detailed presentation of results of homework 1 and 2, IBUU description, and initialization discussions	徐骏	大会报告	核物理	2014.1.8	上海
135	the 4th International Workshop on Nuclear Dynamics in Heavy-Ion Reactions (IWND2014)	Mean-field potential effects on the elliptic flow splitting at RHIC	徐骏	大会报告	核物理	2014.8.15	兰州
136	The international Workshop on simulations of low and intermediate energy heavy ion collisions	Summary talk of code comparison for transport2014 (heavy-ion part)	徐骏	大会报告	核物理	2014.8.15	兰州
137	KITPC program: Present Status of the Nuclear Interaction	Study in-medium spin-orbit interaction with heavy-ion collisions	徐骏	大会报告	核物理	2014.9	北京
138	compressed baryonic matter physics workshop	Relevant topics in asymmetry studies	徐骏	大会报告	核物理	2014.11	武汉

139	The 4th International Workshop on Nuclear Dynamics in Heavy-Ion Reactions (IWND2014)	Nuclear Modification factor and radial flow in Au+Au@1GeV	吕明	大会报告	核物理	2014.8.15	兰州
140	The 2nd workshop on “QCD vacuum and matter under strong magnetic field”	Final state effects on chiral magnetic effect and chiral magnetic wave	马国亮	大会口头报告	相对论重离子碰撞	2014.10.15	北京
141	STAR Regional Meeting & 973 Workshop	Collectivity in small systems from parton scatterings	马国亮	大会口头报告	相对论重离子碰撞	2014.8.19	威海
142	Sino-Thai 2014 Symposium on High Energy Physics and Beyond	Long-range azimuthal correlations in p+p, p+Pb and Pb+Pb collisions from a multi-phase transport model	马国亮	大会口头报告	相对论重离子碰撞	2014.6.1	武汉
143	The 9th Asian Meeting on Synchrotron Radiation Biomedical Imaging	Study on biomedical materials for bone tissue regeneration by synchrotron radiation-based X-ray Imaging	郭瀚	口头报告	X 射线成像	2014.11.5	云南省迪庆州
144	The 6th Asian Conference on High Pressure Research	Recent HP progress at SSRF	杨科	口头报告	同步辐射应用	2014.8.8	北京
145	参加 2014 年度第三届核燃料循环研讨会	Overview of TMSR in China	张岚	大会报告	核化学与核燃料化学	2014-07-21	美国
146	第 18 届熔盐堆临时系统指导委员会会议	Current Status of TMSR in China	蔡翔舟	大会报告	反应堆物理与技术	2014.5.28	上海
147	第九届 GIF 国际论坛核石墨工作组会议	Test Method for Splitting Tensile Strength of Graphite Specimens	曾广礼	大会报告	反应堆物理与技术	2014.9.22	上海
148	Collaborative Work Meeting on Accelerator Driven Sub-critical Systems (ADS) Applications and Use of Low-Enriched Uranium (LEU) in ADS	Recent Progress of TMSR Project	郭威	大会报告	反应堆物理与技术	2014.9.8	安徽合肥
149	HTR2014 国际高温气冷堆技术会议	Seismic Study of TMSR graphite core structure	曾广礼	分会报告	反应堆物理与技术	2014.10.27	山东威海

150	2014 International Actinide Coordination Chemistry Symposium (2014 IACCS)	Theoretical Studies on Coordination Structures and Electronic Spectra of Actinyl Complexes	苏静	展板报告	锕系理论化学	2014.10.24	苏州
151	15th International Nuclear Graphite Specialists Meeting	A Novel Clamp Design for Small Graphite Samples Used in Tensile Splitting Test	张灿	分会报告	核石墨	2014.9.15	杭州
152	16th International Nuclear Graphite Specialists Meeting	The compatibility between graphite and molten salt in molten salt reactor	贺周同	分会报告	材料科学	2014.9.15	杭州